



**HAL**  
open science

# Structural study of the ABC transporter “ *Bacillus subtilis* multidrug resistance ATP ” and characterization of the amphipathic belt wrapping membrane proteins

Veronica Zampieri

## ► To cite this version:

Veronica Zampieri. Structural study of the ABC transporter “ *Bacillus subtilis* multidrug resistance ATP ” and characterization of the amphipathic belt wrapping membrane proteins. Biochemistry, Molecular Biology. Université de Lyon, 2020. English. NNT : 2020LYSE1334 . tel-03538210

**HAL Id: tel-03538210**

**<https://theses.hal.science/tel-03538210v1>**

Submitted on 20 Jan 2022

**HAL** is a multi-disciplinary open access archive for the deposit and dissemination of scientific research documents, whether they are published or not. The documents may come from teaching and research institutions in France or abroad, or from public or private research centers.

L'archive ouverte pluridisciplinaire **HAL**, est destinée au dépôt et à la diffusion de documents scientifiques de niveau recherche, publiés ou non, émanant des établissements d'enseignement et de recherche français ou étrangers, des laboratoires publics ou privés.



N°d'ordre NNT : 2020LYSE1334

## **THESE de DOCTORAT DE L'UNIVERSITE DE LYON**

opérée au sein de  
**l'Université Claude Bernard Lyon 1**

**Ecole Doctorale N° ED 205**  
**Ecole Doctorale Interdisciplinaire des Sciences et Santé**  
**(EDISS)**

**Spécialité de doctorat :**  
**Biochimie**

Soutenue publiquement le 18/12/2020, par :

**Veronica Zampieri**

---

**Structural study of the ABC transporter  
« *Bacillus subtilis* multidrug resistance ATP »  
and characterization of the amphipathic belt  
wrapping membrane proteins**

---

Devant le jury composé de :

Pr. Adriana MIELE, <i>Institut de Chimie et Biochimie Moléculaire et Supramoléculaires</i>	Présidente
Dr. Cécile BREYTON <i>Institut de Biologie Structurale</i>	Rapporteuse
Dr. Mickael BLAISE <i>Institut de Recherche en Infectiologie de Montpellier</i>	Rapporteur
Dr. Martin PICARD, <i>Laboratoire de Biologie Physico-Chimique des Protéines Membranaires</i>	Rapporteur
Dr. Isabelle BROUTIN, <i>Laboratoire de Cristallographie et RMN Biologiques</i>	Examinatrice
Dr. Vincent CHAPTAL, <i>Laboratoire de Microbiologie Moléculaire et Biochimie Structurale</i>	Directeur de thèse
Dr. Pierre FALSON, <i>Laboratoire de Microbiologie Moléculaire et Biochimie Structurale</i>	Co-directeur de thèse



# **Université Claude Bernard – LYON 1**

Administrateur provisoire de l'Université	M. Frédéric FLEURY
Président du Conseil Académique	M. Hamda BEN HADID
Vice-Président du Conseil d'Administration	M. Didier REVEL
Vice-Président du Conseil des Etudes et de la Vie Universitaire	M. Philippe CHEVALLIER
Vice-Président de la Commission de Recherche	M. Jean-François MORNEX
Directeur Général des Services	M. Pierre ROLLAND

## **COMPOSANTES SANTE**

Département de Formation et Centre de Recherche en Biologie Humaine	Directrice : Mme Anne-Marie SCHOTT
Faculté d'Odontologie	Doyenne : Mme Dominique SEUX
Faculté de Médecine et Maïeutique Lyon Sud - Charles Mérieux	Doyenne : Mme Carole BURILLON
Faculté de Médecine Lyon-Est	Doyen : M. Gilles RODE
Institut des Sciences et Techniques de la Réadaptation (ISTR)	Directeur : M. Xavier PERROT
Institut des Sciences Pharmaceutiques et Biologiques (ISBP)	Directrice : Mme Christine VINCIGUERRA

## **COMPOSANTES & DEPARTEMENTS DE SCIENCES & TECHNOLOGIE**

Département Génie Electrique et des Procédés (GEP)	Directrice : Mme Rosaria FERRIGNO
Département Informatique	Directeur : M. Behzad SHARIAT
Département Mécanique	Directeur M. Marc BUFFAT
Ecole Supérieure de Chimie, Physique, Electronique (CPE Lyon)	Directeur : Gérard PIGNAULT
Institut de Science Financière et d'Assurances (ISFA)	Directeur : M. Nicolas LEBOISNE
Institut National du Professorat et de l'Education	Administrateur Provisoire : M. Pierre CHAREYRON
Institut Universitaire de Technologie de Lyon 1	Directeur : M. Christophe VITON
Observatoire de Lyon	Directrice : Mme Isabelle DANIEL
Polytechnique Lyon	Directeur : Emmanuel PERRIN
UFR Biosciences	Administratrice provisoire : Mme Kathrin GIESELER
UFR des Sciences et Techniques des Activités Physiques et Sportives (STAPS)	Directeur : M. Yannick VANPOULLE
UFR Faculté des Sciences	Directeur : M. Bruno ANDRIOLETTI



Alla mia mamma, per avermi sempre incoraggiata ad andare oltre.

# REMERCIEMENTS

Je commence par remercier les rapporteurs de cette thèse le Dr. Mickael Blaise, le Dr. Cécile Breyton et le Dr. Martin Picard ainsi que les autres membres du jury le Dr. Isabelle Broutin et le Pr. Adriana Miele. Je tiens à vous exprimer ma gratitude pour avoir accepté de juger mes travaux de thèse.

Mes remerciements s'adressent ensuite à mes directeurs de thèse dont l'optimisme a souvent été essentiel pour le déroulement de ce projet de thèse. Je vous remercie Dr. Pierre Falson pour m'avoir accueillie au sein de l'équipe et m'avoir fait confiance lors de mon stage de Master 2. Je vous remercie aussi d'avoir partagé votre enthousiasme et vos connaissances. Enfin, merci pour tous les conseils que vous m'avez donné tout au long de la thèse. Je tiens à exprimer ma plus sincère gratitude pour ces années de thèse au Dr. Vincent Chaptal. Je te remercie pour ta patience et ton enthousiasme. Je tiens aussi à te remercier d'avoir su m'écouter, de m'avoir accompagnée dans cet apprentissage scientifique en repoussant mes limites avec de la bienveillance.

Merci aux Drs. Isabelle Broutin and Jean-Michel Jault pour avoir fait partie de mon comité de suivi de thèse. Je vous remercie pour vos précieux conseils.

Je tiens aussi à remercier les collaborateurs : Dr. Ahcène Boumendjel et Kim-Anh Nguyen pour le détergent DCOD, Dr. Luca Monticelli et Dr. Juliette Martin pour les simulations de dynamique moléculaire et Dr. Guillaume Launay pour le développement du serveur Det.Belt.

J'adresse mes remerciements à la plateforme PSF qui m'a permis d'effectuer mes expériences dans de bonnes conditions. Pour cela je remercie le Dr. Virginie Gueguen-Chainon. Je tiens aussi à remercier Eric Diesis pour toutes les discussions en italiens mais également d'avoir toujours été disponible. Enfin, j'adresse mes sincères remerciements au Dr. Frédéric Delolme pour ton encadrement, ta patience, ton écoute et ta disponibilité.

Je remercie les membres de l'équipe du Dr. Jean-Michel Jault. Merci au Dr. Cédric Orelle pour les discussions, l'encadrement, ta disponibilité à m'aider. Je tiens aussi à remercier tous les doctorants qui m'ont toujours bien accueillie quand je passais dans leur laboratoire : Benjamin Bourgey (mon vrai ami), Margot Di Cesare, Waqas Javed, Maty Diagne, Khadija Mathieu et Sylvain Vallet. Merci Maty de m'avoir accompagnée pendant ces trois années de thèse, merci pour les discussions et les encouragements. Ma chère Khadija, merci pour les discussions, tes précieux conseils et ta bienveillance. Je te remercie d'avoir été présente même après la fin de ta thèse. Enfin, merci à Sylvain. Alors, merci monsieur, pour avoir ramené de la bonne humeur pendant la dernière période de ma thèse. Merci d'avoir vu au-delà des apparences et de m'avoir montré de la bienveillance envers mes moments de saturation.

Je tiens aussi à remercier l'ensemble de l'IBCP pour les discussions et les bons moments partagés ensemble. Merci à Chantal, Denis (merci pour le cactus), Guillaume, Joshua, Eva, Anais, Cecilia, Léa, Mathieu et Jad.

Un remerciement particulier à toutes les personnes qui ont fait partie de l'équipe DRMP.

Merci au Dr. Hélène Cortay pour toutes les discussions et les conseils dans le domaine scientifique, professionnel et personnel. Je te remercie aussi pour la bonne humeur que tu as toujours ramenée avec toi au labo ainsi que de m'avoir souvent fait rire pour tes excellents commentaires toujours au bon moment.

A Sandrine. Merci à toi pour m'avoir appris à manipuler et vivre dans un labo. Je ne te remercierai jamais assez d'avoir été plus qu'une enseignante/collègue, tu as été une amie et un binôme. Merci d'avoir répondu à toutes mes questions bêtes, de m'avoir écouté dans les bons et mauvais moments en essayant toujours de me comprendre et me rassurer.

Un remerciement spécial à Marie et Laurent. Merci Marie pour ta bonne humeur, ton humour et ton rire. Je veux te remercier pour la bienveillance que tu m'as toujours montrée. Merci Laurent pour tous les moments passés ensemble.

Merci aussi pour les bons moments passés au labo avec tous les stagiaires qui sont passés : Sébastien, Patricia, Suman, Magda, Rasoul et Anissa. Enfin, merci aux deux stagiaires qui ont contribué à mon projet de thèse Armelle et Flore.

A ma petite tribu de stagiaires : Laurie, Thibaut, Morane, Jorgo et Alexia. Laurie, merci d'avoir apporté ton esprit solaire et ta bonne humeur dans mes journées et surtout pour avoir été mon amie et de mon côté. Thibaut, merci pour ta présence et ton écoute ; toujours présent même après ton départ du labo. Et Chère Morane, merci pour la période passée ensemble. Merci pour le partage et les discussions sur ce que d'habitude les personnes cachent.

Merci à mes deux petits doctorants, Alexia et Jorgo. Même si la majorité du temps vous m'embêtez, je vous remercie d'avoir rempli d'énergie et de bonne humeur cette dernière année de thèse. Jorgo tu fais le dur mais finalement tu ne l'es pas tant que ça. Merci d'avoir été présent dans les moments compliqués et pour les bons moments passés ensemble. Alexia, merci pour toutes les discussions et les moments ensemble. Ça a été un vrai plaisir de te former et d'avoir pu t'aider dans tes premiers pas dans ce projet BmrA. Même si des fois tu en as pas l'impression, je suis heureuse de te laisser mon bébé BmrA, je suis sûre que tu en prendras bien soin.

A Josiane, merci de m'avoir montré comment il est possible d'être forte même dans les situations plus difficiles. Des fois, il n'y a pas besoin de faire trop de bruit, il faut juste être là et avancer. Merci pour toutes les discussions, les goûters, les journées de purif et les câlins dans les jours difficiles.

A Alexis. Mon binôme d'aventure et de désastres. Je te remercie pour toutes les années passées dans ce labo. Merci de m'avoir toujours écoutée, comprise et rassurée. Merci pour tes blagues auxquelles je rigolais sans faille. En vrai, il y a une liste entière de choses pour lesquelles je voudrais te remercier en commençant par le support technique et en finissant par les échanges d'idées. J'espère pouvoir travailler à nouveau avec toi un jour.

A Emile. Merci pour toutes les fois où tu ne m'as pas laissée seule au labo quand je prenais du retard dans mes manip (pour manque d'organisation selon ton dire). Merci aussi de m'avoir poussé à voir les choses d'un autre angle et donc d'agir de manière différente.

A Rachad. Mon ami de pizza and wine therapy. Merci de m'avoir guidé pendant mes débuts au labo. Merci pour ta bienveillance, ton écoute toujours attentionnée et ta présence même à distance. Merci pour cette amitié qui va bien au-delà des paillasses du labo.

Un ringraziamento in particolare alle mie amiche, per avermi mostrato cosa vuol dire essere forti in mille sfumature diverse.

Grazie Silvi per il tuo semplicemente esserci e di avermi mostrato la potenza dell'affidarsi e rischiare. Le nostre chiamate sono sempre una fonte di gioia e carica per me.



Grazie a te Ele, per essere sempre stata presente quando con un messaggio cercavo la tua presenza e il tuo conforto. La vita ha voluto che nonostante la distanza i nostri percorsi siano stati simili. Per questo, ringrazio che tu ci sia stata, perché ogni difficoltà è stata meno difficile, perché la vivevi con me.

Grazie Chiari, per avermi spesso accolta da te con le braccia aperte per darmi un forte abbraccio appena arrivata. Grazie di essere stata un costante punto di riferimento da quando ci siamo conosciute. Ti ringrazio di esserti spesso presa cura di me (soprattutto dandomi da mangiare) specialmente in questo ultimo periodo di tesi. Sei davvero un'amica preziosa.

Merci ma chère coloc, Emilie. Je pense que de simples mots ne sont pas suffisants pour te remercier de ton soutien tout le long de cette thèse. Merci pour nos rendez-vous tous les mercredis, pour tous les repas (surtout ceux préparés par toi), les randonnées, les sorties, pour nos discussions et pour toujours être prête à m'aider. Tu es la meilleure coloc !

A Jessi, che non vuole essere nel mucchio. Sapendo che tanto non ne fai parte e non ne farai mai parte. Perché quando si è famiglia in fin dei conti il legame non ha neanche bisogno di essere descritto.

Alla mia Maura. Ti ringrazio di mostrarmi ogni giorno cosa voglia dire essere forti e vulnerabili allo stesso tempo, di mostrarmi come determinazione e passione ti possano portare ovunque il tuo obiettivo sia. Ti ringrazio che nonostante la nostra grande differenza caratteriale, siamo una il luogo sereno dell'altra. Grazie di esserci stata e di avermi spesso dato la forza per andare avanti.

A te che nonostante tutto sei ancora qui a esserci per me. Ti ringrazio per aver visto in me un potenziale ancora in quel primo anno qui in Francia. Grazie di essere stato la mia famiglia dai primi istanti in questo paese straniero. Voglio soprattutto ringraziarti di avermi incoraggiata in ogni situazione, di avermi sostenuta e di aver tifato per me. Sicuramente non sarei qui ora senza di te. Obrigada pra me ter apredido a viver os momentos difíceis com um pouco de ironia e assim de ter uma linguagem so nossa. I love you so.

Per finire un grazie alla mia grande famiglia così viva, calorosa, semplice e amorosa. Sono fortunata ad essere cresciuta in questo posto caotico e ricco di persone. Grazie di rendere ogni ritorno ricco di abbracci e di bei momenti. Un speciale ringraziamento alla mia guendalina, alla mia compagna di giochi e di vita fin dall'inizio. Grazie Ari di esserci sempre per ascoltarmi senza nessun giudizio volendomi semplicemente bene. Per finire, grazie alla mia sorellona, che nonostante la distanza, mi fa sempre sentire amata. Grazie al mio papà che con il suo modo un poco da brontolo e con lamenti mi fa capire come gli manco e come mi vuole bene. L'ultimo ringraziamento va alla mia mamma. Grazie di essere semplicemente come sei, sei la persona che più mi ha spinto a seguire i miei sogni e a venire in Francia. Grazie di mostrarmi ogni giorno la tua forza.



## Titre : Etude structurale du transporteur ABC « *Bacillus subtilis* multidrug resistance ATP » et caractérisation de la couronne amphiphile des protéines membranaires

Selon l'Organisation Mondiale de la Santé (OMS), la résistance aux antibiotiques est devenue un des problèmes majeurs de la santé publique, surtout due à une utilisation incorrecte de ces molécules. Les bactéries peuvent adopter plusieurs mécanismes dont l'exportation de la molécule par des transporteurs membranaires. Les transporteurs ABC (ATP Binding Cassette) font partie des protéines responsables de ces processus ; elles utilisent l'ATP afin de garantir leur action. La protéine membranaire BmrA (*Bacillus subtilis* multidrug resistance ATP) est un transporteur ABC exprimé chez *Bacillus subtilis* qui est résistant à l'antibiotique Cervimycin C due à cette protéine membranaire. Elle possède aussi un phénotype MDR (multi-drug resistance) car elle peut transporter une large variété de molécules (doxorubicine, Hoechst 33342, etc.). Nous avons résolu la structure de BmrA par cristallographie et par Cryo-EM afin d'étudier son mécanisme. Les structures sont dans une conformation exposant la cavité vers l'extérieur (outward-facing conformation) et une d'entre-elles a le substrat, rhodamine 6G, fixé dans la région transmembranaire. L'analyse des structures de BmrA et celles d'autres transporteurs ABC met en évidence un mouvement en éventail de la région membranaire, que l'on a pu reproduire par des simulations de dynamique moléculaire. La flexibilité de cette région qui rémoigne de la plasticité des transporteurs ABC peut être responsable du relargage de la molécule.

Par ailleurs, la biologie structurale des protéines membranaires est un domaine complexe dû à leur nature amphiphile. La présence d'autres molécules amphiphiles comme les détergents ou les lipides est donc requise pour maintenir en solution ce type de protéines. La couronne qui se forme autour de leur partie hydrophobe a été caractérisée expérimentalement (quantification des détergents liés et estimation de la taille), puis modélisée (développement du serveur Det.Belt) et les résultats transposés à l'analyse des données de Cryo-EM.

Mots clés : BmrA, transporteur ABC, structure protéique, Cryo-EM, cristallographie aux rayons X, substrat, MDR

Title: Structural study of the ABC transporter « *Bacillus subtilis* multidrug resistance ATP » and characterization of the amphipathic belt wrapping membrane proteins

The antibiotic resistance is classified as a major human health threat by the World Health Organization (WHO) mainly due to a misuse of these compounds. Bacteria can adopt the different molecular mechanisms and one of them is the efflux of the compound outside of the cell. The ABC transporters are one of the membrane proteins responsible for this action. Their name derives from the fact that they use the ATP to ensure its activity. The membrane protein BmrA (*Bacillus subtilis* multidrug resistance ATP) is an ABC transporter from *Bacillus subtilis* and it confers the resistance to the antibiotic Cervimycin C. In addition, it displays a multi-drug resistance phenotype (MDR) since it exports various compounds (doxorubicin, Hoechst 33342, etc.) varying in size and shape. Structures of BmrA have been solved using X-ray crystallography and single particle Cryo-EM, aiming at understanding the mechanism of drug export. One of the structures has a substrate bound, rhodamine 6G, and all of them are in outward-facing conformation. The analysis of these structures, and those of other ABC transporters shows a hand-fan movement of a transmembrane region that could be reproduced by molecular dynamic simulations. This movement, typical of the plasticity of these transporters, could be responsible for the release of drugs.

Furthermore, the structural study of membrane proteins is complicated by their amphipathic nature. They require the presence of amphipathic molecules to stay in water solution. The amphipathic belt has been a constant focus during this project. It has been characterized experimentally by quantifying the amount of bound detergent together with the size and shape of the belt. Then, the Det.Belt server has been set up to dynamically draw this belt, depending on the detergents around. Finally, all this information has been used in the context of Cryo-EM to improve data analysis.

Keywords: BmrA, ABC transporter, structure, Cryo-EM, X-ray cristallography, substrate, MDR



## PUBLICATION LIST

“Glycosyl-Substituted Dicarboxylates as Detergents for the Extraction, Overstabilization, and Crystallization of Membrane Proteins”. Kim-Anh Nguyen<sup>1</sup>, Marine Peuchmaur<sup>1</sup>, Sandrine Magnard<sup>1</sup>, Romain Haudecoeur, Cédric Boyère, Saravanan Mounien, Ikram Benammar, Veronica Zampieri, Sébastien Igonet, , Dr. Anass Jawhari, Prof. Ahcène Boumendjel and Dr. Pierre Falson. 2018. *Angewandte Chemie (International Ed. in English)* 57 (11): 2948–52.

“Drug-bound and -free outward-facing structures of a multidrug ABC exporter point to a swing mechanism”. Authors: Vincent Chaptal<sup>1</sup>, Veronica Zampieri<sup>1</sup>, Benjamin Wiseman<sup>1</sup>, Cédric Orelle<sup>3‡</sup>, Juliette Martin<sup>2</sup>, Kim-Anh Nguyen<sup>2</sup>, Sandrine Magnard, Alexia Gobet, Margot Di Cesare, Waqas Javed, Arnaud Kilburg, Marine Peuchmaur, Julien Marcoux, Luca Monticelli, Martin Högbom, Jean-Michel Jault<sup>‡</sup>, Ahcène Boumendjel<sup>‡</sup> and Pierre Falson<sup>1\*</sup>. 2021. Submitted.

“Nanodisc, amphipol or detergent belts in cryoEM reconstructions of membrane proteins are similar and correspond to a common ordered solvent layer”. Veronica Zampieri, Alexia Gobet, Xavier Robert, Pierre Falson, Vincent Chaptal<sup>\*</sup>. Under Review, *Scientific Reports*, Feb. 2021.

## COMMUNICATIONS LIST

Journée scientifique de l'ARC Santé ; L'isle-d'Abeau ; 2017 ; Poster

Colloque de l'Association Française de Cristallographie ; Lyon ; 2018 ; short talk

Journée école doctorale EDISS ; Lyon ; 2018 ; short talk

GDR (Groupement de recherche) Protéines membranaires ; Carqueiranne ; 2019 ; short talk

FEBS meeting ABC2020 ; Innsbruck ; 2020; Poster

Séminaire interne MMSB ; Lyon ; 2020 ; short talk



# CONTENTS

REMERCIEMENTS .....	6
CONTENTS .....	15
FIGURES LIST.....	18
TABLES LIST.....	21
ABBREVIATIONS.....	23
FOREWORD .....	27
<b><u>BIBLIOGRAPHIC REVIEW .....</u></b>	<b>29</b>
I. Resistance to antibiotics.....	31
1. History of antibiotics .....	32
2. Antibiotic resistance .....	37
3. New strategy to counter antibiotic resistance .....	46
II. ABC transporters .....	49
1. Structure.....	50
1.1 The NBD.....	50
1.2 The TMD.....	52
1.3 Focus on type IV transporters .....	56
2. Transport mechanism.....	59
3. Structures of ABC exporters .....	65
4. <i>Bacillus subtilis</i> multi resistance ATP (BmrA) .....	69
III. Structural biology of membrane proteins .....	74
1. Amphipathic belt around the protein .....	75
1.1 Detergent.....	75
1.2 Nanodiscs .....	79
1.3 Polymers.....	82
2. Structural techniques .....	85
2.1 X-ray crystallography.....	87
2.2 Cryo-EM.....	93
IV. Conclusion .....	100
Objectives .....	101
<b><u>MATERIALS AND METHODS .....</u></b>	<b>103</b>
1. Materials.....	105
1.1 Bacterial strains .....	105
1.2 Plasmids and sequences.....	105



1.3 Culture media .....	107
1.4 Compounds .....	108
1.5 Detergents .....	109
2. Methods .....	110
2.1 Membrane scaffold protein preparation .....	110
2.1.1 MSP production.....	110
2.1.2 MSP purification .....	110
3. Mutagenesis .....	111
4. BmrA production .....	112
5. BmrA purifications.....	113
6. Protein quantification.....	115
6.1 BCA assay .....	115
6.2 Nanodrop.....	115
7. SDS-PAGE and Western Blot.....	116
7.1 SDS-PAGE .....	116
7.2 Western Blot .....	116
8. Functional studies.....	118
8.1 ATPase activity.....	118
8.2 Transport essays .....	119
8.3 Binding essays.....	120
8.4 Thermal stability assay.....	121
9. Structural studies.....	122
9.1 X-ray crystallography.....	122
10. Electron microscopy .....	124
10.1 Negative stain .....	124
10.2 Cryo-EM.....	125
10.3 Structure resolution.....	126
11. Detergent quantification .....	127
11.1 Cholate quantification .....	127
11.2 MALDI-TOF detergent quantification .....	127
<b>RESULTS.....</b>	<b>131</b>
Chapter I: BmrA E504A structures .....	133
1. Protein purification .....	136
2. Detergent Belt determination .....	142
3. Crystallogenesis.....	145
4. The DCOD additive .....	149
5. Cryo-protection .....	151

6. Experimental Phase determination assays.....	153
7. Cryo-EM.....	156
8. Resolution of the structures.....	157
9. Highlights of the manuscript relating the analysis of the structures of BmrA.....	161
10. Conclusion .....	162
Title: Drug-bound and -free outward-facing structures of a multidrug ABC exporter point to a swing mechanism .....	164
Chapter II: Preliminaries studies on BmrA .....	212
1. BmrA mutants to explore the flexibility of TM1-TM2 .....	215
1.1 BmrA I46D .....	215
1.2 BmrA I46C-I70C.....	219
2. Nanodisc reconstitution .....	225
2.1 MSP Purification.....	225
2.2 Reconstitution of BmrA into nanodisc.....	227
3. Structure in another conformation .....	233
4. Conclusion and discussion.....	236
Chapter III: Detergent belt representation .....	238
Chapter IV: Study of amphipathic belts in Cryo-EM reconstructions.....	244
Discussion and conclusion.....	278
<b><u>GENERAL DISCUSSION AND CONCLUSION .....</u></b>	<b><u>280</u></b>
<b><u>RESUME FRANÇAIS.....</u></b>	<b><u>286</u></b>
<b><u>REFERENCES.....</u></b>	<b><u>294</u></b>
<b><u>APPENDIX .....</u></b>	<b><u>310</u></b>

## FIGURES LIST

Figure 1. 2050 prediction of death distribution in the world due to antibiotic resistance.....	31
Figure 2. Timeline of the discovery of the antibiotics .....	33
Figure 3. Drug targets in bacteria and the antibiotic family targeting them.....	33
Figure 4. Timeline of resistance strains identification. ....	37
Figure 5. The antibiotic uptake in agriculture worldwide .....	38
Figure 6. Mechanisms of drug resistance used by the bacteria .....	40
Figure 7. Transporter families participating to the export of drugs .....	42
Figure 8. Preclinical projects developed to counter antibiotic resistance.....	47
Figure 9. The ABC transporters organization.....	50
Figure 10. Conserved motifs in the nucleotide binding domain (NBD) .....	52
Figure 11. Overview of the bacterial ABC transporters.....	54
Figure 12. Structure of Sav1866 .....	57
Figure 13. Conformations adopted by the ABC transporters.....	57
Figure 14. Upper view of Sav1866 (from the periplasmic space) .....	58
Figure 15. Coupling helices in the structure of Sav1866 .....	58
Figure 16. Conformational changes of MsbA and P-gp in presence of ATP studied by negative stain in electron microscopy .....	59
Figure 17. Mode of access of the substrate to the binding site .....	60
Figure 18. The constant contact model.....	62
Figure 19. The ATP-switch mechanism .....	64
Figure 20. Structures of TmrAB in multiple conformations .....	68
Figure 21. Cryo-EM micrograph of the ring shape BmrA structure.....	72
Figure 22. Structures of the ring shape BmrA complexes .....	73
Figure 23. Detergent behaviors in hydrophilic environment and examples of detergents .....	77
Figure 24. Structure of the nanodisc.....	80
Figure 25. Structure of SecYE inserted into the nanodisc formed by Apo A1 ( $\Delta$ 1-43) solved by Cryo- EM .....	81
Figure 26. Amphipols .....	82
Figure 27. Polymers SMA (styrene maleic acid copolymer) and DIBMA (diisobutylene-maleic acid copolymer) .....	84
Figure 28. Membrane protein structures.....	86
Figure 29. Detergent in crystals.....	88
Figure 30. Crystal packing of membrane protein .....	89
Figure 31. Histogram of crystal solvent content.....	90
Figure 32. Native-like environment to produce membrane protein crystals.....	91
Figure 33. First 3D model of a membrane protein .....	93
Figure 34. The three steps of the grid preparation for the Cryo-EM .....	94
Figure 35. 3D reconstitution method.....	95
Figure 36. The evolution of the cryo-EM on the resolution of the structure of the ribosome .....	96
Figure 37. Structure of the TRPV1 (PDB 3J5P) .....	97
Figure 38. Detergent visualized by negative stain electron microscopy .....	98
Figure 39. pET-15b plasmid .....	106
Figure 40. Reaction for the detection of ATPase activity .....	118
Figure 41. Curve obtained by a transport assay .....	120
Figure 42. Negative stain protocol .....	125

Figure 43. Detergent quantification method by mass spectrometry .....	129
Figure 44. Dynamic Light Scattering study on the mixture DDM-cholate .....	136
Figure 45. Affinity chromatography of the purification of BmrAE504A .....	137
Figure 46. Second affinity chromatography of the BmrA E504A purification .....	138
Figure 47. BmrA E504A purified with the ratio 1:1 DDM-cholate (0.035% and 0.03%, respectively) .....	139
Figure 48. BmrA E504A purified with the ratio 1:1.33 DDM-cholate (0.035% and 0.04%) .....	140
Figure 49. BmrA E504A purified with the ratio 1:3 DDM-cholate (0.035% and 0.1%) .....	141
Figure 50. Detergent belt around BmrA E504A obtained after the quantification of the detergent bound to BmrA E504A after its purification .....	143
Figure 51. Comparison of the detergent belt .....	144
Figure 52. Results of the screening of the crystallization conditions .....	145
Figure 53. Thermal stability assay of BmrA with/without ligand and/or nucleotide .....	147
Figure 54. Crystals of BmrA with a ligand (GF 120819X or rhodamine 6G) .....	148
Figure 55. The impact of DCOD detergents on the cristallogenesis of BmrA .....	150
Figure 56. Structure of the 3.9 f additive .....	150
Figure 57. Cryo protection mixes of the CryoProtX MD1-61 kit. ....	151
Figure 58. Cryschem sitting drop plate .....	152
Figure 59. Selenium methionine assay .....	153
Figure 60. Heavy atoms soaking essay .....	154
Figure 61. Conditions screening for single particles Cryo-EM .....	156
Figure 62. Resolution of X-ray crystallography structure .....	158
Figure 63. Cryo-EM structure resolution .....	159
Figure 64. Proposal of ABC transporters' mechanism with the insights discovered by this study..	163
Figure 65. Mutants of BmrA in the TM1-2 region are I46D (a) and I46C-I70C (b) .....	215
Figure 66. Quantification of BmrA I46D expression .....	216
Figure 67. Transport activity of the mutant BmrA I46D .....	216
Figure 68. Cleavage test of the mutant BmrA I46D .....	218
Figure 69. Quantification of BmrA I46C-I70C expression .....	219
Figure 70. Transport assays for BmrA I46C-I70C .....	220
Figure 71. Detection of the disulfide bond by SDS-PAGE .....	221
Figure 72. Test of equivalent TMRM for BmrA I46C-I70C .....	222
Figure 73. Revelation of TMRM signal after incubation of the protein in presence of different molecules .....	223
Figure 74. Detection of disulfide bond by the TMRM detection method .....	223
Figure 75. Purification of MSP1D1 .....	226
Figure 76. Purification of MSP1E3D1 .....	226
Figure 77. Purification of BmrA WT reconstituted onto nanodisc formed by MSP1E3D1 .....	227
Figure 78. Micrograph of the grid composed BmrA WT into MSP1E3D1 nanodisc .....	228
Figure 79. Purification of BmrA E504A reconstituted onto nanodisc formed by MSP1E3D1 .....	229
Figure 80. Micrograph of the grid composed BmrA E504A into MSP1E3D1 nanodisc .....	230
Figure 81. Purification of BmrA E504A reconstituted onto nanodisc formed by MSP1D1 .....	231
Figure 82. Micrograph of the grid composed BmrA E504A into MSP1D1 nanodisc .....	232
Figure 83. Binding of the tetraphenylphosphonium (TPP) on BmrA E504A .....	233
Figure 84. Micrographs of BmrA E504A with Tetraphenylphosphonium (TPP) .....	234
Figure 85. Density map obtained by Cryo-EM for BmrA E504 with TPP .....	235
Figure 86. Representation of the detergent belt .....	240
Figure 87. DetBelt server interface .....	241

<b>Figure 88. PDB oriented loaded to the DetBelt server .....</b>	<b>242</b>
<b>Figure 89. The choice of the detergent in the DetBelt server .....</b>	<b>242</b>
<b>Figure 90. Representation of the detergent belt in the DetBelt server.....</b>	<b>243</b>
<b>Figure 91. Résultats de l'étude structurale de BmrA.....</b>	<b>290</b>
<b>Figure 92. Perspectives étude de BmrA .....</b>	<b>291</b>
<b>Figure 93. Etude de la couronne autour des protéines membranaires .....</b>	<b>292</b>

## TABLES LIST

<b>Table 1. Antibiotics targeting the cell wall .....</b>	<b>34</b>
<b>Table 2. Antibiotics targeting the plasma membrane .....</b>	<b>35</b>
<b>Table 3. Antibiotics targeting essential enzymes .....</b>	<b>35</b>
<b>Table 4. Antibiotics targeting the protein synthesis .....</b>	<b>36</b>
<b>Table 5. Conserved motifs in the NBD and their role .....</b>	<b>51</b>
<b>Table 6. Classification of the human ABC transporters .....</b>	<b>53</b>
<b>Table 7. Structure of ABC exporters .....</b>	<b>65</b>
<b>Table 8. Binding experiments done by intrinsic fluorescence on BmrA purified in the detergent DDM .....</b>	<b>70</b>
<b>Table 9. List of the compounds used in this project .....</b>	<b>108</b>
<b>Table 10. List of the detergent used in this project .....</b>	<b>109</b>
<b>Table 11. List of the primers used for the mutagenesis on BmrA .....</b>	<b>112</b>



# ABBREVIATIONS

<b>ABC</b>	ATP-Binding cassette
<b>AcrB</b>	Acriflavine Resistance Protein A
<b>ADP</b>	Adenosine diphosphate
<b>AHS</b>	Access Hydrophobic Surface
<b>AMP-PNP</b>	Adenosine 5'-( $\beta,\gamma$ -imido)trisphosphate
<b>APS</b>	Ammonium persulfate
<b>ATP</b>	Adenosine triphosphate
<b>BmrA</b>	<i>Bacillus subtilis</i> multidrug resistance ATP
<b>BCA</b>	Bicinchoninic acid
<b>Bp</b>	base pair
<b>BSA</b>	Bovine Serum Albumin
<b><i>B. subtilis</i></b>	<i>Bacillus subtilis</i>
<b>CMC</b>	Critical micelle concentration
<b>CFTR</b>	Cystic Fibrosis Transmembrane conductance Regulator
<b>Cryo-EM</b>	Cryogenic Electron Microscopy
<b>CT<math>\mu</math></b>	Centre Technologique des Microstructures
<b>Da</b>	Dalton
<b>DCOD</b>	DiCarboxylate-Oside Detergent
<b>DDM</b>	N-Dodecyl $\beta$ -D-maltoside
<b>DHB</b>	2,5-Dihydroxybenzoic acid
<b>DIBMA</b>	Diisobutylene-maleic acid
<b>DLS</b>	Dynamic Lightening Scattering
<b>DNA</b>	Deoxyribonucleic acid
<b>dNTP</b>	Deoxyribonucleoside triphosphate
<b>DTT</b>	Dithiothreitol
<b>ECL</b>	Extracellular Cellular Loop
<b><i>E. coli</i></b>	<i>Escherichia coli</i>
<b>EDTA</b>	Ethylene Diamine Tetra-acetic Acid
<b>Hepes</b>	(4-(2-hydroxyethyl)-1-piperazineethanesulfonic acid)



<b>His</b>	Histidine
<b>ICD</b>	Intracellular domain
<b>IPTG</b>	Isopropyl- $\beta$ -D-thiogalactoside
<b>Kd</b>	Dissociation constant
<b>LB</b>	Luria Bertani medium
<b>LmrA</b>	<i>Lactococcus</i> multidrug resistance ATP
<b>LPS</b>	Lipopolysaccharides
<b>MALDI-TOF</b>	Matrix Assisted Laser Desorption Ionization – Time of Flight
<b>MATE</b>	Multidrug and toxic compound Extrusion
<b>MFS</b>	Major Facilitator Superfamily
<b>mAu</b>	Milli Absorbance unit
<b>MDR</b>	MultiDrug Resistance
<b>MES</b>	MorpholineEthaneSulfonic acid
<b>MPD</b>	2-Methyl-2,4-pentanediol
<b>MRP1</b>	Multidrug Resistance Protein 1
<b>mRNA</b>	Messenger Ribonucleic acid
<b>NATA</b>	N-Acetyl Tryptophan Amide
<b>MSP</b>	Membrane Scaffold Protein
<b>NAD</b>	Nicotinamide adenine dinucleotide
<b>NADH</b>	Nicotinamide adenine dinucleotide reduced
<b>NBD</b>	Nucleotide Binding Domaine
<b>NTA</b>	Nitrilotriacetic Acid
<b>NTP</b>	Nucleoside Tri Phosphate
<b>OD</b>	Optical Density
<b>OmpF</b>	Outer membrane protein F
<b>PCR</b>	Polymerase Chain Reaction
<b>PDB</b>	Protein Data Bank
<b>PEG</b>	PolyEthylene Glycol
<b>PEP</b>	Phosphoenol pyruvate
<b>P-gp</b>	Permeability-Glycoprotein or P-glycoprotein
<b>Pi</b>	Inorganic phosphate

<b>PK</b>	Pyruvate Kinase
<b>PMSF</b>	Phenylmethylsulfonyl fluoride
<b>RND</b>	Resistance-nodulation-cell division superfamily
<b>Rpm</b>	Revolution per minute
<b>PSF</b>	Protein Science Facility
<b>SAD</b>	Single wavelength Anomalous Diffraction
<b>SBP</b>	Substrate Binding Protein
<b>SDS</b>	Sodium Dodecyl Sulfate
<b>SDS-PAGE</b>	Sodium Dodecyl Sulfate – Polyacrylamide gel electrophoresis
<b>SEC</b>	Size exclusion chromatography
<b>SOC</b>	Super Optimal broth with Catabolite respression
<b>SMA</b>	Styrene Maleic Acid
<b>SMALP</b>	SMA-Lipid-Protein
<b>TB</b>	Terrific Broth
<b>TBS</b>	Tris Buffer Saline
<b>TEMED</b>	N,N,N',N'-Tetramethylenediamine
<b>TEV</b>	Tabacco Etch Virus protease
<b>TM</b>	TransMembrane segment
<b>TMD</b>	TransMembrane Domaine
<b>Tris</b>	Tris(hydroxymethyl)aminomethane
<b>UDM</b>	n-Undecyl $\beta$ -maltoside
<b>UV</b>	Ultraviolet
<b>VO<sub>4</sub><sup>3-</sup></b>	Vanadate
<b>v/v</b>	Volume/volume
<b>WHO</b>	World Health Organization
<b>WT</b>	Wild-type
<b>w/v</b>	Weight/volume



## FOREWORD

Antimicrobial resistance is a major human health issue responsible for 700,000 deaths worldwide in 2015. In 2050, the mortality rate is predicted to rise up 400,000 deaths in Europe, 4,000,000 in Africa and 5,000,000 in Asia. Therefore it will become the first cause of death (O'Neill, 2014). In 2019, the World Health Organization (WHO) created a list of the 12 most alarming bacteria, resistant to one or more class of antibiotics. On the top three, belongs *Acinetocacter baumannii*, *Pseudomonas aeruginosa* and *Enterobacteriaceæ* (Asokan et al. 2019).

Bacteria can resist to a given antibiotic by employing one or more of the following mechanisms: membrane impermeabilization, overexpression and/or mutation of the drug target, metabolization of the drug and export by efflux pumps (Allen et al. 2010). This last one is ensured by membrane proteins belonging to seven different families. The ABC (ATP-binding cassette superfamily) transporters is one of these proteins' families; its name derives from the fact that proteins of this family bind and hydrolyze ATP to function.

My thesis project focuses on one protein of this superfamily, the *Bacillus subtilis* multidrug resistance ATP, BmrA. *Bacillus subtilis* is a Gram (+) bacteria found in the soil and in the gastrointestinal tract. BmrA displays a high homology with others ABC transporters such as LmrA (*Lactococcus lactis* multidrug resistance ATP) and P-gp (human P-glycoprotein) also both implicated in the drug resistance phenomenon. Moreover, BmrA presents a multidrug phenotype since it binds and transports multiple molecules (Steinfels et al. 2004). For all these reasons, the study of the function and structure of BmrA have been undertaken to acquire more knowledge on the ABC transporters' mechanism that is still under debate.

The structural study of membrane proteins is a quite challenging field due to the amphipathic nature of this kind of proteins. From the beginning of the process of determination of BmrA structure, many optimizations were needed: overexpression (Steinfels et al. 2002), purification (Matar-Merheb et al. 2011) and ultimately crystallography. These 2 last steps were the main focus of the DRMP team. In particular, in the lab, Dr. Arnaud Kilburg implemented the purification protocol used for the resolution of the P-gp structure (Aller et al. 2009). He purified the protein with a mixture of DDM and cholate, which allowed the protein to crystallize and to diffract up to 8 Å resolution. My PhD project started here, with

the goal to improve the quality of the crystals to resolve the structure of the protein. I will present in this manuscript these improvements, the resolution of the BmrA structure by X-ray crystallography and Cryo-EM, leading to the preliminary studies based on these structures, and finally two side projects to characterize the detergent belts.

The manuscript starts with a bibliographic review on the antibiotic resistance, ABC transporters and structural studies on membrane proteins. Then, I describe the methods used during this project. The results are articulated as follows:

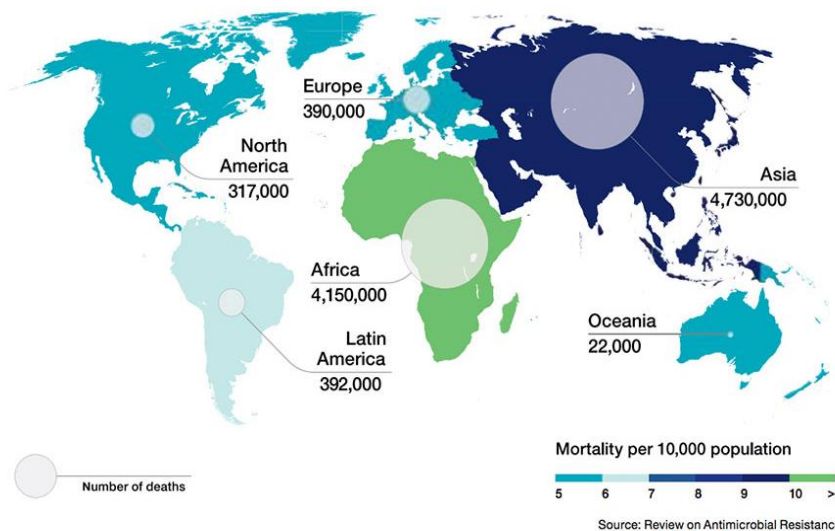
- ❖ **BmrA structures.** I describe the whole process to resolve the structure of BmrA. Then, I compare the structures with those of other ABC transporters.
- ❖ **Preliminaries studies on BmrA.** Mutants in the transmembrane region of the protein have been designed to investigate the plasticity of the BmrA structure. In parallel, the reconstitution of the protein in a more native-like environment has been initiated together with the determination of the cryo-EM structure of BmrA in another conformation.
- ❖ **DetBelt server.** Based on studies carried out by the DRMP team to quantify the amount of detergent bound to the membrane region of membrane proteins by mass spectrometry, I present the setup of a web server useful to visualize or to predict this detergent belt, done in collaboration with the Luca Monticelli's team.
- ❖ **Hydrophobic solvent in Cryo-EM analysis.** This part is focused on the study of the belt formed by amphipathic compounds surrounding the membrane region of a membrane protein, and of its use in the Cryo-EM data analysis.

# BIBLIOGRAPHIC REVIEW



# I. Resistance to antibiotics

WHO declared the antimicrobial resistance as one of the major public health threats concerning all countries around the world. In 2014, Jim O'Neil, reviewing the critical situation of the antimicrobial resistance, estimated that in 2050 it may become the first cause of death (O'Neill 2014). In Europe, every year 670,000 infections are caused by resistant bacteria, among them 33,000 lead to death (European Centre for Disease Prevention and Control ECDC, 2019). In the USA, it concerns 2.8 millions people from which 40,000 died (Redfield 2019). Without any action, in 2050 the deaths will mount up to 10 million worldwide, 390,000 in Europe, 310,000 in USA and up to 4 million in Africa (figure 1). Indeed, this health threat could be an important burden for all the world with a stronger impact on mortality and medical costs in developing countries.



**Figure 1. 2050 prediction of death distribution in the world due to antibiotic resistance**  
(Chaired by Jim O'Neill 2014).

The spreading of antimicrobial resistance induces a decrease in drug effectiveness which then provokes prolonged illness, increased mortality rate and consequently medical costs (Tanwar et al. 2014). The hospital related procedures would be compromised. For example, antibiotics are employed during surgery or chemotherapy treatments to prevent any infection to immunocompromised patients. In addition, others sectors than human health will be impacted: animal health and welfare, food production, livestock and crops, environment and



water sanitation, economic development, commerce and travel/tourism (Measures 2016).

Of note, the current SARS-Covid19 pandemic clearly shows the importance of available and efficient treatment against viruses. To this day 6<sup>th</sup> October 2020, in the whole world, cases of contracted virus are 35,511,291 and the deaths are 1,044,490 (Johns Hopkins Coronavirus Resource Center). This pandemic is showing us that we are not prepared to fight an unknown pathogen microorganism. The absence of treatment costs many lives around the world. There will surely be a strong social and economic crisis after this event. This scenario could be the same for a resistant pathogen microorganism (bacteria, parasite, virus or fungi) on which any already known treatment is inefficient. As such, it becomes more important to study the phenomena of antimicrobial resistance to be prepared to any possible bacterial pandemic.

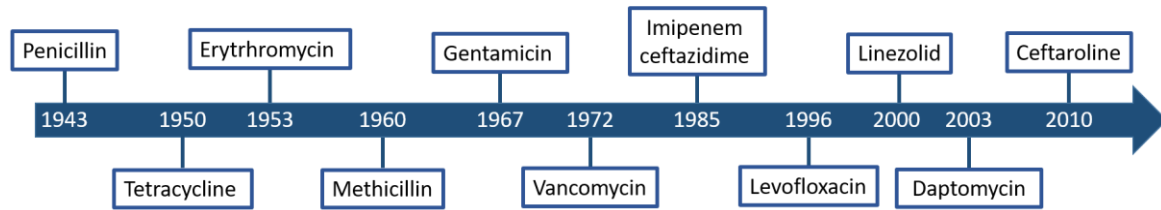
This chapter will focus on antibiotics and the resistance associated to them. Antibiotics inhibit the growth of bacteria or kill them. Their discovery has been a major revolution for human health. The actual problem nowadays is the resistance developed by bacteria which could lead us back to the pre-antibiotic era.

## 1. History of antibiotics

In 1928 Alexander Fleming discovered the first antibiotic by serendipity (Lobanovska and Pilla 2017). He left some of his Petri dishes on the bench during his holidays. The dish containing staphylococci was contaminated by a fungus called *Penicillium notatum*. Fleming noticed that the fungus produced a molecule inhibiting the bacteria growth. He published this discovery in the Experimental Pathology in 1929. This article was the starting point for the research conducted by three scientists at Oxford in 1939, Howard Florey, Ernst Chain and Norman Heatley, who purified penicillin and performed *in vivo* tests on mice. It was then necessary to improve the purity to get successful results on humans. In 1941, "The Penicillin Project" saw Florey and Chain to collaborate with Americans scientists to produce massively this antibiotic, which saved a lot of lives during the World War II. The Nobel Academy awarded Fleming, Florey and Chain the Nobel prize of medicine for the discovery and the development of Penicillin. Dorothy Hodgkin and Barbara Low determined the structure of this antibiotic by X-ray crystallography, confirming the predictions of Edward Abraham collaborator for the purification (Lobanovska and Pilla 2017).

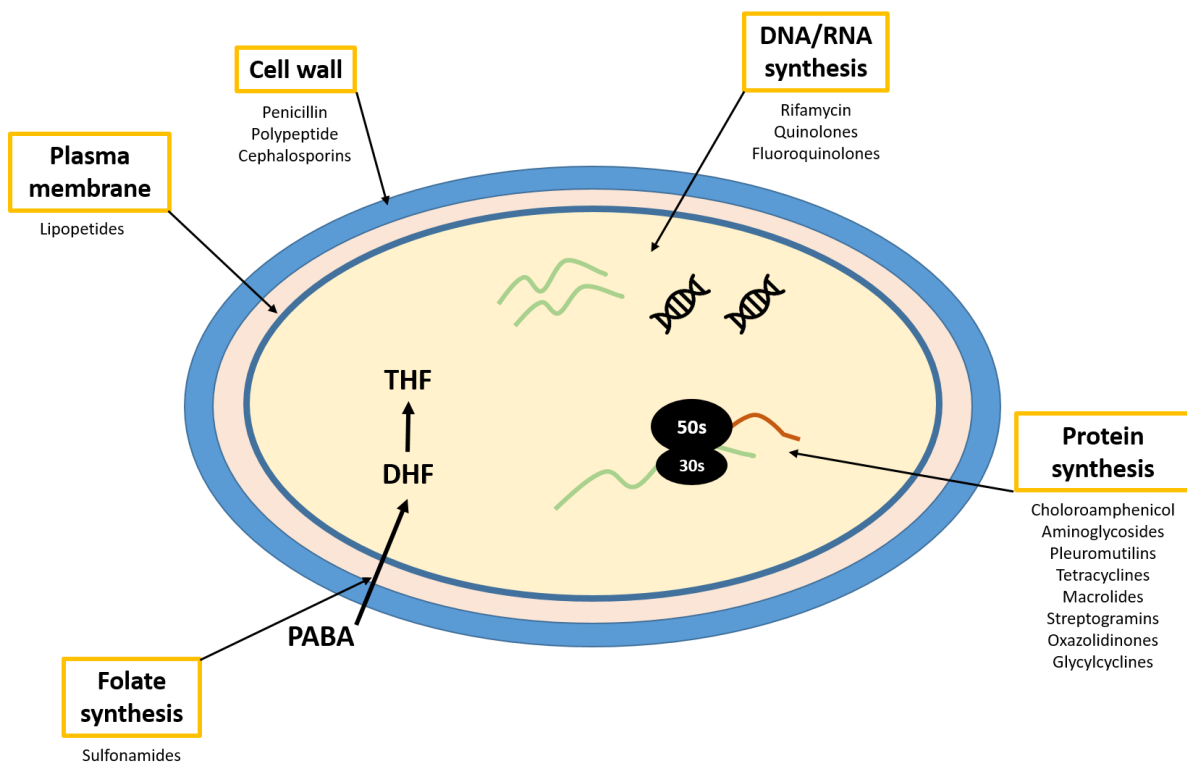
## BILIOGRAPHIC REVIEW

In the following years of this discovery other molecules were discovered (figure 2), found firstly in the soil. This led to the discovery of streptomycin, chloramphenicol and tetracyclin. Afterwards, synthetic antibiotics were produced.



**Figure 2. Timeline of the discovery of the antibiotics**  
(Ventola 2015)

A classification of these bioactive compounds is based on their potential targets which can be the cell wall, cell membrane or essential enzymes and protein synthesis (figure3) (Tortora, Funke, and Case 2015).



**Figure 3. Drug targets in bacteria and the antibiotic family targeting them**  
THF = tetrahydrofolic acid; DHF = dihydrofolate acid; PABA = para-aminobenzoic acid.  
Adapted from Dantas et al., 2014.

## BILIOGRAPHIC REVIEW

- Antibiotics targeting the cell wall

The bacteria cell wall is present in Gram (+) and (-) with variable thickness and location (Epanand et al. 2016). Gram (+) bacteria have a thick wall exposed to the extracellular space while Gram (-) bacteria have a thin wall in between an outer and inner membranes. Cell wall is made of peptidoglycan, essentially N-acetylmuramic and N-acetylglucosamine cross-linked by a peptide. Some antibiotics target the synthesis of the peptidoglycan by inhibiting the enzyme responsible for the cross-link of the polymers (table 1). Weakening the cell wall induces the lysis of the bacteria. These drugs have a low toxicity for human cell since peptidoglycans are specific of bacteria (Bugg and Walsh 1992).

**Table 1. Antibiotics targeting the cell wall**

ANTIBIOTIC FAMILY	ACTION MODE	COMMENTS
<b>PENICILLIN</b>	Inhibits peptidoglycan cross-linking (final step of the biosynthesis)	Their action is bactericidal. Common core structure: $\beta$ -lactam ring Natural penicillin act against Gram (+) bacteria. $\beta$ -lactamases are bacteria enzymes that cleave the $\beta$ -lactam ring which confer a resistance against this antibiotic. (Wise and Park 1965) Semisynthetic penicillins were designed to resist to these enzymes and to expand the spectrum to Gram (-).
<b>POLYPEPTIDE</b>	Inhibits peptidoglycan synthesis	Examples of this antibiotic family are bacitracin and vancomycin. (Bugg and Walsh 1992) Vancomycin has a narrow spectrum and is used against <i>Staphylococcus aureus</i> .
<b>CEPHALOSPORINS</b>	Inhibits peptidoglycan synthesis	Cephalothin and cefixime are examples of this family. Their action is similar to those of penicillin and derivatives. They also are metabolized by $\beta$ -lactamases.

- Antibiotics targeting the plasma membrane

Fatty acids are a major component of the plasma membrane. Their synthesis differs in human and bacteria cell. This class of drugs can target specifically the bacterial fatty acid production. These antibiotics modify the membrane permeability inducing the release of the microorganism's plasma, leading to cell death (table 2) (Epanand et al. 2016).

**Table 2. Antibiotics targeting the plasma membrane**

ANTIBIOTIC FAMILY	ACTION MODE	COMMENTS
<b>LIPOPEPTIDES</b>	Inhibits fatty acid synthesis	Daptomycins and polymixyn B belong to this family. Daptomycins are effective against Gram (+) and polymixyn B against Gram (-).

- Antibiotics targeting essential enzymes

Amongst essential enzymes, the ones participating in DNA replication and transcription are privileged targets for antibiotics (table 3), such as the DNA topoisomerase, DNA gyrase or RNA polymerase (Hooper 1998). Another one is the enzyme responsible for folic acid production, which is essential to synthesize purines and pyrimidines. This class of drugs is in competition with the *Para*-aminobenzoic acid (PABA) which is the precursor of the folic acid (Fernández-Villa, Aguilar, and Rojo 2019). They are not toxic for humans because the latter import it and cannot produce it.

**Table 3. Antibiotics targeting essential enzymes**

ANTIBIOTIC FAMILY	ACTION MODE	COMMENTS
<b>RIFAMPICIN</b>	Inhibits mRNA synthesis	It acts against mycobacteria.
<b>QUINOLONES, FLUOROQUINOLONES</b>	Inhibits DNA gyrase	Quinolones are the first synthetic drug (1960s). Fluoroquinolones were developed later in the 1980's. Bacteria easily develop resistance to these antibiotics.
<b>SULFONAMIDES</b>	Prevent the production of folic acid	There are bacteriostatic and not toxic for human.

- Antibiotics targeting the protein synthesis

Antibiotics inhibit protein expression by targeting the ribosome (table 4). Indeed, ribosomes are different in human and bacteria cells, exemplified by the fact that bacterial ribosomes are composed of 50s and 30s subunits (70s) while the human ones of 60s and 40s (80s). This means that there is no side effect of this class of antibiotics. The compounds bind to one of

## BILIOGRAPHIC REVIEW

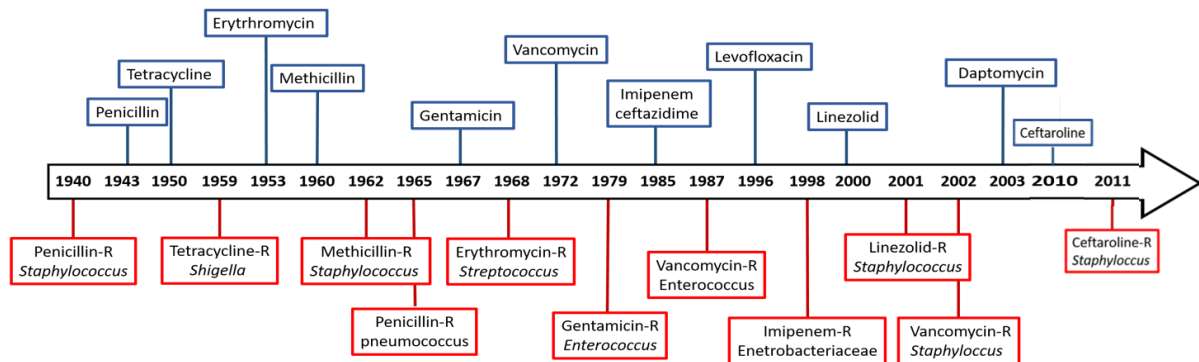
the two ribosomal subunits or to the tRNA site within the ribosome (Kohanski, Dwyer, and Collins 2010).

**Table 4. Antibiotics targeting the protein synthesis**

ANTIBIOTIC FAMILY	ACTION MODE	COMMENTS
<b>CHLORAMPHENICOL</b>	Inhibition of the 50s subunit of the bacterial ribosome	They have a broad spectrum of action.
<b>AMINOGLYCOSIDES</b>	Interaction with 30s subunit	They are bactericidal. Streptomycin belongs to this family. Their targets are Gram (-) bacteria.
<b>TETRACYCLINES</b>	Binding to tRNA	Their action is bacteriostatic. They prevent the addition of any amino acid. They have a broad spectrum of action. Semisynthetic molecules of this family were designed to stay longer in the body.
<b>MACROLIDES</b>	Binding to the 50s subunit	Their action is bacteriostatic. Erythromycin and ketolides are macrolides. They are composed with a macrocyclic lactone ring. These molecules are alternative to penicillin. Ketolides are developed to overcome the resistance. (Katz and Ashley 2005)
<b>STREPTOGRAMINS</b>	Interaction to the 50s subunit	Synercid is a mixture of 2 cyclic peptides. Each one interacts with two distinct parts of the ribosome subunit 50s.
<b>OXAZOLIDINONES</b>	Binding to the 50s subunit	They bind to the 50s subunit near the interaction site with 30s subunit. These synthetic molecules were designed to solve the resistance of vancomycin. They were approved by FDA in 2001.
<b>GLYCYLCYCLINES</b>	Binding to the 30s subunit	It's one of the newer antibiotic class. Tygecyclin is an example of this class. They are similar to the tetracycline.

## 2. Antibiotic resistance

During his Nobel award speech, Fleming warned us that the misuse of penicillin would lead to the development of resistant bacteria strain (Alexander Fleming 1945). Indeed, from the start of antibiotics use the resistance phenomena was observed (figure 4). Microorganisms dispose of an intrinsic resistance but bacteria can also acquire drug resistance through mutations, conjugation or transformation which occurs through five resistance mechanisms (Li and Webster 2018). The current spread of resistant strains is certainly linked to the use, the misuse and the overuse of antibiotics. Each time that an antimicrobial is used there is a risk to induce a resistance mechanism (Levy 1997).



**Figure 4. Timeline of resistance strains identification.**

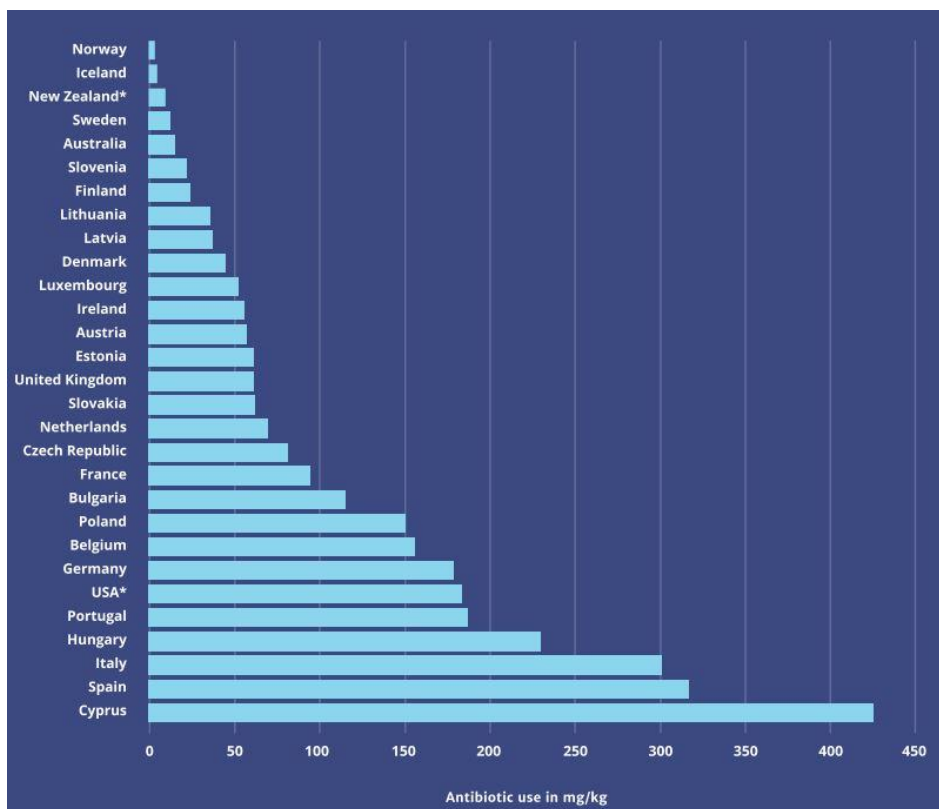
The antibiotic introduction in human health treatment is in blue and the detection of the resistance is in red. Adapted from Ventola 2015.

### a. Causes of the antibiotic resistance spread

Antibiotics are largely used not only for human and animal health care but also for agriculture and livestock production. In these two last categories, the misuse is leading to an overexposure of the bacteria to the drugs which forces adaptation. This kind of drugs are growth promoters and prophylaxis treatment for livestock (O'Neill 2015). As can be seen in figure 5, there is a massive worldwide utilization. For example, in the US 70% of antibiotics are used for this purpose. For the major emerging countries as Brazil, Russia, India, China and South Africa, its use is economically relevant and it is estimated that the uptake would double in the next 20 years. The consequence of this application is that bacteria present in animals are always exposed to these drugs which later on can lead to the development of resistant strains. The transfer to humans is possible *via* the alimentation chain. Another factor is the environmental impact, since 90% of antibiotics are liberated *via* animal excretion which are dispersed in the soil and the groundwater, exposing the bacteria in these areas (Ventola 2015).

## BILIOGRAPHIC REVIEW

Also, in agriculture, pesticides used for fruit trees contain antibiotics as tetracycline and streptomycin and they have the same impact as for the livestock. In addition, some last-resort antimicrobials are used for livestock and agricultural activities. In fact, 31 out of 41 essential human health antibiotics are used for livestock and agricultural activities. In fact, 31 out of 41 essential human health antibiotics are used for agriculture or livestock production, which reduce their effectiveness when used for human diseases. For instance, the colistin is used for agriculture purposes even though it is considered as the last-resort antibiotic in cases of resistance to carbapenem (Liu et al. 2016).



**Figure 5. The antibiotic uptake in agriculture worldwide**  
(O'Neill 2015) (\*Animal biomass estimated based on number of animals)

Another major water and environment pollution is through waste generated by pharmaceutical manufacturing. The APIs (active pharmaceutical ingredients) are synthesized in India and China for economic reasons. Then the biologically active molecule is sent for the final step to the pharmaceutical companies. The waste policies are less restrictive in the lower income countries leading to a dispersion of APIs in the environment surrounding the manufacturing plant (O'Neill 2015).

In humans and animals health care, a problem occurs in the administration process. In 30% to 50% of the cases, treatment duration and the chosen drugs are not appropriate (Ventola

2015). Thus, the choice, the duration and the indication of the treatment are really important factors for an adequate use of the substance. For example, if the duration of the administration is not optimal some microorganisms survive and restart the infection with a high possibility that they developed resistance against the substance. Moreover, the antibiotic dosage is crucial because both high and low concentrations lead to resistance development. For *Pseudomonas aeruginosa*, it has been observed a strain diversification possibly due to the exposure of this microorganism to small amount of drugs (Ventola 2015).

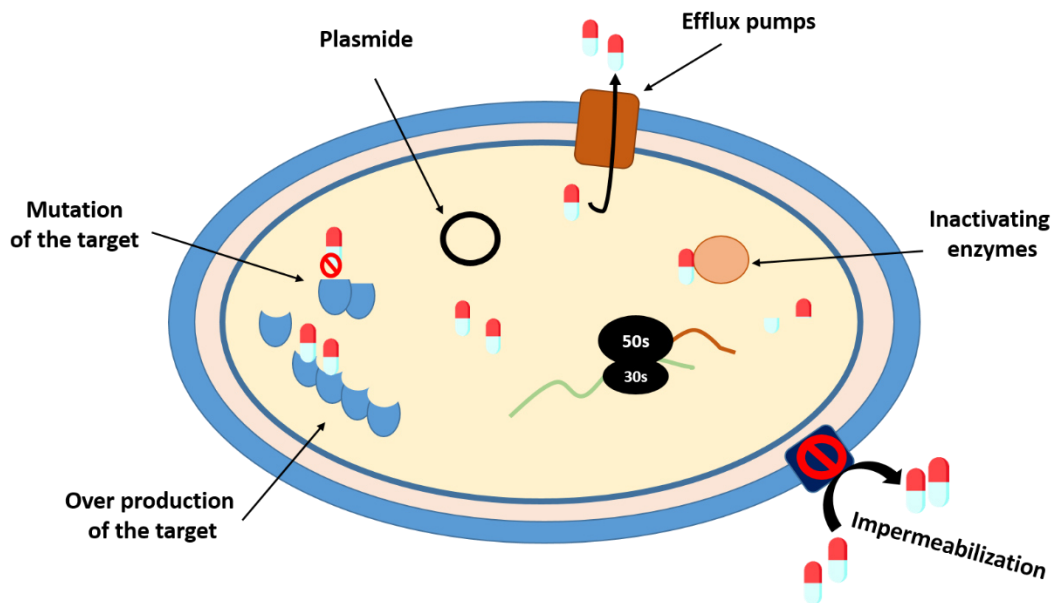
### **b. Mechanisms**

Antibiotics are present in the microorganisms' world. These bioactive molecules are used against other bacteria directly or also in the quorum-sensing reactions. In the latter, the molecules are used at low concentrations and they target either ribosomes, enzymes implicated in the cell wall synthesis or DNA/RNA replication which are the same targets used by antibiotics for humans (Allen et al. 2010). The quorum-sensing is the communication in biofilms that induces modifications on the metabolism to adapt to the environment. This means that bacteria can naturally tolerate low antibiotic concentrations. At a high concentration, a compound can be used by a bacterium against its competitor. It has been observed that the enzymes synthesizing antibiotics are often expressed with proteins conferring resistance to these compounds (Hopwood 2007).

The ability to resist to antibiotics can be intrinsic or acquired. In the case of intrinsic resistance, the bacteria are insensitive to the action of a given compound without any previous exposure to it. The resistance is acquired when bacteria trigger resistance mechanisms against an antibiotic after being in contact with it. Different molecular mechanisms are possible, displayed in figure 6:



## BILIOGRAPHIC REVIEW



**Figure 6. Mechanisms of drug resistance used by the bacteria.**  
(Allen et al. 2010)

- Membrane impermeabilization

Gram (-) bacteria have an outer membrane which is not present in the Gram (+) bacteria. Porins are proteins present in this membrane and their role is to assure the transit of hydrophilic molecules. The membrane proteins are used as passage by the antibiotics to enter the cell and reach the target. A defense mechanism is to mutate these proteins leading to a reduced or even abolished expression of the porin. The opening of the porin can also reduce to restrict the size of the compounds that can transit through it (Fernández and Hancock 2012). Note that impermeabilization of the plasma membrane is also a mechanism leading to resistance, which will be detailed below in the “efflux pump” §.

- Overexpression or modification of the drug target

The antibiotic concentration is crucial for an effective action against the bacteria. The metabolic pathways can be modified leading to an overexpression of the target. The increasing quantity of the target makes inefficient the amount of compound used to allow the resistance of the microorganism. This is the case of the Methicillin-Resistant *Staphylococcus aureus* (MRSA) which expresses different forms of the penicillin-binding protein (PBP). The latter is responsible for the formation of the crosslinking in the construction of the cell wall. The

## BILIOGRAPHIC REVIEW

bacteria produce the wild type PBPs but also a mutated form still active. The mutated PBP has a reduced affinity for penicillin, so it will not be inhibited by it (Fishovitz et al. 2014).

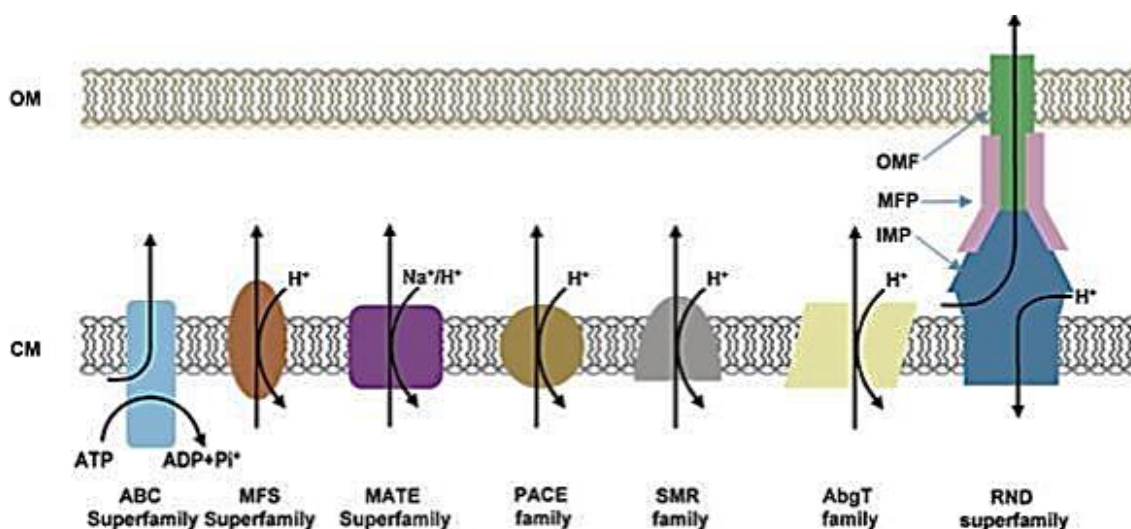
- Inactivating enzymes

Some bacteria express enzymes with the ability to metabolize an antibiotic. The gene corresponding to this enzyme is included in a plasmid to be shared by other bacteria and spread the resistance. This mechanism is more efficient against natural compounds because the corresponding gene is already present in the producing-strains. For example,  $\beta$ -lactamase inactivate all antibiotics containing a  $\beta$ -lactam ring (penicillin, cephalosporin and carbapenems) (Ogawara 2016). This mechanism has been observed in MRSA and *E. coli* (Wright 2000).

- Efflux pumps

Bacteria express membrane proteins which have the ability to transport compounds in or out of the cell (Paulsen 2003). Physiologically, their substrates are amino acids, sugar or lipids. Moreover, these transporters have the capacity to export toxic molecules such as antibiotics for the bacteria. They reduce the bioactive compound concentrations. They also ensure the communication between bacteria necessary for biofilm formation. Moreover, efflux pumps are the first step for drug resistance. This behavior has been observed for example in *Mycobacterium tuberculosis* and *Mycobacterium avium-M. intracellulare* (Schmalstieg et al. 2012; Pasipanodya and Gumbo 2011). These efflux pumps are found in Gram (-) and in Gram (+) bacteria and are located in the cytoplasmic membrane. These secondary active transporters belong to seven membrane protein families described below (figure 7).

The hallmark of these membrane proteins is to translocate drugs by a conformational change by which the drug binding cavity is alternatively exposed to the internal and the external sides of the membrane (Jardetzky 1966).



**Figure 7. Transporter families participating to the export of drugs**  
(Chitsaz and Brown 2017)

- ABC (ATP-binding cassette superfamily)

The ABC transporters are ubiquitously expressed, and they compose one of the largest protein superfamily. Their physiological role is to import nutrient as sugars, lipids, amino acids or to export toxic molecules which in the case of bacteria can correspond to antibiotics. These membrane proteins use the binding and hydrolysis of ATP to ADP to transport compounds. The general mechanism is defined as an alternating access allowing the protein to switch from an inward facing conformation to an outward one. Examples of these efflux membrane proteins are LmrA from *Lactobacillus lactis*, MacB from *Escherichia coli*, MacAB from *Neisseria gonorrhoea* and Sav1866 from *Staphylococcus aureus*. In Gram (-), these ABC proteins take part to a tripartite system as for RND transporters. This superfamily of transporters will be largely discussed in the next chapter.

- RND (Resistance-nodulation division superfamily)

RND transporters are expressed ubiquitously. This superfamily is composed of 8 families amongst which one of them corresponds to the hydrophobic amphiphilic efflux 1 (HAE1) found in Gram (-) bacteria (Tseng et al. 1999). Topologically, they are formed by a three-component system meaning that three distinct proteins compose the full transport. An integral membrane protein is placed in the inner membrane belonging to the IMP family and is composed by 12 TMs and two hydrophilic domains that are situated in the periplasm. The

other membrane protein is placed in the outer membrane and belongs to the OMF family. To form the tripartite complex, a soluble protein belonging to the MFP family links the two membrane proteins in the periplasm. These efflux pumps use the proton motive force to export compounds. Their substrates can be of hydrophobic or amphiphilic nature which are especially found in the periplasm: fatty acids, biocides, organic solvent, antibiotics and organic solvent. RND transporters are overexpressed to induce an MDR phenotype in strains found in human and animal pathogen bacteria. *P. aeruginosa* expresses RND transporters as MexAB-OprM, MexXY-OprM, MexCD-OprJ and MexEF-OprN which export chloramphenicol, fluoroquinolones, tetracycline and beta-lactams (Poole and Srikumar 2001). The membrane protein AcrB from *E. coli* is largely studied as prototype of IMP. The two others proteins of this tripartite system are AcrA (MFP) and the TolC (OMF). The structure of AcrB has been solved many times with or without substrates (Pos 2009). This membrane protein is composed of three monomers. AcrB presents a large drug binding pocket formed by a distal pocket highlighted by the binding of minocycline and doxorubicin; it also displays a proximal pocket corresponding to the binding site of rifampicin and erythromycin. In the distal pocket there is a zone with a high affinity for hydrophobic molecules that is called "hydrophobic trap". Hydrophobic compounds bind to this site and inhibit the efflux of physiological substrates. Four charged residues are responsible for the translocation of the proton which is the motive force for the efflux of substrates (Chitsaz and Brown 2017).

- **MFS (Major facilitator superfamily)**

This superfamily regroups 82 subfamilies of ubiquitous membrane proteins, which constitutes the largest family of secondary transporters (Chitsaz and Brown 2017). With an alternating access mechanism mode, they use an electrochemical gradient of proton or sodium ions to export amino acids, peptides, sugars and drugs. They are classified as symporters, uniporters or antiporters. As the other drug transporters, they have a large cavity composed by aliphatic and aromatic amino acids (Law, Maloney, and Wang 2008). In addition, MFS transporters participate in the drug or multidrug resistance phenomena. *E. coli* account for about 70 MFS, among which 15 are identified as drug transporters. As an example, MdfA exports antibiotics and lipophilic compounds (Heng et al. 2015). Furthermore, MdfA orthologues are expressed in pathogenic strains.

## BILIOGRAPHIC REVIEW

- MATE (**M**ultidrug and **t**oxic compound **e**xtrusion family)

MATE transporters are classified into three families gathering 14 subfamilies. This transporter family counts more than 1000 proteins (Omote et al. 2006; Chitsaz and Brown 2017). Typically, their topology is conserved, constituted of 12 transmembrane helices and a total of 400-550 residues. Their source of energy is sodium and proton gradient used to export cationic molecules. Their cavity is composed by two 6 transmembrane helices bundles displaying four negatively charged residues in the binding site. The mechanism by which they transport drugs remains not fully understood. An example of MATE transporter is the NorM antiporter found in *Vibrio parahaemolyticus* (NorM\_VP) (Morita et al. 1998). This protein exports multiple compounds such as streptomycin, kanamycin, ethidium, norfloxacin and ciprofloxacin, conferring resistance to them. Others examples are NorM\_NG in *N. gonorrhoeae* (Long et al. 2008) and also MepA in *S. aureus* (McAleese et al. 2005).

- SMR (**S**mall **m**ultidrug **r**esistance family)

SMR transporters form the smallest family, classified in three subfamilies regrouping the **p**aired **s**mall **m**ultidrug **r**esistance **p**umps (PSMRs), the **s**mall **m**ultidrug **p**umps (SMP) and the **s**uppressors of **g**roEL mutations (SUGs) (Bay and Turner 2009). Structurally, they are composed of 100-150 residues forming four TMs. Protons gradient is again the source of energy and their binding site has a negatively charged glutamate situated in the first TM. Only one subfamily exports drugs, such as erythromycin, benzalkonium, ethidium, tetracycline. Typical SMR transporters are QacC from *S. aureus* and EmrE from *E. coli* (Rotem and Schuldiner 2004).

- PACE (**P**roteobacterial **a**ntimicrobial compound **e**fflux family)

PACE family belongs to the secondary transporter category and it is also responsible for the export of drugs. They are composed of 150 residues disposed into two domains called BTP for “**b**acterial **t**andem **t**ransmembrane **p**air”. This allowed to regroup ~750 membrane proteins displaying this BTP. They can export benzalkonium, proflavine, acriflavine and dequalinium. An example of PACE transporters is Acel in *A. baumannii* (Chitsaz and Brown 2017).

## BILIOGRAPHIC REVIEW

- AbgT (*p*-aminobenzoyl-glutamate transporter family)

This protein family is composed by antimetabolite transporters and they are the last one to be identify as multidrug resistance actors. MtrF from *N. gonorrhoeae* (Veal 2003) and YdaH of *E. coli* belong to this family (Hussein, Green, and Nichols 1998). Normally, these membrane proteins transport a precursor of folic acid biosynthesis, the *p*-aminobenzoyl-glutamate (Carter et al. 2007). They can also export sulfonamide antimetabolites (Delmar and Yu 2016).

### Biofilms

Another mechanism of resistance is the formation of biofilms which are composed of a polymer matrix and a self-organized consortium of bacteria. Biofilms are made of and exopolysaccharidic matrix in which the bacteria community leaves and is protected by. This network has shown to be resistant to antibiotics. It uses the quorum-sensing to regulate the development of resistance mechanisms. Indeed, known mechanisms used by planktonic bacteria are found in biofilms (Venkatesan, Perumal, and Doble 2015), such as the production of  $\beta$ -lactamase enzymes, overexpression of efflux pumps and modification of the antibiotic target (Høiby et al. 2010). Biofilms are responsible for 60% of nosocomial infections due to their ability to colonize all kind of surface, notably the medical devices (Costerton et al. 1995). Another example is *Pseudomonas aeruginosa* biofilms which are responsible for chronic lung infections. The latter could be lethal for individual with Cystic fibrosis condition (Taylor, Yeung, and Hancock 2014).

### 3. New strategy to counter antibiotic resistance

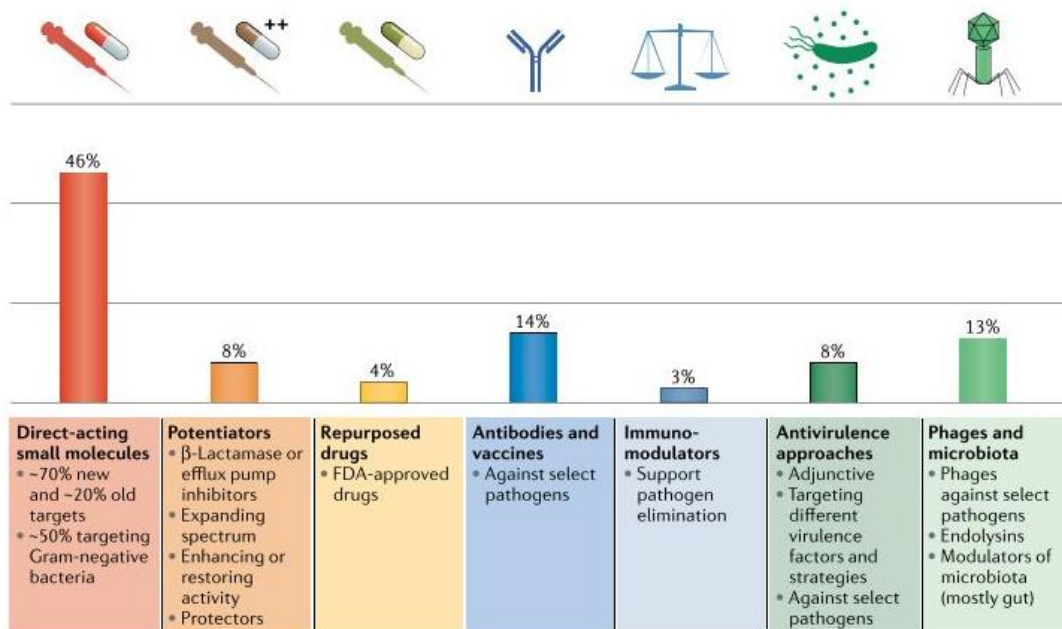
In the last 40 years, no new class of antibiotics has been discovered. This is due to the long and expensive process to identify, produce, validate and commercialize a given compound. Multiple approaches have been used to overcome the catastrophic predictions of the increasing drug resistance pathogens. It is also due to the fact that pharmaceutical companies have preferred the developments of more promising drugs, facing less resistance.

407 preclinical projects are currently developed with the main goal to fight infections. Some of these projects are more traditional, focusing on the discovery of new antibiotics or modifying the already existing ones. Other projects explore alternative therapies as the utilization of the microbiota or of the CRISPR-Cas9 system conjugate with specific phages. Theuretzbacher and his colleagues listed the current projects (figure 8) (Theuretzbacher et al. 2019):

- **New antibiotics** are the main focus of these preclinical projects since the development process is already well established. Three different approaches are used to produce new effective bioactive molecules. The first one corresponds to the modification of known antibiotics to improve their action. The second one is the development of new compounds targeting new bacteria components. Last one is the utilization of new molecules with unknown actions in the bacteria.
- **Potentiators** are molecules used to increase or restore the action of another antibiotic with which it is administrated. An example of potentiators are inhibitors of efflux pumps or of  $\beta$ -lactamases.
- **Repurposed drugs** are compounds currently used for other diseases or other bacteria. These molecules are already approved by the FDA which means that the development and administration are easier.
- **Phage therapy** is currently studied to fight *Staphylococcus aureus*, *Pseudomonas aeruginosa* and also *Clostridioides difficile*. The content of the phage can be natural or engineered. The latter can contain CRISPR-Cas systems which allow a specific modification to target multiple pathogens. A phage-derived peptide called endolysin is used due to its bacteriolytic action. An important possibility with this therapy is that the phage cocktail could be adapted specifically for the infection of one patient.

## BILIOGRAPHIC REVIEW

- **Microbiota-modulation** is a therapy based on the patient gut microbiota and the production of probiotics.
- **Antivirulence compounds** are combined with other antibiotics and their main function is to prevent the biofilm formation or to inhibit the quorum sensing. *P. aeruginosa*, *S. aureus* and *C. difficile* are targeted in this kind of therapy.
- **Antibodies** are pathogen specific therapy which is already approved against *Clostridium botulinum*, *Bacillus anthracis* and *C. difficile*. Their mode of action is the neutralization of toxins or the virulence factors. This therapy is currently studied against *S. aureus* and *P. aeruginosa*. Antibody-drug conjugates are also explored as a strategy.
- **Vaccines** are also a strategy explored to target a group of bacteria or a specific strain which can be also rare. The bacteria that are currently considered are *P. aeruginosa*, *Acinetobacter* species, *Klebsiella pneumoniae* and *N. gonorrhoeae*.
- **Nanobiotics** act against bacteria inducing the production of reactive oxygen that damages the cell membrane or the DNA and inhibits the electrons transport in the membrane.



**Figure 8. Preclinical projects developed to counter antibiotic resistance** (Theuretzbacher et al. 2019).



## BILIOGRAPHIC REVIEW

An interesting example of strategy to identify a new antibiotic is the one used for the Keyicine. Knowing that only 1% or less of the whole microorganisms on this planet has been cultivated and studied in labs, the co-cultivation of two bacteria from different microenvironment could be an effective new approach. The co-cultivated bacteria would be in competition and they could develop compounds against each other. This strategy has been proven effective since N. Adnani and his team co-cultivated *Micromonospora spp* and *Rhodococcus*. Keyicine showed an antimicrobial activity, then it was isolated and proved effective against the multi resistant strain of *Staphylococcus aureus* and the *Eterococcus faecium* (Carignan and Fortier 2018).

Another approach is to prevent the increase of drug resistance development. This could be possible by reducing the utilization of these compounds in the livestock and agriculture. This strategy has been proven to be possible in countries such as Denmark and the Netherlands. These higher income countries have chosen to decrease the compounds uptake and at the same time to improve the global quality of the livestock with better hygiene or more spacious environment. This strategy is not easy to apply for lower income countries for which an infection of the livestock could provoke a huge economical loss. A more adapted solution for these countries must be found (O'Neill 2015).

WHO is mostly active on the prevention of antibiotic resistance. Its actions concern all domains linked to this phenomenon from human healthcare to agriculture. This is the role of the Global Antimicrobial Resistance Surveillance System (GLASS). Up to date, main concerns are vancomycin resistant Enterococci, drug resistant *Streptococcus pneumonia*, methicillin resistant *Staphylococcus aureus*, drug resistant *Mycobacterium turbercolosis*, MDR *Pseudomonas aeruginosa*, ESBL-producing *enterobacteriaceae*, Carbapenem resistant *Enterobacteriaceae*, MDR *Acinetobacter* and drug resistant *Neisseria gonorrhoeae*. Another strategy for individual prevention is the World Antibiotic Awareness Week. Their motto is "Antibiotics: Handle with care" and their goal is to educate people on the drug utilization and on the basic hygienic techniques ("Antibiotic Resistance" 2018)

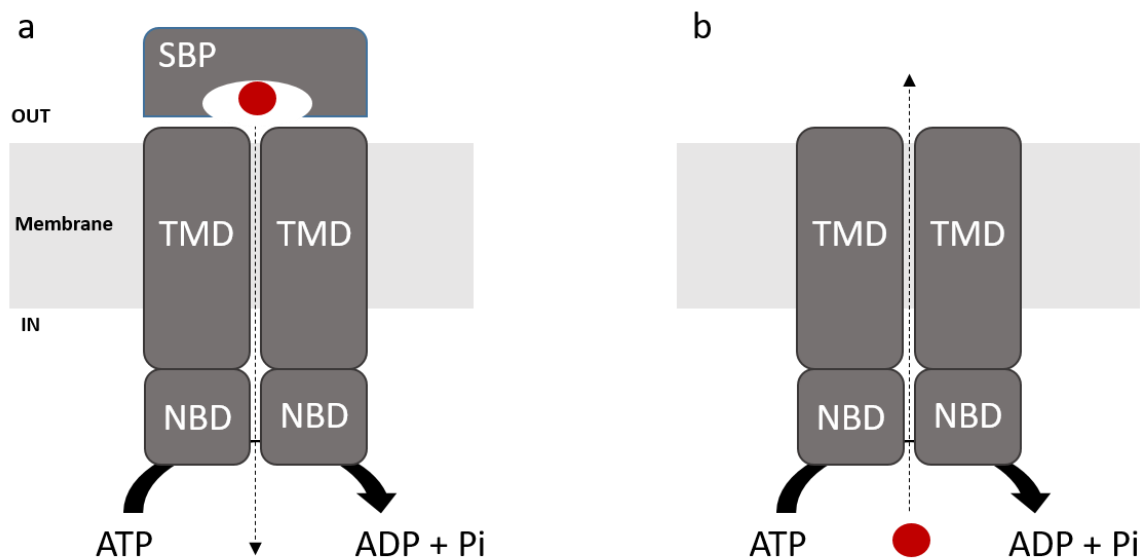
To conclude on this topic, the situation is quite alarming and many strategies are currently developed to prevent the worst scenario. In addition, an important effort is also taken to study the molecular basis of the resistance mechanism of bacteria. This next chapter will be a review on the ABC transporters which are one of the membrane proteins families responsible for the efflux of drugs.

## II. ABC transporters

Discovered about 50 years ago, the ABC («ATP-Binding Cassette») proteins constitute the largest protein family, with an identification based on the presence of the ABC signature, LSSQG, located in their Nucleotide-Binding Domain (Juliano and Ling 1976; Christopher F. Higgins et al. 1986). They are ubiquitously expressed and are implicated in essential activities for cell survival. These primary active transporters use the energy generated by ATP binding and hydrolysis to ensure exchange and/or communication of the cell with the surrounding environment. In doing so, they maintain the cell equilibrium. They take part to many biological process as lipids homeostasis, antigen presentation, signal transduction, detoxification and nutriment uptake (Lewinson and Livnat-Levanon 2017). Their substrates belong to a large spectrum of inorganic and organic molecules with multiple sizes. They transport sugar, amino acids, peptides, nucleosides, vitamins, metals and drugs. The ABC transporters can import or export solutes. Importers are only found in prokaryotes and plants, in which they ensure nutriments uptake (Lewinson and Livnat-Levanon 2017). Exporters are ubiquitously expressed and ensure the efflux of molecules outside the cells. On a bad note, several of these biologically relevant membrane proteins contribute to drugs resistance in human, fungi and bacteria. Example of such transporters is ABCB1 (Gottesman, Fojo, and Bates 2002), ABCG2 (Doyle et al. 1998 ; Miyake et al. 1999) and MRP1 (Cole et al. 1992) responsible for chemioresistance in humans, PatAB responsible for the resistance to fluoroquinolone in *Streptococcus pneumoniae* (Marrer et al. 2006) and Cdr1 responsible for azoles resistance in *Candida albicans* (Holmes et al. 2008). In addition, in human cell some exporters are implicated in various diseases such as Tangier disease (ABCA1), cystic fibrosis (CFTR) and adrenoleukodystrophy (ABCD1).

# 1. Structure

These proteins share a common topology made of a membrane and a cytoplasmic regions. The membrane domain is usually composed of two **transmembrane domains (TMD)** which can count for 4 to 10  $\alpha$ -helices each. This region ensures binding, translocation and release of the solutes. The cytoplasmic region is made of two **nucleotide-binding domains (NBD)** that are responsible for ATP binding and hydrolysis. The NBD contains highly conserved motifs as the ABC signature, the Walker A and B motifs, which will be discussed more in details further in this chapter. In the case of the importers (figure 9a), a **substrate-binding protein (SBP)** is responsible for the substrate binding outside the cell.



**Figure 9. The ABC transporters organization**

(a) An importer is composed by two transmembrane domains (TMDs), two nucleotide-binding domains (NBDs) and the substrate-binding protein (SBP). (b) An exporter is composed of two TMDs and two NBDs. The transported solute is in red and the dotted arrow is the sense of transport. The ATP hydrolysis is symbolized by an arrow.

## 1.1 The NBD

Despite the large spectrum of ABC transporters and their specificities, primary sequences and folds of the NBDs are conserved. Amongst the conserved motifs, some are common with others NTPases while others are found only in ABC transporters. An NBD is composed by a Rec-A like domain,  $\alpha$ -helical subdomain and the  $\beta$ -helical subdomain (table 5). The Rec-A like

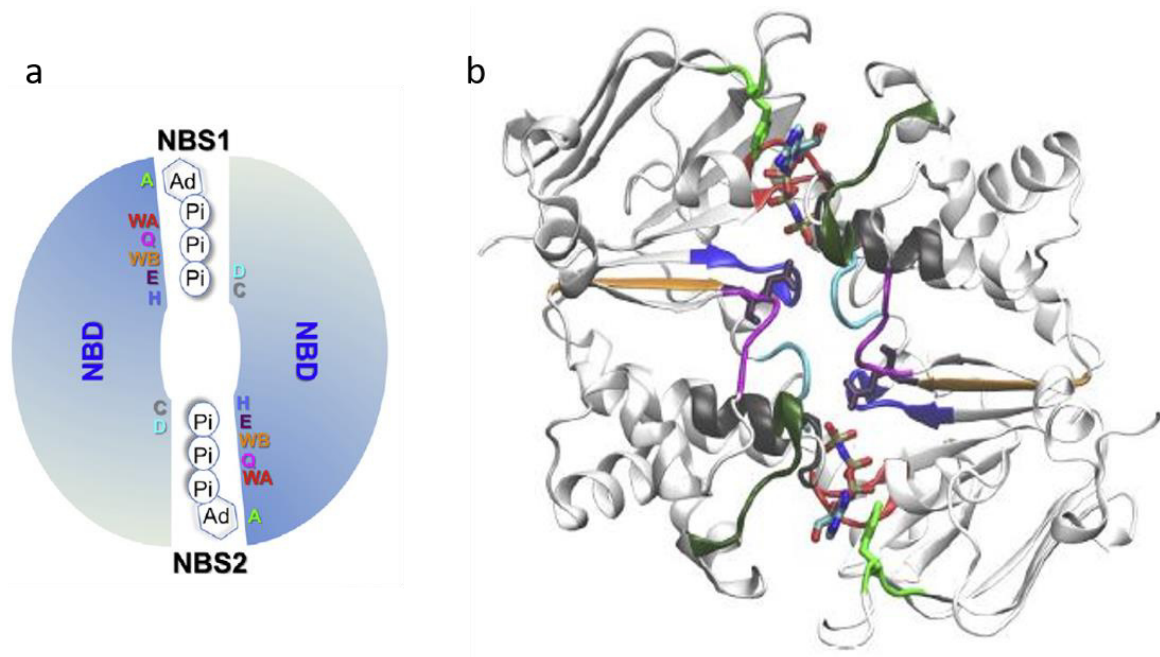
## BILIOGRAPHIC REVIEW

domain is found in others NTPases (Vetter and Wittinghofer 1999) and it is composed by Walker A, Walker B and Q loop motifs. The  $\alpha$ -helical subdomain is specific of the ABC transporter and it contains the signature sequence and the X loop. The  $\beta$ -helical subdomain is composed of the A loop.

**Table 5. Conserved motifs in the NBD and their role**  
(X: every residue possible; h: hydrophobic residue)

Motif	Conserved residues	Role	
Walker A	GXXGXGKX(S/T)	The conserved lysine interacts white the ATP, particularly $\beta$ and $\gamma$ phosphate.	Rec A like domain
Walker B	hhhhDE	The conserved aspartate binds to the $Mg^{2+}$ and the glutamate binds to the catalytic $H_2O$ molecule.	
Q loop	Q	This loop is implicated in the communication between NBD and TMD, its position allows the connection between Rec-A like domain and the $\alpha$ -helical one.	
Signature ABC	LSGGQ	Interaction with $\gamma$ phosphate of the ATP	$\alpha$ -helical subdomain
X loop	TXVGEXG	This loop is responsible for the communication with the TMD.	
A loop	Aromatic residu	Usually a tyrosine helps the positioning of the ATP by a $\pi$ -stacking interaction with the nucleotide ring of the ATP.	$\beta$ -helical subdomain
H loop	H	Interaction with the ATP $\gamma$ phosphate. After the ATP hydrolysis, this residue probably helps the release of the $\gamma$ phosphate. It is also call switch region because of the movement after the hydrolysis.	
D loop	SALD	This loop is in the interface of the two NBD when they are dimerized.	

ATP hydrolysis requires the NBD dimerization. The conformation adopted has been largely studied by structural and biochemical approaches. The first structures solved of isolated NBDs were HisP from *Salmonella typhimurium* (PDB: 1BOU, Sugimoto et al. 1999), MalK from *Thermococcus litoralis* (PDB: 1G29, Diederichs et al. 2000), Rad50 *Pyrococcus furiosus* (PDB: 1F2U, Hopfner et al. 2000). They display different organizations: back-to-back for HisP, face-to-face for MalK and head-to-tail for Rad50, the latter being finally the real one (Kerr 2002). In this state, the D loop and the Signature motif of one NBD interacts with the Walker A and B, Q loop, H loop and the A loop from the other NBD (figure 10).



**Figure 10. Conserved motifs in the nucleotide binding domain (NBD)**

(a) schematic view of the ATP binding in the NBD. The binding site (NBS1 or NBS2) of an ATP molecule is composed by the A loop (in green), Walker A (in red), Q loop (in magenta), Walker B (in orange), H loop (in blue) from one NBD and the D loop (in aquamarine) and the Signature motif (in grey) from the other. (b) Structure of the Sav1866 NBDs binding two AMPPNP, the conserved motifs are in the same color than the image (a). (Orelle, Mathieu, and Jault 2019)

Note that some heterodimeric transporters present a degenerated NBD in which mutations in the consensus motifs as Walker B, H loop and ABC signature prevent ATP hydrolysis. Some examples of this type of ABC transporters are BmrCD from *Bacillus subtilis*, PatAB from *Streptococcus pneumonia*, Cdr1 from *Candida albicans*, MRP1, CFTR, ABCG5/G8 from *Homo sapiens*.

## 1.2 The TMD

These membrane proteins transport different compounds contributing to multiple homeostasies. Their TMD share a common fold, made of  $\alpha$ -helices. Their ability to bind and translocate multiple substrates lies in the high variability of the primary sequence within the TMD. Like NBDs, TMDs dimerize to generate the substrate-binding site and the translocation pathway through the membrane. The communication between the two domains is essentially ensured by the coupling helices disposed between the TM helices in contact with the NBDs. They also interact with characteristic features of the NBDs, like for example the Q-loop which can change position according to the state of the ATP.

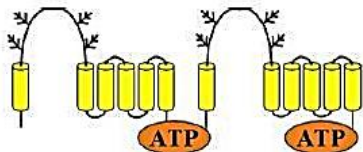
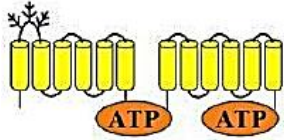
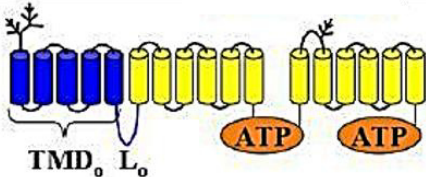
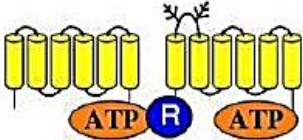


The overall arrangement of the TMD can differ among transporters, which makes it a criterion to classify these transporters:

➤ Classification of human ABC transporters

The 49 human ABC transporters are classified into seven families named from A to G (table 6). The discrimination in these classes are based on the sequence homology, the domains' order and the topological similarities (Dean, Rzhetsky, and Allikmets 2001). On the topological side, the transporters can be full or half transporters. The full transporter gene encodes all the components (generally the two TMDs and the two NBDs). The half transporter gene encodes only a part (generally a TMD and an NBD) and a dimerization is needed for the transporter to become functional (Hyde 1990).

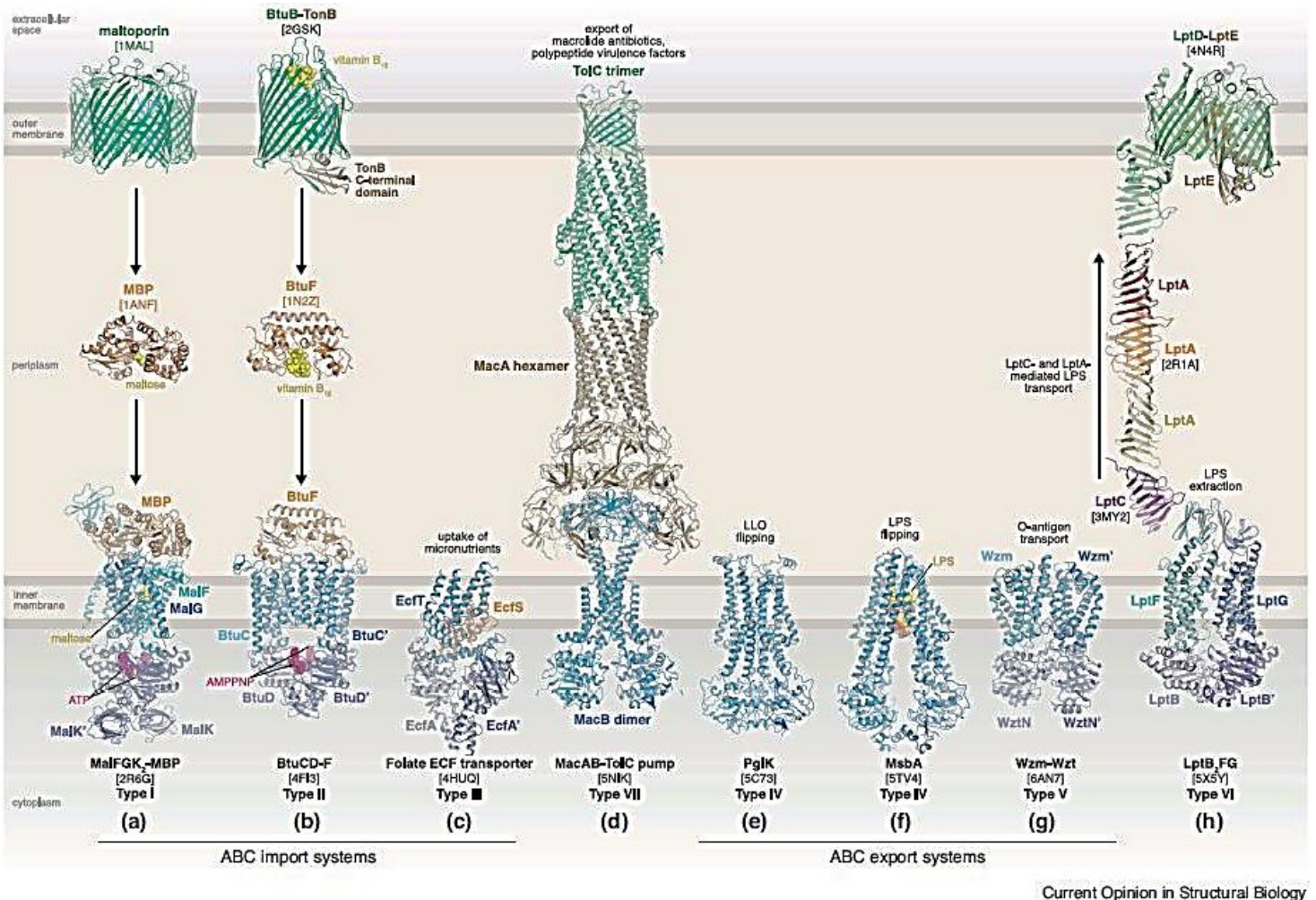
**Table 6. Classification of the human ABC transporters**

They are presented by their subfamily, an image of their organization and a short comment on their components. In the illustration, the cylinders called ATP correspond to the nucleotide-binding domain (NBD). (Dean, Rzhetsky, and Allikmets 2001) and (Loo and Clarke 2008)

Subfamily	Diagram	Description
ABCA		12 full transporters belong to this subfamily. Examples are ABCA4 (ABCR retinol transporter) and ABCA1 (cholesterol transporter).
ABCB		It is the only subfamily containing full transporters (4) and half transporters (7). An example is ABCB1 (P-glycoprotein drug transporter).
ABCC		13 full transporters belong to this subfamily. Examples are ABCC1 (MRP1 drug transporter) and ABCC7 (CFTR Cl <sup>-</sup> channel).
ABCD		4 half transporters are in this subfamily. One of them is ABCD3 (PMP70 peroxisomal transporter)
ABCE/F		These subfamilies are composed only by the NBD. The E subfamily is composed by 1 transporter and the F subfamily counts 3 proteins. An example is ABCF1 (protein translation factor).
ABCG		5 half transporters belong to this subfamily. A particularity of this group is that they are called reverse since the N-terminal side corresponds to the NBD and the C-terminal to the TMD. An example is ABCG2 (BCRP drug transporter)

➤ Classification of the bacterial ABC transporters

A classification of bacterial ABC transporters is also based on their function, their homology of sequence and structure. As a result, this classification counts 7 groups in which there are importers, exporters and extractors (table 11).



Current Opinion in Structural Biology

**Figure 11. Overview of the bacterial ABC transporters**

(a) The importer of type I. Structure of the maltose importer MalFGK2 with the maltose binding protein (MBP) obtained by X-ray (PDB 2R6G). (b) Importer of type II. Structure of the *E. coli* vitamin B12 importer BtuCD with the substrate-binding protein BtuF (PDB 4F13). (c) Type III importer. Structure of the *L. brevis* folate ECF (energy-coupling factor) transporter with the folate-binding protein EcfS. (PDB 4HUQ). (d) Type VII transporter. Structure of the complex MacAB-ToIC pump. (PDB 5N1K). (e) and (f) Exporter type VI. (e) Structure of the *C. jejuni* flippase PglK bound to LLO (lipid-linked oligosaccharide) (PDB 5C73). (f) Structure of *E. coli* the flippase MsbA bound to LPS (PDB 5TV4). (g) Exporter type V. Structure of the *A. aeolicus* channel-forming O-antigen flipping Wzm-Wzt. (PDB 6AN7). (h) Type VI transporter. Structure of the *P. aeruginosa* LPS extracting LptB2FG (PDB 5X5Y). The complex with the LptC, LptA and LptD-E were solved separately. (Thomas and Tampé 2018)

The importers are composed of a membrane protein responsible for the substrate transport and substrate-binding protein (SBP) which role is to bind and drag the substrate to the membrane domain. The importers are divided into three categories. Type I is composed of 5 to 8 helices for the half transporters and usually they dimerize to form the full transporter. In

## BILIOGRAPHIC REVIEW

this groups, there are ModB (molybdate transporter), MalFGK (maltose transporter) and MetI (methionine transporter). Type II is generally composed of 10 transmembrane helices for the half transporter leading to 20 for the full transporter. An example of these importer is BtuCD (vitamin B<sub>12</sub> transporter). Type III has a quite different organization displaying a membrane domain composed by substrate binding protein and also a membrane domain of the transporter. The folate ECF transporters (energy coupling factors) belong to this subfamily.

Exporters are also classified into two groups based on their topological organization of the TMD, even if they all dispose of 6 transmembrane helices for the half transporter leading to 12 for the full transporter. The type IV (or type I exporter) is the only ABC transporter in which the helices are composed by a transmembrane domain and an intracellular domain (ICD) locating the NBD a little further from the membrane. Examples of this class are MsbA (Lipids A exporter) and PglK (lipid-linked oligosaccharide flippase). This subfamily will be discussed in detail further bellow. The type V (or type II exporters) are more similar to the importer with a more compact structural organization. An example is the Wzm-Wzt (channel-forming O-antigen flipping). Similar to this bacterial transporter, there are the human subfamilies A and G.

In Gram (-) bacteria, a tripeptide system allows the efflux of antibiotics or virulence factors. This complex is composed by an ABC transporter located in the inner membrane (here MacB), a trimer protein located in the outer membrane (ToIC) and a connecting protein located in the periplasm (MacA). The ABC transporters of this system belong to the category type VII since its conformation differ from all the others because its TMD contains four helices. From the structure solved for this ABC transporter it is not possible to identify the substrate cavity, but an opening located at the interface of the inner membrane and the periplasm.

The extractors have different folding which corresponds to the type VI. The ABC transporter belonging to this class is part of a system responsible for mature LPS transport from the inner membrane to the outer membrane. LptB<sub>2</sub>FG is the one presented in the figure 11. The transporter is composed by the proteins LptF and LptG for the transmembrane domain and their folding is a  $\beta$ -jellyroll-like. The NBDs are the LptB and LptB'.



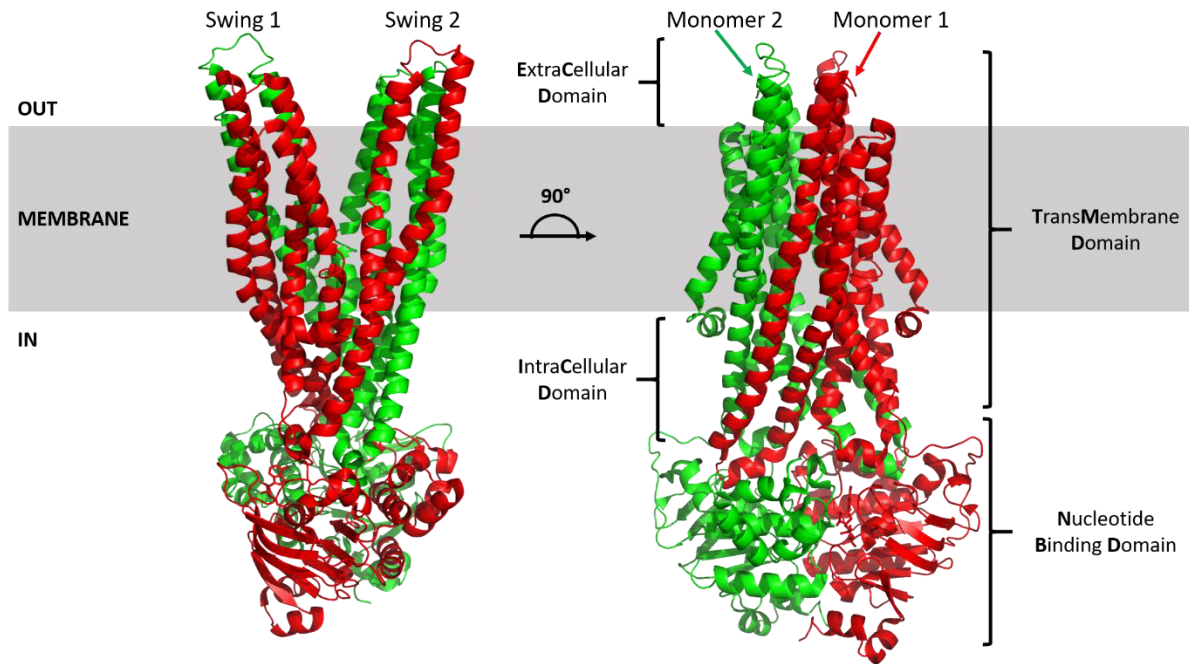
### 1.3 Focus on type IV transporters

The ABC transporters belonging to this category are ubiquitously expressed, some examples are P-glycoprotein (P-gp) from *Homo sapiens*, TmrAB from *Thermus thermophilus*, Sav1866 from *Staphylococcus aureus*, McjD and MsbA from *Escherichia coli*. These transporters are largely studied due to their implication in multidrug resistance for P-gp (chemotherapy resistance) and Sav1866 (antibiotics resistance) or through their relevant role of flippase for MsbA. Note that the first exporter structure solved was the Sav1866 which belongs to this type IV category (Dawson and Locher 2006).

This class of transporters differs significantly from the others for the TM arrangement. The length of the TM helices is approximately of 25 Å. In fact, the transmembrane domain is followed by the Intracellular domain (ICD) located in the cytoplasm and connected to the NBD (figure 12). To form the full transporter, the TM1-2 of one monomer associate with the TM3-6 of the other. As a result, the TMs of one monomer interact with the NBD of the other and this swapping arrangement is a common feature of this type of ABC transporters. Furthermore, important rearrangements occur between the outward-facing and inward-facing conformations (figure 13). The outward-facing conformation display two “wings” composed by TM1-2 from one monomer and TM3-6 from the other monomer (figure 12-13-14) (Rees, Johnson, and Lewinson 2009). For the inward-facing conformation the cavity could be quite open to the inside and the TMs all interact in the upper side (figure 13).

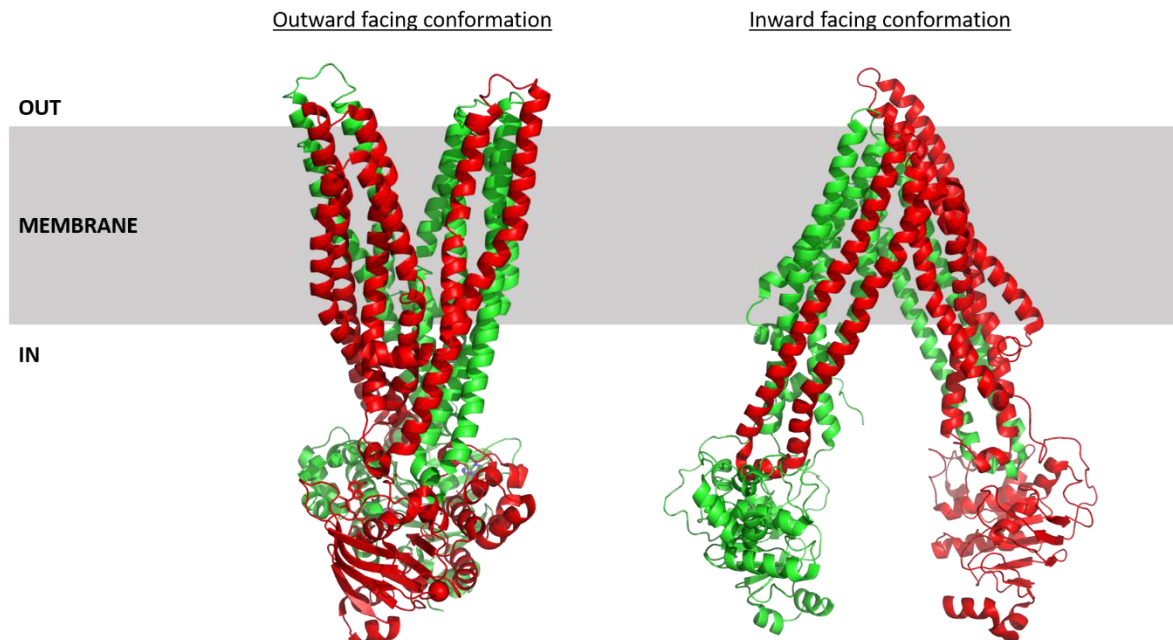
Type IV ABC transporters also share some features with the other transporters, where the coupling helices are at the interface between the TMD and the NBD, and transmit the information of ATP binding, through NBD dimerization, to the transmembrane domain and overall conformational changes (figure 15).

## BILIOGRAPHIC REVIEW



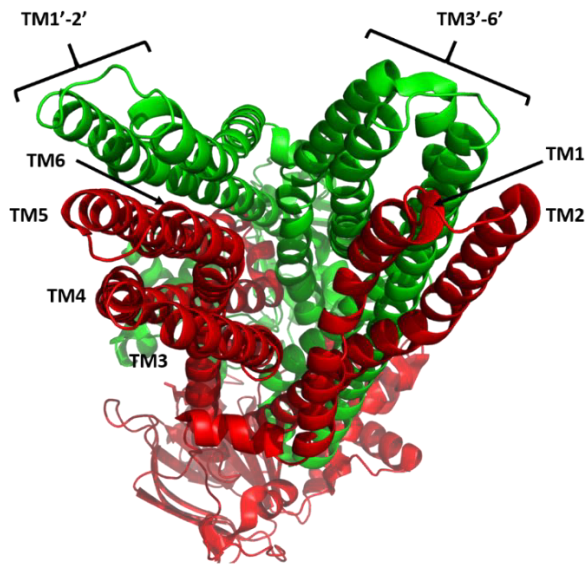
**Figure 12. Structure of Sav1866**

(PDB 2HYD) (Dawson and Locher 2006). The protein is showed inserted in the membrane and in two different orientations. The transporter is in outward facing conformation as the NBDs are bound to the nucleotide and the TMDs are open to the outside of the cell. The two monomers are colored into green and red.

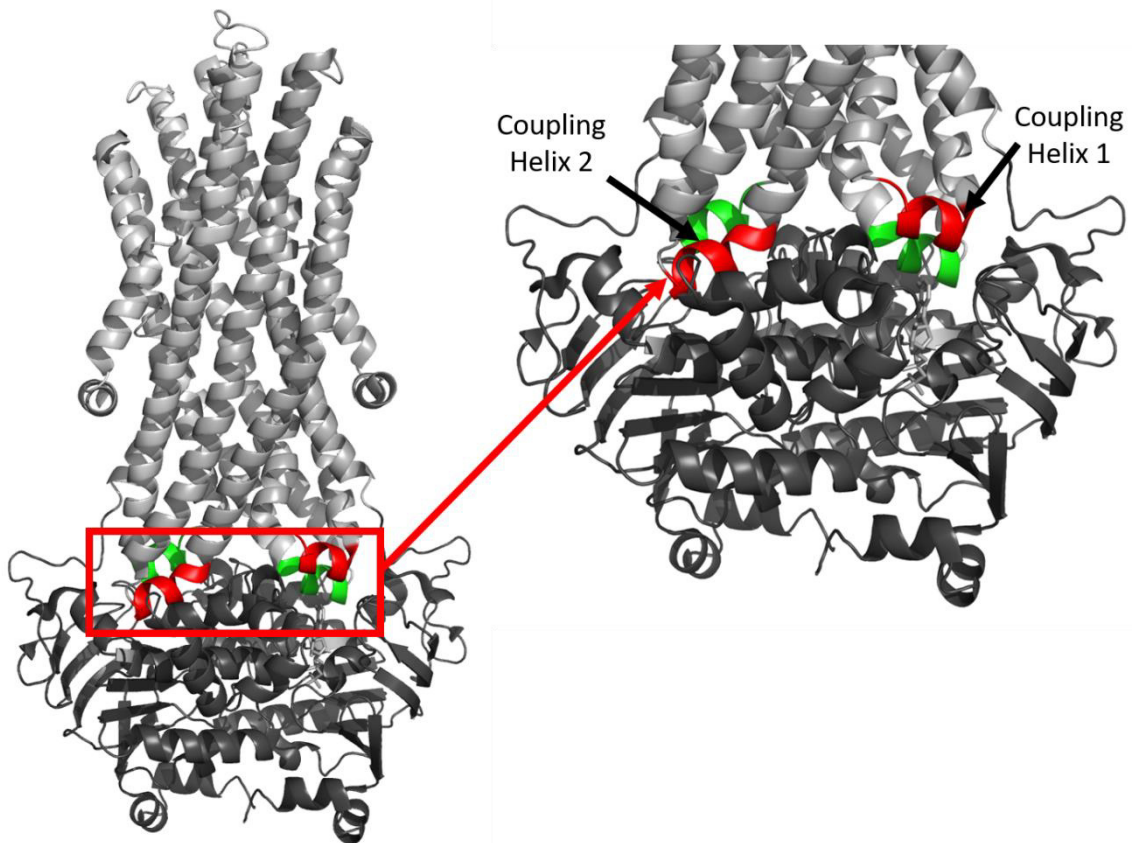


**Figure 13. Conformations adopted by the ABC transporters**

On the left the structure of Sav1866 (PDB 2HYD, Dawson and Locher 2006) is in outward facing conformation exposing the cavity to the outside of the cell. On the right the structure of the ABCB1 (PDB 4KSB, Ward et al. 2013) is in inward facing conformation exposing the cavity to the cytoplasm.



**Figure 14. Upper view of Sav1866 (from the periplasmic space)**  
 The cavity of protein and also the interaction of the TMD of the two monomers (green and red) are shown here. (PDB 2HYD) (Dawson and Locher 2006).

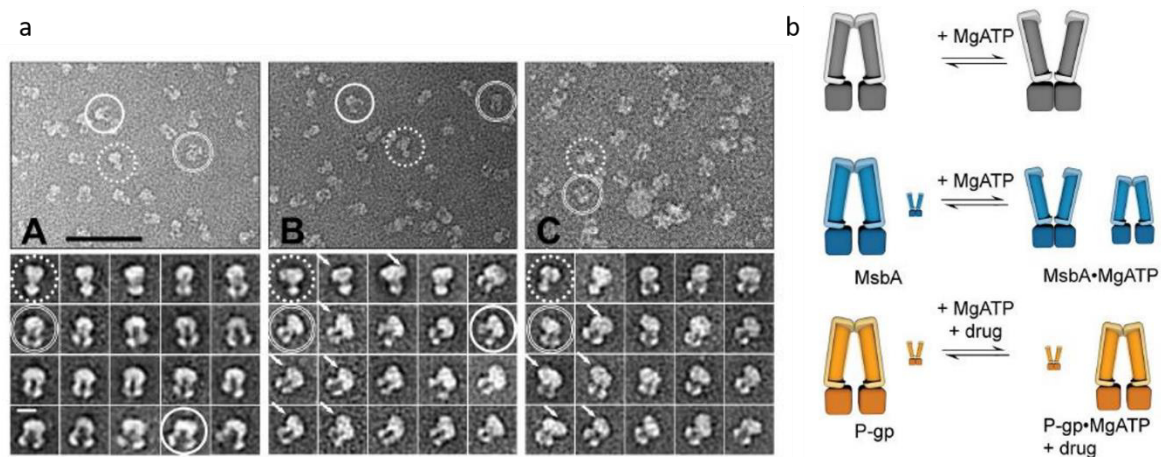


**Figure 15. Coupling helices in the structure of Sav1866**  
 The TMDs are in lighter grey and the NDBs in darker grey. The coupling helix are in red and green for the two monomers. (PDB 2HYD) (Dawson and Locher 2006).

## 2. Transport mechanism

It is widely accepted that ABC exporters use the alternating access mechanism (Jardetzky 1966) to shuttle substrates from inside to outside of the cell. Now, there is plethora of biochemical and structural information showing that these transporters undergo major conformational changes exposing an inner cavity alternatively to the outside or to the inside of the cell. In the Inward Facing conformation (IF) the TMDs are open toward the cytoplasm and the NBDs are not dimerized. In this conformation the substrate can bind. In the Outward Facing conformation (OF) the cavity is exposed to the outside of the cell, the NBDs are dimerized and bind ATP. The opening of the cavity leads to the release of the substrate (figure 13).

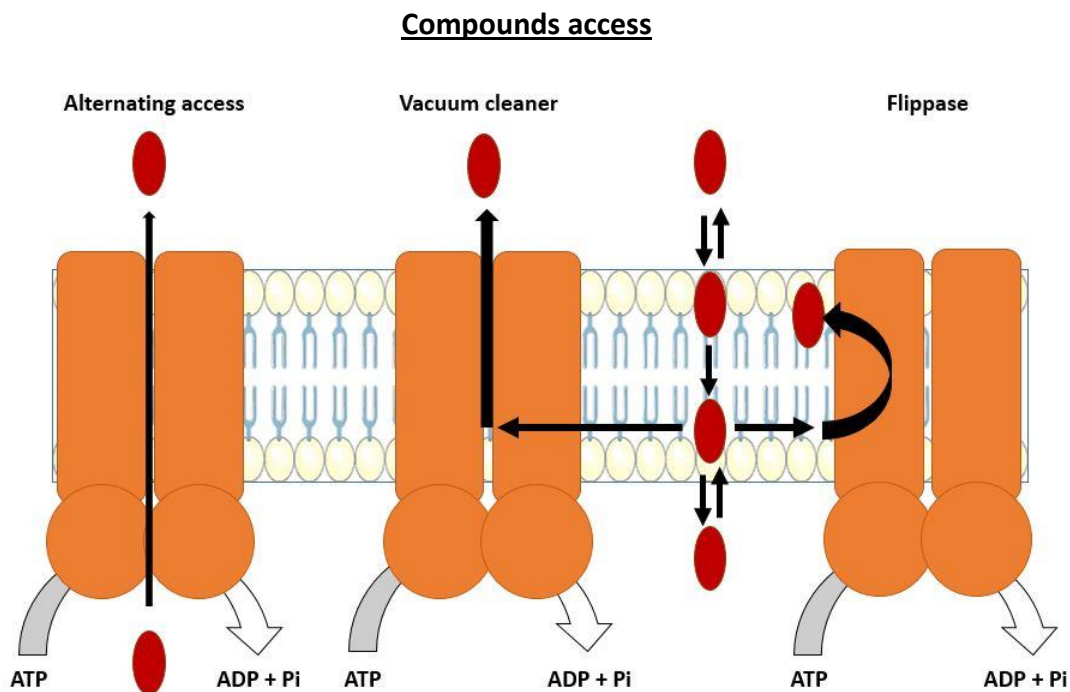
It is important to point that the conformations adopted by the transporter are still a matter of debate to know to which extent the transport mechanism is general. For example, Moeller and his co-workers showed by negative stain electron microscopy the conformation adopted by MsbA and P-gp after the addition of ATP in the sample. These two proteins belong to the same type of transporters but react differently to the addition of the ATP. In fact, they observed that MsbA can undergo an apparent conformational change from the IF to the OF. In contrast, P-gp does not change conformation (figure 16) (Moeller et al. 2015).



**Figure 16. Conformational changes of MsbA and P-gp in presence of ATP studied by negative stain in electron microscopy**

(a) The image A and B correspond to the data of MsbA and the C to P-gp. Micrographs are shown in the up panel and the 2D classification are shown below. (b) Illustration of the information collected in (a) (Moeller et al. 2015).

These data highlight the core of the discussion around the mechanism carried out by ABC transporters. For the accessibility of the compounds to the binding site, there are three mode of action proposed: alternating access, vacuum cleaner and flippase (figure 17). Moreover, not only the conformational changes on the TMDs are element of controversy but also the mode of action of the NBDs. Two model of mechanism have been proposed based on the possibility of the binding of the ATP molecules: the switch model and the constant contact one. Their differences will be discussed here below.



**Figure 17. Mode of access of the substrate to the binding site**

*From the left to the right, there are the alternating access, the hydrophobic vacuum cleaner and the flippase. Image adapted from Sharom 2014.*

The first model is the alternating access, the compound is present in the cytosol and it binds to the protein (inward-facing conformation) to be exported outside of the cell. This is the mechanism proposed for the efflux pumps in general (Jardetzky 1966).

The second proposition is called hydrophobic vacuum cleaner. The majority of the compounds transported are hydrophobic or amphipathic molecules. Consequently, they go in the membrane where they enter into the transporter. Once bound to the protein, they will be exported. This mechanism is observed for the transport of doxorubicin by the P-glycoprotein (Higgins and Gottesman 1992).

## BILIOGRAPHIC REVIEW

The last possible mode of action is the flippase one (Higgins and Gottesman 1992). The protein binds the substrate from the inner leaflet of the membrane and it transport it to the outer leaflet. This is the case of the MsbA which is responsible to the flippase action of the lipid A (hexa-acylated hydrophobic core lipid) (Eckford and Sharom 2010).

The ABC transporters can export a large spectrum of molecules. The polyspecificity of this protein is an important focus of attention. The P-gp has been object of many studies in this context. The protein displays different binding sites since it can export Hoechst 33342 and rhodamine 123 simultaneously (Shapiro and Ling 1997). For instance, the binding site of the Hoechst 33342 is called H and R is the one corresponding to rhodamine 123 (Martinez and Falson 2014). Moreover, other substrates bind to these two sites such as the quercetin for the H site and the daunoribicin and doxorubicin for the R site. In addition, this ABC transporter bind cyclic peptides (QZ59-RRR and QZ59-SSS) (Aller et al. 2009) indicating that the cavity is quite large since it is able to accommodate these substrates (Chufan et al. 2013 ; Martinez and Falson 2014). This large study done on the P-gp shows the plasticity of this kind of proteins. This is not an isolated case since all multidrug resistance transporters can bind a large spectrum of compounds.

### **ATP binding mechanism**

#### *Constant contact model for ATP binding in the NBD*

This model is hypothesized by the observation of A. E. Senior studying the P-gp ( Senior et al., 1995). An experiment of vanadate-trapping seems to indicate that the molecules of ATP are hydrolyzed non-simultaneously. In this hypothesis, a molecule of ATP is always bound to the NBD leading to a constant contact between the NBDs. The steps for the transport activity would be the following ones (figure 18):

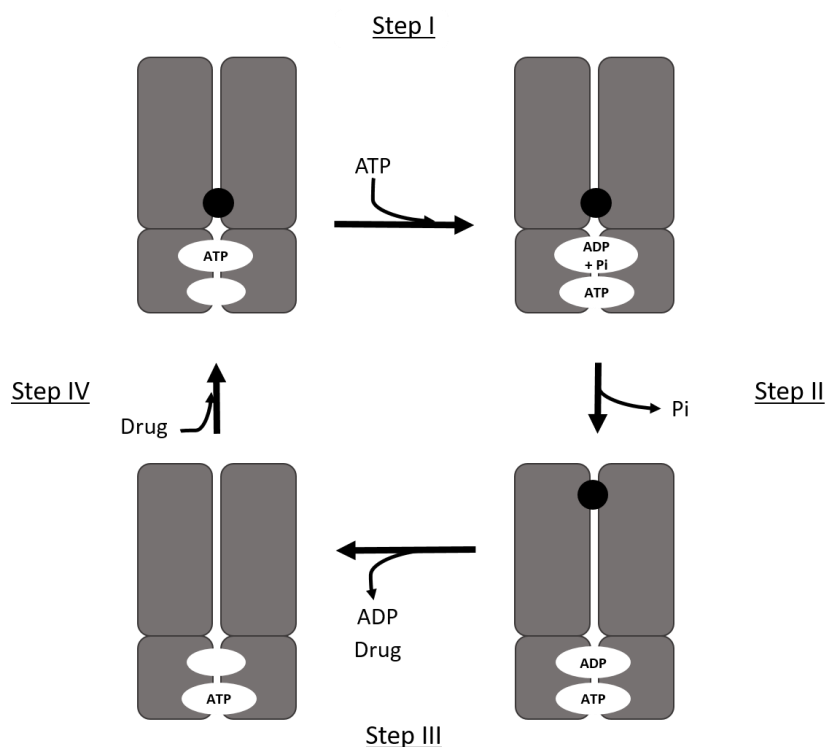
- I. One molecule of ATP is bound to the NBD1. The substrate binds to the site located in the TMD region which is exposed to the cytoplasm.
- II. The hydrolysis of ATP in NBD1 is allowed by the binding of the other molecule of ATP to the NBD2. The site NBD1 contains ADP and Pi.

## BILIOGRAPHIC REVIEW

III. The  $P_i$  is released which produce the relaxation of the NBD1 and the substrate is translocated into a site with lower affinity located in the region of the TMD more exposed to the outside of the cell.

IV. The ADP and the substrate are released.

V. Another substrate bind to the TMDs and in this case, ATP that will ensure the hydrolysis is the one placed in NBD2.



**Figure 18. The constant contact model**

In the step I the drug and the ATP in NBD1 are already bound. The ATP binds to the NBD2 inducing the hydrolysis of the ATP already bound. Step II is the release of the phosphate and the translocation of the drug in the low affinity region in the TMD. Step III is the release of the ADP and the drug. Step IV is the binding of the drug in the high affinity region in the TMD. Figure adapted from Senior et al. 1995.

Supporting this model, P.M. Jones and A.M. George performed molecular dynamics experiments on a mutant of the transporter MJ0796 (PDB 1L2T). They observed that in the simulation with ADP and ATP bound, the site containing ADP was able to open and release the nucleotide and the site containing ATP remained in contact (Jones and George 2009). Furthermore, this hypothesis was confirmed by biochemical experiments performed on the P-gp (Sauna et al. 2007) and on MsbA (Mittal et al. 2012).

## BILIOGRAPHIC REVIEW

### *The ATP-switch model*

This model is based on the observation of the structures in IF and OF conformations. The hypothesis is that the mechanism is based on the switch of these two conformations and the ATP binding/hydrolysis has the key role to regulate these changes. The two molecules of ATP-Mg<sup>2+</sup> bind at the same time which induces the NBDs dimerization leading to the switch from IF to OF conformation. Then the return from OF to IF conformation is possible by using the energy produced by ATP hydrolysis (Christopher F Higgins and Linton 2004). This model is composed by four steps (figure 19):

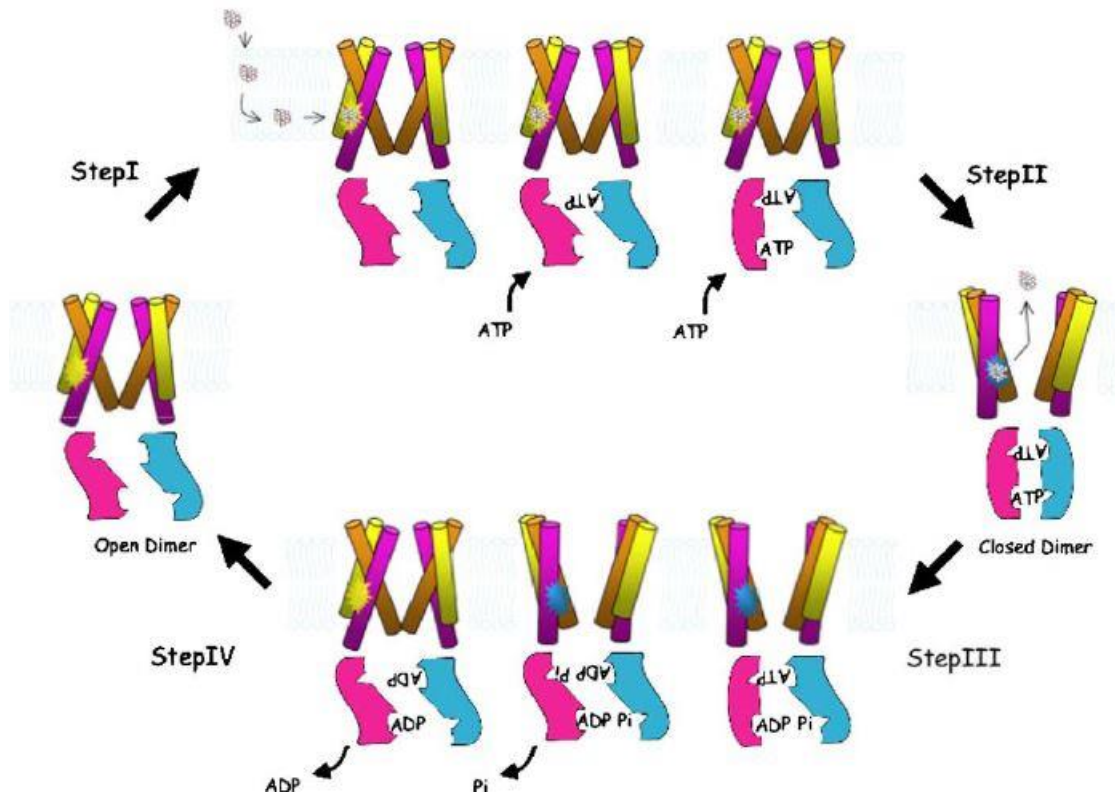
I. The protein is in IF conformation (open dimer). The transport cycle is initiated by the binding of the substrate to his binding site located in the TMDs region. This happening is communicated to the NBDs and it facilitates the binding of the two ATP molecules inducing the dimerization.

II. The transporter is in OF conformation or closed dimer. The NBDs bind the ATP molecules so they are still dimerized. The TMDs region is open to the outside of the cell. The affinity to the substrate is reduced which cause its release.

III. The transporter is in OF conformation post the releasing of the substrate. The ATPs hydrolysis are initiated to induce the conformational change into the IF conformation.

IV. The ATP hydrolysis products ADP and the phosphate are released and the protein is back in IF conformation ready for the next transport cycle.





**Figure 19. The ATP-switch mechanism**

Step I is the binding of the substrate and the two ATPs. Step II is the formation of the closed dimer conformation leading to the release of the substrate. Step III is the hydrolysis of the ATP molecules. Step IV is the return to the starting conformation (Linton and Higgins 2007).

This model was supported by the studies on maltose transporter MalK (Chen et al. 2003) and the mitochondrial transporter Mdl1p (Janas et al. 2003). Furthermore, M.E. Zoghbi and G.A. Altenberg studied the MJ0796 transporter from *M. jannaschii* mechanism by luminescence energy transfer (LRET), concluding that the NBDs dissociate after the hydrolysis of one ATP.

The real process of ABC transporters mechanism is still unclear. The alternating access mechanism was proposed on the basis of the data collected. In view of the many structures that have been solved in the recent years, they suggest that the mechanism might be more complex. On one hand, the lack of structures with the substrate bound prevent the understanding of this step of the cycle. The difficulty to obtain such model is due to the hydrophobic nature of the substrate and the protein which needs the presence of amphipathic molecules as detergent (Locher 2016).

### 3. Structures of ABC exporters

The first structure of an ABC exporter determined was of Sav1866 from *Staphylococcus aureus* by X-ray (Dawson and Locher 2006). Afterwards, many other structures of type IV exporters were solved as for the P-gp or MsbA in outward-facing conformation and inward-facing conformation. In 2016, the first structure of the type V exporter ABCG5/ABCG8 from *Homo sapiens* was solved by X-ray (Lee et al. 2016). With the development of the Cryo-EM, the total number of structures of ABC exporters counts up to more than one hundred. Despite this wealth of structures (table 7), the transport mechanism is still under active debate. This will be discussed further in the chapter I of the results section.

**Table 7. Structure of ABC exporters**

	Organism	PDB code	Res. (Å)	Nucleotide	Ligand	Reference	Method
<b>Sav1866</b>	<i>Staphylococcus aureus</i>	2HYD	3	ADP	-	Dawson and Locher 2006	X-ray
		2ONJ	3.4	AMPPNP	-	Dawson and Locher 2007	
<b>MsbA</b>	<i>Eschericia coli</i>	5TTP	4.8	ADP-VO4	-	Mi et al. 2017	Cryo-EM
		6BPL	2.9	Apo	LPS G907	Ho et al. 2018	
		6BPP	2.9	Apo	LPS G092		
		3B5W	5.3	Apo	-	Ward et al. 2007	
	<i>Vibrio cholerae</i>	3B5X	5.5	Apo	-		
	<i>Salmonella typhimurium</i>	3B5Y	4.5	AMPPNP	-		
		3B60	3.7	AMPPNP	-		
3B5Z		4.2	ADP-VO4	-			
<b>TmrAB</b>	<i>Thermus thermophiles/Vicugna pacos</i>	5MKK	2.7	Apo	-	Nöll et al. 2017	X-ray
		6RAN	4.2	Apo	-	Hofmann et al. 2019	Cryo-EM
		6RAM	3.8	ATP and ADP	-		
		6RAF	3.8	ATP and ADP	-		
		6RAH	2.8	ATP	-		
		6RAG	4.2	ATP and ADP	-		
		6RAJ	3.5	ATP ADP-VO4	-		
		6RAI	2.9	ATP	-		
		6RAL	3.5	ATP and ADP	-		
		6RAK	3.3	ATP ADP-VO4	-		
<b>ABCB1/PgP</b>	<i>Caenorhabditis elegans</i>	4F4C	3.4	Apo	-	Jin et al. 2012	X-ray
	<i>Homo sapiens</i>	6C0V	3.4	ATP	-	Kim and Chen 2018	Cryo-EM
		6QEX	3.6	Apo	Taxol	Alam et al. 2019	Cryo-EM
	<i>Cyanidioschyzon merolae</i>	6A6M	1.9	ANP	-	Kodan et al., 2019	X-ray
		3WMG	2.4	Apo	aCAP	Kodan et al. 2014	X-ray
		3WME	2.7	Apo	-		
		3WMF	2.6	Apo	-		
	<i>Mus musculus</i>	5KPD	3.3	Apo	-	Esser et al. 2017	X-ray
		5KO2	3.3	Apo	-		
5KOY		3.8	ATP	-			

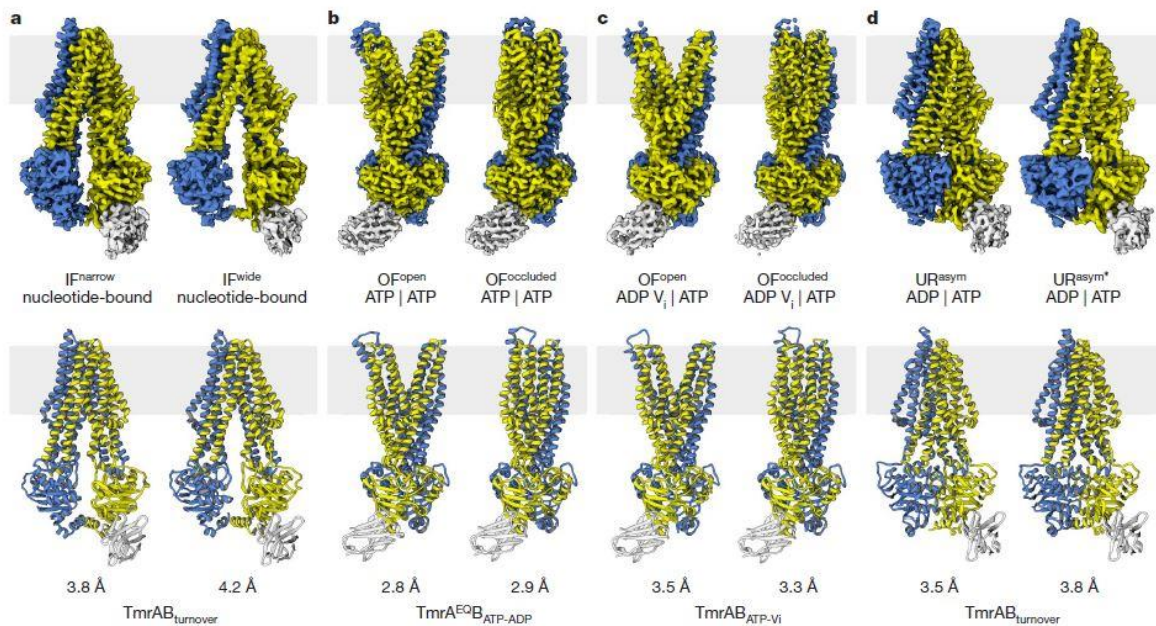
BILIOGRAPHIC REVIEW

		5KPJ	3.5	Apo	M3L		
		5KPI	4.0	Apo	-		
		3G5U	3.8	Apo	-	Aller et al. 2009	X-ray
		3G60	4.4	Apo	QZ59-RRR		
		3G61	4.3	Apo	QZ59-SSS	Li, Jaimes, and Aller 2014	X-ray
		4M1M	3.8	Apo	-		
		4M2S	4.4	Apo	QZ59-RRR		
		4M2T	4.3	Apo	QZ59-SSS		
		4KSB	3.8	Apo	-	Ward et al. 2013	X-ray
		4KSC	4.0	Apo	-		
		4KSD	4.1	Apo	-		
		4LSG	3.8	Apo	-	Chang 2013	X-ray
		4Q9H	3.4	Apo	-	Szewczyk et al. 2015	X-ray
		4Q9I	3.7	Apo	QZ-Ala		
		4Q9J	3.6	Apo	QZ-val		
		4Q9K	3.8	Apo	QZ-Leu		
		4Q9L	3.8	Apo	QZ-Phe		
		4XWK	3.5	Apo	BDE-100	Nicklisch et al. 2016	X-ray
		6QEE	3.9	Apo	Zosuquidar	Alam et al. 2019	Cryo-EM
		6Q81	7.9	ADP	-	Thonghin et al. 2018	Cryo-EM
6GDI	7.9	Apo	-				
<i>Homo sapiens</i> <i>Mus musculus</i>	6FN1	3.5	Apo	Zosuquidar	Alam et al. 2018		
	6FN4	4.1	Apo	-			
<b>TM287/288</b>	<i>Thermotoga maritima</i>	4Q4A	2.6	AMPPNP	-	Hohl et al. 2014	X-ray
		4Q4J	3.2	Apo	-		X-ray
		4Q4H	2.5	Apo	-		X-ray
		3QF4	2.9	AMPPNP	-	Hohl et al. 2012	X-ray
<b>Atm1</b>	<i>Saccharomyces cerevisiae</i>	4MYC	3.1	Apo	-	Srinivasan, Pierik, and Lill 2014	X-ray
		4MYH	3.3	Apo	GSH		
	<i>Novosphingobium aromaticivorans</i>	4MRV	2.5	Apo	-	Lee et al. 2014	X-ray
		4MRP	2.5	Apo	GSH		
		4MRR	2.9	Apo	-		
		4MRS	2.3	Apo	GSSG		
4MRN	2.5	Apo	-				
<b>ABCG5/ABCG8</b>	<i>Homo sapiens</i>	5DO7	3.9	Apo	-	Lee et al. 2016	X-ray
<b>MRP1</b>	<i>Bos taurus</i>	5UJ9	3.4	Apo	-	Johnson and Chen 2017	Cryo-EM
		5UJA	3.3	Apo	LTX		
		6BHU	3.1	ATP	CLR		
<b>ABCB10</b>	<i>Homo sapiens</i>	4AYT	2.8	AMPPCP	-	Shintre et al. 2013	X-ray
		4AYX	2.9	AMPPCP	-		
		4AYW	3.3	AMPPNP	-		
		3ZDQ	2.8	Apo	-		
<b>McjD</b>	<i>Escherichia Coli</i>	5OFR	3.4	ADP-VO4	-	Bountra et al. 2017	X-ray
		5OFP	4.7	Apo	-		
		4PL0	2.7	AMPPNP	-	Choudhury et al. 2014	
		5EG1	3.4	ANP	P6L	Mehmood et al. 2016	
<b>CFTR</b>	<i>Danio rerio</i>	5W81	3.3	ATP	-	Zhang, Liu, and Chen 2017	Cryo-EM
		5UAR	3.7	Apo	-	Zhang and Chen 2016	
	<i>Homo sapiens</i>	5UAK	3.8	Apo	-	Liu et al. 2017	
		6MSM	3.2	ATP	-	Zhang, Liu, and Chen 2018	

## BILIOGRAPHIC REVIEW

	<i>Gallus gallus</i>	6D3R	4.3	ATP	-	Fay et al. 2018	
		6D3S	6.6	ATP	-		
<b>ABCG2</b>	<i>Homo sapiens/ Mus musculus</i>	5NJ3	3.7	Apo	NAG	Taylor et al. 2017	Cryo-EM
		5NJG	3.7	Apo	NAG		
	<i>Homo sapiens</i>	6FFC	3.5	Apo	BWQ	Jackson et al. 2018	
	<i>Homo sapiens/ Mus musculus</i>	6ETI	3.1	Apo	BWQ		
		6FEQ	3.6	Apo	MB136/D 6T		
	<i>Homo sapiens</i>	6HIJ	3.5	Apo	MZ29	Manolaridis et al. 2018	
	<i>Homo sapiens/ Mus musculus</i>	6HCO	3.5	Apo	-		
		<i>Homo sapiens</i>	6HBU	3.1	ATP		
6HZM	3.1		ATP	-			
<b>ABCA1</b>	<i>Homo sapiens</i>	5XJY	4.1	Apo	-	Qian et al. 2017	Cryo-EM
<b>TAP1/TAP2</b>	<i>Homo sapiens</i>	5U1D	3.9	Apo	ICP47	Oldham, Grigorieff, and Chen 2016	Cryo-EM

To conclude this topic, I would like to cite the recent work of Arne Moeller team in collaboration with Robert Tampé team which shows how the improvement in Cryo-EM will allow the observation in depth of these proteins' mechanism (Hofmann et al. 2019). They were able to solve 8 structures of the ABC transporter TmrAB from *Thermus thermophilus* (figure 20). This heterodimeric transporter is a multidrug protein belonging to the type IV exporter. They obtained different conformations at relatively high resolution which represent the possible arrangements adopted by the protein during the transportation of the substrate. They solved structures in inward facing conformation with two different openings, outward facing conformation open and occluded, and post-hydrolytic conformations. Thus, they could have clearer insights of this heterodimeric transporter mechanism, observing the key role of the TM6 in the binding of different substrates, the importance of the release of the phosphate after ATP hydrolysis as initiator of the conformational change and at last the conformations adopted from the OF returning to the IF state.



**Figure 20. Structures of TmrAB in multiple conformations**

(a) and (d) are the results of the same data set. TmrAB was incubated with ATP-Mg<sup>2+</sup> and a substrate. (a) corresponds to the structures in IF conformation and they display different openings of the cavity (IF narrow and IF wide). (b) Structures of a mutant of TmrAB which is the E523Q located the TmrA. The mutation is done to reduce the hydrolysis of the ATP. Two structures in OF are obtained. The openings of the cavity are different: one is occluded and the other is open to the outside of the cell. (c) Structure of the wild type TmrAB in presence of ATP-Vandate. The results are the same than (b). (d) correspond to an asymmetric conformation. The TMDs are closed on the top and opened (1.5 Å and 3 Å) on the cytoplasm side. The NBDs are bound to ATP/ADP. In inward facing conformation with two different opening of the NBDs. (b) Structures are in outward facing conformation in fact the protein is binding ATP On the left the TMD region is open to the outside of the cell, and the other one is occluded. (Hofmann et al. 2019)

The impact of Cryo-EM on the structural biology in general and in particular on the ABC transporter will be discussed in the following chapter.

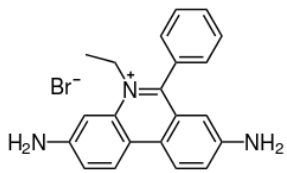
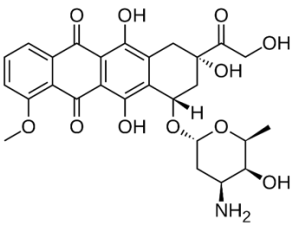
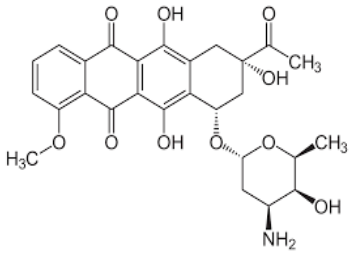
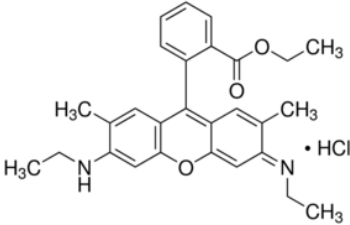
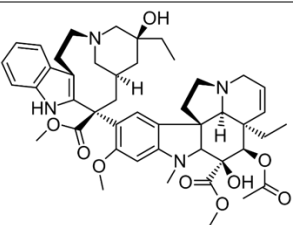
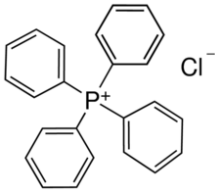
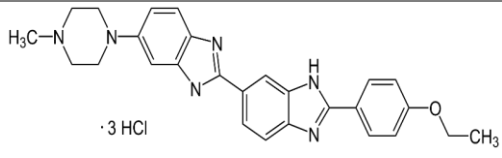
## 4. *Bacillus subtilis* multi resistance ATP (BmrA)

*Bacillus subtilis* is a Gram (+) bacteria which is found in the soil and the gastrointestinal tract. This nonpathogenic microorganism is used as model of Gram (+) bacterium in microbiology studies. A strain of *B. subtilis* has been identified to be resistant to the bioactive molecule Cervimycin C produced by the Gram (-) *Streptomyces tandae*. This antibiotic belongs to the cervimycins (A-D) which have effects against Gram (+) bacteria. The Cervimycins A-D have proven to be effective against MDR staphylococci and vancomycin resistant enterococci (Herold et al. 2005). The *B. subtilis* strain improved the stability of the mRNA of an ABC transporter to resist against this molecule (Krügel et al. 2010). The transporter concerned is *Bacillus subtilis* multi resistance ATP (BmrA). It was identified for the first time by a screening for MDR-like ABC transporter in *B. subtilis* (Steinfels et al. 2002). It is homologous to LmrA (*Lactococcus lactis* multidrug resistance ATP) and to the human P-gp. The highest identity is with LmrA (41.5%) and it presents also a good identity percentage with the N- and C-terminal regions of the human P-gp (28% and 27%).

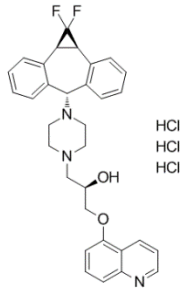
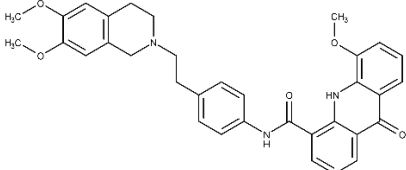
At the beginning, this transporter was called YvcC and it was later renamed BmrA (*Bacillus subtilis* multi resistance ATP) for a series of evidences which proved its capacity to bind various drugs. One of these experiments was the transport of doxorubicin, Hoechst 33342 and 7-aminoactinomycin D when the protein is in inverted-membrane vesicles. Another proof was the binding of multiple molecules (table 8) which are substrates or inhibitors of the P-gp. The last evidence given by Steinfels and his co-workers was that BmrA can efflux the ethidium once entered in the *Bacillus subtilis* (Steinfels et al. 2004).

BILIOGRAPHIC REVIEW

**Table 8. Binding experiments done by intrinsic fluorescence on BmrA purified in the detergent DDM**  
 This table presents the drugs tested, their structures and the  $K_D$  which was measured by this technique. The information was adapted from Steinfels et al. 2004.

Drug		$K_D$ ( $\mu\text{M}$ )
<b>Ethidium bromide</b>		$10.6 \pm 3$
<b>Doxorubicin</b>		$22.1 \pm 4.5$
<b>Daunomycin</b>		$12.2 \pm 3.5$
<b>Rhodamine 6G</b>		$22.4 \pm 5.1$
<b>Vinblastine</b>		$5 \pm 1.1$
<b>Tetraphenylphosphonium</b>		$15.4 \pm 2.7$
<b>Hoechst 33342</b>		$9.5 \pm 2.3$

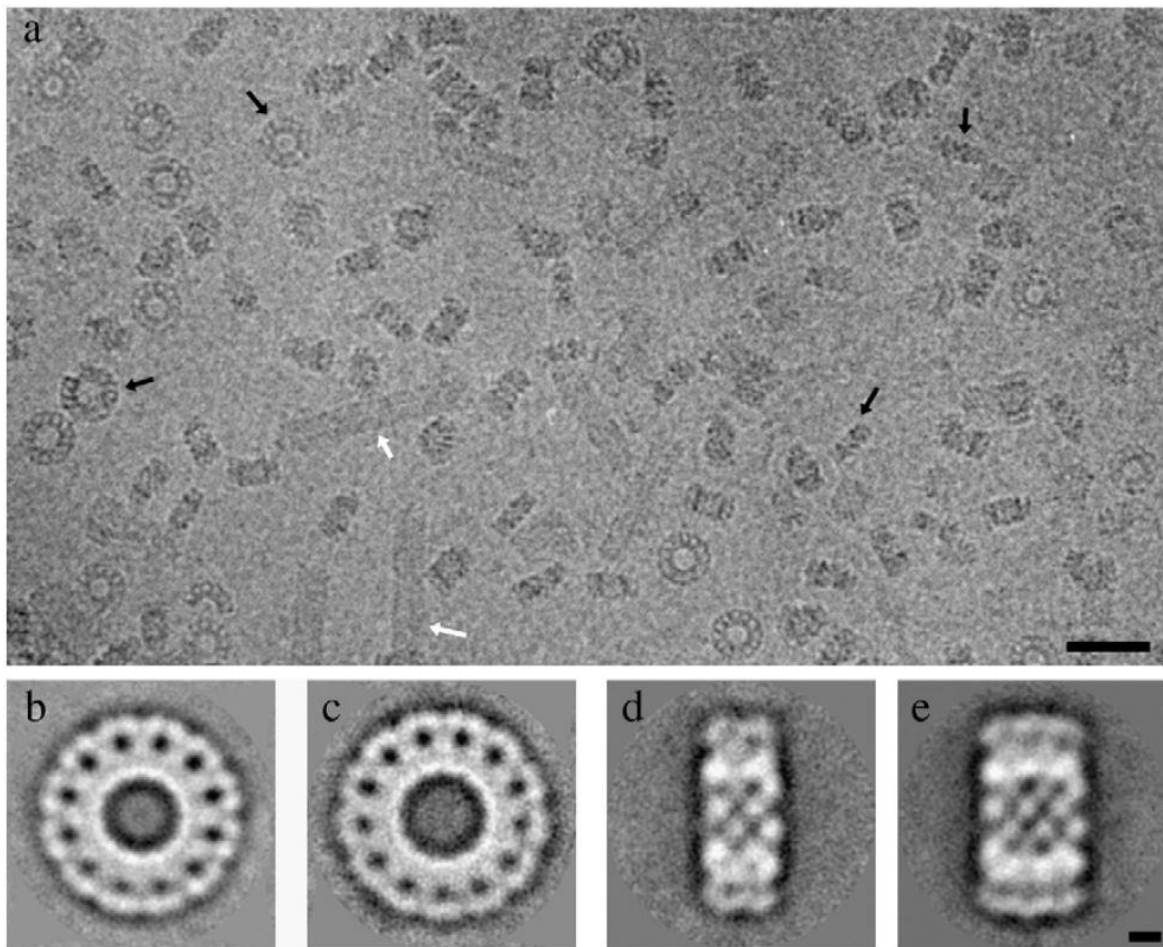
BILIOGRAPHIC REVIEW

<p><b>LY 335979</b></p>		<p>4.4 ± 0.7</p>
<p><b>GF 120918X</b></p>		<p>0.44 ± 0.02</p>

This half transporter is composed by 589 residues (65 kDa) and it requires homodimerization to be active (Ravaud et al. 2006). BmrA can be overexpressed in *E. coli* C41(DE3) achieving 50% of the whole membrane proteins expressed (Steinfels et al. 2002) and it is successfully purified in presence of n-dodecyl- $\beta$ -D-maltoside (DDM) (Ravaud et al. 2006). Even in presence of detergent the protein is active having an ATPase activity of 1.2  $\mu\text{mol}\cdot\text{min}^{-1}\cdot\text{mg}^{-1}$ . This activity reaches 6.5  $\mu\text{mol}\cdot\text{min}^{-1}\cdot\text{mg}^{-1}$  when the protein is reconstituted into proteoliposomes (Orelle et al. 2003 ; Orelle et al. 2008).

Chami and his co-workers were the first to observe ring shaped structures formed by BmrA in presence of lipids (ratio lipid-protein 1.2) and after detergent removal by Bio-beads (Chami et al. 2002).

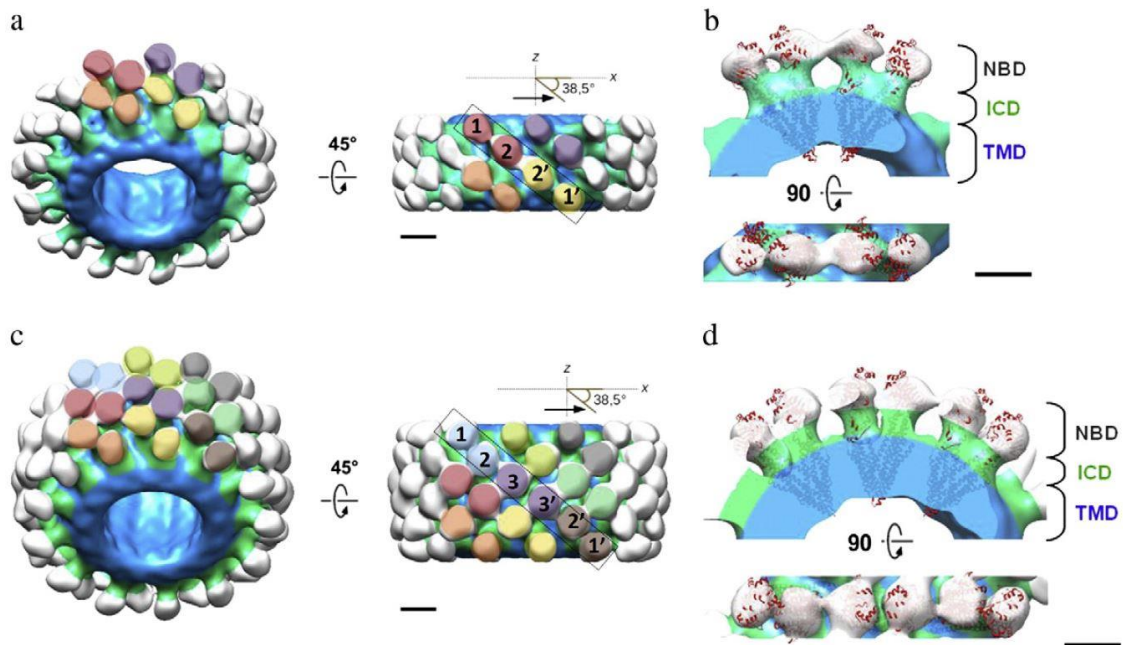




**Figure 21. Cryo-EM micrograph of the ring shape BmrA structure**

(a) Micrograph of the grid showing the particle by the black arrows and the others tubes or membrane by white arrows. The bar corresponds to 25 nm. (b) The up view of the 24 homodimers complex. (c) The up view of the 39 homodimers complex. (d) The side view of the 24 homodimers complex. (e) The side view of the 39 homodimers complex. The bar corresponds to 5 nm. Figure of the publication Fribourg et al. 2014.

Furthermore, this complex proved to be the assembly of 24 or 39 homodimers disposed in inward facing conformation with the NBDs exposed and the TMDs integrated in the lipid leaflets (figure 21). These complexes allowed the resolution of the structures at 23 Å and 25 Å by Cryo-EM (figure 22) (Fribourg et al. 2014). The structures revealed two different distance of opening for the NBDs which are 3 nm and 5 nm which were already observed for the P-gp and MsbA respectively. Moreover, this inward facing conformation has proven to be native-like since the addition of ATP-Mg<sup>2+</sup> induces a conformational change that leads to the destruction of the ring shape structure. This study showed that the dimerization of the NBDs alone was able to induce the conformational change in outward facing conformation, so the binding of ATP-Mg<sup>2+</sup> might be the driving force in this part of the mechanism (Orelle et al. 2008).



**Figure 22. Structures of the ring shape BmrA complexes**

(a) 3D structure of the 24 homodimers complex. (b) The structure of the mouse P-gp (PDB: 3G5U) in inward facing conformation was docked into the density. The structure is visible in red. (c) 3D structure of the 39 homodimers complex. (d) same than (b). The bar corresponds to 5 nm. Figure of the publication Fribourg et al. 2014.

The dynamics of the conformational changes were investigated also by hydrogen/ deuterium exchange (HDX) with mass spectrometry. The transporter was able to undergo important rearrangement in membrane or in detergent. The results of the study show that in the inward facing state (the resting state) the protein is flexible and it can explore different conformation. This flexibility was not overserved in the outward facing state (Mehmood et al. 2012). A recent study which used solid state NMR pinpoints the importance of the X-loop in the communication of NBDs and TMDs suggesting also that a stiffening is needed to provoke the conformational change from inward facing state and outward facing state (Lacabanne et al. 2019).

# III. Structural biology of membrane proteins

Membrane proteins account for up to 20% - 30% of the total amount of proteins expressed (Wallin and Heijne 2008). They are implicated in the exchanges of the cell with the surrounding environment transporting ions or molecules. Due to their localization and their key role for the survival of the cell they represent 60% of the pharmaceutical targets including receptors, channels and transporters (Overington, Al-Lazikani, and Hopkins 2006). Despite their importance, less than 2% of the protein structures found in the PDB (Protein Data Bank) correspond to membrane proteins. To this day, there are 3076 structures of membrane proteins solved, only a third (1077) correspond to unique proteins according to <https://blanco.biomol.uci.edu/mpstruc/>. This underrepresentation is due to their amphipathic nature: the protein exposes hydrophobic residues to be inserted in the membrane and the rest of the protein which is located in the cytoplasm or in the extracellular environment is more hydrophilic. This hydrophobic region of the protein complicates the study of this kind of protein in each step of the manipulation. The protein needs amphipathic molecules to be extracted from the membrane and to be kept in solution. These molecules are often detergents, which interact with the hydrophobic region of the protein and the lipids around it. At high concentration, detergents compete with the lipids and they extract the protein from the membrane by disrupting the membrane. After a purification step, it is possible to substitute them with polymers like amphipols or to reconstitute the protein into a lipidic environment as in a nanodisc or liposome. Recently, polymers with an extraction power have been developed to keep the protein in a more native-like environment. They are called styrene maleic acid co-polymer (SMA) and the diisobutylene-maleic acid (DIBMA).

In this chapter, I will discuss the different kinds of solvent used to keep membrane proteins in water solutions. Afterward, I will focus on the two techniques X-ray crystallography and Cryo-EM used to determine the structure of membrane proteins.

# 1. Amphipathic belt around the protein

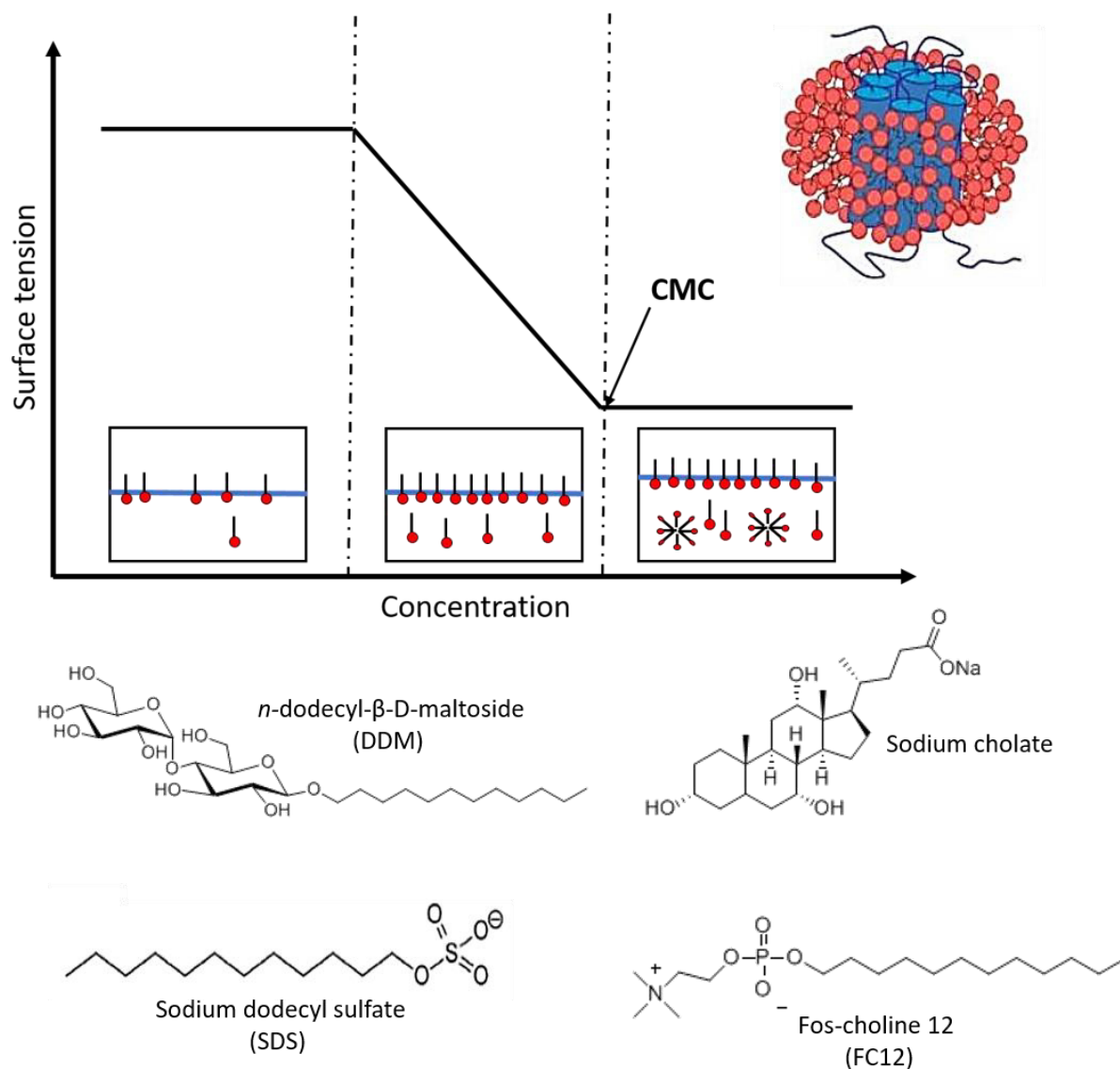
## 1.1 Detergent

Detergents are amphipathic molecules composed of two moieties: one hydrophilic and the other hydrophobic. The hydrophobic part competes with lipids and interacts with the hydrophobic part of the protein. The hydrophilic part (or head for some detergents) interacts with the aqueous environment. Due to their amphipathic nature, when detergent monomers are in aqueous environment at low concentration, the hydrophobic parts group mostly at the air-water interface. Detergent monomers will cover every hydrophobic surface that will lower the free energy of the hydrophobic tail compared to staying as a monomer completely exposed to water. Importantly, detergents are also very labile molecules (this mobility depends on the size of the tail and the nature of the head), and are thus also found as monomers in solution. At a certain concentration called critical micellar concentration (CMC), detergent monomers group together in the water to form large objects called micelles. Increasing the amount of detergents will result in an increase of the amount of micelles in solution, while keeping the monomers constant. Hydrophobic moieties of the detergents gather towards the inside of the micelle, thereby being shielded from water and decreasing their free energy (figure 23). The CMC differs for each detergent since it depends on their nature, and of the type of solvent they are surrounded by; the presence of salt changes the CMC significantly for some detergents. The number of particles into one micelle is called the aggregation number. Based on the nature of the two composing parts, they can be classified into four categories (Seddon, Curnow, and Booth 2004) :

- ✚ Non-ionic detergents are composed by an uncharged head which can be a glycosidic or a polyoxyethylene group. These detergents are usually known to not break protein-protein contacts but only lipids-protein contacts. In fact, they are milder and non-denaturing detergents. Examples of these detergents are Triton X-100, *n*-dodecyl- $\beta$ -D-maltoside (DDM) and *n*-octyl- $\beta$ -D-glucopyranoside (OG). It should be noted that this definition is variable and highly dependent on the application. For example, membrane protein complexes can be individualized by these detergents, therefore “denaturing” the complex, while keeping individual proteins intact.

## BILIOGRAPHIC REVIEW

- ✚ Ionic detergents are composed by cationic or anionic charged head and a hydrocarbon chain as hydrophobic part. They have a strong power of solubilization but they can be very harsh leading to a protein denaturation. An example of this kind of detergent is the well-known sodium dodecyl sulfate (SDS).
- ✚ Bile acid salts are also ionic detergents although they have a steroidal group as backbone which is composed by a polar and apolar face. These detergents have a more rigid structure and the form of their micelles differs from the others in fact they do not have a spherical shape but more a kidney-like shape. They are milder than ionic detergents and also less deactivating. Examples of this kind of detergents are Cholesteryl Hemisuccinate Tris salt (CHS) and sodium Cholate.
- ✚ Zwitterionic detergents are charged detergents with a net charge equal to zero. These detergents have a high capacity of solubilization but with an inactivating impact on the proteins. Examples of these detergents are dodecyldimethyl-*N*-aminooxide (DDAO) or the Fos-choline 8 to 16 (FC8 to FC16)



**Figure 23. Detergent behaviors in hydrophilic environment and examples of detergents**

The upper panel presents the surface tension as a function of detergent concentration. The critical micellar concentration is indicated with an arrow and each change on the tendency of the curve is highlighted by the dotted lines. Each change of state is presented in the rectangle below the curb. In the lower panel, there is an example of detergent for each category : *n*-dodecyl-β-D-maltoside for the non-ionic detergents, sodium dodecyl sulfate for the ionic detergents, sodium cholate for the bile acid salt and fos-choline 12 for the zwitterionic detergents.

An important effort is made to improve the stability and the conservation of membrane protein structure and function. Recently, in the lab, calixarene-based detergents have been designed using the observation that membrane proteins display basic residues in the cytosolic region near the membrane. The architecture of this detergent allows it to interact with these residues and form salt bridges. They are composed of three acidic methylene-carboxylate groups grafted to a calixarene backbone attached to an aliphatic tail (Matar-Merheb et al. 2011). This kind of detergent has proven to be more effective on solubilization and purification of an active form of the MRP4 (human multidrug resistance protein 4) than DDM or FC12

## BILIOGRAPHIC REVIEW

(Hardy et al. 2019). Based on this principle, another series of stabilizing detergents have been designed and to stabilize BmrA substantially (Nguyen et al. 2018). These detergents were key to solving the structure of BmrA as I will present below (cf. results section chapter I).

The choice of the detergent depends on the study which is programmed to be performed on the membrane protein of interest. It is still difficult to predict which detergent will successfully solubilize a protein while maintaining its activity. The only option is to perform a screening of multiple detergents to identify which one is the more adequate to the protein. It is important to notice that sometimes detergents that are more performing in the extraction step are not the most adapted to the functional studies of the protein. In fact, harsh detergents like zwitterionic or ionic detergents can solubilize almost the totality of membrane proteins but they have been proven to denature the protein or extract protein which are not active. Milder detergents as non-ionic detergents extract less membrane proteins but they are mostly active and well folded (Mathieu et al. 2019). It is important to mention that generally the activity of the protein belted by detergents is lower than the activity of the protein reconstituted into lipids. A reported example is the case of BmrA purified with DDM and reconstituted into lipids environment. The activity has been recorded showing a clear increase with the diminution of the detergent and an augmentation of the lipids. (Chaptal et al. 2017).

Detergents need to be present in all the steps from the extraction to the structural or functional studies as if their concentration drops below a certain level, they will partition away from the protein at the risk of the protein precipitation. They are therefore added in all the buffers used during the work. The quantity of detergent bound to the protein or the total quantity in a sample can be difficult to manage. To solve this problem, it is helpful to determine the amount of detergents present using a quantification method such as a colorimetric dosage (Heftmann, Ko, and Bennett 1966) or a radioactive one (Le Maire et al. 1983). These methods are detergent-dependent and they cannot be used when a mixture of two detergents is used. To overcome the limitations of the previous methods, Chaptal and his co-workers developed a method using mass spectrometry, the advantage is that a small quantity of sample is enough and any detergent can be quantified (FC12, DDM, LMNG, etc...). In addition, detergent mixtures are possible to quantify (Chaptal et al. 2017), as will be demonstrated and used later to solve the structure of BmrA (cf. results section chapter I).

## 1.2 Nanodiscs

To study membrane protein in a more native-like environment, the nanodisc system has been developed with the goal to insert proteins back into lipid bilayers (Bayburt and Sligar, 2003). This system mimics the functioning behavior of the human Apolipoprotein A-1 (Apo A-1) which is responsible for the formation of the High-Density Lipoprotein (HDL). This complex of lipid, cholesterol and protein circulates in the blood and it can play a role in the cardiovascular disease (Ilia G. Denisov and Stephen G. Sligar, 2017). The Apo A-1 carries out this function by being composed of ten amphipathic alpha helices, each one composed by 11 to 22 residues, separated by a proline (figure 24a). The membrane scaffold protein (MSP) was designed from the Apolipoprotein A-1 backbone. The first 43 residues of the Apo-1 N-terminal part are not present since this region is not structured. One nanodisc is composed of two MSP that belt a lipid bilayer (figure 24c). The size of the discoidal system is related to the length of the MSP, where insertion of additional helices between Q55 and P56 increase the length of the MSP to yield different flavors of nanodiscs (figure 24b). In addition, in the N-terminal part a tag and a corresponding linker was inserted to allow their purification. To distinguish them a specific nomenclature have been formulated. The terminology MSP1 or MSP2 differentiates between 10 or 20 helices. E indicates if helices are repeated and D is for the presence of the TEV cleavage site (Denisov et al. 2004). There are six MSP available:

- ✚ MSP1 corresponds to the Apo A-1 without the first 43 residues. It presents a 6-histidine tag and also a factor Xa protease site. The diameter of the nanodisc formed is 9.7 nm and the ratio lipids / protein (mol/mol) is 82.
- ✚ MSP1E1 is similar to MSP1 but with the helix 4 repeated to have a nanodisc diameter of 10.4 nm and a ratio lipid / protein (mol/mol) of 106.
- ✚ MSP1E2 is similar to MSP1 but with the helices 4 and 5 repeated to have a nanodisc diameter of 11.1 nm and a ratio of lipid / protein (mol/mol) of 134.
- ✚ MSP1E3 is similar to MSP1 but with the helices 4, 5 and 6 repeated to have a nanodisc diameter of 12 nm and a ratio lipid / protein (mol/mol) of 167.
- ✚ MSP1D1 corresponds to a modified MSP1. In fact, the tag is a hepta histidine tag with the first 11 residues and a TEV protease cleavage site. The substitution of the Xa protease site by the TEV one is due to the more accuracy of the TEV protease.

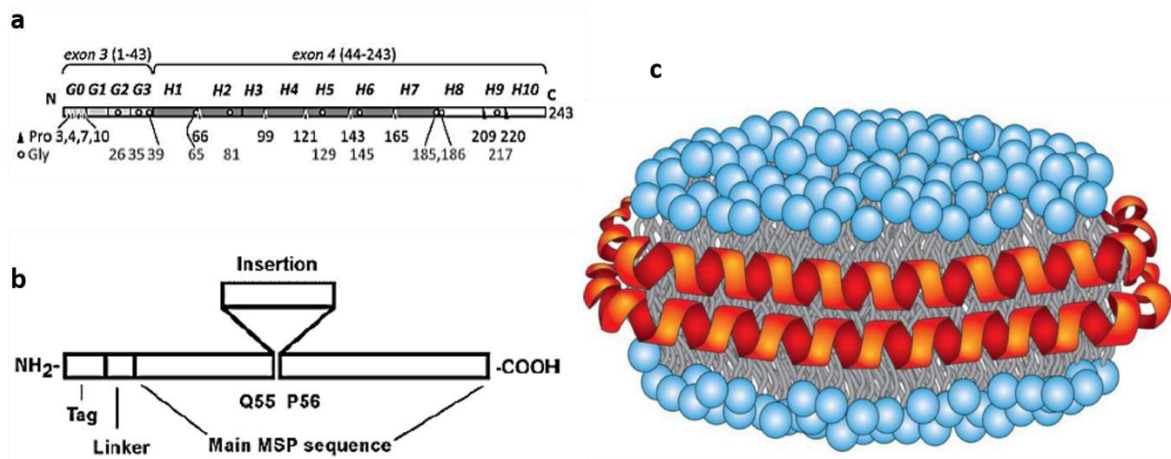


## BILIOGRAPHIC REVIEW

The diameter of the nanodisc is 9.5 nm and the ratio lipid / protein (mol/mol) is of 81.

- ✚ MSP1E3D1 is the same than MSP1E3 with the substitution of the factor Xa protease site with the TEV protease cleavage site.
- ✚ MSP2N2 is composed by a tandem of two MSP. It has also an hepta histidine tag and the TEV protease cleavage site. The diameter of the nanodisc is 17 nm and the ratio lipid / protein (mol/mol) is of 300.

(Note that the thickness of the nanodisc is the same for all of them which is of 5.7 nm (Denisov et al. 2004; Nagle and Tristram-Nagle 2000)).



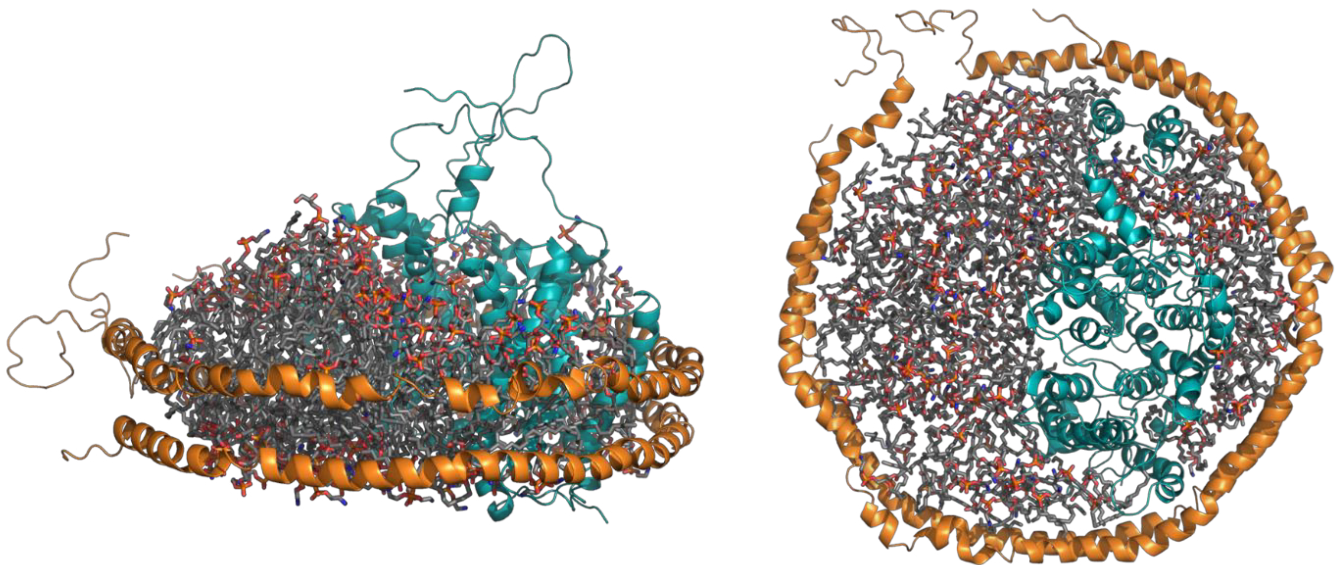
**Figure 24. Structure of the nanodisc**

(a) It is the primary sequence of the Apolipoprotein A1. There are indicated the first non-structured part (1-43) and the second part composed by ten helices. (b) The membrane protein scaffold (MSP) is composed by the tag, the linker which allowed the cleavage by TEV protease or factor Xa, and the site of insertion for the formation of the larger MSP. (c) illustration of a nanodisc. The MSPs are in orange and the lipids in light blue and grey. (a) and (b) are from (Denisov et al. 2004) and (c) from (Ilia G. Denisov and Stephen G. Sligar 2017).

The controlled size of the MSP ensures that the sample obtained after reconstitution is monodisperse and homogenous which are optimal properties for conducting structural studies. In fact, many structures of membrane proteins reconstituted into nanodisc have been solved by Cryo-EM since the sample is also stable at low temperature (Ilia G. Denisov and Stephen G. Sligar 2017). The structure of the complex ribosome-SecYE (translocon of membrane protein) inserted into the nanodisc was solved by Cryo-EM (figure 25). It was possible to determine the structure of the Apo A-1 ( $\Delta$ 1-43) in complex with lipids used to form the nanodisc (Frauenfeld et al. 2011). Many other structures of membrane proteins

reconstituted into nanodisc have been solved as for the TRPV (transient receptor potential cation channel) family although the density of the MSP was not detected (Gao et al. 2016; Pumroy et al. 2019; Hughes et al. 2019). In contrast, in X-ray crystallography technique, nanodisc do not perform well since the complex do not crystallize.

In functional studies, nanodisc represent an interesting system since it is possible to reconstitute the protein in its physiological environment. For example, some human proteins as the ABC transporter ABCG2 need cholesterol to be active, so with the nanodisc system it is possible to introduce cholesterol or an analogue to obtain an active protein (Orlando and Liao 2020; Jackson et al. 2018). In fact, nanodiscs are used to test the interaction with the membrane surface and the binding of substrate or inhibitors. A quite interesting application is in the development of antibodies and vaccines for human therapy. It has been observed that the reconstitution into nanodisc proteins of fragment of virus envelope increased the stability in plasma. This approach has been used for HIV (Ilia G. Denisov and Stephen G. Sligar 2017; Nakatani-Webster et al. 2015).



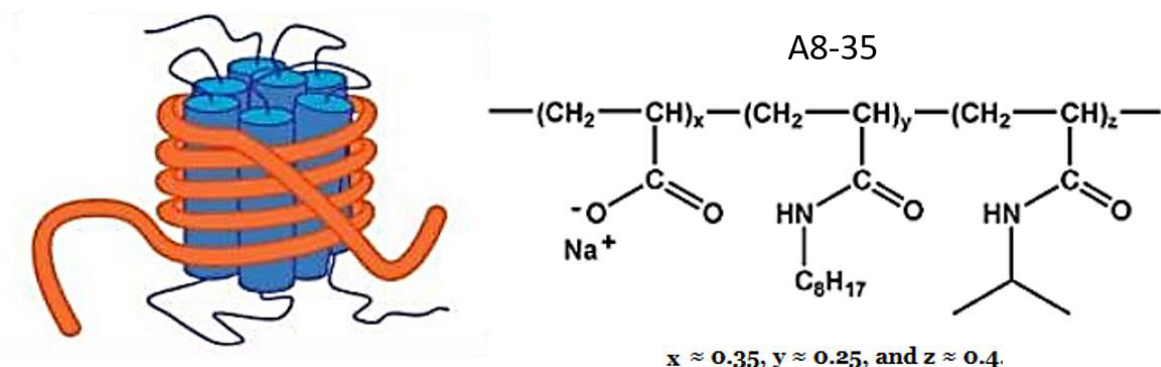
**Figure 25. Structure of SecYE inserted into the nanodisc formed by Apo A1 ( $\Delta 1-43$ ) solved by Cryo-EM**  
 On the left the side view of the complex and on the right the above view. The two Apo A1 ( $\Delta 1-43$ ) are in orange cartoon, the SecY aquamarine cartoon and the lipids are presented in sticks. The lipids were added in the model after the resolution of the structure. Figure adapted from Frauenfeld et al. 2011.

## 1.3 Polymers

### 1.3.1 Amphipols

These polymers are amphipathic molecules composed by a hydrophilic backbone and the hydrophobic sidechains (Tribet, Audebert, and Popot 1996). They are classified as surfactants like detergents. They are also used to keep membrane proteins soluble although due to their low dissociating power there are no evidences that they can extract the proteins from the membrane (Zoonens and Popot 2014). Nonetheless they have a high affinity with the proteins leading to have a low exchange rate. This property allows the complex amphipol/protein to be more stable than with detergents and also there is no need to add them in the buffer (Popot 2010). This means that the buffer would be detergent/amphipol free which is useful for structural studies. Therefore, this polymer has proven to be effective in Cryo-EM since they do not present a strong background. Structures of the TRPV family and the V-ATPase have been solved this way. In addition, to increase even more the stability of the protein it is possible to add lipids which could be useful for functional studies.

The most used amphipol is the A8-35 which contains carboxylate phosphorylcholine acting as the soluble part (figure 26). The nomenclature is due to A for anionic, the first number represents the apparent molecular weight which is here 8 kDa and the last number is the percentage of carboxylic groups which are free in this case and represents 35%. These molecules self-assemble in solution forming a complex of four single polymers resulting in a 40 kDa system (Popot et al. 2011).



**Figure 26. Amphipols**

On the left, a membrane protein (blue) is in complex with amphipols (orange). On the right, the structure molecule corresponds to the more used amphipol A8-35. (Dörr et al. 2016)

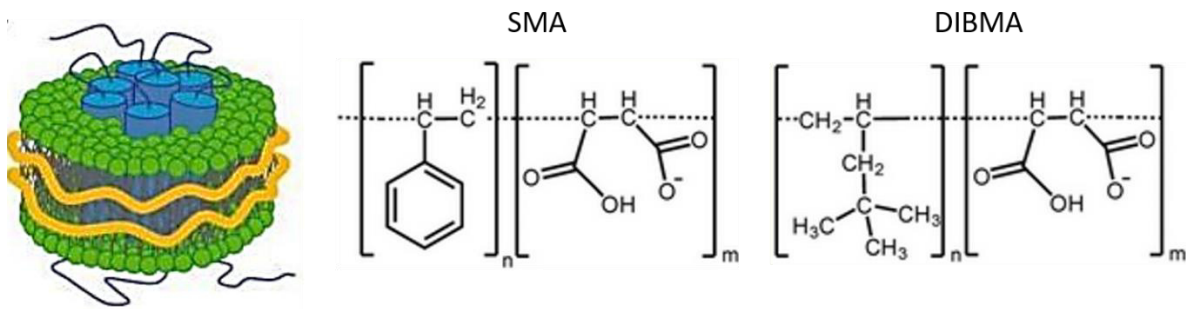
### 1.3.2 SMA and DIBMA

Recently, two other polymers have been designed to preserve the protein in its native environment (figure 27). They are capable of extracting the protein from the membrane keeping the native lipid environment around the protein. The two molecules are the styrene maleic acid co-polymer (SMA) and the diisobutylene-maleic acid (DIBMA). This technology is the only one allowing the purification of membrane protein without the use of detergent.

The first polymer developed is SMA which forms a discoidal lipid bilayer of about 10 nm of diameter and 4.6 nm of thickness. It is classified as a mild extracting agent since it preserves the protein-protein interactions. SMA showed to be successful in the purification of the protein reaching a good final yield and a good purity degree. Such is proved by the resolution of the following membrane proteins : Bacteriorhodopsin from *Haloquadratum walsbyi* by X-ray (PDB 5ITC, Broecker, Eger, and Ernst 2017), AcrB from *Escherichia coli* and Complex III from *Flavobacterium johnsoniae* by Cryo-EM (PDB 6BAJ and 6BTM; Sun et al. 2018 ; Qiu et al. 2018 respectively). However, this polymer presents some disadvantages:

- It absorbs at 260 nm because of the presence of an aromatic styrene group in its structure (figure 27). This means that the determination of the concentration of the protein alone by absorbance is not possible. Moreover, it is not an optimal condition for functional studies as the binding test of a substrate detected by fluorescence.
- It has been observed that it interacts with the divalent ions such as  $Mg^{2+}$ . For instance, this could mean that it is not possible to perform some activity test like the ATPases.

To overcome these two issues, the copolymer DIBMA was developed (figure 27). The latter do not interfere with the absorption method and the interaction with divalent ions is reduced (Oluwole et al. 2017). This copolymer is larger, 15kDa against 7.5-10kDa for SMA, resulting in a larger discoidal lipid bilayer of 25 nm as diameter. Thus DIBMA can extract more than one protein for one lipid discoidal leading to a lower degree of purity for the sample (Gulamhussein et al. 2020).



**Figure 27. Polymers SMA (styrene maleic acid copolymer) and DIBMA (diisobutylene-maleic acid copolymer)**

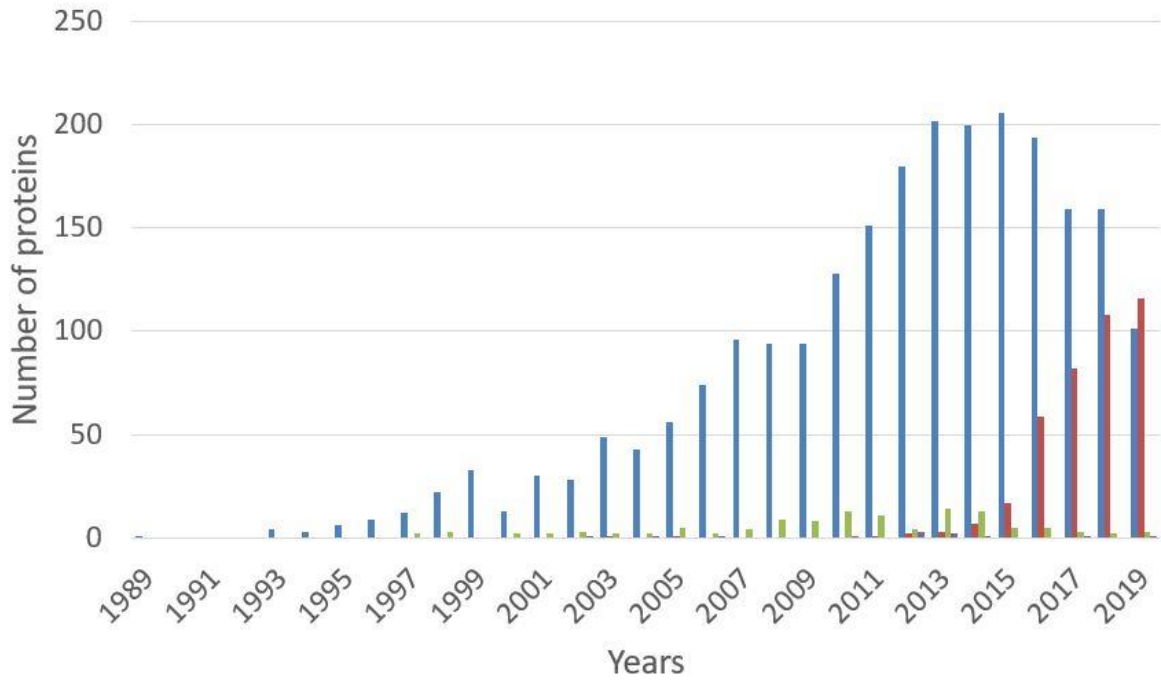
On the left, a membrane protein (blue) is inserted in a lipids bilayer (green) formed by a polymer (yellow). On right, there are the structure of SMA and DIBMA. (Dörr et al. 2016)

## 2. Structural techniques

The techniques mostly used to solve membrane proteins are X-ray crystallography and electron crystallography until the recent major developments of single particle Cryo-EM. It should be noted that NMR is also a structural method to study protein structures and dynamics. Within NMR spectroscopies, only Solid-state NMR can achieve structural details due to the large size of membrane proteins in general. The method is however not as easily implementable yet and is still under development, so I will only focus on X-ray crystallography and single particle Cryo-EM in the rest of the manuscript.

The first structure of a membrane protein was solved in 1985 by X-ray crystallography and it corresponded to the photosynthetic reaction center of *Rhodospseudomonas viridis* (Deisenhofer et al. 1985). In 2003, the structure of the nicotinic acetylcholine receptor pore was determined by cryo electron crystallography (Miyazawa, Fujiyoshi, and Unwin 2003). This method is a combination of diffraction and imaging, since the sample must be a 2D crystal imaged by an electron microscope. However, the main technique used was the X-ray one until the resolution of a structure at near-atomic resolution by single particle Cryo-EM in 2013. It was the structure of the ion channel TRPV1 (code PDB is 3J5P) (Liao et al. 2013). Since then, this method has grown very popular to solving membrane protein structures, as exemplified by the graphic below, plotting the number of structures solved and the corresponding year. There is an evident augmentation during the last 5 years (figure 28).

In X-ray crystallography studies, a critical step for many proteins is the formation of crystals, this step is bypass by Cryo-EM. The sample is immediately deposited on the grid just after the purification step. Even if some optimizations are also needed to obtain high resolution data, the Cryo-EM offers always information about the sample. Thus, a density map is automatically obtained as an output even at low resolution which can still give information on the protein as its flexibility.



**Figure 28. Membrane protein structures**

*This graph presents the number of structures solved per year and per technique. Structures solved by X-ray crystallography (blue), NMR (green) and Cryo-EM (red). Personal communication from data collected from the PDB by Xavier Robert (MMSB).*

## 2.1 X-ray crystallography

X-ray diffraction crystallography has been the major method used to solve the structure of macromolecules, developed during the XXe century. This technique relies on the diffraction power of the crystal which is an ordered arrangement of molecule in three dimensions of space. The crystal packing is determined by protein-protein contacts. A high concentration of protein is usually the key to obtain a crystal and this constitutes one of the largest bottlenecks for the application of this technique to membrane proteins. It is often difficult to overexpress the protein because they easily become toxic to the expression system since the membrane space is limited (Borges-Walmsley, McKeegan, and Walmsley 2003). To overcome this problem many studies have been geared towards developing tools for overexpressing recombinant membrane proteins. A pioneer work has been the development by Miroux and Walker of two *E. coli* strains derived from standard BL21 that accommodate the overproduction of membrane proteins: C41 and C43 (Miroux and Walker 1996). These strains decrease the strength of the T7 promotor which gives cells time to accommodate with the production of membrane proteins. Many other studies have followed in different expression systems, all with the goal to overexpress the large amount of protein needed for crystallography.

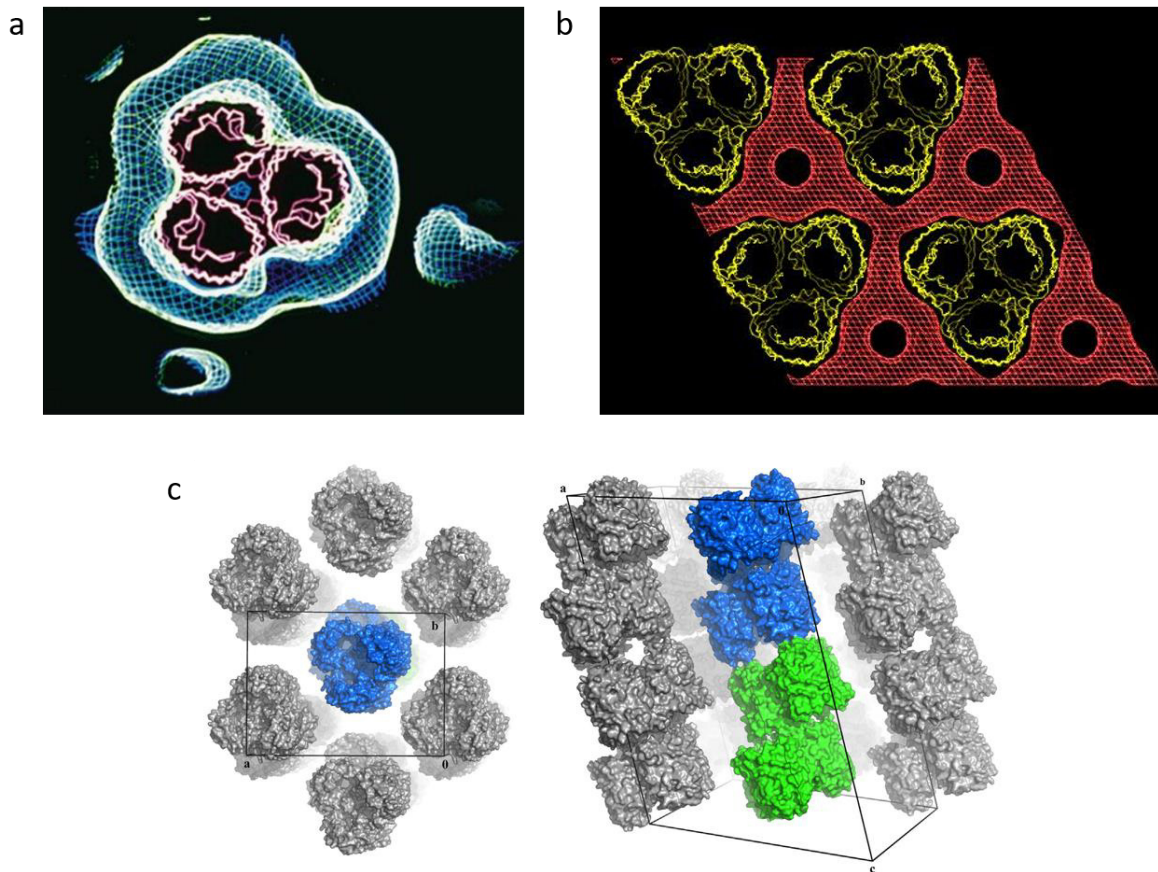
In addition to this issue, the membrane proteins need the detergent to be extracted and kept in solution as discussed above. The presence of the detergent belt around the protein prevents protein:protein contacts, and therefore often precludes the formation of the crystal (figure 30b) (Ostermeier and Michel 1997). Once a crystal has been obtained, detergents now play an active role in the crystal packing as clearly shown for the *E. coli* porin OmpF over the years (figure 29). Neutron diffraction of OmpF crystals first shows the detergent torus wrapping around the protein within the crystal (figure 29a). Then the authors showed how detergents were expanding from one protein to the other within the packing, to create a continuum (figure 29b). Additionally, it was shown in centered monoclinic crystals of OmpF that the detergent itself was responsible for lateral contact between OmpF columns, thereby playing the role of “normal” protein:protein contacts in crystals (figure 29c) (Chaptal et al. 2016).

Following this idea, investigators tried to vary detergents in the process of making or optimizing a crystal. This has been seldom documented, based on the difficulty of measuring



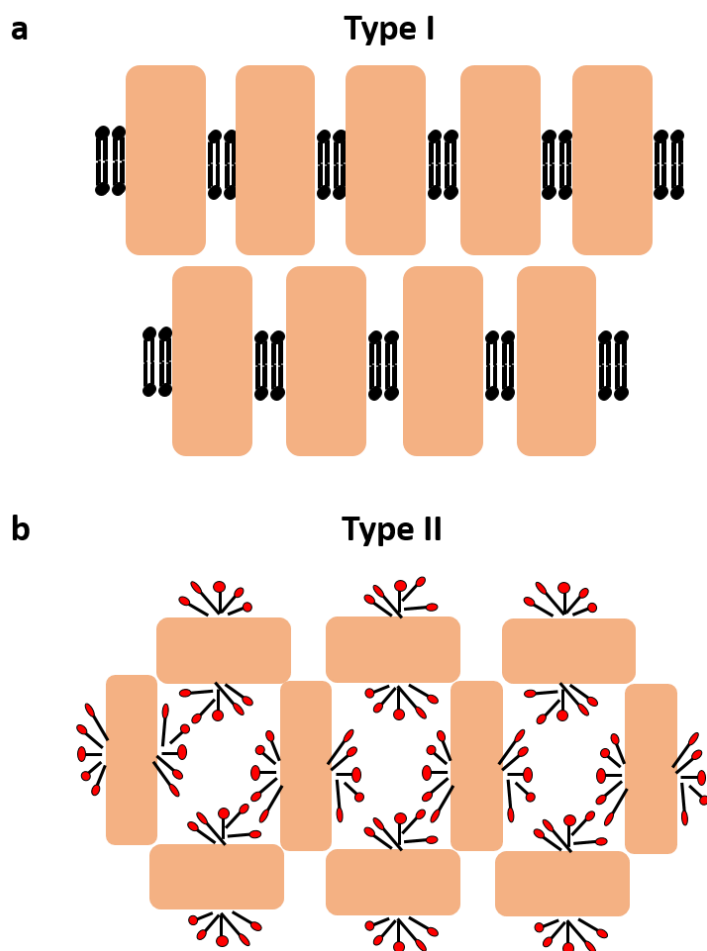
## BILIOGRAPHIC REVIEW

and following detergents in purifications. One famous example is the influence of LDAO concentration on the diffraction of the ADP/ATP exchanger (Eva Pebay-Peyroula et al. 2003). In the result section, I will describe the rational design of a smaller detergent belt to improve BmrA's crystals diffraction.



**Figure 29. Detergent in crystals**

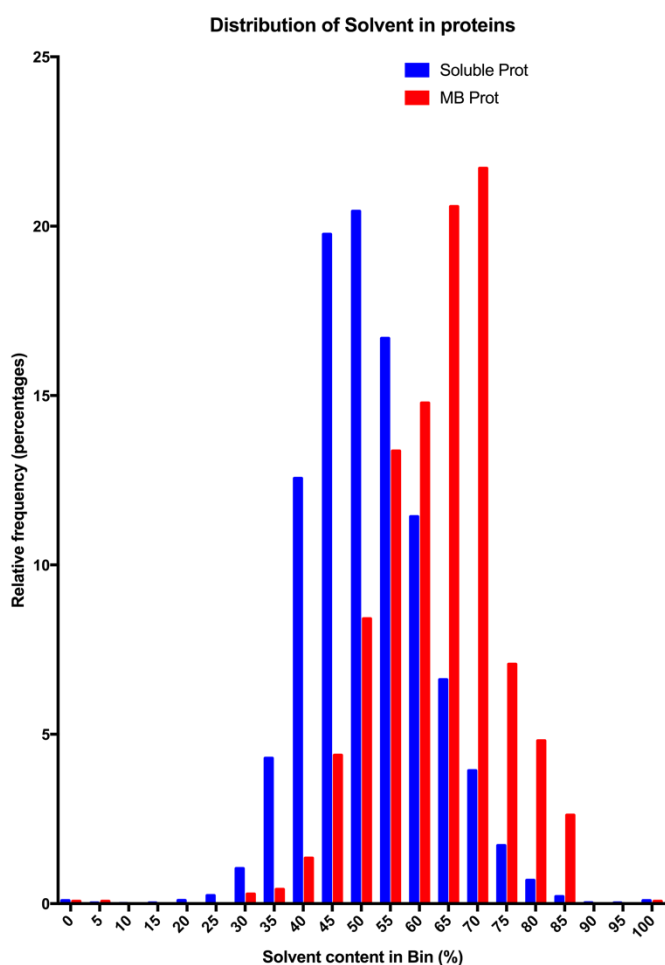
(a) The detergent belt around the membrane protein OmpF was determined by neutron diffraction. The detergent is in light blue and the structure of OmpF is in pink. (b) This is the upper view of the crystal arrangement of OmpF (yellow) and the solvent/detergent (red). The protein is in yellow and the solvent in red. (c) This is a crystal packing of OmpF. The detergents are responsible for the crystals contacts. The density maps are presented in blue, green and grey. (E. Pebay-Peyroula et al. 1995 ; Chaptal et al. 2016)



**Figure 30. Crystal packing of membrane protein**

(a) Type I packing is formed by 2D crystal of membrane protein stacked. This type of crystal arrangement is especially formed by lipid cubic phase or bicelles methods. Nevertheless, it is possible to obtain also in presence of detergents. The protein is the orange cylinder and the lipids or the bicelles are in black. (b) Type II packing is composed by a packing done by the polar contacts of the membrane protein and the detergent belt around the protein. It is the type of packing found for protein in detergent. The proteins are the orange cylinder and the detergent are in red (polar head) and black (hydrophobic part). This figure is adapted from Ostermeier and Michel 1997.

Once the membrane protein crystal grew and diffracted enough to collect data, other difficulties have to be faced in the data processing part. In the soluble protein crystal, the solvent ranges from 20% to 85% with a majority of cases around 45%. In the membrane protein crystal, the solvent ranges from 30% to 85% with a majority of cases around 70% (figure 31). This average higher percentage of solvent for the membrane protein is due to the presence of detergent belt. Unfortunately, the latter is not considered as an active part of the packing but only as solvent by the treatment program to solve the structures. This leads to a loss of information in the treatment process of the data for membrane proteins, and a greater error on the phase calculation, with an impact on the quality of the electron density maps. This effect is greater at lower resolution, which usually also correlates with higher solvent content.



**Figure 31. Histogram of crystal solvent content**

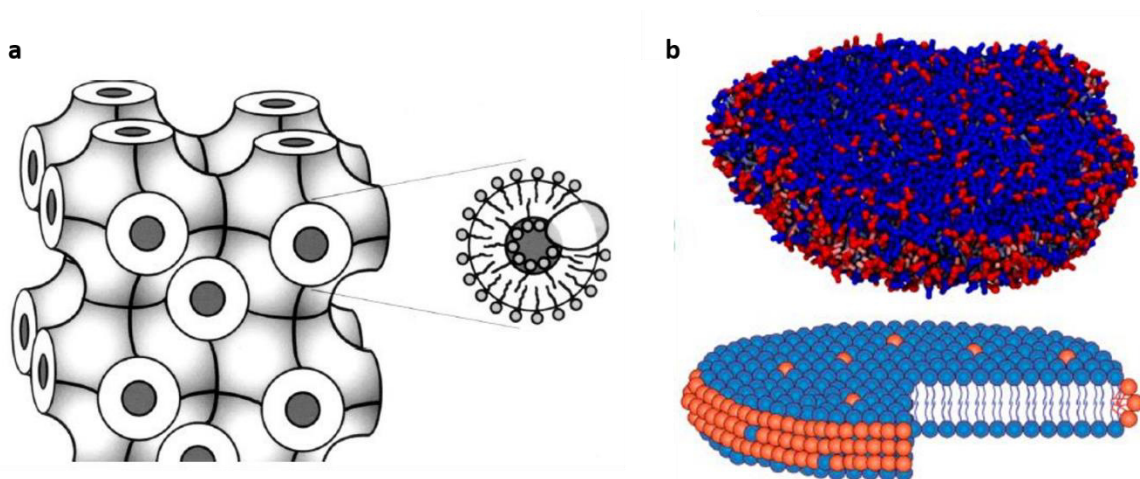
*It was measured for the whole PDB, January 2016. Personal communication, Vincent Chaptal.*

To solve the problem of the detergent environment, other techniques were developed; lipid cubic phase or bicelles. This kind of hydrophobic environment form a type I packing which is composed of a stack of 2D crystal (figure 32).

- Lipid cubic phase is composed of monoacylglycerol (MAG) or monooleic and water organized into a three-dimensional matrix in which the protein can insert in the bilayer. This method allows the formation of crystal type I in a more native-like environment (Caffrey 2015). The advantages are that the presence of the lattice promotes the nucleation step (seeding) and secondly the protein conserves its structural integrity and its activity (Landau and Rosenbusch 1996). This matrix is stable, quasisolid and it allows the diffusion of hydrophobic and hydrophilic molecules. The structure of the sensory rhodopsin II was solved using this method (PDB code is 1H68) (Royant et al. 2001). The disadvantage is its important viscosity and defined structural shape that doesn't accommodate all proteins (for example BmrA never entered cubic phases or

bicelles), and also that the crystals formed are quite small which means they are difficult to detect (Faham and Bowie 2002).

- Bicelles are a mixture of lipids and detergents (or large and small tail lipids) organized into a bilayer allowing the membrane protein to be inserted into a more native-like environment than detergents only. This method allowed to solve the structure of the bacteriorhodopsin from *Halobacterium salinarum* at 2 Å resolution (PDB code is 1KME). The disadvantage is the high frequency to obtain aggregates or the high rate of false positive. Moreover, like for cubic phase not all protein crystallizes in this environment. (Faham and Bowie 2002).



**Figure 32. Native-like environment to produce membrane protein crystals**  
 (a) Cubic lattice formed by lipids. (b) Bicelles which are a mix of detergent and lipids.

Finally, the anisotropy in the collected data is a frequent problem encountered in the case of membrane proteins. The anisotropy is defined as the loss of diffraction power in one or two of the three spatial directions. Practically the diffraction pattern is not equal into the three directions, but is more an ellipse. This translates into a loss of information of the structure to solve (lack of completeness at high resolution). It is important to mention that anisotropy is not only a problem of membrane proteins because it is also observed for soluble proteins but less frequently. Since the crystallography software were at first developed based on soluble proteins, which often diffract to better resolution than the membrane ones, the anisotropy was not handled well. The data are then truncated where the diffraction was present for the three directions and not all the data were taken into consideration to solve the structure. To overcome this issue, the UCLA anisotropy server, followed by Staraniso were developed to

## BILIOGRAPHIC REVIEW

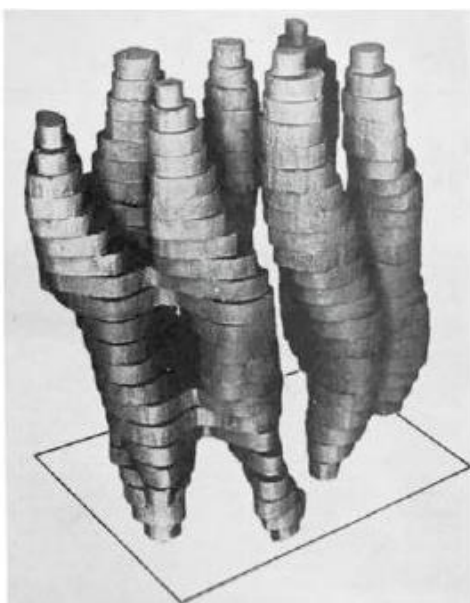
deal with this specific kind of data. A recent study of Robert and his co-workers revealed that anisotropy seemed to be independent of the type of packing or crystallization mode, the nature and the size of the protein (Robert et al. 2017). The main conclusion of their study is that the diffraction power of membrane protein crystals is different from the soluble ones due to the intrinsically different nature of these kind of macromolecules.

To conclude, the X-ray diffraction crystallography was the most used and performed technique to solve membrane protein structures even if many adjustments have to be made during the process. This technique still allows to this day the solving of membrane proteins structures.

## 2.2 Cryo-EM

In 1997, while attending a 3D electron microscopy meeting Richard Henderson stated that the cryo electron microscopy would dominate all the others techniques used in biological structural studies (Moallem 2009). Twenty years later, he was awarded by the chemistry Nobel prize with Joachim Frank and Jacques Dubochet for their implication in the development of this technique. Each of them participated in each milestone that led to the global utilization of the Cryo-EM. This method marked a real revolution in the structural studies making it possible to solve the structures of macromolecules which are resistant to X-ray crystallography, like membrane proteins or protein complexes.

The first one to tackle the structural studies of membrane proteins by electron microscopy was Richard Henderson. His study determined the first atomic model of this kind of protein with the collaboration of Unwin (Henderson and Unwin 1975). They purified 2D crystal of the Bacteriorhodopsin and diffracted them using an electron microscope. As a result, they were now capable of constructing the first representation of a membrane protein (figure 33). However, the resolution was at 7 Å so it was not enough to solve the atomic structure. In fact, the first atomic resolution membrane protein structure (3 Å) was solved by X-ray crystallography in 1985 (Deisenhofer et al. 1985). In 1990, the structure of the Bacteriorhodopsin was fanally solved at 3.5 Å resolution by electron crystallography (Henderson et al. 1990).



**Figure 33. First 3D model of a membrane protein**

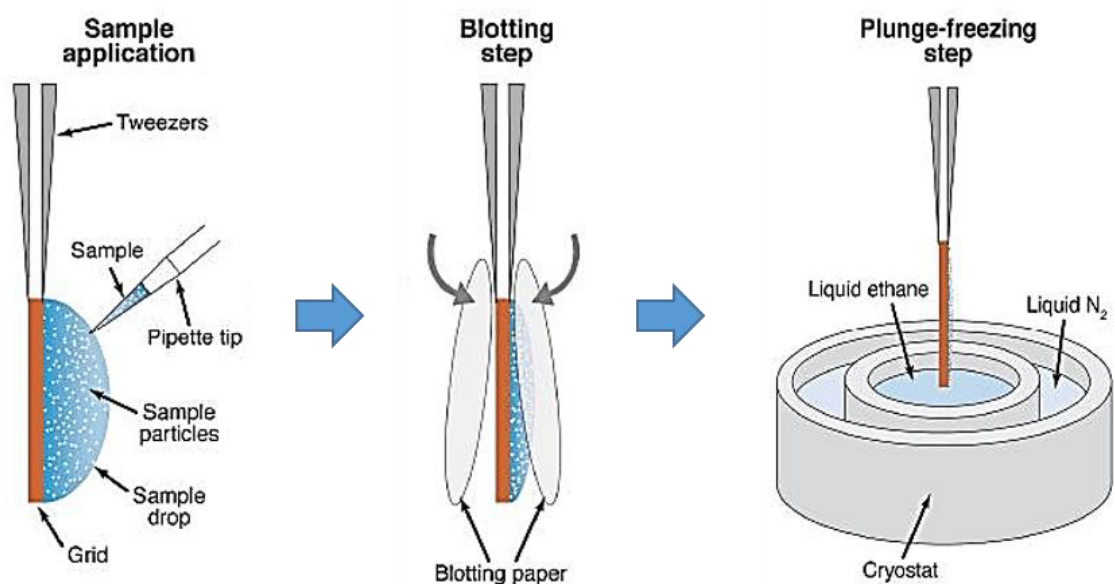
*The method used is electron crystallography (Henderson and Unwin 1975).*

## BILIOGRAPHIC REVIEW

The second milestone was the discovery of the water vitrification (Brüggeller and Mayer 1980) and its utilization in the sample freezing (Dubochet and McDowell 1981; Dubochet et al. 1982). This water state was a turning point because this amorphous state could help the preservation of organic specimens at low temperature reducing also the radiation damages. Therefore, the sample would be frozen in a thin layer of vitrified water and maintained at low temperature in liquid nitrogen. On an historical note, the cryo part in cryo-EM is due to this application. To prepare the specimens with this method, the plunge freezing system was developed (figure 34):

- ✚ The grid is composed by a carbon film with tiny holes. Before adding the sample, it is treated by a glow discharge to render it hydrophilic for the sample to enter the holes.
- ✚ The sample is added to the grid and the excess is blotted away by a filter paper.
- ✚ The grid is rapidly plunged into liquid ethane by a mechanical device.
- ✚ The sample preparation is stocked into liquid nitrogen.

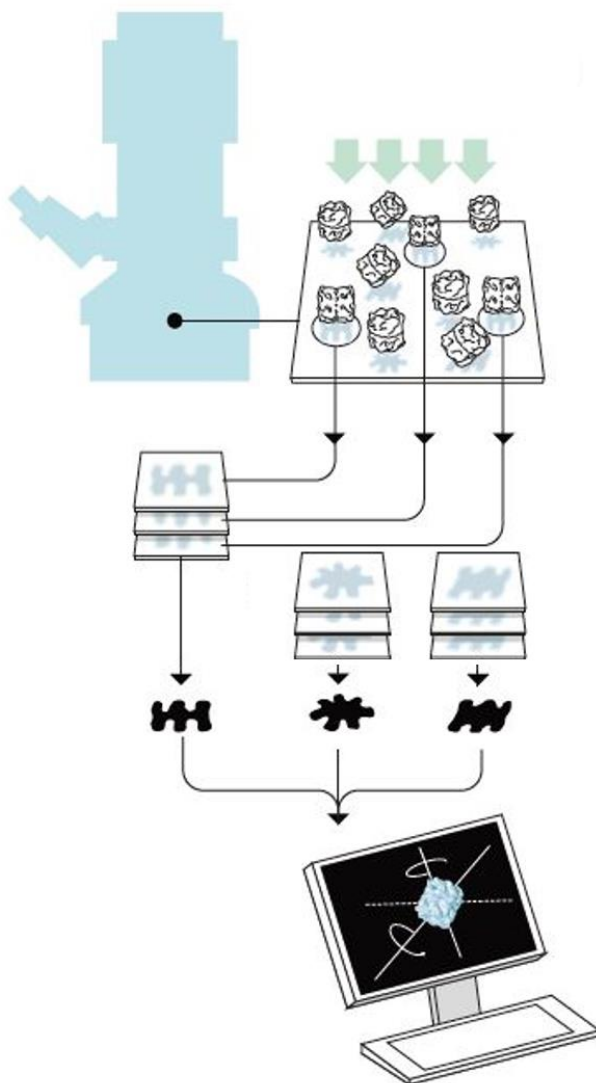
The main critical steps are the blotting of the sample and the type of grid since the former has an impact on the concentration and the distribution of the sample on the grid, and the latter as the particles distribute differently in different hole types and ice thickness. Nowadays, these steps are semi-automated thanks to mechanical devices such as the Vitrobot to increase the reproducibility.



**Figure 34. The three steps of the grid preparation for the Cryo-EM**

*The first step is sample application, the second one is the blotting of the excess of the sample and the third one is an plunge freezing (Sgro and Costa 2018).*

A major milestone was the implementation by Joachim Frank of images analysis processes that allowed to solve the 3D structure from the collection of 2D images of the sample. Since the proteins are distributed into this layer of vitrified water in random orientations, Frank developed a program to discriminate the proteins from the background, recognize the same pattern and then merge together the same orientations (Joachim Frank 1975; Saxton and Frank 1976; J. Frank et al. 1978). To complete this work, he developed a software capable of determining the 3D structure using the 2D classification. This allowed to solve a structure at 40 Å resolution of the ribosome (figure 35) (Wagenknecht et al. 1989).



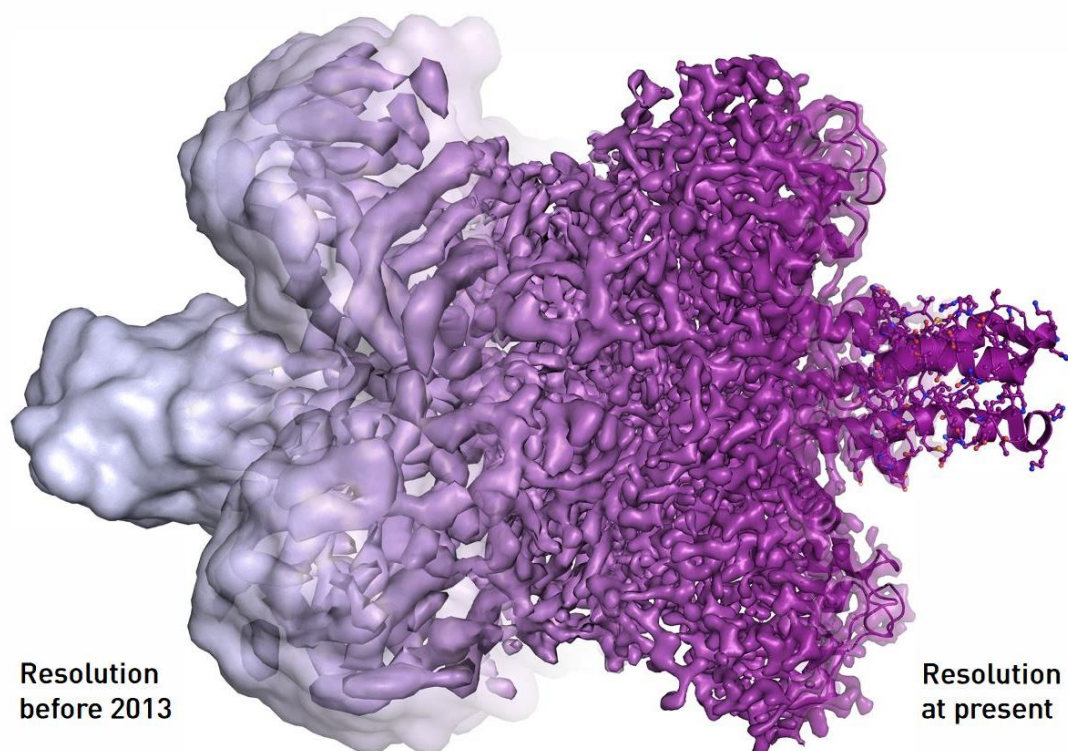
**Figure 35. 3D reconstitution method**

*After data collection, the 2D images are classified and then the 3D model is determined on the basis of this classification. This illustration has been realized by Johan Jarnestad/The Royal Swedish Academy of Sciences.*



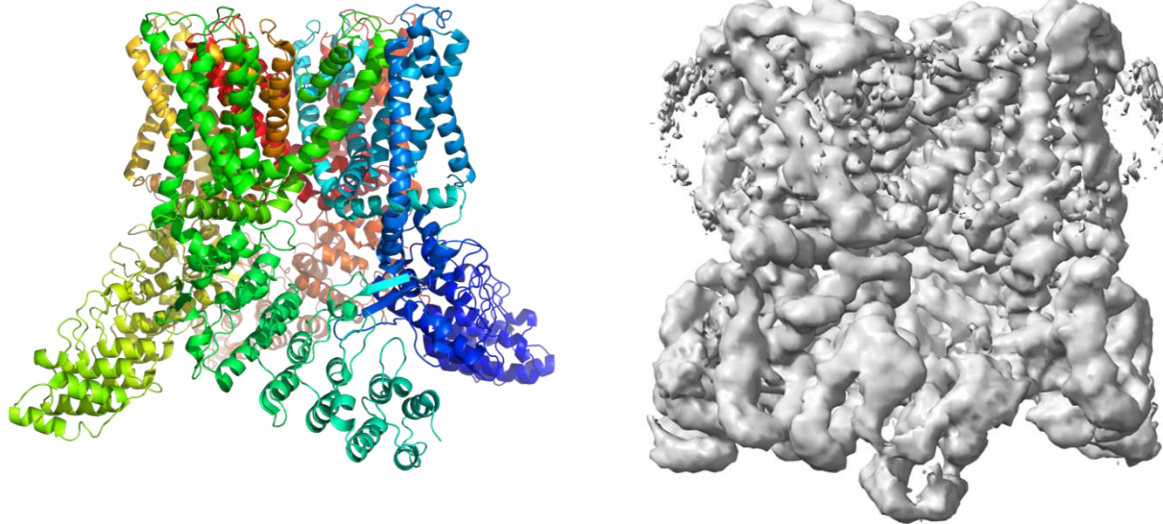
Even if the Cryo-EM was improving, it could not reach the high resolution of the X-ray. In fact, the information obtained of the sample was mostly a blob at low resolution. For this, the structural biology performed by this technique was called on a funny note the “blobology”.

Technical development allowed not only the determination of protein structure at high resolution, but also the passage from a niche method to a worldwide utilization. The development of direct-electrons detectors (DED) elevated the blobology to a high resolution. This detector could record every single electron event allowing the collection of information not only at high frequency for the atomic resolution but also at low frequency which maintained a good contrast. This is essential to ensure particle peaking and alignment step (McMullan, Faruqi, and Henderson 2016). This technology substituted the CCD (charged-coupled device), which was converting the electron event into photo. The last step was the implementation of software able to treat the data correctly and rapidly but also to be easily used by the structural scientists without expertise in this domain. The first software was RELION implemented by Sjors Scheres (Scheres 2012), then CryoSPARC and cisTEM were developed (Punjani et al. 2017; Grant, Rohou, and Grigorieff 2018). These programs ensure the data treatment pipeline from the micrographs to the 3D reconstitution.



**Figure 36. The evolution of the cryo-EM on the resolution of the structure of the ribosome**  
*This illustration has been realized by Martin Högbom /The Royal Swedish Academy of Sciences.*

All these milestones together allowed the resolution of the membrane protein TRPV1 at 3.27 Å in the year 2013 (figure 37) (Liao et al. 2013).



**Figure 37. Structure of the TRPV1 (PDB 3J5P)**

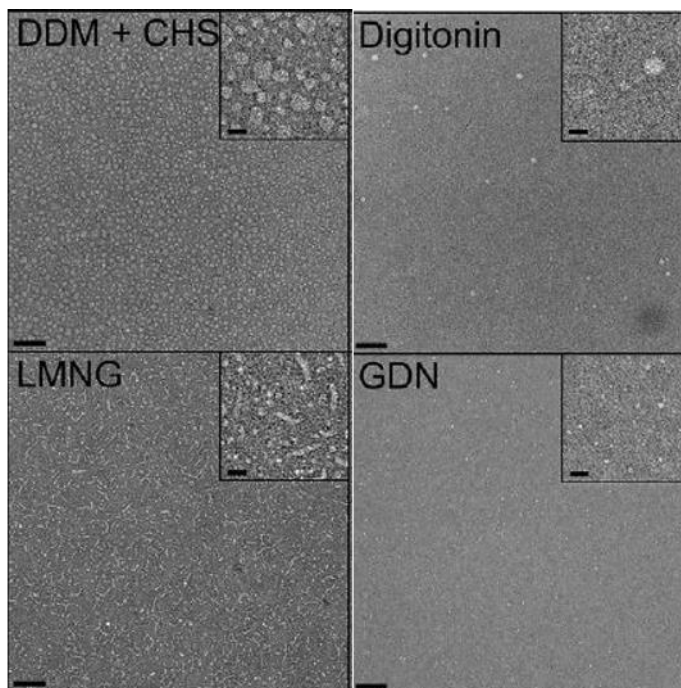
*It is the first membrane protein structure solved by single particle cryo-EM. On the left, the protein is displayed in cartoon and each colors present a subunit. On the right, there is the density map of the protein (Liao et al. 2013).*

The impact on the membrane protein structural studies was the real revolution since it facilitated some complex steps on the resolution of the structure:

- ✚ **Sample quantity.** In X-ray, the quantity of protein required is in mg scale to have enough protein concentration to induce the crystal formation with a high resolution diffraction power. Crystal optimization was also very greedy for protein. In Cryo-EM, the protein concentration needed is in the µg scale. The reduction of the sample concentration by a factor of 10 is a great advantage for membrane proteins given the complexity of its production and purification.
- ✚ **Detergent presence.** In X-ray, the detergent is a real problem as already mentioned above. In Cryo-EM, the presence of the detergent is more tolerated and it can even sometimes contribute to the good dispersion on the grid. In fact, they are surfactants which means they can modify the surface tension which is a critical parameter before the bottling and the freezing steps. In addition, the detergent belt could take an active role in the structure determination since it could help during the alignment step. Still,

## BILIOGRAPHIC REVIEW

the detergent choice must be done carefully because the free micelle will also be present on the grid contributing to the background. Some detergents or mixture of detergents can organize themselves into tubes such as LMNG or DDM-CHS. An extensive review on this topic has been carried out by Gewering and his co-workers. They tested a variety of buffers with different detergents visualizing them by negative stain on an electron microscope (figure 38) (Gewering et al. 2018). It is clear that some detergents can display a higher background (LMNG) than others (GDN or digitonin).



**Figure 38. Detergent visualized by negative stain electron microscopy**

On the top left pannel, the mixture of DDM and CHS is displayed. On the bottom left panel, it's the LMNG which is displayed. On the top right panel, it's the digitonin. Finally, on the right bottom panel, it's the GDN. The sample is visualized in white. In each top right corner, there is a zoom in of one part of the grid and its scale is of 20 nm. The scale in the all micrograph is of 100 nm.

✚ **Protein flexibility.** In contrast to X-ray, in Cryo-EM there is no need for a rigid packing of proteins all in the same conformation. The protein distributes within holes of the grids, and their natural fluctuation is captured by rapid freezing. This means that the protein can adopt a more natural conformation and also that it could be possible to determine multiple conformations of the same protein.

The development of this technique is not yet at its full potential. Many improvements will be introduced in the next future such as the introduction of the Volta phase plate or the reduction of the sample quantity to be utilized. The Volta phase plate will improve the collection of data at focus helping the contrast of the images by placing in the objective lens of the microscope a thin metallic layer. The quantity needed to prepare a grid is in the range of microliters. In

## BILIOGRAPHIC REVIEW

this case, the improvement would be to use only some nanoliters. Such would be really useful for membrane protein which are difficult to overexpress and also purify at high quantity (Cheng 2018). The “spotiton” device has been developed for this purpose, using the ink jet printer technology to “spit” protein onto a grid, alleviating the need to blot the sample. This has been turned into a commercial “cameleon” by TTP Labtech.

Therefore, the single particle Cryo-EM allows the analysis of the protein in different conformations on the same grid. This means that data could be collected at once for a single sample in all possible different conformations. This opportunity is a huge improvement in the study of the protein and its mechanism since it will be possible to study the multiple conformations in the same conditions. Since, the structure gives also important information on the functional point of view, the more structures solved the more it would be possible to determine the protein mechanism.

## IV. Conclusion

This bibliographic review summarizes the worrying situation on the antimicrobial resistance phenomena which will be in the near future the first cause of human death (O' Neill 2014). Human pathogen bacteria belong to these dangerous microorganisms. The antibiotics are used to fight against them and their discovery marked a new era in the human medicine. The use and the misuse of these bioactive compounds is leading to an incrimination of the resistance spreading. Amongst the mechanisms which can be adopted by the bacteria, there are the efflux pumps. They are membrane proteins having the ability to export the drug against their concentration gradient. It seems that these exporters are activated as first step of the drug resistance. The bacteria reduces the inner concentration of the antibiotic by exporting them and then they develop other resistance mechanism for the long term (Schmalstieg et al. 2012). They can be classified into seven families, and amongst them there are ABC transporters. Despite the fact that the study of these proteins started 40 years ago (Juliano and Ling 1976; Christopher F. Higgins et al. 1986), their mechanism is still unclear in the details. They display a large spectrum of possible substrates; they are called polyspecific. The complexity of their characterization is centered mostly in the structural studies. The latter is quite challenging for membrane proteins due to their hydrophobic region needed for the insertion in the lipid bilayer. The presence of amphipathic molecules is indispensable to keep the protein soluble. The addition of these compounds adds a variable complex to control. The recent development of the Cryo-EM is changing the structural field of membrane proteins. This technological advancement allowed the study of many structures of ABC transporters. Despite the large number of structures now available, the mechanism is still subject of discussion since it is unclear in the details.

# Objectives

The goals of my PhD project were to study the mechanism of ABC transporters and also to acquire more insights on the behavior of membrane proteins. The structural study of the ABC exporter BmrA from *Bacillus subtilis* was used to reach these goals. This study of BmrA started many years ago and many optimizations were already set up at the start of my PhD (Wiseman et al. 2014; Ravaud et al. 2006; Matar-Merheb et al. 2011; Chaptal et al. 2017). Thus, I concentrated my effort on the optimization of the crystallography and Cryo-EM experiments. An extensive effort targeted the control of the detergent belt to improve the crystal diffraction power for X-ray analysis. This led to the resolution of the structure. In parallel, the protein structure was also determined by Cryo-EM. Then, the objective was to investigate more the transmembrane region movement observed from the structure solved. Mutants were designed to characterize this movement testing their transport and ATPase activities. Furthermore, the protein was inserted into a lipid environment to analyze its behavior in more native-like environment. In parallel, a particular attention on the amphipathic environment around the protein was a constant in all this project. I participated in the development of a sever allowing the representation of the detergent belt around the proteins. Finally, an assessment of the amphipathic belt in the density map was carried out. These two last projects aim to acquire an understanding on the behavior of the amphipathic belt which is useful for the study of membrane proteins.



# MATERIALS AND METHODS





# 1. Materials

## 1.1 Bacterial strains

**BL21(DE3)** strain from *E. coli* is used to the over-expression of the soluble membrane protein scaffold (MSP). It contains the sequence for the T7 ARN polymerase which under the control of the lucUV5 promoter. The expression is initiated by the IPTG (Isopropyl  $\beta$ -D-1-thiogalactopyranoside).

**CD43(DE3)  $\Delta$ acrB** strain from *E. coli* is used for the over-expression of BmrA WT and the others BmrA mutants. This strain is derived from the *E. coli* BL21(DE3) strain in which there is a mutation in the sequence of the promoter slowing down the expression of the protein; this is useful for the expression and folding of membrane protein. This *E. coli* strain has been deleted of the sequence corresponding to the membrane protein AcrB which has proven to be a stubborn contaminant of the purification of BmrA (Wiseman et al. 2014). *E. coli* CD43(DE3)  $\Delta$ acrB strain was gifted by Pr. Klaas Martinus Pos.

## 1.2 Plasmids and sequences

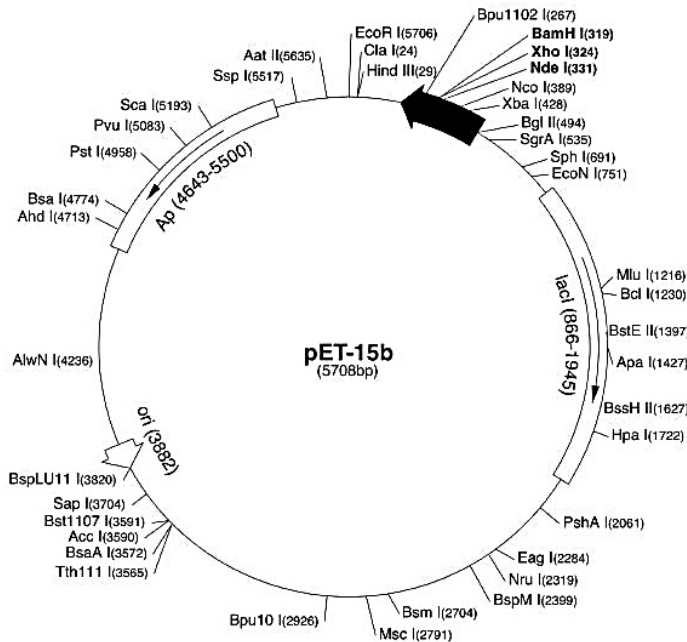
**pMSP1D1 and pMSP1E3D1** are the plasmid used for the expression of the two membrane scaffold proteins MSP1D1 and MSP1E3D1. These commercial plasmids are from Addgene. They contain the lacI promoter, T7 terminator, Kanamycin gene resistance and a 6 histidine tag.

The sequences of the MSP1D1 and MSP1E3D1 are composed by the tag (here 6 histidine tag), the TEV cleavage sequence and then the sequence corresponding to the membrane protein scaffold. The MSP1E3D1 is an extended form of MSP1D1, it has the sequence corresponding to the helices 3, 4 and 5 repeated twice.

**pET15b (+)** is the plasmid used for the expression of BmrA WT and mutants (figure 39). It contains the T7 promoter, transcription starter and terminator which is compatible with the

## MATERIELS AND METHODS

bacteria strain used for the expression. As antibiotic resistance gene, there is the ampicillin one which allows the selection of the bacteria transformed with this plasmid.



**Figure 39. pET-15b plasmid**  
This is the plasmid in which the sequence of BmrA WT and mutants are inserted. Image of the plasmid is from Anatrice web site.

BmrA WT and mutant primary sequences are displayed here below, the mutations are indicated in red:

### BmrA WT

```
MPTKKQKSKSKLKPFALVRRTNPSYGKLAFAFALASVVTTLVSLLIPLLTQQLVDGFSMSNLSGTQIGLIALVFF
VQAGLSAYATYALNYNGQKIISGLRELLWKKLIKLPVSYFDTNASETVSRVTNDTMVVKELITTHISGFITGIIIS
VIGSLTILFIMNWKLTLLVVLVVPLAALILVPIGRKMFISRETQDETARFTGLLNQILPEIRLVKASNAEDVEY
GRGKMGISSFLKLGVREAKVQSLVGPLISLVLMAALVAVIGYGGMQVSSGELTAGALVAFILYLFQIIMPMGQIT
TFFTQLQKSIGATERMIEILAEEDTDTVTGKQIENAHLP IQLDRVSFGYKPDQLILKEVSAVIEAGKVTAIVGPS
GGGKTTLFKLLERFYSPTAGTIRLGDEPVDTYSLSWREHIGYVSQESPLMSGTIRENICYGLERDVTDAEIEKA
AEMAYALNFIKELPNQFDTEVGERGIMLSGGQRQRIATARALLRNPSILMLDEATSSLDQSEKSVQQALEVLME
GRTTIVIAHRLSTVVDADQLLFVEKGEITGRGTHHELMASHGLYRDFAEQQLKMNADLENKAG
```

### BmrA E504A

```
MPTKKQKSKSKLKPFALVRRTNPSYGKLAFAFALASVVTTLVSLLIPLLTQQLVDGFSMSNLSGTQIGLIALVFF
VQAGLSAYATYALNYNGQKIISGLRELLWKKLIKLPVSYFDTNASETVSRVTNDTMVVKELITTHISGFITGIIIS
VIGSLTILFIMNWKLTLLVVLVVPLAALILVPIGRKMFISRETQDETARFTGLLNQILPEIRLVKASNAEDVEY
GRGKMGISSFLKLGVREAKVQSLVGPLISLVLMAALVAVIGYGGMQVSSGELTAGALVAFILYLFQIIMPMGQIT
TFFTQLQKSIGATERMIEILAEEDTDTVTGKQIENAHLP IQLDRVSFGYKPDQLILKEVSAVIEAGKVTAIVGPS
GGGKTTLFKLLERFYSPTAGTIRLGDEPVDTYSLSWREHIGYVSQESPLMSGTIRENICYGLERDVTDAEIEKA
AEMAYALNFIKELPNQFDTEVGERGIMLSGGQRQRIATARALLRNPSILMLDATSSLDQSEKSVQQALEVLME
GRTTIVIAHRLSTVVDADQLLFVEKGEITGRGTHHELMASHGLYRDFAEQQLKMNADLENKAG
```

## MATERIELS AND METHODS

### BmrA I46D

MPTKKQKSKSKLKPFALVRRNTNPSYGKLAFAALSVVTTLVSLLDPLLTKQLVDGFSMSNLSGTQIGLIALVFF  
VQAGLSAYATYALNYNGQKIISGLRELLWKKLIKLPVSYFDTNASETVSRVTNDTMVVKELITTHISGFITGIIS  
VIGSLTILFIMNWKLTLLVVLVVVPLAALILVPIGRKMFSISRETQDETARFTGLLNQILPEIRLVKASNAEDVEY  
GRGKMGISSLFKLGVREAKVQSLVGPLISLVLMAALVAVIGYGGMQVSSGELTAGALVAFILYLFQIIMPMGQIT  
TFFTQLQKSIGATERMIEILAEEDTDTGKQIENAHLPQLDRVSFGYKPDQLILKEVSAVIEAGKVTAIVGPS  
GGGKTTLFKLLERFYSPTAGTIRLGDEPVDTSLESWREHIGYVVSQESPLMSGTIRENICYGLERDVTDAEIEKA  
AEMAYALNFIKELPNQFDTEVGERGIMLSGGQRORIAIARALLRNPSILMLDEATSSLDSQSEKSVQQALEVLME  
GRTTIVIAHRLSTVVDADQLLFVEKGEITGRGTHHELMASHGLYRDFAEQQLKMNADLENKAG

### BmrA I46C-I70C

MPTKKQKSKSKLKPFALVRRNTNPSYGKLAFAALSVVTTLVSLLCPLLTKQLVDGFSMSNLSGTQCGLIALVFF  
VQAGLSAYATYALNYNGQKIISGLRELLWKKLIKLPVSYFDTNASETVSRVTNDTMVVKELITTHISGFITGIIS  
VIGSLTILFIMNWKLTLLVVLVVVPLAALILVPIGRKMFSISRETQDETARFTGLLNQILPEIRLVKASNAEDVEY  
GRGKMGISSLFKLGVREAKVQSLVGPLISLVLMAALVAVIGYGGMQVSSGELTAGALVAFILYLFQIIMPMGQIT  
TFFTQLQKSIGATERMIEILAEEDTDTGKQIENAHLPQLDRVSFGYKPDQLILKEVSAVIEAGKVTAIVGPS  
GGGKTTLFKLLERFYSPTAGTIRLGDEPVDTSLESWREHIGYVVSQESPLMSGTIRENICYGLERDVTDAEIEKA  
AEMAYALNFIKELPNQFDTEVGERGIMLSGGQRORIAIARALLRNPSILMLDEATSSLDSQSEKSVQQALEVLME  
GRTTIVIAHRLSTVVDADQLLFVEKGEITGRGTHHELMASHGLYRDFAEQQLKMNADLENKAG

## 1.3 Culture media

**LB medium** (Lysgeny Broth, Fisher BioReagents): 5 g/L of yeast extract, 10 g/L of tryptone, 10 g/L of NaCl.

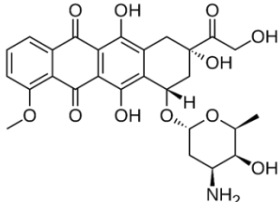
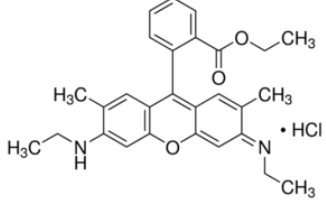
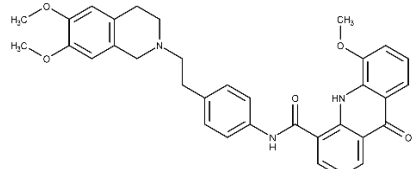
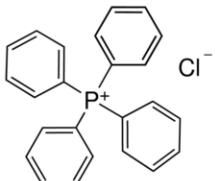
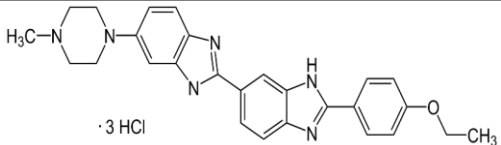
**LB-Agar medium:** LB medium described above with the addition of 1.5% agar.

**TB medium** (Terrific Broth, Sigma Aldrich): 24 g/L of yeast extract, 12 g/L of tryptophan, 9.4 g/L of K<sub>2</sub>PO<sub>4</sub> and 2.2 g/L of KH<sub>2</sub>PO<sub>4</sub>.

**SOC medium** (Super Optimal broth with catabolite repression): 2% of tryptone, 10 mM NaCl, 2.5 mM KCl, 10 mM MgSO<sub>4</sub>, 10 mM MgCl<sub>2</sub>, 20 mM glucose et 0.5% yeast extract.

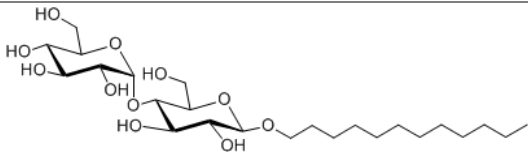
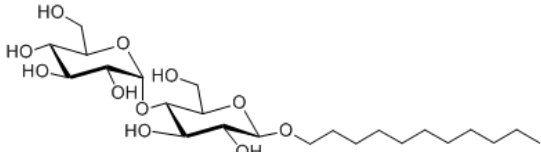
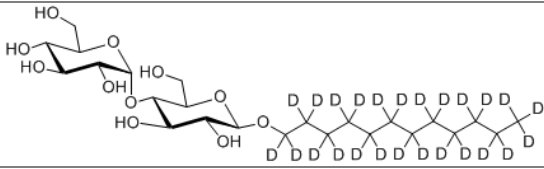
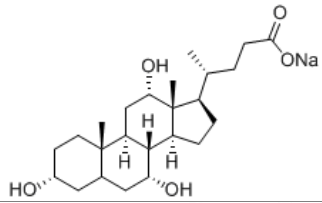
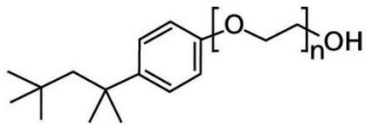
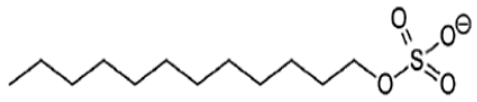
## 1.4 Compounds

Table 9. List of the compounds used in this project

Compound	Structure	Supplier
Doxorubicin		Sigma Aldrich
Rhodamine 6G		Sigma Aldrich
GF 120918 X		Sigma Aldrich
Tetraphenylphosphonium		Sigma Aldrich
Hoechst 33342		Sigma Aldrich

## 1.5 Detergents

Table 10. List of the detergent used in this project

Detergent	Structure	CMC (mM)	Molecular weight (g/mol)	Supplier
<b>DDM</b> n-Dodecyl- $\beta$ -D-Maltopyranoside		0.17	510.6	Anatrace
<b>UDM</b> n-Undecyl- $\beta$ -D-Maltopyranoside		0.59	496.6	Anatrace
<b>DDM<sup>D</sup></b> Deuterated n-Dodecyl- $\beta$ -D-Maltopyranoside		0.2	535.8	Anatrace
<b>Sodium Cholate</b>		9-15	430.6	Sigma Aldrich
<b>Triton X100</b>		0.22	624.8	Euromedex
<b>SDS</b> Sodium Dodecyl Sulfate		8.2	288.3	Euromedex

# 2. Methods

## 2.1 Membrane scaffold protein preparation

Membrane scaffold protein (MSP) is used to reconstitute BmrA into nanodiscs. Two MSP forms have been purified to test different sizes of nanodisc. The gene for the expression of the MSP contains the sequence for the protein and the 6 histidine tag. To remove the tag, there is a cleavage site of TEV (Denisov et al. 2004). The purification is done into two steps: the first one is the purification of the protein with the 6 histidine tag and the second one is to recuperate the MSP without the tag.

### 2.1.1 MSP production

BL21 bacteria made competent by a treatment with  $\text{CaCl}_2$  are incubated with MSP plasmid (pMSP1D1 or pMSP1E3D1) for 30 minutes in the ice. The volume used for the bacteria is of 200  $\mu\text{L}$  and 1  $\mu\text{L}$  of plasmid (10  $\text{ng}/\mu\text{L}$ ). Then, the sample is incubated 45 seconds at  $42^\circ\text{C}$ . The SOC medium (300  $\mu\text{L}$ ) is added and the mixture is incubated for an hour at  $37^\circ\text{C}$ . Fifty microliters of this sample are loaded on a petri dish which contains LB-agar medium with Kanamycin (40  $\mu\text{L}/\text{mL}$ ). The petri dish is then incubated overnight at  $37^\circ\text{C}$ .

The next day, two colonies are picked and each one is placed in a flask containing 50 mL of LB – kanamycin medium. These are incubated overnight at  $37^\circ\text{C}$  and at 190 rpm.

The following day, the culture media are added to 3 flasks containing each 1 L of terrific broths (TB) medium with 40  $\mu\text{g}/\text{mL}$  of kanamycin. The volume of culture media added is calculated to obtain an OD of 0.1. The flasks are then incubated at  $37^\circ\text{C}$  and agitated at 190 rpm. When the OD is of 2, the IPTG is added at a concentration of 1 mM. After 3h, the bacteria are centrifuged during 15 minutes at  $4^\circ\text{C}$  and at 6000 rpm. The pellets are placed at  $-80^\circ\text{C}$ .

### 2.1.2 MSP purification

The bacteria pellet is solubilized with 50 mL of buffer (40 mM Tris pH 7.4; 100 mM NaCl; 1 % (w/v) Triton X100; 0.5 mM EDTA; 1 mM PMSF) and 2  $\mu\text{L}$  Benzonase (24 U/mL, Merck). The bacteria are lysed by 2 passages at 18,000 psi through a microfluidizer 100 (Microfluidics IDEX Corp) and then centrifuged during 30 minutes at 30,000 g at  $4^\circ\text{C}$ . The supernatant is charged

## MATERIELS AND METHODS

onto Ni<sup>2+</sup>-NTA column pre-equilibrated in 40 mM Tris pH 7.4, 100 mM NaCl, 1 % (w/v) Triton X100, 0.5 mM EDTA and 1 mM PMSF. The washing is then realized with 10 column volume (5 mL) with the three following buffers: first wash buffer is composed by 40 mM Tris pH 8, 300 mM NaCl and 1% (w/v) Triton X100; the second one by 40 mM Tris pH8, 300 mM NaCl, 50 mM sodium cholate and 20 mM Imidazole; the last one by 40 mM Tris pH8, 300 mM NaCl, and 50 mM Imidazole. The protein is eluted by 40 mM Tris pH 8, 300 mM NaCl and 500 mM Imidazole. The fractions of the elution pic are pooled together and the TEV (2 mg/mL) is added calculating 1 mg of TEV for 40 mg of MSP. The mixture is then dialyzed (cutoff 12-14 kDa) in a first time into 300 mL 40 mM Tris, 100 mM NaCl and 0.5 mM EDTA for 3 hours and then into 700 mL of the same buffer overnight at 4°C. To the protein dialyzed, 20 mM Imidazole are added. The protein is loaded on the Ni<sup>2+</sup>-NTA column equilibrated with 20 mM Tris pH 7.4 and 100 mM NaCl. The flow through is collected and it contains the MSP without the tag. The protein which was not cleaved is eluted with 40 mM Tris pH 8, 300 mM NaCl and 500 mM Imidazole. The protein cleaved is dialyzed two times as previously described and finally concentrated at 5,000 g with a 100 kDa cutoff Amicon Ultra-15. The concentrated sample is frozen in liquid nitrogen and stored at -80°C.

### 3. Mutagenesis

The two mutants designed are BmrA I46D and BmrA I46C-I70C. The double mutant is done into step. The BmrA WT plasmid pET15b is used. The site directed mutagenesis is performed with the commercial kit Quickchange (Agilent Technologies). Beforehand, the primers are designed to contain the mutation in the middle, the percentage of CG has to be at 40% and lastly the fusion temperature is higher than 78°C (table 11). One hundred and twenty-five nanogramme of each primer are added to 1 µL reaction buffer at 10X, 1 µL of plasmid pET15b at 10 ng/µL, 0.2 µL dNTP mix, 0.3 µL Quick solution, 0.2 µL Quickchange lightening enzyme (ADN polymerase). The final volume is of 10 µL and it is completed with sterile water. Afterward, the mix is incubated for 2 minutes at 95°C, then it undergoes into 18 PCR (Polymerase chain reaction) cycles (20 seconds at 95°C, 10 seconds at 60°C and 30seconds/Kb plasmid at 68°C) and, finally, it stays for 5 minutes at 68°C. Two microliters of *Dpn* I enzyme is added to degraded the parental plasmid. The sample is stocked at -20°C. To amplified the plasmid, a transformation into TOP 10 strains is employed. Finally, the plasmid is purified using



the NucleoSpin Plasmid/Plasmid (NoLid) kit (Macherey-Nagel) and the mutation is checked by sequencing it.

*Table 11. List of the primers used for the mutagenesis on BmrA*

Mutant	Primers	Tm	CG%
<b>I46C</b>	5'-acgctggtcagcctgctctgtccattattaacgaagcag-3'	78	51
	3'-tgcgaccagtcggacgagacaggaataattgcttcgtc-5'	78	51
<b>I70C</b>	5'-caggcacgcaaatacggttgtagcgcgctggtggtt-3'	80	51
	3'-gtccgtgctttagcacaacacgcgcgaccacaaa-5'	80	51
<b>I46D</b>	5'-acgctggtcagcctgctcgatccattattaacgaagcag-3'	78	51
	3'-tgcgaccagtcggacgagctaggaataattgcttcgtc-3'	78	51

## 4. BmrA production

### Transformation

CD43(DE3)  $\Delta$ acrB bacteria are treated with  $\text{CaCl}_2$  to make them competent. Fifty microliters of these competent bacteria are incubated with 1  $\mu\text{L}$  of pET15b (+) plasmid (0.1  $\mu\text{g}/\mu\text{L}$ ) for 30 minutes in the ice. The mixture is placed for 45 seconds at 42°C, then 300  $\mu\text{L}$  of SOC medium are added and placed under gentle agitation for one hour at 37°C. Twenty microliters of this sample are loaded on a petri dish which contains LB-agar medium with ampicillin (5  $\mu\text{g}/\text{mL}$ ). The petri dish is then incubated overnight at 37°C.

### Expression

A colony is incubated in 3 mL LB medium with 50  $\mu\text{g}/\text{mL}$  of ampicillin for 7-8 h at 37 °C. Thirty microliters of this pre-culture are added to 1 L LB medium with 50  $\mu\text{g}/\text{mL}$  of ampicillin. The culture is incubated at 22 °C and when an  $\text{OD}_{600}$  of 0.6 is reached, the IPTG (0.7 mM) is added. BmrA is expressed during 5-6 hours at 22°C. Bacteria pellet is collected at 5000 x g for 15 min., 4 °C and then stored at – 80°C.

### Membrane preparation

The bacteria pellet is suspended in 10 mL 50 mM Tris-HCl pH 8.0, 5 mM  $\text{MgCl}_2$  and 1 mM PMSF and lysed by 3 passages at 18,000 psi through a microfluidizer 100 (Microfluidics IDEX Corp).

## MATERIELS AND METHODS

The solution was centrifuged 30 minutes at 15,000 x g at 4 °C. The membrane fraction was pelleted by centrifugation for 1 h at 180,000 x g at 4°C, suspended in 50 mM Tris-HCl pH 8.0, 1 mM PMSF and 1 mM EDTA and centrifuged again. The final pellet was suspended in 20 mM Tris-HCl pH 8.0, 0.3 M sucrose and 1 mM EDTA and frozen in liquid nitrogen.

### 5. BmrA purifications

The membrane with overexpressed BmrA are solubilized, the sample is then purified by two steps of affinity chromatography followed by a size exclusion chromatography.

#### **Solubilization of the protein**

The membranes are solubilized with a buffer containing 4.5% (w/v) Triton X100 (20 mM Tris-HCl pH 8.0, 100 mM NaCl, 15% glycerol (v/v), anti-protease tablets, 0.1 mM TCEP) at 5 mg/mL. The solution is incubated at 4°C and under gentle agitation for 90 minutes and then centrifuged 40 minutes at 100,000 x g.

#### **Affinity chromatography**

The first purification step is an affinity chromatography since the protein is expressed with a 6 histidine tag. The resulting supernatant from the solubilization step is loaded onto a Ni<sup>2+</sup>-NTA column which is equilibrated in 20 mM Tris-HCl pH 8.0, 100 mM NaCl, 15% (v/v) glycerol, anti-protease tablets, 4.5% Triton X100 and 20 mM imidazole. The resin is washed with 20 mM Hepes-HCl pH 8.0, 100 mM NaCl, 20 mM imidazole, 0.0675% (w/v) DDM and 0.04% (w/v) sodium cholate. The protein is eluted by adding 200 mM imidazole to the same buffer. BmrA fractions are pooled and diluted ten times in 20 mM Hepes-HCl pH 8.0, 100 mM NaCl, 0.0675% (w/v) DDM and 0.04% (w/v) sodium cholate and loaded again on the same resin for another step of affinity chromatography.

#### **Concentration**

The pool of BmrA fractions is concentrated on 50 kDa cutoff Amicon Ultra-15 devices, with the centrifuge speed at 1000 x g for 10-15 min.

#### **Size exclusion chromatography**

The concentrated protein sample is loaded onto Superdex 200 10/300 using as mobile phase 20 mM Hepes-HCl pH 7.5, 100 mM NaCl, 0.035% (w/v) DDM and 0.03% (w/v) sodium cholate for DDM-cholate molar ratio of 1:1. The quantity of detergent in this buffer varies basing on

## MATERIELS AND METHODS

the detergent ratio desired. For the ratio DDM-cholate 1:1.33, there are 0.035% (w/v) DDM and 0.04% (w/v) sodium cholate; for the ratio DDM-cholate 1:3 there are 0.035% (w/v) DDM and 0.1% (w/v) sodium cholate. The elution peak is then pooled and stored at 4 °C before use. Cholate has the tendency to remain in the SEC column, consequently to avoid contamination the Superdex resin is washed with 1 M NaOH.

### Nanodisc reconstitution

The MSP1D1 et MSP1E3D1 are the two membrane scaffold proteins used to reconstitute BmrA in a lipidic bilayer. The lipids used are from *E. coli*. The reconstitution into nanodisc is effectuated after the purification of the protein with detergent.

Beforehand, *E. coli* lipids (Avanti Polar) are prepared at 25 mg/ml into 20 mM of Hepes pH 7.5, 100 mM NaCl and 10% (w/v) sodium cholate. Four hundred micrograms of purified BmrA E504A in 450 µL of Hepes-HCl pH 7.5, 100 mM NaCl, 0.035% DDM and 0.03% sodium cholate were mixed 38 µL of *E. coli* lipids for 5 min at room temperature. The mix was then added of 420 µg purified MSP1E3D1 in 46 µL of 40 mM Tris-HCl, pH 7.4, 100 mM NaCl and 0.5 mM EDTA. Twenty mM Hepes-HCl pH 7.5 and 100 mM NaCl were added up to 1 mL final and incubated 1 hour more at room temperature. The final molar ratio of BmrA/MSP/lipids was 1/5/400 in 20 mM Hepes-HCl pH 7.5, 100 mM NaCl. Lastly, SM-2 biobeads (40 mg, Biorad) were then added to the mixture, placed 3 hours or overnight under gentle agitation at room temperature.

The protein solution is then loaded on a Ni<sup>2+</sup>-NTA equilibrated by 20 mM Hepes pH 7.5 and 100 mM NaCl. Twenty mM of imidazole is added to the buffer for the washing step and 200 mM for the elution of the protein. The fractions are then pooled and concentrated 50 kDa cutoff Amicon Ultra-15 devices, with the centrifuge speed at 1000 x g for 10-15 min. Ultimately, the concentrated sample is loaded onto Superdex 200 10/300 column using as mobile phase 20 mM Hepes-HCl pH 7.5 and 100 mM NaCl.

## 6. Protein quantification

### 6.1 BCA assay

The protein quantification in the membrane is realized using the bicinchoninic acid (BCA) assay. The solution is composed by the BCA and copper (II) ion  $\text{Cu}^{2+}$ . In alkaline medium, the proteins react with  $\text{Cu}^{2+}$  and reduced then into copper (I) ion  $\text{Cu}^+$  which reacts with BCA. Such increases the intensity of the colorimetric reaction. The absorbance is read at a wavelength of 562 nm since the complex  $\text{BCA-Cu}^+$  is purple. The amount of  $\text{Cu}^+$  formed is proportional to the protein concentration in the sample.

Practically, a plate of 96 wells is used to performed this dosage. A calibration curve is done using bovine serum albumin (BSA). The protein sample is diluted (around 10 times) and final volume is of 20  $\mu\text{L}$ . The reactive agent volume is of 180  $\mu\text{L}$ . Before the lecture of the absarbane, the plate is incubated at 37°C for 30 minutes. The spectrometer used is Xenus of SAFAS (monaco).

### 6.2 Nanodrop

This method is used for the determination of the protein concentration after the purification step and in routine for the functional and structural studies. It is based on the capacity of absorbance of aromatic residues as tyrosine and tryptophan at 280 nm. Their absorbance is proportional to the protein concertation and follows the Beer-Lambert law ( $\text{OD} = \epsilon \cdot l \cdot C$ ). Knowing the molar attenuation coefficient of the protein of interest, it is easily possible to determine the concentration. It can be calculated introduction the sequence in the Expasy calculator ([expasy.org/protparam/](http://expasy.org/protparam/)). In the case of BmrA, it is of 6,22  $\text{L} \cdot \text{mol}^{-1} \cdot \text{cm}^{-1}$ .

Practically, the UV-visible Nanodrop spectrometer is used which advantage is to eliminate the path length ( $l$ ) since the sample is deposited in the optic trajectory directly. Two microliters of sample and also of the corresponding buffer are needed and the measure is realized at 280 nm.

## 7. SDS-PAGE and Western Blot

### 7.1 SDS-PAGE

The sodium dodecyl sulfate – polyacrylamide gel electrophoresis is a method used to visualize proteins contained in a sample and to check the purity. This method relies in the protein migration on the basis of their size. The sample is treated with SDS which is an ionic detergent, therefore the proteins are globally denaturated and charged negatively.

Beforehand, the sample is incubated with the Laemmli buffer 4X (0.25 M Tris pH 6.8, 8% (w/v) SDS, 40% of glycerol, 0.7 M of  $\beta$ mercaptoethanol and 2.5 mg of bromophenol blue).

The gel is of 0.75 mm thickness and it is composed by a stacking gel on the top and then a resolving gel:

- Stacking gel: 4% (v/v) acrylamide/bisacrylamide (Euromedex), 0.5 M Tris pH 6.8, 10% (w/v) SDS, 10% of ammonium persulfate (APS) and 0.1% of TEMED (N, N, N, N'-Tetramethyl-ethylenediamine).
- Resolving gel: 10% (v/v) acrylamide/bisacrylamide, 1.5 M Tris pH 8.8, 8% (w/v) SDS, 10% of ammonium persulfate (APS) and 0.1% of TEMED (N, N, N, N'-Tetramethyl-ethylenediamine).

The gel is placed in a tank containing of TG-SDS buffer (Euromedex) composed by 25 mM Tris pH 8.5, 192 mM glycine and 0,1% (w/v) SDS. Then, the samples and a molecular weight ladder (170 kDa, Euromedex) are loaded in the gel wells. A voltage of 120 V is imposed for 1h30.

Afterward, the gel is placed into Coomassie Brilliant Blue solution (0.025% (w/v) Coomassie R250, 1% (v/v) methanol, 25% (v/v) isopropanol and 10% (v/v) acetic acid) and then into a discoloration solution of 10% (v/v) acetic acid to visualize the proteins.

### 7.2 Western Blot

The western blot is a method to visualize specifically the protein of interest by the interaction with a specific antibody. BmrA is expressed with a 6 histidine tag, the antibody used to detect the protein is against the tag.

The proteins are transferred from the gel (described above) onto a nitrocellulose membrane (GE Healthcare Life Sciences). The system composed by gel, nitrocellulose membrane, two sponges and whatman paper is placed in a tank covered with 1X Tris-glycine buffer. A 0.2 A

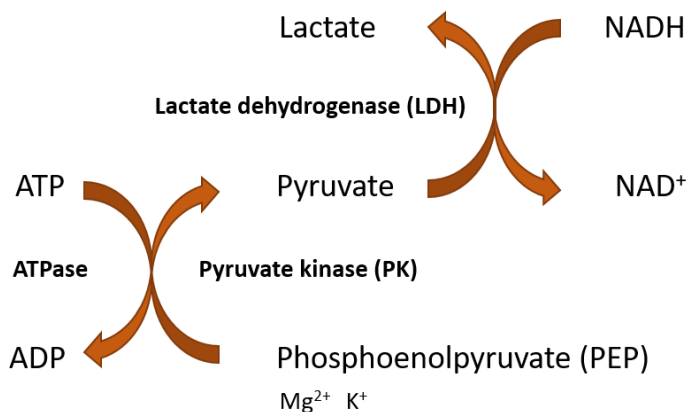
## MATERIELS AND METHODS

current is imposed during 1h20. Afterwards, the membrane is saturated with a 3% (w/v) BSA (bovine serum albumin), 0.1% (v/v) TBS-T (Tris-buffered saline-tween) buffer during one hour and incubated with HRP-antibody at 1/20,000 dilution during 1 hour at room temperature. A wash step is performed with 0.1% (v/v) TBS-T buffer. The revelation of the membrane is done with the commercial kit Pierce™ ECL Western Blotting Substrate (Thermofisher); the chemiluminescence reaction is due to the presence of the peroxidase HRP and its substrate luminol. The system Fusion Fx (Vilber Lourmat) is used to record the signal.

## 8. Functional studies

### 8.1 ATPase activity

The ATPase activity of the protein is tested after purification and/or in membrane. The protein hydrolyzes the ATP into ADP. Then, the pyruvate kinase (PK) transforms phosphoenolpyruvate (PEP) to pyruvate which is transformed to lactate by the lactate dehydrogenase (LDH). This last reaction requires the oxidation of the NADH (figure 40). The NAD<sup>+</sup> absorb at wavelength of 340 nm.



*Figure 40. Reaction for the detection of ATPase activity*

Vanadate mix: 1 mM sodium orthovanadate (Na<sub>3</sub>VO<sub>4</sub>), 5 mM ATP, 5 mM sodium azide (NaN<sub>3</sub>), 2 mM sodium sulfide (Na<sub>2</sub>S) and buffer 30 mM Tris-HCl pH 8, 100 mM NaCl, 10 mM KCl and 2 mM MgCl<sub>2</sub>. The same mix is prepared without Na<sub>3</sub>VO<sub>4</sub>.

Enzyme mix: 5 mM ATP, 0.6 mM NADH, 5 mM NaN<sub>3</sub>, 2 mM Na<sub>2</sub>S, 1 mM PEP, 0.1 mg/mL PK and 0.1 mg/mL LDH and buffer 30 mM Tris-HCl pH 8, 100 mM NaCl, 10 mM KCl and 2 mM MgCl<sub>2</sub>.

All the compounds of the mix are previously prepared. The enzyme PK and the inhibitors (Na<sub>2</sub>S and NaN<sub>3</sub>) are prepared just before the utilization. The stock solution of PK is centrifuged at 14,000 x g for 1 minute, the pellet obtained is suspended with 30 mM Tris-HCl pH 8 and 100 mM NaCl. The Na<sub>2</sub>S and NaN<sub>3</sub> are inhibitors of the respiratory chain and they are prepared in water and under the fume hood. The Na<sub>3</sub>VO<sub>4</sub> is incubated at 100°C during 5 to 10 minutes. In addition, the NADH is added to the mix just before the measure since it is sensible to the light.

For the ATPase activity of the protein in membrane, 24 µL of protein sample is incubated with 46 µL of mix with Na<sub>3</sub>VO<sub>4</sub> or without it for 10 minutes at 30°C. Twenty µL of this mix is

deposited in the well of the 96 wells-plate. 180  $\mu$ L of enzyme mix is added just before the measure. The absorbance is recorded at 340 nm for 15 to 20 minutes with the SAFAS Xenius (Monaco) spectrometer. The slope of the curve is then measured which is in absorbance/minutes. The specific activity is calculated reporting to the quantity of protein present in the sample.

In the case of the protein purified, the overall protocol is the same. It is not necessary to incubate the sample with the vanadate mix and the inhibitors are not needed too.

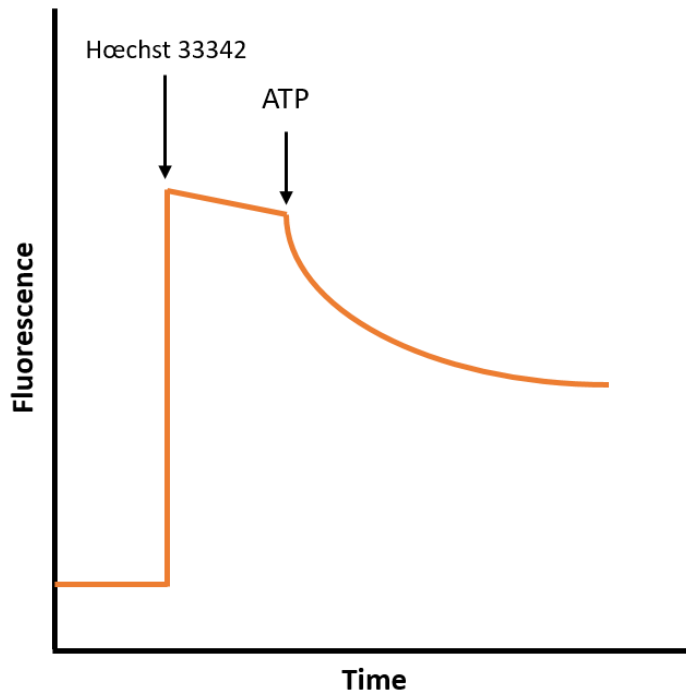
### 8.2 Transport essays

Another method to test the activity of the ABC transporters is the transport essays. The proteins are inserted in inverted membrane vesicles and they can transport compounds from outside to inside. To visualize the transports, fluorescent molecules are used as H $\ddot{o}$ echst 33342 and doxorubicin.

The inverted membrane vesicles are pre-incubated with the fluorescent compound which binds in the substrate binding side in the ABC transporter and also in the membrane. The changing of their environment from a hydrophilic one to the hydrophobic one increases the overall fluorescence of the sample. The adding of the ATP induces the transport of the compound by the transporter which is visualized by a decreasing of the fluorescence.

The inverted vesicles are produced by the membrane preparation described just above (cf. membrane preparation of BmrA). In a 1 mL quartz cuvette, 100  $\mu$ g of protein in inverted vesicles are added to the buffer (50 mM Hepes pH8, 5 mM MgCl<sub>2</sub>, 8.5 mM NaCl, 60  $\mu$ g/mL PK, 4 mM PEP) at 25°C. After 2 minutes of incubation, 2  $\mu$ M of H $\ddot{o}$ echst 33342 or 10  $\mu$ M of doxorubicin are added. After others 2-5 minutes, the transport is initiated by 2 mM of ATP. The Photon Technology International fluorimeter is used to record the transport. The fluorescence is recorded at emission 590 nm with a bandwidth of 4 nm upon excitation at 480 nm with a bandwidth of 2 nm for the Doxorubicin and emission at 457 nm upon excitation at 355 nm for the H $\ddot{o}$ echst 33342.





**Figure 41. Curve obtained by a transport assay**

The inverted membrane vesicles are incubated with buffer and  $Mg^{2+}$  which correspond to the first line. The increasing of fluorescence is due to the adding of the fluorescent molecules (here Hoechst 33342). The decreasing corresponds to the adding of the ATP which induce the transport of the compound inside of the vesicle. The slope of this last part of the curve is the transport activity of BmrA.

The ATP slope corresponds to the activity of the protein (figure 41). Its value is measured in fluorescence/minutes and then divided by the quantity of BmrA present in the membrane vesicles.

### 8.3 Binding essays

This test is used to verify if a given molecule binds to the protein; in addition, it is possible to determine the affinity constant parameter. This technique measures the fluorescence of the tryptophan (intrinsic fluorescence) or the molecule (extrinsic fluorescence). The changing of the fluorescence indicates the binding of the compound.

The protein samples (triplicates) are placed at  $0.5 \mu\text{M}$  in quartz cuvettes. As control, the buffer and NATA (N-acetyl-tryptophan-amide) are tested in parallel. The final volume is of  $200 \mu\text{L}$ . The compound is added in increasing concentration to each cuvette. For the intrinsic fluorescence, the exciting wavelength is of  $290 \text{ nm}$ , the fluorescence is recorded between  $310$  and  $380 \text{ nm}$ . For extrinsic fluorescence, the wavelengths depend on the compound tested. The buffer and NATA are used to check the measure the non-specific fluorescence.

## 8.4 Thermal stability assay

Purified BmrA E504A is incubated with different compounds (rhodamine 6G and GF 120918X) and nucleotide. The stability of the sample is tested with a thermal stability assay (Ashok, Nanekar, and Jaakola 2015).

The samples tested are: BmrA E504A, BmrA E504A with ATP-Mg<sup>2+</sup>, BmrA E504A with GF, BmrA E504A with Rhodamine 6G, BmrA E504A with each compound and ATP-Mg<sup>2+</sup>. The incubation is during 30 minutes for each molecule. The samples (50 µL) are incubated at different temperatures from 25°C to 90°C using the PCR thermal cycler (PeqSTAR 2x gradient; Peqlab). Then, they are centrifuged at 20 000 x g during 40 minutes. The supernatants are loaded onto an SDS-PAGE. The intensity of each bands is measured with ImageJ software.

## 9. Structural studies

### 9.1 X-ray crystallography

The purified BmrA E504A is concentrated by centrifugation-filtration at 500 x g with a 50 kDa cutoff Amicon Ultra-15 at 22°C. The protein concentration reached is between 7 to 10 mg/mL. Then, BmrA E504A is incubated with 5 mM ATP-Mg<sup>2+</sup> for 30 minutes and sometimes with substrates as 100 µM rhodamine 6G and 50 µM GF 120918 X.

The crystallogenesi s step was performed at 19 °C. Crystals were obtained by vapor diffusion on hanging drops. Crystallogenesi s was done by mixing with a Mosquito 500 nL of reservoir precipitation solution and 500 nL of BmrA E504A sample. The mix is deposited on a plastic cover and sealed onto the plate to form a closed system. The plate is then placed in the Formulatrix which images periodically the drops, it is indeed possible to follow the crystal formation. Successful crystals appear after 3 days, grown up to 5-8 days and progressively disappeared if the incubation lasted longer.

A screening of the precipitation solution was done using the Suite PEG I and Suite PEG II (Hampton), which yield initial condition that were further optimized by varying the PEG concentrations and molecular weight, and pH. The successful conditions were 30%-34% PEG 300 at pH 7-8 and 20%-25% PEG 1000 at pH 8-8.5. These conditions were further optimized with the addition of additives which are detergent designed and synthesized by the team in collaboration with A. Boumenjel team (Nguyen et al. 2018). 48 compounds were tested in the crystallogenesi s process.

The successful conditions are 400 nL 0.1 M Tris-HCl pH 8.5, 25% PEG 1000, 50 nL compound 3.9f and 500 nL BmrA E504A sample.

#### **Crystal cryocooling**

The first cryoprotection solution tested was the 20% glycerol and 0.1 M Tris pH 7.5-8.5. However, this solution was not adapted to BmrA crystals since they crack just after the contact with it. To improve this step, a large screening of cryoprotection solutions was undertaken following the protocol of CryoProtX MD1-61 (Vera and Stura 2014). The mixtures proposed by this kit have been tested and further optimized. The successful solution is 12.5% (v/v) diethylene glycol, 18% (v/v) 2-methyl-2,4-pentanediol, 7% (v/v) ethylene glycol, 12.5% (v/v) 1,2-

propanediol, 12.5% (v/v) dimethyl sulfoxide. In addition, 5 mM ATP-Mg and 3.9 f have been added to the cryoprotection mix to ensure their concentration inside the crystal.

The systems for the crystals harvesting was also optimized. The final process uses Cryschem sitting drop plates. The reservoir is filled with water to increase the humidity around the protein and the crystal drop is placed in the middle. The cryoprotection solution (1  $\mu$ L) is added around the crystal drop into 3 drops and then gently brought in contact with the crystal. After a minute of incubation, the crystal is fished out and cryocooled in liquid nitrogen. Crystals are stored in liquid nitrogen before being analyzed at the synchrotron.

The process of optimization of the cryoprotection solution will be discussed in more details in the results section (cf. results chapter I).

### Phase determination

In X-ray crystallography analysis, the amplitude and phase are essential to solve the structure of the protein. Although, the phase is not recorded with protein crystals. To obtain this information different options are possible such as molecular replacement and heavy metal atoms bound to the protein. The molecular replacement uses the phase information of another solved structure and this is the one technique used for BmrA structure resolution. Heavy atoms can absorb the X-ray more than the other atoms in the protein; this is called anomalous scattering.

An important effort has been employed to determine the phase experimentally. Three approaches have been used:

- **Selenium methionine.** The methionine of the protein is derivated into selenium methionine. The expression of the protein is performed into poor medium; the amino acids are added individually. The selenium methionine replaces the methionine. These residues have the property generated anomalous scattering. A high resolution is not needed in this case since if it is not possible to solve the phase, it is still possible to place the sequence.
- **Heavy metals.** The cysteine residues can bind heavy metals as potassium tetrachloroplatinate ( $K_2PtCl_4$ ), potassium hexachloroplatinate ( $K_2PtCl_6$ ), potassium gold (III) chloride ( $K(AuCl_4)$ ), mercuric chloride ( $HgCl_2$ ), mercury (II) acetate ( $Hg(OAc)_2$ ) and mercury chloride ( $HgCl_2$ ). This metal generate also anomalous scattering. To test

## MATERIELS AND METHODS

which one binds successfully to the protein, the compound TMRM (Tetramethylrhodamine methyl ester) is used which is visible at UV wavelength. The protein is incubated with 5 equivalents to the different heavy metals. To the sample, the TMRM compound is added and loaded into an SDS-PAGE. After the sample migration, the gel is revealed at the UV lamp and then colored with Coomassie Brilliant Blue followed by the discoloration with 10% (v/v) acetic acid.

- **TbXO<sub>4</sub>**. It is crystallophore compound containing Terbium which has a strong anomalous power. It is added to the cryoprotection solution. Eric Girard gifted us with some sample of TbXO<sub>4</sub>. A microtube contains the powder for a solution at 100 mM of compound. It is centrifuged shortly before the resuspension in 10  $\mu$ L of cryoprotection solution. Then, the solution is centrifuged again at 10,000 rpm for 2 minutes and used to fish out the crystals. Once at the synchrotron, an energy scan is performed to verify its presence. Then the data collection is realized at  $\lambda = 1.649 \text{ \AA}$  and  $E = 7.52 \text{ keV}$ .

### Data collection and treatment

The crystals were analyzed at ESRF and SOLEIL synchrotron on various screening sessions. The data collection that allowed the resolution of the structure was performed at SOLEIL synchrotron on PX2 beam line. It was collected by shooting the crystal in a helicoidally way and at full transmission. The resolution obtain is of 3.9  $\text{\AA}$  however a high anisotropy is present since in the two other directions the resolution is at 4.6 and 5.2  $\text{\AA}$ . The server Staraniso was used to use all the data collected. The completeness in the highest resolution shell was of 78%. The data were then indexed with XDS. To solve the phase, the molecular replacement was performed using Sav 1866 (PDB 2hyd) and MsbA (PDB 3b60). This was done by Phaser software. The successful model was the MsbA one. The resolution of the structure is discussed later together with the cryo-EM one.

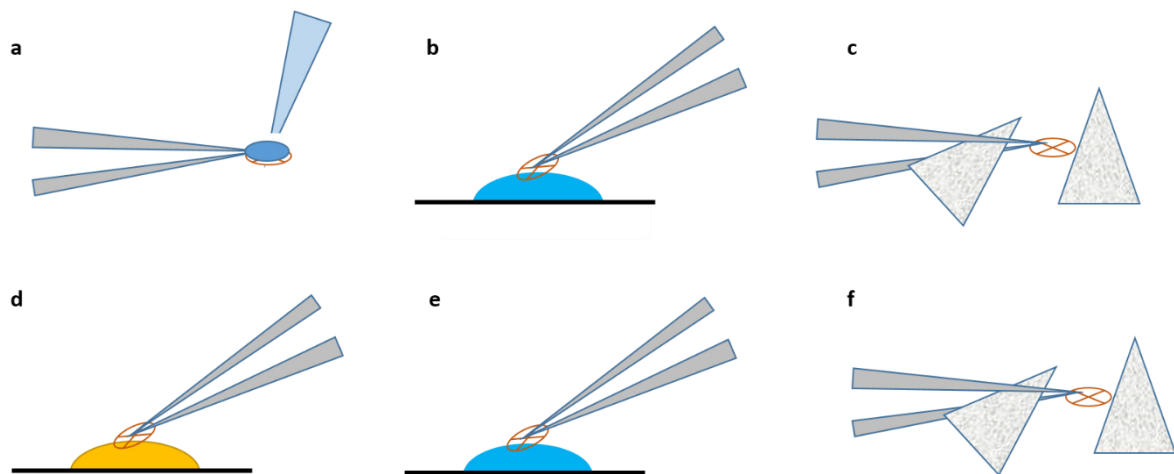
## 10. Electron microscopy

### 10.1 Negative stain

The grids are furnished by the CT $\mu$  microscopy platform at Lyon 1. They are copper grids covered with a layer of carbon cover up by a layer of copper. Five microliters of sample are

## MATERIELS AND METHODS

loaded on the grid which is previously exposed to argon glow discharge to become hydrophilic. After 2 minutes, the grid is washed in a water drop for 30 seconds. The excess is absorbed with Whatman paper. The grid is placed in contact with a drop of PTA (phosphotungstic acid) or Uranyl 4% (furnished by the platform) for 30 seconds. It is then washed in a water drop and the excess is absorbed by another Whatman paper (figure 42). The grids are observed with the JOEL 1400 Flash transmission electron microscopy at the CTμ microscopy platform at Lyon 1.



**Figure 42. Negative stain protocol**

(a) the sample is loaded on the grid and incubated during 2 minutes. (b) the grid is washed in a water drop during 30 seconds. (c) the excess is absorbed with Whatman paper. (d) The grid is placed on a Uranyl 4X for 30 seconds and (e) then washed on a water drop for other 30 seconds. (f) Finally, the excess is absorbed with Whatman paper.

## 10.2 Cryo-EM

The grid preparation, the data collection and treatment were performed at the Stockholm University. The data collection and treatment were carried out by Benjamin Wiseman.

### Grid preparation

The preparation of the grid is performed using the Vitrobot devices. Beforehand the Cflat 1.2/1.3 Au grids are argon glow discharged for 40 seconds at 20 mA (PELCO easiGlow device). The grid is placed in the Vitrobot chamber which is at 100% humidity. The sample loaded is composed by 3.4 mg/mL BmrA E504A, 5 mM ATP-Mg<sup>2+</sup> and 0.1 mM rhodamine 6G. The excess is blotted for 3 seconds. Then, the grid is plunged automatically by the device in liquid ethane and it is conserved in nitrogen liquid.

### Data collection and treatment

The grids screening was performed on a Talos Arctica microscope. The data collection of the best grid was done using Titan Krios G3 electron microscope (300 KeV) with a K2 camera. Two data collection session took place to acquire 3477 movies. The electron dose used is of 6.4 electrons/pixel/s and 1.06 Å/pixel, the total exposure is of 6 seconds and the defocus ranges from 1.2 to 3.2 μm. CTFIND4 was used to estimate the contrast transfer function (CTF) parameters. The total data treatment was performed with cryoSPARC v2 from the motion correction (alignparts lmbfgs), the 2D and 3D classification and refinement. The total of particles used for the final map is of 128372. At first, the ab-initio model was done without any symmetry applied, then the C2 symmetry was imposed improving the resolution of 0.3 Å in overall resolution.

### 10.3 Structure resolution

The density maps for the two structures were obtained almost at the same time with a slight advance of the X-ray one. The model building was performed in Coot for both of them. For the X-ray crystallography structure, the refinement of the model was carried out with autoBUSTER. At first, the model was a poly-Ala to place the transmembrane helices. Then, once residues' chains lateral and ATP-Mg<sup>2+</sup> densities appeared the sequence was assigned. To improve the resolution TLS refinement were imposed at first one TLS for chain and then 1 TLS of a dimer TMD and 1 for a dimer of NBD. This led to 30 and 35 for R and Rfree. The geometry clashes were corrected using ISOLDE. Finally, the correction of Ramachandran and rotamers outliers were carried out and the final parameters of R and Rfree are of 26% and 31% respectively. For the cryo-EM structure, the X-ray model available was used to positioned the structure in this density map. The first map used is the one with the C2 symmetry imposed and sharpened using Phenix. The model was built using Coot and ISOLDE. Once the model was built in this first map, it was checked in the not sharpened C2 map, and then in the C1 map. In the C1 map, two additional densities were detected in the transmembrane region and two molecules of Rhodamine 6G were docked in it. Finally, the statistics of the structures were carried out with MolProbability and EMringer Model.

The two structures are deposited in the Protein Data Bank 6R72 and 6R81.

## 11. Detergent quantification

### 11.1 Cholate quantification

The detergent sodium cholate belongs to the bile acid salts class. A colorimetric dosage for this kind of detergents has been developed using sulfuric acid (Heftmann, Ko, and Bennett 1966). The former reacts with the cholate ring resulting in a yellow color. The absorbance at 389 nm is proportional to the detergent in the sample.

This quantification is effectuated using a 96 wells-plate. A calibration curve is realized with 0; 0.1, 0.3, 0.5 and 0.7  $\mu\text{g}/\mu\text{L}$  of sodium cholate. The sample is tested at different volumes with a final volume of 10  $\mu\text{L}$ . Then, 190  $\mu\text{L}$  of sulfuric acid are added to all the wells. The plate is covered up and placed under agitation for 10 minutes at 600 rpm at room temperature. The SAFAS Xenius (Monaco) spectrometer is used to measure the absorbance.

### 11.2 MALDI-TOF detergent quantification

The mass spectrometer MALDI-TOF (Matrix Assisted Laser Desorption Ionization – Time Of Flight) can be used to quantify the detergent in sample. This approach is used to quantify the DDM (figure 43).

The molecules are identified by their mass/charge ratio which is determined by the time of flight between the ionization source and the detector. The sample is mixed with matrix (aromatic molecule) and deposited on a stainless-steel plate. The mix crystallize at room temperature and pressure. The matrix absorbs the energy produced by the UV laser which induces the sublimation of the sample and the molecules ionization into positive charged ions.

To be able to quantify the detergent, a known quantity of another detergent is added. This is called internal standard. It needs to have different molecular weight but similar biophysical proprieties than the detergent of interest. For example, in the case of the DDM the standard is UDM or deuterated DDM.

UDM and DDM solution are prepared at 1% (w/v) in buffer 20 mM Hepes pH 7.5 and 100 mM NaCl. For the calibration curve, three different ratio UDM/DDM are prepared: 1/3; 1/1 and 3/1. The concentration of UDM is constant in the three mix, the varying quantity is of DDM.



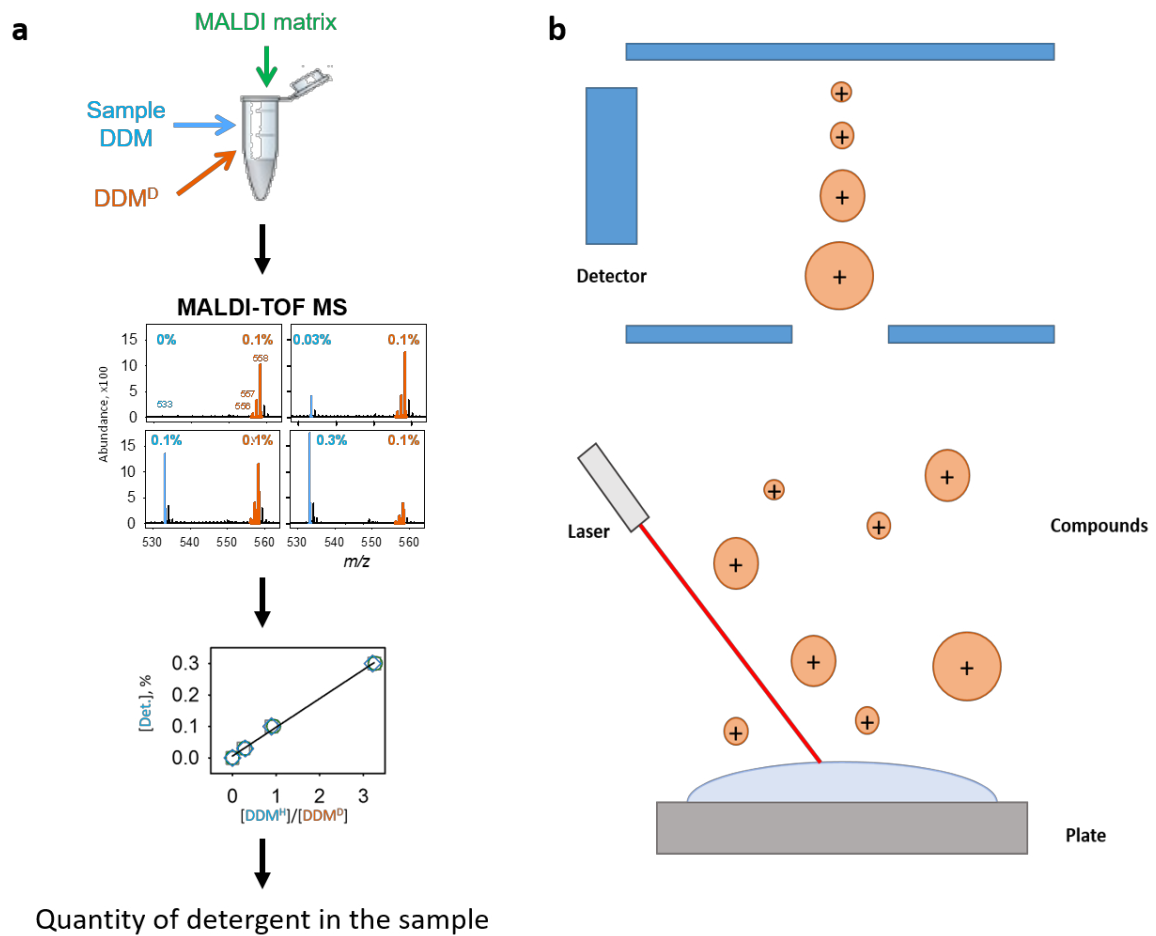
## MATERIELS AND METHODS

The final volume is of 100  $\mu\text{L}$ , therefore 5  $\mu\text{L}$  are added of UDM and 1.7, 5 or 15  $\mu\text{L}$  of DDM according to the ratio desired. The volume of the sample containing DDM can vary from 5  $\mu\text{L}$  to 47.5  $\mu\text{L}$  based on an approximation of the molecules bound to the protein. In the case of the DDM, 200 molecules are estimated bound to BmrA (in presence of cholate). To the sample, 2.5  $\mu\text{L}$  of UDM and the buffer are added and stocked at  $-20^{\circ}\text{C}$  before utilization. All the volumes are systematically weighed on the precision scale.

The sample is then diluted 10 times or 50 times with the matrix 2,5-dihydroxybenzoic acid (DHB, at 10 mg/ml in water) and sodium iodide (NaI, 10 mg/ml in acetone) solution. The NaI is necessary to ionize the sample into  $\text{MNa}^+$  form. On the plate, 1  $\mu\text{L}$  of this mixture is deposited and it crystallizes at room temperature. For each sample, three drops are tested.

The mass spectrometer is a Voyager-DE Pro MALDI-TOF (Sciex, Framingham, MA) which has nitrogen laser of wavelength of 337 nm. For this kind of quantification, there is an automatic acquisition method since the parameters are already optimized. Such are 5000 V voltage, extraction delay of 170 ns, mass range of  $m/z$  350 à 1000. Each spot is shot 100 times at 9 different places. The spectra obtained are accumulated and calibrated for the mass. A program was developed to treat automatically the data and determine the ratio of the intensity of the detergent to test and the standard (DDM/UDM). The same process is effectuated for each spot and a mean is calculated for each sample.

The same protocol is implemented for the others detergent (OG and FC12). In the case of FC12 the matrix is  $\alpha$ -Cyano-4-hydroxycinnamic acid (CHCA).



**Figure 43. Detergent quantification method by mass spectrometry**

(a) The sample is placed in presence of the MALDI matrix and standard detergent (here DDMD). The sample is analyzed by the mass spectrometer which measured the abundance of each molecule. The quantity of detergent is then calculated thank to a calibration curve done in parallel. (b) The MALDI-TOF functioning is exemplified by this illustration. The crystallized sample on the plate is shot with an UV laser. The molecules ionized are free from the plate. The detector records the time of light (rate) of the molecules identifying their  $m/z$ . (Chaptal et al. 2017)



# RESULTS



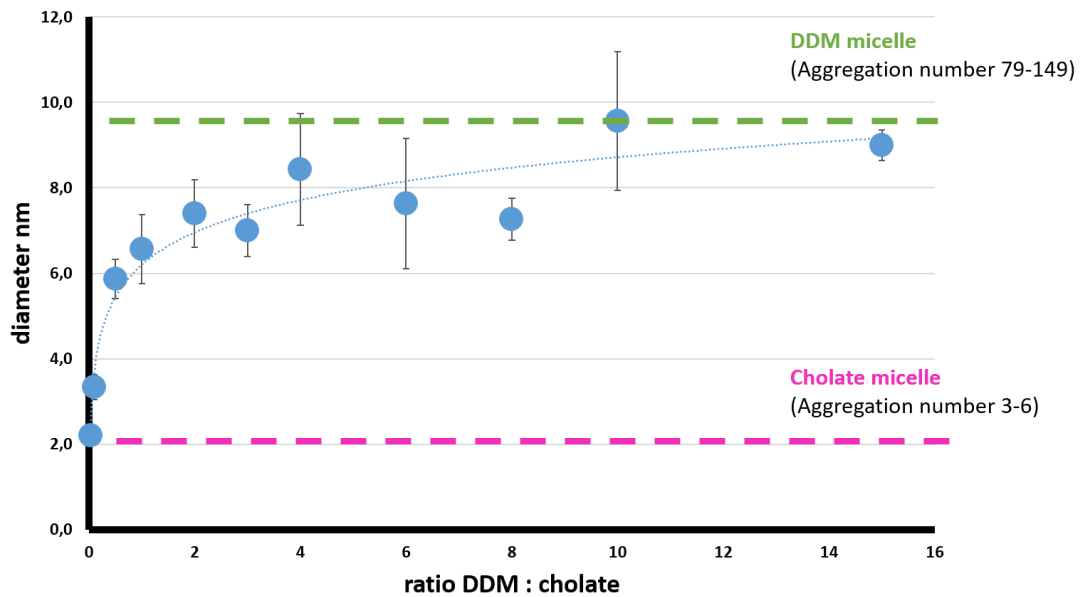
# Chapter I: BmrA E504A structures



This first chapter will detail the process to obtain the two structures of BmrA E504A which were solved by both X-ray crystallography and single particle Cryo-EM. This study followed and continued the PhD project of Dr. Arnaud Kilburg. He performed the structural study using X-ray crystallography since the Cryo-EM was not enough developed to solve structures at high resolution. The stability and the homogeneity of the sample are critical parameters for X-ray crystallography studies. The inactive mutant BmrA E504A was chosen because it is stable in the outward facing conformation since it can fix the nucleotides without hydrolyzing them.

Initially, the protein was purified with DDM obtaining low resolution diffracting crystals. Then, he used the mixture of detergents DDM-cholate (3:1) on the basis of the results obtained on the P-gp (Aller et al. 2009). The crystals had a better diffracting power even if after a lot of optimization, the diffracting power could not bypass the resolution limit of 6 Å. The addition of sodium cholate improved the X-ray crystallography experiments. To further understand this detergent mixture, a study on its behavior was performed by dynamic light scattering (DLS). The size of the micelles was recorded in function of the ratio of DDM-cholate (figure 44). The increasing concentration of sodium cholate in the sample decreases the size of the micelle. In addition, DLS can measure the homogeneity of the sample by looking at the distribution of the size of objects that are present; the mixture DDM-cholate forms mix micelles of the same size. I tested three ratios of DDM-cholate during my PhD project, they were the 1:1, 1:3 and 1:1.33 DDM-cholate.





**Figure 44. Dynamic Light Scattering study on the mixture DDM-cholate**

The green dotted line represents the size of the DDM micelle and the magenta one the cholate. The graph shows the size of the micelles (diameter) in function of the DDM-cholate ratio. The blue dots are the size of the micelles corresponding to different ratios.

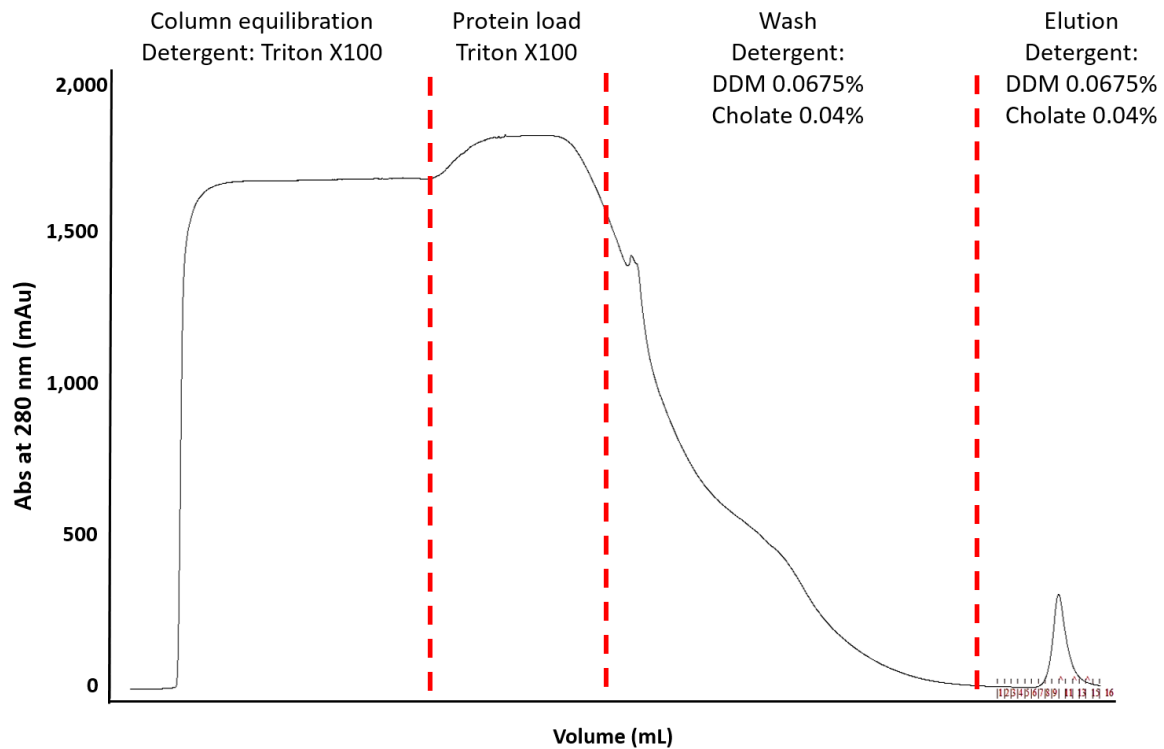
## 1. Protein purification

The mutant BmrAE504A was over-expressed in the C43(DE3)  $\Delta$ AcrB *E. coli* strains reaching 50% of the protein expression amongst all the others. The membranes were then solubilized by Triton X100 which is a mild detergent leading to an extraction yield of around 70%. This detergent however, is not the most efficient one to solubilize BmrA. DDM or FC12 for example could extract almost the totality of BmrA. Still, the protein extracted by Triton X100 led to better results in the crystallogenesi step than the other detergents (cf. Kilburg PhD results). In short, DDM could extract all of BmrA, but the crystals were small and nucleation was everywhere in the drop. The crystals could never be optimized. The exchange of Triton X100 to DDM alone did not improve the crystallization, yielding slightly better crystals than DDM alone. Introduction of the DDM-cholate mixture was a game changer allowing to yield larger crystals that could really be worked with and optimized, and reaching interesting diffracting power. The purification was thus already optimized when I arrived so I did not modify it any further.

The first affinity chromatography was crucial for the detergent exchange since the protein was in presence of Triton X100 at the beginning and in presence of the mixture DDM-cholate at

the end of it. This process was checked by the absorbance at 280 nm since the detergent Triton X100 absorbs at this wavelength (figure 45).

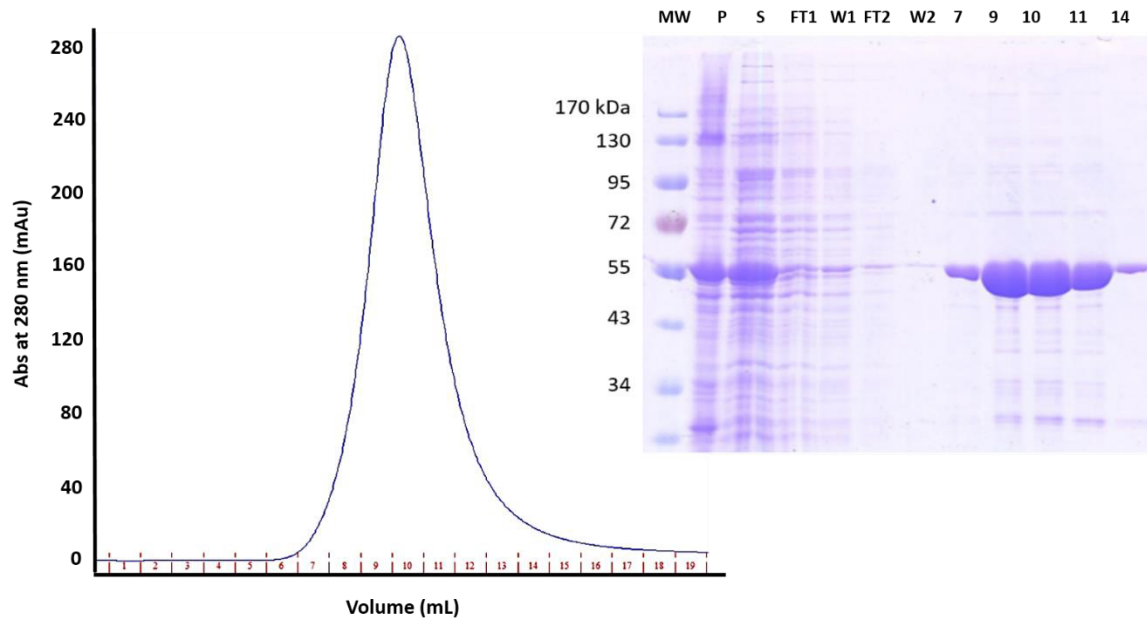
BmrA E504A was eluted in single step with a buffer containing 200 mM Imidazole. In addition, this step had a good yield since the purified protein was eluted at relatively high concentration for a membrane protein.



**Figure 45. Affinity chromatography of the purification of BmrAE504A**

The different steps are marked with red dotted lines. From left to right, the equilibration of the column, the protein loading, the washing and the elution of the protein of interest.

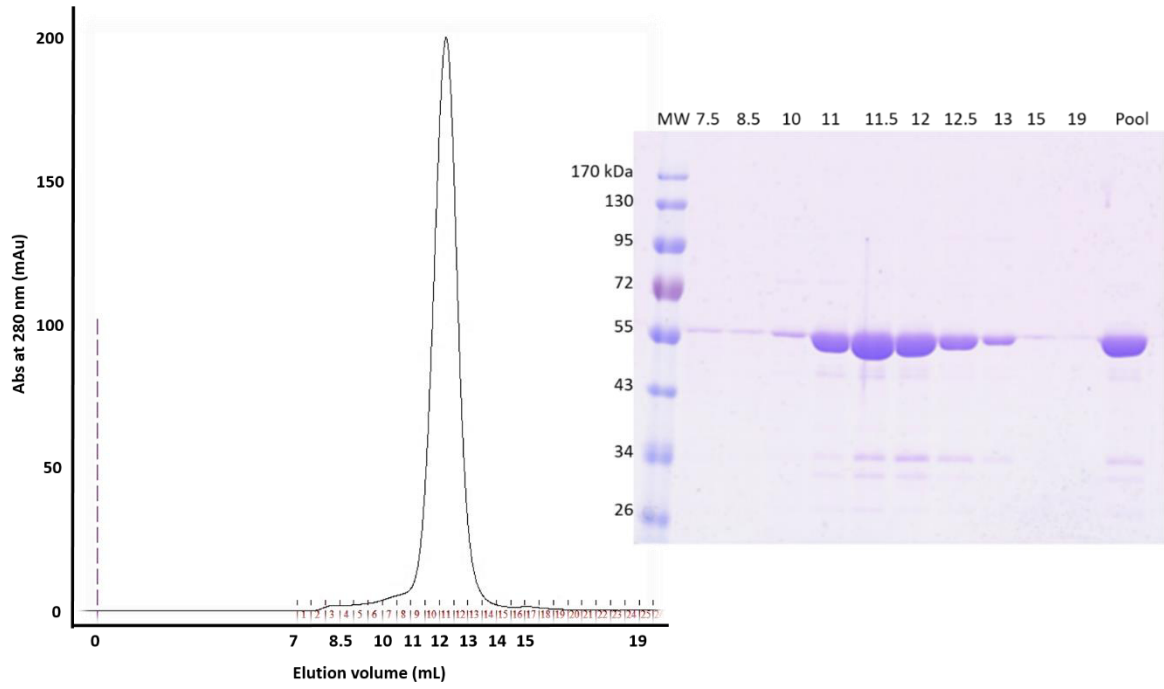
Afterward, the fractions of the peak were pooled and diluted for another step of affinity chromatography to increase the capacity of binding to the Ni-NTA resin. This second step was necessary to reach a high purity degree of the sample for the crystallogenesis step. It eliminated contaminants still present after the first one (figure 46).



**Figure 46. Second affinity chromatography of the BmrA E504A purification**

On the left, the elution peak of BmrA E504A and on the right, the SDS-PAGE containing samples from the two steps of affinity chromatography. The samples are: C for pellet, S for supernatant, FT1 and W1 for flow through and wash of the first affinity chromatography, FT2 and W2 for flow through of the second affinity chromatography, 7 to 14 for the fractions of the peak.

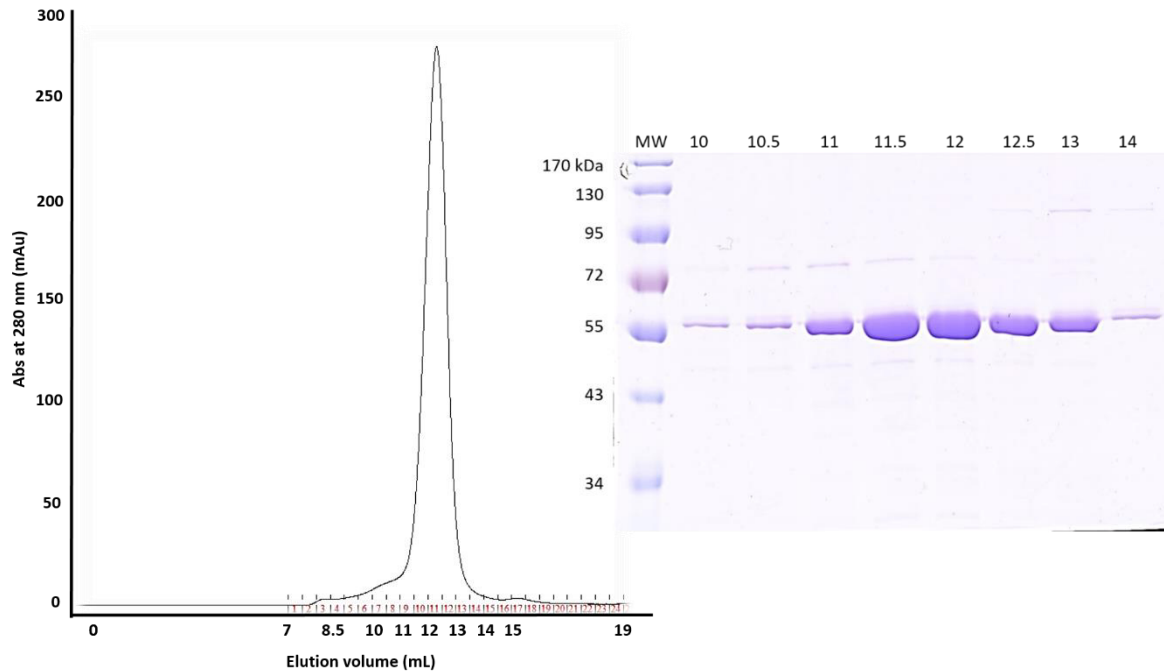
The fractions corresponding to the peak were pooled together and concentrated to be loaded onto the size exclusion chromatography. The goal of this step was to evaluate the purity degree of the sample, to eliminate the imidazole and lastly to exchange the ratio of DDM-cholate. That last one aimed to reduce the detergent belt around the protein. The protein was purified with molar ratio of 1:1, 1:1.33 and 3:1 DDM-cholate. In these three conditions, the protein seemed to be well purified since the peaks were well-defined and symmetrical (figure 47, 48 and 49). Then, the SDS-PAGE were run to check sample purity. The one corresponding to the ratio 1:1 DDM-cholate showed BmrA E504A at 55 kDa and another band at 34 kDa (figure 47). The protein of interest was of 65 kDa although it migrates to 55 kDa. This phenomenon had been already observed by Ravaud and co-workers (Ravaud et al. 2006). This could be explained by the fact that membrane proteins bind more SDS detergent molecules inducing a higher negative charge. For this reason, BmrA migrated further than expected. The band at 34 kDa had not been identified even though it did not appear to be a problem for the rest of the experiments.



**Figure 47. *BmrA E504A* purified with the ratio 1:1 DDM-cholate (0.035% and 0.03%, respectively)** Size exclusion profile of *BmrA* and SDS-Page corresponding to this purification. The samples deposited correspond to the fractions of the peak and their pool.

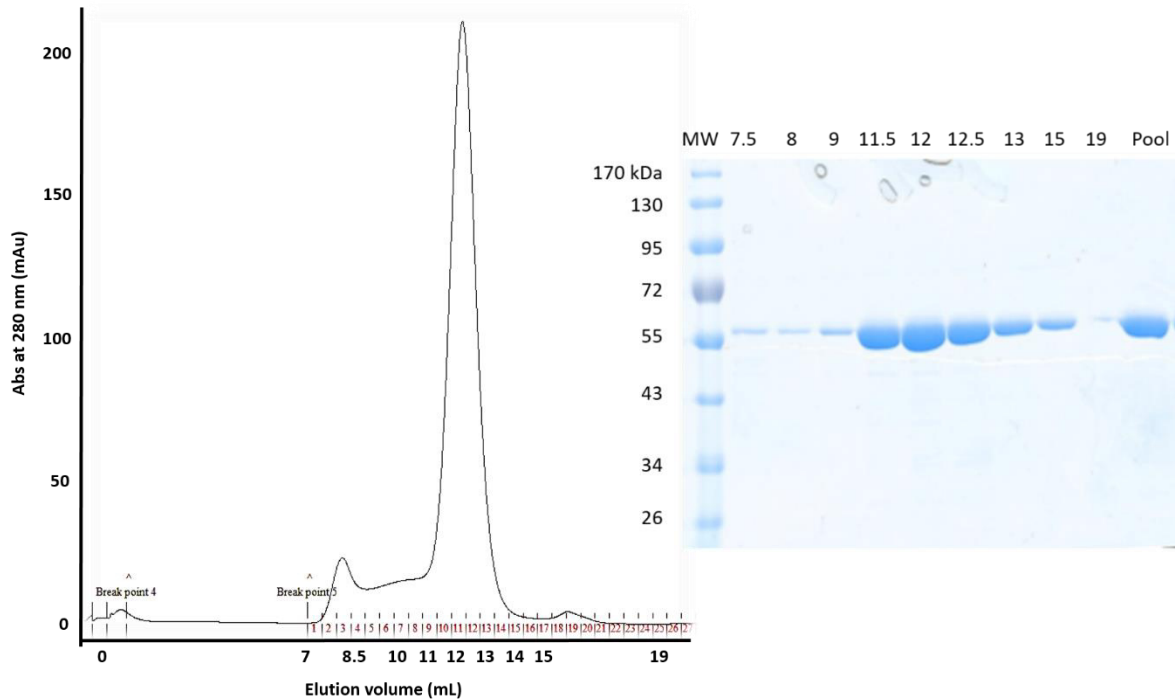
## RESULTS: CHAPTER I

The SDS-PAGE corresponding to the ratio 1:1.33 DDM-cholate purification revealed a band for the protein of interest at 55 kDa and an additional band at 72 kDa for some samples (figure 48). This latter band had not been identified either. In this case too, it did not seem to perturb the following steps.



**Figure 48. *BmrA E504A* purified with the ratio 1:1.33 DDM-cholate (0.035% and 0.04%)**  
Size exclusion profile and SDS-Page corresponding to the purification with the ratio 1 :1.33 DDM-cholate.  
The samples deposited correspond to the fractions of the peak.

In the case of the ratio 1:3 DDM-cholate purification, no contaminant was present (figure 49). In the chromatogram, it was possible to detect a small peak at the beginning (fraction 2 and 3). It corresponded to a protein aggregated which is not present for the others detergent mixture.



**Figure 49. *BmrA E504A* purified with the ratio 1:3 DDM-cholate (0.035% and 0.1%)**

Size exclusion profile and the SDS-Page corresponding to the purification with 1 :3 DDM-cholate. The samples deposited correspond to the fractions of the peak and the corresponding pool.

Once the protein was purified, the detergent quantification and the structural studies (X-ray crystallography and Cryo-EM experiments) were carried out.

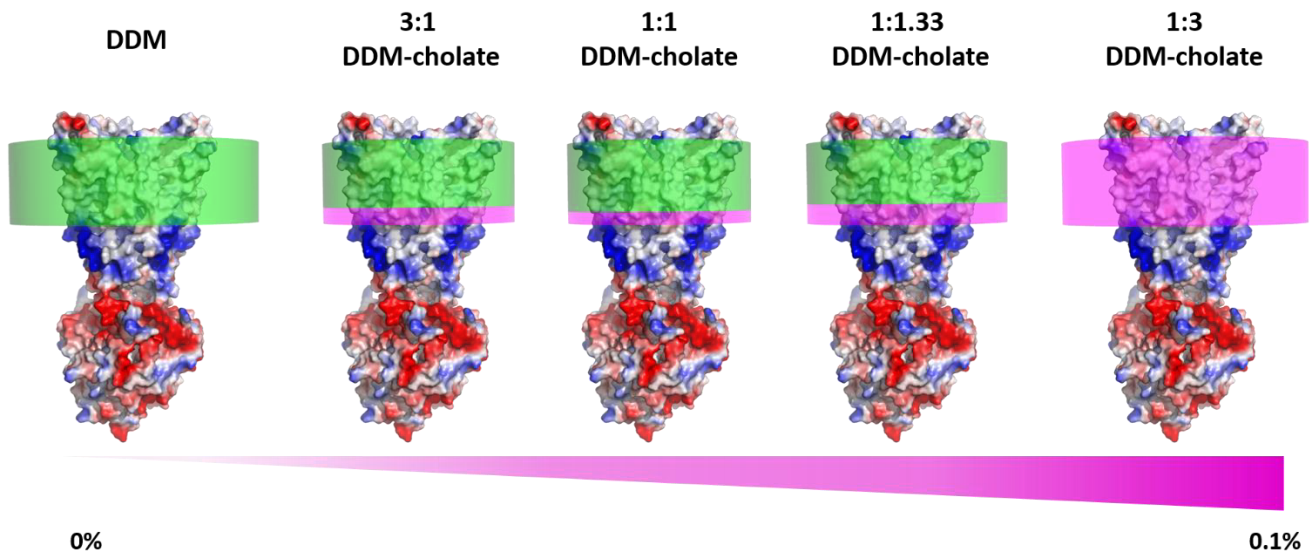
## 2. Detergent Belt determination

The quantification of the detergent bound to BmrA E504A was performed just after the purification step. A sample of each fraction was tested for the quantification of the sodium cholate and of the DDM.

A colorimetric dosage was performed for the quantification of the sodium cholate. The samples were incubated with sulfuric acid and the absorbance was measured at 390 nm. These quantifications revealed that  $21 \pm 5$  molecules of sodium cholate were bound to BmrA purified with the ratio 1:1 DDM-cholate. For the ratio 1:1.33 DDM-cholate,  $57 \pm 28$  molecules were measured.  $573 \pm 81$  sodium cholate were detected for the ratio 1:3 DDM-cholate.

To quantify DDM, 0.05% (w/v) of UDM, used here as standard, was added to the sample. The samples were diluted to 1/10 with the MALDI matrix DHB-NaI.  $150 \pm 23$  and  $186 \pm 10$  molecules of DDM were bound to BmrA for the ratio 1:1 and 1:1.33 DDM-cholate respectively. It was impossible to detect the quantity of DDM bound for the ratio 1:3 DDM-cholate. The reason could be that few molecules of DDM were bound, consequently they were not detectable by the MALDI-TOF device.

Once the quantity of detergent bound to the protein was determined, it was possible to model it using the DetBelt server (cf. Results chapter III). The server calculates the average volume occupied by the detergent around the protein (figure 50).

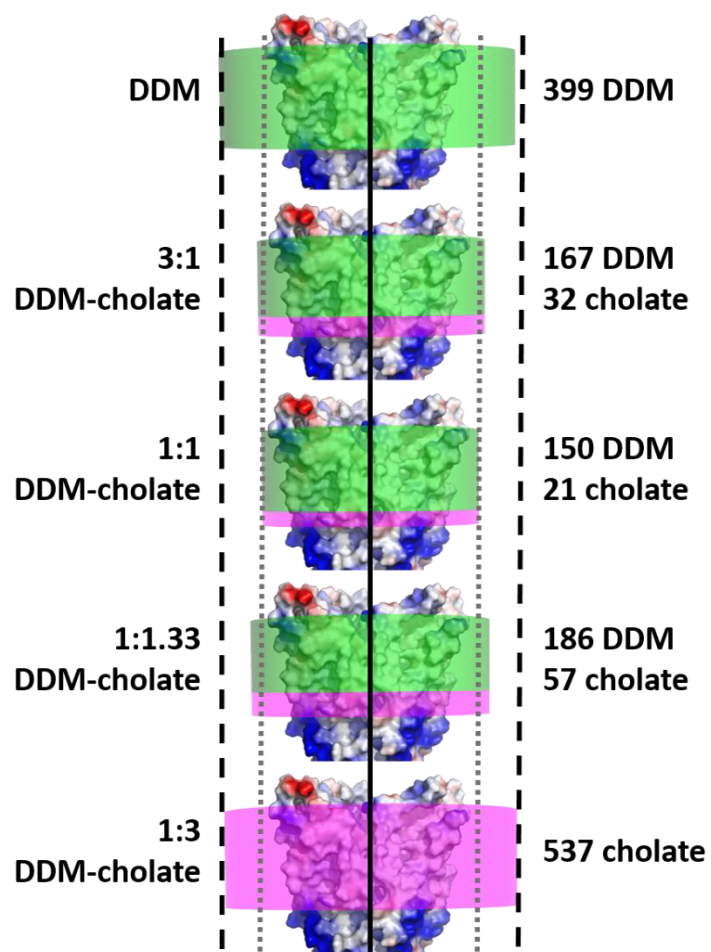


**Figure 50. Detergent belt around BmrA E504A obtained after the quantification of the detergent bound to BmrA E504A after its purification**

From left to right, there are displayed DDM, mixture 3:1 DDM-cholate, 1:1 DDM-cholate, 1:1.33 DDM-cholate and 1:3 DDM-cholate. The green corresponds to the volume occupied by DDM and the magenta one by cholate. The protein is displayed in surface and colored in electrostatic indices. The representation of the belt was realized with the Det.Blet server which will be discussed in the chapter III.

The detergent belt obtained with DDM alone and 3:1 DDM-cholate were added to evaluate the size change. The belt decreases with the increase in sodium cholate up to a minimum for the ratio 1:1, and then increases for the ratio of 1:1.33 and 1:3. As a consequence, the smallest was the one formed by the ratio 1:1 DDM-cholate. The bigger ones were formed by DDM alone and 1:3 DDM-cholate (Figure 51).



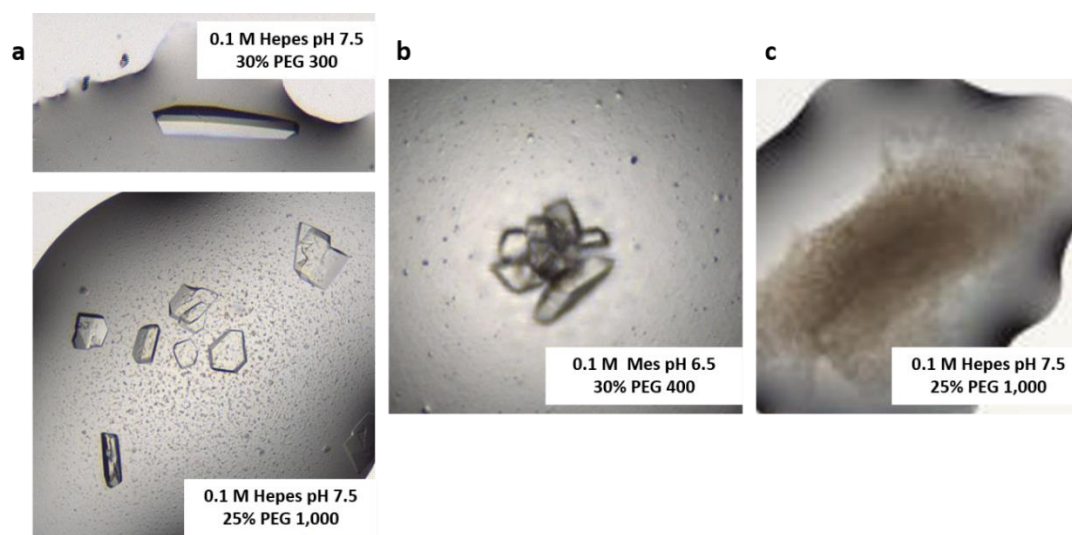


**Figure 51. Comparison of the detergent belt**

*These are the detergent belt presented in figure 50. The black dotted lines indicate the limits of the bigger detergent belt. The gray dotted lines indicate the limits of the smaller detergent belt.*

### 3. Crystallogenesis

Once the protein was purified, crystallogenesis essays were undertaken. The protein was concentrated at 500 x g using the 50 kDa cutoff Amicon Ultra-15 device. This rate was chosen to prevent the over concentration of detergent micelles. The value of concentration aimed was of 10 mg/mL although it was not reachable every time; the lowest concentration tested was of 6 mg/mL. The sample was incubated with 5 mM ATP-Mg<sup>2+</sup> for 30 minutes. Preliminary precipitant conditions' screening was performed for the three ratios of DDM-cholate. The commercial kits tested were the suite PEG I and PEG II from Hampton which vary the concentration of salt and pH in the solution. The protein was purified with the ratio 1:1 DDM-cholate crystallized in 0.1 M Hepes pH 7.5 and 30% PEG 300 and also in 0.1 M Hepes pH 7.5 and 25% PEG 1,000 (figure 52a). For the ratio 1:1.33, crystals appeared only from the condition composed by 0.1 M Mes pH 6.5 and 30% PEG 400 (Figure 52b). The protein aggregates in all conditions tested for the ratio 1:3 DDM-cholate (figure 52c). The diffraction power of the crystals obtained had been tested at the Synchrotron facility SOLEIL. The crystals of BmrA in 1:1 DDM-cholate had a diffraction pattern reaching near 4 Å resolution. For the ratio 1:1.33 DDM-cholate, the diffraction power of the crystals reached low resolution only. Therefore, the optimization of the conditions had been carried out only for ratio 1:1 DDM-cholate.

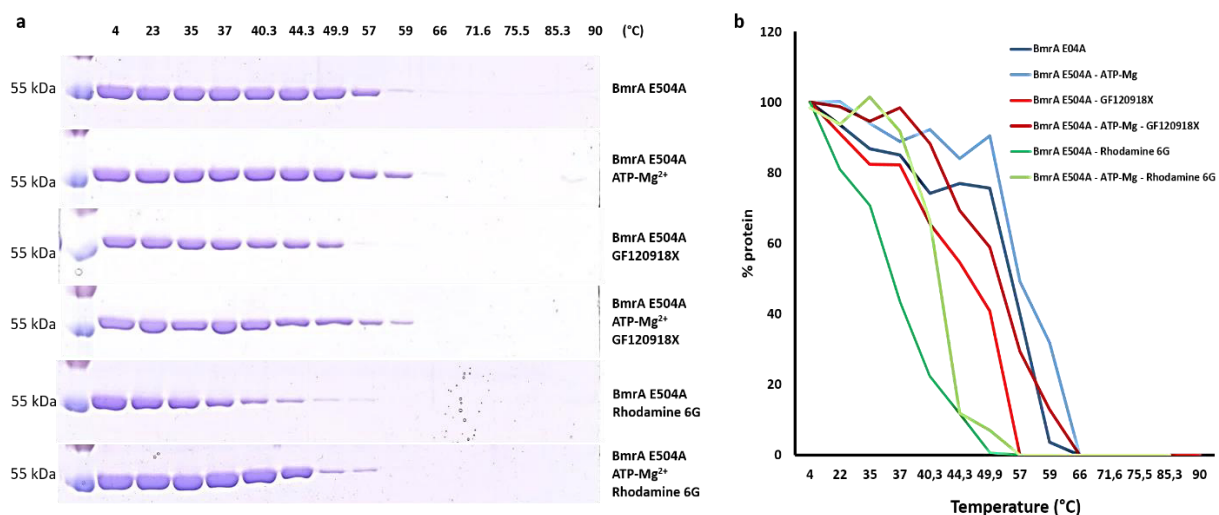


**Figure 52. Results of the screening of the crystallization conditions**

(a) These crystals are obtained from the BmrA E504A purified with 1:1 DDM-cholate. The precipitant conditions are 0.1 M Hepes pH 7.5 – 30% PEG 300 and 0.1 M Hepes pH 7.5 – 25% PEG 1, 000. (b) These crystals result from the incubation of purified protein in 1:1.33 and 0.1 M mes pH 6.5 - 30% PEG 400. (c) BmrA E504A with 1:3 DDM-sodium cholate aggregates in all condition tested, here is shown 0.1 M Hepes pH 7.5 and 25% PEG 1,000. All the samples contain 5 mM of ATP-Mg<sup>2+</sup>.

The conditions for the crystallization of the sample were finely optimized. Various quantity of PEG and pH of the buffer were explored around the successful conditions which were 0.1 M HEPES pH 7.5 – 30% PEG 300 and 0.1 M HEPES pH 7.5 – 25% PEG 1,000. Both PEG 300 and 1,000 were tested in the range between 20% and 35%. The buffer was tested from pH 6.5 (MES) to 8.5 (Tris). The crystals diffracted better when generated into PEG 1,000 solution. However, the diffraction power was still above 4 Å resolution. One important modification was the temperature at which the protein was concentrated and incubated with ATP-Mg<sup>2+</sup>. At the beginning, it was done at 4°C and then the crystal growth at 19°C. This BmrA mutant fixed better ATP-Mg<sup>2+</sup> at 22°C; it seemed like the temperature variation could provoke movement of the protein to bind the compounds and this translated in poor quality of crystals. Finally, after the purification step, the sample was always kept at room temperature.

In parallel, the co-crystallization of BmrA E504A with a ligand was attempted. The molecules tested were rhodamine 6G and GF 120918X (inhibitor of the human homologue of BmrA, P-gp). The binding of the two compounds was tested on BmrA purified with DDM and their  $K_D$  were of  $22.4 \pm 5.1$  and  $0.44 \pm 0.02$   $\mu$ M (Steinfels et al. 2004). A thermal stability assay was realized to test the protein in their presence. The sample tested in both cases are: BmrA E504A, BmrA E504A with ATP-Mg<sup>2+</sup>, BmrA E504A with the compound, BmrA E504A with ATP-Mg<sup>2+</sup> and the compound (figure 53). The results showed that BmrA E504A was stable up to 57°C, while the addition of the ATP-Mg<sup>2+</sup> increased the half denaturing temperature to 59°C. Both compounds decreased the stability of the protein which could be restored with the addition of ATP-Mg<sup>2+</sup>. The instability of the protein with the ligand was probably due to the conformation modification.

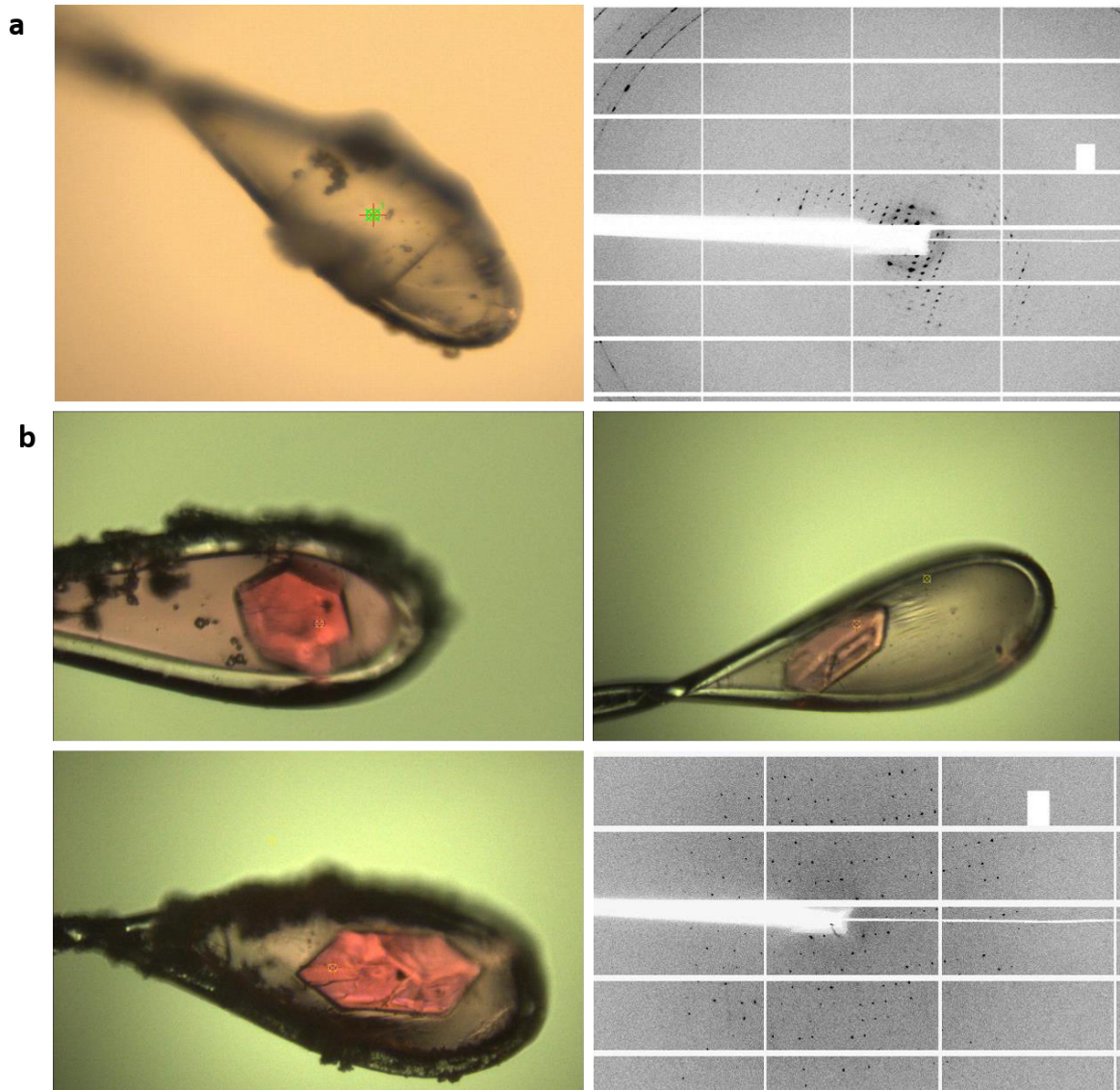


**Figure 53. Thermal stability assay of BmrA with/without ligand and/or nucleotide**

(a) the SDS-PAGE resulted from the thermal stability assays performed to study the stability of the protein in various conditions. From up to down, the samples tested are BmrA E504A, BmrA E504A with ATP-Mg<sup>2+</sup>, BmrA E504A with GF 120918X, BmrA E504A with GF 120918X and ATP-Mg<sup>2+</sup>, BmrA E504A with rhodamine 6G, BmrA E504A with rhodamine 6G and ATP-Mg<sup>2+</sup>. They were placed from 4°C up to 90°C and then loaded onto the SDS-PAGE (only part of the gel with BmrA shown here). (b) The data obtained for these gel bands using ImageJ.

The crystallogensis assay was performed with the BmrA E504A, ATP-Mg<sup>2+</sup> and both compounds separately. The protein was incubated at first with the ligand and then with the nucleotide. The conditions tested for the crystal growth were the same than for BmrA E504A and ATP-Mg<sup>2+</sup>.

In the case of GF 120918X, the crystals grew in 27% PEG 1,000 at pH 8.5 (0.1 M Tris) as precipitant solution after a few days of incubation at 19°C. Unfortunately, these crystals could only diffract up to 8 Å resolution (figure 54a). In the case of rhodamine 6G, crystals grew in presence of 23% PEG 1,000 at pH 8.5 (0.1 Tris) as precipitant solution (figure 54b). They could diffract up to 5 Å resolution. Further optimization was performed although it did not lead to overcome this maximum of diffraction resolution.



**Figure 54. Crystals of BmrA with a ligand (GF 120819X or rhodamine 6G)**

(a) The crystal obtained for BmrA E504A with GF 120819X and its diffraction pattern. (b) The three examples of crystals obtained for BmrA E504A with rhodamine 6G. There is also an example of diffraction pattern.

The crystallogensis experiments were carried out with the sample BmrA E504A and ATP-Mg<sup>2+</sup> since it was the more performing one. The next step of optimization was the use of DCOD additive.

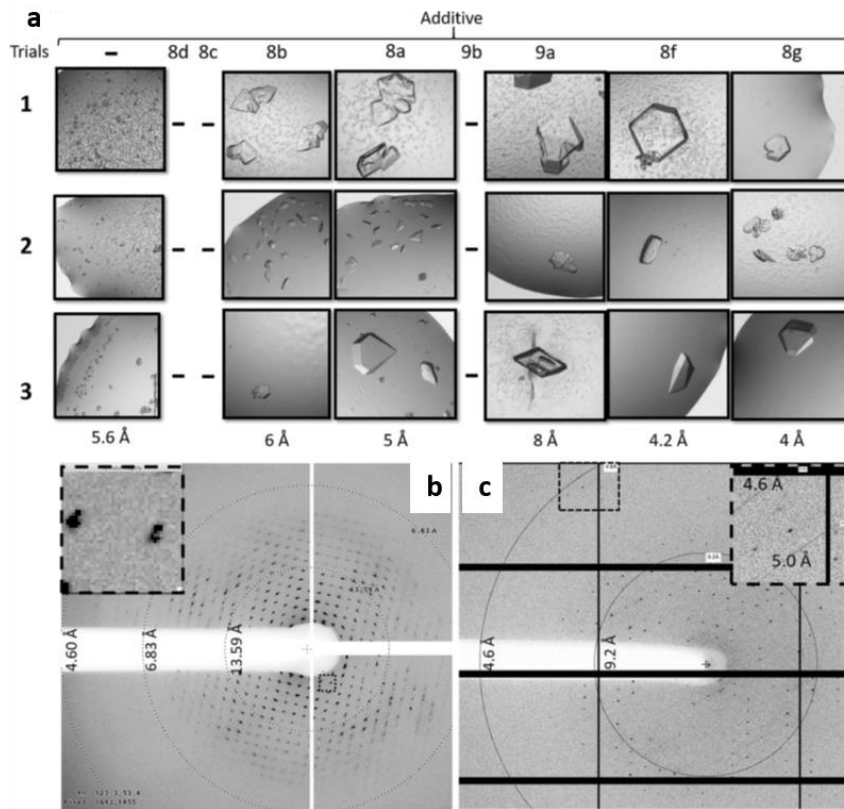
## 4. The DCOD additive

Membrane proteins display an important amount of basic residues at the interface of the membrane and the cytoplasm, also known as the “positive inside rule” (von Heijne 1992). The DCOD detergents exploit this characteristic by aiming to stabilize more the protein. The general DCOD structure is composed by a hydrophobic chain, maltose heads and carboxylic groups. The hydrophobic chain is supposed to interact with the hydrophobic part of the protein and the carboxylic groups with the arginine and lysine residues forming salt bridges. This last one is the more stabilizing factor.

These detergents were designed in collaboration with A. Boumendjel team. The chemical production of the compounds was carried out in his laboratory and the test of the protein stability was performed in our laboratory by S. Magnard. The tests revealed that in presence of this detergents BmrA was stable up to 90°C.

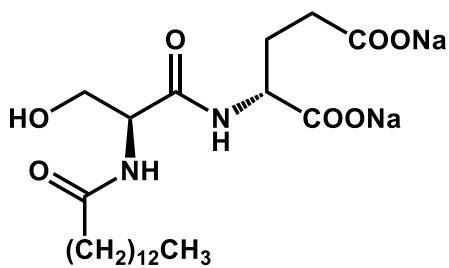
Their influence was also studied in the crystallogensis experiments; they were used as additive which meant that they were added just before the drop formation by the robot Mosquito. The sample was composed by BmrA E504A purified with 1:1 DDM-sodium cholate and ATP-Mg<sup>2+</sup>. The precipitant condition tested was the optimized one which was between 20%-27% PEG 1,000 and Tris pH 8.5. The additive was added at 10 times the CMC. The drop was composed by 450 nL of protein sample, 50 nL of additive and 500 nL of precipitant solution, yielding a final concentration of additive around the value of the CMC. The amount of additive added this way was less than 10 monomers per BmrA dimer. The crystals appeared after 3 days as for the ones without additive. The real improvement brought by the DCOD additives was to solve a spot-doubling issue (figure 55). Crystals without additive often displayed spots too close to another which could be the participation of two crystals (pseudomerothedral Twinning) or a not efficient protein packing. The pseudomerothedral twinning option was excluded since the doubling spots were present at low resolution in the diffracting pattern and the cells parameters were not compatible for this space group. These detergents seemed to solve this complication which could prevent the resolution of the protein even when the high resolution was reached.

This whole study was published and the paper can be found in the appendix section, page 311.



**Figure 55. The impact of DCOD detergents on the crystallogenesis of BmrA**  
 (a) Crystals resulted from the addition with the additive (8d, 8c, 8b, 8a, 9b, 9a, 8f and 8g). (b) Diffraction pattern without additive. On the corner, there a zoom on the spots. (c) Diffraction pattern with additive. There is a zoom on the spots in the corner

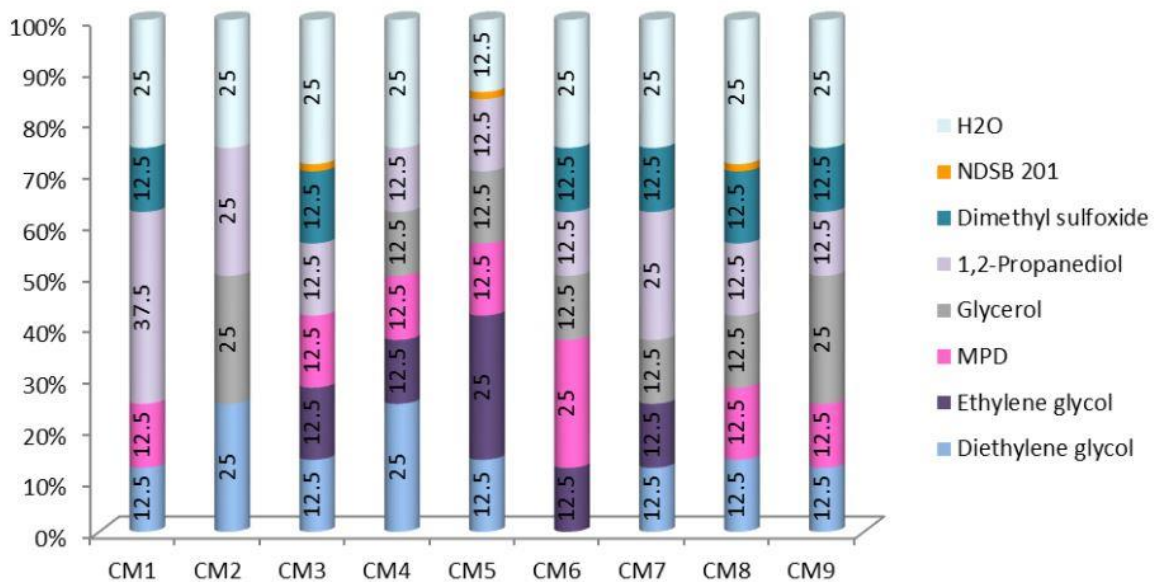
A DCOD additive was crucial to improve the crystallogenesis of BmrA E504A. One of these allowed the resolution of BmrA structure. This compound was not amongst the ones published in the paper; it is called 3.9 f. Its presence induced the deletion of the doubling spots' problem as shown in the figure here below (figure 56).



**Figure 56. Structure of the 3.9 f additive**

## 5. Cryo-protection

The crystals grew from day 3 of incubation at 19°C up to day 5. The crystals were harvested the 6<sup>th</sup> day because they dissolved at day 8. They were frozen into liquid nitrogen and stored until their analysis at a Synchrotron facility. During this step, the ice could be an issue to overcome since its presence could prevent the collection of high resolution diffraction data. To solve this problem, cryo-protection solutions were used. In a typical cryo-protection experiment, the crystals are fished out from the drop, placed in a drop of cryo-protection solution, fished out again and then frozen. Generally, a solution containing glycerol is used. In the case of BmrA E504A, the crystals broke once in contact with a glycerol solution. We struggled a lot with cryo-protection of BmrA crystals. Until one day, at the synchrotron facility, we met Enrico Stura who is an expert in the cryo-protection solution (Vera and Stura 2014). He studied the basis of this process designing different mixture composed by precipitant and solubilizer compounds to preserve the equilibrium of the crystal once collected in the loop. He created the commercial CryoProtX MD1-61 kit which we tested (figure 57). Amongst the precipitants, there were MPD (2-methyl-2,4-pentandiol) and DMSO (Dimethyl sulfoxide). The solubilizer were glycerol, ethylene and propylene glycols.



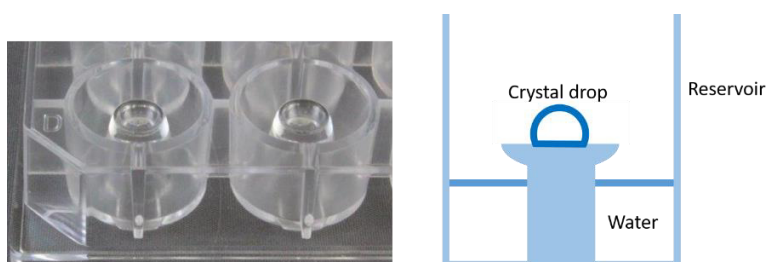
**Figure 57. Cryo protection mixes of the CryoProtX MD1-61 kit.**  
(Figure from the datasheet of the kit delivered by Molecular dimensions)



The mixes tested were the CM1, CM2, CM3 and CM4. A crystal was placed in a drop of this mix and was monitored. Three situations were possible: the crystal cracked, dissolved or was stable. If the crystals cracked, the cryoprotection solution can be fixed by diminishing the quantity of precipitant and to add more solubilizer. If the crystal dissolved however, the quantity of solubilizer had to be increased and the precipitant decreased.

CM2 and CM4 induced the complete dissolution of the crystal. It was probably due to the presence of the glycerol which had already proven to not be a good cryo-protectant for BmrA crystals. Both CM1 and CM3 stabilized more the crystal and did not contain glycerol. A further optimization was needed since the crystal seemed to dissolve a little. The quantity of precipitant was then increased and the solubilizer was decreased; the final solution was 12.5% (v/v) di-ethylene glycol, 18% (v/v) 2-methyl-2,4-pentanediol, 7% (v/v) ethylene glycol, 12.5% (v/v) 1,2-propanediol, 12.5% (v/v) dimethyl sulfoxide and NDSB 201.

Once the optimal mix was found, the technique of fishing and cryo cooling also needed optimization. At first, the crystal was directly added to the cryoprotection solution drop, but cracked or dissolved immediately. Then, the cryoprotection solution was added to the crystal drop; this method was more successful than the first one although the crystals were still damaged by it. Finally, the cryoprotection solution was added to the crystal drop in a progressive way to do not induce a drastic change in the crystal surrounding. To decrease any other disturbance, ATP-Mg<sup>2+</sup> and the additive 3.9 f were added to the solution. A further optimization was to conserve a humid environment; Cryschem sitting drop plates (figure 58) were used and the reservoir was filled with water. The humidity conserved the crystal drop in a surrounding more similar to the one in the growth conditions. Together, these improvements allowed data collection at high resolution needed to solve the BmrA E504A structure (PDB 6R72).



**Figure 58. Cryschem sitting drop plate**

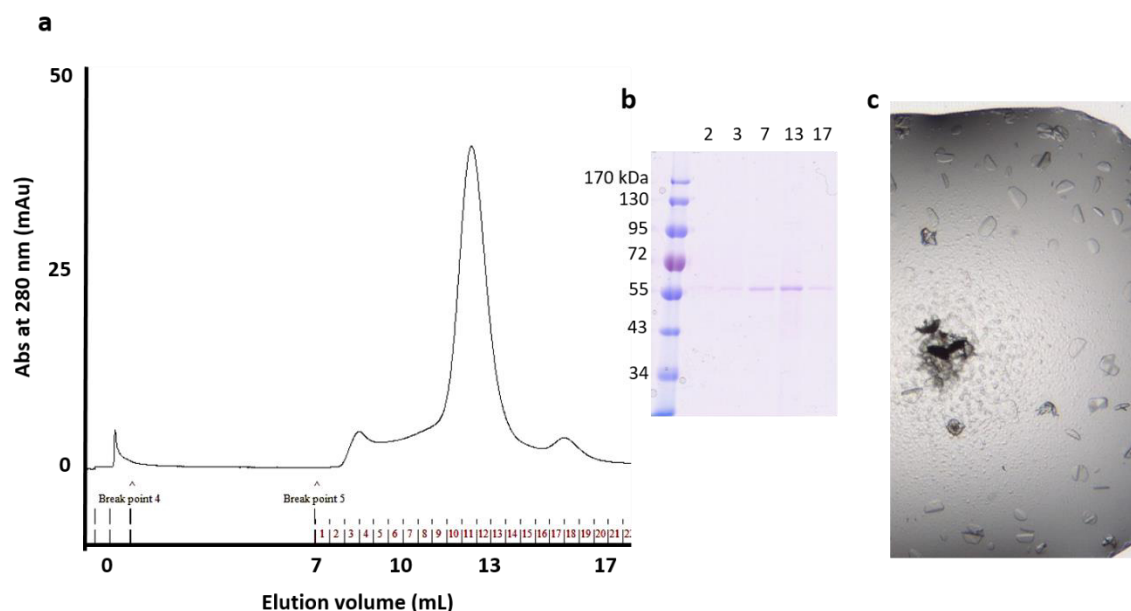
*On the left, the photo of the plate and on the right, an illustration of the crystal fishing out setting*

## 6. Experimental Phase determination assays

As described in the methods section, we explored 3 ways to perform the heavy atoms incorporation on BmrA, which were not successful. The heavy atoms soaking aggregated the protein and no crystal growth could be observed. The selenium methionine derived BmrA yield crystals that did not diffract.

### Selenium methionine

The protein was successfully produced and purified as is shown in the figure 59a-b. Some crystals were obtained (figure 59c) but they were really little and had no diffraction power. It could be that the protein is less stable in these conditions. No other assay with selenium methionine were performed since the molecular replacement worked.



**Figure 59. Selenium methionine assay**

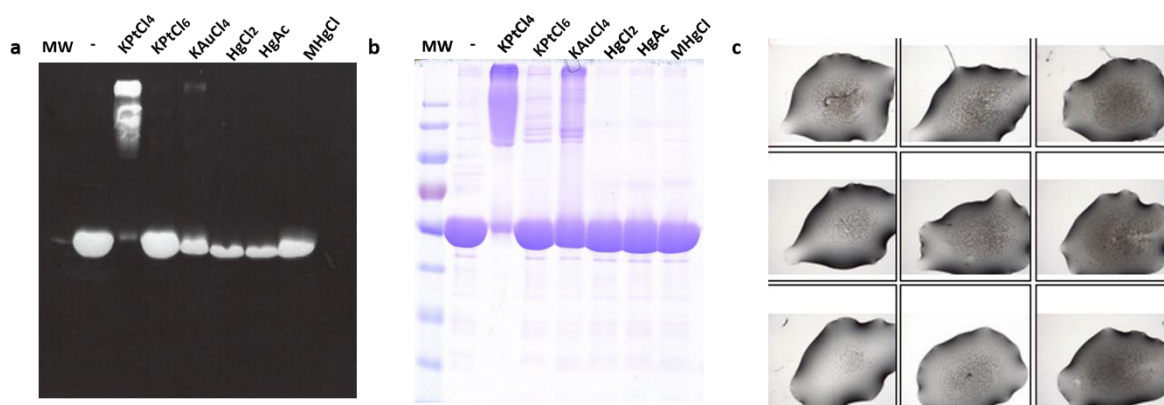
(a) SEC purification profile of BmrA with the selenium methionine. (b) The corresponding SDS-PAGE. (c) Crystals obtained.

### Heavy atoms soaking

Another experimental phasing aspect was the derivation of the protein with heavy atoms. Cysteine residues bind heavy atoms and BmrA E504A contains one cysteine residue for each monomer. A way to detect the derivation of the cysteine by a heavy atom was to probe the accessibility of the cysteine. It could be done by using TetraMethylRhodamineMaleimide (TMRM), which is conveniently fluorescent under UV light. The TMRM will bind to accessible

cysteines, and when the protein is analyzed by SDS-PAGE, we can observe a fluorescent band where the protein is. If the cysteines are not accessible to TMRM, for example because they have been derivated by a heavy atom, an absence of fluorescence will be detected. This is a convenient and easy way to screen which heavy atom is able to bind to a cysteine.

A screening of heavy atoms (HA) was performed on the purified protein. 5 molar equivalents of heavy atoms were added to the sample and incubated during 10 minutes. Then, the TMRM compound was added up to saturated concentration. The sample were loaded into the SDS-PAGE and revealed using a UV lamp and then stained with Commassie blue to visualize the total protein band. Figure 60a-b show a typical result from this screening. The negative control corresponded to no HA addition, and results in the full TMRM signal under UV light. Platinum were not good compounds for BmrA, resulting in either aggregation (KPtCl<sub>4</sub>) or no binding (KPtCl<sub>6</sub>). Gold resulted in a partial decrease of the signal compared to mercury derivatives. HgCl<sub>2</sub> or HgAc gave the best result, not aggregating the protein and decreasing TMRM binding (therefore derivating the cysteine). These two compounds were then tested for crystallogenesis. The protein was incubated with the ATP-Mg<sup>2+</sup>, then with the mercury acetate and chloride, followed by standard crystallogenesis. No crystals were obtained in these conditions and the protein tended to precipitate in the drop (figure 60c).



**Figure 60. Heavy atoms soaking assay**

(a) UV revelation of the SDS-PAGE loaded with the sample composed by BmrA and each heavy atom. (b) The corresponding gel colored with Commassie Brilliant Blue. (c) The crystallogenesis experiment.

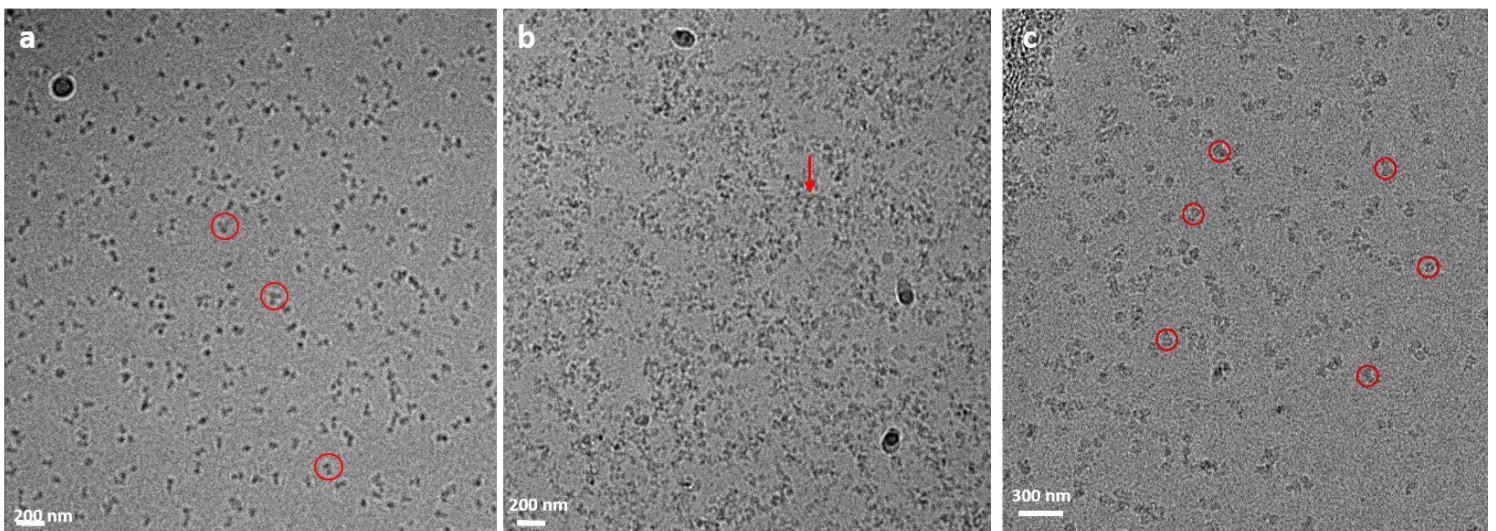
### **TbXO<sub>4</sub>**

The crystallophores TbXo<sub>4</sub> was also tested for the phase determination. This compound is a lanthanide complex which has the property to improve the nucleation step and enable the phase determination (Engilberge et al. 2017). The presence of a cluster of terbium heavy atom is the key element for the resolution of the phase, having a strong anomalous signal and structure solution is resolved at low resolution. This crystallophore was used as additive in the crystallogenesis drop and also in addition to the cryoprotection solution. The best results were obtained when added to the cryoprotection solution. Several datasets have been collected at the peak of the terbium for a SAD experiment, with a maximum resolution of 6 Å. We faced an isomorphous problem, with cell parameters varying too much to be able to merge enough data to reach sufficient completeness. Consequently, it was not possible to solve the phase with this compound.

## 7. Cryo-EM

At the same time as we tried to solve the structure by crystallography, cryo-EM came out to be a very promising tool to solve structures of membrane proteins. We performed single particle cryo electron microscopy experiments in collaboration with the Martin Högbom team at Stockholm University. The optimized sample of BmrA E504A was tested for a screening step realized using a Glacios 200 KeV. The conditions screened were different concentrations of protein with ATP-Mg<sup>2+</sup>; the addition of the additive detergent 3.9 f or a substrate rhodamine 6G were tested too.

The sample composed by BmrA E504 with ATP-Mg<sup>2+</sup> showed a good homogeneity. The optimal concentration was of 5 mg/mL; it allowed to have a good amount of particles and also in a good dispersion in the grids (figure 61a). On the other hand, the sample containing the detergent 3.9 f seemed to aggregate the protein (figure 61b). Consequently, this condition was not analyzed any further. Lastly, the sample composed by BmrA E504A - ATP-Mg<sup>2+</sup> - rhodamine 6G was tested; it showed a good particles homogeneity and dispersion (figure 61c). The latter was the grid used for the data collection with the Titan 300 KeV.

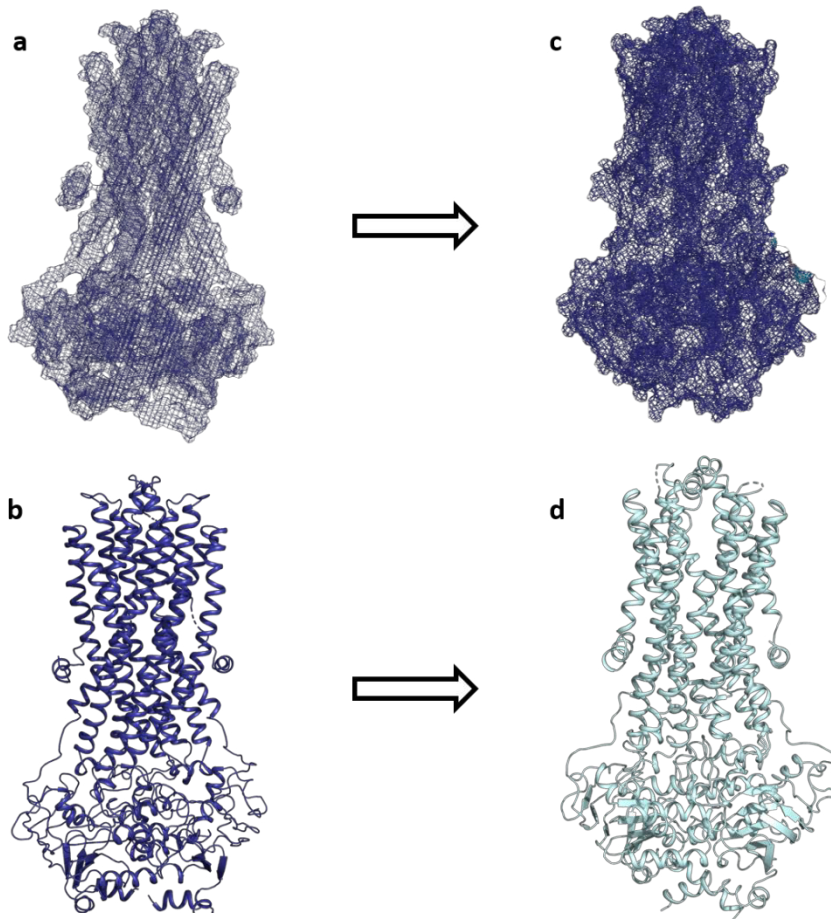


**Figure 61. Conditions screening for single particles Cryo-EM**

(a) This micrograph corresponds to the sample BmrA E504A with ATP-Mg<sup>2+</sup>. The protein is concentrated at 5 mg/mL. The red circles indicate the particles corresponding to the protein of interest. (b) This micrograph corresponds to BmrA E504A with ATP-Mg<sup>2+</sup> and the detergent additive 3.9 f. The white line measures 200 nm. (c) It is the micrograph of the sample composed by BmrA E504A with ATP-Mg<sup>2+</sup> and the rhodamine 6G. The scale bar (white line) is of 200 or 300 nm as listed.

## 8. Resolution of the structures

The first data obtained were from X-ray crystallography. They displayed a high level of anisotropy since the diffraction was of 3.9 x 4.6 x 5.2 Å resolution. Data were processed up to the highest resolution where diffraction could be detected: 3.7 Å. The statistics output by typical scaling softwares such as Aimless or xscale did not make sense as they try to scale data in shells, and there is absence of data in the highest resolution shells for BmrA dataset. The Staraniso server gives interesting statistics as it first calculates the diffraction ellipsoid and outputs anisotropic statistics. In doing so, we were able to identify that by cutting the data at 3.9 Å, we still retained 78% anisotropic completeness in the highest resolution shell. We therefore collected all the data that could be collected for this crystal. For reference, spherical completeness was only 22%. Given the fact that experimental phase determination did not work, the molecular replacement was used to solve the structure. Many models were tested as lots of structures of ABC transporters are available, and as a whole or cut in parts. The successful models were the outward-facing conformation of the ABC transporter Sav1866 and MsbA (PDB 2hyd and 3b60). The latter displayed better scores of molecular replacement solution. The group space was of P2<sub>1</sub> and there were 2 dimers in the asymmetric unit. The first step was to build a poly-Ala model to initially improve the map which was very poor (figure 62a-b). After some cycles of refinement in autoBUSTER, this poly-Ala model was then mutated back to the BmrA sequence once some features started to appear corresponding to the residues side chains. A big improvement in the statistic was observed once the TLS (Translation-Libration-Screw-rotation) were applied one on the transmembrane region (TMD) and one on the nucleotide binding domain (NBD). Some details appeared after this refinement as the density for the ATP and the break in the TM1-TM2 region. For the good placement of residues and of the ATP, the building was guided by the red and green density that appeared after a refinement step. For instance, especially the position of the ATP was the result of this iterative process. Coot and ISOLDE are the programs used for the building of the model, the second one allowed to correct clashes since it can perform local molecular dynamics guided by the map. The figures 62 c and d show the final density map and model. The final scores are R for 26% and Rfree for 32.1%. The structure has been deposited under the PDB accession code 6r72.

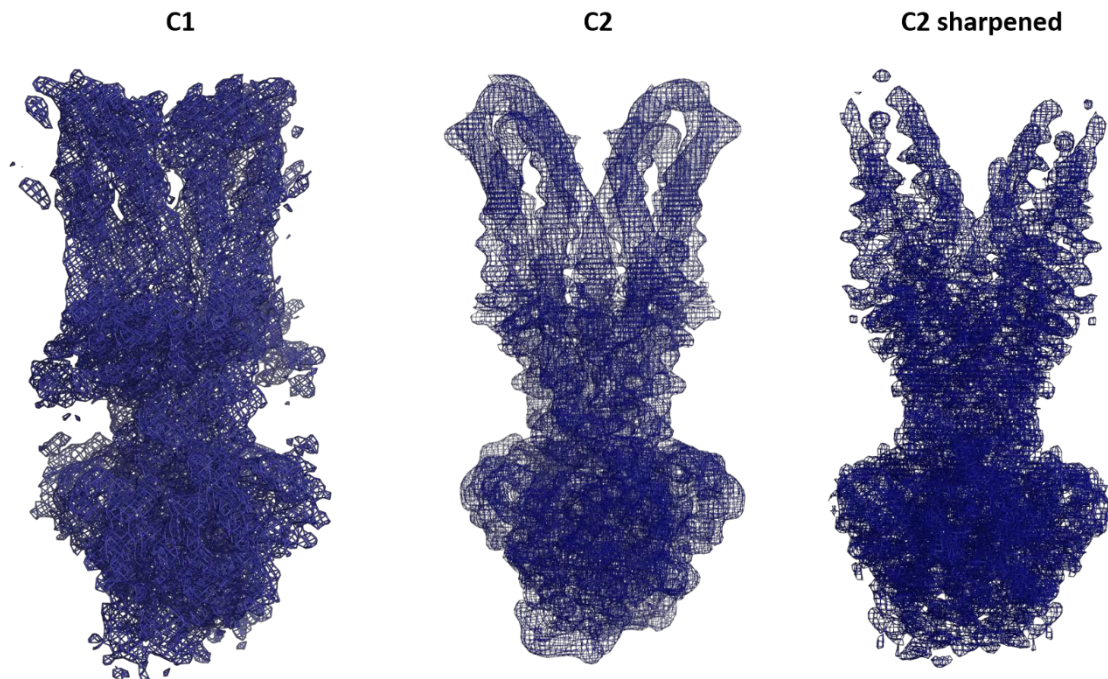


**Figure 62. Resolution of X-ray crystallography structure**

(a) Density map after the molecular replacement. (b) first model. (c) Final density map. (d) Final structure

The cryo-EM acquisition and data processing were performed by Benjamin Wiseman in Stockholm university. Two data-collection sessions were performed leading to a total of 3477 movies and 1,588,361 particles. The whole processing was performed using cryoSPARC v2. Two rounds of 2D classifications were performed before the first ab-initio 3D classification and refinement step. Two rounds of the latter were needed before the merging of the two data-collections. Lastly, a non-uniform refinement was performed to obtain the density map at 4.2 Å resolution. This map had no symmetry imposed (C1). Since BmrA is a homodimer, a C2 symmetry was applied to improve the resolution to 3.9 Å (figure 63). I used the X-ray model of BmrA available at this time to start the building in the Cryo-EM C2 density map (figure 63). Coot and ISOLDE were used as for the X-ray building. The sharpening treatment was performed on the C2 density map using Phenix which is employed for the refinement process. The NDBs part was quite noisy, to bypass this problem the information on the position of the ATP were taken from the X-ray density map. Knowing that the X-ray data process is interactive and displayed the correct position of the nucleotide. Once the model

building was finished in the C2 sharpened map, the fit was checked in the C2 without sharpening treatment and then in the C1 map. In the latter, there was an additional density on the transmembrane region which was attributed to the ligand rhodamine 6G due to its presence in the sample and confirmed by binding assays.



**Figure 63. Cryo-EM structure resolution**

*From to the left to the right, the C1 density map (no symmetry), C2 density map and then C2 sharpened density map.*



### ***Quantification of the particles for both techniques***

Interestingly, the two structures were solved at 3.9 Å resolution. We compared “for fun” how many “particles” were necessary to solve both structures.

- For the Cryo-EM model, the particles used for the *ab-initio* 3D reconstitution are:

$$\sim 1 \times 10^5 \text{ particles}$$

- For X-ray crystallography, we can calculate the amount of particles illuminated by the X-ray beam:

The space group is P2<sub>1</sub>, so each cell contains 4 BmrA homodimers

(1 homodimer = 1 particle in Cryo-EM)

Cell dimensions are 117.8 × 110.8 × 155.6 Å and 90°; 93.2°; 90°

Its volume is of 2,025,932 Å<sup>3</sup> → ~ 2 × 10<sup>6</sup> Å<sup>3</sup>

The smallest beam size used to diffract the crystal is 5 μm

Let's thus consider a crystal of 5x5x5 μm ; its volume is of 125 μm<sup>3</sup> → 1.25 × 10<sup>14</sup> Å<sup>3</sup>

$$\text{particles in this small crystal} = \frac{\text{volume of this crystal} \times \text{particles in each cell}}{\text{volume of the cell}}$$

$$\text{Particles in the crystal} = \frac{1.25 \times 10^{14} \times 4}{2 \times 10^6} = 2.5 \times 10^8 \text{ particles}$$

For X-ray crystallography, there are minimum 2.5 × 10<sup>3</sup> more particles needed to obtain the same result than in Cryo-EM experiment.

The real crystal was in reality much bigger: 200 X 50 x 50 μm. This crystal is made of 1 × 10<sup>12</sup> particles.

## 9. Highlights of the manuscript relating the analysis of the structures of BmrA

The data collected by both techniques allowed the resolution of the structure of BmrA E504A in an outward-facing conformation. The ATP-Mg<sup>2+</sup> is bound in both structures and also the cavity is open to the extracellular side. In the case of the Cryo-EM sample, the substrate rhodamine 6G is present bound in the protein in the transmembrane domain. The superposition of the two models results in 0.8 Å r.m.s.d. (without the TM1-TM2 loop), this means that they share almost the same structure. Two exceptions are present: the substrate binding and the different position for the loop between TM1 and TM2.

To investigate further these observations, two main axes were followed:

- **Comparison of BmrA structures and the others ABC transporters.**

All the structures in the same conformation are superposed. Interestingly, this reveals a common fold made of TM3-6 and the NBD, with a notable difference in the position of TM1-2 in all the structures, showing various different degree of cavity opening which could be described as a hand-fan movement (Figure 4a-e in the paper appended below). This observation could demonstrate the flexibility of the protein in the outward-facing conformation, and hints on how the cavity opening occurs during the drug release part of the mechanism.

- **Molecular dynamic simulation on BmrA structures inserted in the membrane**

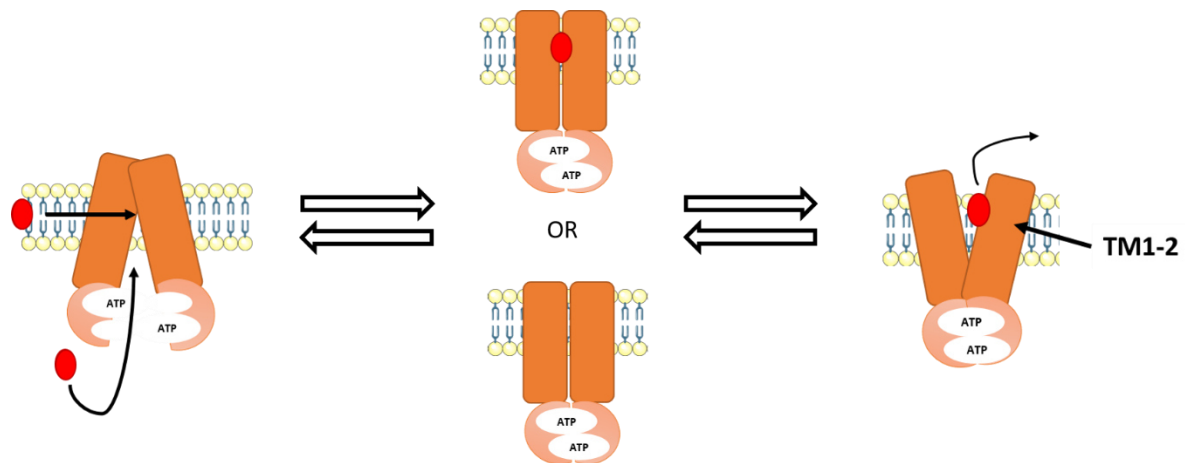
Luca Monticelli's team performed all-atom molecular dynamic simulations on both structures inserted in a lipids bilayer of POPE/POPG (3/1). Four simulations were carried out for each structure for 500 ns each. The closing movement of transmembrane domain is recorded in six out of eight cases. This conformational change occurs by an asymmetric behavior of each monomer highlighting the ability of the protein to adopt different pattern albeit its homodimer nature. Another crucial observation is that the superposition of all the structures obtained from these simulations displays also a hand-fan movement of the TM-1-2 (Figure 4f and 5 in the paper appended below).

These results describe the flexibility of ABC transporters which is linked to their ability to export different types of drug. The export of these compounds is probably possible due to the plasticity of the protein which is driven by the hydrophobicity as a force.

## 10. Conclusion

The whole information of BmrA structures, the analysis of the biological context and the molecular dynamic simulation, allowed the observation of the TM1-2 movement which could give important insight of ABC transporter mechanisms. In TM1-2 hand fan movement relays the ability of these proteins to transport different kind of molecules. Its flexibility is required to adapt the opening of the cavity for the efflux of the compound. The other main observation was the closing of the cavity once the protein was inserted in a membrane. This indicates that the protein releases the compound and then immediately goes back in occluded conformation. The mechanism (figure 64) would be the following:

- The protein is in the inward-facing conformation, it can bind a compound and the ATP-Mg<sup>2+</sup>.
- It switches to occluded conformation with the TMDs and NDBs dimerized.
- The structure deforms locally in the apex of the transporter, with a flexibility highlighted by different positions of TM1-2; the compound is released with a degree of cavity opening depending on the size of the compound. A small compound can be expelled with a small opening; a larger compound requires a larger opening.
- The cavity closes immediately after substrate release due to the hydrophobicity of the cavity.
- The nucleotides are hydrolyzed, which induces the changing of conformation back to the inward-facing conformation.



**Figure 64. Proposal of ABC transporters' mechanism with the insights discovered by this study**

Starting on the left, the protein is in inward facing conformation and it binds the ligand and the ATP. Then the protein is in occluded conformation, the ligand is in the binding cavity. The movement of the TM1-2 allows the release of the ligand. Once it is liberated, the TMs switch in occluded conformation due to the hydrophobic force of the protein cavity. The ATP hydrolysis is the next step which allow the switching in inward facing conformation.

These results open the way to other projects. The first one is a further investigation of this TM1-2 hand-fan movement, the second one is about the behavior of the protein in lipidic environment. Lastly, to determine the full mechanism of the protein other structures are needed. These projects have been started and the preliminary results are displayed in the next chapter.

## FRONT MATTER

# Title: Drug-bound and -free outward-facing structures of a multidrug ABC exporter point to a swing mechanism

**Short title: Outward-facing structures of a multidrug ABC pump**

## Authors

Vincent Chaptal<sup>1†</sup>, Veronica Zampieri<sup>1†</sup>, Benjamin Wiseman<sup>1,2†</sup>, Cédric Orelle<sup>3‡</sup>, Juliette Martin<sup>4‡</sup>, Kim-Anh Nguyen<sup>5‡</sup>, Sandrine Magnard<sup>1</sup>, Alexia Gobet<sup>1</sup>, Margot Di Cesare<sup>3</sup>, Waqas Javed<sup>3</sup>, Arnaud Kilburg<sup>1</sup>, Marine Peuchmaur<sup>6</sup>, Julien Marcoux<sup>7</sup>, Luca Monticelli<sup>4</sup>, Martin Högbom<sup>2</sup>, Jean-Michel Jault<sup>3¥</sup>, Ahcène Boumendjel<sup>5¥</sup> and Pierre Falson<sup>1\*</sup>.

## Affiliations

<sup>1</sup> Drug Resistance & Membrane Proteins group, Molecular Microbiology and Structural Biochemistry Laboratory, CNRS UMR 5086, University of Lyon, IBCP, 7, passage du Vercors, 69367 Lyon, France.

<sup>2</sup> Department of Biochemistry and Biophysics, Arrhenius Laboratories for Natural Sciences, Stockholm University, Stockholm, Sweden.

<sup>3</sup> Bacterial nucleotide-binding proteins group, Molecular Microbiology and Structural Biochemistry Laboratory, CNRS UMR 5086, University of Lyon, IBCP, 7, passage du Vercors, 69367 Lyon, France.

<sup>4</sup> Modeling Biological Macromolecules group, Molecular Microbiology and Structural Biochemistry Laboratory, CNRS UMR 5086, University of Lyon, IBCP, 7, passage du Vercors, 69367 Lyon, France.

<sup>5</sup> Laboratoire Radiopharmaceutiques Biocliniques, Faculté de Médecine de Grenoble, UMR UGA - INSERM U1039, Grenoble, France.

<sup>6</sup> University of Grenoble Alpes, CNRS, DPM UMR 5063, 38041 Grenoble, France.

<sup>7</sup> Institut de Pharmacologie et de Biologie Structurale (IPBS), UMR 5089, Université de Toulouse, CNRS, UPS, 31000 Toulouse, France.

†‡¥ Equal contributions as first (†), second (‡) and penultimate (¥) co-authors, respectively.

\* Correspondence to Pierre Falson, Drug Resistance & Membrane Proteins group, Molecular Microbiology and Structural Biochemistry Laboratory (CNRS UMR 5086), University of Lyon, IBCP, 7, passage du Vercors, 69367 Lyon, France. +33 (0) 6 46580266, [pierre.falson@univ-lyon1.fr](mailto:pierre.falson@univ-lyon1.fr).

## Abstract

Multidrug ABC transporters translocate drugs across membranes by a mechanism for which the molecular features of drug release are so far unknown. Here, we resolved two ATP-Mg<sup>2+</sup>-bound outward-facing (OF) conformations of the *Bacillus subtilis* (homodimeric) BmrA, one by X-ray crystallography without drug, and another by single-particle cryo-EM with rhodamine 6G (R6G). Two R6G molecules bind to the drug-binding cavity at the level of the outer leaflet, between transmembrane (TM) helices 1-2 of one monomer and TM5'-6' of the other. R6G induces a rearrangement of TM1-2, highlighting a flexibility that was confirmed by H/D exchange and molecular dynamics simulations. The latter also shows a fast post-release occlusion of the cavity driven by hydrophobicity. Altogether, these data support a new swing mechanism for drug transport.

### Teaser

Drug release from a multidrug efflux pump occurs through a swing mechanism driven by hydrophobicity and plasticity of the drug-binding pocket.

## MAIN TEXT

### Introduction

Multidrug ATP-Binding Cassette (ABC) exporters transport a large panel of drugs conferring a multidrug resistance (MDR) cell phenotype that leads to chemotherapy failures against pathogenic microbes and cancers. Early conceptualized (1), ABC exporters mainly switch between a high drug affinity inward-facing (IF) conformation in which the drug-binding pocket in the membrane domain is exposed to the inner membrane leaflet, and a low drug affinity OF conformation favoring drug release outside the cells. These proteins are made of two transmembrane domains (TMDs) typically built with twelve transmembrane helices and two nucleotide-binding domains (NBD). Drugs bind to the TMD, accessible from the inner membrane leaflet in the IF conformation. Two ATP molecules bind at the interface between the two nucleotide-binding domains (NBD) (2, 3), thereby stabilizing the dimer and favoring the drug occlusion that leads the reorganization of the TMD in an OF conformation (4).

Several exporter structures have been obtained (5-13), complemented with biochemical and biophysical characterizations (eg (14-16)), altogether contributing to a mechanistic understanding of the IF to OF transition. Moreover, the molecular mechanism by which structurally-divergent drugs bind to the IF conformation is presently better understood thanks to the structure of the human ABCB1 in complex with the anticancer drug taxol (14). This structure revealed that the ligand recognition is driven by the intrinsic plasticity of TM4 and TM10, required to accommodate the structure of the drug.

The question remains open as to how the structural variability of drugs is handled by those exporters to expel them and which molecular features of the protein in the OF conformation are driving this release step (17). So far, since the first structure released in 2006 (5) and almost 50 years after their discovery (18) no OF structure of a MDR ABC exporter with a bound drug has been solved. To that aim, the ATP-bound cryo-EM structure of ABCC1 in the presence of its substrate, Leukotriene C4, was resolved, however the location of the substrate was not determined (19). Previously, the crystal structure of the antibacterial peptide transporter McjD was obtained in complex with AMP-PNP and two molecules of nonyl-glucoside that were used as crystallization additive were bound in the putative drug-binding cavity (8). Interestingly, molecular dynamics simulation based on that structure predicted a marked flexibility of the TM1-2 region (20), pointing to a possible role of this region in the release of substrates. However, so far, structural information is lacking to corroborate this hypothesis, mainly due to the poor affinity of the transported substrate in the OF conformation.

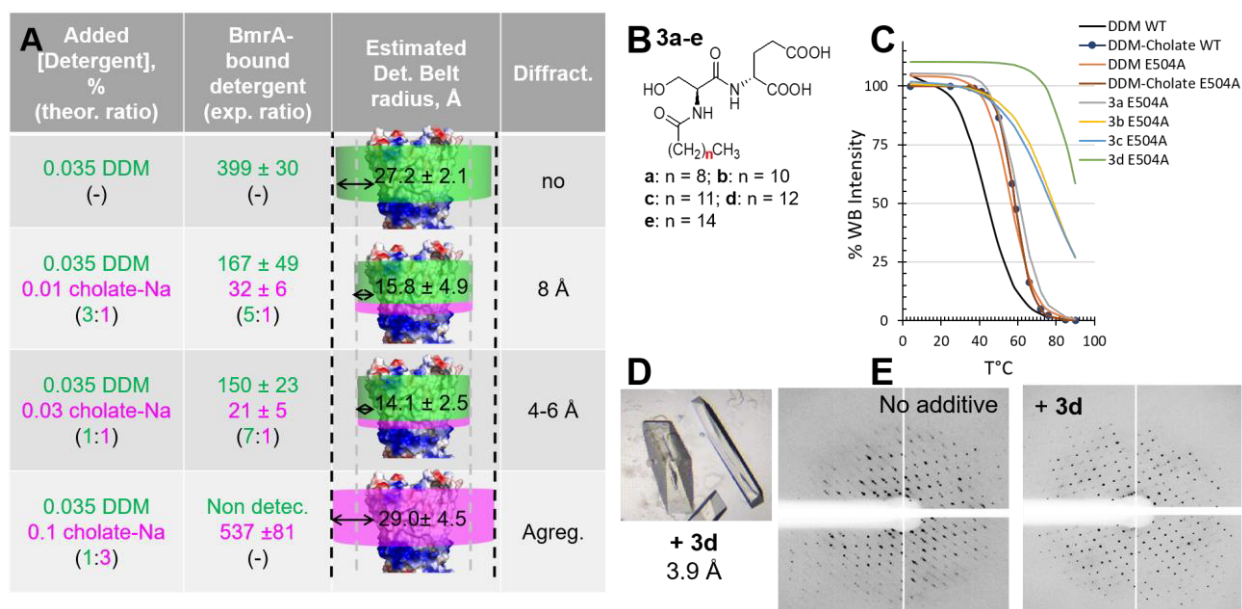
Here we tackled the question by resolving two OF conformations of BmrA, a type IV ABC transporter (21, 22) from *B. subtilis* (23) conferring resistance to cervimycin C, an antibiotic produced by

*Streptomyces tandæ* against Gram-positive bacteria (24). Using an ATPase inactive mutant, E504A (25), we resolved its X-ray structure in complex with ATP-Mg<sup>2+</sup>, which required several key steps optimization and to design specific stabilizers. We also resolved its cryo-EM structure in complex with ATP-Mg<sup>2+</sup> and rhodamine 6G, a drug commonly transported by ABC exporters (26). Comparison of these structures enlightens how the drug binds before its release and shows how the flexibility of the TM1-2 segment drives this process, and this was confirmed by H/D exchange coupled to mass spectrometry (HDX-MS) and molecular dynamics simulations.

## Results

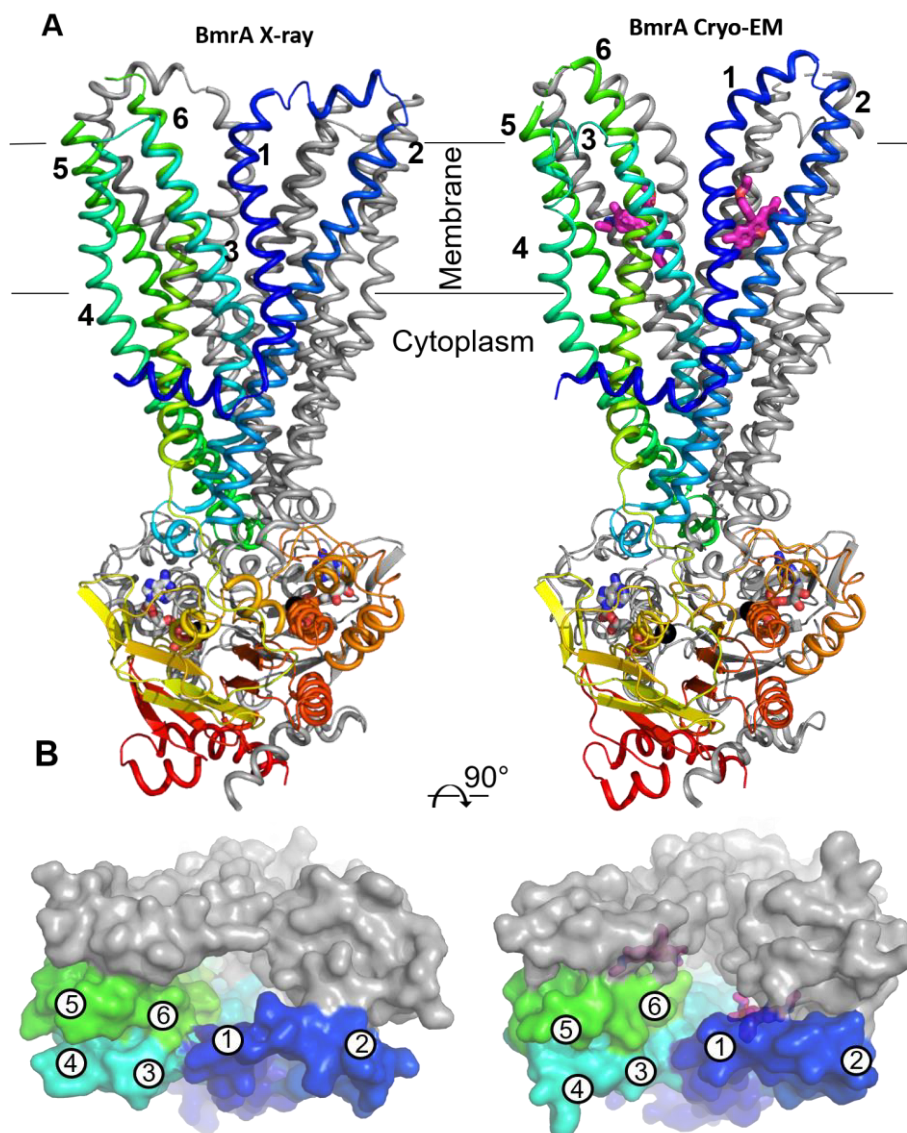
### Crystal structure of BmrA in OF conformation in complex with ATP-Mg<sup>2+</sup>.

We first stabilized BmrA in its OF conformation by introducing the E504A mutation that prevents hydrolysis of ATP (25, 27) and substrate transport (Fig. S1) as also reported for other transporters (14). The protein crystallized following the procedure set-up for the mouse P-glycoprotein, using triton X-100 for extraction and a mixture of N-dodecyl- $\beta$ -D-n-maltopyranoside (DDM) and cholate for purification (28). Quantification of detergents bound to BmrA (29) was helpful to produce high-quality crystals, as increasing cholate reduced the amount of DDM bound to BmrA up to 50% which proportionally reduced the estimated detergent-belt size (Fig. 1A). Diffraction patterns of the resulting crystals displayed a lattice-doubling problem that prevented their processing and which we overcame by designing a series of tailored amphiphiles **3a-e** (Fig. 1B; Chemistry section in Supplementary Materials) with a scaffold based on glycosyl-substituted dicarboxylates surfactants (30). Of note, these additives increase the thermal stability of BmrA up to ~30 °C for **3d** (Fig. 1C, Data set 2), which helped produce better diffracting protein crystals (Fig. 1DE).



**Figure 1. Crystallization of BmrA. (A) Quantification of detergents bound to BmrA. see Methods and Data set 1 for details. (B) Structure of the thermostabilizing amphiphilic additives. (C) Thermostabilisation of BmrA. For clarity, fits (2-3 independent assays) are displayed, with circles for the reference condition (DDM + cholate). Full data is provided in the Data set 2. (D) BmrA crystals in presence of 3d. (E) Lattice problem resolution with 3d.**

We reached 3.9 Å resolution for the BmrA E504A-ATP-Mg<sup>2+</sup> complex (Fig. 2, left panels; Figs. S2-S3, Table S1). Two dimers of BmrA were found in the asymmetric unit, with a r.m.s.d. of 0.7 Å over 525 residues (Fig. S2). The structure displays the characteristic type-IV fold of ABC transporters (21), in which the NBDs bind two ATP-Mg<sup>2+</sup> in a head-to-tail mode, freezing the BmrA-E504A mutant in complex with ATP-Mg<sup>2+</sup> in a typical OF conformation. The E504A mutation stabilizes the efflux pump in an OF pre-hydrolytic state, similar to the one displayed by the wild-type (WT) BmrA trapped in the transition state for ATP hydrolysis in the presence of vanadate (31). The extracellular side of BmrA displays an opening to a cavity likely corresponding to the drug-exit path. Importantly in the context of this study, the crystal structure shows that the loop connecting TM1 to TM2 is stabilized by few crystal contacts between half of the monomers (Fig. S2B-D), while the other half remains free of movement. All the loops nevertheless distribute around similar positions showing both the correctness of this position and the flexibility of this region (Fig. S2E).



**Figure 2.** X-ray and cryo-EM structures of the BmrA E504A mutant in complex with ATP-Mg<sup>2+</sup> and R6G. (A) Cartoons of the transporter, normal to the plane of the membrane. One monomer is in grey and the other one is rainbow colored. TM helices are numbered for the colored monomer. ATP and R6G are displayed as



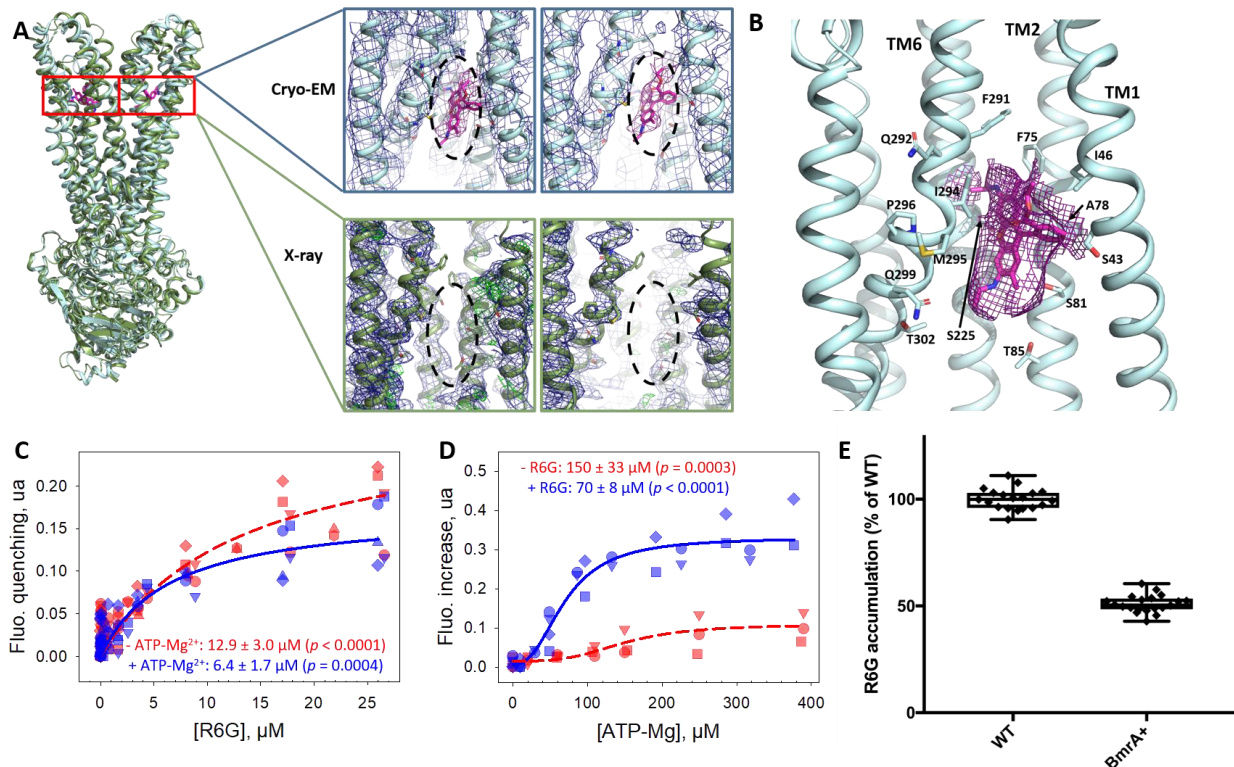
*sticks colored by atom type and Mg<sup>2+</sup> as black sphere. (B) Surface representation of BmrA viewed from the extracellular side to highlight the difference in the OF cavity.*

### **Cryo-EM structure of BmrA in the OF conformation in complex with R6G and ATP-Mg<sup>2+</sup>.**

Incubating BmrA with known ligands (23) gave the best crystals with R6G, which we could however not optimize beyond 5 Å (Fig. S4). This led us to move to single-particle cryo-EM (Fig. 2, Fig. S5) that allowed to build the structure using the highest resolution map using C2 symmetry. Refinement up to 3.9 Å was carried out using both sharpened and unsharpened maps, as the former lost details on the TM1-TM2 hinge movement (Fig. S6-S8). The resulting fold is very similar to that of the crystal structure with the difference in conformation of the region TM1-2 where TM1 is shifted towards TM2, resulting in a more pronounced opening of the cavity (Fig. 2B, Table S1).

We observed two additional densities in the cryo-EM density map (Fig. 3AB), seen more clearly without the application of symmetry. R6G, cholate or the polar head of DDM could be positioned in these densities, although in the case of the last two no equivalent densities was observed in the X-ray map. We therefore carried out a series of biochemical assays with the WT and E504 mutant to discriminate between these possible ligands. Both proteins were purified in DDM or DDM-cholate, followed by a reconstitution into nanodiscs (32), on which we probed the binding of the three compounds. We observed by intrinsic fluorescence that R6G binds to BmrA E504A purified in DDM/cholate with a 2-fold higher affinity when ATP-Mg<sup>2+</sup> is present (Fig. 3C). The reverse effect was also observed, ATP-Mg<sup>2+</sup> binding with 2-fold higher affinity when R6G is added (Fig. 3D). When purified in DDM, both WT and mutant BmrA displayed similar affinity for R6G ( $4.8 \pm 0.9$  and  $3.3 \pm 0.7$   $\mu\text{M}$ ,  $p < 0.0001$ ), while specific interaction could be detected neither with cholate (Fig. S9A) nor DDM (or decyl maltoside at higher concentrations), on BmrA-nanodiscs complexes (Fig. S9B). On the contrary, R6G bound to the same complexes with affinities as high as  $\sim 0.07 \pm 0.09$   $\mu\text{M}$  ( $p = 0.4$ ) and  $\sim 0.03 \pm 0.02$   $\mu\text{M}$  ( $p = 0.1$ ) for WT and mutant, respectively. Of note, R6G binds to nanodiscs themselves with an affinity of 3-7  $\mu\text{M}$  (Fig. S9CD). These results indicate that cholate and DDM do not bind to the drug-binding site of BmrA in contrast to R6G, which binds in the sub-micromolar to micromolar range depending on the local environment. This led us to assume that this density reveals the occupancy of R6G, as displayed in Fig. 2 and Fig. 3. Finally, we evaluated the capacity of BmrA to transport R6G by quantifying the intracellular R6G level in a *B. subtilis* strain overexpressing BmrA (24) (BmrA+) compared to the parent strain, upon incubation with the dye (Fig. 3E). We observed that R6G accumulates  $\sim 50\%$  less in the former strain supporting that R6G is indeed exported by BmrA out of the bacteria.

The two R6G molecules bind at the level of the outward leaflet, between TM1-2 of one monomer, and TM5'-6' of the other one. They are maintained in the cavities by a movement of TM1 towards TM2, resulting in a capped hydrophobic space sealed by residues I46, F75, L258', M259' and F291'. Several of these residues correspond to those found in the taxol-binding pocket of human ABCB1 (14) (Fig. S10).

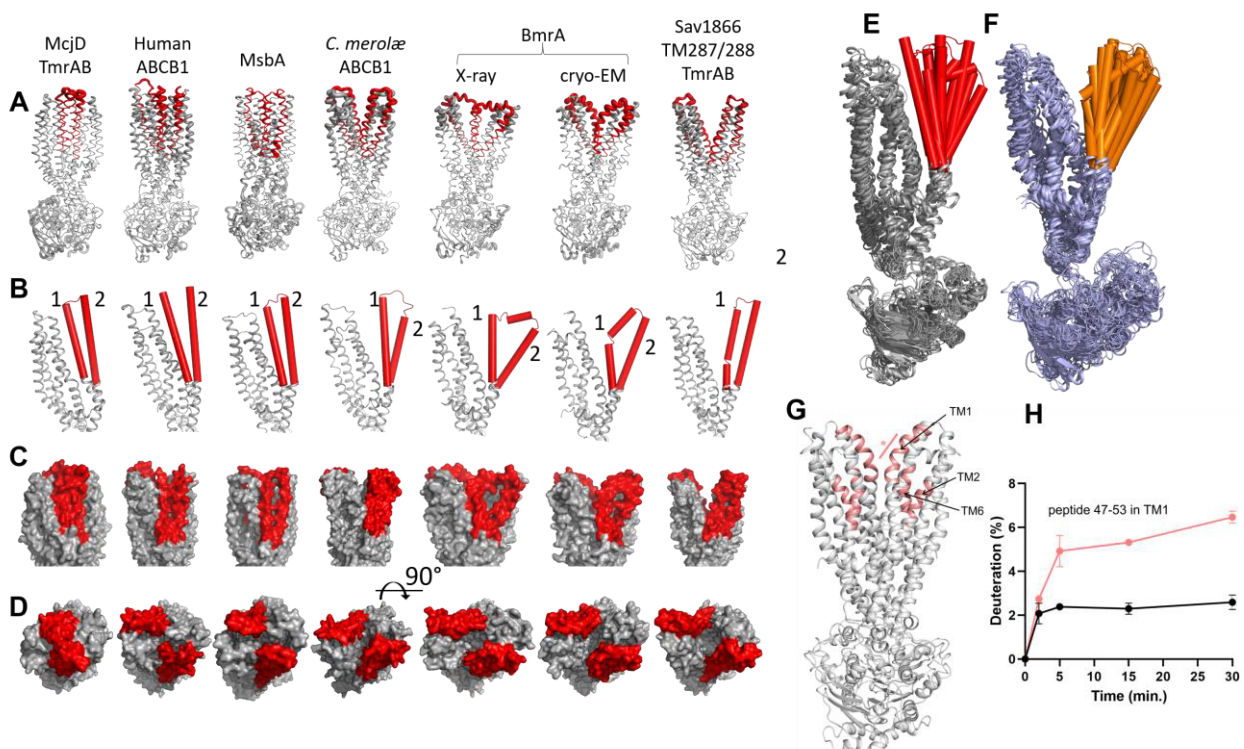


**Figure 3. Rhodamine 6G in the cryo-EM structure of *BmrA* E504A mutant in complex with ATP-Mg<sup>2+</sup> and its effect on *BmrA* activity. (A) Superposition of the X-ray and cryo-EM structures and zoom in the two R6G-binding sites in the cryo-EM structure compared to the X-ray structure. Density maps are shown in blue and green, respectively. R6G structure and density are in magenta. (B) Detail of one R6G-binding site. (C) Binding of R6G on *BmrA* E504A/DDM-cholate, with (blue) or without (red) 5 mM ATP-Mg<sup>2+</sup> probed by intrinsic fluorescence. Symbols correspond to 4 independent experiments, fitted with equation 1. (D) Binding of ATP-Mg<sup>2+</sup> with (blue) or without (red) 100 μM R6G on *BmrA* E504A/DDM-cholate probed by intrinsic fluorescence. Symbols correspond to 3-4 independent experiments, fitted with equation 2. (E) R6G accumulation in *B. subtilis* strains 168 (WT) and 8R, a mutant of *B. subtilis* 168 strain overexpressing *BmrA* (*BmrA*<sup>+</sup>), probed by fluorescence. Cells incubated with 5 μM R6G for 30 min at 37 °C were then washed, lysed, and their intracellular R6G content probed by fluorescence on supernatants, taking as reference the WT strain. Data are the average of 3 independent 3-10 replicates ( $p < 10^{-10}$ ).**

### Structural differences between the X-ray and cryo-EM structures of *BmrA* highlight the mobility of the TM1-TM2 region.

Although quite similar, the X-ray and Cryo-EM structures of *BmrA* display important local differences rendering the drug-exit path significantly different between them (Fig. 2). The differences originate from a displacement of the TM1-2 region, in the proximity of a kink starting in TM1 at residue P47, towards the end of TM1. Such displacement allows the central part of TM1 to shift from TM3 in the X-ray structure towards TM2 in the cryo-EM structure. These differences between structures solved under nearly identical conditions highlight a major local plasticity at the level of TM1-2. To evaluate its functional relevance, we compared these structures with those of previously resolved nucleotide-bound type IV ABC transporters: *E. coli* McjD (8, 11), *T. thermophilus* TmrAB (13), human (4) and *C. merolae* (15) ABCB1, *E. coli* MsbA (16), *S. aureus* Sav1866 (5), and *T. maritima* TM287/288 (33). We tentatively ranged them from the most occluded to the widest open (Fig. 4A-E). This showed that TM1 in the X-ray structure of *BmrA* is oriented similarly as in McjD, ABCB1 and MsbA while TM2 is shifted towards the OF conformation typically observed as in Sav1866. The loop connecting TM1 and TM2 has unwound on each side, allowing and/or accompanying the movement of TM2. In the cryo-EM

structure, a consecutive displacement of TM1 shifting towards TM2 is seen, with an unwinding that takes place downward on TM1. The most open structures of Sav1866 and TM287/288 show TM1 and TM2 segments close together and separated from those forming the TM3-6 core. This motion of TM1-2 is concomitant with a wide opening of the cavity and a physical separation of the two TM3-6 cores that behave as rigid bodies. The movement would be granted by the intrinsic flexibility of ABC transporters on their external side, as hinted by the B-factors displayed in Fig. 4A. Superposing the topologically conserved regions encompassing TM3-6 core and NBD of all structures allowed to visualize the wide range of conformations of TM1-2, suggesting a hand fan motion (Fig. 4E). We could reproduce such amplitude by molecular dynamics on the present BmrA structures (Fig. 4F and detailed in the next section below). Finally, we confirmed the functional mobility of TM1-2 by probing the structural dynamics of the WT BmrA reconstituted in nanodiscs by HDX-MS experiments. We sought to identify the transmembrane regions that display an increased accessibility/flexibility when



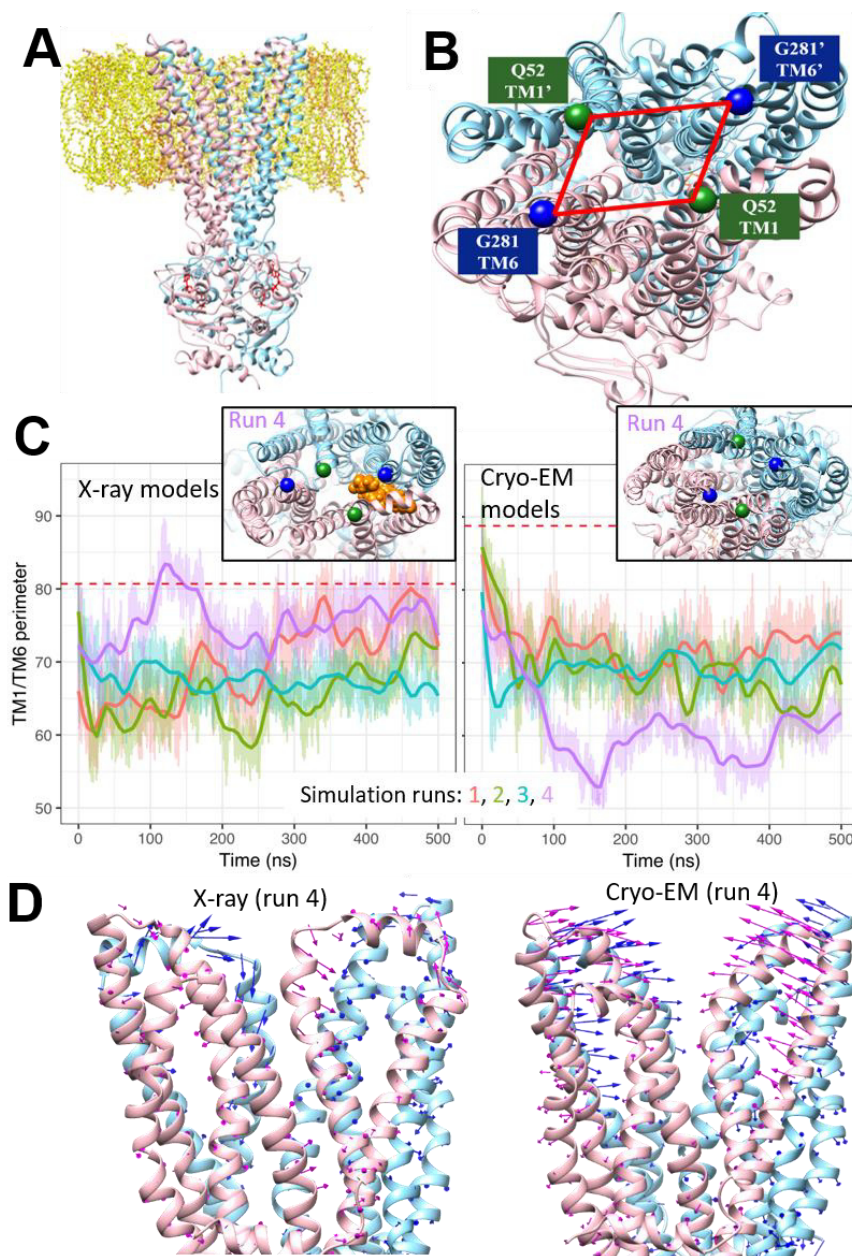
**Figure 4. TM1-2 positions and mobility in OF BmrA and other type IV ABC transporters. (A-D) Views (PDB codes) of McjD (4pl0, 5ofr), TmrAB (left: 6rai, 6rak; right: 6rah-6raj), human (6c0v) and *C. merolae* ABCB1 (6a6m), MsbA (5ttt), BmrA (this study), Sav1866 (2hyd) and TM287/288 (6qv0, 6qv1, 6qv2), superimposed from TM3 to TM6 and displayed from left to right from the most occluded to the widest open conformation. Cartoon thickness in panel A is proportional to B-factor. Structures are colored in grey with TM1-2 in red. (B) Close-up view of TM1-6 of each monomer and of the N-terminal half of ABCB1 with the TM1-2 segment in red cylinders. (C) View as in panel B displayed in surface. (D) View of the external side. (E) Superimposition of the different structures shown in A. (F) Molecular dynamic simulations of BmrA as detailed in Fig. 5 and corresponding section. (G, H) HDX-MS experiment of WT BmrA reconstituted in nanodiscs. Data were recorded after 15 min  $D_2O$  exchange and only the transmembrane peptides with increased deuterium uptake in the Vi-trapped conformation as compared to the apo state are shown (salmon color,  $p < 0.01$ ). The star indicates the position of the peptide 47-53 for which the deuterium uptake is plotted as a function of time in panel H, either in the Vi-trapped (salmon) or apo (black) states.**

transitioning to the OF state, using BmrA either in its apo state or stabilized in its OF conformation upon vanadate-induced (Vi) nucleotide trapping (Fig. S11 and Fig. 4GH). We observed only a few transmembrane peptides that display a significantly higher deuterium uptake in the OF conformation stabilized by Vi-trapping, all localized in TM1, TM2 and TM6 (Fig. 4G). This is exemplified by the peptide 47-53 (shown by a star in panel H). Altogether, these results are consistent with the mechanical

plasticity of TM1-2 inferred from the X-ray and cryo-EM structures of BmrA, which looks like a key-feature of MDR pumps allowing the release of substrates varying in size and shape.

### **Molecular dynamics simulations of X-ray and cryo-EM structures of BmrA.**

In order to get a dynamic view of the drug-exit site of BmrA, we performed all-atom molecular dynamics simulations on the present (drug-less) X-ray and cryo-EM ATP-Mg<sup>2+</sup> bound structures, reconstituted in a POPE/POPG (3/1) lipid bilayer (Fig. 5A). Hence, we carried out four simulations of 500 ns on each structure in identical conditions using different starting velocities. We got an estimation of the size of the drug-exit cavity by measuring the variation with time of the perimeter formed by the C- $\alpha$  of residues Q52<sub>TM1</sub> and G281<sub>TM6</sub> of each monomer (Fig. 5BC). As shown, the initial perimeter of the cryo-EM structure, up to 90 Å, was larger than that of the X-ray one, up to 80 Å. Considering the simulation settings and the limited resolution of the structures we expected to observe only changes driven by strong forces. All the models undergo a closure (Fig. 5C, Fig. S12), reaching a common perimeter of ~70 Å. BmrA shifts towards the most occluded states, as the one observed in MsbA and ABCB1 in Fig. 4. This closure is rapid, generally occurring within the initial 100 ns, as also proposed for the extracellular gate of TmrAB (13), and followed by large-scale structural fluctuations (Fig. 5D, Fig. S13). Of note, a closure was also obtained in simulations with longer equilibration steps (not shown). An unexpected and interesting result came from the fourth simulation generated from the X-ray structure that, by contrast to the others, rapidly opened its drug exit cavity up to ~80 Å. This specific behavior allowed a lipid to bind between TM1-2 and 6 (left inset Fig. 5c) in a location close to that seen for rhodamine 6G, which highlights the hydrophobic nature of the ligand.



**Figure 5. Dynamics of BmrA TMD region. (A) Starting model of BmrA inserted in a lipid bilayer. Chains A and B are colored in pink and cyan, ATP in red and lipids in yellow. (B) Close-up view showing the distance measured between residues Q52(TM1) - G281(TM6) - Q52'(TM1)' - G281'(TM6)'. (C) Time-evolution of the (Q52-G281-Q52'-G281') distance for each of the four simulations from X-ray and cryo-EM models. Red dashed lines indicate the initial values of the distances. Insets display snapshots of each run 4, taken at T = 336 ns and 370 ns, respectively, with on the left a lipid in orange bound to the drug-binding pocket. (D) Displacement of each C- $\alpha$  of each monomer A (pink) and B (blue) from initial X-ray (left) and cryo-EM (right) structures from the average structures.**

## Discussion

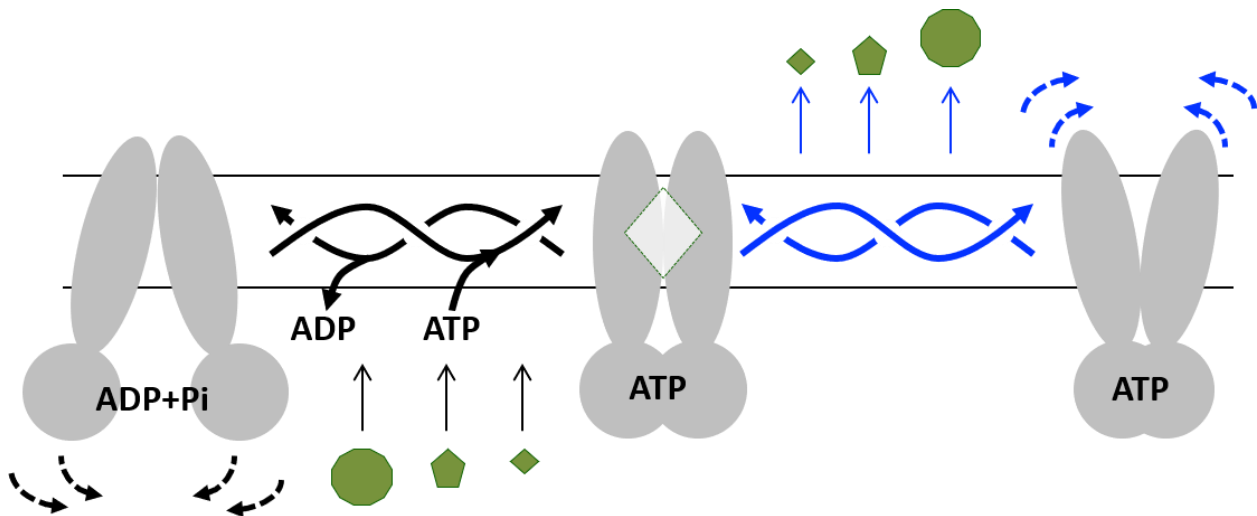
The two BmrA structures presented here are the missing link in the landscape of structures of multidrug ABC transporters resolved in OF conformations and one of them reveals for the first time a structure of a type IV MDR ABC transporter with its transported substrate in a drug-release competent state. The R6G molecules are located at the level of the outer leaflet and are poised to be released from the transporter. Several parameters have contributed to stabilize this ternary complex, among

them the positive effect of R6G and ATP-Mg<sup>2+</sup> on their mutual affinities. The present structures reveal a drug-release site made of flexible and rigid transmembrane helices, TM1-2 and TM3-6, respectively. Combined with HDX-MS and molecular dynamics simulations, they provide new information on the mechanism of drug release from the drug-binding pocket and show how the transporter resets to an occluded conformation by closing back on itself immediately after drug release. The flexibility of multidrug ABC transporters has been well established in IF states, sampling different conformations that facilitate recognition of multiple compounds (31, 34, 35). The current study reveals that such a flexibility is also sampled in OF conformations, possibly with a lower amplitude. We propose that this flexibility is required to adapt the site to various substrates' sizes, essential to secure their release to the extracellular side, and also to reset the transporter back to an occluded state, thereby preventing any trans-inhibition mechanism as reported recently (36). Such flexibility is also consistent with the fast dynamics of the extracellular gate of TM287/288 observed in EPR experiments (37) and suggests that no additional energy input is needed for drug release.

A key point arises when comparing the fast closure revealed by the simulations with the stabilized outward states observed in both X-ray and cryo-EM structures. A similar flexibility of the external part of the transmembrane segments is observed in the structures and simulations. In the case of experimental structures, the hydrophobic nature of the substrate cavity together with the accessibility to water favor its filling with amphipathic detergents as seen previously (29), which stabilize these OF conformations. Although detergent molecules are too mobile and flexible to be observed at these resolutions, they do however constitute excellent tools to capture such transient states. In the case of simulations in lipid membrane, the hydrophobic pocket is exposed to water, which is extremely unfavorable and leads to a rapid motion of TM1-2 that closes the pocket to shield it from water. This motion appears sufficient *per se* to reset the transporter back to an occluded conformation. The hydrophobicity of the drug-binding pocket is so important that in one simulation a single lipid molecule moved into the cavity (Fig. 5C), causing the cavity to remain open. This result fits well with the presence of a detergent molecule in the binding pocket of McjD (8) together with the very recent discovery of a lipid inside the structure of the Major Facilitator Superfamily protein LrmP (38). Altogether, this data highlights the hydrophobicity of the drug-binding pocket as the main driving force for the closing movement, independently of any ATP hydrolysis.

These findings lead us to reexamine the transport mechanism, often depicted as a cycle with a deterministic set of conformations that the transporter goes through to finally come back to its initial state. Rather, we propose a swing mechanism (Figure ) that relies on the flexibility of both the IF and OF conformations. The intrinsic flexibility of the exporter in the IF state allows it to sample multiple conformations. This grants the accommodation of a wide array of chemically unrelated drugs, the hallmark of multidrug transporters. Binding of ATP leads to the occluded conformation, concomitant with the plastic deformation of the outward-most part of the exporter, resulting in drug release. Here, this OF plasticity is beneficial for the release of multiple types of substrates. Hydrophobicity of the substrate binding pocket then triggers the closing of the transporter, without energy input, leading to the hypothesis that ATP hydrolysis occurs after drug release, as already proposed (19). The exporter thus swings back towards the IF conformation, ready for another swing. Playing together, intrinsic

plasticity and hydrophobicity of the substrate binding pocket alleviate the need for precisely defined steps for transport.



**Figure 6. Swing mechanism of efflux.** Left: IF conformation of the transporter displaying flexibility at the NBD level, with thus different degrees of opening of the substrate-binding cavity (black dotted arrows) and allowing for diverse shape and size of substrates. Middle: Occluded conformation. Right: OF substrate-release conformation. Release occurs via a plastic deformation of the external part of the transmembrane region. Deformation of the apex is adapted to the size or chemical property of the substrates (blue dotted arrows). Hydrophobicity of the drug-binding pocket triggers the immediate closing of the external part of the transporter, which swings back to the occluded state. ATP hydrolysis occurs followed by ADP and Pi release resulting in the opening in the IF conformation again, ready for another swing. Twisted arrows exemplify the different routes the transporter can take to reach any conformation, granted by the local deformability of the transmembrane helices.

## Materials and Methods

included in the Supplementary Materials.

## References

1. O. Jardetzky, Simple allosteric model for membrane pumps. *Nature* **211**, 969-970 (1966).
2. K. Linton, C. Higgins, Structure and function of ABC transporters: the ATP switch provides flexible control. *Pflügers Archiv European Journal of Physiology* **453**, 555-567 (2007).
3. K. P. Locher, Mechanistic diversity in ATP-binding cassette (ABC) transporters. *Nature Structural & Molecular Biology* **23**, 487 (2016).
4. Y. Kim, J. Chen, Molecular structure of human P-glycoprotein in the ATP-bound, outward-facing conformation. *Science* **359**, 915-919 (2018).
5. R. J. Dawson, K. P. Locher, Structure of a bacterial multidrug ABC transporter. *Nature* **443**, 180-185 (2006).

6. A. Ward, C. L. Reyes, J. Yu, C. B. Roth, G. Chang, Flexibility in the ABC transporter MsbA: Alternating access with a twist. *Proceedings of the National Academy of Sciences* **104**, 19005-19010 (2007).
7. A. B. Ward *et al.*, Structures of P-glycoprotein reveal its conformational flexibility and an epitope on the nucleotide-binding domain. *Proceedings of the National Academy of Sciences of the United States of America* **110**, 13386-13391 (2013).
8. H. G. Choudhury *et al.*, Structure of an antibacterial peptide ATP-binding cassette transporter in a novel outward occluded state. *Proceedings of the National Academy of Sciences* **111**, 9145-9150 (2014).
9. A. Blees *et al.*, Structure of the human MHC-I peptide-loading complex. *Nature* **551**, 525 (2017).
10. Z. L. Johnson, J. Chen, Structural Basis of Substrate Recognition by the Multidrug Resistance Protein MRP1. *Cell* **168**, 1075-1085.e1079 (2017).
11. K. Bountra *et al.*, Structural basis for antibacterial peptide self-immunity by the bacterial ABC transporter McjD. *EMBO J* **36**, 3062-3079 (2017).
12. H. Goddeke *et al.*, Atomistic Mechanism of Large-Scale Conformational Transition in a Heterodimeric ABC Exporter. *J Am Chem Soc* **140**, 4543-4551 (2018).
13. S. Hofmann *et al.*, Conformation space of a heterodimeric ABC exporter under turnover conditions. *Nature* **571**, 580-583 (2019).
14. A. Alam, J. Kowal, E. Broude, I. Roninson, K. P. Locher, Structural insight into substrate and inhibitor discrimination by human P-glycoprotein. *Science* **363**, 753-756 (2019).
15. A. Kodan *et al.*, Inward- and outward-facing X-ray crystal structures of homodimeric P-glycoprotein CmABCB1. *Nat Commun* **10**, 88 (2019).
16. W. Mi *et al.*, Structural basis of MsbA-mediated lipopolysaccharide transport. *Nature* **549**, 233-237 (2017).
17. O. Lewinson, C. Orelle, M. A. Seeger, Structures of ABC transporters: handle with care. *FEBS Lett*, (2020).
18. R. L. Juliano, V. Ling, A surface glycoprotein modulating drug permeability in Chinese hamster ovary cell mutants. *Biochim Biophys Acta* **455**, 152-162 (1976).
19. Z. L. Johnson, J. Chen, ATP Binding Enables Substrate Release from Multidrug Resistance Protein 1. *Cell* **172**, 81-89.e10 (2018).
20. R. X. Gu *et al.*, Conformational Changes of the Antibacterial Peptide ATP Binding Cassette Transporter McjD Revealed by Molecular Dynamics Simulations. *Biochemistry* **54**, 5989-5998 (2015).
21. C. Thomas, R. Tampé, Structural and Mechanistic Principles of ABC Transporters. *Annu Rev Biochem* **89**, 605-636 (2020).
22. C. Thomas *et al.*, Structural and functional diversity calls for a new classification of ABC transporters. *FEBS Lett*, (2020).



23. E. Steinfels *et al.*, Characterization of YvcC (BmrA), a multidrug ABC transporter constitutively expressed in *Bacillus subtilis*. *Biochemistry* **43**, 7491-7502 (2004).
24. H. Krügel *et al.*, Cervimycin C resistance in *Bacillus subtilis* is due to a promoter up-mutation and increased mRNA stability of the constitutive ABC-transporter gene bmrA. *FEMS Microbiology Letters* **313**, 155-163 (2010).
25. C. Orelle, O. Dalmas, P. Gros, A. Di Pietro, J. M. Jault, The conserved glutamate residue adjacent to the Walker-B motif is the catalytic base for ATP hydrolysis in the ATP-binding cassette transporter BmrA. *J Biol Chem* **278**, 47002-47008 (2003).
26. S. Nim *et al.*, Atomic modelling and systematic mutagenesis identify residues in multiple drug binding sites that are essential for drug resistance in the major *Candida* transporter Cdr1. *Biochimica et Biophysica Acta (BBA) - Biomembranes* **1858**, 2858-2870 (2016).
27. C. Orelle *et al.*, Conformational Change Induced by ATP Binding in the Multidrug ATP-Binding Cassette Transporter BmrA. *Biochemistry* **47**, 2404-2412 (2008).
28. S. G. Aller *et al.*, Structure of P-glycoprotein reveals a molecular basis for poly-specific drug binding. *Science* **323**, 1718-1722 (2009).
29. V. Chaptal *et al.*, Quantification of Detergents Complexed with Membrane Proteins. *Sci Rep* **7**, 41751 (2017).
30. K. A. Nguyen *et al.*, Glycosyl-Substituted Dicarboxylates as Detergents for the Extraction, Overstabilization, and Crystallization of Membrane Proteins. *Angew Chem Int Ed Engl* **57**, 2948-2952 (2018).
31. D. Lacabanne *et al.*, Flexible-to-rigid transition is central for substrate transport in the ABC transporter BmrA from *Bacillus subtilis*. *Commun Biol* **2**, 149 (2019).
32. I. G. Denisov, Y. V. Grinkova, A. A. Lazarides, S. G. Sligar, Directed Self-Assembly of Monodisperse Phospholipid Bilayer Nanodiscs with Controlled Size. *Journal of the American Chemical Society* **126**, 3477-3487 (2004).
33. C. A. J. Hutter *et al.*, The extracellular gate shapes the energy profile of an ABC exporter. *Nature Communications* **10**, 2260 (2019).
34. S. Mehmood, C. Domene, E. Forest, J. M. Jault, Dynamics of a bacterial multidrug ABC transporter in the inward- and outward-facing conformations. *Proceedings of the National Academy of Sciences of the United States of America* **109**, 10832-10836 (2012).
35. P. C. Wen, B. Verhalen, S. Wilkens, H. S. McHaourab, E. Tajkhorshid, On the origin of large flexibility of P-glycoprotein in the inward-facing state. *J Biol Chem* **288**, 19211-19220 (2013).
36. K. Barth *et al.*, Conformational Coupling and trans-Inhibition in the Human Antigen Transporter Ortholog TmrAB Resolved with Dipolar EPR Spectroscopy. *J Am Chem Soc* **140**, 4527-4533 (2018).
37. M. H. Timachi *et al.*, Exploring conformational equilibria of a heterodimeric ABC transporter. *Elife* **6**, e20236 (2017).

38. V. Debruycker *et al.*, An embedded lipid in the multidrug transporter LmrP suggests a mechanism for polyspecificity. *Nat Struct Mol Biol* **27**, 829-835 (2020).

### Acknowledgments

**General:** We thank Pr. Klaas Martin Pos for the gift of the CD43(DE3) $\Delta$ *AcrB* *E. coli* strain and Pr. Hans Krügel for those of *B. subtilis* 168 and 8R. We thank Dr. Lorena Martinez for her input in the BmrA purification process in introducing the cholate-DDM mixture. We thank Synchrotron SOLEIL and ESRF staffs, the crystallogenes platform from SFR Bioscience UMS 3444 and IBCP. We thank Drs. Clemens Von Rhein and Pierre Legrand for their help in anisotropic data processing. Cryo-EM sample screening, optimization and data collection was performed at the Cryo-EM Swedish National Facility in Stockholm, Sweden, funded by the Knut and Alice Wallenberg, Family Erling Persson and Kempe Foundations, SciLifeLab, Stockholm University, and Umeå University. BW especially thanks Marta Carroni and Julian Conrad from the Swedish National Facility in Stockholm for their technical assistance in Cryo-EM data collection

**Funding:** This work was supported by the *Centre National de la Recherche Scientifique* (CNRS), *l'Institut National de la Santé et de la Recherche Médicale* (INSERM), Lyon University, Grenoble-Alpes University, the French Research Agency (ANR), and Auvergne-Rhône-Alpes region (ARC1) as follows: ARC1-CLAMP # 13 009802 01 to AB, VC and PF; ANR-CLAMP-13-BSV5-0001-01 to PF, AB, VC and AK; ANR-NMX-14-CE09-0024-03 to PF, J-MJ and VC; ANR-CAVEOTANK-17-CE11-0015-03 to PF and VC; ANR-CLAMP2- 18-CE11-0002-01 to PF, AB, MH and VC; ANR-17-EURE-0003 (CBH-EUR-GS) to AB and MP; ANR-19-CE11-0023-01 to CO, VC, J-MJ and PF. Molecular dynamics calculations were carried out at CINES, GENCI grant A0040710138 to LM. Financial support was also provided to MH by the Swedish Research Council (2017-04018) and the Knut and Alice Wallenberg Foundation (2017.0275). AK and VZ PhDs were funded by ARC1 and EDISS school, respectively. K-AN PhD was funded by EDCSV of Grenoble-Alpes University. BW postdoc was funded by the ANR projects CAVEOTANK and CLAMP2. The HDX-MS experiments were supported by the French Ministry of Research (Investissements d'Avenir Program, Proteomics French Infrastructure, ANR-10-INBS-08), the Fonds Européens de Développement Régional Toulouse Métropole and the Région Midi-Pyrénées.

**Author contributions:** VC, VZ, AK and SM purified BmrA and carried out the crystallogenes experiments. MH granted access to cryo-EM equipment and BW carried out the cryo-EM experiments. VZ, VC and PF carried out the detergent quantifications. VC, VZ and BW resolved the structures. CO and VZ prepared the E504A mutant and carried out the transport and ATPase assays. AB and PF conceived the crystallization additives and KAN, MP, AB synthesized them. SM and PF carried out the thermostability assays. JMartin and LM carried out the dynamic simulations. WJ, MDC and JMarcoux performed the HDX-MS experiments which were supervised by J-MJ and CO. J-MJ and CO contributed to the analysis of the results. VZ, AG, MdC, SM, CO, J-MJ, VC and PF carried out the biochemical experiments. PF managed the overall project. The manuscript was written through contributions of all authors who gave their approval to its final version.

**Competing interests:** Crystallization additives are patented under the French patent n° 1751922 deposited 09/03/2017 and can be requested for research only. The authors declare no other competing interests.

**Data and materials availability:** Crystal and cryo-EM structures of BmrA-E504A have been deposited in the Protein Data Bank and Electron Microscopy Data Bank with the following codes, PDB 6r72, 6r81 and EMD-4749 (C2 symmetry), and PDB 7BG4 and EMD-12170 (no symmetry, with R6G).

The HDX-MS data have been deposited to the ProteomeXchange Consortium via the PRIDE partner repository (38) with the data set identifier PXD022185. All data is available in the main text and the supplementary materials.

## **Supplementary Materials**

Materials and Methods

Figures S1-S13

Tables S1

External Data set S1, S2

Evaluation structure reports VR1-3

advances.sciencemag.org/cgi/content/full/sciadv.[ms.no.]/DC1

## Supplementary Materials for

### **Drug-bound and -free outward-facing structures of a multidrug ABC exporter point to a swing mechanism**

Vincent Chaptal<sup>†</sup>, Veronica Zampieri<sup>†</sup>, Benjamin Wiseman<sup>†</sup>, Cédric Orelle<sup>‡</sup>, Juliette Martin<sup>‡</sup>, Kim-Anh Nguyen<sup>‡</sup>, Sandrine Magnard, Alexia Gobet, Margot Di Cesare, Waqas Javed, Arnaud Kilburg, Marine Peuchmaur, Julien Marcoux, Luca Monticelli, Martin Högbom, Jean-Michel Jault<sup>¥</sup>, Ahcène Boumendjel<sup>¥</sup> and Pierre Falson\*.

<sup>†‡¥</sup> Equal contributions as first (†), second (‡) and penultimate (¥) co-authors, respectively.

\*Corresponding author. Email: [pierre.falson@univ-lyon1.fr](mailto:pierre.falson@univ-lyon1.fr)

#### **This PDF file includes:**

Materials and Methods

Supplementary Text

Figs. S1 to S13

Tables S1

Captions for Data S1 to S2

References 39 to 55

#### **Other Supplementary Materials for this manuscript include the following:**

Data S1: Quantification of detergents bound to BmrA in crystallization assays

Data S2: Thermostability assays of BmrA with designed compounds

Validation reports for structures VR1-3

## Supplementary Text

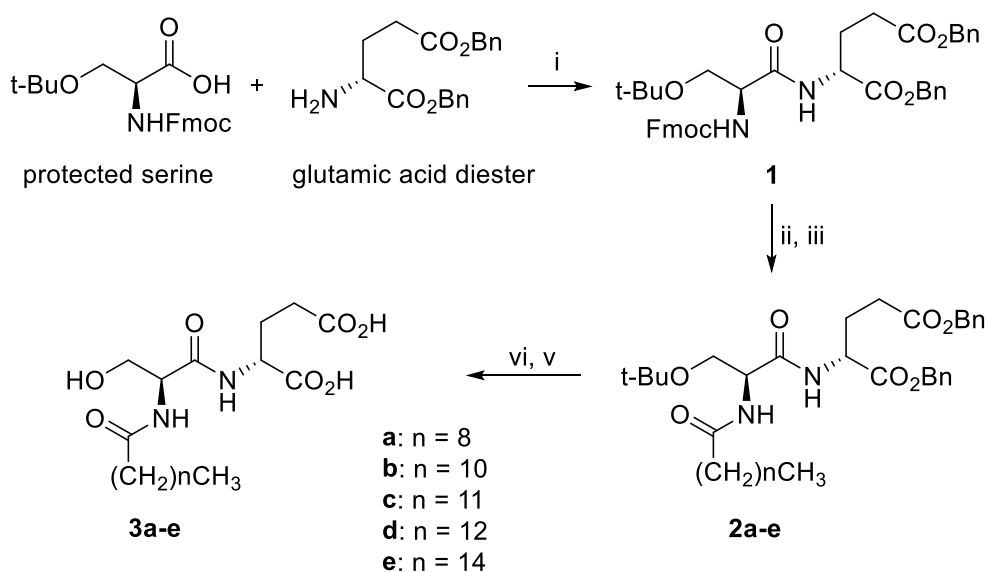
## Materials and Methods

## Chemistry

Solvents and reagents were purchased from commercial sources and used without further purification. Reactions were monitored by thin layer chromatography (TLC) using commercial silica gel 60 F<sub>254</sub> coated plates from Macherey-Nagel. Visualization were carried out under UV light at 254 and 365 nm and/or heating with a solution of sulfuric acid/acetic acid/water or phosphomolybdic acid/cerium sulfate/sulfuric acid/water or ninhydrin stain or iodine vapor. Purifications were performed by gravity column chromatography using silica gel 60 (230-400 mesh) from Macherey-Nagel or by automatic Reveleris® X2 flash chromatography system. MPs were measured using a Büchi B540 melting point apparatus and are uncorrected. Electrospray ionization (ESI) mass spectra were obtained on an Esquire 3000 Plus Bruker Daltonis instrument with a nanospray inlet. Accurate mass measurements (HRMS) were carried out on an ESI/QTOF with the Waters Xevo G2-S QTOF device. Analyses were performed by the analytical service of *Institut de Chimie Moléculaire de Grenoble* (ICMG). Spectra were recorded in deuterated solvents on Bruker Avance spectrometers at 400 or 500 MHz for <sup>1</sup>H and 100 or 125 MHz for <sup>13</sup>C NMR, respectively. Chemical shifts ( $\delta$ ) are reported in parts per million (ppm) relative to the solvent [<sup>1</sup>H:  $\delta$ (acetone-*d*<sub>6</sub>) = 2.05 ppm,  $\delta$ (DMSO-*d*<sub>6</sub>) = 2.50 ppm,  $\delta$ (CD<sub>3</sub>OD) = 3.31 ppm,  $\delta$ (CDCl<sub>3</sub>) = 7.26 ppm; <sup>13</sup>C:  $\delta$ (DMSO-*d*<sub>6</sub>) = 39.5 ppm,  $\delta$ (CD<sub>3</sub>OD) = 49.0 ppm,  $\delta$ (CDCl<sub>3</sub>) = 77.2 ppm,  $\delta$ (acetone-*d*<sub>6</sub>) = 206.3 ppm]. Multiplicity of signals is reported as followed: s (singlet), bs (broad singlet), d (doublet), t (triplet), q (quartet), qt (quintet), st (septet), dd (doublet of doublet), ddd (doublet of doublet of doublet), dt (doublet of triplet) ddt (doublet of doublet of triplet) and m (multiplet). Coupling constants (J) are given in Hertz (Hz). When direct signal assignments were difficult, additional spectra were acquired (J-mod, COSY, HMQC or HMBC).

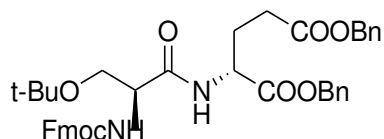
## Synthesis of amphiphiles 3a-3e as crystallization additives

Crystallization additives were obtained according to the synthetic scheme shown below.



Reagents and Conditions. i. TBTU, DIEA, DMF; ii. Et<sub>2</sub>NH, CH<sub>2</sub>Cl<sub>2</sub>; iii. R-CO-Cl, DMAP, pyridine, CH<sub>2</sub>Cl<sub>2</sub>; vi. H<sub>2</sub>, Pd/C, MeOH; v. TFA, CH<sub>2</sub>Cl<sub>2</sub>.

Synthesis of compound 1. Dibenzyl (R)-2-[(S)-2-[(9H-fluoren-9-yl)methoxycarbonyl] amino]-3-tert-butoxypropanamido} glutarate.



To a solution of protected serine (3.5 g, 9.12 mmol) in anhydrous DMF (15 mL/mmol) were successively added the glutamic acid diester (9.0 g, 18.24 mmol, 2 equiv.), TBTU (1.2 equiv.) and DIPEA (5 equiv.). The mixture was stirred at room temperature (rt) under N<sub>2</sub> atmosphere for 3 h. After completion of the reaction, water (15 mL/mmol) was added. The compound precipitated and was crystallized in a mixture of CH<sub>2</sub>Cl<sub>2</sub>/Et<sub>2</sub>O to provide compound 1 (5.14 g, 81% yield).

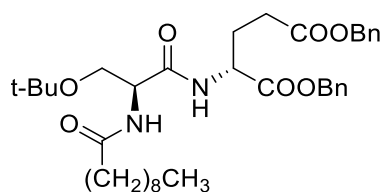
R<sub>f</sub> = 0.50 (cyclohexane/EtOAc 7:3); MP = 126-128 °C; <sup>1</sup>H NMR (400 MHz, CDCl<sub>3</sub>) δ ppm 1.19 (s, 9H), 1.99-2.11 (m, 1H), 2.22-2.35 (m, 1H), 2.32-2.55 (m, 2H), 3.41 (dd, *J* = 8.3, 8.3 Hz, 1H), 3.75-3.87 (m, 1H), 4.23 (t, *J* = 7.1 Hz, 1H), 4.24-4.33 (m, 1H), 4.40 (d, *J* = 6.8 Hz, 2H), 4.68-4.76 (m, 1H), 5.09 (s, 2H), 5.17 (s, 2H), 5.78 (bs, 1H), 7.21-7.46 (m, 15H), 7.61 (d, *J* = 7.0 Hz, 2H), 7.76 (d, *J* = 7.5 Hz, 2H). <sup>13</sup>C NMR (100 MHz, CDCl<sub>3</sub>) δ ppm 27.4 (3xCH<sub>3</sub>), 27.5 (CH<sub>2</sub>), 30.0 (CH<sub>2</sub>), 47.1 (CH), 51.8 (CH), 54.6 (CH), 61.7 (CH<sub>2</sub>), 66.5 (CH<sub>2</sub>), 67.2 (CH<sub>2</sub>), 67.4 (CH<sub>2</sub>), 74.3 (C), 120.0 (2xCH), 125.1 (2xCH), 127.1 (2xCH), 127.7 (2xCH), 128.2-128.7 (10xCH), 135.1 (C), 135.7 (C), 141.3 (2xC), 143.7 (2xC), 156.1 (C), 170.1 (C), 171.2 (C), 172.3 (C); MS (ESI+) *m/z* (%) 426 (100), 570 (3), 715 (1) [M+Na]<sup>+</sup>; HRMS (ESI+) *m/z*, calculated for C<sub>41</sub>H<sub>45</sub>N<sub>2</sub>O<sub>8</sub> 693.3176, found 693.3156.

### Synthesis of compounds 2.

*Fmoc deprotection.* To a solution of compound 1 (1 equiv.) in anhydrous dichloromethane (20 mL/mmol) was added diethylamine (20 equiv.). The reaction mixture was stirred at rt under N<sub>2</sub> atmosphere overnight. The volatiles were removed under reduced pressure. To eliminate the residual diethylamine, the crude product was diluted in dichloromethane, washed with a saturated sodium bicarbonate (NaHCO<sub>3</sub>) solution, dried over MgSO<sub>4</sub>, filtered and concentrated under reduced pressure and used for the next steps without further purification.

*Amide formation.* The crude compound obtained in the previous step (1 equiv.) was dissolved in anhydrous dichloromethane (30 mL/mmol). The acyl chloride derivative was added (2 equiv.), together with dimethylaminopyridine (DMAP) (0.5 equiv.) and pyridine (34 equiv.). The reaction mixture was stirred at rt under N<sub>2</sub> atmosphere overnight. The reaction mixture was acidified to pH = 3 with an aqueous solution of HCl 10% and extracted with dichloromethane. The combined organic layers were washed with brine and dried over MgSO<sub>4</sub>, filtered, and concentrated under reduced pressure. The crude product was purified by silica gel column chromatography.

**Compound 2a.** Dibenzyloxycarbonyl (R)-2-[(S)-3-tert-butoxy-2-(decanamido)propanamido]glutarate

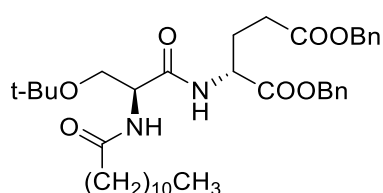


The crude product was prepared starting from 1 (500 mg, 0.70 mmol) and commercially available decanoyl chloride (267 mg, 1.40 mmol). After purification by column chromatography on silica gel

(cyclohexane/EtOAc 8:2 to 7:3), the pure product **2a** (195 mg, 0.31 mmol, 45%) was obtained as a white solid.

$R_f$  = 0.18 (cyclohexane/EtOAc 7:3). MP = 82-85 °C;  $^1\text{H}$  NMR (400 MHz,  $\text{CDCl}_3$ )  $\delta$  ppm 0.87 (t,  $J$  = 6.9 Hz, 3H), 1.16 (s, 9H), 1.19-1.35 (m, 12H), 1.55-1.66 (m, 2H), 1.96-2.07 (m, 1H), 2.21 (t,  $J$  = 7.8 Hz, 2H), 2.21-2.30 (m, 1H), 2.32-2.50 (m, 2H), 3.31 (dd,  $J$  = 8.7, 8.7 Hz, 1H), 3.80 (dd,  $J$  = 8.7, 4.2 Hz, 1H), 4.44-4.50 (m, 1H), 4.65-4.72 (m, 1H), 5.08 (s, 2H), 5.15 (s, 2H), 6.40 (d,  $J$  = 6.4 Hz, 1H, NH), 7.27-7.36 (m, 11H);  $^{13}\text{C}$  NMR (100 MHz,  $\text{CDCl}_3$ )  $\delta$  ppm 14.1 ( $\text{CH}_3$ ), 22.7 ( $2\times\text{CH}_2$ ), 25.6 ( $\text{CH}_2$ ), 27.4 ( $3\times\text{CH}_3$ ), 27.5 ( $\text{CH}_2$ ), 29.3-29.44 ( $4\times\text{CH}_2$ ), 30.0 ( $\text{CH}_2$ ), 31.9 ( $\text{CH}_2$ ), 36.6 ( $\text{CH}_2$ ), 51.8 (CH), 53.0 (CH), 61.3 ( $\text{CH}_2$ ), 66.5 ( $\text{CH}_2$ ), 67.3 ( $\text{CH}_2$ ), 74.3 (C), 128.3-128.7 ( $10\times\text{CH}$ ), 135.2 (C), 135.8 (C), 170.4 (C), 171.2 (C), 172.3 (C), 173.3 (C); MS (ESI+)  $m/z$  (%) 626 (30)  $[\text{M}+\text{H}]^+$ , 648 (100)  $[\text{M}+\text{Na}]^+$ ; HRMS (ESI+)  $m/z$ , calculated for  $\text{C}_{36}\text{H}_{53}\text{N}_2\text{O}_7$  625.3853, found 625.3846.

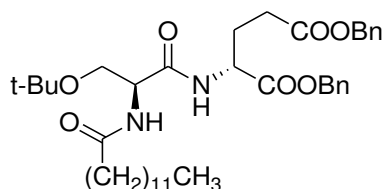
**Compound 2b.** Dibenzyl (R)-2-[(S)-3-tert-butoxy-2-(dodecanamido)propanamido]glutarate



The crude product was prepared starting from **1** (400mg, 0.58 mmol) and commercially available dodecanoyl chloride (252 mg, 1.15 mmol). After purification by column chromatography on silica gel (cyclohexane/EtOAc 8:2 to 7:3), the pure product **2b** (182 mg, 0.28 mmol, 48%) was obtained as a white solid.

$R_f$  = 0.12 (cyclohexane/EtOAc 8:2); MP = 67-69 °C;  $^1\text{H}$  NMR (400 MHz,  $\text{CDCl}_3$ )  $\delta$  ppm 0.88 (t,  $J$  = 6.9 Hz, 3H), 1.17 (s, 9H), 1.19-1.35 (m, 16H), 1.56-1.67 (m, 2H), 1.96-2.08 (m, 1H), 2.21 (t,  $J$  = 7.6 Hz, 2H), 2.21-2.32 (m, 1H), 2.32-2.50 (m, 2H), 3.30 (dd,  $J$  = 8.7, 8.7 Hz, 1H), 3.81 (dd,  $J$  = 8.7, 4.2 Hz, 1H), 4.42-4.49 (m, 1H), 4.64-4.72 (m, 1H), 5.09 (s, 2H), 5.16 (s, 2H), 6.38 (d,  $J$  = 6.3 Hz, 1H, NH), 7.23-7.39 (m, 11H);  $^{13}\text{C}$  NMR (100 MHz,  $\text{CDCl}_3$ )  $\delta$  ppm 14.2 ( $\text{CH}_3$ ), 22.8 ( $\text{CH}_2$ ), 25.6 ( $\text{CH}_2$ ), 27.5 ( $3\times\text{CH}_3$ ), 27.6 ( $\text{CH}_2$ ), 29.4-29.7 ( $6\times\text{CH}_2$ ), 30.0 ( $\text{CH}_2$ ), 32.0 ( $\text{CH}_2$ ), 36.7 ( $\text{CH}_2$ ), 51.9 (CH), 53.1 (CH), 61.4 ( $\text{CH}_2$ ), 66.6 ( $\text{CH}_2$ ), 67.5 ( $\text{CH}_2$ ), 74.4 (C), 128.4-128.8 ( $10\times\text{CH}$ ), 135.2 (C), 135.9 (C), 170.4 (C), 171.3 (C), 172.4 (C), 173.4 (C); MS (ESI+)  $m/z$  (%) 131 (30), 199 (40), 654 (50)  $[\text{M}+\text{H}]^+$ , 677 (100), 699 (20); HRMS (ESI+)  $m/z$ , calculated for  $\text{C}_{38}\text{H}_{57}\text{N}_2\text{O}_7$  653.4166, found 653.4158.

**Compound 2c.** Dibenzyl (R)-2-[(S)-3-tert-butoxy-2-(tridecanamido)propanamido]glutarate.

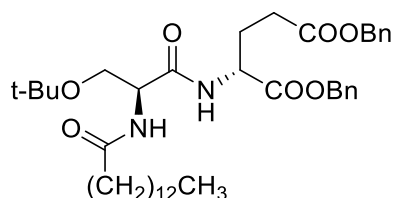


The crude product was prepared starting from **1** (500 mg, 0.70 mmol) and commercially available tridecanoyl chloride (326 mg, 1.40 mmol). After purification by column chromatography on silica gel (cyclohexane/EtOAc 8:2 to 7:3), the pure product **2c** (233 mg, 0.35 mmol, 50%) was obtained as a white solid.

$R_f$  = 0.24 (cyclohexane/EtOAc 7:3); MP = 68-71 °C;  $^1\text{H}$  NMR (400 MHz,  $\text{CDCl}_3$ )  $\delta$  ppm 0.88 (t,  $J$  = 6.9 Hz, 3H), 1.17 (s, 9H), 1.20-1.36 (m, 18H), 1.55-1.67 (m, 2H), 1.96-2.08 (m, 1H), 2.21 (t,  $J$  = 7.6 Hz, 2H), 2.21-2.32 (m, 1H), 2.32-2.50 (m, 2H), 3.31 (dd,  $J$  = 8.7, 8.7 Hz, 1H), 3.80 (dd,  $J$  = 8.7, 4.2 Hz, 1H), 4.44-4.50

(m, 1H), 4.63-4.73 (m, 1H), 5.08 (s, 2H), 5.15 (s, 2H), 6.41 (d,  $J = 6.4$  Hz, 1H, NH), 7.25-7.37 (m, 11H);  $^{13}\text{C}$  NMR (100 MHz,  $\text{CDCl}_3$ )  $\delta$  ppm 14.1 ( $\text{CH}_3$ ), 22.7 ( $\text{CH}_2$ ), 25.5 ( $\text{CH}_2$ ), 27.4 ( $3\times\text{CH}_3$ ), 27.5 ( $\text{CH}_2$ ), 29.3-29.7 ( $7\times\text{CH}_2$ ), 29.9 ( $\text{CH}_2$ ), 31.9 ( $\text{CH}_2$ ), 36.5 ( $\text{CH}_2$ ), 51.8 (CH), 53.0 (CH), 61.3 ( $\text{CH}_2$ ), 66.5 ( $\text{CH}_2$ ), 67.3 ( $\text{CH}_2$ ), 74.2 (C), 128.3-128.6 ( $10\times\text{CH}$ ), 135.2 (C), 135.8 (C), 170.4 (C), 171.2 (C), 172.3 (C), 173.3 (C); MS (ESI+)  $m/z$  (%) 668 (20)  $[\text{M}+\text{H}]^+$ , 690 (100)  $[\text{M}+\text{Na}]^+$ ; HRMS (ESI+)  $m/z$ , calculated for  $\text{C}_{39}\text{H}_{59}\text{N}_2\text{O}_7$  667.4322, found 667.4334.

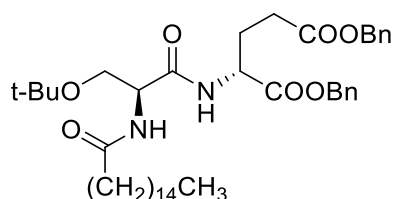
**Compound 2d.** Dibenzyl (R)-2-[(S)-3-t-butoxy-2-(tetradecanamido)propanamido] glutarate.



The crude product was prepared starting from **1** (400 mg, 0.58 mmol) and commercially available tetradecanoyl chloride (285 mg, 1.15 mmol). After purification by column chromatography on silica gel (cyclohexane/EtOAc 8:2 to 7:3), the pure product **2d** (187 mg, 0.27 mmol, 48%) was obtained as a white solid.

$R_f = 0.07$  (cyclohexane/EtOAc 8:2); MP = 71-73 °C;  $^1\text{H}$  NMR (400 MHz,  $\text{CDCl}_3$ )  $\delta$  ppm 0.88 (t,  $J = 6.9$  Hz, 3H), 1.17 (s, 9H), 1.20-1.36 (m, 20H), 1.56-1.67 (m, 2H), 1.97-2.08 (m, 1H), 2.21 (t,  $J = 7.6$  Hz, 2H), 2.23-2.50 (m, 3H), 3.29 (dd,  $J = 8.7, 8.7$  Hz, 1H), 3.80 (dd,  $J = 8.7, 4.2$  Hz, 1H), 4.41-4.49 (m, 1H), 4.63-4.72 (m, 1H), 5.09 (s, 2H), 5.14 (d,  $J = 12.3$  Hz, 1H), 5.18 (d,  $J = 12.3$  Hz, 1H), 7.25-7.39 (m, 11H);  $^{13}\text{C}$  NMR (100 MHz,  $\text{CDCl}_3$ )  $\delta$  ppm 14.2 ( $\text{CH}_3$ ), 22.8 ( $\text{CH}_2$ ), 25.6 ( $\text{CH}_2$ ), 27.5 ( $3\times\text{CH}_3$ ), 27.6 ( $\text{CH}_2$ ), 29.4-29.8 ( $8\times\text{CH}_2$ ), 30.0 ( $\text{CH}_2$ ), 32.0 ( $\text{CH}_2$ ), 36.7 ( $\text{CH}_2$ ), 51.9 (CH), 53.1 (CH), 61.4 ( $\text{CH}_2$ ), 66.6 ( $\text{CH}_2$ ), 67.5 ( $\text{CH}_2$ ), 74.4 (C), 128.4-128.8 ( $10\times\text{CH}$ ), 135.2 (C), 135.8 (C), 170.5 (C), 171.3 (C), 172.4 (C), 173.4 (C); MS (ESI+)  $m/z$  (%) 131 (65), 199 (100), 682 (60)  $[\text{M}+\text{H}]^+$ ; HRMS (ESI+)  $m/z$  calculated for  $\text{C}_{40}\text{H}_{61}\text{N}_2\text{O}_7$  681.4479, found 681.4447.

**Compound 2e.** Dibenzyl (R)-2-[(S)-3-tert-butoxy-2-(hexadecanamido)propanamido] glutarate



The crude product was prepared starting from **1** (300 mg, 0.43 mmol) and commercially available hexadecanoyl chloride (238 mg, 0.87 mmol). After purification by column chromatography on silica gel (cyclohexane/EtOAc 8:2), the pure product **2e** (93 mg, 0.13 mmol, 30%) was obtained as a white solid.

$R_f = 0.11$  (8:2 cyclohexane/EtOAc). MP = 69-71 °C.  $^1\text{H}$  NMR (400 MHz,  $\text{CDCl}_3$ )  $\delta$  ppm 0.88 (t,  $J = 6.8$  Hz, 3H), 1.17 (s, 9H), 1.20-1.37 (m, 24H), 1.55-1.68 (m, 2H), 1.97-2.09 (m, 1H), 2.21 (t,  $J = 7.6$  Hz, 2H), 2.16-2.51 (m, 3H), 3.29 (dd,  $J = 8.7, 8.7$  Hz, 1H), 3.81 (dd,  $J = 8.7, 4.2$  Hz, 1H), 4.39-4.49 (m, 1H), 4.62-4.72 (m, 1H), 5.09 (s, 2H), 5.14 (d,  $J = 12.3$  Hz, 1H), 5.18 (d,  $J = 12.3$  Hz, 1H), 6.36 (d,  $J = 6.3$  Hz, 1H), 7.20-7.40 (m, 11H);  $^{13}\text{C}$  NMR (100 MHz,  $\text{CDCl}_3$ )  $\delta$  ppm 14.3 ( $\text{CH}_3$ ), 22.8 ( $\text{CH}_2$ ), 25.7 ( $\text{CH}_2$ ), 27.5 ( $3\times\text{CH}_3$ ), 27.6 ( $\text{CH}_2$ ), 29.4-29.8 ( $10\times\text{CH}_2$ ), 30.1 ( $\text{CH}_2$ ), 32.1 ( $\text{CH}_2$ ), 36.7 ( $\text{CH}_2$ ), 51.9 (CH), 53.1 (CH), 61.4 ( $\text{CH}_2$ ), 66.6 ( $\text{CH}_2$ ), 67.5 ( $\text{CH}_2$ ), 74.5 (C), 128.4-128.8 ( $10\times\text{CH}$ ), 135.2 (C), 135.9 (C), 170.5 (C), 171.3 (C), 172.4 (C), 173.5 (C); MS (ESI+)  $m/z$  (%) 199 (15), 710 (100)  $[\text{M}+\text{H}]^+$ , 732 (15)  $[\text{M}+\text{Na}]^+$ ; HRMS (ESI+)  $m/z$  calculated for  $\text{C}_{42}\text{H}_{65}\text{N}_2\text{O}_7$  709.4792  $[\text{M}+\text{H}]^+$ , found 709.4805.

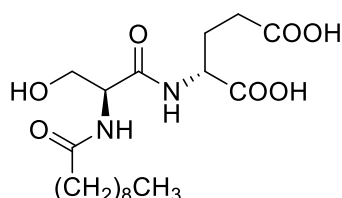


**Synthesis of compounds 3**

*Catalytic hydrogenolysis.* To a degassed solution of a compound **2** (1 equiv.) in MeOH (100 mL/mmol) was added Pd/C 10% (200 mg/mmol). The reaction mixture was stirred at rt under H<sub>2</sub> atmosphere from 4 h to overnight. After filtration over Celite® to remove the catalyst, the solvent was evaporated under reduced pressure. The residue was used directly for the next step or washed with cyclohexane and/or dichloromethane to obtain the product which was used as is for the *t*-Bu deprotection step.

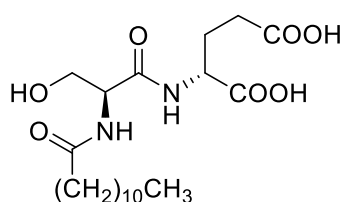
*t*-Butyl deprotection. To a solution of *t*-Bu-intermediate, obtained in the previous step (1 equiv.) in anhydrous dichloromethane (12 mL/mmol) at 0 °C was added dropwise TFA (4 mL/mmol). The reaction mixture was stirred at rt under N<sub>2</sub> atmosphere overnight. The volatiles were removed under reduced pressure and the residue was dissolved in DCM. A solution of NaOH (2 M) was added to pH = 11-12. The aqueous layer was washed with EtOAc before being acidified to pH 1-2 with concentrated HCl and extracted 3 times with EtOAc. The combined organic layers were dried over MgSO<sub>4</sub>, filtered and concentrated under reduced pressure. The residue was washed with DCM to obtain the pure product.

**Compound 3a.** (R)-2-[(S)-2-(Decanamido)-3-hydroxypropanamido]glutaric acid.



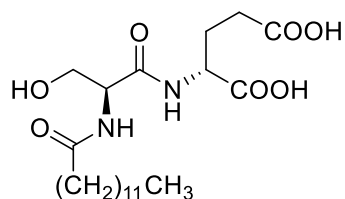
The pure product (white solid, 182 mg, 0.47 mmol, 94%) was prepared starting from **2a** (310 mg, 0.50 mmol). MP = 53-57 °C; <sup>1</sup>H NMR (400 MHz, CD<sub>3</sub>OD) δ ppm 0.89 (t, *J* = 6.8 Hz, 3H), 1.22-1.38 (m, 12H), 1.56-1.69 (m, 2H), 1.90-2.03 (m, 1H), 2.14-2.26 (m, 1H), 2.29 (t, *J* = 7.3 Hz, 2H), 2.36-2.43 (m, 2H), 3.73-3.84 (m, 2H), 4.42-4.52 (m, 2H); <sup>13</sup>C NMR (100 MHz, CD<sub>3</sub>OD) δ ppm 14.4 (CH<sub>3</sub>), 23.7 (CH<sub>2</sub>), 26.8 (CH<sub>2</sub>), 27.9 (CH<sub>2</sub>), 30.3-30.5 (4xCH<sub>2</sub>), 31.1 (CH<sub>2</sub>), 33.0 (CH<sub>2</sub>), 36.9 (CH<sub>2</sub>), 53.3 (CH), 56.6 (CH), 63.1 (CH<sub>2</sub>), 172.5 (C), 174.9 (C), 176.5 (C), 176.5 (C); MS (ESI-) *m/z* (%) 387 (100) [M-H]<sup>-</sup>, 404 (20); HRMS (ESI-) *m/z* calculated for C<sub>18</sub>H<sub>31</sub>N<sub>2</sub>O<sub>7</sub> 387.2131 [M-H]<sup>-</sup>, found 387.2140.

**Compound 3b.** (R)-2-[(S)-2-(Dodecanamido)-3-hydroxypropanamido]glutaric acid.



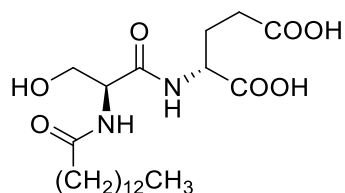
The pure product (white solid, 1.68 g, 4.04 mmol, 70%) was prepared starting from **2b** (3.76 g, 5.80 mmol). MP = 100-102 °C; <sup>1</sup>H NMR (400 MHz, CD<sub>3</sub>OD) δ ppm 0.90 (t, *J* = 6.9 Hz, 3H), 1.22-1.38 (m, 16H), 1.57-1.67 (m, 2H), 1.91-2.01 (m, 1H), 2.15-2.26 (m, 1H), 2.29 (t, *J* = 7.2 Hz, 2H), 2.37-2.44 (m, 2H), 3.72-3.81 (m, 2H), 4.43-4.51 (m, 2H); <sup>13</sup>C NMR (100 MHz, CD<sub>3</sub>OD) δ ppm 14.4 (CH<sub>3</sub>), 23.7 (CH<sub>2</sub>), 26.8 (CH<sub>2</sub>), 27.9 (CH<sub>2</sub>), 30.4-30.7 (6xCH<sub>2</sub>), 31.0 (CH<sub>2</sub>), 33.1 (CH<sub>2</sub>), 36.9 (CH<sub>2</sub>), 53.1 (CH), 56.6 (CH), 63.1 (CH<sub>2</sub>), 172.6 (C), 174.6 (C), 176.4 (C), 176.5 (C); MS (ESI-) *m/z* (%) 157 (40), 199 (30), 387 (80), 415 (100) [M-H]<sup>-</sup>; HRMS (ESI-) *m/z* calculated for C<sub>20</sub>H<sub>35</sub>N<sub>2</sub>O<sub>7</sub> 415.2444 [M-H]<sup>-</sup>, found 415.2447.

**Compound 3c.** (R)-2-[(S)-2-(Tridecanamido)-3-hydroxypropanamido]glutaric acid.



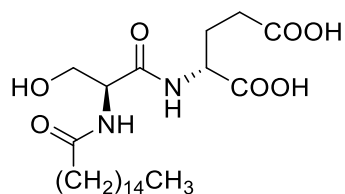
The pure product (white solid, 115 mg, 0.27 mmol, 89%) was prepared starting from **2c** (198 mg, 0.30 mmol). MP = 58-63 °C;  $^1\text{H}$  NMR (400 MHz,  $\text{CD}_3\text{OD}$ )  $\delta$  ppm 0.89 (t,  $J$  = 6.9 Hz, 3H), 1.21-1.41 (m, 18H), 1.54-1.68 (m, 2H), 1.90-2.04 (m, 1H), 2.14-2.27 (m, 1H), 2.29 (t,  $J$  = 7.4 Hz, 2H), 2.36-2.48 (m, 2H), 3.71-3.83 (m, 2H), 4.43-4.53 (m, 2H);  $^{13}\text{C}$  NMR (100 MHz,  $\text{CD}_3\text{OD}$ )  $\delta$  ppm 14.4 ( $\text{CH}_3$ ), 23.7 ( $\text{CH}_2$ ), 26.8 ( $\text{CH}_2$ ), 27.8 ( $\text{CH}_2$ ), 30.3-30.9 (7x $\text{CH}_2$ ), 31.0 ( $\text{CH}_2$ ), 33.0 ( $\text{CH}_2$ ), 36.9 ( $\text{CH}_2$ ), 53.1 (CH), 56.6 (CH), 63.1 ( $\text{CH}_2$ ), 172.6 (C), 174.6 (C), 176.4 (C), 176.5 (C); MS (ESI-)  $m/z$  (%) 429 (100)  $[\text{M}-\text{H}]^-$ , 446 (30); HRMS (ESI-)  $m/z$  calculated for  $\text{C}_{21}\text{H}_{37}\text{N}_2\text{O}_7$  429.2601  $[\text{M}-\text{H}]^-$ , found 429.2599.

**Compound 3d.** (R)-2-[(S)-2-(Tetradecanamido)-3-hydroxypropanamido]glutaric acid



The pure product (white solid, 57 mg, 0.13 mmol, quantitative) was prepared starting from **2d** (87 mg, 0.13 mmol). MP = 109-112 °C;  $^1\text{H}$  NMR (400 MHz,  $\text{CD}_3\text{OD}$ )  $\delta$  ppm 0.90 (t,  $J$  = 6.8 Hz, 3H), 1.19-1.39 (m, 20H), 1.57-1.67 (m, 2H), 1.90-2.02 (m, 1H), 2.16-2.26 (m, 1H), 2.29 (t,  $J$  = 7.4 Hz, 2H), 2.36-2.45 (m, 2H), 3.71-3.84 (m, 2H), 4.43-4.52 (m, 2H);  $^{13}\text{C}$  NMR (100 MHz,  $\text{CD}_3\text{OD}$ )  $\delta$  ppm 14.4 ( $\text{CH}_3$ ), 23.7 ( $\text{CH}_2$ ), 26.8 ( $\text{CH}_2$ ), 27.9 ( $\text{CH}_2$ ), 30.4-30.9 (8x $\text{CH}_2$ ), 31.1 ( $\text{CH}_2$ ), 33.0 ( $\text{CH}_2$ ), 36.9 ( $\text{CH}_2$ ), 53.3 (CH), 56.6 (CH), 63.1 ( $\text{CH}_2$ ), 172.6 (C), 174.9 (C), 176.5 (C), 176.5 (C); MS (ESI-)  $m/z$  (%) 443 (100)  $[\text{M}-\text{H}]^-$ ; HRMS (ESI-)  $m/z$  calculated for  $\text{C}_{22}\text{H}_{39}\text{N}_2\text{O}_7$  443.2757  $[\text{M}-\text{H}]^-$ , found 443.2754.

**Compound 3e.** (R)-2-[(S)-2-(Hexadecanamido)-3-hydroxypropanamido]glutaric acid



The pure product (white solid, 36 mg, 0.08 mmol, 65%) was prepared starting from **2e** (83 mg, 0.18 mmol). MP = 111-113 °C;  $^1\text{H}$  NMR (400 MHz,  $\text{CD}_3\text{OD}$ )  $\delta$  ppm 0.90 (t,  $J$  = 6.8 Hz, 3H), 1.19-1.37 (m, 24H), 1.55-1.68 (m, 2H), 1.90-2.03 (m, 1H), 2.15-2.26 (m, 1H), 2.29 (t,  $J$  = 7.4 Hz, 2H), 2.36-2.44 (m, 2H), 3.72-3.82 (m, 2H), 4.43-4.52 (m, 2H);  $^{13}\text{C}$  NMR (100 MHz,  $\text{CD}_3\text{OD}$ )  $\delta$  ppm 14.4 ( $\text{CH}_3$ ), 23.7 ( $\text{CH}_2$ ), 26.8 ( $\text{CH}_2$ ), 27.9 ( $\text{CH}_2$ ), 30.4-30.8 (10x $\text{CH}_2$ ), 31.1 ( $\text{CH}_2$ ), 33.1 ( $\text{CH}_2$ ), 36.9 ( $\text{CH}_2$ ), 53.2 (CH), 56.6 (CH), 63.1 ( $\text{CH}_2$ ), 172.6 (C), 174.7 (C), 176.5 (C), 176.5 (C); MS (ESI-)  $m/z$  (%) 471 (100)  $[\text{M}-\text{H}]^-$ ; HRMS (ESI-)  $m/z$  calculated for  $\text{C}_{24}\text{H}_{43}\text{N}_2\text{O}_7$  471.3070, found 471.3057.

## Biochemistry

**Products.** Products were from Sigma except when indicated. SOC medium was from Invitrogen, LB broth medium from Roth, ampicillin and Triton X100 from Euromedex, anti-protease tablets from

Roche, Ni<sup>2+</sup>-NTA resin from Generon, DDM and DM from Anatrace, Amicon Ultra-15 devices from Millipore and Superdex 200 10/300 GL from GE.

**BmrA expression.** BmrA expression was adapted from methods previously reported (23, 39). The E504A mutant was generated and fused to a 6-histidine *N*-terminal Nickel-affinity tag in the pET15(+) plasmid and overexpressed in the CD43(DE3) $\Delta$ *acrB* *E. coli* strain, a gift of Pr. Klaas Martinus Pos. A freshly transformed colony was incubated in 3 mL LB containing 50  $\mu$ g/mL for 7-8 h at 37 °C. Thirty microliters of this preculture were added to 1 L LB containing 50  $\mu$ g/mL of ampicillin, which was then incubated at 22 °C until reaching 0.6 OD<sub>600</sub>. BmrA expression was induced by 0.7 mM IPTG followed by a 5-6 h incubation at 22 °C. Bacteria were collected at 5000 xg for 15 min., 4 °C and then suspended in 10 mL 50 mM Tris-HCl pH 8.0, 5 mM MgCl<sub>2</sub> and 1 mM PMSF. Bacteria were lysed by 3 passages at 18,000 psi through a microfluidizer 100 (Microfluidics IDEX Corp). The solution was centrifuged 30 min. at 15,000 xg at 4 °C. The membrane fraction was pelleted by centrifugation for 1 h at 180,000 xg at 4°C, suspended in 50 mM Tris-HCl pH 8.0, 1 mM PMSF and 1 mM EDTA and centrifuged again. The final pellet was suspended in 20 mM Tris-HCl pH 8.0, 0.3 M sucrose and 1 mM EDTA, frozen in liquid nitrogen and stored at -80 °C.

**BmrA purification.** Membranes were solubilized at 5 mg/mL in 20 mM Tris-HCl pH 8.0, 100 mM NaCl, 15% glycerol (v/v), anti-protease tablets, 0.1 mM TCEP and 4.5% (w/v) Triton X100, under gentle agitation for 90 min. and then centrifuged 40 min. at 100,000 xg. The supernatant was loaded onto a Ni<sup>2+</sup>-NTA equilibrated in 20 mM Tris-HCl pH 8.0, 100 mM NaCl, 15% (v/v) glycerol, anti-protease tablets, 4.5% Triton X100 and 20 mM imidazole. The resin was washed with 20 mM Hepes-HCl pH 8.0, 100 mM NaCl, 20 mM imidazole, 1.3 mM DDM and 1 mM sodium cholate. The protein was eluted by adding 200 mM imidazole to the same buffer. BmrA fractions were pooled and diluted ten times in the Hepes buffer (same composition as above) without imidazole and loaded again on the same resin for another step of affinity chromatography. The pool of BmrA fractions was concentrated on 50 kDa cutoff Amicon Ultra-15 devices, with the centrifuge speed set at 1000 xg for 10-15 min, and then loaded onto Superdex 200 10/300 using as mobile phase 20 mM Hepes-HCl pH 7.5, 100 mM NaCl, 0.7 mM DDM and 0.7 mM sodium cholate (DDM:cholate molar ratio of 1:1). The same step was also carried out at DDM-cholate ratio of 3:1 or 1:3. Cholate was systematically removed from the Superdex resin by a washing with 1M NaOH. The elution peak was then pooled and stored at 4 °C before use. BmrA was particularly stable when not concentrated as previously reported (30).

**Thermostabilisation assays** were carried out as previously reported (30). Membranes of BmrA diluted at 2 g proteins/L were solubilized with 10 mM DDM, with or without 1 mM of compounds **3a-3e** in a final volume of 2 mL, for 2 h at 4 °C. Solutions were clarified by centrifugation at 100,000 xg for 1 h at 4 °C and supernatants were aliquoted (50  $\mu$ l) and individually submitted 30 min to a temperature of 25 to 90 °C using a PCR thermal cycler (PeqSTAR 2x gradient; Peqlab). Samples were then centrifuged 40 min at 20,000 xg and supernatants were analyzed by SDS-PAGE and Western-blot using anti-His antibody. The relative intensity of BmrA at each temperature was quantified on Western blot using Image Lab software 4.1 (Bio-Rad). Each condition was performed twice or thrice. Intensity was plotted as a function of the temperature and normalized. Data were fitted with equation 5 (see data fit section).

**Detergents quantification.** DDM bound to BmrA was quantified by mass spectrometry as described (29). Cholate was quantified as previously reported (40). Modelling of the detergent belt radius was done following the same protocol and using the DeltBelt server ([www.deltbelt.ibcp.fr](http://www.deltbelt.ibcp.fr)).

**ATPase activity.** The ATPase activity of BmrA was measured as previously described (30, 41). The protein in solution in 20 mM Hepes-HCl pH 7.5, 100 mM NaCl, 0.7 mM DDM and 0.7 mM cholate was

diluted in the ATPase activity assay buffer containing either 1 mM DDM or a mixture of 0.7 mM DDM and 0.7 mM cholate, and the ATPase activity recorded.

**Membrane-scaffold protein (MSP) production and purification.** The MSP1E3D1 protein was expressed in BL21 *E. coli* (p1E3D1 plasmid, Addgene) as previously described (32). Bacteria were suspended in 50 mL of 40 mM Tris-HCl pH 7.4, 100 mM NaCl, 1 % (w/v) Triton X100, 0.5 mM EDTA, 1 mM PMSF. Two microliters of Benzonase (24 U/mL, Merck) were added and the bacteria were lysed by 2 passages at 18,000 psi through a microfluidizer 100 (Microfluidics IDEX Corp) and then centrifuged during 30 min. at 30,000 xg, 4°C. The supernatant was loaded onto a 0.5-mL Ni<sup>2+</sup>-NTA column (GE Healthcare) resin pre-equilibrated with 5 resin-volumes of 40 mM Tris-HCl pH 7.4, 100 mM NaCl, 1 % (w/v) Triton X100, 0.5 mM EDTA and 1 mM PMSF. The resin was then washed with 10 resin-volume with 3 different buffers: wash buffer 1 composed of 40 mM Tris-HCl pH 8.0, 300 mM NaCl and 1% (w/v) Triton X100; wash buffer 2 composed of 40 mM Tris-HCl pH 8.0, 300 mM NaCl, 50 mM sodium cholate and 20 mM Imidazole; wash buffer 3 composed of 40 mM Tris-HCl pH 8.0, 300 mM NaCl, 50 mM Imidazole. MSP1E3D1 was eluted with 15 mL of 40 mM Tris-HCl pH 8.0, 300 mM NaCl and 500 mM Imidazole. The fractions of the elution pic were pooled and the TEV (2 mg/mL) was added to remove the His tag, at a ratio of 1 mg TEV for 40 mg MSP1E3D1. The mixture was then dialyzed (cutoff 12-14 kDa), a first time against 300 mL 40 mM Tris-HCl, pH 7.4, 100 mM NaCl and 0.5 mM EDTA for 3 hours and then against 700 mL of the same buffer, overnight at 4°C. After dialysis 20 mM imidazole was added and the solution loaded on a 0.5 mL Ni<sup>2+</sup>-NTA column equilibrated with 20 mM Tris-HCl pH 7.4 and 100 mM NaCl. The flow-through containing MSP1E3D1 was collected. The uncleaved fraction was eluted with 40 mM Tris-HCl pH 8.0, 300 mM NaCl and 500 mM Imidazole, dialyzed two times as above and finally concentrated spinning at 5,000 xg with a 100 kDa cutoff Amicon Ultra-15. The concentrated samples were frozen in liquid nitrogen and stored at -80°C.

**BmrA nanodisc reconstitution.** BmrA was reconstituted into nanodiscs as previously described (42) with the following modifications. Six hundred micrograms of purified BmrAE504A in 200 µL of HEPES-HCl pH 7.5, 100 mM NaCl, 0.035% DDM and 0.03% sodium cholate were mixed with 1.4 mg of *E. coli* lipids (Avanti Polar) in 56 µL of 99 mM cholate, 20 mM HEPES-HCl pH 7.5, 100 mM NaCl for 10 min at room temperature. The mix was then added of 665 µg MSP1E3D1 in 35 µL of 40 mM Tris-HCl, pH 7.4, 100 mM NaCl and 0.5 mM EDTA. The volume was completed to 1 mL with HEPES-HCl pH 7.5, 100 mM NaCl and incubated 1 h at room temperature. The final molar ratio of BmrA/MSP/lipids was 1/5/400 in 20 mM HEPES-HCl pH 7.5, 100 mM NaCl. SM-2 biobeads (170 mg/100 µg BmrA, Biorad) were then added to the mixture, placed 3 h under gentle agitation at room temperature. Empty nanodiscs were removed from the BmrA-nanodiscs by Ni<sup>2+</sup>-NTA chromatography. The resin was equilibrated with 20 mM HEPES-HCl pH 7.5, 100 mM NaCl, then loaded with the sample, washed with 20 mM HEPES-HCl pH 7.5, 100 mM NaCl, 20 mM imidazole. The BmrA-nanodiscs complex was then eluted with 20 mM HEPES-HCl pH 7.5, 100 mM NaCl, 200 mM imidazole. Imidazole was then removed from the solution by passing through a HiTrap desalting column equilibrated with 20 mM HEPES-HCl pH 7.5, 100 mM NaCl.

**Ligand binding on BmrA in detergents.** R6G, ATP-Mg<sup>2+</sup> and cholate binding was carried out by incubating 15 min on ice 0.5 µM BmrA, WT or E504A mutant prepared in DDM or DDM-cholate with or without 5 mM ATP-Mg<sup>2+</sup> in 20 mM HEPES-HCl pH 7.5, 100 mM NaCl, including 0.7 mM DDM and/or 0.7 mM cholate depending on the experiments. The binding of R6G was probed by intrinsic fluorescence recorded on a SAFAS Xenius spectrophotofluorimeter set up at a constant photo multiplier voltage of 570 V. Tryptophan residues or *N*-acetyl tryptophan amide (NATA) used as negative control were excited at 280 nm, and their fluorescence emission spectra were recorded between 310 and 380 nm, with a 5-nm bandwidth for excitation and emission. Experiments were done

in a quartz cuvette in a final volume of 200  $\mu\text{L}$ , in which increasing amounts of R6G were added. Resulting emission curves were integrated and deduced from the same experiments carried out with NATA, used at the same concentration than that of BmrA tryptophan residues. Data were plotted as a function of R6G concentration. Binding of ATP-Mg<sup>2+</sup> was carried out in the same way, pre-incubating BmrA E504A with or without 100  $\mu\text{M}$  R6G for 15 min on ice.

**Ligand binding to BmrA-nanodiscs complexes and empty nanodiscs.** R6G, DDM and DM binding assays were carried out as above. Assays with empty nanodiscs (without BmrA) were carried out at the same nanodiscs concentration as that of BmrA-nanodiscs, complexes. This allowed to correct the fluorescence quenching due to the interaction between empty nanodiscs alone and ligands. Two cuvettes of NATA were also used: one for BmrA-nanodiscs complex and the other one for the empty nanodiscs. Data were analyzed in the same way as above.

**Doxorubicin transport by BmrA** was recorded as previously described (23). Ten micromolar of doxorubicin and 2 mM ATP were added to 100  $\mu\text{g}$  *E. coli* inverted membrane vesicles containing overexpressed BmrA. Transport was initiated upon addition of 2 mM MgCl<sub>2</sub> and monitored at 25 °C in 1-mL quartz cuvettes recording the fluorescence on a Photon Technology International fluorimeter at 590 nm with a bandwidth of 4 nm upon excitation at 480 nm with a bandwidth of 2 nm. Transport was initiated by adding 2 mM ATP-Mg<sup>2+</sup>.

**R6G accumulation in *Bacillus subtilis* strains.** R6G accumulation assay was performed in *B. subtilis* strain 168 (WT) and 8R (overexpressing *BmrA* (24) kindly provided by Pr. Hans Krügel). Strains were grown overnight in LB medium at 37 °C with agitation, and then diluted to 0.05 OD<sub>600nm</sub> with fresh medium. Once the culture reached 0.5 OD<sub>600nm</sub>, they were incubated with 5  $\mu\text{M}$  R6G for 30 min more. Then 2 mL of each culture ( $\sim 1$  OD<sub>600nm</sub>) was centrifuged at 15,000  $\times g$  for 10 min at 4 °C. The pellets were washed with 1 mL LB medium and centrifuged. The pellets were suspended in 500  $\mu\text{L}$  of 50 mM Tris-HCl pH 8.0, 150 mM NaCl, 1 mg/mL lysozyme and incubated for 1 h at 37 °C with agitation. The cells were then incubated with 0.5% SDS for 15 min more. R6G fluorescence was recorded with a SAFAS Xenius spectrofluorimeter in a black 96 well-plate using 200  $\mu\text{L}$  of cell lysates setting excitation to 526 nm and recording fluorescence between 541 and 650 nm.

**Data fit.** Data were fitted using Microsoft Excel (365), SigmaPlot (v12.5) and GraphPad (v8) using/setting up the following equations:

**Equation 1 (Intrinsic fluorescence quenching, ligand binding, one site saturation):**

$f = F_{max} * \text{abs}([L]) / (K_D + \text{abs}([L]))$ ,  $F_{max}$  = maximal intrinsic fluorescence without ligand,  $[L]$  = ligand concentration,  $K_D$ , ligand dissociation constant.

**Equation 2 (allosteric intrinsic fluorescence increase):**

$f = F_{min} + (F_{max} - F_{min}) / (1 + ([L] / K_D)^{-h})$ ,  $F_{min}$  = minimal intrinsic fluorescence without ligand,  $F_{max}$  = maximal intrinsic fluorescence with ligand,  $[L]$  = ligand concentration,  $K_D$ , ligand dissociation constant,  $h$  = Hill number.

**Equation 3 (Sigmoidal, 3 parameters):**  $f = F_{max} / (1 + \exp(-([L] - [L]_{50}) / b))$ ,  $F_{max}$  = maximal intrinsic fluorescence,  $[L]$  = ligand concentration,  $\mu\text{M}$ ,  $[L]_{50}$  = ligand concentration at half-maximal intrinsic fluorescence,  $\mu\text{M}$ .

**Equation 4 (Intrinsic fluorescence quenching, ligand binding, two sites saturation):**  $f = F_{max1} * \text{abs}([L]) / (K_{D1} + \text{abs}([L])) + F_{max2} * \text{abs}([L]) / (K_{D2} + \text{abs}([L]))$ ,  $F_{max1}$ ,  $F_{max2}$  = maximal intrinsic fluorescence without ligand,  $[L]$  = ligand concentration,  $K_{D1}$ ,  $K_{D2}$ , ligand dissociation constants.

## HDX experiments

HDX-MS experiments were performed using a Synapt G2-Si mass spectrometer coupled to a NanoAcquity UPLC M-Class System with HDX Technology (Waters™). All the reactions were carried out manually. Labeling was initiated by diluting 5  $\mu$ L of typically 15  $\mu$ M BmrA in nanodiscs, in 95  $\mu$ L D<sub>2</sub>O labeling buffer, 5 mM Hepes pD 8.0, 50 mM NaCl. For the Vanadate-trapped condition, the labeling buffer additionally contained 10 mM ATP, 10 mM MgCl<sub>2</sub> and 1 mM Vanadate. Samples were labeled for 2, 5, 15 and 30 minutes at 20 °C. Subsequently, the reactions were quenched by adding 22  $\mu$ L of ice-cold quenching buffer, 0.5 M glycine, 8 M guanidine-HCl pH 2.2, 0.035% DDM and 0.03% sodium cholate, to 100  $\mu$ L of labelled sample, in ice bath. After 1 min, the 122- $\mu$ L quenched sample was added into a microtube containing 200  $\mu$ g of activated zirconium magnetic beads (MagReSyn Zr-IMAC from Resyn Biosciences, USA), to remove the phospholipids (43). After 1 min. magnetic beads were removed and the supernatant injected immediately through a 100- $\mu$ L loop. Labelled proteins were then subjected to in-line digestion at 15 °C using a pepsin column (Waters Enzymate™ BEH Pepsin Column 300 Å, 5  $\mu$ m, 2.1 x 30 mm). The resulting peptides were trapped and desalted for three minutes on a C4 pre-column (Waters ACQUITY UPLC Protein BEH C4 VanGuard pre-column 300 Å, 1.7  $\mu$ m, 2.1 x 5 mm, 10K - 500K) before separating them with a C4 column (Waters ACQUITY UPLC Protein BEH C4 Column 300 Å, 1.7  $\mu$ m, 1 x 100 mm) using a linear acetonitrile gradient of 5-40% in 15 min and then four alternative cycles of 5% and 95% until 25 min. The valve position was adjusted to divert the sample after 11.2 min of each run from C4 column to waste to avoid contaminating the mass spectrometer with detergent. Two full kinetics were run for each condition, one after the other, to get duplicate of each deuteration timepoint. Blanks, with equilibration buffer, 5 mM Hepes pH 8.0, 50 mM NaCl, were injected after each sample injection and pepsin column washed during each run with pepsin wash (1.5 M guanidine-HCl, 4% acetonitrile, 0.8% formic acid pH 2.5) to minimize the carryover. Electrospray ionization Mass spectra were acquired in positive mode in the m/z range of 50–2000 and with a scan time of 0.3 s. For the identification of non-deuterated peptides, data was collected in MS<sup>E</sup> mode and the resulting peptides were identified using PLGS™ software (ProteinLynx Global SERVER 3.0.2 from Waters™). Deuterated peptides were identified using DynamX 3.0 software (Waters™), using the following parameters: minimum intensity of 1000, minimum products per amino acid of 0.3 and file threshold of 2. Deuterios 2.0 software (44) was used for data analysis, visualization and statistical treatments. The mass spectrometry data have been deposited to the ProteomeXchange Consortium via the PRIDE (45) partner repository with the dataset identifier PXD022185.

## Biophysics

**Products.** Crystallization solutions were from Grenier bio-one. The Mosquito crystallization robot is from TTP Labtech. Crystallization plates and cover were from Grace Bio-Labs. The cryoprotection kit was from Molecular Dimensions. Cryschem plates were from Hampton Research. Vitrobot grid freezing device is from FEI. The Talos Arctica and Titan Krios G3 are from Thermo Scientific.

## **X-ray**

*Protein crystallization.* The crystallography step was performed at 19 °C. Crystals were obtained by vapor diffusion on hanging drops. E504A BmrA mutant was concentrated by centrifugation-filtration to 7-10 mg/mL spinning at 500 xg on a 50 kDa cutoff Amicon Ultra-15 at 22 °C. BmrA E504A mutant was then incubated with 5 mM ATP-Mg for 30 min. Crystallogenesis was done by mixing with a Mosquito 450 nL of reservoir solution containing 100  $\mu$ L 0.1 M Tris-HCl pH 8.5, 23-27% PEG 1000 with 50 nL of compounds 3a-3e and 500 nL of BmrA E504A sample. the mix was deposited on a plastic cover,

sealed onto the plate and imaged periodically with a Formulatrix. Crystals appear after 3 days, grown up to 5-8 days and progressively disappeared if the incubation lasted longer.

*Crystal cryocooling.* As BmrA E504A mutant crystals were sensitive to cryoprotection, it was therefore performed using the CryoProtX MD1-61 kit. Best results were obtained with a final solution containing 12.5% (v/v) di-ethylene glycol, 18% (v/v) 2-methyl-2,4-pentanediol, 7% (v/v) ethylene glycol, 12.5% (v/v) 1,2-propanediol, 12.5% (v/v) dimethyl sulfoxide, supplemented with 5 mM ATP-Mg and 1 mM compounds **3a-3e**. One microliter of cryo-solution was divided in 3 drops under the binocular, close to the drop containing the crystal and then gently brought in contact using the freezing loop, at the opposite side where the crystal was sitting, in the course of 1 min. This operation was performed in Cryschem sitting drop plates, with the drop sitting in the middle of a water-filled reservoir to saturate the solution with humidity. Crystals were then harvested and placed on a fresh drop of cryo-solution for 1 min. before harvesting and cryocooling in liquid N<sub>2</sub>. Crystals were stored in liquid N<sub>2</sub> before being analyzed at the synchrotron.

*Diffraction data acquisition.* Diffraction screening has been performed at ESRF and SOLEIL synchrotrons on multiple beamlines over the years. Best data set was collected on PX2 at SOLEIL, consisting of a low-resolution pass at low transmission, and a high-resolution dataset at full transmission collected helicoidally. Crystal polymorphism was strongly present, precluding data merging among several crystals. Crystals diffracted very anisotropically, going to 3.9 Å resolution in the strongest diffracting direction. Data were processed in XDS as spherical to the highest resolution possible (3.9 Å) even though spherical statistics were not usable. Staraniso analysis for diffraction anisotropy revealed that completeness was 78% in the highest resolution shell, therefore revealing that all the data collectable for this crystal had been collected. Data was cut at the diffraction limits suggested by the Staraniso server. Anisotropic diffraction table is available in supplementary Table 1.

*X-ray structure and model building.* Phases were solved by molecular replacement using Phaser on amplitudes, with data corrected for anisotropy using Staraniso, and using the outward facing conformation dimer of Sav1866 (PDB code ID 2hyd) or MsbA (PDB code ID 3b60) as search models. Although Sav1866 and MsbA structures are very similar, the MsbA model yielded higher molecular replacement solution scores. Crystals belonged to the P21 space group with 2 dimers in the asymmetric unit. The molecular replacement solution was clear, but the electron density was very noisy due to the large conformational changes observed on BmrA, and that resulted in poor overall phases. The core of the protein was nevertheless clearly visible with helices as tubes. The nucleotide-binding domain was very blurry as well as external loops. The model was turned into poly-Ala to place helices of the transmembrane region, and initial movement of the TM1-TM2 hinge. Refinement was carried out in autoBUSTER using corrected amplitudes, applying strict NCS. Iterative manual building in Coot followed by refinement resulted in visible continuous electron density with decreasing R-factors. Density for large amino acids appeared, as well as for ATP. Sequence was assigned, and iterative refinement continued with introduction of TLS refinement (1 TLS per chain, 4 total). It yielded R-factors around 30 and 35 for R and R<sub>free</sub> respectively, with small grooves in the helices. Re-definition of TLS (1 for a dimer of TMD, 1 for a dimer of NBD, 4 total) resulted in a dramatic decrease of R-factors by 3 points, and much clearer electron density features, helices with large grooves and side chain density. Unwinding of TM3 next to residue 136 was apparent, as well as helix breaks in the trans-membrane region and clear density for ATP. Some incorrect modeling of ATP became apparent with negative and positive density showing where the correct position was then defined. NCS was relaxed and correct modeling of geometry clashes was carried out in ISOLDE. Registry was built by starting to assign using initial first large density features clearly visible as refinement converged for the TMD, then using superpositions for the NBD. Registry at key locations was then probed by replacing several amino-

acids, or by trying to turn helices by one amino-acid clockwise or counterclockwise and probed by refinement. Newly refined structures clearly showed positive or negative densities indicative of incorrectly modeled features. Ramachandran and rotamers outliers were corrected, yielding a final model with R = 26.0% and R<sub>free</sub> = 32.1%. The final model was deposited in the Protein Data Bank under the accession code 6r72.

### **Cryo-EM**

*Sample preparation.* Purified BmrA E504A mutant at 3.4 mg/mL in DDM-cholate 1:1 (0.035%-0.03%) was incubated with 0.1 mM R6G followed by 5 mM ATP-Mg. Three microliters of this mixture were applied to cryo-EM Au-grids (Cflat 1.2/1.3 3Au) previously discharged in air for 40 s at 20 mA (PELCO easiGlow), blotted for 3 s, and plunge frozen in liquid ethane with a Vitrobot grid freezing device.

*Data acquisition, image processing.* Best grids screened with a Talos Arctica were then imaged with a Titan Krios G3 electron microscope equipped with a K2 camera and operating at 300 keV. A total of 3477 movies of 40 frames each were acquired over 2 data-collection sessions in electron counting mode at 1.06 Å/pixel, 6.4 electrons/pixel/s, with a total exposure time of 6 s and combined into a single MRC stack using EPU automatic data collection control software using defocus values ranging from 1.2 to 3.2 μm. Contrast transfer function (CTF) parameters were estimated from the averaged movie with CTFIND4 and 2170 particle images were selected manually and subjected to 2D classification in cryoSPARC v2. Automatic particle selection was performed with templates from the 2D classification. Beam induced particle motion between fractions was corrected with a new implementation of alignparts lmbfgs in cryoSPARC v2. The number of particle images were reduced to 128372 by further 2D and 3D classifications and refinements. Models were calculated ab initio and refined without the application of symmetry with cryoSPARC v2. For each data collection session automatically picked particles were cleaned with 2 rounds of 2D classification followed by a preliminary round of 3D classification to further remove obvious junk particles such as empty detergent micelles that were not eliminated during the 2D classification process. Although no discrete conformation could be isolated to high resolution, removal of additional particles improved the resolution of the final maps suggesting significant non-discrete or continuous flexing. Since these maps suggested a significant amount of small, non-discrete flexing, better resolved maps were obtained using cryoSPARC v2's non-uniform refinement feature. An additional refinement with the application of C2 symmetry was performed that resulted in a gain of 0.3 Å in overall resolution which helped to slightly improve the interpretability of the map in the model building process. The asymmetric and C2 symmetrized maps have been deposited in the Electron Microscopy database under the accession codes EMD-4749 and EMD-12170 respectively.

*Model building and refinement.* The X-ray model was docked into a 3.9 Å C2 symmetrized cryo-EM density map and improved with iterative rounds of manual building in Coot and Isolde followed by real\_space\_refine in Phenix. Of Note, sharpening the C2 symmetry map using Phenix led to improved features in the trans-membrane domain, but worse in outer loops and the NBD. The final model was thus built using both sharpened and unsharpened maps. The final model was validated with MolProbity and EMRinger and deposited in the Protein Data Bank under the accession code 6R81 and electron microscopy database EMD-4749.

Two small densities were visible in the C2 symmetrized map at the locations of R6G. Re-examination of the data with no symmetry led to the identification of clearer densities in which R6G could be placed and suitably refined. Notably, both densities are not equivalent in the two halves of BmrA, suggesting that in both binding sites there is a heterogeneity/flexibility of binding, reminiscent of substrate release. Understandably, the application of C2 symmetry masked the quality of the reconstructions at these locations since these sites are not identical with respect to R6G binding. Thus BmrA was refined



in the presence of R6G, following the same procedure as above using the asymmetric map. Final model and maps were deposited in the Protein Data Bank under the accession code 7BG4 and electron microscopy database EMD-12170. Model statistics are provided in supplementary Table 1.

### Bioinformatics

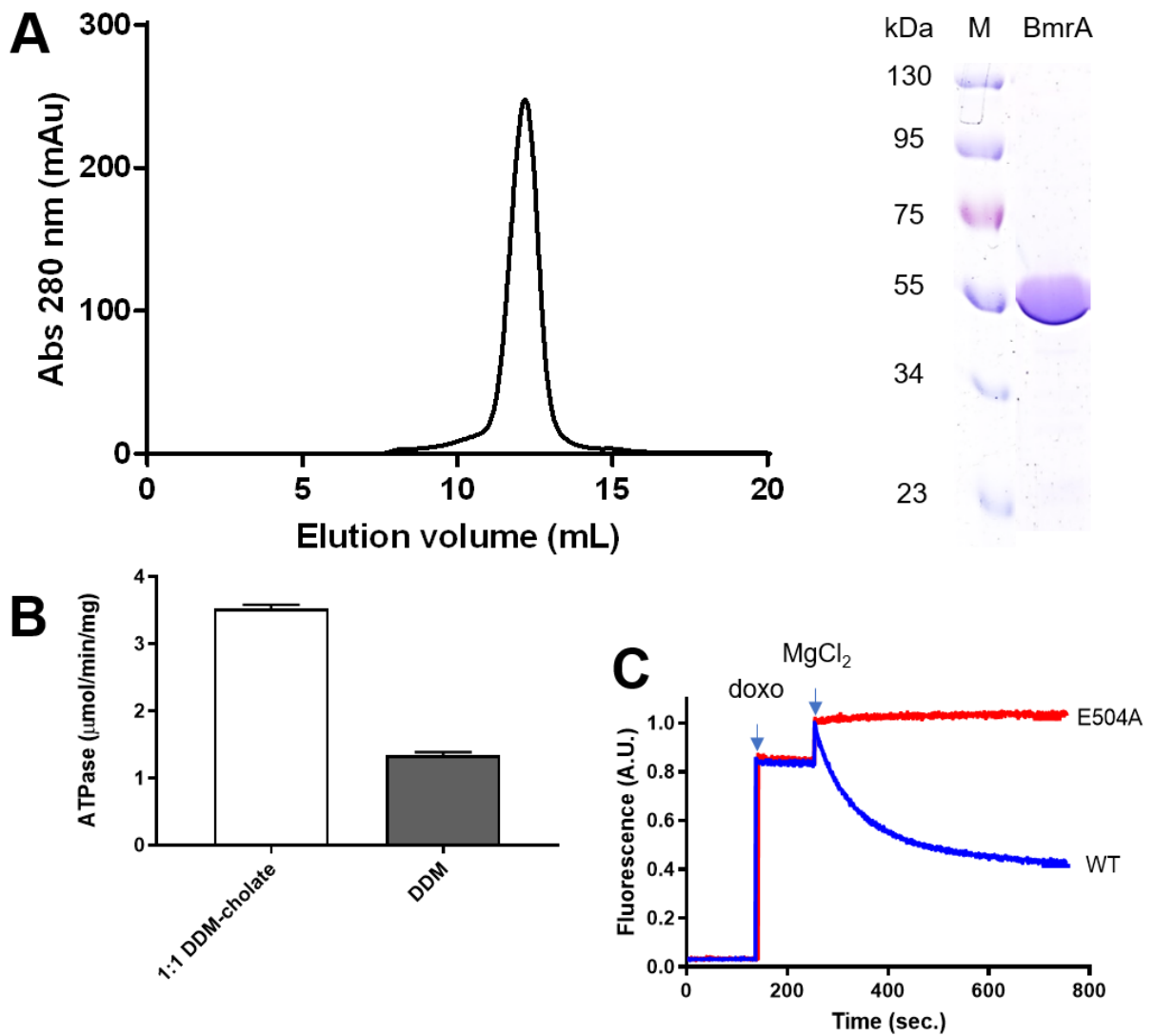
Both the X-ray and the cryo-EM(C2) structures span residues 10 to 589, and both miss a few residues (271-278 in the X-ray structure, 273-278 in the cryo-EM structure), corresponding to the loop region between TM5 and TM6. Complete models of dimeric wild-type BmrA were generated using Modeler (v9.12), for both the X-ray and the cryo-EM structures, using the structure of the ABC transporter related protein from *Novosphingobium aromaticivorans* (PDB code ID 4mrs) (46) as a template for the missing residues, and the alignment generated by HHPred (47). The N-termini were capped with acetyl groups, and the missing N-terminal residues were not modeled. Both models contained ATP molecules and Mg<sup>2+</sup> ions, as observed in both the X-ray and the cryo-EM structures. The models were then oriented using the OPM server (<http://sunshine.phar.umich.edu/server.php>) (48) and embedded into a mixed POPE/POPG bilayer (ratio 3/1) using the CHARMM-GUI membrane builder (49), and the replacement method. The systems were solvated and 150 mM KCl was added to the solution, yielding a total of ~157,000 atoms in tetragonal boxes of dimensions ~100x100x165 Å<sup>3</sup>.

All simulations were run with the GROMACS (v2016.4) software package (50, 51). The CHARMM36 force field was used for both the lipids and the protein, together with the CHARMM TIP3P water model. Non-bonded interactions were calculated with a cutoff of 1.2 Å, with a shift function on the potential to avoid discontinuities. Neighbor lists were updated using the Verlet scheme. Long-range electrostatic interactions were calculated with the Particle Mesh Ewald method (52). Bonds involving hydrogen atoms were constrained using the P-LINCS algorithm (53).

Each system was minimized by steepest descent and then equilibrated using a 6-cycle equilibration scheme, using position restraints on the protein and gradually reducing the force constant. Equilibration and production runs were performed at 303.15 K and 1 bar; the temperature was kept constant with the velocity rescale algorithm (54) and the pressure with the Parrinello-Rahman barostat (55). The integration time step was set to 2 fs. For each system, four replicates were simulated for 500 ns each. The first 200 ns of each simulation were treated as equilibration, and average quantities (average structures, inter-atomic distances, RMSD, RMSF, B factors) were computed on the remaining 300 ns. Two additional replicates were run with long equilibration steps (275 ns before 500 ns of production) to confirm the closing movement of the cavity.

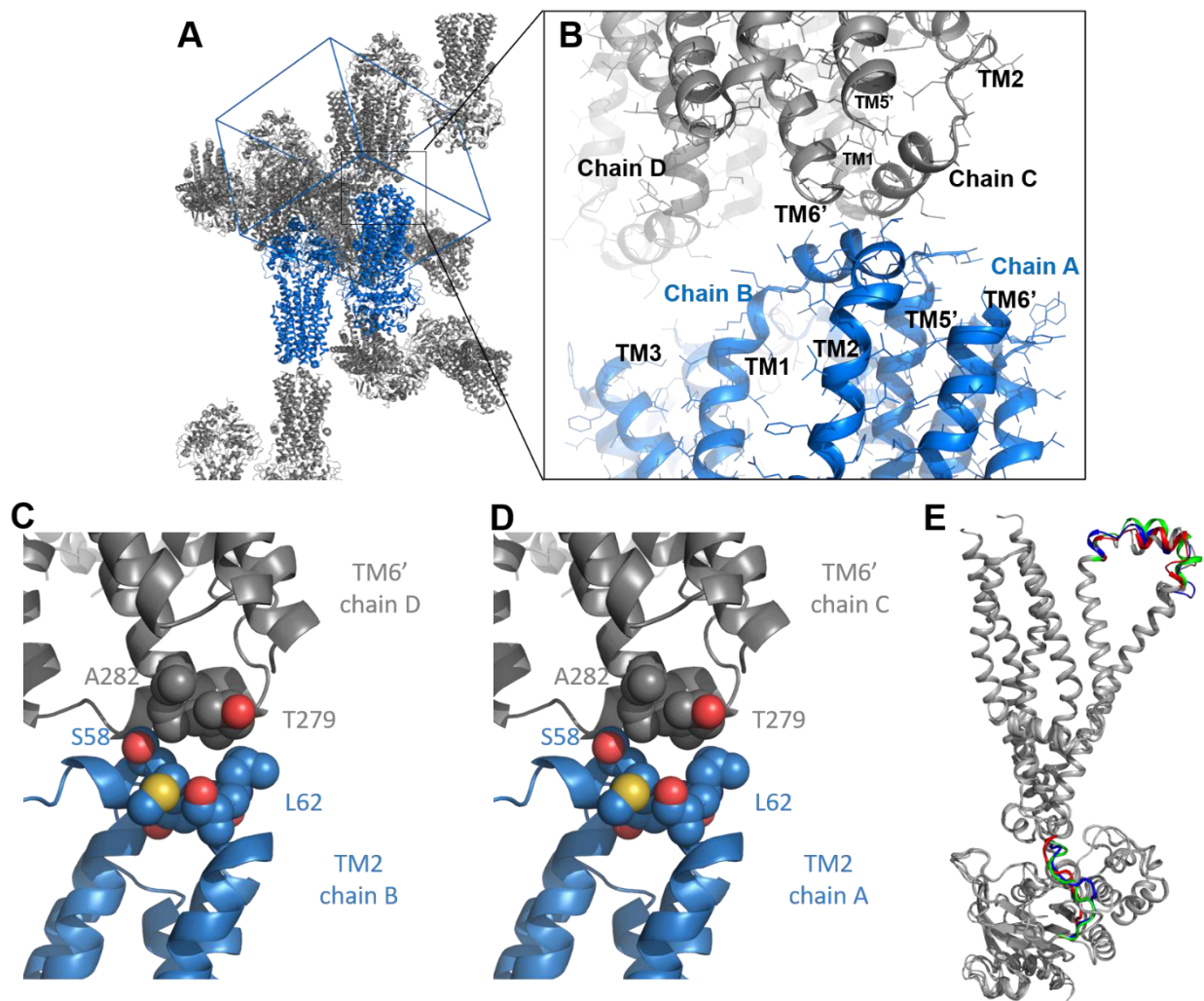
Due to the relatively large size and the transmembrane nature of BmrA, we expect functional motions of the transport cycle to take place on time scales much longer than the simulation time (probably 3-4 orders of magnitude longer), which are currently not accessible by all-atom molecular dynamics. Therefore, we only expect to observe relatively fast conformational changes, and changes driven by strong driving forces.

Fig. S1.



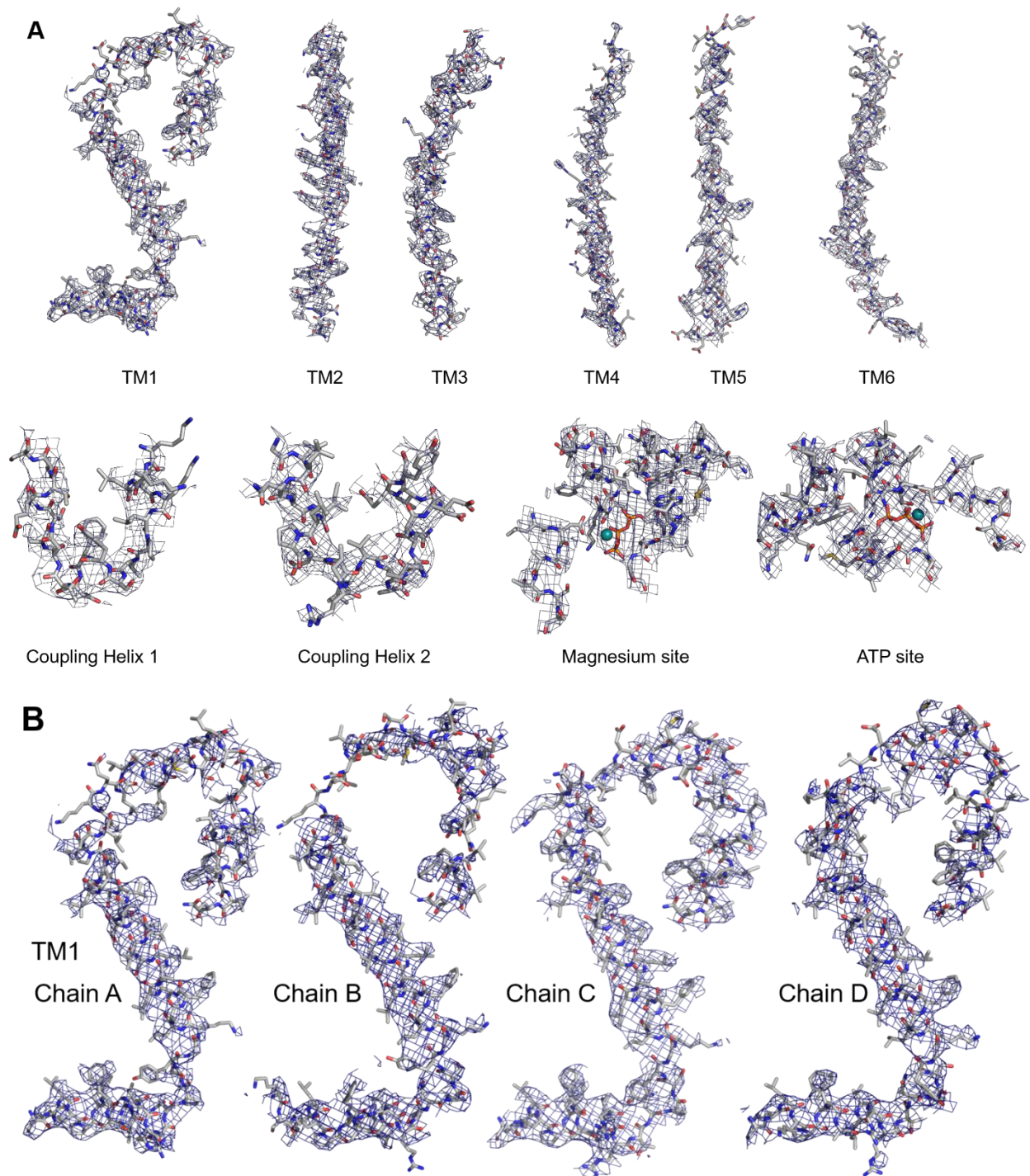
**Fig. S1. Purification of BmrA, ATPase activity and transport assay. (A) Preparative SEC profile of detergent purified BmrA (left panel). The peak fraction was analyzed by SDS-Page (right panel). (B) ATPase activities of WT BmrA purified with DDM or DDM-cholelate mixture. (C) Doxorubicin (doxo) transport activity of WT BmrA and the inactive E504A mutant.**

Fig. S2.



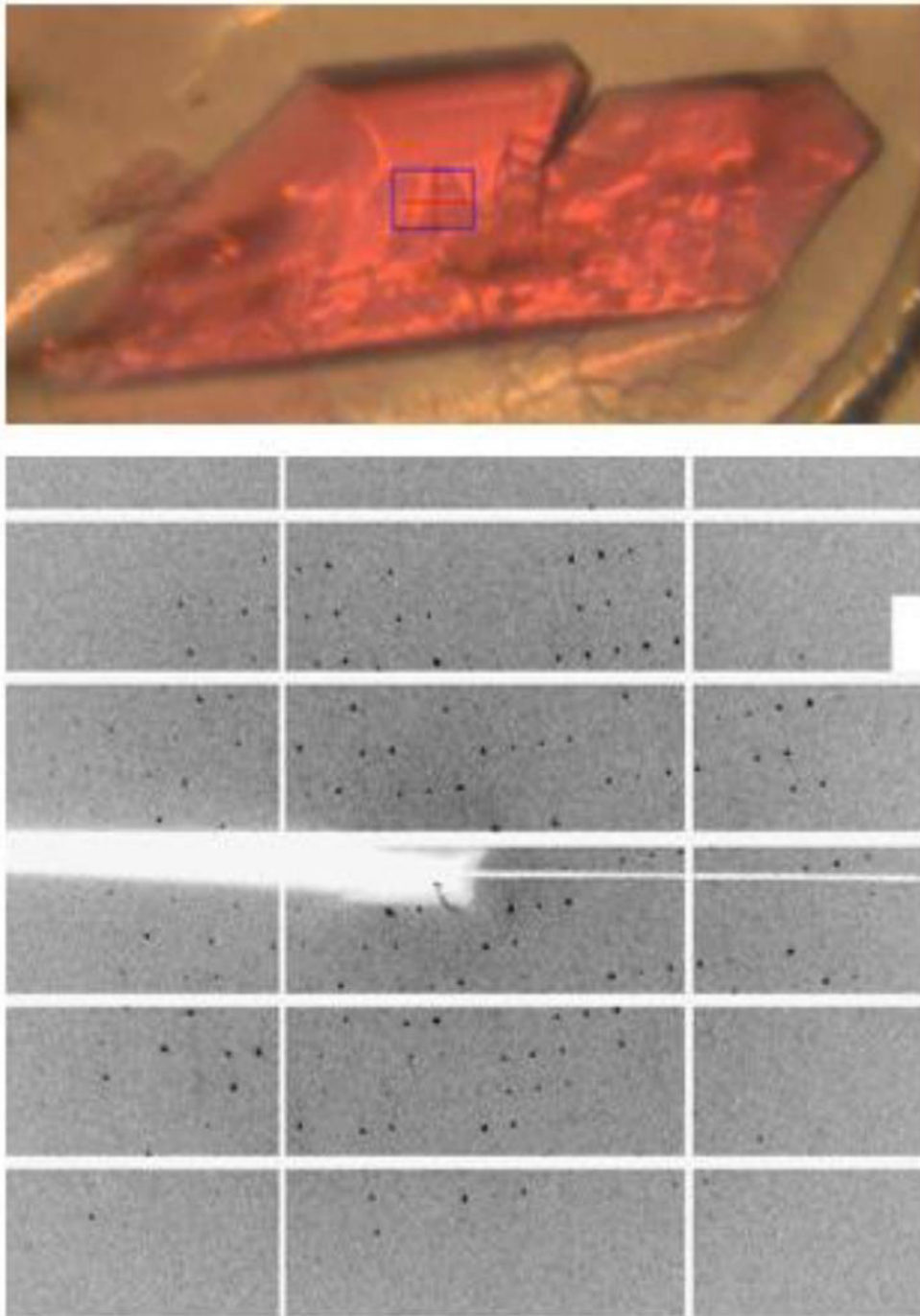
**Fig. S2. Crystallographic packing and difference between monomers in the asymmetric unit. (A) Overall crystal packing. The 4 BmrA monomers A-D of the asymmetric unit, assembled in 2 dimers, AB colored in blue, and the symmetric dimer CD in grey. Proteins are represented as cartoon, and the cell is drawn in blue. (B, C, D) Close-up views of the interaction between TM1-2 of the B/D and C/A monomers. (E) Differences between monomers in the X-ray structure. Structures are represented in cartoon, colored in grey. Flexible regions are highlighted in green (chain B), blue (chain C) and red (chain D). Each 4 monomers of the asymmetric unit of the crystallographic structure were superposed onto chain A.**

Fig. S3.



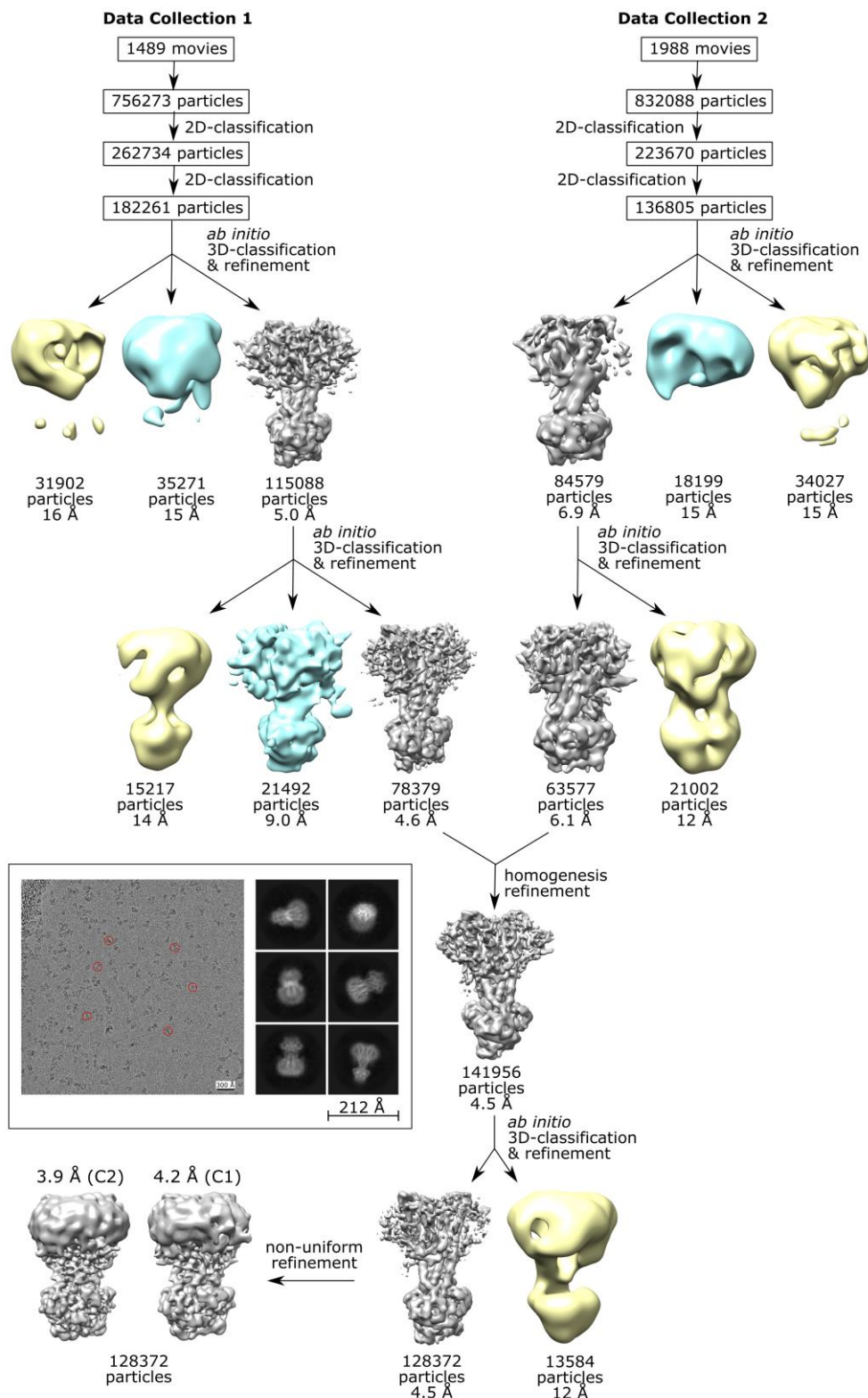
**Fig. S3. X-ray densities of BmrA. (A) TM helices, coupling helices and ATP-Mg<sup>2+</sup> binding site of chain A. (B) Densities of the TM1-extracellular loop 1 for each chain.**

Fig. S4.



*Fig. S4. Crystallization of BmrA E504A in complex with ATP-Mg<sup>2+</sup> and R6G.*

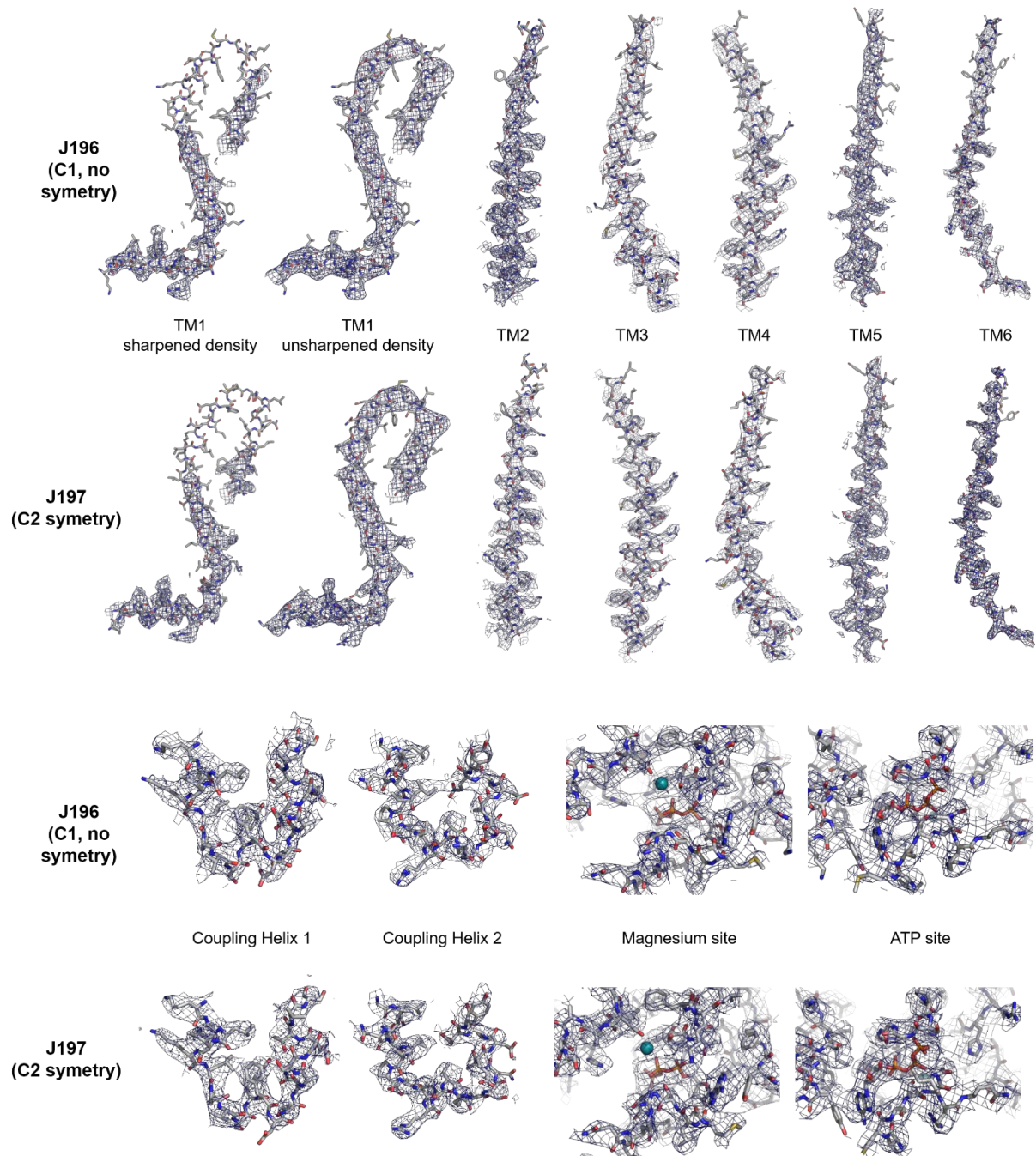
Fig. S5.



**Fig. S5. Image collection, 2D-3D classification, and processing workflow of cryo-EM image analysis of BmrA in OF conformation.** Micrographs from two separate data collection sessions were processed in parallel and the best particles from each session were later combined to produce the final maps. For each session, picked particles were cleaned using 2 rounds of 2D classification followed by a 3D classification. Heterogeneity within the dominating outward-facing conformation was further assessed with additional rounds of 3D classification that removed an additional 35% of the outward-facing particles. Although removal of these particles improved

*the resolution of the dominating outward-facing conformation, discrete conformations could not be refined to high resolution suggesting that a large degree of small, non-discrete flexing was interfering with particle alignment. Due to the significant flexing amount, the final maps were refined using cryoSPARC's non-uniform refinement feature resulting in better resolved maps. An additional refinement with the application of C2 symmetry was performed that resulted in an improvement in resolution. Boxed: example micrograph with particles used for 2D classification (red circles), and corresponding representative 2D class averages.*

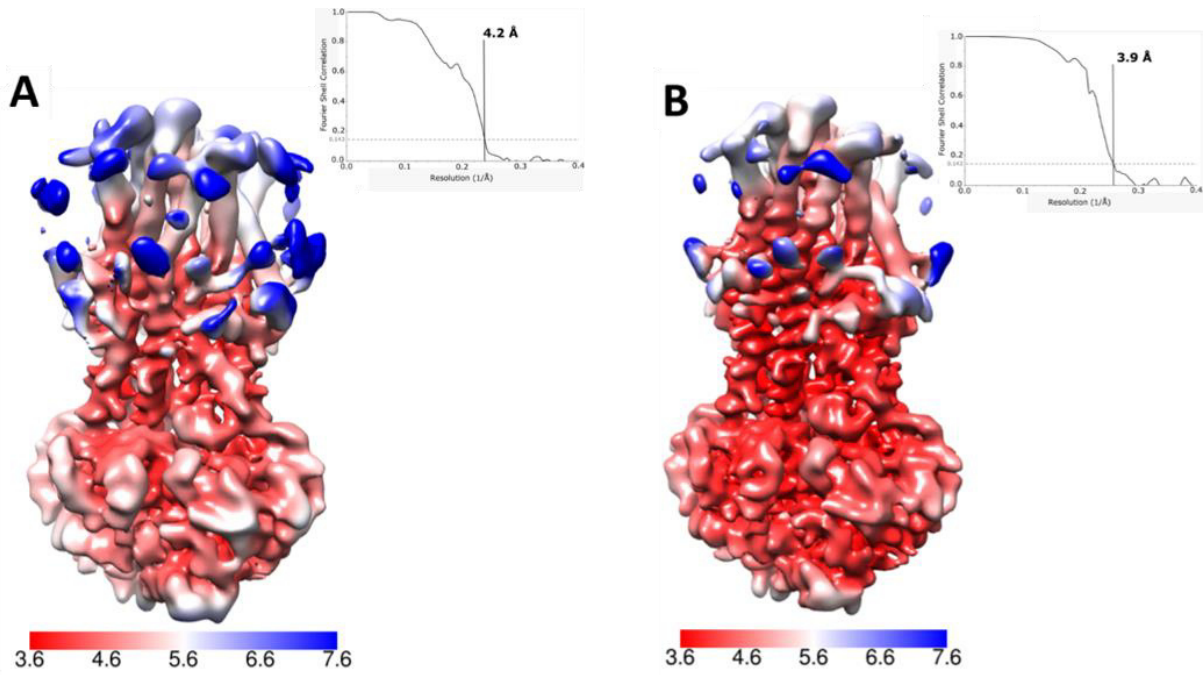
Fig. S6.



**Fig. S6. Cryo-EM densities of BmrA. Sharpened EM densities of the TM helices (and also unsharpened for TM1), coupling helices and the Magnesium and ATP binding sites for J196 (C1, no symmetry) and J197 (C2 symmetry map).**

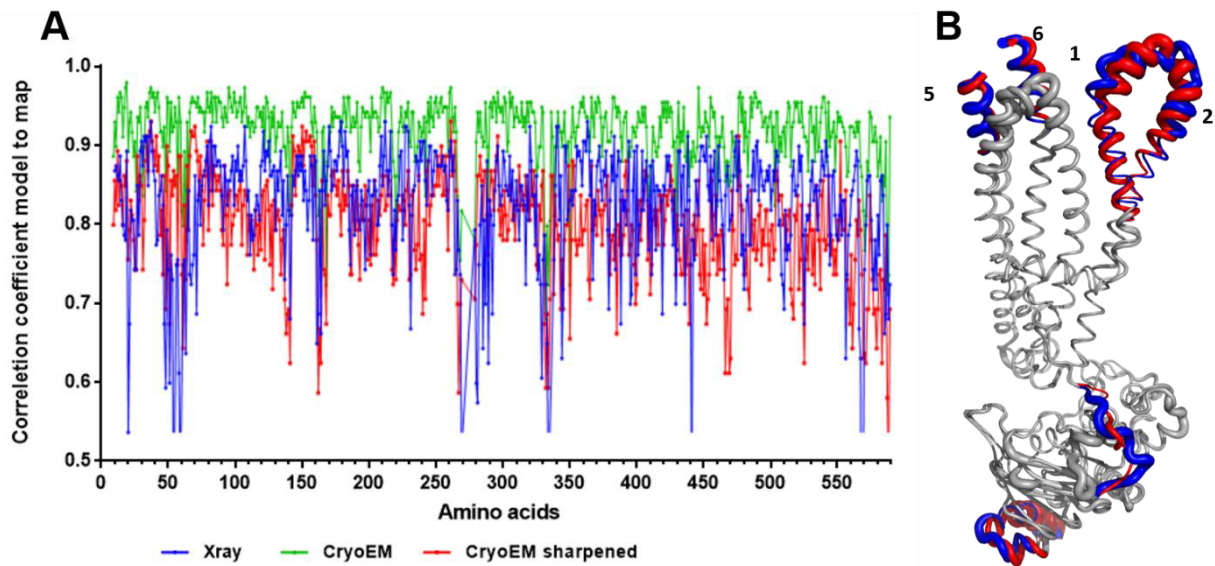


Fig. S7



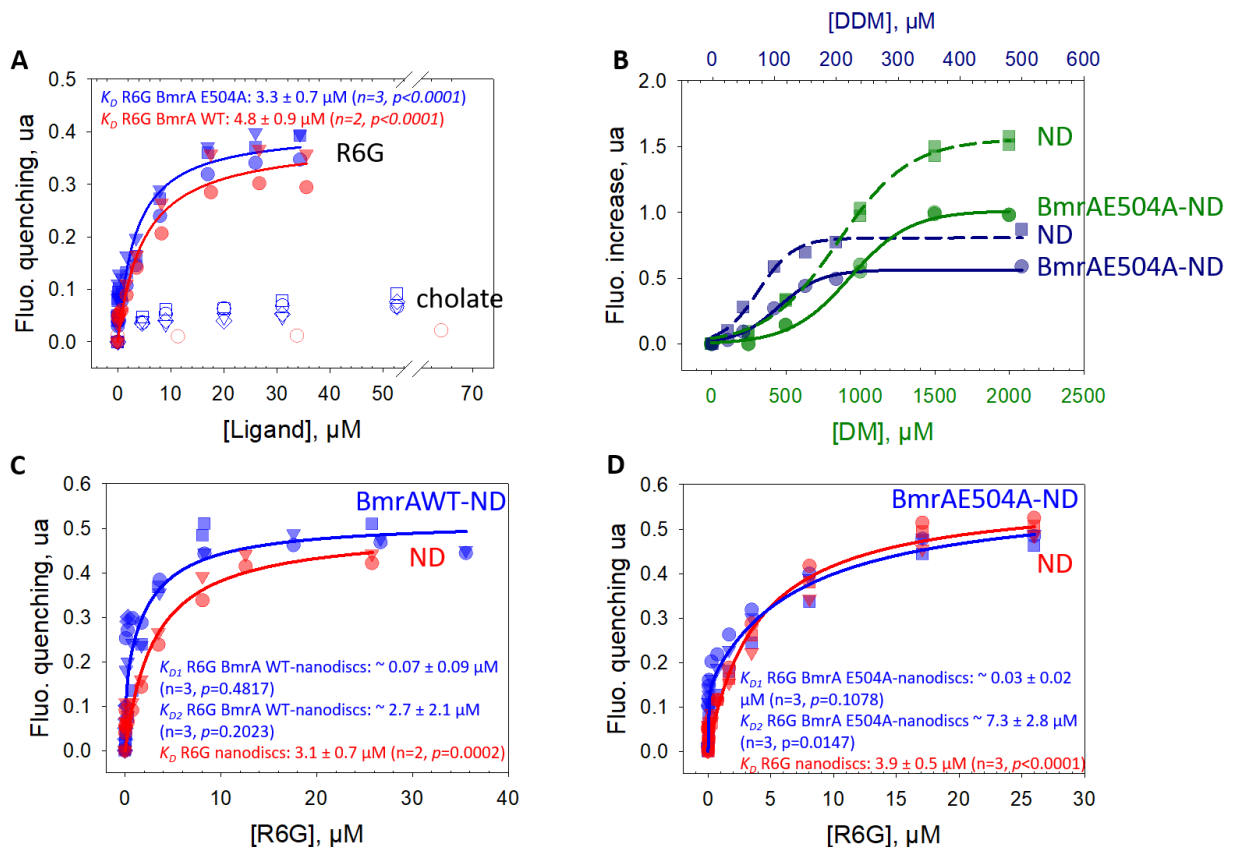
**Fig. S7. Assessment of the cryo-EM data. Local-resolution estimation of the C1 (A) and C2 (B) density maps and their corresponding Fourier Shell Correlation (FSC).**

Fig. S8.



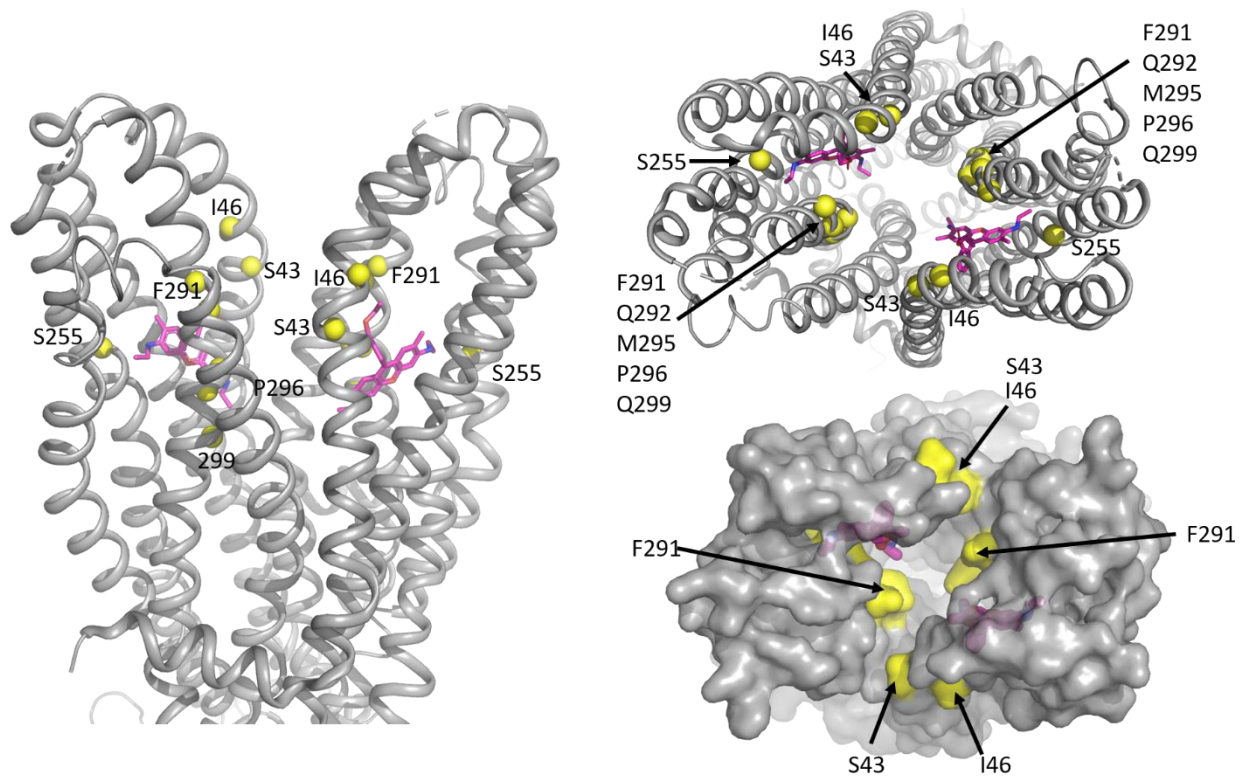
**Fig. S8. Correlation coefficient model to map and identification of the flexible parts of X-ray and cryo-EM structure. (A)** The value of correlation coefficient model to map was calculated for each model against the corresponding density map. The results are plotted as a function of the amino acid sequence (X-ray in blue, cryo-EM unsharpened in green and sharpened in red). **(B)** The X-ray and the cryo-EM structures are superposed; the flexible parts are colored in red and blue for the cryo-EM and X-ray structure, respectively. These flexible parts correspond to the lowest CC values. The cartoon is represented with the thickness of the sausage corresponding to the B-factor, the higher the B-factor, the larger the sausage.

Fig. S9.

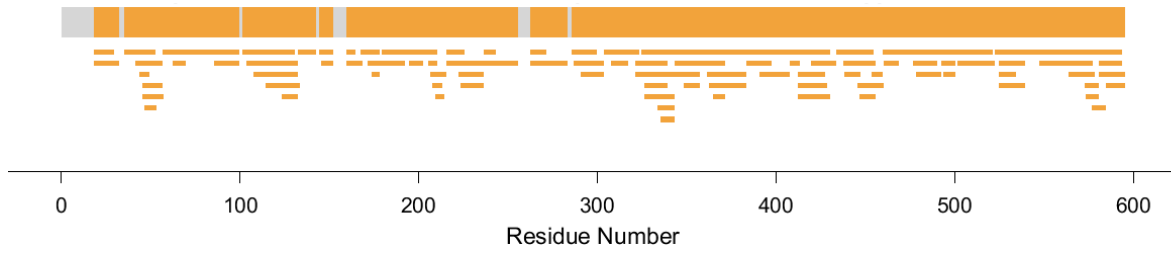


**Fig. S9. Binding of compounds to BmrA probed by intrinsic fluorescence. (A) Binding of R6G (filled symbols) and cholate (empty symbols) to BmrA WT (red) or E504A mutant (blue) purified in DDM. Data were fitted with equation 1. No significant fluorescence change was observed upon cholate addition in same conditions. (B) Effect of DDM (blue) and decyl maltoside (DM, green) on empty nanodiscs (ND) and BmrA-nanodiscs complexes. BmrA E504A was purified in DDM and then reconstituted into nanodiscs to which DM or DDM were added. The same experiments were done with empty nanodiscs (ND). Data were fitted using equation 3, giving a half-maximal fluorescence increase detergent concentration,  $[DDM]_{50}$ , of  $\sim 106 \pm 6 \mu\text{M}$  ( $n = 1$ ,  $p < 0.0001$ ) and  $\sim 74.1 \pm 7.7 \mu\text{M}$  ( $n = 1$ ,  $p < 0.0006$ ), and  $[DM]_{50}$  of  $931 \pm 23 \mu\text{M}$  ( $n = 2$ ,  $p < 0.0001$ ) and  $850 \pm 21 \mu\text{M}$  ( $n = 2$ ,  $p < 0.0001$ ) for the BmrA-nanodiscs complexes and empty nanodiscs, respectively. (C, D) Binding of R6G to BmrA WT-nanodiscs (C, blue), BmrA E504A-nanodiscs (D, blue) and corresponding empty nanodiscs (C or D, red). The amount of empty nanodiscs used in these experiments correspond to that of MSP1E3D1 proteins in complex with BmrA, estimated by SDS-PAGE using each purified protein as standard. Data best fitted with equation 1 for empty nanodiscs (one site saturation) and equation 4 for BmrA-nanodiscs complexes (two sites saturation).**

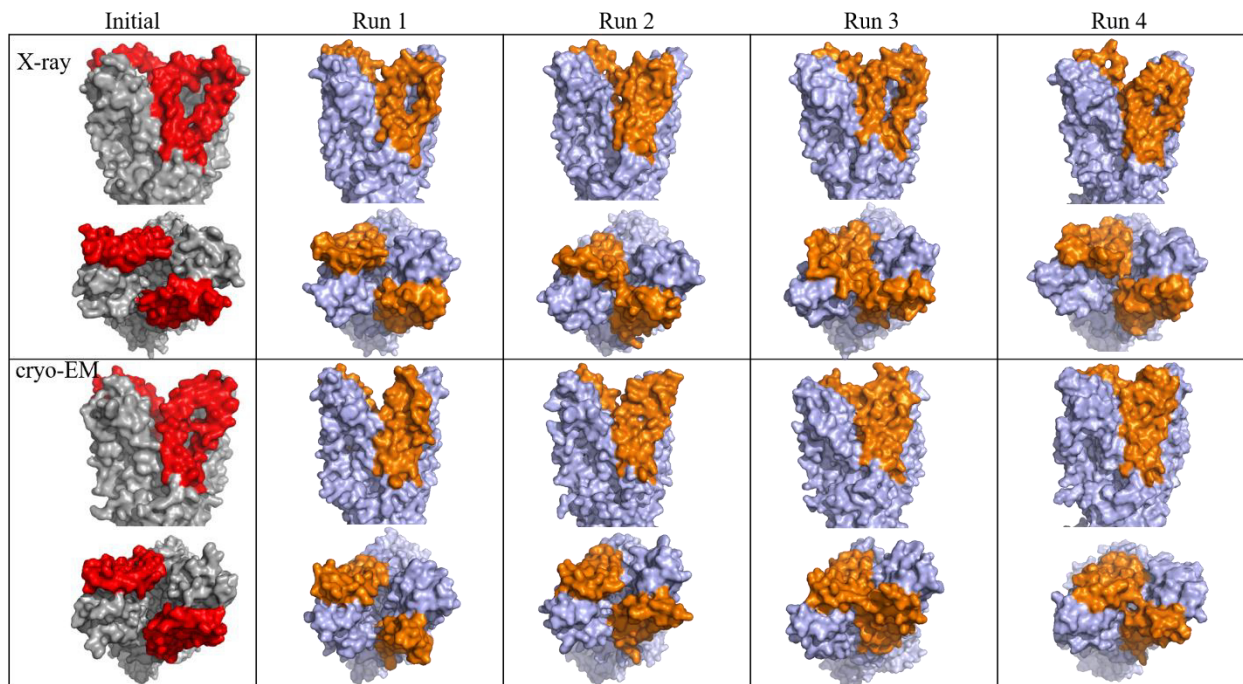
Fig. S10.



**Fig. S10.** *BmrA* residues equivalent to those of the human ABCB1 involved in Taxol binding. Cryo-EM *BmrA* structure is displayed in grey in which residues in yellow correspond to those involved in taxol binding in the human ABCB1 (14).

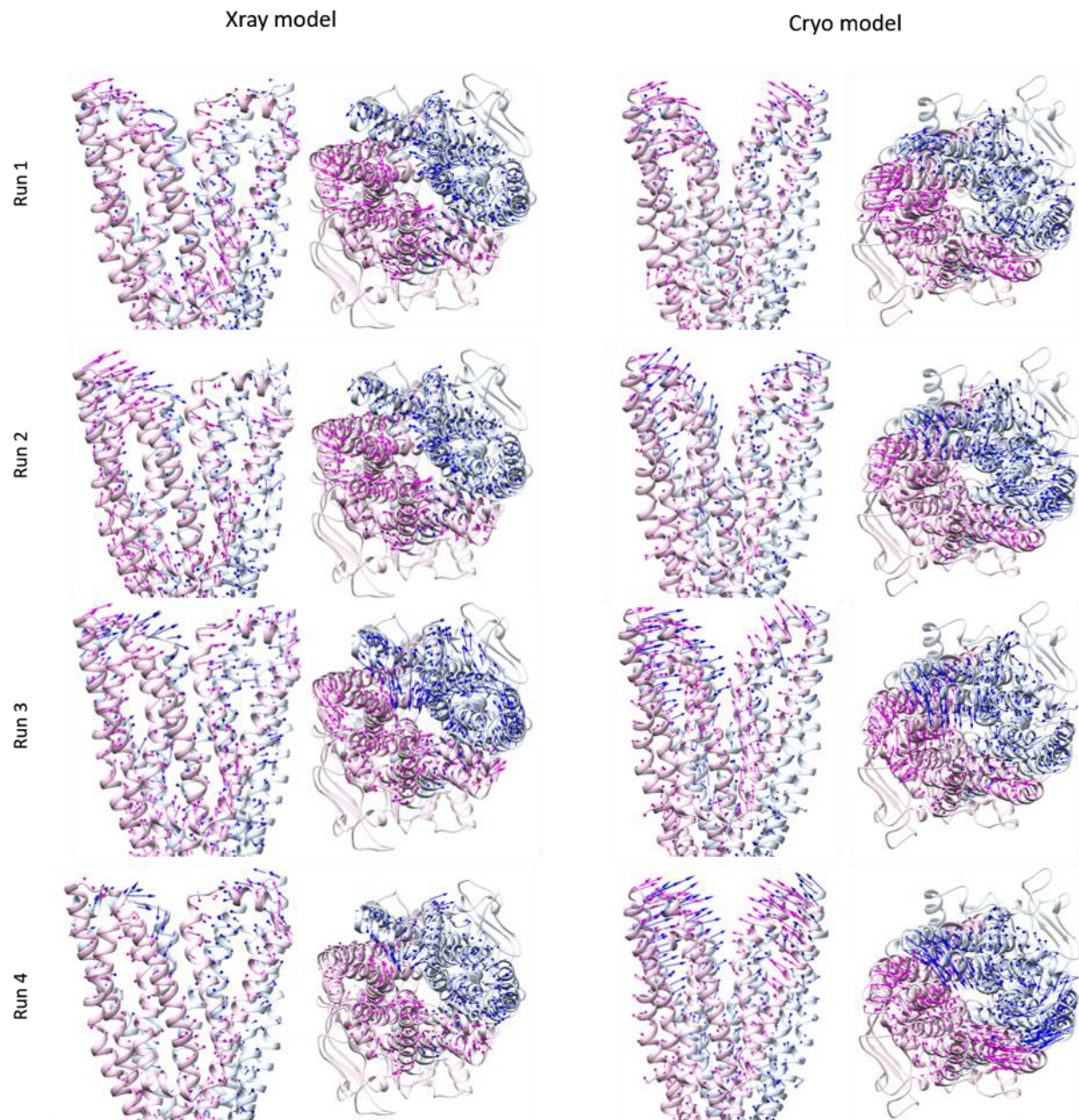
**Fig. S11.**

**Fig. S11.** *BmrA* peptide coverage map obtained in the HDX-MS experiment. The common peptides identified in both states (apo and Vi-trapped) of WT *BmrA* reconstituted in nanodiscs are indicated in orange. The overall sequence coverage was approximately 93%.

**Fig. S12.**

**Fig. S12. Molecular dynamic simulation results. The X-ray and cryo-EM structures are in grey and red (TM1-2). The final structures after 500 ns of simulation resulting from the four simulation runs are in light blue and orange (TM1-2). The side view (upper panel) and the top view (lower panel), from the outside of the membrane, are shown for each simulation.**

Fig. S13.



**Fig. S13.** Conformational changes of the TM region in the 8 simulations. Chain A is shown in pink and chain B in blue. Arrows indicate the displacement of the TM regions from the starting structures to the average structures.

**Table S1.****Table S1.** X-ray & cryo-EM data collection and refinement statistics.

X-ray	Non-corrected data	Corrected data
Data collection		
Space group	P2 <sub>1</sub>	P2 <sub>1</sub>
Cell dimensions		
<i>a, b, c</i> (Å)	117.8, 110.8, 155.6	117.8, 110.8, 155.6
<i>α, β, γ</i> (°)	90,93.2,90	90,93.2,90
Resolution (Å)	48.6-3.92(4.3-3.95) <sup>a</sup>	80.6-3.95(4.3-3.95)
<i>R</i> <sub>merge</sub>	0.068(3.7)	-(-)
<i>I</i> / <i>σ</i>	11.58(1.39)	11.65(1.39)
Completeness (%)	56.5(11.0)	92(71.5)
Redundancy	3.5(3.4)	-(-)
Ellipsoid <sup>b</sup>		0.851 a* + 0.525 c* b* -0.36 a* + 0.933 c*
Refinement		
Resolution (Å)		28.5-3.95
No. reflections		20484
<i>R</i> <sub>work</sub> / <i>R</i> <sub>free</sub>		26.0/32.1
No. atoms		17680
Protein		17552
Ligand/ion		128
B-factors (Å <sup>2</sup> )		
Protein		114.4
Ligand/ion		47.3
R.m.s deviations		
Bond lengths (Å)		0.013
Bond angles (°)		1.97
Ramachandran (%)		



## RESULTS: CHAPTER I

Favored	92.26
Allowed	7.39
Outliers	0.35

### Cryo-EM data collection, refinement and validation statistics

	EMD-12170	EMD-4749
	PDB: 7BG4	PDB: 6R81
<b>Data collection and processing</b>		
Magnification	130000	130000
Voltage (kV)	300	300
Electron exposure (e <sup>-</sup> /Å <sup>2</sup> )	38.4	38.4
Defocus range (μm)	1.2 to 3.2	1.2 to 3.2
Pixel size (Å)	1.06	1.06
Symmetry imposed	C1	C2
Initial particle images (no.)	486404	486404
Final particle images (no.)	128372	128372
Map resolution (Å)	4.2	3.9
FSC threshold	0.143	0.143
Map resolution range (Å)	3.6 to 25	3.5 to 9.1
<b>Refinement</b>		
Initial model used (PDB code)	6R81	6R72
Model resolution (Å)	4.3	4.2
FSC threshold	0.5	0.5
Model resolution range (Å)	3.6 to 7.6	3.6 to 7.6
Map sharpening <i>B</i> factors (Å <sup>2</sup> ) <sup>c</sup>	187, 238	187, 218
<b>Model composition</b>		
Non-hydrogen atoms	8927	8861
Protein residues	1141	1141
Ligands	6	4

RESULTS: CHAPTER I

---

<i>B</i> factors (Å <sup>2</sup> )		
Protein	95.8	170
Ligand	109	153
R.m.s. deviations		
Bond lengths (Å)	0.004	0.011
Bond angles (°)	0.834	1.61
Validation		
MolProbity score	2.24	2.33
Clashscore	16.2	14.1
Poor rotamers (%)	0.21	1.25
Ramachandran plot		
Favored (%)	90.6	88.1
Allowed (%)	9.40	11.5
Disallowed (%)	0.00	0.40

---

<sup>a</sup> Highest resolution shell is shown in parenthesis.

<sup>b</sup> Definition of ellipsoid: Data has been fitted to the ellipsoid defined by the following parameters:

Ellipsoid definition: 0.1742 0.2691 0.2191 2.0533

Diffraction limits & principal axes of ellipsoid fitted to diffraction cut-off surface:

4.564	0.8858	0.0000	0.4640	$0.851 \_a\_ * + 0.525 \_c\_ *$
3.717	-0.0000	1.0000	-0.0000	$\_b\_ *$
5.739	-0.4640	-0.0000	0.8858	$-0.360 \_a\_ * + 0.933 \_c\_ *$

Worst diffraction limit after cut-off:

5.976 at reflection -1 1 26 in direction  $-0.038 \_a\_ * + 0.038 \_b\_ * + 0.999 \_c\_ *$

Best diffraction limit after cut-off:

3.917 at reflection -2 28 5 in direction  $-0.070 \_a\_ * + 0.982 \_b\_ * + 0.175 \_c\_ *$

<sup>c</sup> Note that 2 different map sharpening levels were used to aid model building.

**Data S1. (separate file)**

Detergent quantitation.

**Data S2. (separate file)**

Thermostability assays.

**References**

39. B. Wiseman *et al.*, Stubborn contaminants: influence of detergents on the purity of the multidrug ABC transporter BmrA. *PLoS One* **9**, e114864 (2014).
40. E. Heftmann, S. T. Ko, R. D. Bennett, Response of steroids to sulfuric acid in thin-layer chromatography. *J Chromatogr* **21**, 490-494 (1966).
41. C. Orelle *et al.*, A multidrug ABC transporter with a taste for GTP. *Sci Rep* **8**, 2309 (2018).
42. F. J. Alvarez, C. Orelle, A. L. Davidson, Functional reconstitution of an ABC transporter in nanodiscs for use in electron paramagnetic resonance spectroscopy. *J Am Chem Soc* **132**, 9513-9515 (2010).
43. C. M. Hebling *et al.*, Conformational analysis of membrane proteins in phospholipid bilayer nanodiscs by hydrogen exchange mass spectrometry. *Anal Chem* **82**, 5415-5419 (2010).
44. A. M. Lau, J. Claesen, K. Hansen, A. Politis, Deuterios 2.0: Peptide-level significance testing of data from hydrogen deuterium exchange mass spectrometry. *Bioinformatics*, (2020).
45. Y. Perez-Riverol *et al.*, The PRIDE database and related tools and resources in 2019: improving support for quantification data. *Nucleic Acids Res* **47**, D442-d450 (2019).
46. J. Y. Lee, J. G. Yang, D. Zhitnitsky, O. Lewinson, D. C. Rees, Structural Basis for Heavy Metal Detoxification by an Atm1-Type ABC Exporter. *Science* **343**, 1133-1136 (2014).
47. L. Zimmermann *et al.*, A Completely Reimplemented MPI Bioinformatics Toolkit with a New HHpred Server at its Core. *Journal of Molecular Biology* **430**, 2237-2243 (2018).
48. M. A. Lomize, I. D. Pogozheva, H. Joo, H. I. Mosberg, A. L. Lomize, OPM database and PPM web server: resources for positioning of proteins in membranes. *Nucleic Acids Research* **40**, D370-D376 (2011).
49. J. Lee *et al.*, CHARMM-GUI Input Generator for NAMD, GROMACS, AMBER, OpenMM, and CHARMM/OpenMM Simulations Using the CHARMM36 Additive Force Field. *Journal of Chemical Theory and Computation* **12**, 405-413 (2016).
50. M. J. Abraham *et al.*, GROMACS: High performance molecular simulations through multi-level parallelism from laptops to supercomputers. *SoftwareX* **1-2**, 19-25 (2015).

51. B. Hess, C. Kutzner, D. van der Spoel, E. Lindahl, GROMACS 4: Algorithms for Highly Efficient, Load-Balanced, and Scalable Molecular Simulation. *Journal of Chemical Theory and Computation* **4**, 435-447 (2008).
52. U. Essmann *et al.*, A smooth particle mesh Ewald method. *The Journal of Chemical Physics* **103**, 8577-8593 (1995).
53. S. Páll, B. Hess, A flexible algorithm for calculating pair interactions on SIMD architectures. *Comput. Phys. Commun.* **184**, 2641-2650 (2013).
54. G. Bussi, D. Donadio, M. Parrinello, Canonical sampling through velocity rescaling. *The Journal of Chemical Physics* **126**, 014101 (2007).
55. M. Parrinello, A. Rahman, Polymorphic transitions in single crystals: A new molecular dynamics method. *Journal of Applied Physics* **52**, 7182-7190 (1981).

# Chapter II: Preliminaries studies on BmrA



This chapter is about the preliminary studies started on the basis of the results obtained by the structures of BmrA E504A. Three main axes are: 1/the design of mutants in the TM1-TM2 region, 2/ the reconstitution of the protein in a lipidic environment and 3/ the structure determination of other conformations.

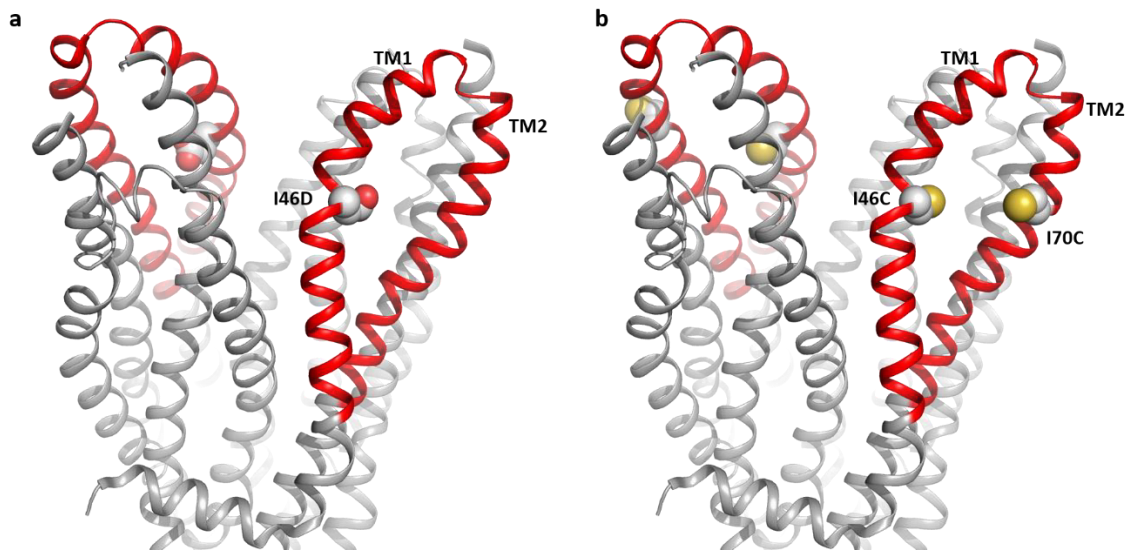
The first axe focuses on the mechanistic implication of the TM1-TM2 in the release of the drug by the transporter. Two mutants were designed aiming to rigidify this region in one case and in the other to make it more mobile. ATPase activity and transport assays were performed to characterize them and their implication. The results of this study are detailed in the next paragraph.

The two structures of BmrA are obtained in the presence of detergents. These amphipathic molecules are known to bind not only to the exposed hydrophobic part of the protein but also to the cavity (resulting in a competitive inhibition of substrate binding). This could translate in an opening of the protein which is not necessarily explored in the native context of the membrane or in the stabilization of the protein in a conformation not physiological. The goal was to reconstitute the protein into a lipid bilayer using the nanodisc support. Furthermore, a cryo-EM screening was realized aiming to solve the structure in this condition. The second paragraph here below will explain it.

Lastly, the resolution of the structure in other conformations is crucial to understand the full mechanism cycle. BmrA structures are in outward-facing conformation with and without a ligand. The focus on this new experiment was to determine the structure of the protein in inward-facing conformation with and without a drug. The preliminary results are presented in the last paragraph of this chapter.

## 1. BmrA mutants to explore the flexibility of TM1-TM2

The mutants designed were in the TM1-TM2 region: BmrA I46D (Figure 65a) and BmrA I46C-I70C (figure 65b). BmrA I46D should induce more flexibility in this region cleaving the first part of the TM. BmrA I46C-I70C should rigidify the TM1-TM2 by a disulfide bond.



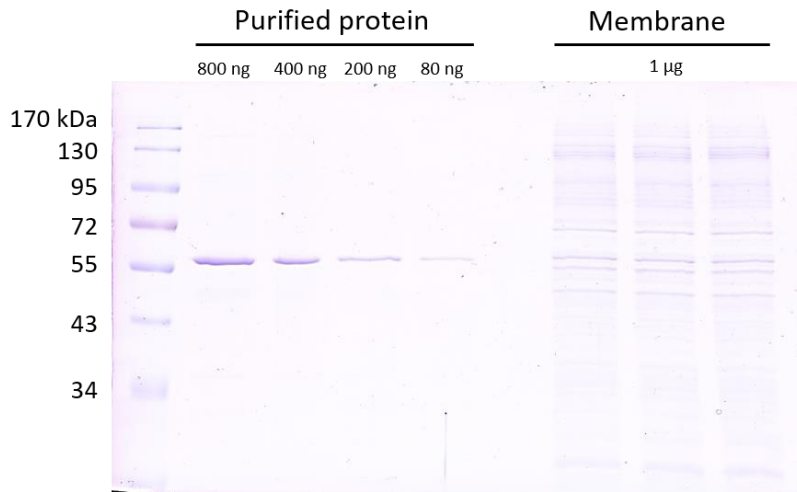
**Figure 65. Mutants of BmrA in the TM1-2 region are I46D (a) and I46C-I70C (b)**  
They both are located in the TM1 and TM2 region which is displayed in red. The structures displayed here correspond to the Cryo-EM model.

### 1.1 BmrA I46D

The aspartate residue is placed just before a proline, the interaction between DP is labile in acidic solution. Once the bond is cleaved, TM1 is detached from the rest of the protein and TM2 would gain more mobility.

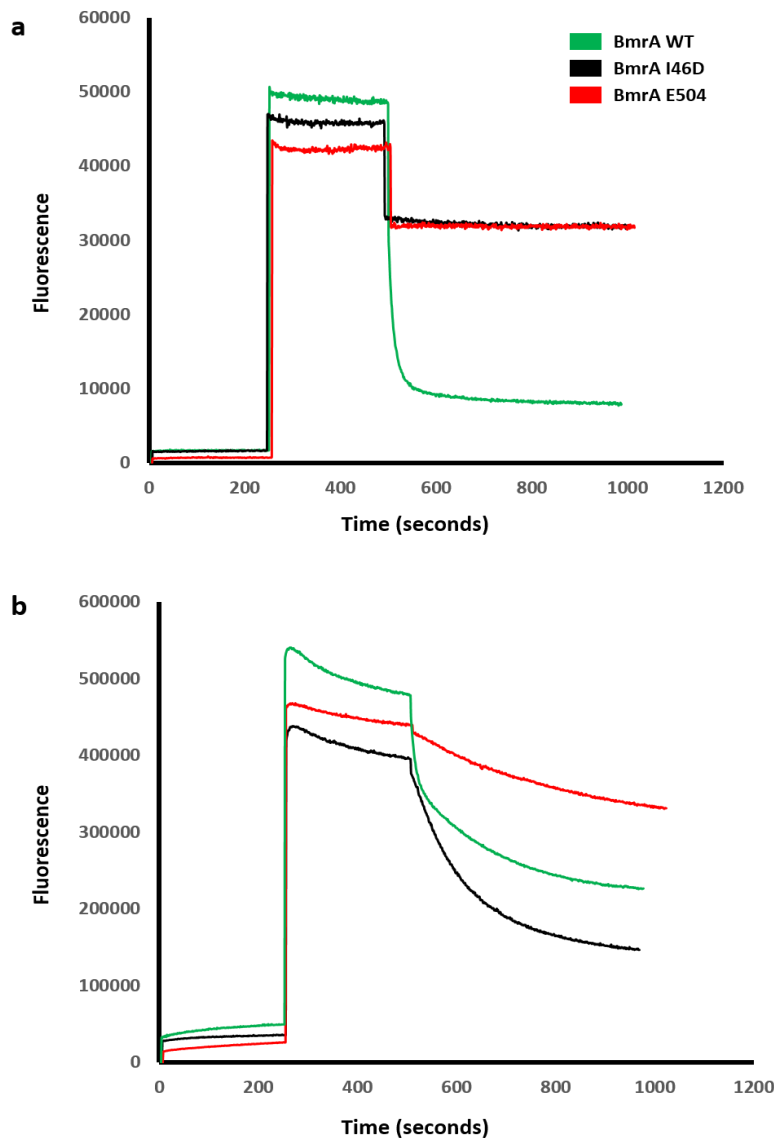
This mutant showed a lower expression yield than BmrA WT and BmrA E504A (figure 66). In addition, its activity was two times less than the one of BmrA WT. Its activity was of  $0.45 \pm 0.19$   $\mu\text{mol}/\text{min}/\text{mg}$  against  $1.08 \pm 0.2$   $\mu\text{mol}/\text{min}/\text{mg}$  for the WT. The transport assays showed also differences from the WT which could export efficiently both Hoechst 33342 and doxorubicin. BmrA I46D exported Hoechst 33342 at 70% compared to the wild type (figure 67b). Although, it could not transport doxorubicin (figure 67a). An explicative hypothesis is that this residue is in the binding site of the drug which could no longer fix in the mutant.





**Figure 66. Quantification of BmrA I46D expression**

This SDS-PAGE displays on the left the purified and on the right membrane sample. The purified protein is loaded at different quantity from 800 ng to 80 ng. The membrane sample is loaded three times at 1 µg.

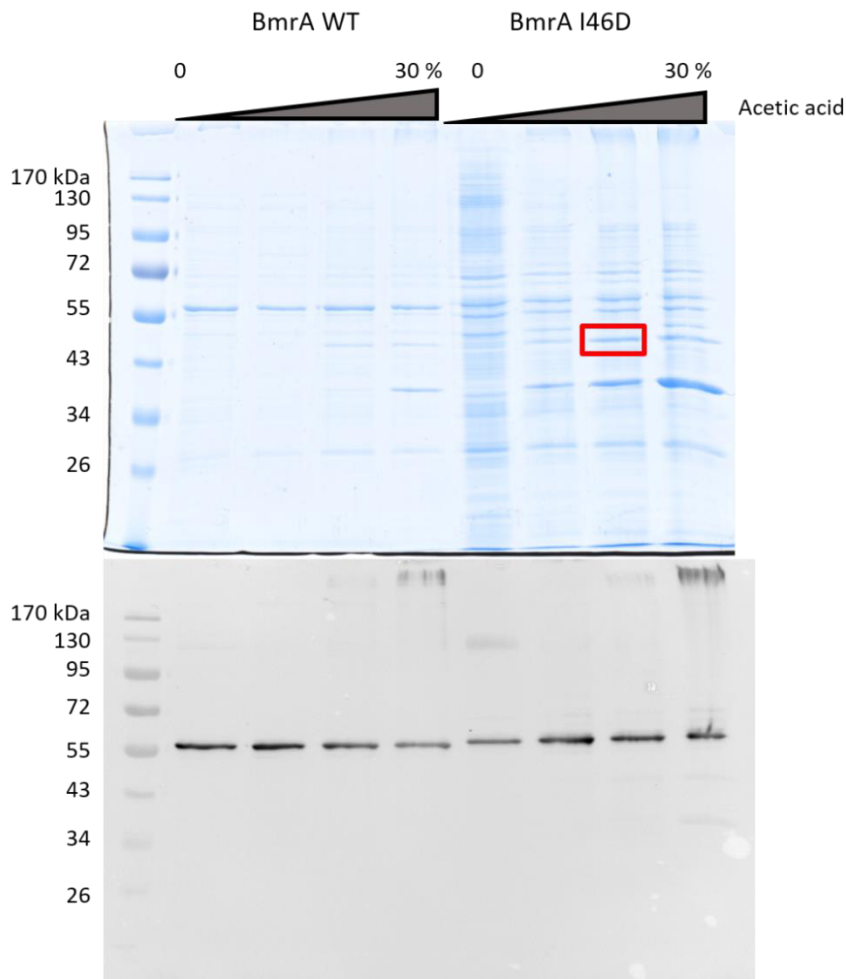


**Figure 67. Transport activity of the mutant BmrA I46D**

(a) These curves correspond to the transport assay of the doxorubicin by the inverted-membrane vesicles containing BmrA WT (green), BmrA I46D (black) and BmrA E504A (red). The latter is used as negative control. (b) The results of the Hæchst 33342 transport by the inverted-membrane vesicles containing BmrA WT (green), BmrA I46D (black) and BmrA E504A (red). Each sample contains 100 µg de protein total.

Once the mutant was characterized without the cleavage, the protein was incubated with increasing concentration of acetic acid (10% to 30%) to disrupt the bond between the aspartate and the proline residues. The cleavage was checked on Western Blot since the histidine tag detected by the antibody is attached to the N-terminal region which corresponds to the TM1.

The SDS-PAGE and the Western Blot revealed a band which appeared for the mutant after the addition of the acetic acid (figure 68). It was visible at 10% and becomes more evident with 20% and 30%. This band could correspond to the cleaved BmrA I46D since the protein without the TM1 would have a molecular weight of around 60 kDa. The band detected was between 43 and 55 kDa, the band corresponding to BmrA monomer is at 55 kDa, this meant that the band suspected could be the cleaved mutant. In addition, in the Western Blot this band was not detected. To check this hypothesis, the band was analyzed by mass spectrometry confirming that it was BmrA without the first 43 residues. This result suggested that the cleavage took place. Also, this band was also visible in the WT control when 30% of acid was added. This could mean that part of the band identified for the mutant was a non-specific degradation of BmrA.



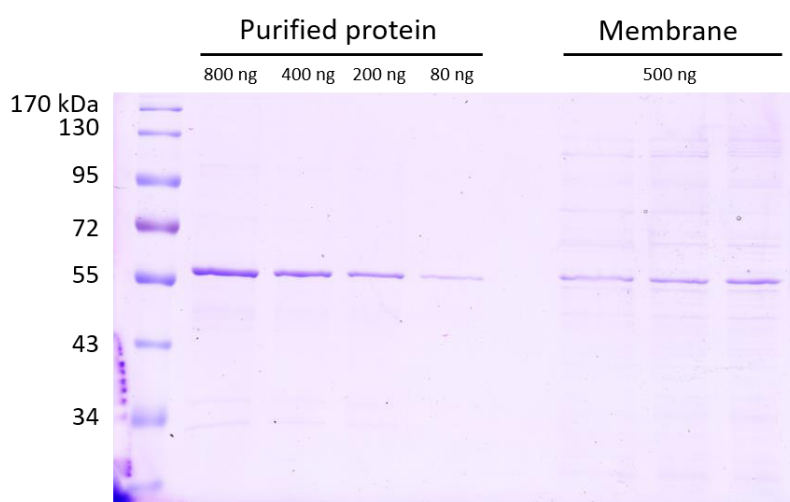
**Figure 68. Cleavage test of the mutant BmrA I46D**  
 On the upper panel, the SDS-PAGE loaded with the sample for BmrA WT on the left and BmrA I46D on the right. On the below panel, there is the Western Blot corresponding. The antibody is directed against the histidine tag. The sample are incubated with acetic acid at 10% (v/v), 20% (v/v) and 30% (v/v). There is a control of the samples without acid. The red rectangle indicate the band that could correspond to the cleaved protein.

Further investigation is needed to characterize this mutant. These preliminary results already highlight a perturbation of the protein due to a single residue mutation in the transmembrane domain. The aspartate residue which is charged replaces the hydrophobic isoleucine residue; this could prevent the binding of substrate as for the Doxorubicin and also perturb the interactions in this highly hydrophobic region. An arrangement problem could occur preventing the usual expression yield to be reached, and also perturbing the correct protein function since it is less active in all the activities (ATPase one and transport).

## 1.2 BmrA I46C-I70C

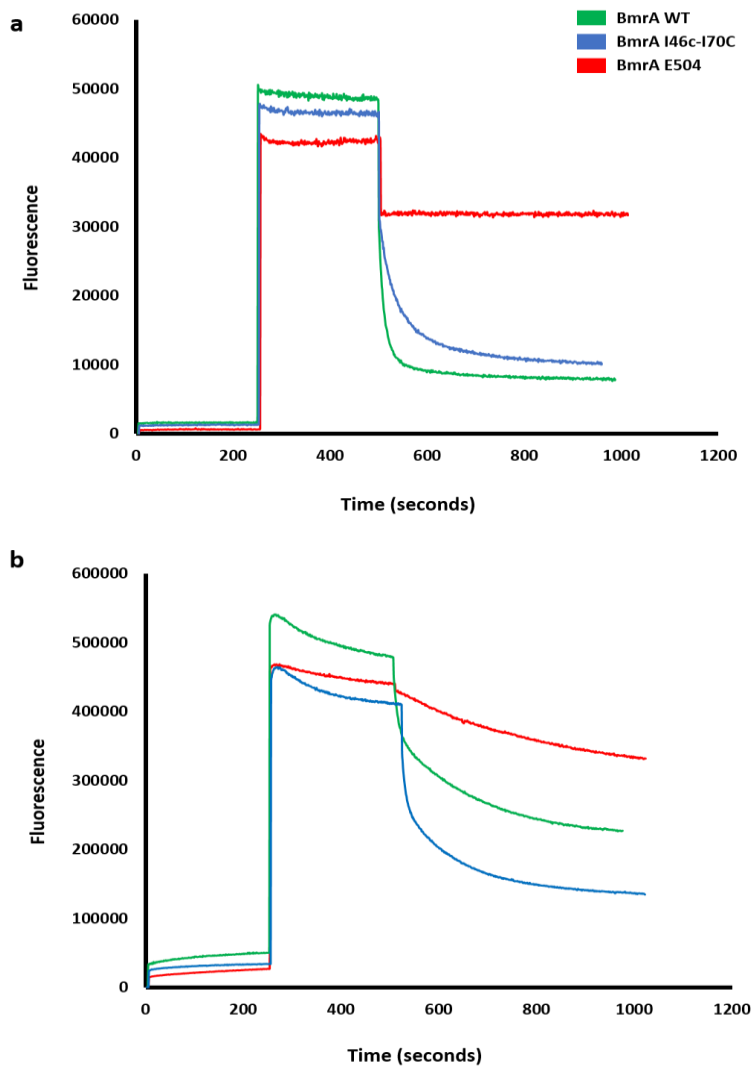
The double mutant BmrA I46C-I70C was designed to rigidify the protein inducing a crosslink between TM1 and TM2. These two residues were placed in the upper membrane region of the TM1 and TM2. Their distance is around of 4-7 Å in the ABC transporters' structures solved in a more occluded outward-facing conformation.

Its expression had almost the same yield of the wild type with 52% of BmrA I46C-I70C (figure 69) against 43% for BmrA WT. The ATPase activity was also practically equivalent since for BmrA I46C-I70C is of  $0.96 \pm 0.15$   $\mu\text{mol}/\text{mg}/\text{min}$  and for BmrA WT is  $1.08 \pm 0.17$   $\mu\text{mol}/\text{mg}/\text{min}$ . Finally, the transport assays gave some differences in the results; the mutant transported 2.5 times less the Doxorubicin and 3 times less the H $\ddot{o}$ chst 33342 than BmrA WT (figure 70).



**Figure 69. Quantification of BmrA I46C-I70C expression**

*This SDS-PAGE displays on the left the purified and on the right membrane sample. The purified protein is loaded at different quantity from 800 ng to 80 ng. The membrane sample is loaded three times at 500 ng.*



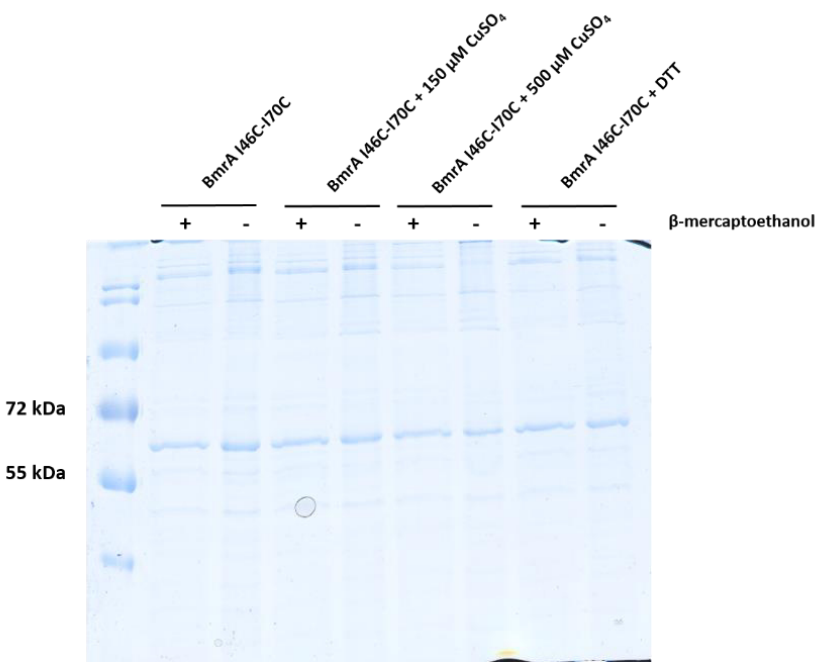
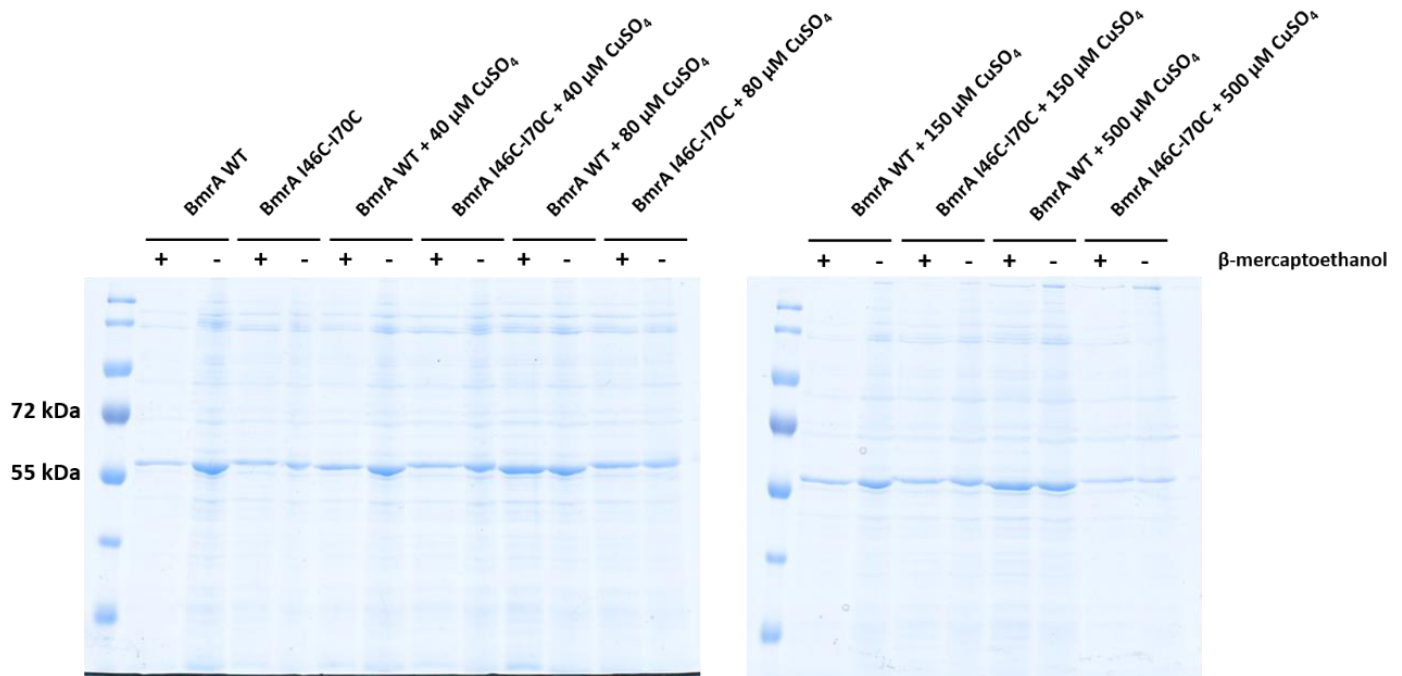
**Figure 70. Transport assays for BmrA I46C-I70C**

(a) The transport assay of the doxorubicin. Inverted membrane vesicles contain overexpressed BmrA WT (green), BmrA I46C-I70C (blue) or BmrA E504A (red). (b) The curves correspond to the transport of Hoechst 33342. The experiment is realized for inverted membrane vesicles overexpressing BmrA WT (green), E504A (red) or I46C-I70C (blue). Each sample contains 100  $\mu\text{g}$  de protein total.

To induce or disrupt the disulfide bond, the protein was incubated with an oxidant or a reducing agent.  $\text{CuSO}_4$  was added to the sample as oxidant and DTT (Dithiothreitol) was used as reducing agent. Each reagent was tested at different concentration and also with different times of incubation (from 30 minutes to overnight). Afterward, the transport assays were performed and in parallel also the detection of the presence of the disulfide bound.

This crosslink has to occur in the upper part of the TM1-TM2 belonging to the same monomer. This means that its detection is challenging; the migration difference on the SDS-PAGE will be quite subtle. The protein was incubated with both the oxidant and reducing reagent and loaded onto the gel. Many attempts were carried out to detect a difference of migration using membrane sample and also purified protein. The gel of 10%, 12% and 14% acrylamide/bisacrylamide were tested without any visible difference. I also tried to increase the migration time allowing the protein to separate more. None of these assays were

successful as shown in the figure 71. I next tried to visualize differences by Western Blot, which is a more sensitive technique. I was however unable to visualize a difference in migration (results not shown here).



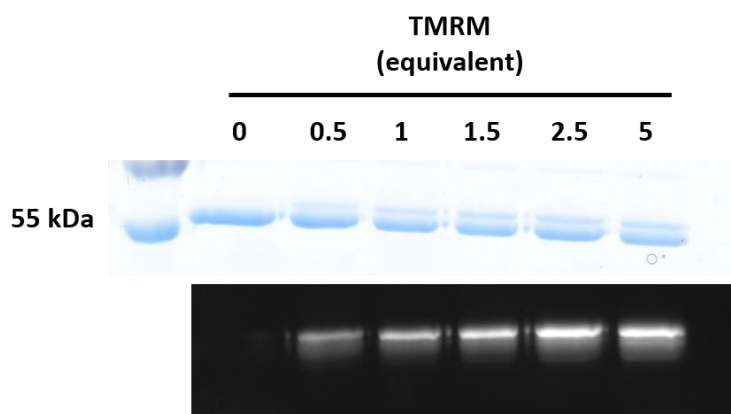
**Figure 71. Detection of the disulfide bond by SDS-PAGE**

The upper panel present the SDS-PAGE at 10% acrylamide/bisacrylamide. The samples alternate membranes containing BmrA WT and the mutant BmrA I46C-I70C. The membranes are incubated with 40 μM to 500 μM of CuSO<sub>4</sub>. The samples are loaded with or without the reducing agent β-mercaptoethanol. The panel here on the left, is a SDS-PAGE at 14% acrylamide/bisacrylamide. The samples loaded are membrane expressing the mutant BmrA I46C-I70C incubated with 150 μM and 500 μM CuSO<sub>4</sub> or DTT. They are incubated with or without β-mercaptoethanol in the Laemmli buffer.

Lastly, the same method used to visualize the heavy atoms binding (see chapter I, “Heavy atoms soaking” section) was implemented to this case too since the TMRM compound fixes to free cysteine residues. BmrA WT contains only one native cysteine per monomer, the

mutant BmrA I46C-I70C brings two additional ones. If the two cysteine residues are implicated in a crosslink, the TMRM will fix only the native cysteine. On the opposite situation, the TMRM will fix to three residues. A basal signal is always present due to the binding of the TMRM to the native cysteine. The signal will be three times more intense if the disulfide bound is not present.

The first step was to test the saturation of the signal, different quantity of TMRM were incubated with BmrA I46C-I70C (figure 72). TMRM signal was at its maximum between 2.5 and 5 molar equivalents of protein. In this case, all the cysteine could bind TMRM. For the rest of the experiment, the quantity of TMRM was used at 5 equivalents of the protein.



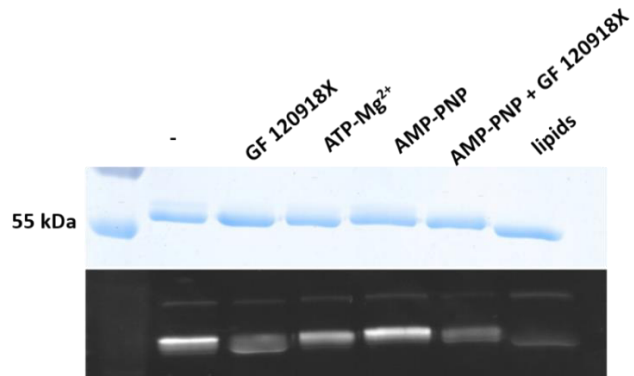
**Figure 72. Test of equivalent TMRM for BmrA I46C-I70C**

The protein is incubated with different molar equivalent of TMRM. The sample is loaded onto SDS-PAGE which is revealed at UV lamp and also colored with Brilliant Blue Commassie.

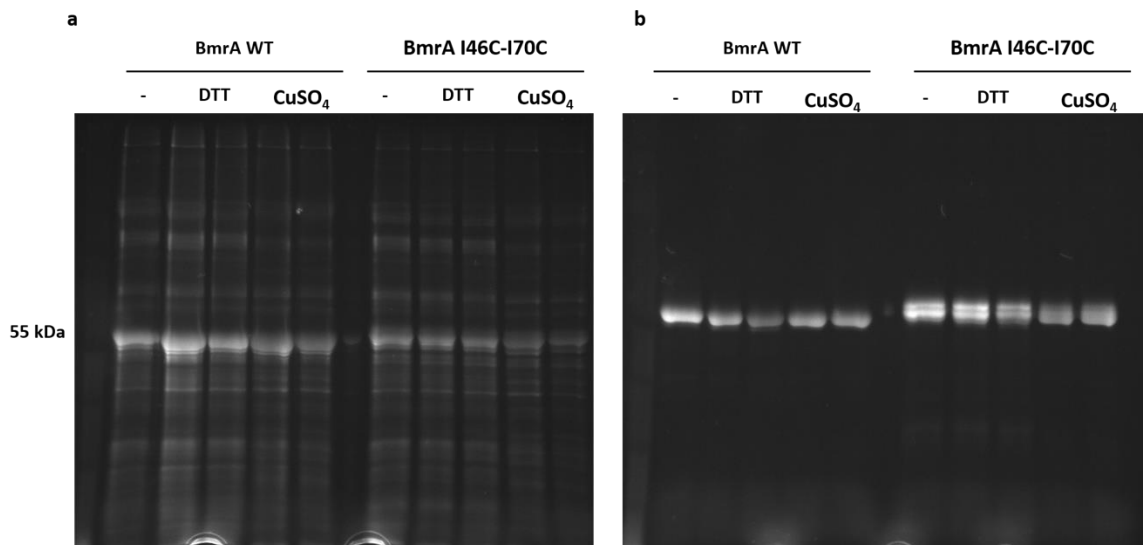
The protein was then incubated with different molecules which could induce a conformational modification. These molecules were ligand GF 120918X (100  $\mu$ M), ATP-Mg<sup>2+</sup> (2 mM), AMP-PNP (analogue non-hydrolysable of the ATP) and lipids. The TMRM signal showed a diminution when the protein was incubated with the ligand GF 120918X and lipids. This could indicate that the binding of these compounds to the protein prevented the labeling by TMRM (figure 73).

**Figure 73. Revelation of TMRM signal after incubation of the protein in presence of different molecules**

The protein is incubated with are ligand GF 120918X, ATP-Mg<sup>2+</sup>, AMP-PNP (analogue non-hydrolysable of the ATP) and lipids. The TMRM is then added. The sample is loaded onto SDS-PAGE which is revealed at UV lamp and also colored with Brilliant Blue Commassie.



After this first validation of the method, the protein was incubated with a reducing agent (DTT) and an oxidant (CuSO<sub>4</sub>). The sample were then incubated with the TMRM and loaded onto SDS-PAGE. The experiment was performed on membrane overexpressing BmrA WT and BmrA I46C-I70C (figure 74a) and on purified samples (figure 74b). In both cases, no significant difference was detected in presence of DTT or CuSO<sub>4</sub>. This assay was repeated several times without any significant result.



**Figure 74. Detection of disulfide bond by the TMRM detection method**

(a) The membrane containing BmrA WT and BmrA I46C-I70C are incubated with DTT or CuSO<sub>4</sub>. The TMRM is added, its signal is detected with a UV lamp. (b) The same process is performed with the purified protein.

In parallel of the detection assays, I followed transport activity. The membrane sample was incubated with DTT or CuSO<sub>4</sub> for 30 minutes before the measures. A range of concentration of the two reagents were tested. In the case of the DTT, the sample seemed to be stable up to 1 mM. In the case of the CuSO<sub>4</sub>, at first the sample seemed to be stable up to 1 mM,



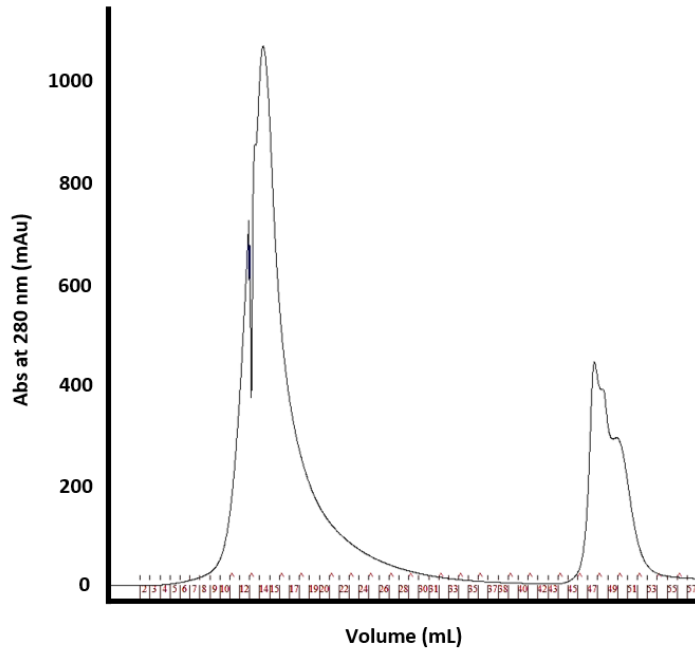
although with time it revealed an instability losing transport ability. This could be due to the fact that the reaction was not stopped which could induce a progressive degradation of the sample, and off target effects. These results are still preliminary and need further investigation.

## 2. Nanodisc reconstitution

The nanodisc system allows the insertion of a purified protein in a lipid bilayer for functional and structural studies. The structures solved represent the protein purified with detergents. In this chapter, I show some assays of the reconstitution of BmrA WT and BmrA E504A into two different sizes of nanodiscs (MSP1E3D1 of 128 Å diameter and MSP1D1 of 97 Å). At first, BmrA WT was inserted into the nanodisc formed by MSP1E3D1. The goal was to validate the reconstitution with an ATPase activity assay, the quality of the sample was then checked by negative stain electron microscopy and single-particle Cryo-EM. Then, the mutant BmrA E504A was reconstituted in the same conditions, although the screening grids of Cryo-EM showed that the sample was not homogeneous. As a consequence, I tried the reconstitution in a smaller nanodisc but unfortunately it could be seen on the Cryo-EM images that the protein was not inserted into the nanodisc. All these experiments are detailed in the following paragraphs beginning with the purification of the two MSP.

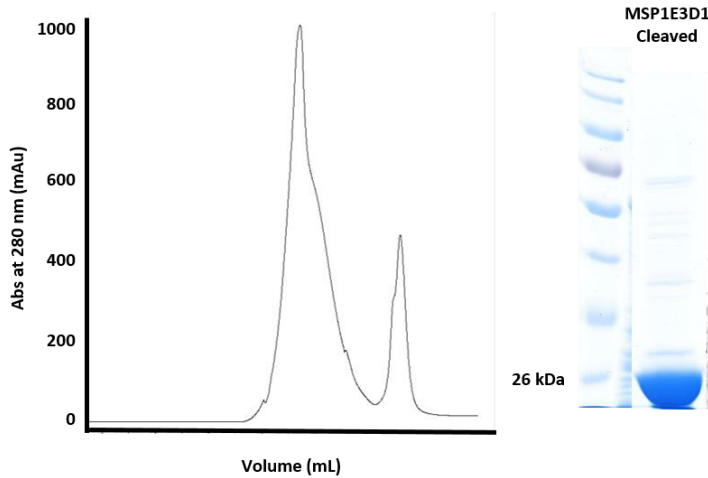
### 2.1 MSP Purification

The MSP1E3D1 and MSP1D1 were over-expressed in BL21 *E. coli* bacterial strain. The purification was composed by three steps: a first affinity chromatography, dialyze in presence of TEV enzyme and a second reverse-affinity chromatography. The first step was needed to separate the protein of interest from all the others proteins present in the cellular lysate, the protein was expressed with a histidine tag. The cleavage by TEV enzyme allowed to eliminate the tag which prevent the purification of the nanodisc without BmrA inserted. The second step of affinity chromatography separated the MSP without the tag and the ones not cleaved by the TEV enzyme. The two figure 75 and 76 present the chromatogram of this last step of purification. The figure 75 corresponds to MSP1D1; the first peak was the flow through which is the protein without the tag and the second peak is the ones with the tag which is eluted thank to imidazole. The same profile was obtained for the MSP1E3D1 as it is shown by the figure 76. The presence of the two peaks means that the tag was cleaved. In spite the fact that the TEV enzyme could not eliminate the tag of all MSP, the purified proteins without the tag was enough to perform reconstitution assay.



**Figure 75. Purification of MSP1D1**

The chromatogram corresponds to the second affinity chromatography of the purification of MSP1D1. The first peak corresponds to the cleaved protein (MSP1D1 without the histidine tag). The second peak is the protein which has the histidine tag.



**Figure 76. Purification of MSP1E3D1**

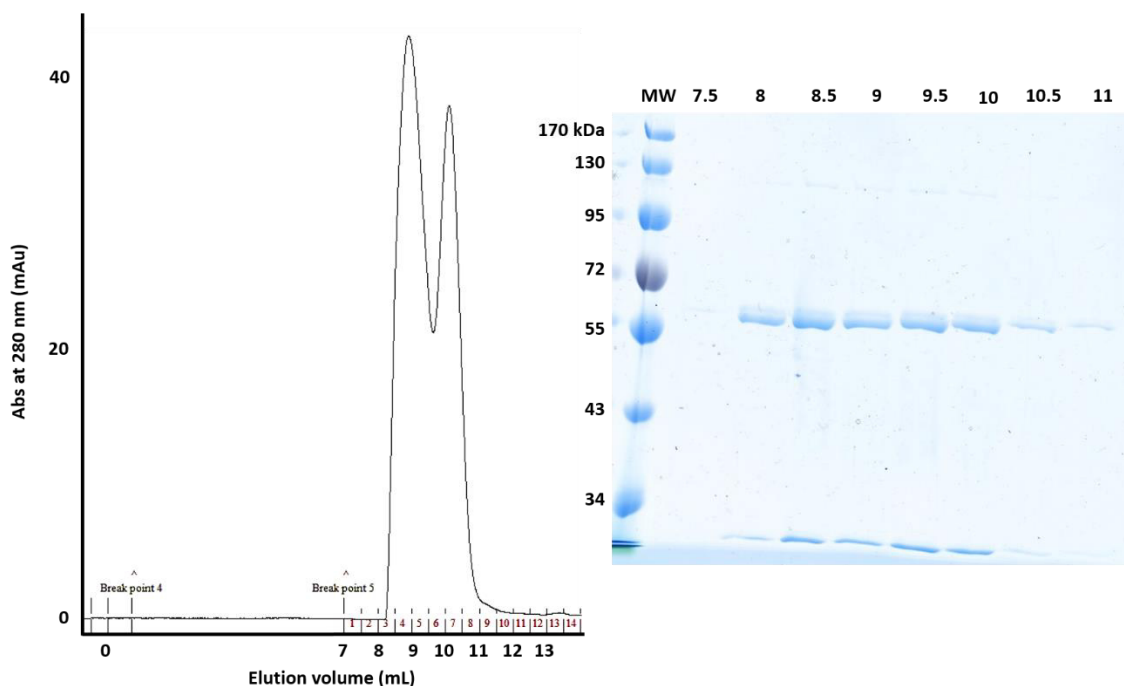
The chromatogram corresponds to the second affinity chromatography of the purification of MSP1D1. The first peak corresponds to the cleaved protein (MSP1D1 without the histidine tag). The second peak is the protein which has the histidine tag. The gel on the right shows the purified sample corresponding to the cleaved one.

## 2.2 Reconstitution of BmrA into nanodisc

BmrA WT and BmrA E504A were purified at first in the detergent's mixture ratio 1:1 DDM-cholate. The fractions of peak were used for the reconstitution step which was realized overnight at room temperature. Below are the purification results of each reconstitution and the corresponding the cryo-EM screens.

### BmrA WT – MSP1E3D1

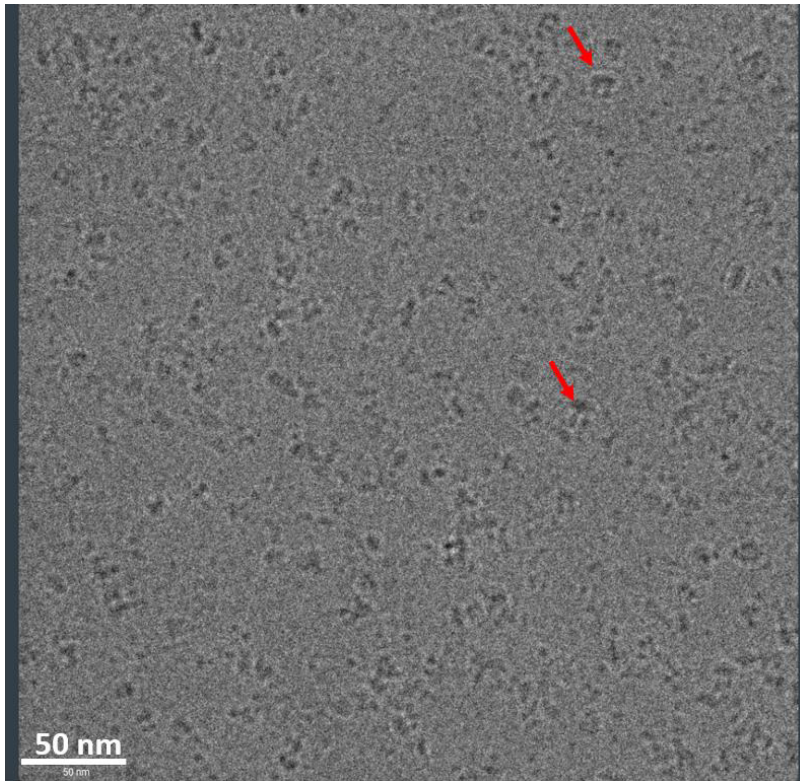
BmrA WT was reconstituted into the larger nanodisc which was formed by MSP1E3D1. The size exclusion chromatography profile showed that the sample was composed by two different populations. BmrA purified in detergent is eluted at 11.5 mL, the peaks showing in the figure 77 are centered at 8.5 and 10 mL. The nanodisc should increase the size and the volume of the protein, the shift of the elution volume could indicate the insertion of the protein. The SDS-PAGE was loaded with the fractions corresponding to the two peaks. Each fraction displayed a good degree of purity, only the BmrA and the MSP1E3D1 were present. It is difficult to understand here the reason of the presence of two peaks.



**Figure 77. Purification of BmrA WT reconstituted onto nanodisc formed by MSP1E3D1**

On the left, the chromatogram corresponding to the size exclusion chromatography of BmrA WT into nanodisc formed by MSP1E3D1. On the right, the SDS-PAGE displays the fractions of the peak presented on the left.

The fractions were loaded on the grids and tested for Cryo-EM experiment without the addition of any ligands or nucleotides. The fraction eluted at 9 mL was the one presenting better homogeneity and dispersion of the sample (figure 78). The size of the particles could correspond to BmrA WT reconstituted into nanodisc since the size of the protein is of about 120 Å x 60 Å. It was possible to see some particles which have resemblance with BmrA in inward-facing conformation (red arrows).

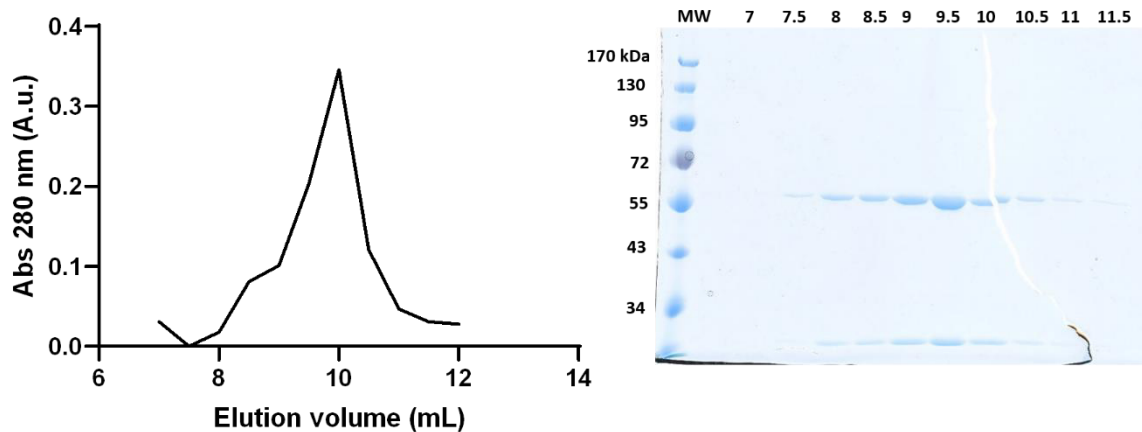


**Figure 78. Micrograph of the grid composed BmrA WT into MSP1E3D1 nanodisc**

*This micrograph corresponds to the sample composed by BmrA WT inserted into MSP1E3D1 nanodisc. It's the fraction 5 which correspond to the first SEC peak. The red arrows indicate particles which could be BmrA in inward-facing conformation. The scale is of 50 nm (left corner).*

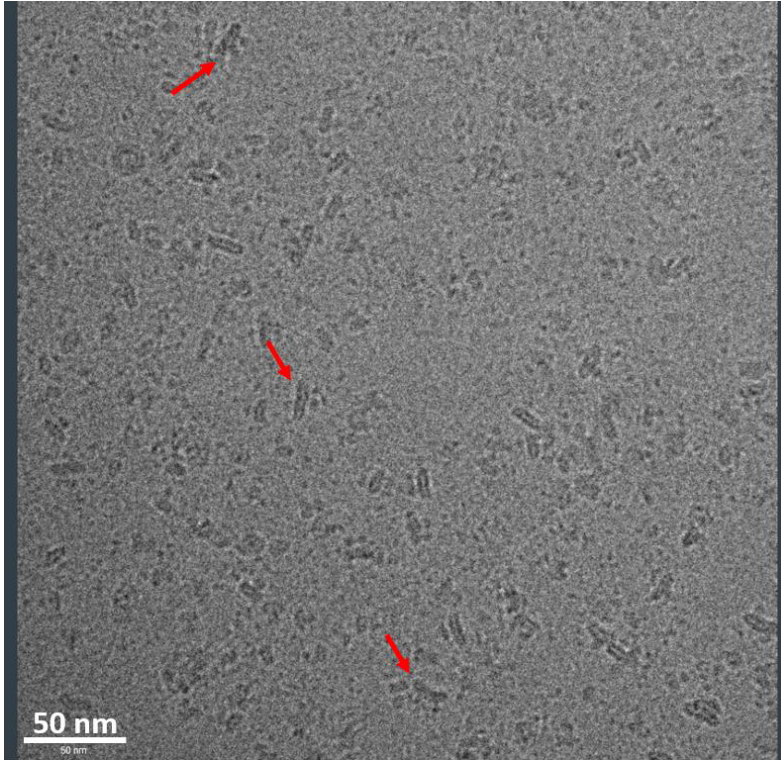
**BmrA E504A – MSP1E3D1**

The same protocol used for BmrA WT was implemented for the inactive mutant. The SEC profile was quite different than the one obtained for the wild type. There was a unique peak centered at 9.5 mL, although there was a shoulder which could correspond to the first peak in the wild type purification (figure 79). The gel showed a purified sample containing BmrA and MSP1E3D1 for each fraction.



**Figure 79. Purification of BmrA E504A reconstituted onto nanodisc formed by MSP1E3D1**  
 On the left, the SEC profile corresponds to BmrA E504A into nanodisc formed by MSP1E3D1. On the right, the SDS-PAGE displays the fractions of the peak presented on the left.

The fractions of the peaks were tested for the Cryo-EM assay; this time the protein was incubated with ATP-Mg<sup>2+</sup>. The sample seemed heterogenous and the particles were not well spread out. In figure 80, it is possible to identify particles which could correspond to BmrA inserted into the nanodisc (red arrows). It seemed that two proteins were inserted into same nanodisc which could be due to the size of the MSP1E3D1. This MSP has a diameter of 128 Å, it could accommodate up to two dimers of BmrA since in the outward-facing conformation the width of the membrane part is of ~ 50 Å. This problem was not observed for the wild type. The fact that the nucleotide was present in this case could not have influenced the insertion since it is added afterward. The explanation could be that the mutant is less flexible than the wild type.

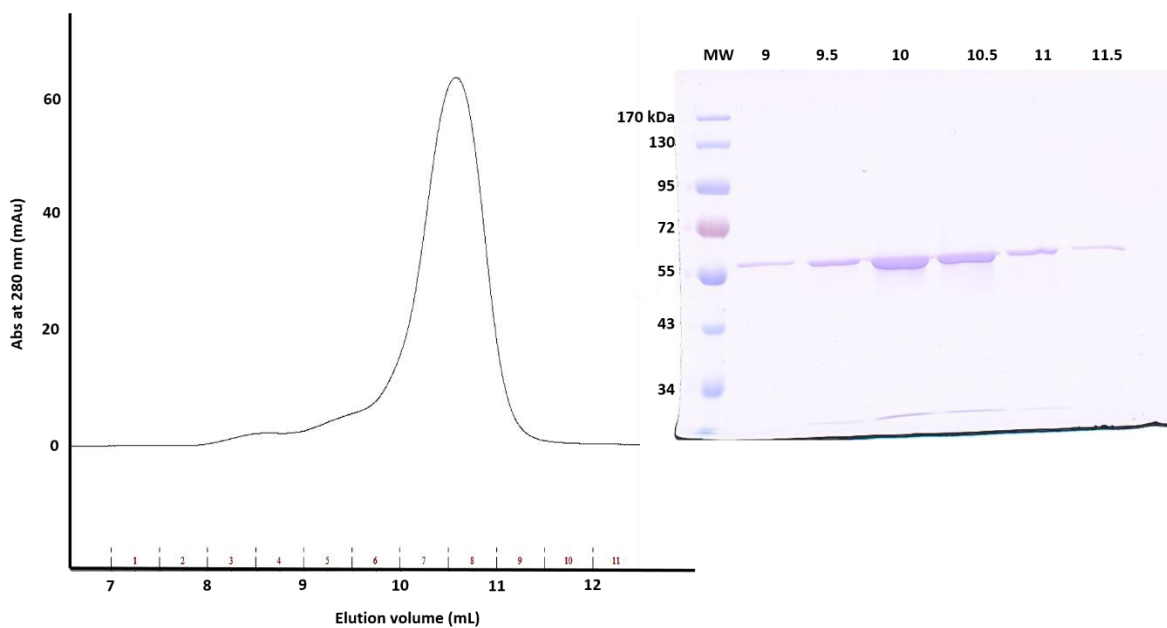


**Figure 80. Micrograph of the grid composed BmrA E504A into MSP1E3D1 nanodisc**

*This micrograph corresponds to the sample composed by BmrA E504A inserted into MSP1E3D1 nanodisc. The protein is incubated with ATP-Mg<sup>2+</sup>. It correspond to the fraction centered at 9.5 ml. The red arrows indicate particles which could correspond to BmrA. The scale in the left corner corresponds to 50 nm.*

**BmrA E504A – MSP1D1**

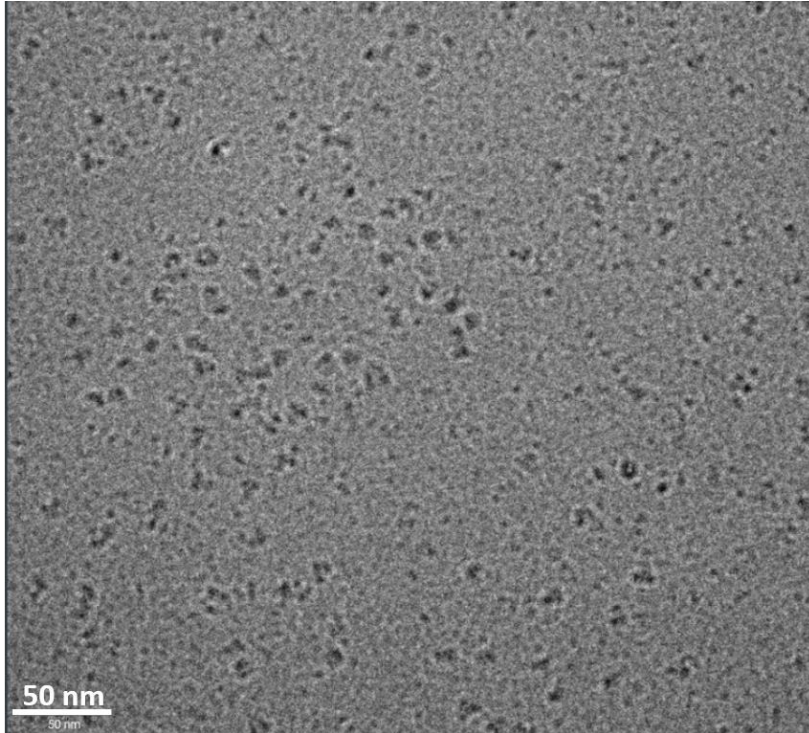
To bypass the insertion problem of the mutant into MSP1E3D1, the MSP1D1 nanodisc was tested. This MSP forms nanodisc of 78 Å of diameter. The SEC chromatogram displayed a unique peak centered at 10 mL, it shifted on the right in comparison to the protein reconstituted into MSP1E3D1 (figure 81). This meant that the particles were smaller and it was the result desired. The SDS-PAGE showed a well purified sample but the MSP1D1 band was weak in comparison with the BmrA's one (figure 81).



**Figure 81. Purification of BmrA E504A reconstituted onto nanodisc formed by MSP1D1**  
On the left, the SEC profile and on the right, the SDS-PAGE corresponding.

Afterwards, the purified fractions were incubated with ATP-Mg<sup>2+</sup> and tested for Cryo-EM assay. The sample showed heterogeneity and the protein seemed to not be inserted into the nanodisc composed by MSP1D1 (figure 82). This observation was correlated with the SDS-PAGE result that showed little amount of MSP present with BmrA.





**Figure 82. Micrograph of the grid composed BmrA E504A into MSP1D1 nanodisc**

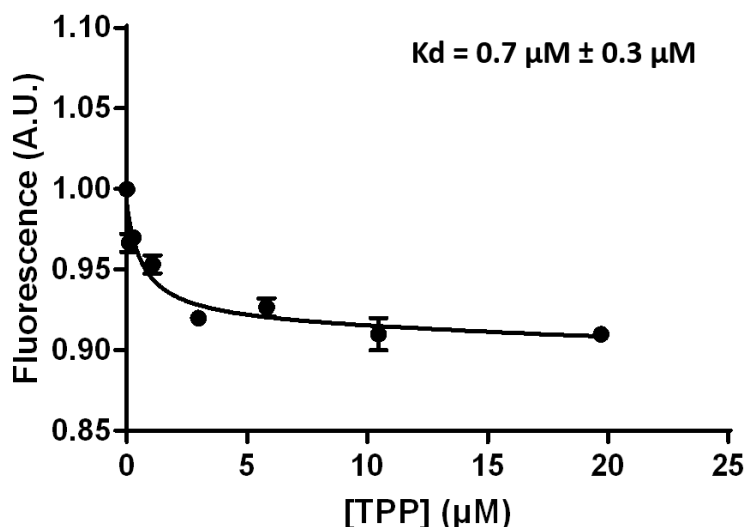
*This micrograph corresponds to the sample composed by BmrA E504A inserted into MSP1D1 nanodisc. The protein is incubated with ATP-Mg<sup>2+</sup>. It corresponds to the fraction centered at 10 ml. The scale in the left corner correspond to 50 nm.*

This last result is still encouraging since the particles are visible and that for the BmrA wild type this protocol worked. The conditions for the reconstitution of the mutant need some more optimization.

### 3. Structure in another conformation

Since the structures above were of BmrA in outward facing conformation with and without a ligand, the goal was now to determine another structure of the protein in the inward-facing conformation in presence of another substrate molecule. The latter was the tetraphenylphosphonium (TPP) which is a charged compound containing a phosphonium in the middle of four phenyl groups. Its  $K_D$  was measured at  $15.4 \pm 2.7 \mu\text{M}$  on BmrA purified with DDM (Steinfels et al. 2004). The choice of this compound relied on the presence of the phosphonium which is useful for the absorption of the electrons and in principle should help in detecting its presence.

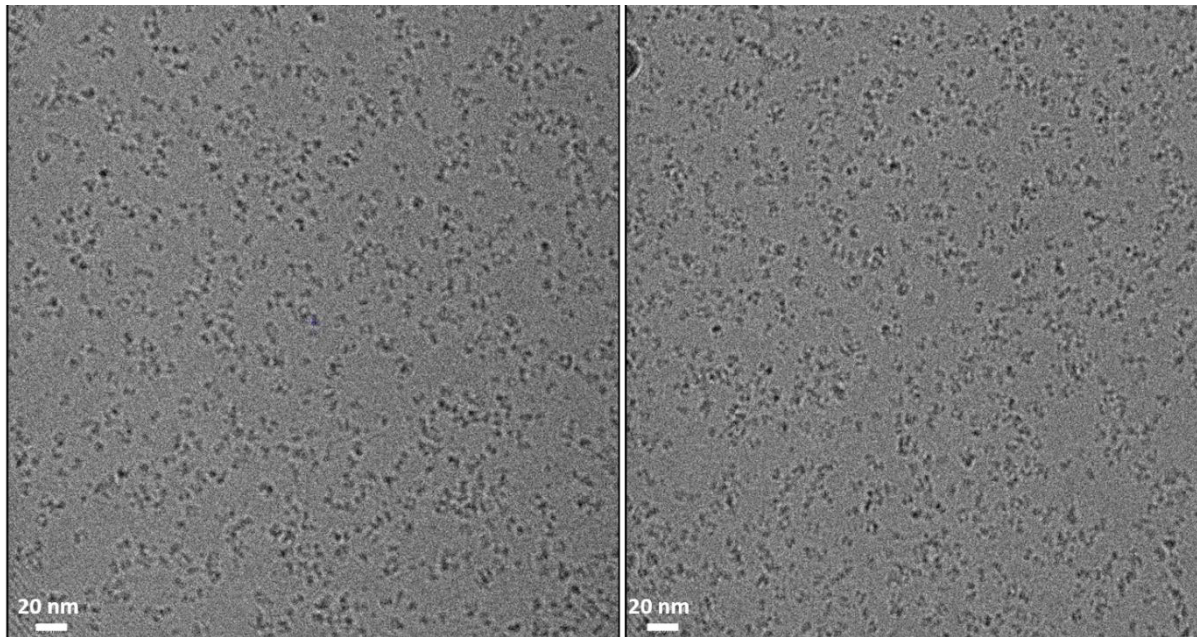
A binding assay was performed to check the binding to BmrA E504A purified with the mixture 1:1 DDM-cholate. The quenching of the intrinsic fluorescence of the protein was recorded and plotted in function of different concentration of TPP (0-29  $\mu\text{M}$ ). The compound bound to the protein with an affinity constant of  $0.7 \mu\text{M}$  (figure 83). The error on the measure of the  $K_D$  was quite high; this assay needs to be performed again to ensure the real value of the binding.



**Figure 83. Binding of the tetraphenylphosphonium (TPP) on BmrA E504A**  
The fluorescence binding assay is performed to determine the binding of the TPP on BmrA E504A.

Afterwards, a single particle Cryo-EM assay was performed on this sample composed of BmrA E504A and TPP. This part was also realized at the Karolinska Institute with our collaborators (Martin Högbom team). The sample preparation protocol was the same used previously. The protein was incubated with  $200 \mu\text{M}$  of TPP, loaded on the grid and screened with the Talos

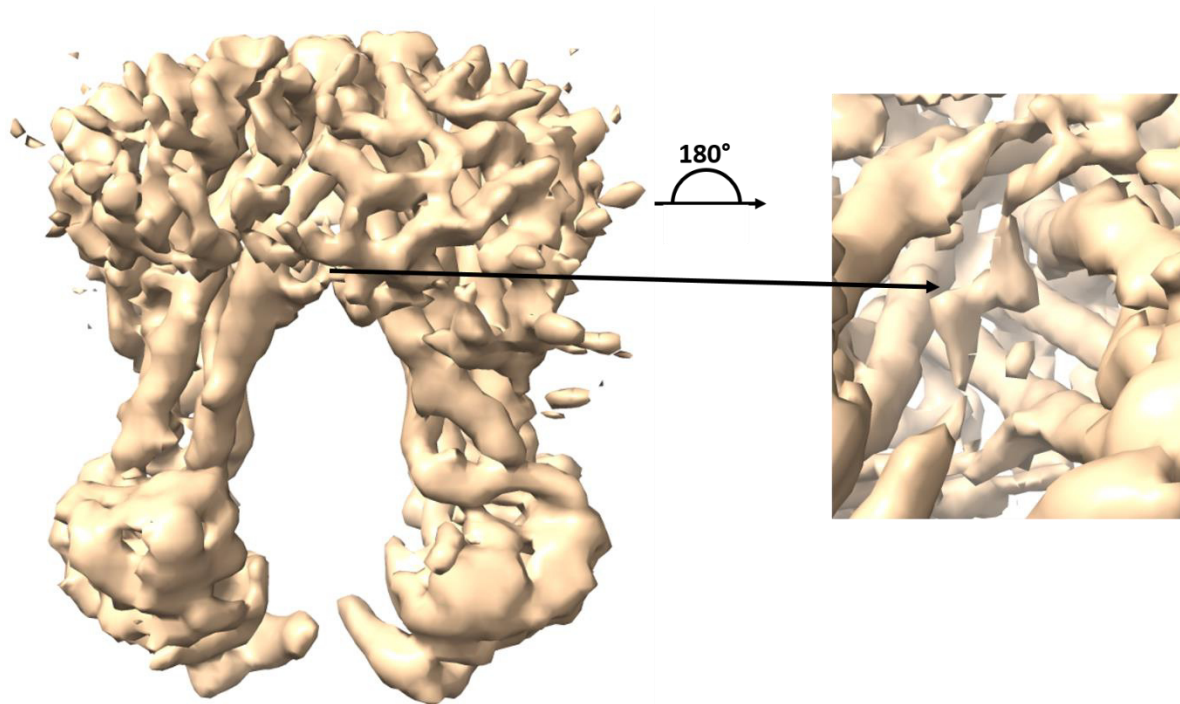
Arctica. The sample was slightly heterogeneous (figure 84) although the particles are well spread out.



**Figure 84. Micrographs of BmrA E504A with Tetraphenylphosphonium (TPP)**

*These two figures correspond to the micrograph obtained for the sample BmrA E504A in presence the compound TPP. The scale is of 20 nm.*

The data collection of this grid was performed on the Titan Krios G3 electron microscope. The 2D classification and the 3D reconstitution showed the protein in the inward-facing conformation. Due to the high flexibility of the protein in this conformation, the high resolution was difficult to reach even after three data collections. The protein seems to explore different degree of opening. The 3D reconstitution shows a very low resolution for the NDBs although TMDs are better defined. In addition, a density corresponding to the TPP appears to be present (figure 85).



**Figure 85. Density map obtained by Cryo-EM for BmrA E504 with TPP**

*On the left, the density map of the whole protein. On the right, the density which could correspond to the substrate TPP or a detergent molecule.*

These data collected are not enough to solve a structure at high resolution of the protein and to determine the binding site of the ligand. Thus, with this low resolution it is difficult to identify if the additional density corresponds to the TPP compound or to a detergent molecule.

## 4. Conclusion and discussion

This whole chapter presents the three projects that had been undertaken since the resolution of the structures of BmrA. Each one of them investigates questions aroused from the structural analysis and the key points are the movement of the TM1-2, the detergent environment and finally the binding of a drug in a given conformation. We attempted to answer these questions, an experimental procedure has been set up for each project.

Two mutants have been designed to prove the movement of the TM1-2. The idea was to have two mutations which could provoke opposite reaction. BmrA I46D has the intent to induce more mobility to the TM1-2. Its characterization before any incubation with the acetic acid shows a difference in the drug transport and the ATPase activity. This finding is interesting since it shows that a single mutation in the transmembrane domain can induce a perturbation of the protein and a drug specific reaction. The loss of the doxorubicin transport might suggest that this drug bind in this particular region of the cavity. The provoking of the bound aspartate and proline residues cleavage needs more optimization. On the other hand, BmrA I46C-I70C aims to rigidify the movement binding together TM1-2. It conserves the activity of the wild type when no treatment has been done yet. The challenging part is the detection of the presence of the disulfide bound. No conclusion could be drawn since the detection test presented in this manuscript revealed to not be adapted. The fact that this bond is placed on the same monomer and in the upper region of the transmembrane domain makes it more difficult to study and analyze. To solve this problem, other methods need to be tested as for example the quantification of  $-SH$  using a GSH calibration curve. In conclusion, these two mutants present an interesting way to characterize the movement of the TM1-2 although the limitations imposed by this transmembrane region complicates their study.

The second project concerns the questioning about the detergent environment. The scientific community studying membrane proteins constantly wonders about the impact of detergent on the protein and the relevance of the results obtained. These amphipathic molecules are crucial to the extraction and purification step; it is difficult to forgo their use. It is already proved in the literature that membrane proteins are less active in detergent than in lipids (Chaptal et al. 2017). Nevertheless, they still can at some level bind ligand and maintain an activity. A lot of membrane protein's structures are solved with the protein in presence of

detergent. This leads to the questioning of their physiological relevance. Since the two structures of BmrA are in detergent, the aim of this project is to determine the same structure in lipid to observe the conformation adopted by the protein in this environment. The nanodisc formed by MSP has been chosen as system. The results obtained are quite encouraging, the BmrA wild type reconstitution has been successfully done. On the other hand, the inactive mutant has been more complex to reconstitute and to give good results in the cryo-EM analysis. Other assays are needed to optimize this sample.

The last project undertaken is the study of the protein in another conformation with a compound bound. The mechanism of the ABC transporters is still unclear in the details. The structure of the protein in different conformations is needed to have more insights. A few years ago, the structural study of a membrane protein was a real challenge, the resolution of one structure in a given conformation was a project that could take years. The cryo-EM development made possible to speed up these studies of this kind of proteins. Afterward the resolution of the structure of BmrA in outward-facing conformation with and without a substrate elucidates the drug release mechanism part. It was clear that the inward-facing conformation was the next conformation to analyze. The sample was good enough to perform a data collection on a Titan Krios G3 electron microscope. Unluckily, the protein in this conformation displays a high flexibility which prevents the obtaintion of the high resolution even after multiple rounds of data collection. A solution could be to use the protein reconstituted in nanodisc for the structural study of this conformation. The protein in nanodisc might be less flexible due to the size restriction imposed by the MSP.

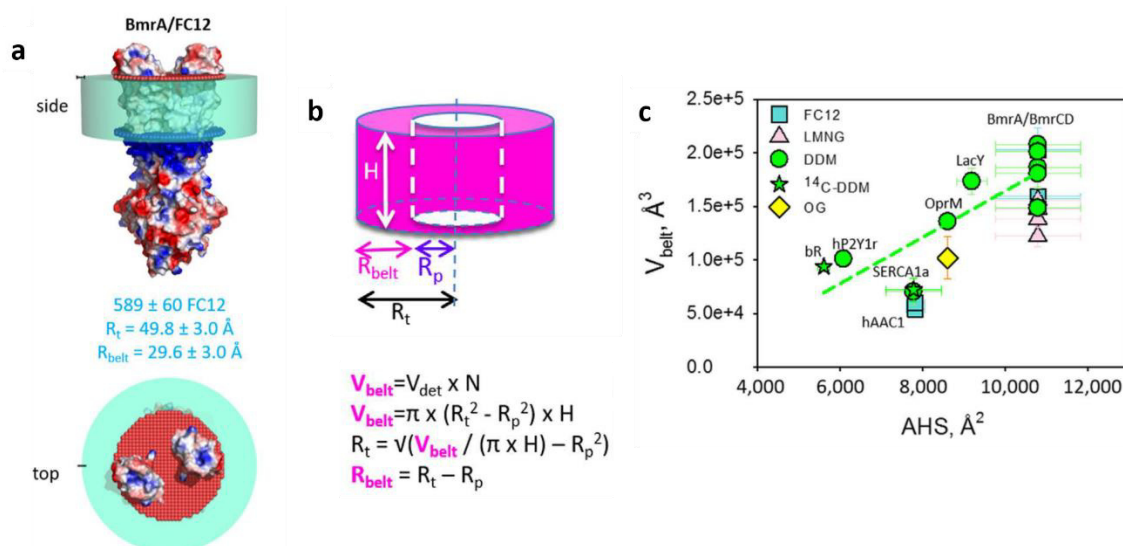
To conclude, the two structures of BmrA have opened the way too many others projects to better understand the ABC transporter mechanism. Even if the results here presented are still preliminary, they show already interesting observations which needs to be explored more.

# Chapter III: Detergent belt representation

## RESULTS: CHAPTER III



This chapter is focused on the representation of the detergent belt around the protein. As explained in the introduction section, the detergent plays an important role in the handling of membrane proteins. These amphipathic molecules are responsible of keeping the protein soluble in a hydrophilic environment. Although, they present a real challenge due to their strong exchangeability. It is complex to visualize the detergent belt by structural biology techniques. The DRMP team set up a method to quantify the detergent bound to membrane proteins (cf. methods) (Chaptal et al. 2017). This quantification allows to estimate the volume of this belt. The volume of a single molecule is calculated by the software Voidoo and then it is multiplied by the number of detergent quantified. This belt is represented as a hollow cylinder around the hydrophobic part of the protein (figure 86).



**Figure 86. Representation of the detergent belt**

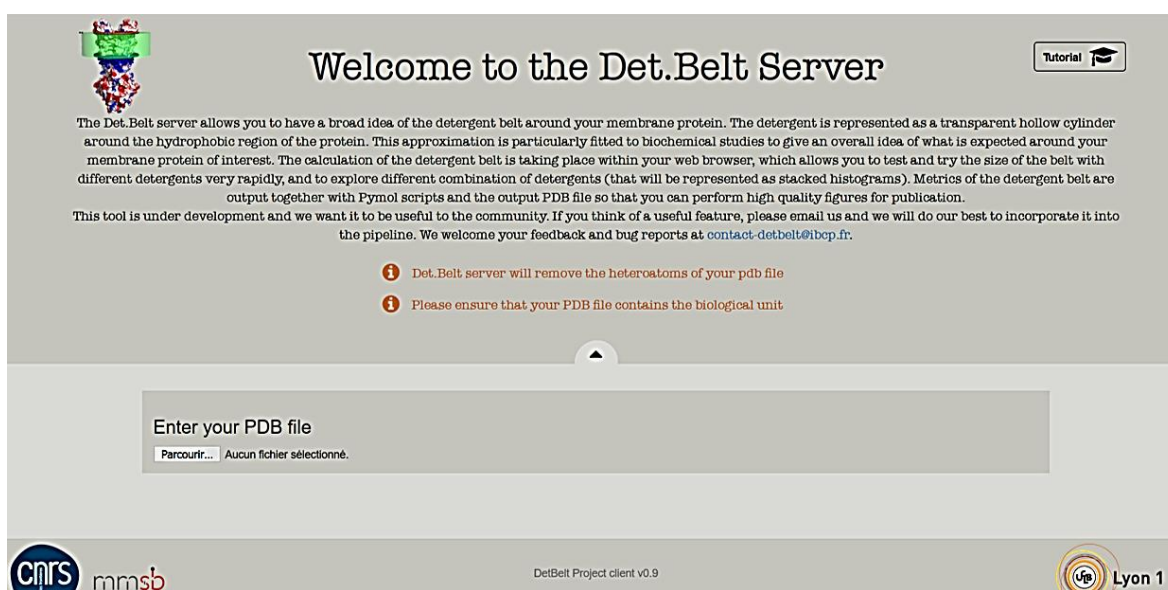
(a) This figure represents the Fos-choline 12 belt around BmrA. There are the side and the top view. The quantity of detergent was determined by the MALDI-TOF detergent quantification. (b) This how the hollow cylinder corresponding to the detergent belt is calculated. The whole volume is number of detergent determined multiplied by the volume of one molecule. (c) This panel is the curve of the volume of the detergent belt in function of the accessible hydrophobic surface (AHS). (Chaptal et al. 2017)

To give an idea of this detergent belt, the server Det.Belt has been developed in collaboration with Guillaume Launay and Juliette Martin in the team of Luca Monticelli (informatics development). First, the PDB of the protein is oriented in the membrane and it is possible thanks to the PPM server ([opm.phar.umich.edu/ppm\\_server](http://opm.phar.umich.edu/ppm_server)). The PDB obtained is then loaded to the Det.Belt server which calculates the accessible hydrophobic surface (AHS) by the use of the *naccess* program. The quantity of the detergent is input by the user or estimated using the curve showed in the figure 86. This curve has been calculated on the results of the quantification of various detergents bound to different proteins which varies on AHS

parameter. The server represents the detergent belt and gives the information following AHS, global volume, half-height, inner and the outer radius. Multiple detergents and lipids are in the data set of this sever. As a consequence, it is possible to represent different detergent belts for the protein of interest, and have a “biochemist look” at what the belt would look like for any detergent, and estimate the amount of molecules embarked by the protein. Finally, PDB format, the zip archive, the PyMOL and text file can be download. This server is available at <http://www.detbelt.ibcp.fr> and a tutorial is also available to guide users.

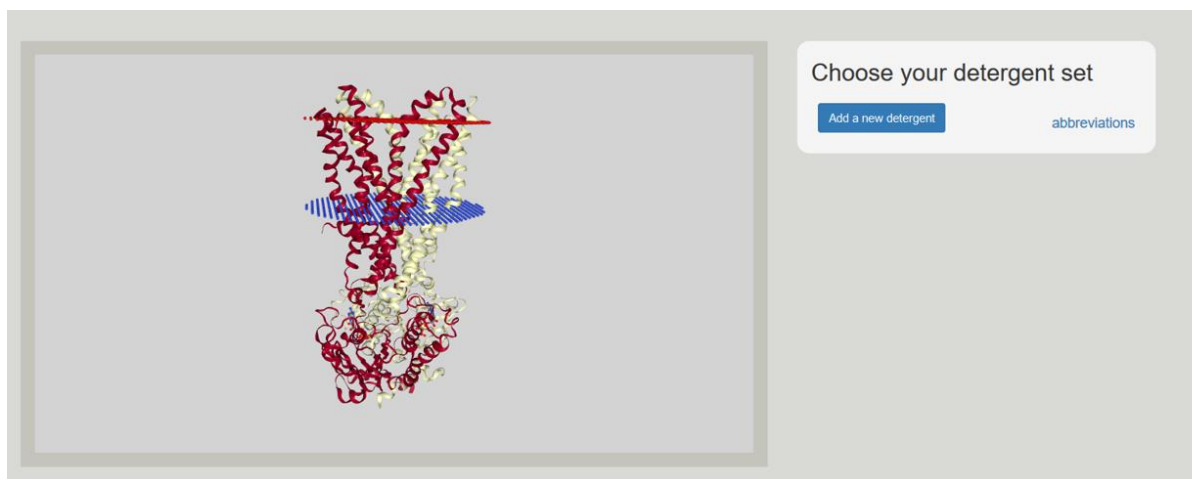
In this project, I participated to the implementation of the detergents data base. I collected the parameters of each detergent (CMC, molecular weight, aggregation number, etc.) and calculated its volume using Voidoo. This allows the user to choose the detergent of interest for their study.

The figures 87, 88, 89, 90 show how to use this server.



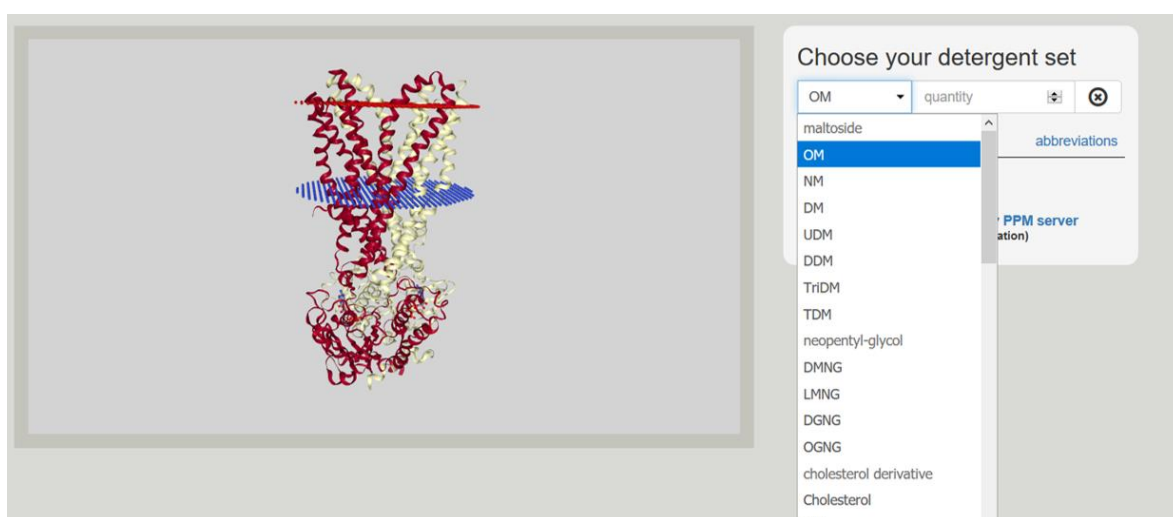
**Figure 87. DetBelt server interface**

*The welcome interface of the DetBlet server. In the upper corner in the right, there is the link to the tutorial. In the middle of the page, there is where it is possible to load the PDB file.*



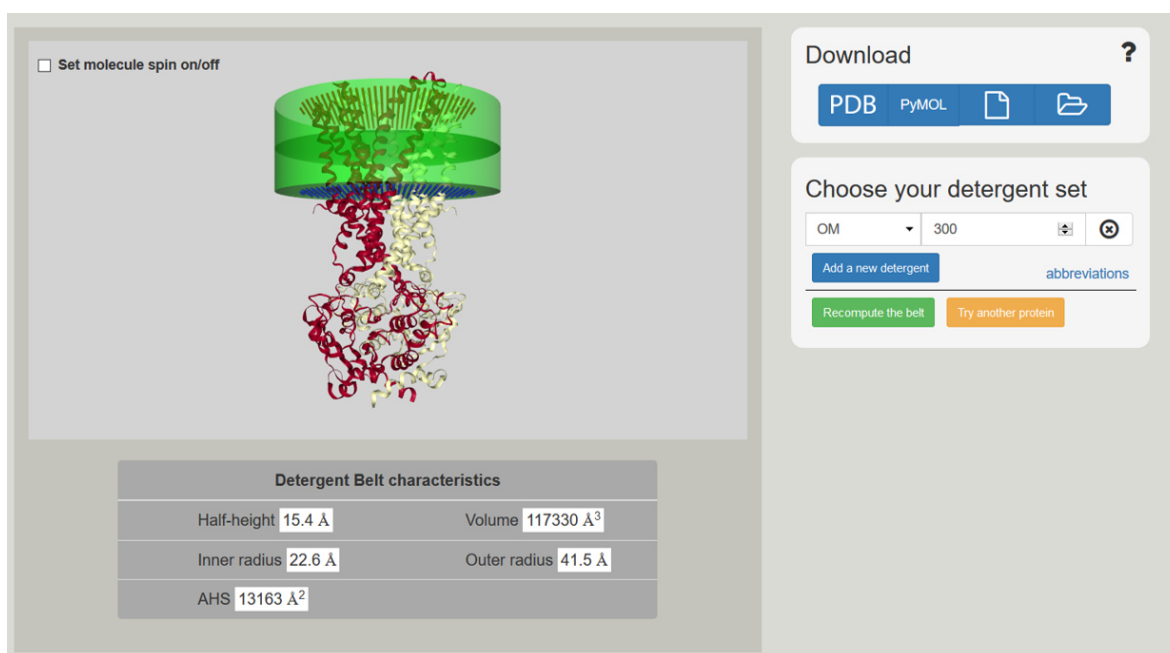
**Figure 88. PDB oriented loaded to the DetBelt server**

The PDB is previously oriented using the PPM server ([opm.phar.umich.edu/ppm\\_server](http://opm.phar.umich.edu/ppm_server)) and then loaded in the DetBelt server. The protein is represented in cartoon and colored in red and yellow. The limits of the membrane are displayed in red for the extracellular side and blue for the cytoplasmic side.



**Figure 89. The choice of the detergent in the DetBelt server**

In the right side of the interface, there is the menu with all the possible choices of detergent.



**Figure 90. Representation of the detergent belt in the DetBelt server**

The detergent belt composed by 300 molecules of *n*-Octyl- $\beta$ -D-Maltopyranoside (OM) is modeled by a green hollow cylinder placed around the hydrophobic part of the protein. Below the protein, there are shown the information about the belt as the half-height, the volume, the AHS, the inner and the outer radius. Finally, in the upper corner in the right, there is the download possibilities.

The server belt was used to visualize the volume of the detergent belt determined experimentally. This was a useful way to rationalize the impact of the mixture of detergent used and its impact on the crystallogensis experiment. For instance, it was used to create all the figures of BmrA with the detergent belt (cf. Chapter I). Furthermore, it is useful to estimate in advance the possible size of the detergent belt adapting it for the experiment desired.

# Chapter IV: Study of amphipathic belts in Cryo- EM reconstructions

## RESULTS: CHAPTER IV

The solvent belt around the membrane region of the proteins is a crucial parameter in all the step of their studies. The Cryo-EM data treatment is no exception. This belt participates to the diffusion of the electron and it is visible in the density map. A bottleneck step for the Cryo-EM data treatment is the selection of the particles and the averaging of 2D and 3D classes. They are based on the alignment of the particles and the belt contributes strongly in this process. We investigated whether the type of belt surrounding the membrane protein has an influence on the reconstruction, on how the belt is visible in the structure. For this, we downloaded the whole PDB and extracted the membrane proteins solved by Cryo-EM and that have been solved in multiple environments. To these, we also added all the GPCRs and the ABC transporters as they each share their common fold, and thus we could investigate the influence of the belts on their 3D reconstructions. I measured the belt size for all the proteins listed in Table 2 in the paper appended bellow. More than 90 structures have been analyzed in the three main types of amphipathic solvent belts: detergents, nanodiscs and amphipols. Surprisingly, the main observation of this study is that the size of the belt does not change significantly amongst the different reconstructions and the types of solvent. The quasi totality of the measures is between 14 and 36 Å of diameter. The average size is around 19 and 29 Å.

## Critical assessment of the belt surrounding membrane proteins in cryo-EM structures.

Veronica Zampieri, Alexia Gobet, Xavier Robert, Pierre Falson and Vincent Chaptal

Drug Resistance & Membrane Proteins group, Molecular Microbiology and Structural Biochemistry Laboratory (CNRS UMR 5086), University of Lyon, IBCP, 7, passage du Vercors, 69367 Lyon, France.

Membrane protein structure determination has become almost a routine job with the recent development of single particle electron microscopy in cryogenic conditions (Cryo-EM). A skyrocketing amount of membrane protein structures becomes available improving our knowledge of many biological processes. However, most of them are poorly resolved and the new frontier is now to reach the atomic resolution. In order to reach this grail of a nice quality structure, it is necessary to extract the protein from the native membrane, and purify it to homogeneity so it can be applied on a grid and imaged on a microscope. And there lies the specificity of membrane proteins: they display a part of their structure that spans the membrane, abundant in hydrophobic residues, rendering them insoluble in water. There is thus a need for some molecule to shield this trans-membrane region from water and from other hydrophobic molecule or even other proteins around, else the result will be aggregation and loss of the precious gem.

Many recipes are available today to maintain membrane proteins in solution. The historical way, still very much used today, is to use detergents to extract membrane proteins from the membrane and then purify them in detergent solutions. They are small molecules that display a hydrophilic head and a hydrophobic tail. Both moieties vary in nature, length and size, allowing screening for best conditions. By nature, detergents are very mobile and form a dynamic belt wrapping around the trans-membrane part of the protein[1]. Due to this dynamic property, detergents can have sometimes negative impacts on membrane proteins structure and function. Therefore, detergents with increased stabilizing properties have been more recently conceived for limiting such mobility either by having a design close to lipids (LMNG) or by generating specific interactions [Nguyen Angewandte Chemie]. On the other hand, their amphipathic nature is unique to stabilize given conformations. Besides, other tools have been developed to forgo the need of detergents. Among them, the derivation of the lipid A apolipoprotein engineered a series of Membrane Scaffold Proteins (MSP) that, assembled together with lipids, allow to reconstitute a near-native membrane environment around the membrane protein[2]. In the same vein, amphipols are polyvinyl polymers that wrap around detergent-extracted membrane proteins and stabilize them without the need for detergents and lipids[3]. More recently, new polymers have been designed to directly extract membrane proteins with lipids around from native membranes, allowing their purification without detergents [4].

All these compounds generate a local amphipathic environment around the membrane region of membrane proteins that maintains them in water-based solutions. This layer is a belt of which membrane proteins are indissociable. Despite its huge influence on the protein function this belt could be only observed in few membrane protein crystals (PebayPeroula) but cryo-EM now allows for its visualization much easily. We have taken this opportunity to investigate the influence of the compounds forming this belt on the visualization of the hydrophobic space that it shields. We show that whatever the compounds forming the belt, the later create on average similar reconstructions,

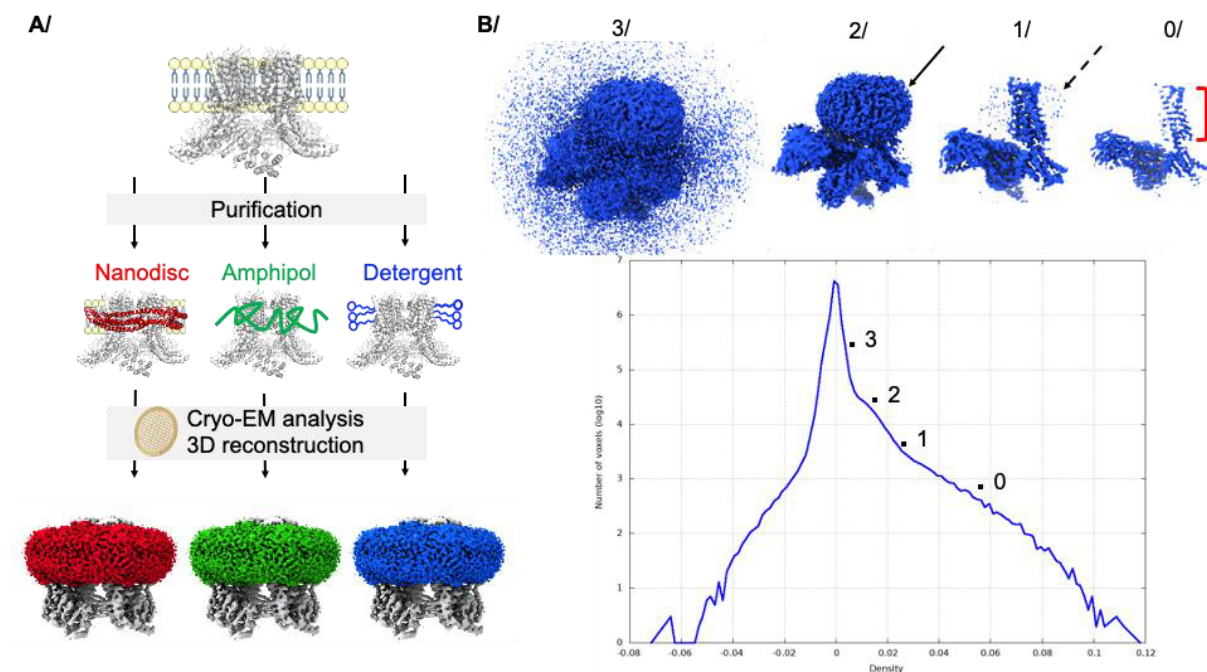


whether it originates from the same protein, or from protein from different shapes and structures. This allowed us to further identify the position of that belt in map-density distributions, opening the way to the rationalization of masks for particle alignment during 3D reconstruction of membrane proteins structures.

## 2. Results

### 2.1. 3D reconstruction of membrane proteins structures resolved by cryo-EM in various environments

In order to discriminate whether there is an influence of the type of compounds forming the belt around the membrane protein on the structure reconstruction from cryo-EM data, we selected in the Protein Data Bank for comparison membrane proteins having been resolved in detergents, nanodiscs and amphipols (Fig. 1A. and Table 1). The idea behind this selection was first to keep the protein fold constant in order to normalize its influence on the reconstruction and second, to be able to focus on the belts alone. The identification of the belt is obvious to a trained eye, capable of detecting the trans-membrane parts of a protein in a structure; it is characterized by an expansion of lower-level density in the vicinity of the membrane region as a decrease in the map density. After the observation of map-density distributions of each structure of this dataset, an apparent feature appeared for identifying the belt, as exemplified in Figure 1B. At high density levels, the very ordered parts of the structure are visible, on which reconstruction was anchored. Typically, trans-membrane helices are key features used in 3D reconstructions of membrane proteins and are visible at this level. With decreasing density levels, the number of voxels increases in a concave shape (level 0). The higher ordered layers of the belt start to appear when the curve becomes convex (level 1, dotted arrow). It becomes more and more apparent over the course of about one log when the curve inflexes concavely (level 2) before a sharp increase in number of voxels leading to appearance of low-level noise all through the box (level 3). Throughout reconstructions, it is apparent that the more visible the belt, the clearer and sharper the transition is between levels 1 and 2.



RESULTS: CHAPTER IV

**Fig. 1.** Visualization of the different types of belts surrounding membrane proteins. **A/** General scheme of membrane protein purification from the membrane, kept in detergent (blue) or reconstituted in nanodisc (red) or amphipol (green), and imaged by cryo-EM to obtain a 3D reconstruction. The channel TRPV1 is used as an example of reconstruction (EMD-8117), with belts colored accordingly. **B/** Typical map-density distribution and representative density levels of reconstructions (EMD-20079). Level 0 corresponds to parts of the structure with strong density; the red bar shows the trans-membrane domain. Level 1 corresponds to the appearance of high density for the belt, depicted by the dotted arrow. Level 2 represents the maximum density observed at low-level density, depicted by the solid arrow. Level 3 corresponds to low density noise.

Table 1. Membrane proteins selected for the study

PROTEIN	PDB ID	EMD	YEAR	SYM.	RES. (Å)	HYDROPHOBIC ENVIRONMENT	PUBLICATION
TRPV1	3J5P	5778	2013	C4	3.3	amphipol	Liao 2013
	3J5Q	5776	2013	C4	3.8	amphipol	Cao 2013
	3J5R	5777	2013	C4	4.2	amphipol	Cao 2013
	5IRX	8117	2016	C4	2.9	Nanodisc (MSP2N2)	Gao 2016
	5IRZ	8118	2016	C4	3.3	Nanodisc (MSP2N2)	Gao 2016
	5IS0	8119	2016	C4	3.4	Nanodisc (MSP2N2)	Gao 2016
TRPV2	6U84	20677	2019	C4	3.7	Nanodisc (MSP2N2)	Pumroy2019
	5AN8	6455	2015	C4	3.8	amphipol	Zubcevic 2016
	6OO3	20143	2019	C4	2.9	Nanodisc (MSP2N2)	Zubcevic2019
	6BO4	7118	2018	C4	4.0	LMNG	Dosey 2019
	5HI9	6580	2016	C4	4.4	DMNG	Huynh2015
TRPV3	6DVW	8919	2018	C4	4.3	Digitonin	Singh 2018
	6DVY	8920	2018	C4	4.0	Digitonin	Singh 2018
	6DVZ	8921	2018	C4	4.2	GDN	Singh 2018
	6LGP	882	2019	C4	3.3	Nanodisc (MSP2N2)	Shimada 2020
	6MHO	9115	2018	C4	3.4	Poly (Maleic Anhydride-alt-1-Decene)/PMALC8	Zubcevic 2018
	6UW4	20917	2020	C4	3.1	nanodisc (MSP2N2)	Deng 2020
	6MHS	9117	2018	C4	3.2	Poly (Maleic Anhydride-alt-1-Decene)/PMALC8	Zubcevic 2018
	6UW6	20918	2020	C4	3.7	nanodisc (MSP2N2)	Deng 2020
	6UW9	20920	2020	C4	4.3	nanodisc (MSP2N2)	Deng 2020
	6UW8	20919	2020	C4	4.0	nanodisc (MSP2N2)	Deng 2020
	6PVL	20492	2019	C4	4.4	GDN	Singh 2019
	6PVM	20493	2019	C4	4.5	GDN	Singh 2019
	6PVO	20495	2019	C4	5.2	GDN	Singh 2019
	6PVN	20494	2019	C4	4.1	GDN	Singh 2019
6PVP	20496	2019	C4	4.5	GDN	Singh 2019	
TRPV5	6B5V	7058	2017	C4	4.8	DMNG	Hughes 2018
	6O1N	593	2019	C4	2.9	Nanodisc (MSP2N2)	Dang 2019
	6PBF	20292	2019	C4	4.2	Nanodisc (MSP2N2)	Hughes 2019
TRPV6	6D7T	7825	2018	C4	4.4	amphipol	Singh 2018
	6E2F	8961	2018	C1	3.9	amphipol	Singh AK 2018
	6E2G	8962	2018	C1	3.6	amphipol	Singh AK 2018
LRRC8A	5ZSU	6952	2018	C3	4.3	Digitonin	Kasuya 2018
	6O00	564	2019	C6	4.2	Nanodisc (MSP1E3D1)	Kern 2019
	6DJB	7935	2018	C3	4.4	digitonin	Kefauver 2018
TMEM16	6BGI	7095	2017	C2	3.8	Nanodisc (MSP2N2)	Dang 2017
	6BGJ	7096	2017	C2	3.8	LMNG	Dang 2017

RESULTS: CHAPTER IV

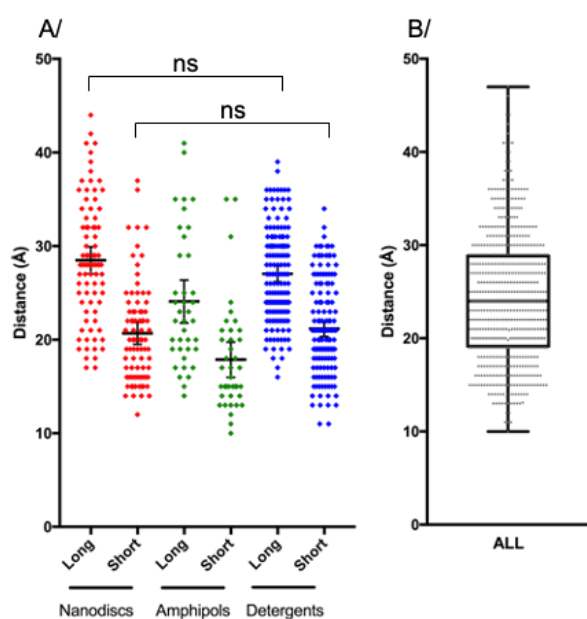
V-ATPase	5TJ5	8409	2016	C1	3.9	amphipol	Mazhab-Jafari 2016
	6C6L	7348	2018	C1	3.5	Nanodisc (MSP1E3D1)	Roh 2018
	6O7T	644	2019	/	3.2	GDN	Vasanthakumar 2019
OTP3	6NF6	9361	2019	C2	3.3	nanodisc (MSP2N2)	Saotome 2019
	6O84	650	2019	/	3.9	DDM CHS	Chen 2019
OSCA	6MGV	9112	2018	C2	3.1	nanodisc (MSP2N2)	Cruz 2018
	6OCE	20017	2019	C2	4.9	UDM-CHS	Maity 2019
PKD TRP	5T4D	8354	2016	C4	3.0	nanodisc	Shen2016
	6A70	6991	2018	C1	3.6	digitonin	Su2018
	5K47	8200	2016	C4	4.2	UDM	Grieben 2017
	5MKF	3524	2017	C1	4.2	amphipol	Wilkes 2017
	5MKE	3523	2017	C4	4.3	amphipol	Wilkes 2017
MsbA	5TTP	8467	2017	C2	4.8	Nanodisc (MSP1D1)	Mi 2017
	5TV4	8469	2017	C1	4.2	Nanodisc (MSP1D1)	Mi 2017
Pgp	6QEE	4536	2019	C1	3.9	Nanodisc (MSP1D1)	Alam 2019
	6C0V	7325	2018	C1	3.4	DDM-CHS	Kim 2018
	6FN1	4281	2018	C1	3.6	amphipol	Alam 2018
	6FN4	4282	2018	C1	4.1	LMNG-CHS	Alam 2018
	6QEX	4539	2019	/	3.6	Nanodisc (MSP1D1)	Alam 2019
CFTR	6D3R	7793	2018	C2	4.3	digitonin	Fay 2018
	6MSM	9230	2018	C1	3.2	digitonin	Zhang 2018
	5UAK	8516	2017	C1	3.9	digitonin	Liu 2017
	5UAR	8461	2016	C1	3.7	digitonin	Zhang 2016
	6O2P	0611	2019	C1	3.3	LMNG-CHS	Liu 2019
	5W81	8782	2017	C1	3.4	LMNG	Zhang 2017
MRP1	5UJ9	8559	2017	C1	3.5	digitonin	Johnson 2017
	5UJA	8560	2017	C1	3.3	digitonin	Johnson 2017
	6BHU	7099	2017	C1	3.1	digitonin	Johnson 2018
TAP1/TAP2	5UID	8482	2017	C1	3.9	C12E8	Oldham 2016
ABCG2	5NJG	3654	2017	C2	3.7	nanodisc (MSP1D1)	Taylor 2017
	6ETI	3953	2018	C2	3.1	Nanodisc (MSP1D1)	Jackson 2018
	6FEQ	4246	2018	C2	3.6	Nanodisc (MSP1D1)	Jackson 2018
	6FFC	4256	2018	C2	3.5	Nanodisc (MSP1D1)	Jackson 2018
	6HCO	0196	2018	C2	3.5	Nanodisc (MSP1D1)	Manolaridis 2018
	6HZM	0190	2018	C2	3.1	Nanodisc (MSP1D1)	Manolaridis 2018
ABCA1	5XJY	6724	2017	C1	4.1	Digitonin	Qian 2017
LptB2FGC	6MI7	9125	2019	C1	4.2	Nanodisc (MSP1D1)	Li 2019
	6S8N	10125	2019	C1	3.1	LMNG	Tang 2019
GPCR	5UZ7	8623	2017	C1	4.1	MNG/CHS	Liang 2017
	6B3J	7039	2018	C1	3.3	MNG/CHS	Liang 2018
	6CMO	7517	2018	C1	4.5	Digitonine	Kang 2018
	6D9H	7835	2018	C1	3.6	LMNG/CHS	Draper-Joyce 2018
	6E3Y	8978	2018	C1	3.3	LMNG/CHS	Liang 2018
	6G79	4358	2018	C1	38	DM	Garcia-Nafria 2018
	6N4B	0339	2019	C1	3	LMNG/GDN	Krishna Kumar 2019
	6NBF	0410	2019	C1	3	LMNG/GDN/CHS	Zhao 2019
	6NI3	9376	2019	C1	3.8	LMNG	Nguyen 2019
	6OIJ	20078	2019	C1	3.3	LMNG/GDN	Maeda 2019
	6OIK	20079	2019	C1	3.6	LMNG/GDN	Maeda 2019
	6OS9	20180	2019	C1	3	LMNG/GDN	Kato 2019
	6OT0	20190	2019	C1	3.9	MNG/GDN/ CHS/ Digitonin	Qi 2019
	6OY9	20222	2019	C1	3.9	LMNG	Gao 2019
	6PWC	20505	2019	C1	4.9	digitonin	Yin 2019
6QNO	4598	2019	C1	4.4	/	Tsai 2019	

## 2.2. 3D reconstructions of membrane proteins in nanodiscs or detergents yield similar average belt sizes

Using the map-density histogram, we calculated for each entry the belt size by measuring the distance between the protein edge and the solvent boundaries at level 2 (SFig. 1., Table 2). Belt reconstructions are not spherical but rather follow the protein shape. We thus measured long and short distances of the belts that we separated in two categories for further processing. Figure 2 displays the distribution plot of these lengths for the proteins data set. For each type of belt, there is an apparent spread of the lengths, with 95% comprised between 14 and 36 Å, and no length below 10 Å around the protein. Statistical analysis of long distances observed in detergents and nanodiscs belts show that they follow the same distribution, as well as small distances for these two categories. On average, the belt is visible up to 21-27 Å around the proteins.

The smaller amount of structures resolved using amphipols precludes the statistical analysis on means using parametric statistics. However, non-parametric statistics on ranks reveals first an ambiguity about long distances where the current data set cannot distinguish whether the distances are different or similar (more structures are needed to solve the debate), and second unambiguously state that short distances measured in amphipols follow the same distribution as for nanodiscs or detergents belts. Put together, these results point to a common average distance distribution of the belts surrounding membrane protein observed after 3D reconstruction of cryo-EM data.

In order to distinguish if there is some inter-family or inter-solvent specificities hidden within the global distribution, we further separated proteins for individual analysis.



**Fig. 2.** Distance distributions between the protein edge and the belt boundary. **A/** Distances separated by type of belts. Nanodiscs (red), amphipols (green) and detergents (blue). Each dot corresponds to a distance, the horizontal bar is the mean with the error bar displaying the 95% confidence interval of the mean (reported in brackets below). Long and short distances are separated for clarity. Nanodiscs, long 28 Å [27-30] and short 21 Å [20-22]. Amphipols, long 24 Å [22-26] and short 18 Å [16-20]. Detergents, long 27 Å [26-28] and short 21 Å [20-22]. **B/** All distances represented by a grey dot. The box corresponds to the 25<sup>th</sup> (19 Å) and 75<sup>th</sup> (29 Å) percentile with an equal mean and median of 24 Å. 95% of total distances are comprised between 14 and 36 Å.

Table 2. Measures of the diameter of the belt

PROTEIN	PDB ID	EMD	Diameter of the belt					
TRPV1	3J5P	5778	22	20	16	15	14	14
	3J5Q	5776	25	24	23	22	21	20
	3J5R	5777	29	22	24	21	19	18
	5IRX	8117	33	29	28	16	15	15
	5IRZ	8118	36	32	32	17	17	14

RESULTS: CHAPTER IV

	5IS0	8119	36	32	32	19	18	17
TRPV2	6U84	20677	40	41	36	20	23	22
	5AN8	6455	29	29	27	17	16	16
	6OO3	20143	34	32	29	20	15	15
	6BO4	7118	28	24	21	21	15	11
	5HI9	6580	24	25	22	15	15	14
TRPV3	6DVW	8919	28	23	22	21	19	17
	6DVY	8920	29	25	20	19	15	14
	6DVZ	8921	28	27	25	24	23	21
	6LGP	882	32	27	26	21	23	19
	6MHO	9115	35	32	25	23	21	17
	6UW4	20917	25	21	20	19	18	16
	6MHS	9117	24	20	19	18	17	15
	6UW6	20918	34	33	28	24	23	22
	6UW9	20920	28	24	21	20	19	18
	6UW8	20919	26	25	24	23	23	19
	6PVL	20492	25	23	23	22	21	16
	6PVM	20493	32	30	29	27	23	18
	6PVO	20495	29	23	22	21	20	19
	6PVN	20494	31	24	23	21	18	15
	6PVP	20496	35	31	29	22	21	19
TRPV5	6B5V	7058	25	21	20	18	16	15
	6O1N	593	35	34	27	17	15	14
	6PBF	20292	37	39	36	25	22	21
TRPV6	6D7T	7825	20	19	17	15	15	13
	6E2F	8961	41	31	25	24	22	20
	6E2G	8962	21	20	18	17	14	13
LRRC8A	5ZSU	6952	29	29	27	26	26	25
	6O00	564	37	34	35	32	32	30
	6DJB	7935	22	22	20	19	18	16
TMEM16	6BGI	7095	41	37	29	29	27	26
	6BGJ	7096	30	30	30	17	13	11
V-ATPase	5TJ5	8409	19	19	17	16	15	13
	6C6L	7348	20	18	18	16	15	12
	6O7T	644	24	24	20	19	19	18
OTP3	6NF6	9361	29	22	21	20	19	15
	6O84	650	30	30	27	27	27	26
OSCA	6MGV	9112	28	28	28	25	21	19
	6OCE	20017	36	34	33	31	30	30
PKD TRP	5T4D	8354	30	26	24	23	16	15
	6A70	6991	24	23	20	19	19	17
	5K47	8200	23	22	16	15	12	11
	5MKF	3524	17	15	14	13	13	10
	5MKE	3523	30	26	24	23	16	15
MsbA	5TTP	8467	28	24	22	20	20	16
	5TV4	8469	27	20	19	18	16	15
Pgp	6QEE	4536	44	42	38	37	36	32
	6C0V	7325	32	27	26	29	19	26
	6FN1	4281	40	35	35	35	35	31
	6FN4	4282	36	34	34	34	32	30
	6QEX	4539	32	30	30	29	28	24
BmrA	6R81	4749	20,9	19,8	14	13,7	13,1	13
CFTR	6D3R	7793	30	28	27	25	19	19
	6MSM	9230	35	31	30	29	29	24
	5UAK	8516	32	30	29	24	21	21

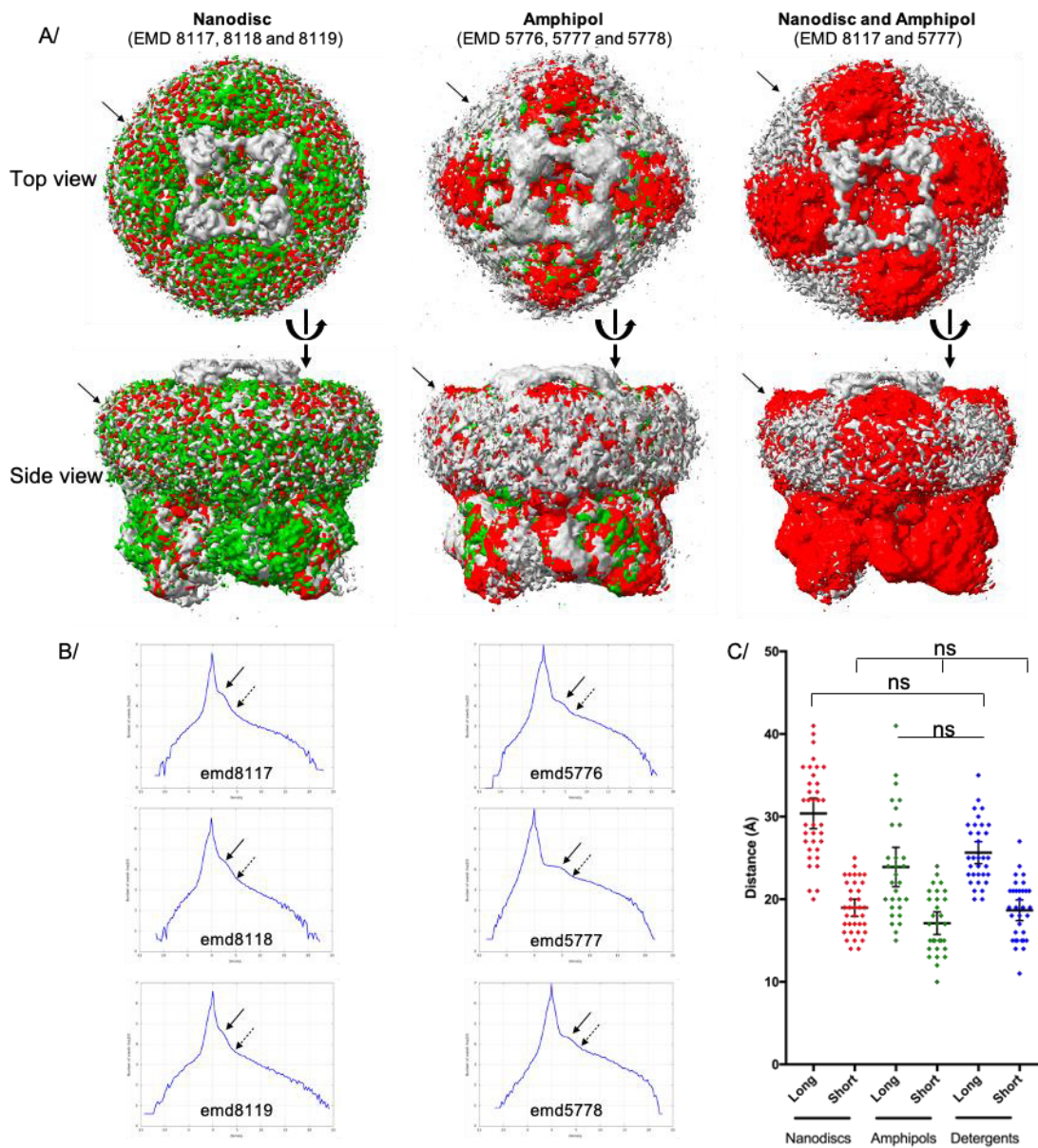
	5UAR	8461	43	41	33	29	28	25
	6O2P	0611	39	33	28	29	27	22
	5W81	8782	36	35	30	27	23	19
MRP1	5UJ9	8559	32	27	26	24	22	22
	5AUJ	8560	29	25	22	20	20	19
	6BHU	7099	27	26	24	21	21	14
TAP1/TAP2	5UJ9	8482	25	24	23	20	18	18
ABCG2	5NJG	3654	20	19	17	16	15	15
	6ETI	3953	19	19	17	16	14	14
	6FEQ	4246	31	31	27	25	22	22
	6FFC	4256	29	28	26	25	25	24
	6HCO	196	33	32	31	28	28	26
	6HZM	190	26	25	23	23	22	22
ABCA1	5XJY	6724	35	31	28	27	26	25
LptB2FGC	6MI7	9125	28	25	23	22	21	20
	6S8N	10125	22	19	18	18	16	14
GPCR	5UZ7	8623	36	30	28	27	22	21
	6B3J	7039	30	27	24	24	17	17
	6CMO	7517	35	32	32	30	30	28
	6D9H	7835	23	22	19	19	17	16
	6E3Y	8978	24	20	18	16	13	13
	6G79	4358	22	21	20	19	16	15
	6N4B	0339	29	27	26	26	25	24
	6NBF	0410	36	36	32	29	28	27
	6NI3	9376	21	19	19	18	17	16
	6OIJ	20078	26	26	23	20	20	19
	6OIK	20079	33	31	31	28	27	22
	6OS9	20180	25	25	24	23	20	18
	6OT0	20190	31	31	30	29	28	22
	6OY9	20222	24	24	24	21	20	16
	6PWC	20505	38	36	34	30	29	29
	6QNO	4598	21	17	16	15	15	13

### 2.3. The TRPV family

The Transient Receptor Potential Vanilloid (TRPV) family consists of six ion channels, varying in ion-selectivity according to the sub-family. Despite being functionally distinct, they share a common fold, being active as a tetramer formed around 6 trans-membrane helices per monomer[4]. In the present dataset, we identified structures of TRPV1 in nanodiscs and amphipols, TRPV2 in nanodiscs, amphipols and detergent (LMNG and DMNG), and TRPV5 in nanodiscs and DMNG (Table 1). The fact that TRPV proteins share a conserved fold gives a unique opportunity to compare varying belts. We also included structures of TRPV3 and 6 that were resolved in only one condition, benefiting from the fact that they share the same fold.

The signal of the belt varies in intensity between the diverse 3D reconstructions, for unclear reasons (Fig. 3A). For example, the nanodisc-belts of TRPV1 and 2 appear with a strong signal in these five reconstructions, while its intensity is much milder in the two reconstructions of TRPV5. Similar trends can be seen with amphipols or detergents across the different reconstructions. Nevertheless, each belt boundary is clearly visible and was measured for all thirty proteins (Fig. 3C). Distance distributions follow a similar trend as the global one (Fig. 2A.), where differences amongst belts are undistinguishable. The same ambiguity remains between long distances of nanodiscs and amphipols belts, but this is challenged by the lack of difference this time between amphipols and detergents ones.

More reconstructions would help to differentiate the trend. Nevertheless, the fact that short distances follow the same distributions across the three types of belts, together with the undistinguishable long distances for nanodiscs and detergents belts suggest a similar average size.

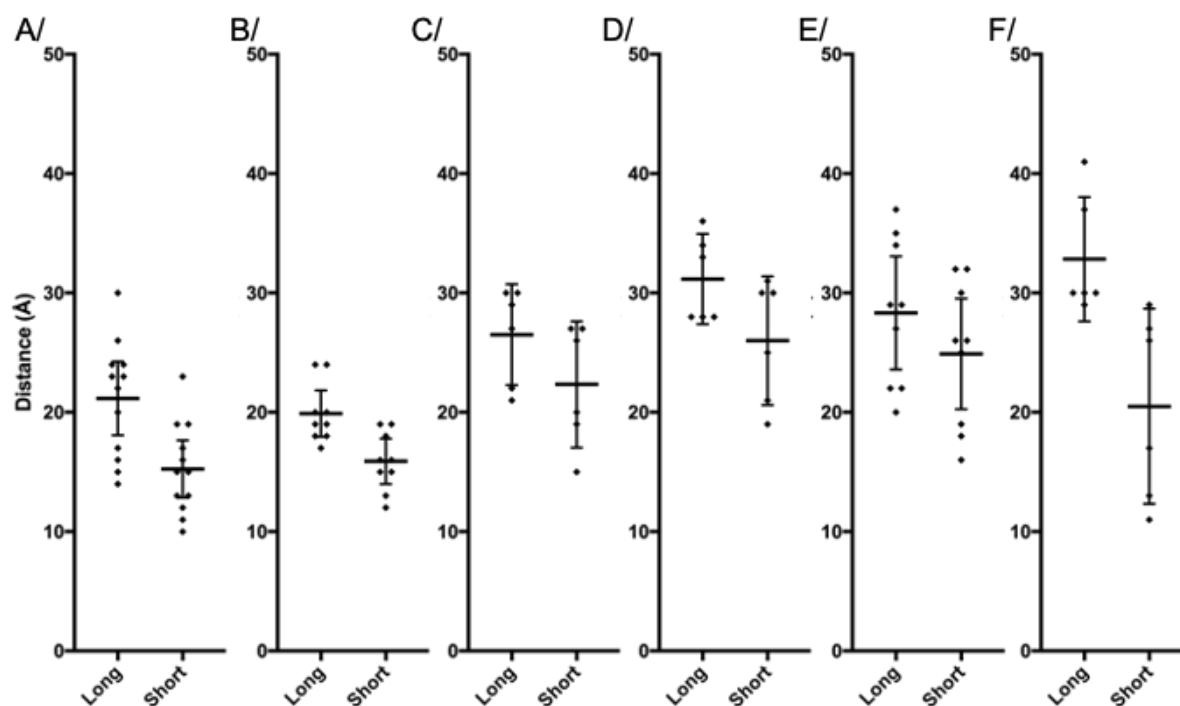


**Fig. 3.** Belts surrounding TRPV proteins. **A/** Example of the TRPV1 proteins resolved with nanodiscs or amphipols belts. The EMD accession codes are listed and each structure is colored in grey, red or green, and overlaid. Top and side views are depicted, the solid arrow points to the position of the belt. **B/** Map-density distribution for each entry. On each distribution, the dotted arrow shows the belt appearance at level 1, and the solid arrow at level 2. **C/** Distance distributions for all TRPV proteins, with the same color-coding as Fig.2. Statistical analysis was carried out using ANOVA and Kruskal-Wallis functions.

#### 2.4. Similar average belts lengths across multiple protein types resolved using different shielding compounds

We have identified in the dataset multiple protein structures that have been resolved only a few times with different belts. The limited amount of structures prevents a statistical analysis on each protein.

Instead, these proteins were evaluated in a group, thereby offering the opportunity to compare proteins with completely distinct folds, and originating from various sources and hydrophobic environments (Fig. 4., Table 1). Within each protein, belt distances cluster rather well, showing a narrow distribution of distances, sampling apparently randomly across the distribution of all proteins shown in Fig. 2. Comparison of all these proteins reveals that their means group in similar ranges, with overlapping confidence interval of the mean, invoking a comparable hydrophobic belt around all these proteins.



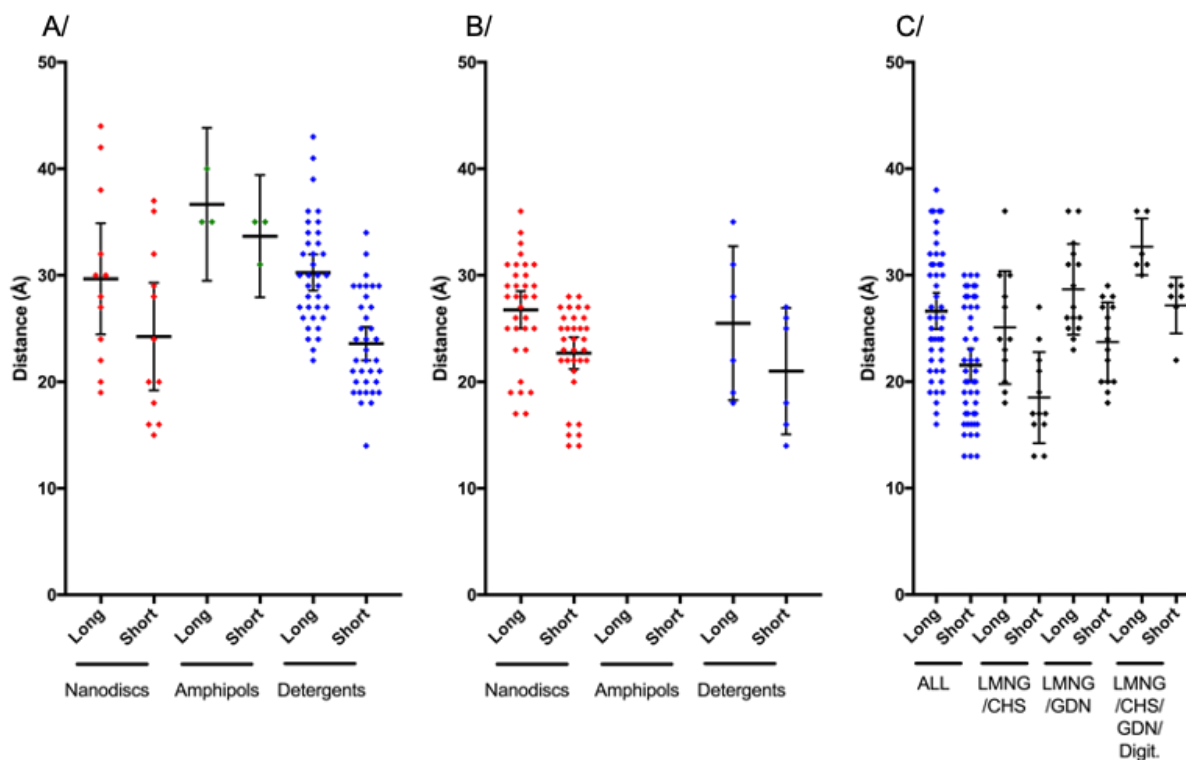
**Fig. 4.** Distance distributions between the protein edge and the belt boundary for several types of proteins. Given the limited amount of structures in each family, nanodiscs, amphipols and detergents have been reported together. Each dot corresponds to a distance, the horizontal bar is the mean with the error bar displaying the 95% confidence interval of the mean (in brackets below). Long and short distances are separated for clarity. **A/** PDK-TRP family, long 21 Å [18-24] and short 15 Å [13-18]. **B/** V-ATPase, long 20 Å [18-22] and short 16 Å [14-18]. **C/** OTP3, long 27 Å [22-31] and short 22 Å [17-28]. **D/** OSCA, long 31 Å [27-35] and short 26 Å [21-31]. **E/** LRRC8A, long 28 Å [24-33] and short 25 Å [20-30]. **F/** TMEM16, long 33 Å [28-38] and short 21 Å [12-29].

### 2.5. The superfamily of ABC transporters

ATP-binding Cassette (ABC) transporters are a large superfamily of transporters, harnessing the energy of ATP-binding and hydrolysis to translocate a wide range of substrate across many biological membranes. They are ubiquitous, and involved in many important cell-homeostasis functions[5]. While no single ABC transporter has been solved by cryo-EM in different hydrophobic environment, these proteins display a common fold and all together have been solved in nanodiscs, amphipols and detergents. They also offer the advantage that there is a large amount of structures, solved by several groups around the world using their own methodologies, and that their structures have been resolved in multiple conformations offering a unique view of the belt distribution around proteins in motion. Type V (or Type-I exporter, ABCB1-like) and type VI (or Type-II exporter, ABCG2-like) have been



separated for clearer analysis (Fig. 5AB). Within the type V, no difference is detected between the distributions of distances. Between type V and VI, the distances are also inseparable, claiming that the hydrophobic belt around ABC transporters is always of similar size, regardless of the conformation or the arrangement of trans-membrane helices.



**Fig. 5.** Distance distributions around ABC transporters and GPCRs. **A/** Type V ABC transporter (ABCB1-like). Nanodiscs, long 30 Å [24-35] and short 25 Å [19-29]. Amphipols, long 37 Å [29-44] and short 34 Å [28-39]. Detergents, long 30 Å [29-32] and short 24 Å [22-25]. **B/** Type VI ABC transporter (ABCG2-like). Nanodiscs, long 27 Å [25-28] and short 23 Å [21-24]. Detergents, long 26 Å [18-33] and short 21 Å [15-27]. **C/** GPCR, all structures, in detergents: long 27 Å [25-28] and short 22 Å [20-23]. For structures solved in the mixture LMNG/CHS: long 25 Å [22-29] and short 19 Å [16-21]; LMNG/GDN: long 29 Å [26-31] and short 24 Å [22-26], and for the complex mixture of LMNG/CHS/GDN with or without digitonin: long 33 Å [30-36] and short 27 Å [24-30].

## 2.6. Similar detergent belt reconstructions around GPCRs

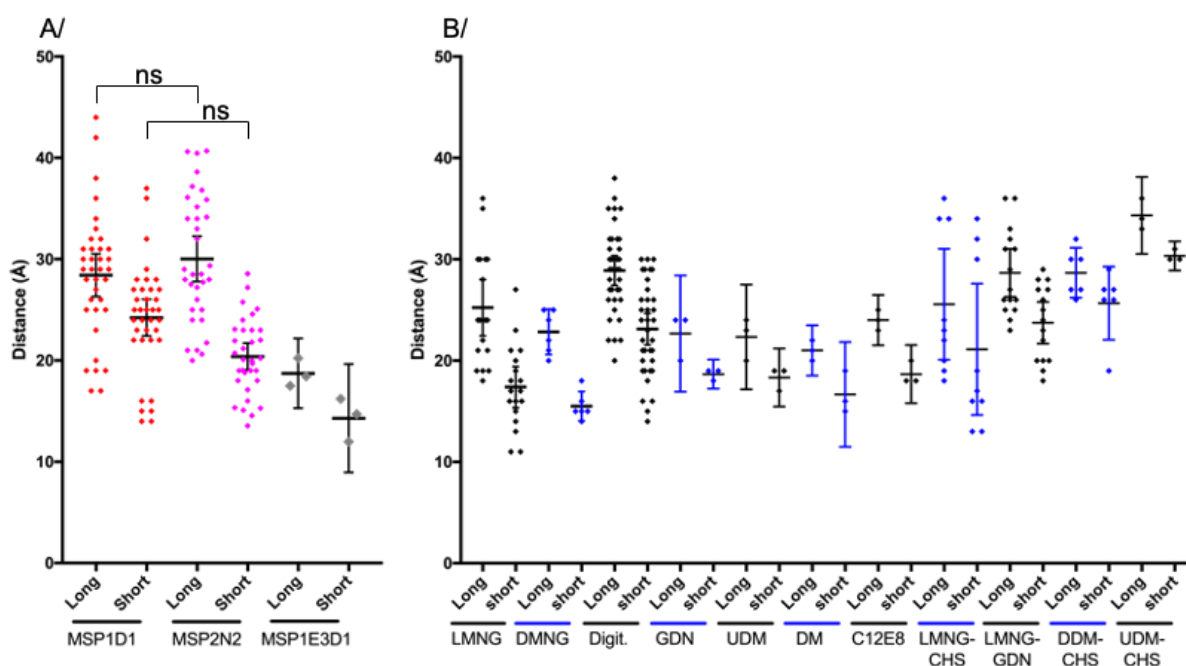
Twenty one unique structures of GPCR were found in the present database, belonging to the A, B, C or F classes (or G, R, F or S, respectively, according to the GRAFS nomenclature[6]), all solved in detergents. The vast majority used LMNG as a base, alone or in combination with other cholesterol-like detergents such as CHS, GDN or digitonin. All structures have been resolved in complex with their cognate G proteins, and/or  $\beta$ -arrestin, in various flavors. Like for ABC transporters, all these GPCR structures share an overall fold that grants the direct comparison of their associated belts, with local differences between structures, making it more worthwhile to analyze differences in the detergent belt measurement. The detergent belt distance distribution (Fig. 5.) is inseparable from the ABC transporter ones, or from the global distance distribution of all membrane proteins solved by cryo-EM

(Fig. 2.). Following this trend, the popular detergent mixes, for these GPCR structures, between LMNG and CHS, GDN or digitonin yield similar detergent belt reconstructions on average.

### 2.7. Different types of nanodiscs yield similar reconstructions; detergent belts are all of equivalent size.

We checked whether a difference in distance distribution can be observed among the type of hydrophobic solvent. For instance, different flavors of Membrane Scaffold Proteins (MSP) are available to form nanodiscs, varying the length of a helical fragment within the MSP to make it longer or shorter[2]. In the current dataset, proteins have been solved with 3 types of MSP, the short MSP1D1 and its longest version MSP1E3D1 comprising 3 helical insertion. MSP2N2 is formed by the fusion of two MSP1D1.

Figure 6A shows the distance distribution of the nanodisc-belt sorted by nanodisc type revealing that they are undistinguishable after reconstruction. Long and short distances of two types of nanodiscs formed by MSP1D1 and MSP2N2 follow the same distribution, with means equivalent to the mean obtained for all measurements in Fig. 2. Following this observation, distances were also separated by type of detergent to distinguish if a detergent or a detergent mixture give rise to distinct size of belts. Distances measured from different types of detergents are all virtually indissociable, and distribute in the same range as distances observed for nanodiscs and all other measurements together (Fig. 2.).



**Fig. 6.** Distance distributions of the different nanodiscs or detergents belts. **A/** Distances measured for nanodiscs belts. MSP1D1, long 28 Å [26-31] and short 24 Å [22-26]. MSP2N2, long 32 Å [30-35] and short 20 Å [18-22]. MSP1E3D1, long 19 Å [15-22] and short 14 Å [9-20]. **B/** Distances measured for the most represented detergents in this dataset. LMNG (Lauryl Maltose Neopentyl Glycol), long 25 Å [22-28] and short 17 Å [15-19]. DMNG (Decyl Maltose Neopentyl Glycol), long 23 Å [20-25] and short 16 Å [14-18]. Digit. (Digitonin), long 29 Å [27-30] and short 23 Å [22-25]. GDN (Glyco-disgitonin), long 23 Å [17-28] and short 19 Å [17-20]. UDM (Undecyl- $\beta$ -D-galactopyranoside), long 22 Å [17-28] and short 18 Å [15-21]. DM (Decyl- $\beta$ -D-galactopyranoside), long 21 Å [19-24] and short 17 Å [12-22]. C12E8 (Octaethylene Glycol Monododecyl Ether), long 24 Å [22-27] and short 19 Å [16-22]. LMNG-CHS (CHS: Cholesteryl-hemisuccinate), long 26 Å [20-31] and short 21 Å [15-28]. LMNG-GDN, long 29 Å [26-31] and short 24 Å [22-26]. DDM-CHS (DDM: Dodecyl-

$\beta$ -D-galactopyranoside), long 29 Å [26-31] and short 26 Å [22-29]. UDM-CHS, long 34 Å [31-38] and short 30 Å [29-32]. Numbers are the mean followed by the 95% confidence interval of the mean in brackets.

### 3. Discussion

In order to discriminate if the compound used to shield the membrane region of a membrane protein has an influence on the observation of the corresponding belt by cryo-EM, we performed a statistical analysis of a curated database of selected membrane proteins solved in several hydrophobic environments. By visualizing every structure, we identified in map-density distributions a signature of belt appearance (levels 1 & 2 in Fig. 1B.). We further identified its boundaries for every protein and measured its size for statistical analysis. 95% of all measured lengths distribute between 14 and 36 Å around the surface of trans-membrane segments, and half of the belts are comprised between 19 and 29 Å. The belts were further separated by type of forming compound to probe whether nanodiscs, amphipols or detergents yield tighter or larger belts. The results presented in Figure 2 show that the size distribution is the same whatever the compound, and is therefore statistically indistinguishable on average.

This result correlates well with other types of measurements of the same compounds by other methods. Molecular dynamics simulations of membrane proteins embedded in amphipols or detergents show a belt around the transmembrane regions, with some degree of flexibility[1, 7-9]. Indeed, the belt formed by these amphipathic compounds is very fluid, revealing local clusters of individual molecules, forming and deforming with time. When measured using neutron diffraction of membrane protein crystals[10], an averaging technique like cryo-EM, the detergent belt appears as a homogeneous belt around the protein. The size of the belt observed was then highly dependent on the type of crystal as the detergent could merge between belts of symmetric molecules[11]. All these techniques have been limited to the size of the system for molecular dynamic simulations, or “neutron-diffraction quality” crystals combined with deuterated detergents; here, cryo-EM allows for the visualization of any compound, with belt measurements matching other measuring methods.

3D variability of the detergent belt has been visualized in cryo-EM[12]. This observation follows the averaging principle also observed using neutron diffraction of membrane protein crystals.

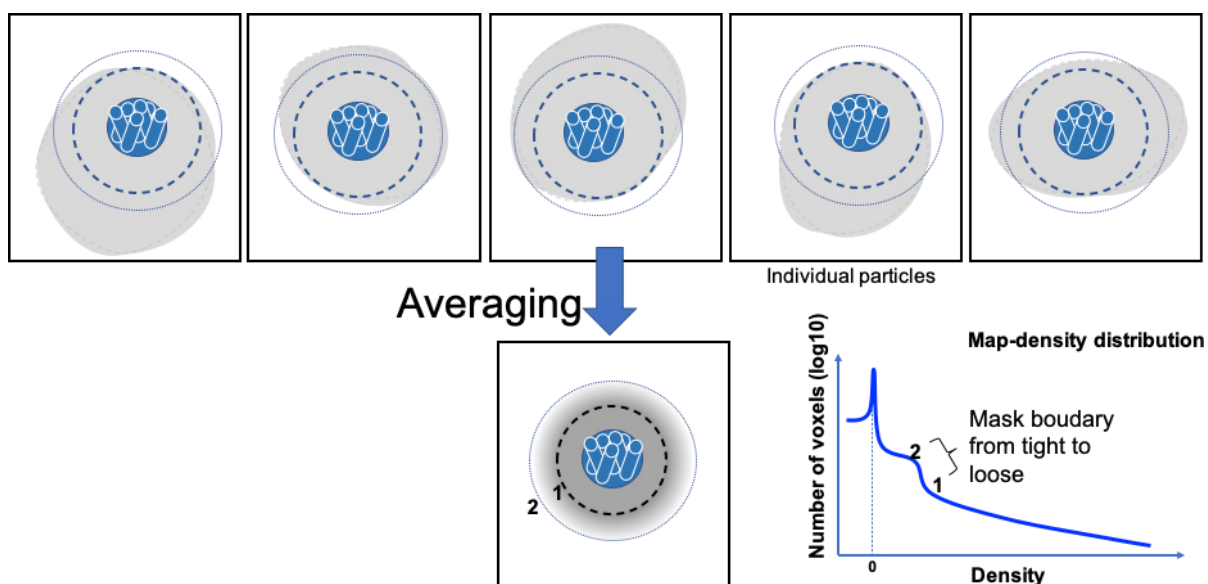
Nanodiscs formation with a membrane protein embedded is in itself a smart process, where the three ingredients (Membrane Scaffold Protein, lipids and membrane protein) are mixed together, and detergents removed using biobeads. The membrane protein-nanodiscs complex is then separated from empty nanodiscs using affinity chromatography and/or size exclusion chromatography. The object comprising the membrane protein of interest is in reality quite heterogeneous, containing a mixture of large and small nanodiscs, with more or less lipids embarked. Also, within the nanodisc, the membrane protein can move from side to side and does not always stay in the middle. This explains why the membrane scaffold protein is never observed in 3D reconstructions of membrane proteins in nanodiscs.

Following this idea, we further explored if we could identify within a set of protein, or type of belt, a combination that could influence the size of the belt seen around membrane proteins. We could not establish any significant difference in the measurement distributions, all falling within the overall distribution described in Figure 2. Hereabouts, the incorporation of ABC transporters and GPCRs in this dataset yields an important viewpoint. From detergent quantification we know that the amount of detergent present around membrane proteins is directly proportional to the accessible hydrophobic area[1]. The amount of detergent around ABC transporters (12 trans-membrane helices) is thus inherently larger than the one around GPCRs (7 trans-membrane helices). One would thus expect to

visualize a larger belt around ABC transporters by cryo-EM, but the size of the belt is following the same distribution (Fig. 5.).

Finally, there is the observation that the belt observed around membrane proteins by cryo-EM is circular, somewhat reminiscent of the ones observed by neutron diffraction of crystals. This is partly due to symmetries enforced during reconstructions, but at the heart, mostly due to particle averaging. Particle alignments are anchored on secondary structures, among which trans-membrane helices are a lighthouse in a fog of the belt. The belt observed during reconstruction is thus made out of several layers distributing radially away from the protein boundary (Fig. 7.). Level 1 corresponds to the highest density, and represents the common minimum ordered layer, where the amphipathic compounds are always in contact with the protein hydrophobic region. This layer concomitantly increases in size and decreases in density as it radiates away from the protein boundary, representing areas of space less and less populated by the belt. This is influenced by the fluid properties of the belt, as the sample is vitrified in liquid ethane. Each individual particle of a dataset represents a snapshot carrying a given belt-size.

Since the belt has intrinsic properties to diffract electrons, it has a strong influence on the reconstructions. For example, for a 130 kDa ABC transporter, the DDM belt (400 monomers) determines an additional 200 kDa[1]. It is thus understandable that even if this detergent belt is not ordered, it still accounts for an important part of electron diffraction around the membrane protein. Habitually, masks are created to exclude the detergent, and to only use the information originating from proteins to perform particles alignments. Here we show where the belt is usually visualized, and the reasons underlying its visualization. The data presented here suggests that including the ordered part of the belt in masks can only be beneficial during reconstruction.



**Fig. 7.** Influence of the averaging on belt visualization. Top: set of particles all centered on the trans-membrane helices, with the same orientation. The inner dash circle represents the volume around the membrane protein where the belt is always present. The outer dotted circle represents the spread upto where the solvent belt can be visualized. The belt is shown in gray, with various shapes to highlight its variability around the trans-membrane domain. Bottom: The result of the averaging is a clear definition of transmembrane helices, and a gradient of presence for the solvent radiating away from the protein boundary. The level 1 and 2 correspond to the levels presented on the map-density distribution.

## 4. Material and methods

### 4.1. Membrane proteins structure database extraction

Based on the mpstruc database (<https://blanco.biomol.uci.edu/mpstruc/>) that lists all the membrane proteins of known 3D structure, we created a dataset containing only entries solved by Cryo-EM. We wrote a Bash shell script in order to automatically extract information from these entries. This allowed us to determine those which have been solved in multiple hydrophobic environments (nanodiscs, amphipols or detergents) and to sort them in distinct subsets. Then, for each entry, we extracted from the Electron Microscopy Data Bank (EMDB) the map-density distribution data in order to render graphs plotting the density distribution (*i.e.* the number of voxels as a function of the density).

### 4.2. Map comparison

Maps were retrieved from EMDB and opened in ChimeraX[13]. Maps were first manually aligned, then aligned using the volume tool within ChimeraX. Threshold levels to compare the maps were adjusted to include the highest level of low contour information, without including noise voxels appearing in the box. This level corresponds to the slope change in the map-density histogram.

### 4.3. Measures of the solvent belt around the protein

The measure of solvent belt thickness was performed in ChimeraX using the tool “tape” which is included in the software. The density map histogram was used to increase or decrease the contour information. At first, the density map showed the maximum of the solvent belt information and vertical lines were drawn to signal the limit the solvent belt. Then the density map contour was reduced in order to see clearly the protein density. Horizontal lines were drawn to link the vertical lines and the protein density. The tape tool measures the distance. This experiment was performed six times and in distinct spots of the solvent belt.

### 4.4. Statistical analysis

Statistical analysis was performed only on the total amount of measures to have substantial quantity of measures to be meaningful. For this reason, measures in amphipols were excluded from the analysis, as well as analysis of individual types of proteins or hydrophobic environments. ANOVA was used to distinguish differences between means. Non-parametric Kruskal-Wallis analysis yields the same statistical meaning as the one gave by ANOVA. For all figures, means were computed as well as the 95% confidence interval of the mean.

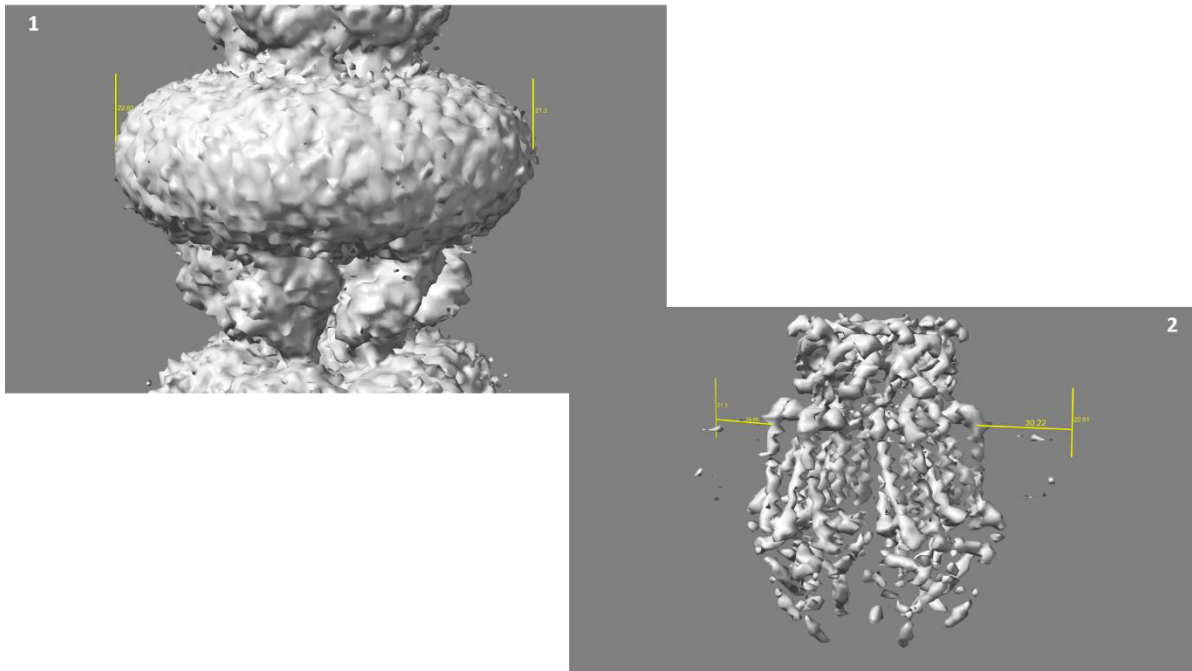
## Acknowledgments

This work was supported by the CNRS, Lyon University and the French National Research Agency, ANR-CLAMP2- 18-CE11-0002-01 to PF and VC and ANR-19-CE11-0023-01 to VC and PF.

## References

1. Chaptal, V., et al., *Quantification of Detergents Complexed with Membrane Proteins*. Sci Rep, 2017. **7**: p. 41751.
2. Bayburt, T.H. and S.G. Sligar, *Membrane protein assembly into Nanodiscs*. FEBS Lett, 2010. **584**(9): p. 1721-7.
3. Marconnet, A., et al., *Solubilization and Stabilization of Membrane Proteins by Cycloalkane-Modified Amphiphilic Polymers*. Biomacromolecules, 2020.
4. van Goor, M.K., et al., *High-resolution structures of transient receptor potential vanilloid channels: Unveiling a functionally diverse group of ion channels*. Protein Sci, 2020. **29**(7): p. 1569-1580.
5. Thomas, C. and R. Tampé, *Structural and Mechanistic Principles of ABC Transporters*. Annu Rev Biochem, 2020. **89**: p. 605-636.
6. Fredriksson, R., et al., *The G-Protein-Coupled Receptors in the Human Genome Form Five Main Families: Phylogenetic Analysis, Paralogon Groups, and Fingerprints*. Molecular Pharmacology, 2003. **63**(6): p. 1256-1256-1272.
7. Perlmutter, J.D., J.-L. Popot, and J.N. Sachs, *Molecular Dynamics Simulations of a Membrane Protein/Amphipol Complex*. The Journal of Membrane Biology, 2014. **247**(9): p. 883-895.
8. Etzkorn, M., et al., *How Amphipols Embed Membrane Proteins: Global Solvent Accessibility and Interaction with a Flexible Protein Terminus*. The Journal of Membrane Biology, 2014. **247**(9): p. 965-970.
9. Wolfe, A.J., et al., *Quantification of Membrane Protein-Detergent Complex Interactions*. The Journal of Physical Chemistry B, 2017. **121**(44): p. 10228-10241.
10. Pebay-Peyroula, E., et al., *Detergent structure in tetragonal crystals of OmpF porin*. Structure, 1995. **3**(10): p. 1051-9.
11. Penel, S., et al., *Detergent binding in trigonal crystals of OmpF porin from Escherichia coli*. Biochimie, 1998. **80**(5-6): p. 543-51.
12. Punjani, A. and D.J. Fleet, *3D Variability Analysis: Directly resolving continuous flexibility and discrete heterogeneity from single particle cryo-EM images*. bioRxiv, 2020: p. 2020.04.08.032466.
13. Goddard, T.D., et al., *UCSF ChimeraX: Meeting modern challenges in visualization and analysis*. Protein Sci, 2018. **27**(1): p. 14-25.

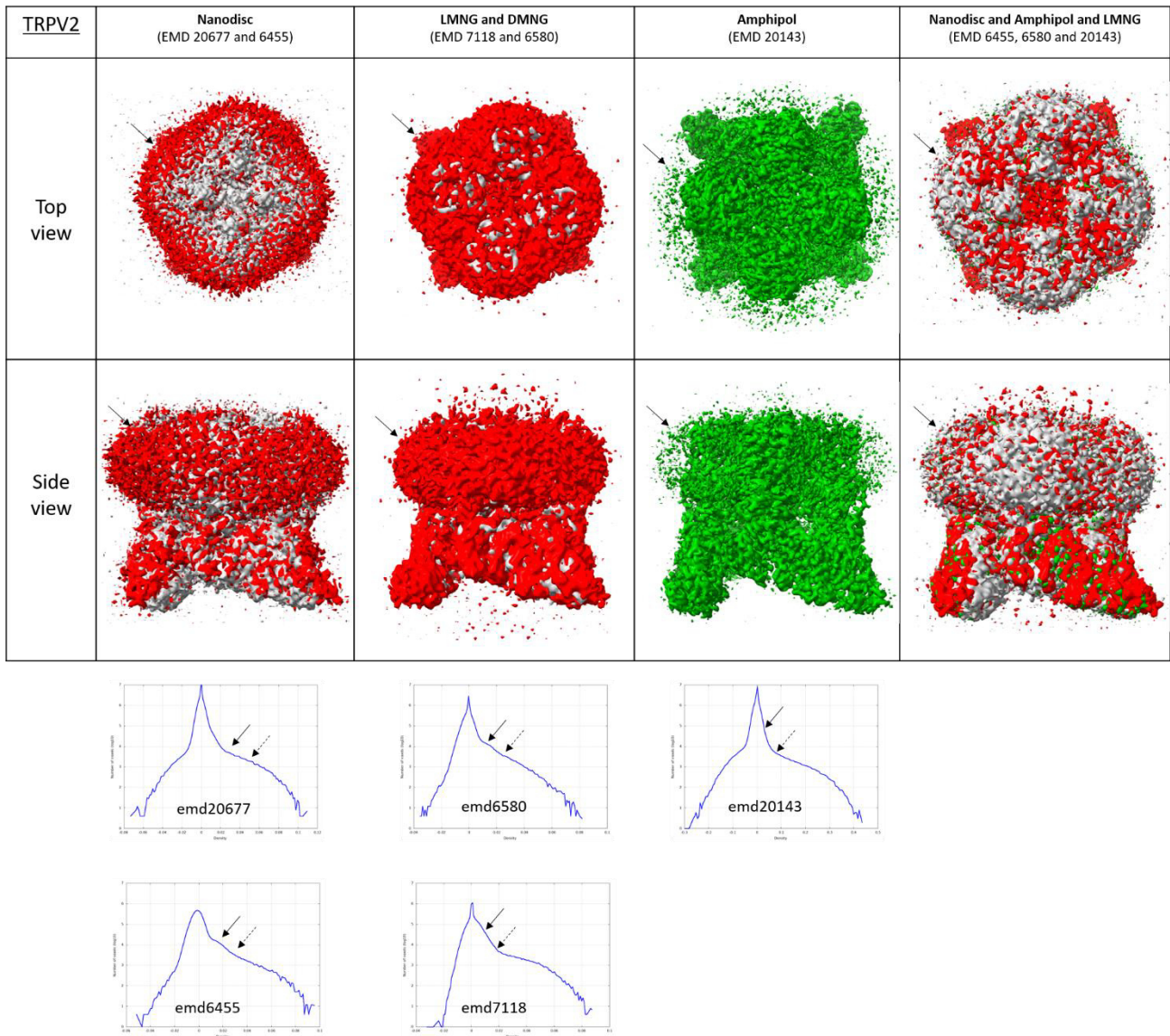
Supplementary figure



SFig 1. Method of measurement of the belt diameter

(1) The first step is to draw the lines at the edge of the belt. (2) Then, the density of the belt is reduced and measure the distance between the protein and the lines drawn in the first step.

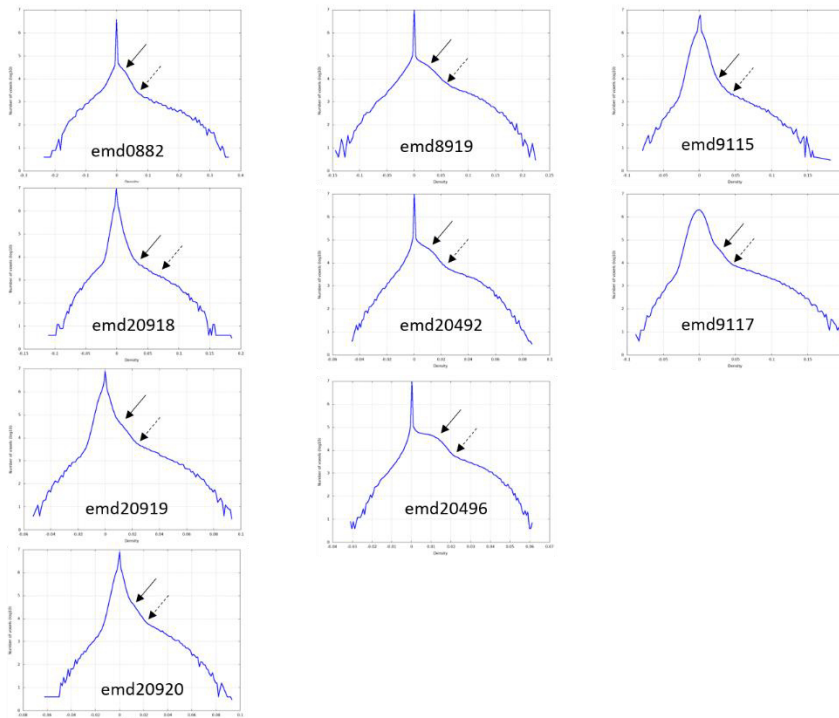
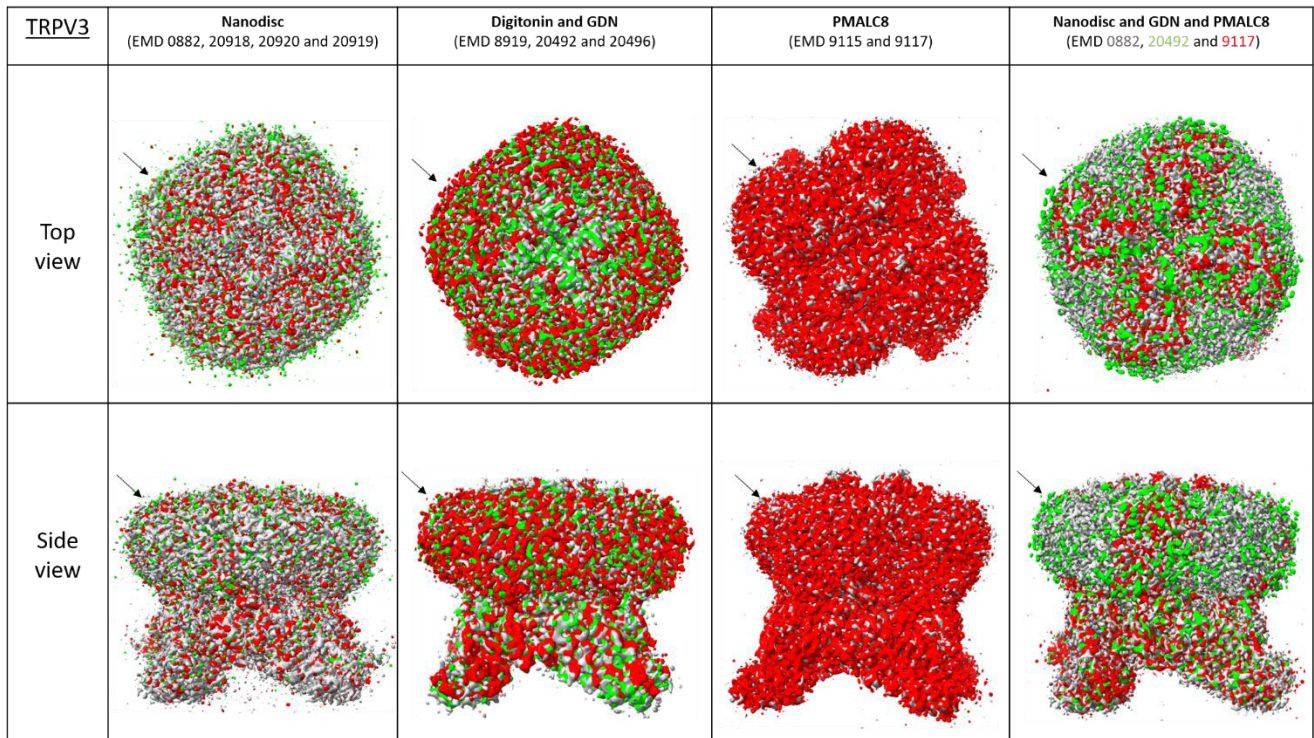
RESULTS: CHAPTER IV



SFig 2. TRPV2 density map superimpositions and the corresponding histograms

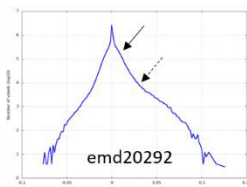
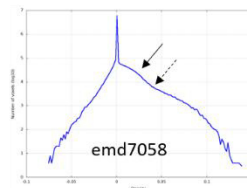
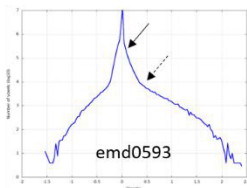
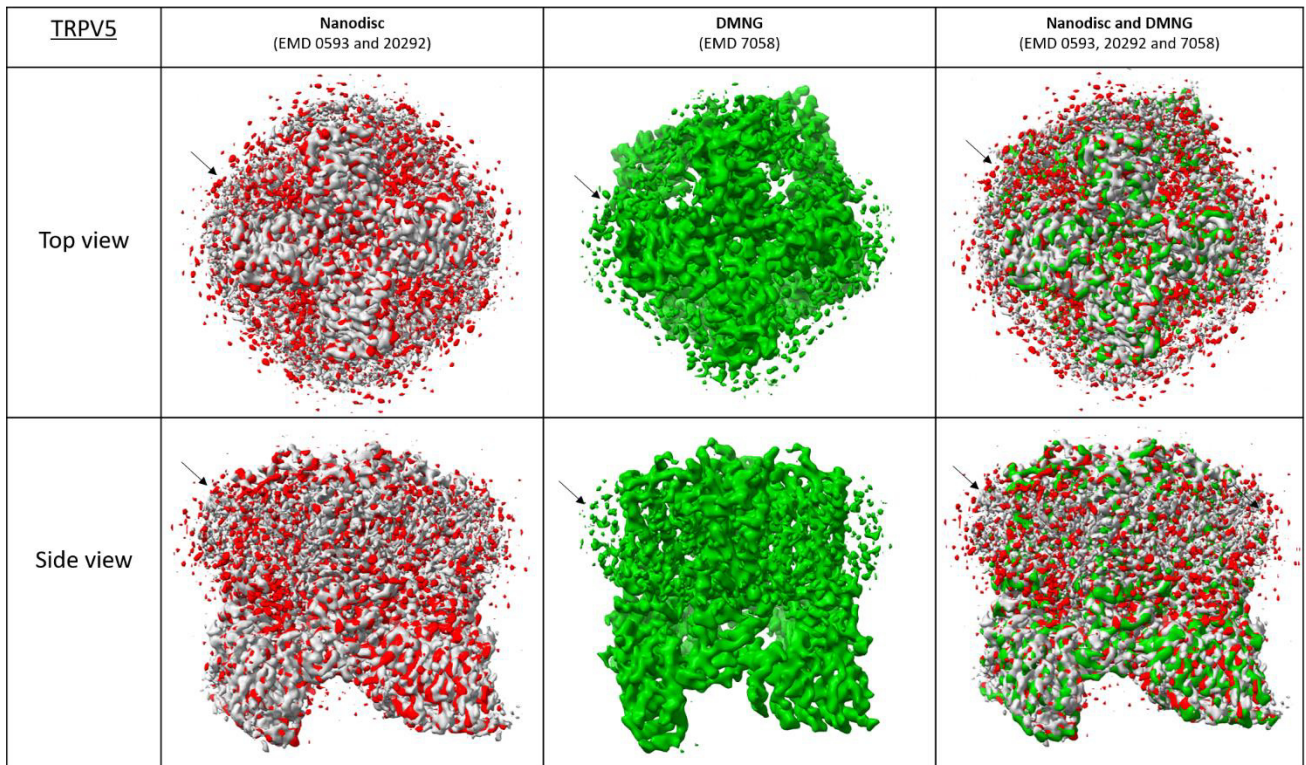


RESULTS: CHAPTER IV



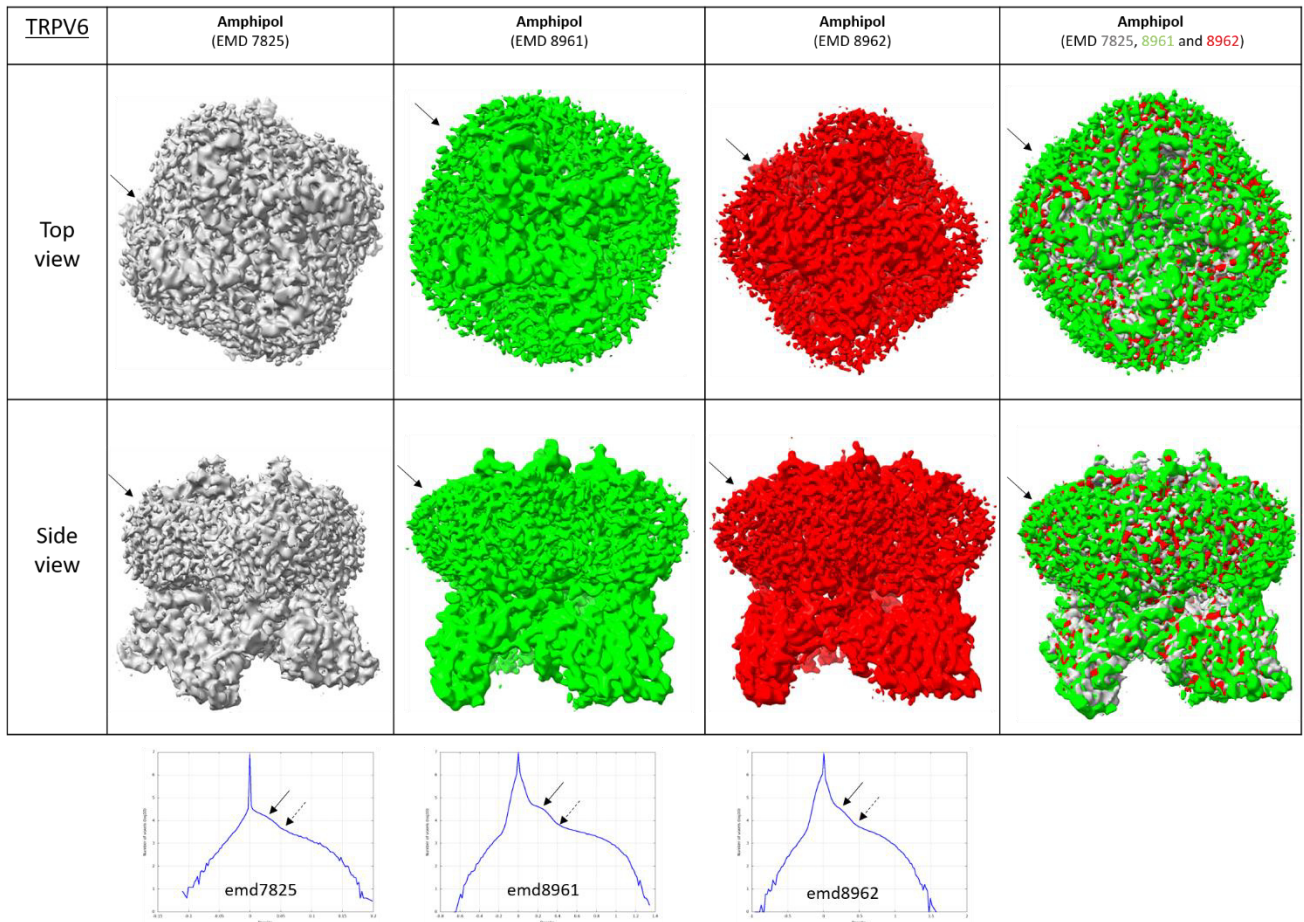
SFig 3. TRPV3 density map superimpositions and the corresponding histograms

RESULTS: CHAPTER IV



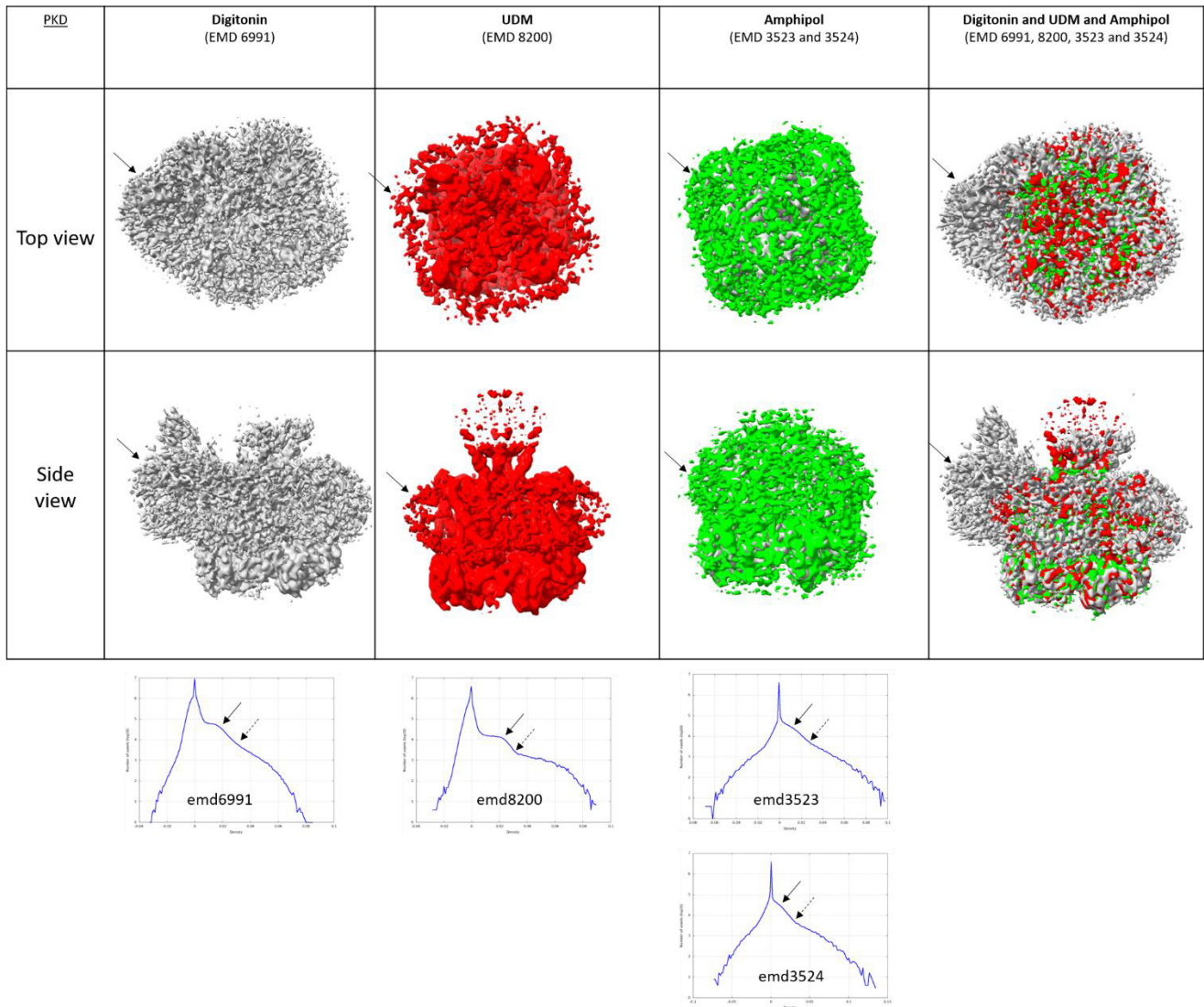
SFig 4. TRPV5 density map superimpositions and the corresponding histograms

RESULTS: CHAPTER IV



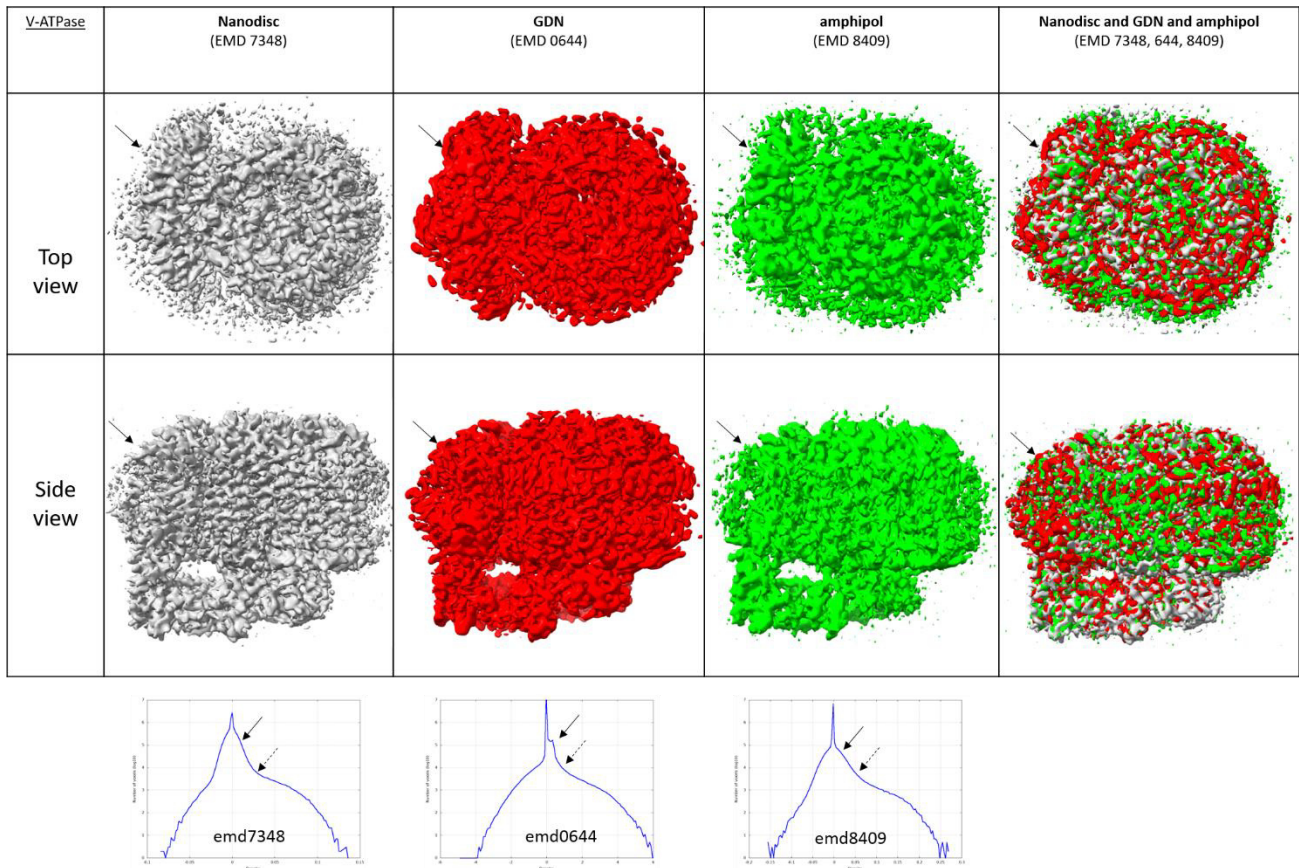
SFig 5. TRPV6 density map superimpositions and the corresponding histograms

RESULTS: CHAPTER IV



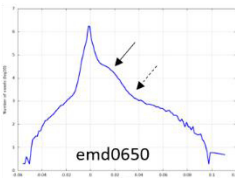
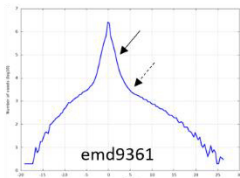
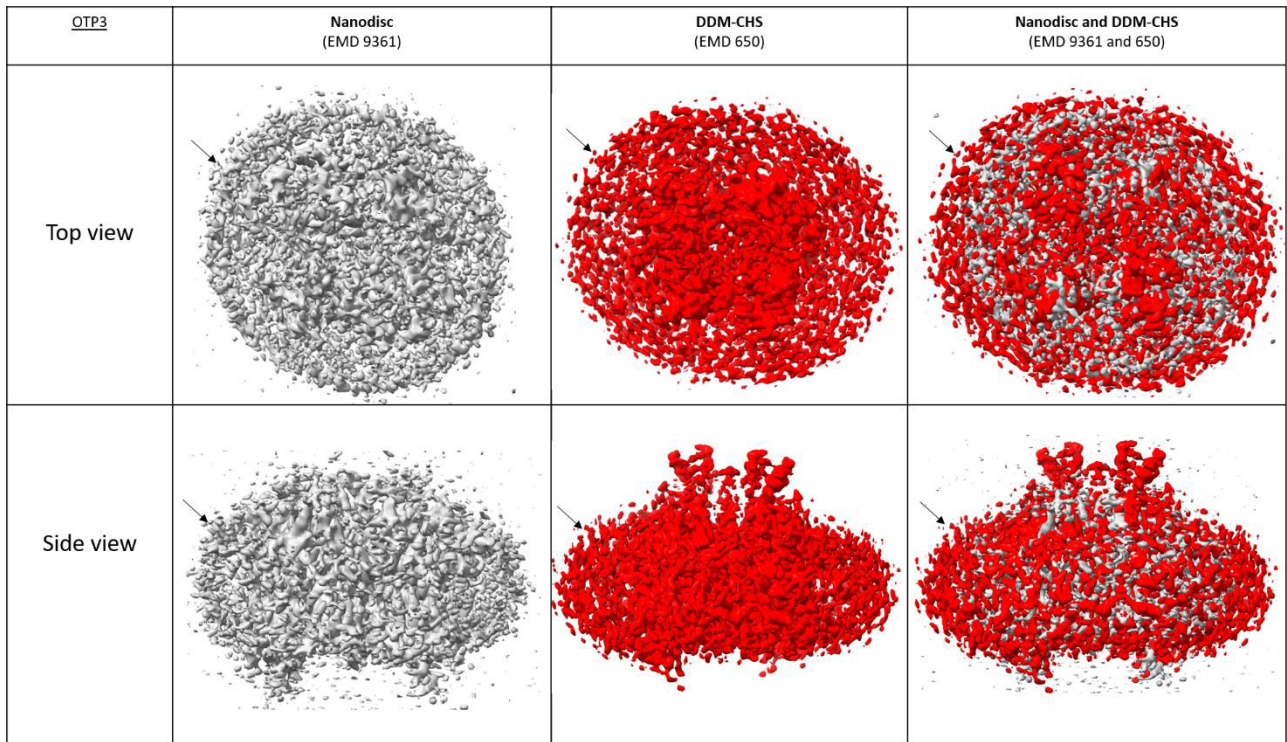
SFig 6. PDK density map superimpositions and the corresponding histograms

RESULTS: CHAPTER IV



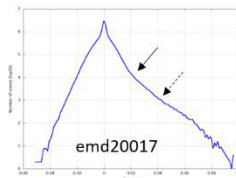
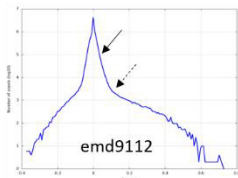
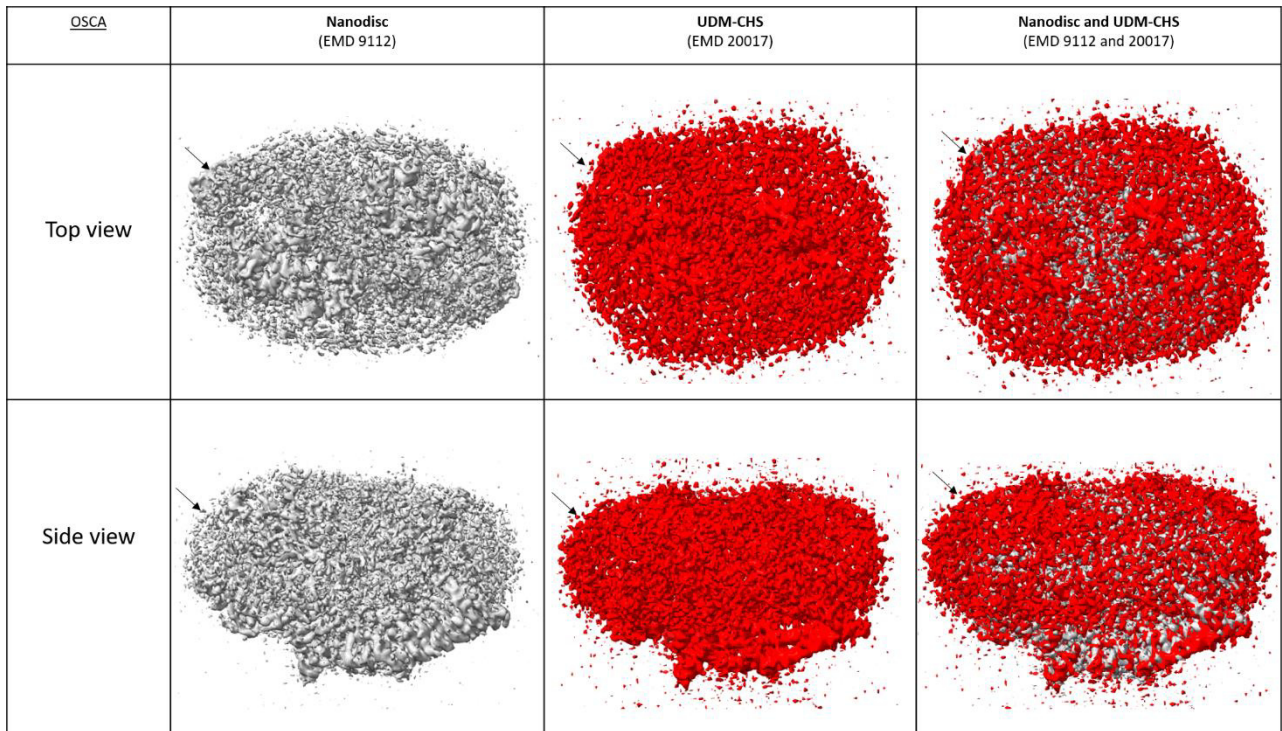
SFig 7. V-ATPase density map superimpositions and the corresponding histograms

RESULTS: CHAPTER IV



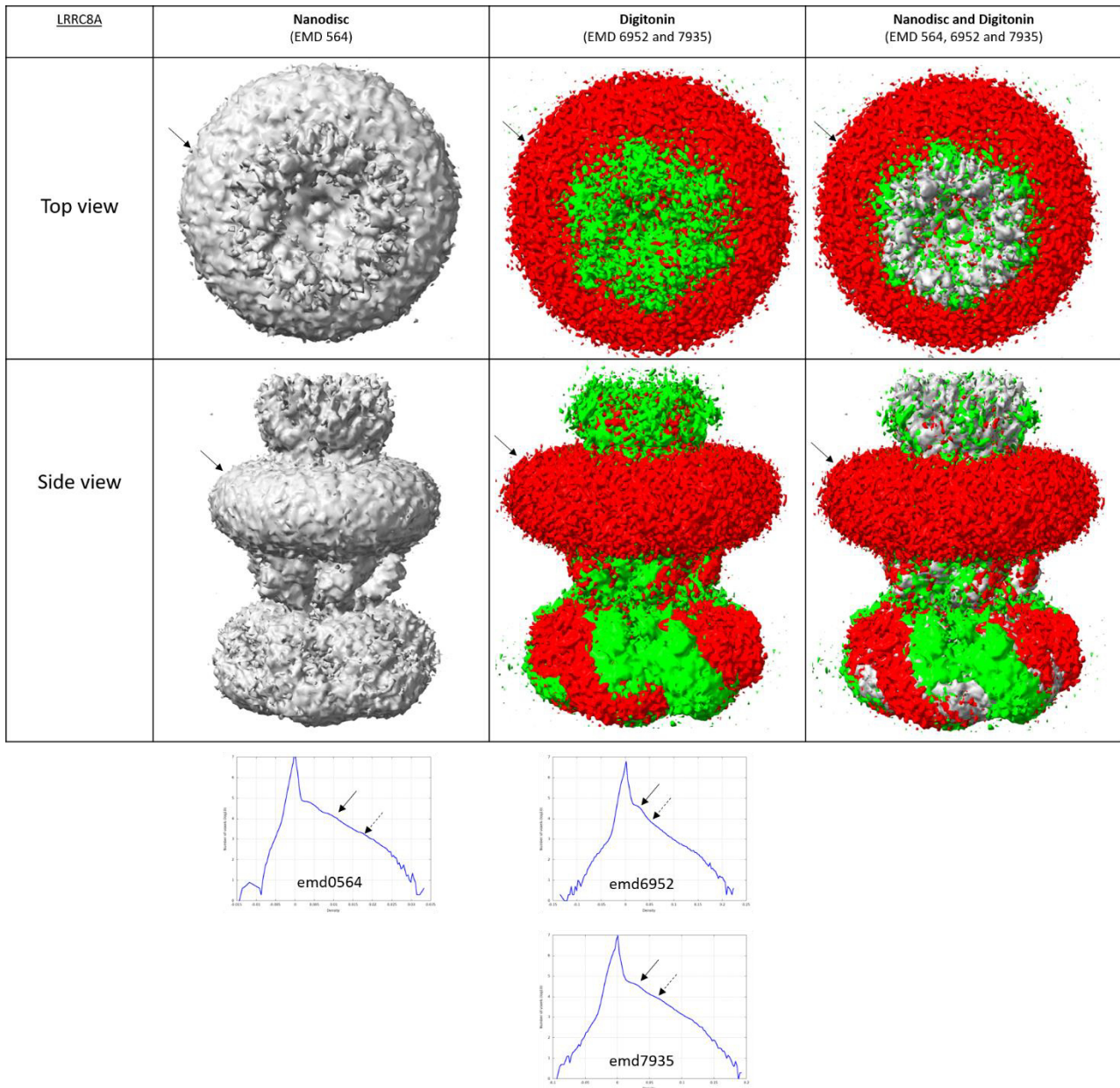
SFig 8. OTP3 density map superimpositions and the corresponding histograms

RESULTS: CHAPTER IV



SFig 9. OSCA density map superimpositions and the corresponding histograms

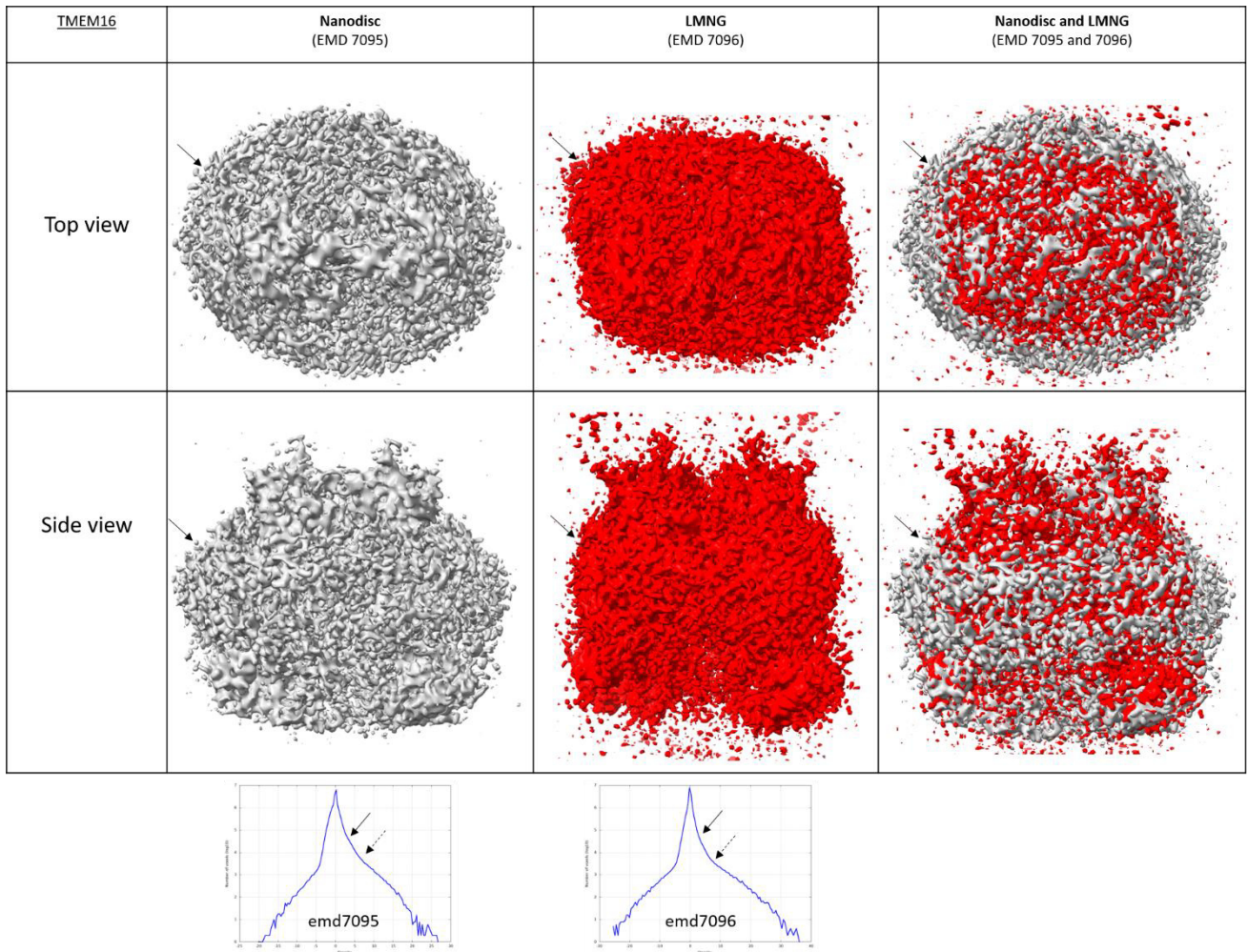
RESULTS: CHAPTER IV



SFig 10. LRRC8A desinty map superimpositions and the corresponding histograms

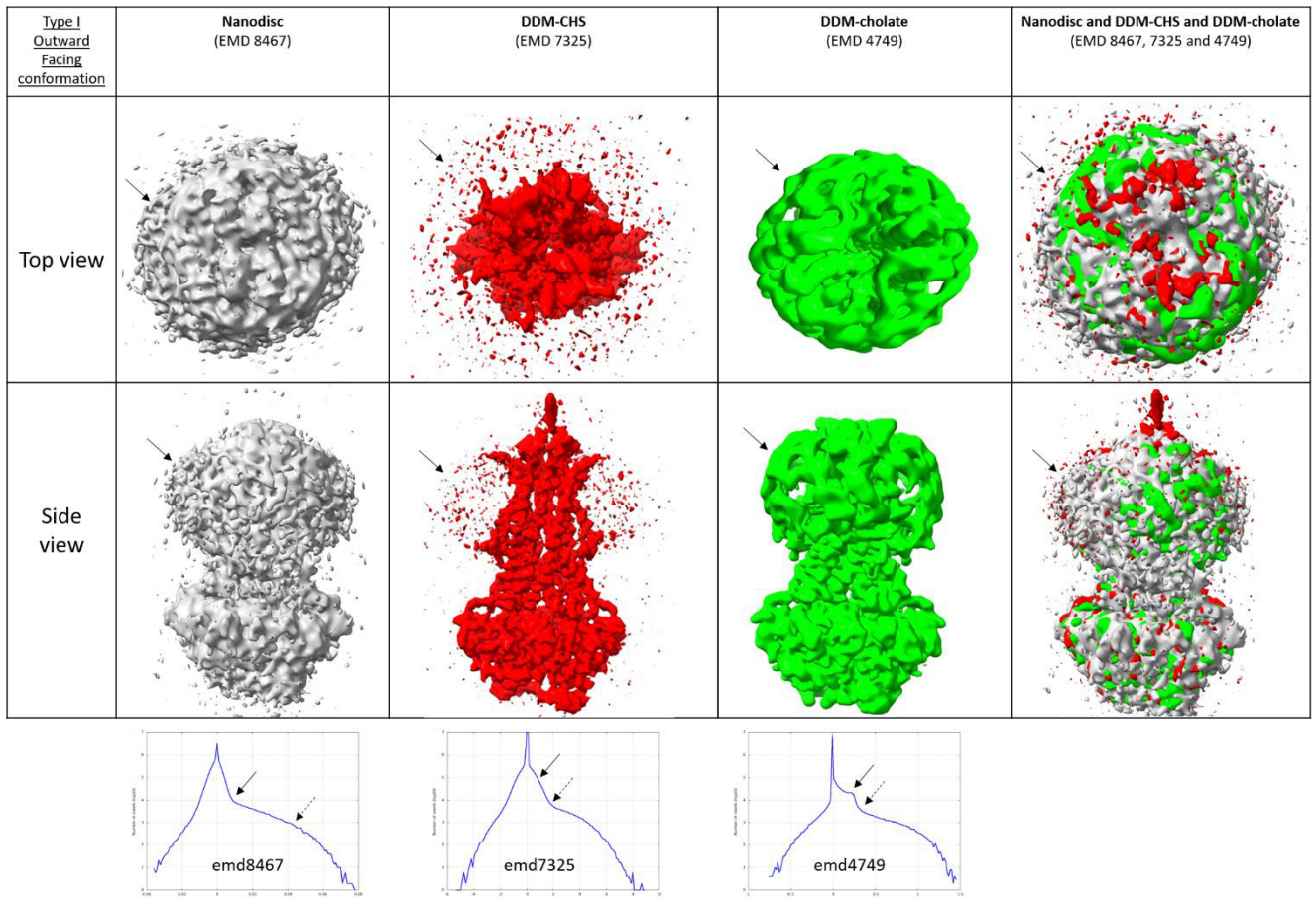


RESULTS: CHAPTER IV



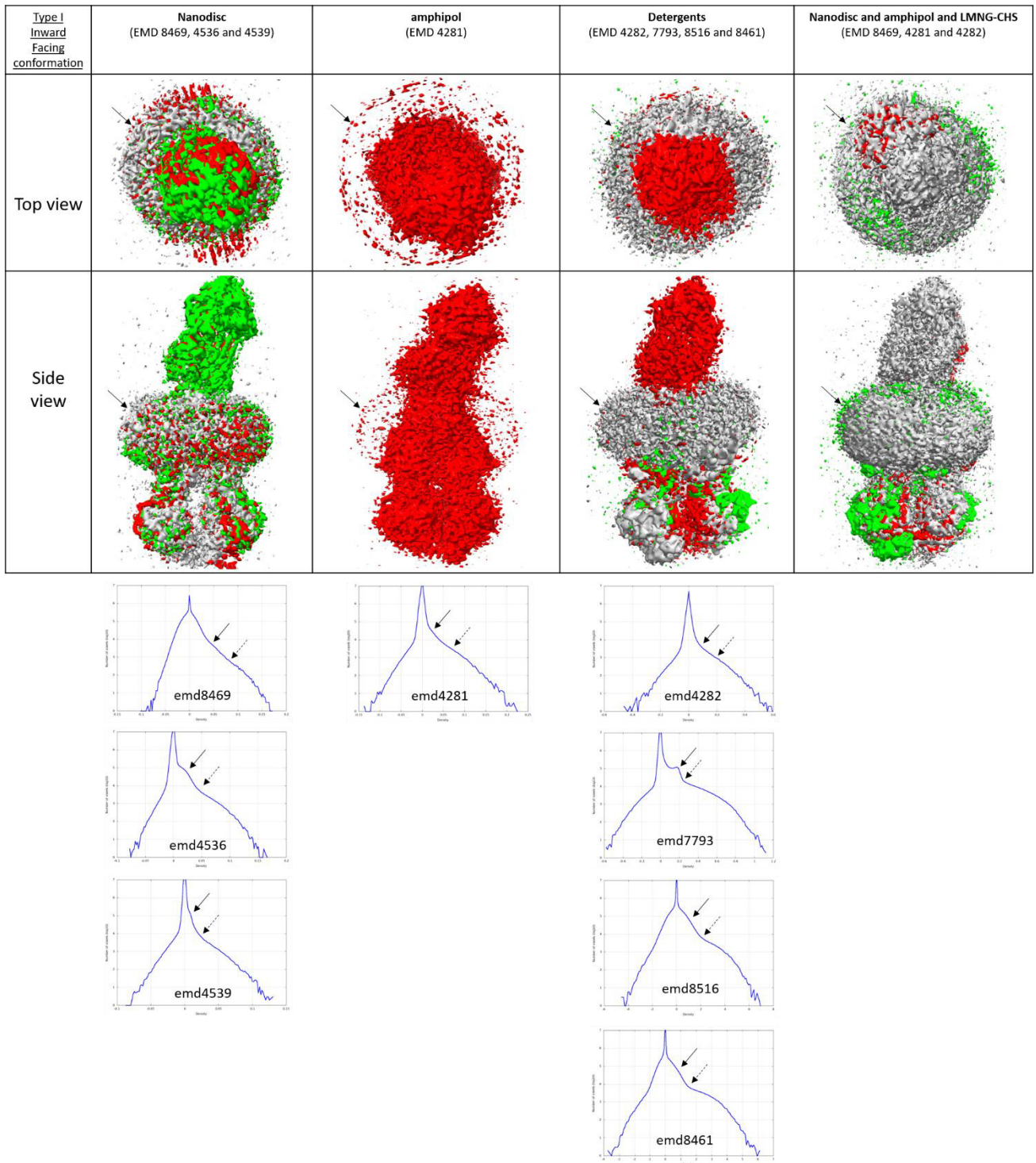
SFig 11. TMEM16 density map superimpositions and the corresponding histograms

RESULTS: CHAPTER IV



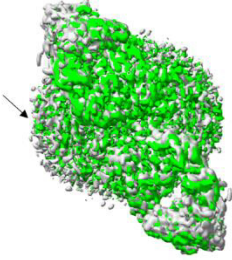

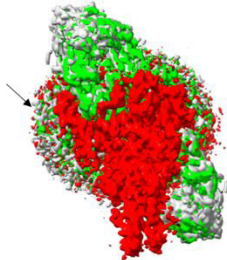
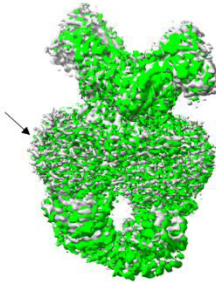
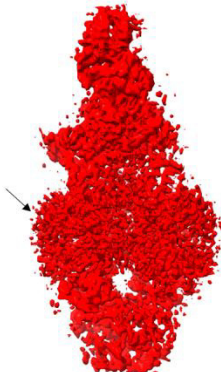
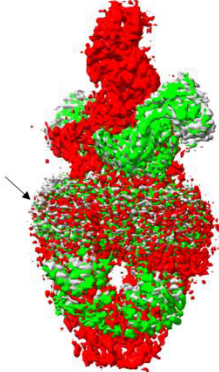
SFig 12. ABC type I (outward-facing conformation) density map superimpositions and the corresponding histograms

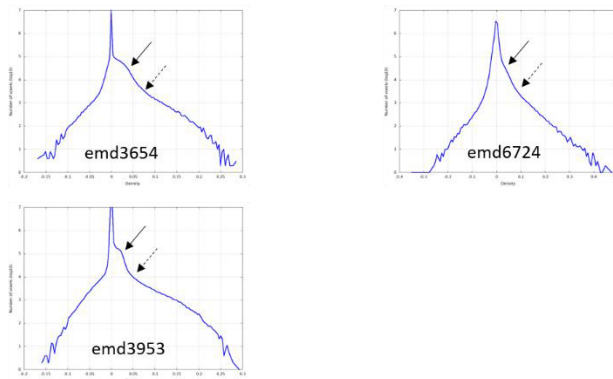
RESULTS: CHAPTER IV



SFig 13. ABC type I (inward-facing conformation) density map superimpositions and the corresponding histograms

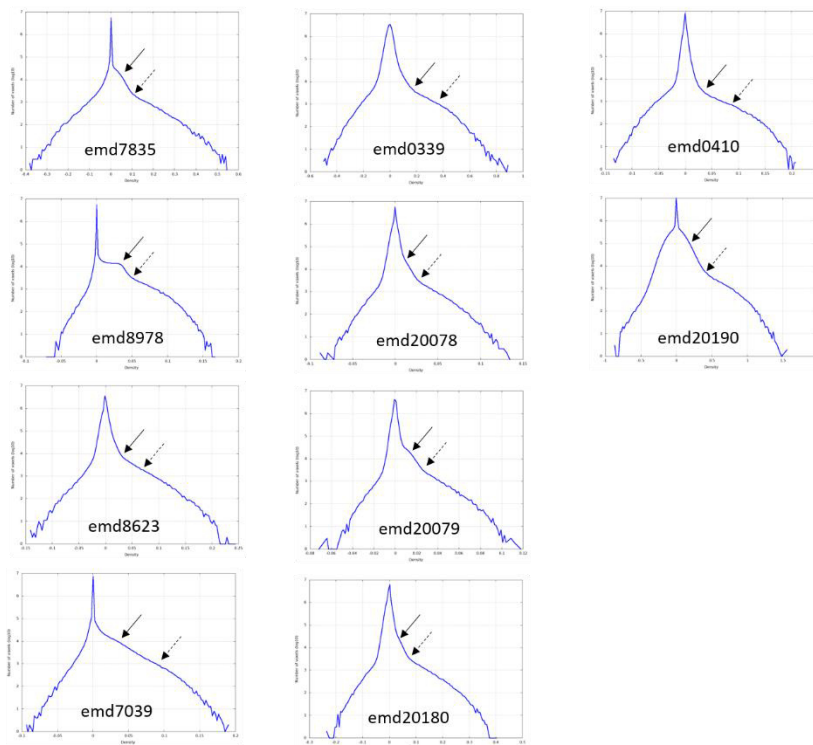
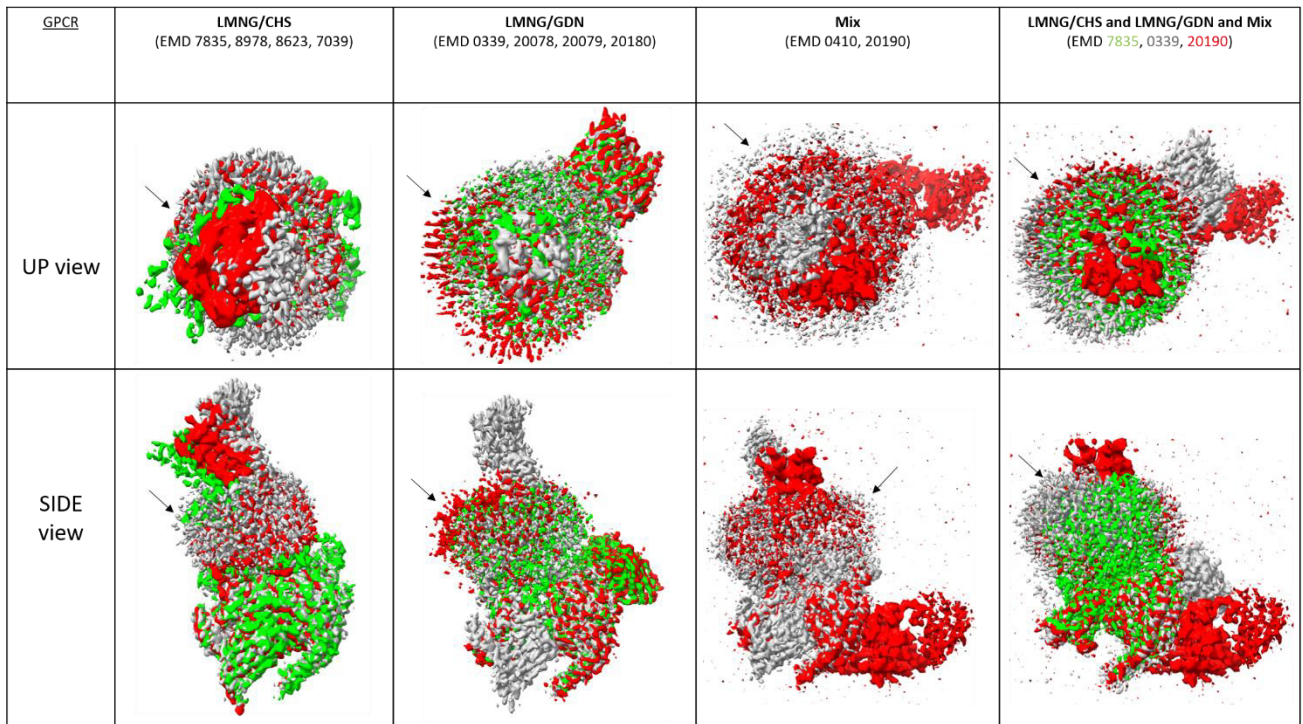
RESULTS: CHAPTER IV

<u>Type II</u>	Nanodisc (EMD 3654 and 3953)	Digitonin (EMD 6724)	Nanodisc and Digitonin (EMD 3654, 3953 and 6724)
Top view			
Side view			



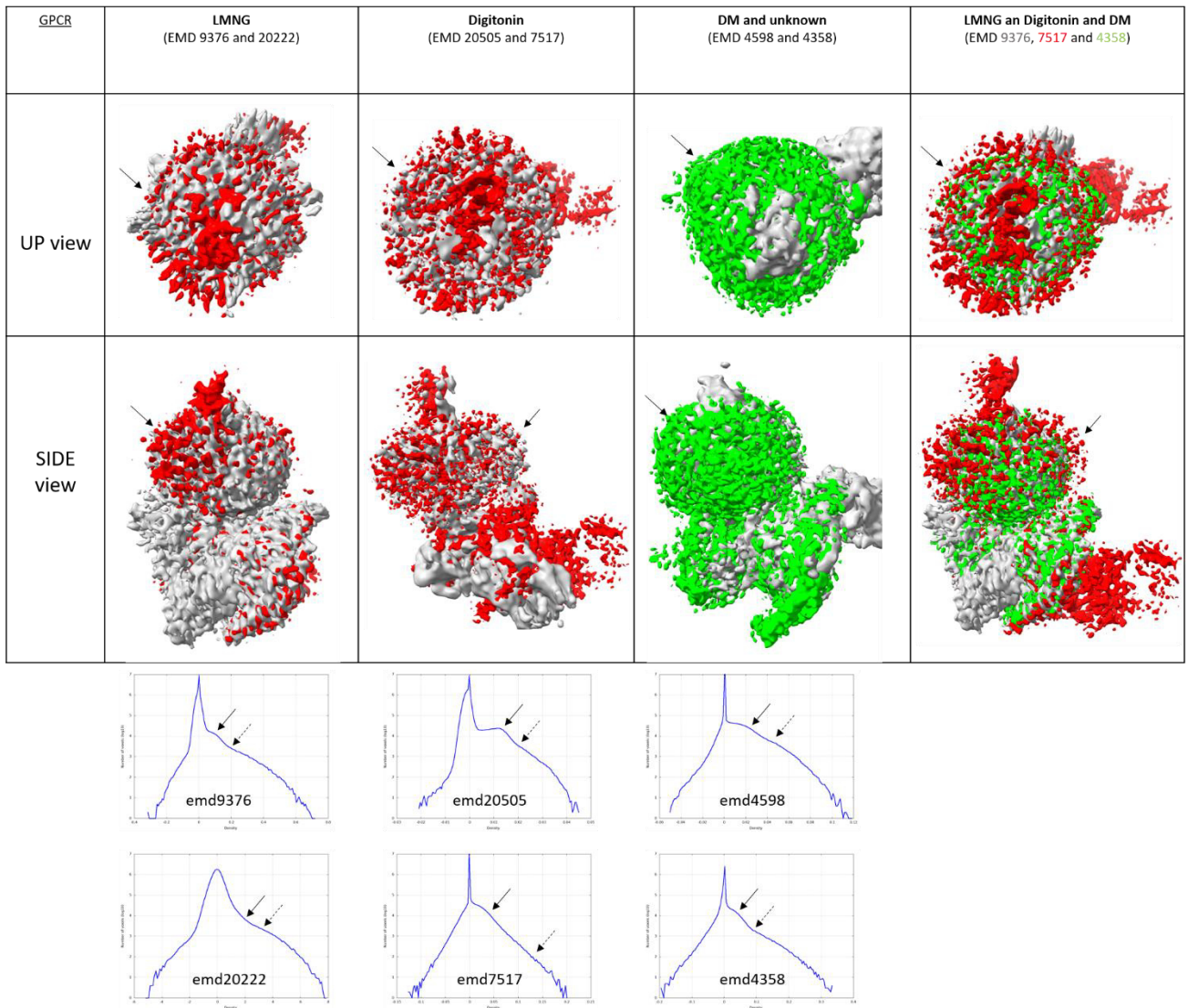
SFig 14. ABC type II density map superimpositions and the corresponding histograms

RESULTS: CHAPTER IV



SFig 15. GPCR (part 1) density map superimpositions and the corresponding histograms

RESULTS: CHAPTER IV



SFig 16. GPCR (part 2) density map superimpositions and the corresponding histograms

## Discussion and conclusion

The amphipathic belt around the protein is an essential information in the data treatment of membrane proteins. In Cryo-EM, it is even a more crucial parameter due to its implication in the particles' alignment. A common practice is to mask this belt in the data treatment to have a better resolution of the protein. The challenge is that it is a fluid and it can vary from one particle to the other. In the case of nanodisc, the protein is probably inserted in slightly different region of the membrane bilayer. The resulting density map is an average of all the belts of each particle. This leads to a loss of information. Our study points to the fact that all density maps show the same range of hydrophobic solvent belt's sizes, leading to the hypothesis that cryoEM yields the visualization of a common minimum for each belt. All this observation together helps to understand better the behavior of the belt in the density maps.





# GENERAL DISCUSSION AND CONCLUSION



Antimicrobial resistance is a major human health threat and bacteria plays an essential role to this phenomenon; for instance, the World Health Organization postulate a list of microorganisms to monitor and it contains several bacteria (“WHO Publishes List of Bacteria for Which New Antibiotics Are Urgently Needed”). The most alarming ones are *Acinetobacter baumannii*, *Pseudomonas aeruginosa* and *Enterobacteraceae* which are resistant to carbapenem. In this same list we can also find *Enterococcus faecium* resistant to vancomycin, *Salmonellae* resistant to fluoroquinolone, *Staphylococcus aureus* resistant to methicillin and vancomycin. Antibiotics have been developed to kill or inhibit bacteria. Their discovery was a real revolution for medicine which marks the end of the pre-antibiotic era. Nevertheless, their misuse lead to increasing development of resistance mechanism and the development of multi-drug resistance strains. The molecular mechanisms are: modification or overexpression of the target; impermeabilization of the membrane; inactivating enzymes and efflux pumps.

The study of membrane proteins is a complex field due to the amphipathic nature of these types of proteins. They need to be in constant presence of amphipathic molecules (detergents or lipidic bilayer) to be soluble and ensure the experiments’ feasibility. The choice of the detergent or reconstitution system (nanodisc) is crucial to assure the stability and the activity of the protein. For structural techniques, the hydrophobic solvent belt is a crucial parameter. In X-ray crystallography experiments, the belt plays an active role in the crystal formation since it can participate or prevent the protein:protein contacts. In Cryo-EM, this region participates to particle alignment since it is visible by this method. Their presence could help the data treatment but it can also perturb the correct alignment of the protein and reduce the resolution.

The common theme of my PhD project was the focus on the amphipathic belt wrapping the hydrophobic part of the protein. Indeed, “*Bacillus subtilis* multidrug resistance ATP” is used not only as model of ABC transporters but also membrane proteins. The main goal was to give insights on the multiple aspects and efforts needed in the study of this kind of proteins which are often therapeutic target or implicated in important biological processes. The results obtained show strategies to improve the membrane protein sample and also add information to the knowledge on the ABC transporters’ mechanism.

The structural study of BmrA started almost twenty years ago, the choice of the detergent for the extraction and purification of the protein was a major improvement allowing the

resolution of the structure. The strategy was to rationalize the behavior of the detergent belt to be able to optimize it. The quantification of detergent played a key role in this process. The development of the Det.Belt server helped in the visualization of the volume occupied by the detergent belt. On the other hand, the idea of using a steroid detergent was implemented by other studies although the new approach was to investigate the behavior of the mixture and to see the impact of the crysalllogenesis step. It is probably possible to apply the same approach to other protein that are difficult to crystallize.

The design of the DCOD detergent is also an attempt to rationally stabilize the membrane protein. The idea was to exploit the presence of basic residues placed near the hydrophobic part of the protein. These detergents proved effective to increase the stability of the protein in solution and also to improve the X-ray crystallography experiment. These molecules allowed the resolution encountered in the diffraction pattern of the BmrA crystal. It seems that this additive decreased the flexibility of the protein and this can be a solution for other protein like BmrA.

The nanodisc were also used to study BmrA. The idea was to verify the behavior of the protein in a more native-like environment. The molecular dynamic simulations of the protein inserted in the membrane showed an occluded conformation. The goal of the nanodisc reconstitution was to observe experimentally the conformation adopted by the protein in absence of the detergent. Nanodisc are frequently used for the structural study of membrane protein by Cryo-EM. We initiated some sample preparation, but it requires more optimization.

Finally, in crystallography experiments, the belt is not visible in the final data since it is too mobile to diffract. In Cryo-EM analysis however, the belt is present and can participate or prevent the correct particle alignment. The resulting belt in the density map is the result of the averaging of each particle. To optimize the data processing, the belt is often masked. The masks are done empirically without any rational approach. Our study aims to characterize the different kind of belts to assess their sizes. It resulted that there is no statistical difference amongst them, they all have a diameter between 19 and 39 Å. This indicate that an automatically produced mask could be developed for membrane protein data treatment. This whole project investigated further the behavior of the hydrophobic solvent belt and gave inputs on how to treat it in some steps on the structural studies of membrane proteins.

On ABC transporters mechanism, the main observations of this study brought new insights to understand their function. The first one is the resolution of the first ABC exporter type I in outward-facing conformation with a substrate bound. Beforehand, only two examples were present in the literature presenting the structure almost in this state. The structure of McjD from *E. coli* is solved with a detergent molecule bound in the cavity (nonyl beta-D-glucopyranoside) (Choudhury et al. 2014). Then the other example is MRP1 structure which is in presence within the substrate even though its density is not visible in the density map (Johnson and Chen 2017b). The second one is the hand-fan movement of the transmembrane region which allowed its identification in all the other ABC exporters type I structures in outward-facing conformation. This TM1-2 movement is then confirmed by the molecular dynamic simulation performed on BmrA structures. This observation indicates that it exemplifies the opening of the cavity necessary for the drug release. ABC exporters can frequently transport multiple drugs, that are different in size and shape. This flexibility and adaptability probably lay in this possible motion of TM1-2. Furthermore, the results of the simulation indicate that the protein in a membrane environment has the tendency to close. This is probably due to the large quantity of hydrophobic residues present in the cavity. All together these results show details of the mechanism of the protein. For instance, once the substrate is liberated thanks to the movement of TM1-2, the protein closes immediately driven by the hydrophobicity of the cavity. Then, the ATP hydrolysis occurs to allow the conformation change. In conclusion, this project was aiming to acquire more knowledge on the ABC transporter mechanism; thanks to the two structures, it was possible to elucidate a part of it, while other structures are necessary to uncover the whole process.



# RESUME FRANÇAIS





La résistance aux antimicrobiens est devenue un problème majeur pour la santé humaine qui a attiré l'attention de l'Organisation Mondiale de la Santé (OMS). Cette dernière a en effet mis en place des études visant à comprendre les perspectives d'évolutions de ce phénomène. Les estimations projettent qu'à partir de l'année 2050 10 millions d'individus décèderont à cause d'une infection résistante à tout traitement disponible (O' Neill 2014). Si cela s'avère vrai, ce phénomène sera la première cause de mortalité humaine surpassant ainsi le cancer et le diabète. Les antimicrobiens spécifiques des bactéries sont appelés antibiotiques. Les bactéries développent des mécanismes de résistances tels que la mutation ou surexpression de la cible, l'imperméabilisation de la membrane, l'inactivation de la molécule par une enzyme et l'efflux des antibiotiques par des protéines membranaires. Les transporteurs ABC (ATP-Binding Cassette) font partie de ces protéines. Ce mécanisme qui semble être adopté comme première ligne de défense par les bactéries fait que la concentration interne de la molécule diminue, ce qui donne le temps à la bactérie de mettre en place d'autres mécanismes de défense. Malgré leur importance biologique, le mécanisme de ces transporteurs reste peu compris en raison de leur flexibilité et polyspécificité. En effet, ces protéines lient et exportent des molécules qui varient en taille et forme, faisant que plusieurs exportateurs confèrent un phénotype MDR (Multi-Drug Resistance). Plusieurs structures de ces protéines ont récemment été résolues. Il manque cependant des représentations pour certaines conformations empêchant de caractériser le mécanisme complet.

Par ailleurs, le domaine de la biologie structurale des protéines membranaires est assez complexe en raison de leur nature amphiphile. Elles possèdent une partie hydrophobe exposée à l'extérieur qui permet à la protéine de s'insérer dans la membrane. Afin de pouvoir les étudier, des molécules amphiphiles sont nécessaires. On retrouve dans cette catégorie les détergents, les amphipols, les nanodisques et les polymères DIBMA et SMA. Leur présence étant nécessaire tout au long de la manipulation de ces protéines, cela peut être désavantageux pour certaines techniques comme la cristallographie. En effet, la couronne qui se forme autour de la partie hydrophobe de la protéine peut empêcher la formation de l'empilement cristallin.

Le transporteur ABC BmrA (*Bacillus subtilis* multidrug resistance ATP) est impliqué dans la résistance à l'antibiotique cervimycine C chez la bactérie gram (+) *Bacillus subtilis*. Étant donné que ce transporteur peut fixer plusieurs molécules, il présente aussi un phénotype MDR. Parmi

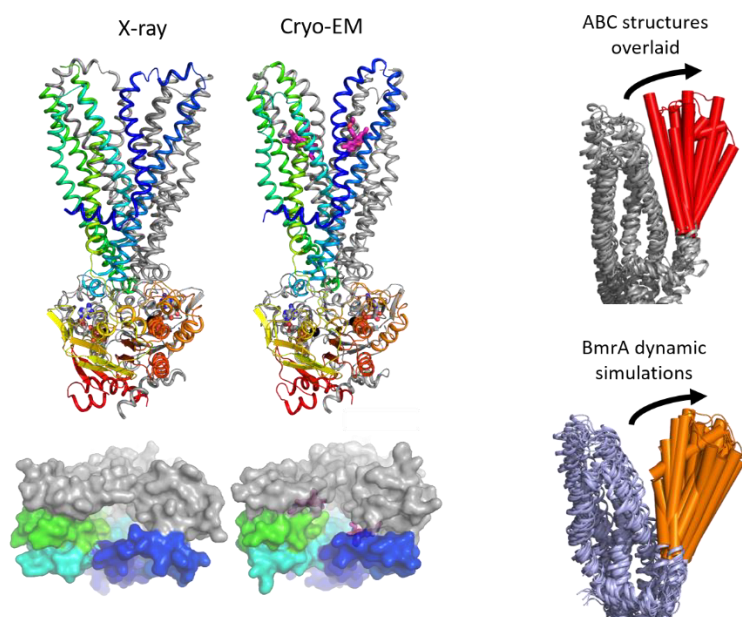
## RESUME FRANÇAIS

ces molécules on peut citer des agents utilisés dans le traitement contre le cancer (daunorubicine et doxorubicine), des inhibiteurs d'autres transporteurs ABC (GF 120918 X et LY 335979) et des colorants cellulaires (bromure d'éthidium et rhodamine 6G). Cette protéine est utilisée comme modèle pour étudier le mécanisme des transporteurs ABC ainsi que pour l'étude structurale des protéines membranaires. Le but de mon projet de thèse était d'en résoudre la structure. La première partie de ma thèse a porté sur la résolution des deux structures de BmrA et leur analyse. La deuxième partie porte sur les projets qui découlent des observations issues de l'étude structurale. Tout le long de ces projets, la couronne qui entoure la partie hydrophobe de la protéine a été caractérisée expérimentalement, modélisée et étudiée dans le contexte des analyses de données de Cryo-EM.

L'étude structurale de BmrA a débutée il y a plusieurs années. Les étapes d'expression et de purification ont été optimisées en amont de ma thèse (Thèse de Rima Matar). La dernière optimisation a été l'extraction de la protéine par le détergent Triton X100 et l'utilisation du mélange DDM et sodium cholate lors des étapes de purification (Thèse d'Arnaud Kilburg). Des études par DLS (Dynamic Light Scattering) du mélange DDM-cholate ont montré que la taille de la micelle diminue en augmentant la concentration de cholate.

Dans un premier temps, l'échantillon a été optimisé pour résoudre la structure par cristallographie. Trois mises au point principales ont été nécessaires : réduction de la taille de la couronne de détergent, utilisation des additifs DCOD pour améliorer le cliché de diffraction (Nguyen et al. 2018) et optimisation de la solution de cryo-protection. La structure a pu être déterminée en présence d'ATP car on a utilisé le mutant BmrA E504A qui peut fixer le nucléotide mais pas l'hydrolyser. Ce même échantillon a été étudié par Cryo-EM et dans ce cas la rhodamine 6G, substrat de BmrA, est aussi présente. On a ainsi déterminé la structure de BmrA en présence d'ATP et d'un substrat et il s'agit de la première de ce type pour les transporteurs ABC. Les deux structures sont dans la même conformation qui est appelée outward-facing dans laquelle la cavité de la protéine est exposée vers l'extérieur de la cellule et les nucléotides sont fixés au niveau de la partie soluble de la protéine (NBD) (figure 91). La seule différence se trouve dans la région transmembranaire (TMD) : la boucle entre les hélices transmembranaires 1 et 2 adopte une position différente. Ensuite, les deux structures sont comparées avec d'autres structures de transporteurs ABC dans cette conformation. Il en ressort alors que pour chaque transporteur les TM1-2 sont placés différemment (figure 91).

Quand on superpose ces structures on remarque que les hélices présentent un mouvement qui ressemble à celui d'un éventail. Cela a aussi été observé lors de simulation de dynamique moléculaire exécutées sur les deux structures (figure 91). La capacité de BmrA à exporter différents types de molécules est probablement expliqué par la flexibilité de cette région. De plus, les simulations ont montré qu'une fois insérée dans une membrane, les régions TM1-2 se ferment aussitôt. Cela permet d'élucider une partie du mécanisme de ces protéines : le relargage du substrat est possible grâce au mouvement du TM1-2 qui se ferme dès que le substrat n'est plus présent.

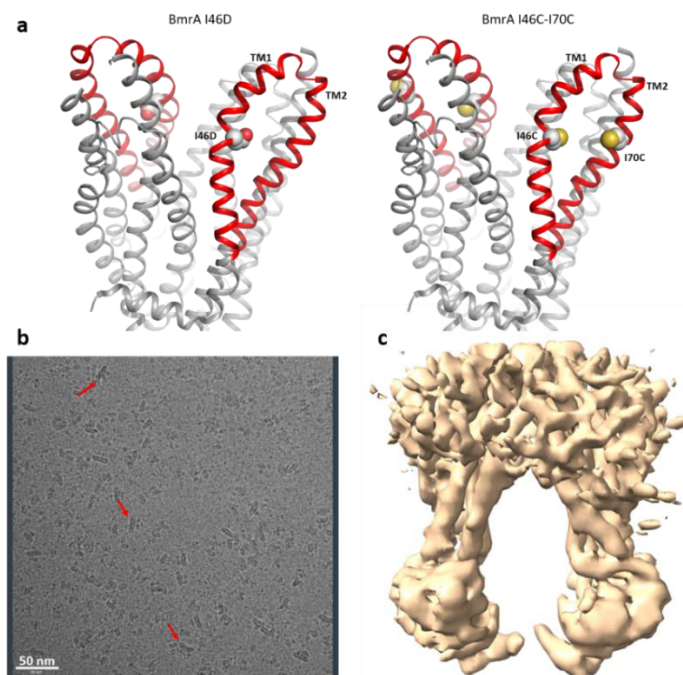


**Figure 91. Résultats de l'étude structurale de BmrA**

A gauche, les structures obtenues pour BmrA sont présentées avec une vue de côté et la vue de dessus correspondante. En haut à droite il y a la superposition des structures de BmrA et des transporteurs ABC et en dessous, il y a les résultats des simulations de dynamique moléculaire. Les flèches noires indiquent le mouvement observé pour les TM1-2 (rouge ou orange).

Ces résultats ont engendré d'autres perspectives d'études : des mutations au niveau des régions TM1-2 afin de caractériser biochimiquement ce mouvement, l'étude structurale de la protéine insérée dans une bicouche lipidique et enfin déterminer la structure de la protéine dans une autre conformation. Ces trois projets constituent des perspectives intéressantes pour l'étude de BmrA. Les deux mutants sont BmrA I46D et BmrA I46C-I70C (figure 92a). Le 1<sup>er</sup> a pour but de rendre la boucle plus flexible. En effet, le résidu aspartate est suivi d'une proline et par hydrolyse acide la liaison peptidique DP peut être rompue. Le double mutant permettrait, au contraire, de rendre la boucle plus rigide par création d'un pont disulfure. Les résultats sont encore à un stade préliminaire. A ce jour, la seule différence notable entre BmrA WT et les mutants réside dans l'activité ATPasique et de transport. Ensuite, afin d'étudier la structure de la protéine dans un contexte plus réaliste, BmrA a été insérée dans une bicouche

lipidique entourée par une MSP (Membrane Scaffold Protein). Cette construction est appelée nanodisques. Deux MSP de taille différente ont été testé : MSP1E3D1 et MSP1D1. Des mises au points sont encore nécessaire pour rendre l'échantillon homogène afin d'obtenir des données de Cryo-EM exploitables (figure 92b). Enfin, les transporteurs ABC peuvent adopter une conformation appelée inward-facing dans laquelle la cavité est exposée vers l'intérieur et les NBDs sont non liés aux nucléotides. Des données de Cryo-EM ont été collectées pour résoudre cette structure mais la protéine étant trop flexible dans cette conformation, il reste pour l'instant compliqué de l'obtenir à haute résolution (figure 92c).

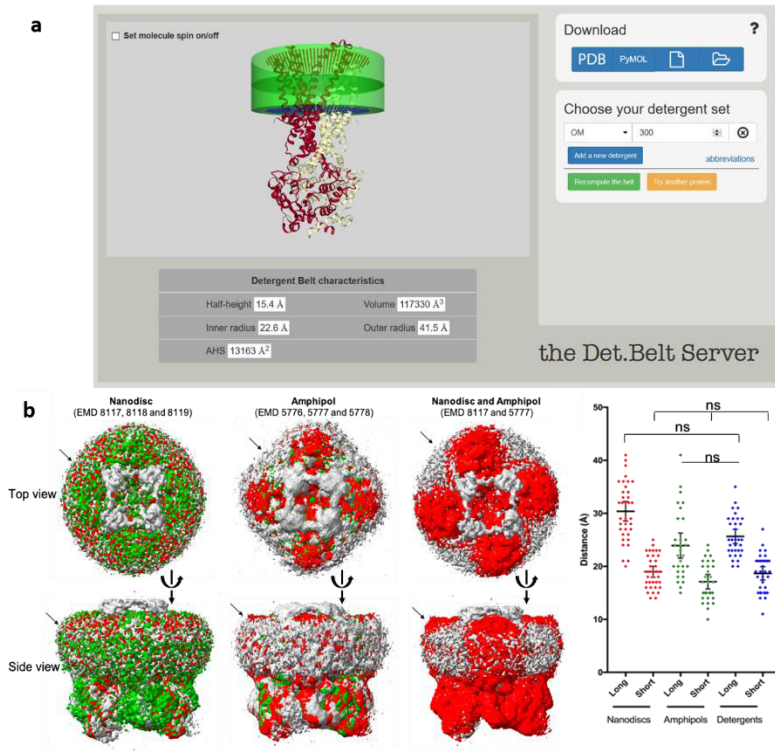


**Figure 92. Perspectives étude de BmrA**

(a) La région transmembranaire est présentée pour les deux mutants BmrA I46D et BmrA I46C-170C. Les TM1-2 sont en rouge et les mutations sont présentées en sphères. (b) BmrA est reconstituée en nanodisques en utilisant MSP1E3D1. Celui-ci est une image d'une analyse d'échantillon par Cryo-EM. Les flèches indiquent des particules pouvant correspondre à BmrA. (c) C'est la carte de densité de BmrA en conformation inward-facing.

Pour conclure, la couronne autour de la partie hydrophobe de la protéine a toujours été prise en considération et étudiée tout au long de cette thèse. L'équipe avait déjà développé une méthode afin de quantifier les détergents liés à la protéine. Cette information permet d'estimer le volume occupé par ces molécules et ainsi, de modéliser la couronne sous forme de cylindre creux. Afin de rendre cela accessible à tous, en collaboration avec l'équipe de Luca Monticelli, le server Det.Belt a été développé (figure 93a). Ce dernier permet de représenter la couronne de détergent autour de la protéine membranaire d'intérêt. Ensuite, on a effectué une étude sur la couronne de détergent issus de données structurales de Cryo-EM. Dans ce contexte, la couronne est visible et participe à l'étape critique de l'alignement des particules. La comparaison de cartes de densités de plus de 100 structures de protéines membranaires

montrent qu'il n'y a pas de différence significative au niveau de la taille de la couronne (figure 93b). Cela suggère que des masques pour ces régions peuvent être développés automatiquement pour enlever sa contribution dans le traitement des données.



**Figure 93. Etude de la couronne autour des protéines membranaires**

(a) Image de l'interface du server Det.Belt. La couronne est représentée par le cylindre creux vert. (b) cette image présente l'étude effectuée sur la couronne dans l'analyse des données de Cryo-EM. A gauche, il y a les cartes de densité superposées pour les différents types de couronne pour la protéine membranaire (TRPV1). A droite, l'étude statistique de la taille de la couronne.



# REFERENCES

- Alam, Amer, Julia Kowal, Eugenia Broude, Igor Roninson, and Kaspar P Locher. 2019. "Structural Insight into Substrate and Inhibitor Discrimination by Human P-Glycoprotein" 756 (February): 753–56.
- Alam, Amer, Raphael Küng, Julia Kowal, Robert A. McLeod, Nina Tremp, Eugenia V. Broude, Igor B. Roninson, Henning Stahlberg, and Kaspar P. Locher. 2018. "Structure of a Zosuquidar and UIC2-Bound Human-Mouse Chimeric ABCB1." *Proceedings of the National Academy of Sciences of the United States of America* 115 (9): E1973–82. <https://doi.org/10.1073/pnas.1717044115>.
- Alan E. Senior, Marwan K. Al-Shawi, and Ina L. Urbatsch. 1995. "The Catalytic Cycle of P-Glycoprotein." *FEBS Letters* 377 (3): 285–89. [https://doi.org/10.1016/0014-5793\(95\)01345-8](https://doi.org/10.1016/0014-5793(95)01345-8).
- Alexander Fleming. 1945. "Penicillin." 1945. <https://www.nobelprize.org/uploads/2018/06/fleming-lecture.pdf>.
- Allen, Heather K., Justin Donato, Helena Huimi Wang, Karen A. Cloud-Hansen, Julian Davies, and Jo Handelsman. 2010. "Call of the Wild: Antibiotic Resistance Genes in Natural Environments." *Nature Reviews Microbiology* 8 (4): 251–59. <https://doi.org/10.1038/nrmicro2312>.
- Aller, Stephen G, Jodie Yu, Andrew Ward, Yue Weng, Srinivas Chittaboina, Patina M Harrell, Yenphuong T Trinh, Qinghai Zhang, Ina L Urbatsch, and Geoffrey Chang. 2009. "Structures of P-Glycoproteins Reveals a Molecular Basis for Poly-Specific Drug Binding." *Science* 323 (5922): 1718–22. <https://doi.org/10.1126/science.1168750>.Structure.
- "Antibiotic Resistance." 2018. World Health Organization. 2018. <https://www.who.int/news-room/fact-sheets/detail/antibiotic-resistance>.
- Ashok, Y., R. Nanekar, and V.-P. Jaakola. 2015. "Defining Thermostability of Membrane Proteins by Western Blotting." *Protein Engineering, Design and Selection* 28 (12): 539–42. <https://doi.org/10.1093/protein/gzv049>.
- Asokan, Govindaraj V., Tufoof Ramadhan, Eman Ahmed, and Hala Sanad. 2019. "WHO Global Priority Pathogens List: A Bibliometric Analysis of Medline-PubMed for Knowledge Mobilization to Infection Prevention and Control Practices in Bahrain." *Oman Medical Journal* 34 (3): 184–93. <https://doi.org/10.5001/omj.2019.37>.
- Bay, Denice C., and Raymond J. Turner. 2009. "Diversity and Evolution of the Small Multidrug Resistance Protein Family." *BMC Evolutionary Biology* 9 (1): 140. <https://doi.org/10.1186/1471-2148-9-140>.
- Bayburt, Timothy H., and Stephen G. Sligar. 2003. "Self-Assembly of Single Integral Membrane Proteins into Soluble Nanoscale Phospholipid Bilayers." *Protein Science: A Publication of the Protein Society* 12 (11): 2476–81. <https://doi.org/10.1110/ps.03267503>.
- Borges-Walmsley, M. Ines, Kenneth S. McKeegan, and Adrian R. Walmsley. 2003. "Structure and Function of Efflux Pumps That Confer Resistance to Drugs." *The Biochemical Journal* 376 (Pt 2): 313–38. <https://doi.org/10.1042/BJ20020957>.
- Bountra, Kiran, Gregor Hagelueken, Hassanul G Choudhury, Valentina Corradi, Kamel El Omari, Armin Wagner, Indran Mathavan, et al. 2017. "Structural Basis for Antibacterial Peptide Self-immunity by the Bacterial ABC Transporter McjD." *The EMBO Journal* 36 (20): 3062–79. <https://doi.org/10.15252/embj.201797278>.
- Broecker, Jana, Bryan T. Eger, and Oliver P. Ernst. 2017. "Crystallogenesis of Membrane Proteins Mediated by Polymer-Bounded Lipid Nanodiscs." *Structure* 25 (2): 384–92. <https://doi.org/10.1016/j.str.2016.12.004>.
- Brüggeller, Peter, and Erwin Mayer. 1980. "Complete Vitrification in Pure Liquid Water and Dilute Aqueous Solutions." *Nature* 288 (5791): 569–71. <https://doi.org/10.1038/288569a0>.
- Bugg, T. D., and C. T. Walsh. 1992. "Intracellular Steps of Bacterial Cell Wall Peptidoglycan Biosynthesis: Enzymology, Antibiotics, and Antibiotic Resistance." *Natural Product Reports* 9 (3): 199–215. <https://doi.org/10.1039/np9920900199>.



- Caffrey, Martin. 2015. "A Comprehensive Review of the Lipid Cubic Phase or in Meso Method for Crystallizing Membrane and Soluble Proteins and Complexes." *Acta Crystallographica. Section F, Structural Biology Communications* 71 (Pt 1): 3–18. <https://doi.org/10.1107/S2053230X14026843>.
- Carignan, Alex, and Louis-charles Fortier. 2018. "La Keyicine Quand Deux Têtes Valent Mieux" 34: 377–79.
- Carter, Eric L., Lindsey Jager, Lars Gardner, Christel C. Hall, Stacey Willis, and Jacalyn M. Green. 2007. "Escherichia Coli Abg Genes Enable Uptake and Cleavage of the Folate Catabolite P-Aminobenzoyl-Glutamate." *Journal of Bacteriology* 189 (9): 3329–34. <https://doi.org/10.1128/JB.01940-06>.
- Chaired by Jim O'Neill. 2014. "Antimicrobial Resistance : T Ackling a Crisis for the Health and Wealth of Nations," no. December: 20.
- Chami, Mohamed, Emmanuelle Steinfelds, Cédric Orelle, Jean-Michel Jault, Attilio Di Pietro, Jean-Louis Rigaud, and Sergio Marco. 2002. "Three-Dimensional Structure by Cryo-Electron Microscopy of YvcC, an Homodimeric ATP-Binding Cassette Transporter from Bacillus Subtilis11 Edited by W. Baumeister." *Journal of Molecular Biology* 315 (5): 1075–85. <https://doi.org/10.1006/jmbi.2001.5309>.
- Chaptal, Vincent, Frédéric Delolme, Arnaud Kilburg, Sandrine Magnard, Cédric Montigny, Martin Picard, Charlène Prier, et al. 2017. "Quantification of Detergents Complexed with Membrane Proteins." *Scientific Reports* 7: 41751. <https://doi.org/10.1038/srep41751>.
- Chaptal, Vincent, Arnaud Kilburg, David Flot, Benjamin Wiseman, Nushin Aghajari, Jean-Michel Jault, and Pierre Falson. 2016. "Two Different Centered Monoclinic Crystals of the E. Coli Outer-Membrane Protein OmpF Originate from the Same Building Block." *Biochimica et Biophysica Acta (BBA) - Biomembranes* 1858 (2): 326–32. <https://doi.org/10.1016/j.bbamem.2015.11.021>.
- Chen, Jue, Gang Lu, Jeffrey Lin, Amy L Davidson, and Florante A Quiocho. 2003. "A Tweezers-like Motion of the ATP-Binding Cassette Dimer in an ABC Transport Cycle." *Molecular Cell* 12 (3): 651–61. <https://doi.org/10.1016/j.molcel.2003.08.004>.
- Cheng, Yifan. 2018. "Single-Particle Cryo-EM-How Did It Get Here and Where Will It Go." *Science* 361 (6405): 876–80. <https://doi.org/10.1126/science.aat4346>.
- Chitsaz, Mohsen, and Melissa H. Brown. 2017a. "The Role Played by Drug Efflux Pumps in Bacterial Multidrug Resistance." *Essays in Biochemistry* 61 (1): 127–39. <https://doi.org/10.1042/EBC20160064>.
- Choudhury, Hassanul G., Zhen Tong, Indran Mathavan, Yanyan Li, So Iwata, Séverine Zirah, Sylvie Rebuffat, Hendrik W. van Veen, and Konstantinos Beis. 2014. "Structure of an Antibacterial Peptide ATP-Binding Cassette Transporter in a Novel Outward Occluded State." *Proceedings of the National Academy of Sciences of the United States of America* 111 (25): 9145–50. <https://doi.org/10.1073/pnas.1320506111>.
- Chufan, Eduardo E., Khyati Kapoor, Hong-May Sim, Satyakam Singh, Tanaji T. Talele, Stewart R. Durell, and Suresh V. Ambudkar. 2013. "Multiple Transport-Active Binding Sites Are Available for a Single Substrate on Human P-Glycoprotein (ABCB1)." *PloS One* 8 (12): e82463. <https://doi.org/10.1371/journal.pone.0082463>.
- Cole, S. P., G. Bhardwaj, J. H. Gerlach, J. E. Mackie, C. E. Grant, K. C. Almquist, A. J. Stewart, E. U. Kurz, A. M. Duncan, and R. G. Deeley. 1992. "Overexpression of a Transporter Gene in a Multidrug-Resistant Human Lung Cancer Cell Line." *Science (New York, N.Y.)* 258 (5088): 1650–54. <https://doi.org/10.1126/science.1360704>.
- Costerton, J. W., Z. Lewandowski, D. E. Caldwell, D. R. Korber, and H. M. Lappin-Scott. 1995. "Microbial Biofilms." *Annual Review of Microbiology* 49: 711–45. <https://doi.org/10.1146/annurev.mi.49.100195.003431>.
- Dawson, Roger J. P., and Kaspar P. Locher. 2006. "Structure of a Bacterial Multidrug ABC Transporter." *Nature* 443 (7108): 180–85. <https://doi.org/10.1038/nature05155>. <https://doi.org/10.1016/j.febslet.2007.01.073>.

- Dean, M, A Rzhetsky, and R Allikmets. 2001. "The Human ATP-Binding Cassette (ABC) Transporter Superfamily." *Genome Research* 11 (7): 1156–66. <https://doi.org/10.1101/gr.184901>.
- Deisenhofer, J., O. Epp, K. Miki, R. Huber, and H. Michel. 1985. "Structure of the Protein Subunits in the Photosynthetic Reaction Centre of Rhodospseudomonas Viridis at 3Å Resolution." *Nature* 318 (6047): 618–24. <https://doi.org/10.1038/318618a0>.
- Delmar, Jared A., and Edward W. Yu. 2016. "The AbgT Family: A Novel Class of Antimetabolite Transporters: AbgT Family of Antimetabolite Transporters." *Protein Science* 25 (2): 322–37. <https://doi.org/10.1002/pro.2820>.
- Denisov, I. G., Y. V. Grinkova, A. A. Lazarides, and S. G. Sligar. 2004. "Directed Self-Assembly of Monodisperse Phospholipid Bilayer Nanodiscs with Controlled Size." *Journal of the American Chemical Society* 126 (11): 3477–87. <https://doi.org/10.1021/ja0393574>.
- Diederichs, K., J. Diez, G. Grellner, C. Müller, J. Breed, C. Schnell, C. Vonrhein, W. Boos, and W. Welte. 2000. "Crystal Structure of MalK, the ATPase Subunit of the Trehalose/Maltose ABC Transporter of the Archaeon Thermococcus Litoralis." *The EMBO Journal* 19 (22): 5951–61. <https://doi.org/10.1093/emboj/19.22.5951>.
- Dörr, Jonas M., Stefan Scheidelaar, Martijn C. Koorengevel, Juan J. Dominguez, Marre Schäfer, Cornelis A. van Walree, and J. Antoinette Killian. 2016. "The Styrene–Maleic Acid Copolymer: A Versatile Tool in Membrane Research." *European Biophysics Journal* 45 (1): 3–21. <https://doi.org/10.1007/s00249-015-1093-y>.
- Doyle, L. A., W. Yang, L. V. Abruzzo, T. Krogmann, Y. Gao, A. K. Rishi, and D. D. Ross. 1998. "A Multidrug Resistance Transporter from Human MCF-7 Breast Cancer Cells." *Proceedings of the National Academy of Sciences of the United States of America* 95 (26): 15665–70. <https://doi.org/10.1073/pnas.95.26.15665>.
- Dubochet, J., J. Lepault, R. Freeman, J. A. Berriman, and J.-C. Homo. 1982. "Electron Microscopy of Frozen Water and Aqueous Solutions." *Journal of Microscopy* 128 (3): 219–37. <https://doi.org/10.1111/j.1365-2818.1982.tb04625.x>.
- Dubochet, J., and A. W. McDowell. 1981. "Vitrification of Pure Water for Electron Microscopy." *Journal of Microscopy* 124 (3): 3–4. <https://doi.org/10.1111/j.1365-2818.1981.tb02483.x>.
- Dvir Rotem and Shimon Schuldiner. 2004. "EmrE, a Multidrug Transporter from Escherichia Coli, Transports Monovalent and Divalent Substrates with the Same Stoichiometry." *Journal of Biological Chemistry* 279 (47): 48787–93. <https://doi.org/10.1074/jbc.M408187200>.
- Eckford, Paul D. W., and Frances J. Sharom. 2010. "The Reconstituted Escherichia Coli MsbA Protein Displays Lipid Flippase Activity." *Biochemical Journal* 429 (Pt 1): 195–203. <https://doi.org/10.1042/BJ20100144>.
- Engilberge, Sylvain, François Riobé, Sebastiano Di Pietro, Louise Lassalle, Nicolas Coquelle, Charles-Adrien Arnaud, Delphine Pitrat, et al. 2017. "Crystallophore: A Versatile Lanthanide Complex for Protein Crystallography Combining Nucleating Effects, Phasing Properties, and Luminescence." *Chemical Science* 8 (9): 5909–17. <https://doi.org/10.1039/C7SC00758B>.
- Epand, Richard M., Chelsea Walker, Raquel F. Epand, and Nathan A. Magarvey. 2016. "Molecular Mechanisms of Membrane Targeting Antibiotics." *Biochimica et Biophysica Acta (BBA) - Biomembranes*, Antimicrobial peptides, cell membrane and microbial surface interaction, 1858 (5): 980–87. <https://doi.org/10.1016/j.bbamem.2015.10.018>.
- Esser, Lothar, Fei Zhou, Kristen M. Pluchino, Joseph Shiloach, Jichun Ma, Wai-Kwan Tang, Camilo Gutierrez, et al. 2017. "Structures of the Multidrug Transporter P-Glycoprotein Reveal Asymmetric ATP Binding and the Mechanism of Polyspecificity." *The Journal of Biological Chemistry* 292 (2): 446–61. <https://doi.org/10.1074/jbc.M116.755884>.
- European Centre for Disease Prevention and Control. Surveillance of and antimicrobial resistance in Europe 2018. Stockholm: ECDC. 2019. "Surveillance of Antimicrobial Resistance in Europe 2018," 110.
- Faham, Salem, and James U. Bowie. 2002. "Bicelle Crystallization: A New Method for Crystallizing Membrane Proteins Yields a Monomeric Bacteriorhodopsin Structure." *Journal of Molecular Biology* 316 (1): 1–6. <https://doi.org/10.1006/jmbi.2001.5295>.

- Fay, Jonathan F., Luba A. Aleksandrov, Timothy J. Jensen, Liying L. Cui, Joseph N. Kousouros, Lihua He, Andrei A. Aleksandrov, Drew S. Gingerich, John R. Riordan, and James Z. Chen. 2018. "Cryo-EM Visualization of an Active High Open Probability CFTR Anion Channel." *Biochemistry* 57 (43): 6234–46. <https://doi.org/10.1021/acs.biochem.8b00763>.
- Fernández, Lucía, and Robert E. W. Hancock. 2012. "Adaptive and Mutational Resistance: Role of Porins and Efflux Pumps in Drug Resistance." *Clinical Microbiology Reviews* 25 (4): 661–81. <https://doi.org/10.1128/CMR.00043-12>.
- Fernández-Villa, Daniel, Maria Rosa Aguilar, and Luis Rojo. 2019. "Folic Acid Antagonists: Antimicrobial and Immunomodulating Mechanisms and Applications." *International Journal of Molecular Sciences* 20 (20). <https://doi.org/10.3390/ijms20204996>.
- Fishovitz, Jennifer, Juan A. Hermoso, Mayland Chang, and Shahriar Mobashery. 2014. "Penicillin-Binding Protein 2a of Methicillin-Resistant Staphylococcus Aureus." *IUBMB Life* 66 (8): 572–77. <https://doi.org/10.1002/iub.1289>.
- Frank, J., W. Goldfarb, D. Eisenberg, and T.S. Baker. 1978. "RECONSTRUCTION OF GLUTAMINE SYNTHETASE USING COMPUTER AVERAGING." *Ultramicroscopy* 3 (3): 283–90.
- Frank, Joachim. 1975. "Averaging of Low Exposure Electron Micrographs of Non-Periodic Objects." *Ultramicroscopy* 1 (2): 159–62. [https://doi.org/10.1016/S0304-3991\(75\)80020-9](https://doi.org/10.1016/S0304-3991(75)80020-9).
- Frauenfeld, Jens, James Gumbart, Eli O. Van Der Sluis, Soledad Funes, Marco Gartmann, Birgitta Beatrix, Thorsten Mielke, et al. 2011. "Cryo-EM Structure of the Ribosome-SecYE Complex in the Membrane Environment." *Nature Structural and Molecular Biology* 18 (5): 614–21. <https://doi.org/10.1038/nsmb.2026>.
- Fribourg, Pierre Frederic, Mohamed Chami, Carlos Oscar S Sorzano, Francesca Gubellini, Roberto Marabini, Sergio Marco, Jean Michel Jault, and Daniel Lévy. 2014. "3D Cryo-Electron Reconstruction of BmrA, a Bacterial Multidrug ABC Transporter in an Inward-Facing Conformation and in a Lipidic Environment." *Journal of Molecular Biology* 426 (10): 2059–69. <https://doi.org/10.1016/j.jmb.2014.03.002>.
- Gao, Yuan, Erhu Cao, David Julius, and Yifan Cheng. 2016. "TRPV1 Structures in Nanodiscs Reveal Mechanisms of Ligand and Lipid Action." *Nature* 534 (7607): 347–51. <https://doi.org/10.1038/nature17964>.
- Gerard J. Tortora, Berdell R. Funke, and Christine L. Case. 2015. *Microbiology: An Introduction, Global Edition*. Edited by Pearson Education Limited. 12th ed. <https://www.dawsonera-com.docelec.univ-lyon1.fr/readonline/9781292099156>.
- Gewering, Theresa, Dovile Janulienė, Anne B. Ries, and Arne Moeller. 2018. "Know Your Detergents: A Case Study on Detergent Background in Negative Stain Electron Microscopy." *Journal of Structural Biology* 203 (3): 242–46. <https://doi.org/10.1016/j.jsb.2018.05.008>.
- Gottesman, Michael M., Tito Fojo, and Susan E. Bates. 2002. "Multidrug Resistance in Cancer: Role of ATP-Dependent Transporters." *Nature Reviews Cancer* 2 (1): 48–58. <https://doi.org/10.1038/nrc706>.
- Grant, Timothy, Alexis Rohou, and Nikolaus Grigorieff. 2018. "CisTEM, User-Friendly Software for Single-Particle Image Processing." *ELife* 7. <https://doi.org/10.7554/eLife.35383>.
- Gulamhussein, Aiman A., Romez Uddin, Brian J. Tighe, David R. Poyner, and Alice J. Rothnie. 2020. "A Comparison of SMA (Styrene Maleic Acid) and DIBMA (Di-Isobutylene Maleic Acid) for Membrane Protein Purification." *Biochimica et Biophysica Acta (BBA) - Biomembranes* 1862 (7): 183281. <https://doi.org/10.1016/j.bbamem.2020.183281>.
- Hardy, David, Roslyn M. Bill, Alice J. Rothnie, and Anass Jawhari. 2019. "Stabilization of Human Multidrug Resistance Protein 4 (MRP4/ABCC4) Using Novel Solubilization Agents." *Slas Discovery* 24 (10): 1009–17. <https://doi.org/10.1177/2472555219867074>.
- Heftmann, E., S. T. Ko, and R. D. Bennett. 1966. "Response of Steroids to Sulfuric Acid in Thin-Layer Chromatography." *Journal of Chromatography* 21 (3): 490–94. [https://doi.org/10.1016/s0021-9673\(01\)91347-0](https://doi.org/10.1016/s0021-9673(01)91347-0).

- Heijne, G. von. 1992. "Membrane Protein Structure Prediction. Hydrophobicity Analysis and the Positive-inside Rule." *Journal of Molecular Biology* 225 (2): 487–94. [https://doi.org/10.1016/0022-2836\(92\)90934-c](https://doi.org/10.1016/0022-2836(92)90934-c).
- Henderson, R., J. M. Baldwin, T. A. Ceska, F. Zemlin, E. Beckmann, and K. H. Downing. 1990. "Model for the Structure of Bacteriorhodopsin Based on High-Resolution Electron Cryo-Microscopy." *Journal of Molecular Biology* 213 (4): 899–929. [https://doi.org/10.1016/S0022-2836\(05\)80271-2](https://doi.org/10.1016/S0022-2836(05)80271-2).
- Henderson, R., and P. N. Unwin. 1975. "Three-Dimensional Model of Purple Membrane Obtained by Electron Microscopy." *Nature* 257 (5521): 28–32. <https://doi.org/10.1038/257028a0>.
- Heng, Jie, Yan Zhao, Ming Liu, Yue Liu, Junping Fan, Xianping Wang, Yongfang Zhao, and Xuejun C Zhang. 2015. "Substrate-Bound Structure of the E. Coli Multidrug Resistance Transporter MdfA." *Cell Research* 25 (9): 1060–73. <https://doi.org/10.1038/cr.2015.94>.
- Herold, Kerstin, Friedrich A Gollmick, Ingrid Groth, Martin Roth, Klaus-dieter Menzel, Ute Mçllmann, Udo Gräfe, and Christian Hertweck. 2005. "Cervimycin A – D : A Polyketide Glycoside Complex from a Cave Bacterium Can Defeat Vancomycin Resistance," 5523–30. <https://doi.org/10.1002/chem.200500320>.
- Higgins, C. F., and M. M. Gottesman. 1992. "Is the Multidrug Transporter a Flippase?" *Trends in Biochemical Sciences* 17 (1): 18–21. [https://doi.org/10.1016/0968-0004\(92\)90419-a](https://doi.org/10.1016/0968-0004(92)90419-a).
- Higgins, Christopher F., Ian D. Hiles, George P. C. Salmond, Deborah R. Gill, J. Allan Downie, Ian J. Evans, I. Barry Holland, et al. 1986. "A Family of Related ATP-Binding Subunits Coupled to Many Distinct Biological Processes in Bacteria." *Nature* 323 (6087): 448–50. <https://doi.org/10.1038/323448a0>.
- Higgins, Christopher F, and Kenneth J Linton. 2004. "The ATP Switch Model for ABC Transporters." *Nature Structural & Molecular Biology* 11 (10): 918–26. <https://doi.org/10.1038/nsmb836>.
- Ho, Hoangdung, Anh Miu, Mary Kate Alexander, Natalie K. Garcia, Angela Oh, Inna Zilberleyb, Mike Reichelt, et al. 2018. "Structural Basis for Dual-Mode Inhibition of the ABC Transporter MsbA." *Nature* 557 (7704): 196–201. <https://doi.org/10.1038/s41586-018-0083-5>.
- Hofmann, Susanne, Dovile Janulienė, Ahmad R. Mehdipour, Christoph Thomas, Erich Stefan, Stefan Brüchert, Benedikt T. Kuhn, et al. 2019. "Conformation Space of a Heterodimeric ABC Exporter under Turnover Conditions." *Nature* 571 (7766): 580–83. <https://doi.org/10.1038/s41586-019-1391-0>.
- Hohl, Michael, Christophe Briand, Markus G. Grütter, and Markus A. Seeger. 2012. "Crystal Structure of a Heterodimeric ABC Transporter in Its Inward-Facing Conformation." *Nature Structural & Molecular Biology* 19 (4): 395–402. <https://doi.org/10.1038/nsmb.2267>.
- Hohl, Michael, Lea M. Hürlimann, Simon Böhm, Jendrik Schöppe, Markus G. Grütter, Enrica Bordignon, and Markus A. Seeger. 2014. "Structural Basis for Allosteric Cross-Talk between the Asymmetric Nucleotide Binding Sites of a Heterodimeric ABC Exporter." *Proceedings of the National Academy of Sciences of the United States of America* 111 (30): 11025–30. <https://doi.org/10.1073/pnas.1400485111>.
- Høiby, Niels, Thomas Bjarnsholt, Michael Givskov, Søren Molin, and Oana Ciofu. 2010. "Antibiotic Resistance of Bacterial Biofilms." *International Journal of Antimicrobial Agents* 35 (4): 322–32. <https://doi.org/10.1016/j.ijantimicag.2009.12.011>.
- Holmes, Ann R., Ya-Hsun Lin, Kyoko Niimi, Erwin Lamping, Mikhail Keniya, Masakazu Niimi, Koichi Tanabe, Brian C. Monk, and Richard D. Cannon. 2008. "ABC Transporter Cdr1p Contributes More than Cdr2p Does to Fluconazole Efflux in Fluconazole-Resistant *Candida Albicans* Clinical Isolates." *Antimicrobial Agents and Chemotherapy* 52 (11): 3851–62. <https://doi.org/10.1128/AAC.00463-08>.
- Hooper, D. C. 1998. "Bacterial Topoisomerases, Anti-Topoisomerases, and Anti-Topoisomerase Resistance." *Clinical Infectious Diseases: An Official Publication of the Infectious Diseases Society of America* 27 Suppl 1 (August): S54-63. <https://doi.org/10.1086/514923>.

- Hopfner, Karl-peter, Annette Karcher, David S Shin, Lisa Craig, L Matthew Arthur, James P Carney, and John A Tainer. 2000. "Structural Biology of Rad50 ATPase : ATP-Driven Conformational Control in DNA Double-Strand Break Repair and the ABC-ATPase Superfamily" 101: 789–800.
- Hopwood, David A. 2007. "How Do Antibiotic-Producing Bacteria Ensure Their Self-Resistance before Antibiotic Biosynthesis Incapacitates Them?" *Molecular Microbiology* 63 (4): 937–40. <https://doi.org/10.1111/j.1365-2958.2006.05584.x>.
- Hughes, Taylor Et, John Smith Del Rosario, Abhijeet Kapoor, Aysenur Torun Yazici, Yevgen Yudin, Edwin C. Fluck, Marta Filizola, Tibor Rohacs, and Vera Y. Moiseenkova-Bell. 2019. "Structure-Based Characterization of Novel TRPV5 Inhibitors." *ELife* 8. <https://doi.org/10.7554/eLife.49572>.
- Hussein, Mouyassar J, Jacalyn M Green, and Brian P Nichols. 1998. "Characterization of Mutations That Allow P-Aminobenzoyl- Glutamate Utilization by Escherichia Coli." *J. BACTERIOL.* 180: 9.
- Ilia G. Denisov and Stephen G. Sligar. 2017. "NANODISCS IN MEMBRANE BIOCHEMISTRY AND BIOPHYSICS." *Chem Rev.* <https://doi.org/10.1021/acs.chemrev.6b00690>.
- Jackson, Scott M., Ioannis Manolaridis, Julia Kowal, Melanie Zechner, Nicholas M. I. Taylor, Manuel Bause, Stefanie Bauer, et al. 2018. "Structural Basis of Small-Molecule Inhibition of Human Multidrug Transporter ABCG2." *Nature Structural & Molecular Biology* 25 (4): 333–40. <https://doi.org/10.1038/s41594-018-0049-1>.
- Janas, Eva, Matthias Hofacker, Min Chen, Simone Gompf, Chris van der Does, and Robert Tampé. 2003. "The ATP Hydrolysis Cycle of the Nucleotide-Binding Domain of the Mitochondrial ATP-Binding Cassette Transporter Mdl1p." *Journal of Biological Chemistry* 278 (29): 26862–69. <https://doi.org/10.1074/jbc.M301227200>.
- Jardetzky, O. 1966. "Simple Allosteric Model for Membrane Pumps." *Nature* 211 (5052): 969–70. <https://doi.org/10.1038/211969a0>.
- Jin, Mi Sun, Michael L. Oldham, Qiuju Zhang, and Jue Chen. 2012. "Crystal Structure of the Multidrug Transporter P-Glycoprotein from Caenorhabditis Elegans." *Nature* 490 (7421): 566–69. <https://doi.org/10.1038/nature11448>.
- Johns Hopkins Coronavirus Resource Center. n.d. "COVID-19 Map." Johns Hopkins Coronavirus Resource Center. Accessed August 17, 2020. <https://coronavirus.jhu.edu/map.html>.
- Johnson, Zachary Lee, and Jue Chen. 2017a. "Structural Basis of Substrate Recognition by the Multidrug Resistance Protein MRP1." *Cell* 168 (6): 1075-1085.e9. <https://doi.org/10.1016/j.cell.2017.01.041>.
- Jones, Peter M., and Anthony M. George. 2009. "Opening of the ADP-Bound Active Site in the ABC Transporter ATPase Dimer: Evidence for a Constant Contact, Alternating Sites Model for the Catalytic Cycle." *Proteins: Structure, Function, and Bioinformatics* 75 (2): 387–96. <https://doi.org/10.1002/prot.22250>.
- Juliano, R. L., and V. Ling. 1976. "A Surface Glycoprotein Modulating Drug Permeability in Chinese Hamster Ovary Cell Mutants." *Biochimica Et Biophysica Acta* 455 (1): 152–62. [https://doi.org/10.1016/0005-2736\(76\)90160-7](https://doi.org/10.1016/0005-2736(76)90160-7).
- Katz, Leonard, and Gary W. Ashley. 2005. "Translation and Protein Synthesis: Macrolides." *Chemical Reviews* 105 (2): 499–528. <https://doi.org/10.1021/cr030107f>.
- Kerr, Ian D. 2002. "Structure and Association of ATP-Binding Cassette Transporter Nucleotide-Binding Domains." *Biochimica et Biophysica Acta (BBA) - Biomembranes* 1561 (1): 47–64. [https://doi.org/10.1016/S0304-4157\(01\)00008-9](https://doi.org/10.1016/S0304-4157(01)00008-9).
- Kim, Youngjin, and Jue Chen. 2018. "Molecular Structure of Human P-Glycoprotein in the ATP-Bound, Outward-Facing Conformation." *Science (New York, N.Y.)* 359 (6378): 915–19. <https://doi.org/10.1126/science.aar7389>.
- Kodan, Atsushi, Tomohiro Yamaguchi, Toru Nakatsu, Keita Matsuoka, Yasuhisa Kimura, Kazumitsu Ueda, and Hiroaki Kato. n.d. "Inward- and Outward-Facing X-Ray Crystal Structures of Homodimeric P-Glycoprotein CmABCB1." *Nature Communications*, no. 2019: 1–12. <https://doi.org/10.1038/s41467-018-08007-x>.

- Kodan, Atsushi, Tomohiro Yamaguchi, Toru Nakatsu, Keita Sakiyama, Christopher J. Hipolito, Akane Fujioka, Ryo Hirokane, et al. 2014. "Structural Basis for Gating Mechanisms of a Eukaryotic P-Glycoprotein Homolog." *Proceedings of the National Academy of Sciences of the United States of America* 111 (11): 4049–54. <https://doi.org/10.1073/pnas.1321562111>.
- Kohanski, Michael A, Daniel J Dwyer, and James J Collins. 2010. "How Antibiotics Kill Bacteria: From Targets to Networks." *Nature Reviews. Microbiology* 8 (6): 423–35. <https://doi.org/10.1038/nrmicro2333>.
- Krügel, Hans, Andreas Licht, Gesine Biedermann, Andreas Petzold, Jürgen Lassak, Yvonne Hupfer, Bernhard Schlott, et al. 2010. "Cervimycin C Resistance in *Bacillus Subtilis* Is Due to a Promoter Up-Mutation and Increased mRNA Stability of the Constitutive ABC-Transporter Gene *BmrA*." *FEMS Microbiology Letters* 313 (2): 155–63. <https://doi.org/10.1111/j.1574-6968.2010.02143.x>.
- Lacabanne, Denis, Cédric Orelle, Lauriane Lecoq, Britta Kunert, Claire Chuilon, Thomas Wiegand, Stéphanie Ravaut, Jean Michel Jault, Beat H. Meier, and Anja Böckmann. 2019. "Flexible-to-Rigid Transition Is Central for Substrate Transport in the ABC Transporter *BmrA* from *Bacillus Subtilis*." *Communications Biology* 2 (1): 1–9. <https://doi.org/10.1038/s42003-019-0390-x>.
- Landau, Ehud M., and Jürg P. Rosenbusch. 1996. "Lipidic Cubic Phases: A Novel Concept for the Crystallization of Membrane Proteins." *Proceedings of the National Academy of Sciences of the United States of America* 93 (25): 14532–35.
- Law, Christopher J., Peter C. Maloney, and Da-Neng Wang. 2008. "Ins and Outs of Major Facilitator Superfamily Antiporters." *Annual Review of Microbiology* 62: 289–305. <https://doi.org/10.1146/annurev.micro.61.080706.093329>.
- Le Maire, M., S. Kwee, J. P. Andersen, and J. V. Møller. 1983. "Mode of Interaction of Polyoxyethyleneglycol Detergents with Membrane Proteins." *European Journal of Biochemistry* 129 (3): 525–32. <https://doi.org/10.1111/j.1432-1033.1983.tb07080.x>.
- Lee, Jonas Y., Janet G. Yang, Daniel Zhitnitsky, Oded Lewinson, and Douglas C. Rees. 2014. "Structural Basis for Heavy Metal Detoxification by an *Atm1*-Type ABC Exporter." *Science (New York, N.Y.)* 343 (6175): 1133–36. <https://doi.org/10.1126/science.1246489>.
- Lee, Jyh-Yeuan, Lisa N. Kinch, Dominika M. Borek, Jin Wang, Junmei Wang, Ina L. Urbatsch, Xiao-Song Xie, et al. 2016. "Crystal Structure of the Human Sterol Transporter ABCG5/ABCG8." *Nature* 533 (7604): 561–64. <https://doi.org/10.1038/nature17666>.
- Levy, S. B. 1997. "Antibiotic Resistance: An Ecological Imbalance." *Ciba Foundation Symposium* 207: 1–9; discussion 9–14. <https://doi.org/10.1002/9780470515358.ch1>.
- Lewinson, Oded, and Nurit Livnat-Levanon. 2017. "Mechanism of Action of ABC Importers: Conservation, Divergence, and Physiological Adaptations." *Journal of Molecular Biology* 429 (5): 606–19. <https://doi.org/10.1016/j.jmb.2017.01.010>.
- Li, Bingyun, and Thomas J. Webster. 2018. "Bacteria Antibiotic Resistance: New Challenges and Opportunities for Implant-Associated Orthopedic Infections." *Journal of Orthopaedic Research* 36 (1): 22–32. <https://doi.org/10.1002/jor.23656>.
- Li, Jingzhi, Kimberly F. Jaimes, and Stephen G. Aller. 2014. "Refined Structures of Mouse P-Glycoprotein." *Protein Science: A Publication of the Protein Society* 23 (1): 34–46. <https://doi.org/10.1002/pro.2387>.
- Liao, Maofu, Erhu Cao, David Julius, and Yifan Cheng. 2013. "Structure of the TRPV1 Ion Channel Determined by Electron Cryo-Microscopy." *Nature* 504 (7478): 107–12. <https://doi.org/10.1038/nature12822>.
- Linton, Kenneth J., and Christopher F. Higgins. 2007. "Structure and Function of ABC Transporters: The ATP Switch Provides Flexible Control." *Pflügers Archiv - European Journal of Physiology* 453 (5): 555–67. <https://doi.org/10.1007/s00424-006-0126-x>.
- Liu, Fangyu, Zhe Zhang, László Csanády, David C. Gadsby, and Jue Chen. 2017. "Molecular Structure of the Human CFTR Ion Channel." *Cell* 169 (1): 85–95.e8. <https://doi.org/10.1016/j.cell.2017.02.024>.

- Liu, Yi-Yun, Yang Wang, Timothy R. Walsh, Ling-Xian Yi, Rong Zhang, James Spencer, Yohei Doi, et al. 2016. "Emergence of Plasmid-Mediated Colistin Resistance Mechanism MCR-1 in Animals and Human Beings in China: A Microbiological and Molecular Biological Study." *The Lancet. Infectious Diseases* 16 (2): 161–68. [https://doi.org/10.1016/S1473-3099\(15\)00424-7](https://doi.org/10.1016/S1473-3099(15)00424-7).
- Lobanovska, Mariya, and Giulia Pilla. 2017. "Penicillin's Discovery and Antibiotic Resistance: Lessons for the Future?" *Yale Journal of Biology and Medicine* 90 (1): 135–45.
- Locher, Kaspar P. 2016. "Mechanistic Diversity in ATP-Binding Cassette (ABC) Transporters." *Nature Structural & Molecular Biology* 23 (6): 487–93. <https://doi.org/10.1038/nsmb.3216>.
- Long, Feng, Corinne Rouquette-Loughlin, William M. Shafer, and Edward W. Yu. 2008. "Functional Cloning and Characterization of the Multidrug Efflux Pumps NorM from *Neisseria Gonorrhoeae* and YdhE from *Escherichia Coli*." *Antimicrobial Agents and Chemotherapy* 52 (9): 3052–60. <https://doi.org/10.1128/AAC.00475-08>.
- Loo, Tip W., and David M. Clarke. 2008. "Mutational Analysis of ABC Proteins." *Archives of Biochemistry and Biophysics* 476 (1): 51–64. <https://doi.org/10.1016/j.abb.2008.02.025>.
- Manolaridis, Ioannis, Scott M. Jackson, Nicholas M.I. Taylor, Julia Kowal, Henning Stahlberg, and Kaspar P. Locher. 2018. "Cryo-EM Structures of a Human ABCG2 Mutant Trapped in ATP-Bound and Substrate-Bound States." *Nature* 563 (7731): 426–30. <https://doi.org/10.1038/s41586-018-0680-3>.
- Marrer, Estelle, Karen Schad, Andreas T. Satoh, Malcolm G. P. Page, Maggie M. Johnson, and Laura J. V. Piddock. 2006. "Involvement of the Putative ATP-Dependent Efflux Proteins PatA and PatB in Fluoroquinolone Resistance of a Multidrug-Resistant Mutant of *Streptococcus Pneumoniae*." *Antimicrobial Agents and Chemotherapy* 50 (2): 685–93. <https://doi.org/10.1128/AAC.50.2.685-693.2006>.
- Martinez, Lorena, and Pierre Falson. 2014. "Multidrug Resistance ATP-Binding Cassette Membrane Transporters as Targets for Improving Oropharyngeal Candidiasis Treatment." *Advances in Cellular and Molecular Otolaryngology* 2 (1): 23955. <https://doi.org/10.3402/acmo.v2.23955>.
- Matar-Merheb, Rima, Moez Rhimi, Antoine Leydier, Frédéric Huché, Carmen Galián, Elodie Desuzinges-Mandon, Damien Ficheux, et al. 2011. "Structuring Detergents for Extracting and Stabilizing Functional Membrane Proteins." *PLoS ONE* 6 (3): 1–10. <https://doi.org/10.1371/journal.pone.0018036>.
- Mathieu, Khadija, Waqas Javed, Sylvain Vallet, Christian Lesterlin, Marie Pierre Candusso, Feng Ding, Xiaohong Nancy Xu, Christine Ebel, Jean Michel Jault, and Cédric Orelle. 2019. "Functionality of Membrane Proteins Overexpressed and Purified from *E. Coli* Is Highly Dependent upon the Strain." *Scientific Reports* 9 (1): 1–15. <https://doi.org/10.1038/s41598-019-39382-0>.
- McAleese, Fionnuala, Peter Petersen, Alexey Ruzin, Paul M. Dunman, Ellen Murphy, Steven J. Projan, and Patricia A. Bradford. 2005. "A Novel MATE Family Efflux Pump Contributes to the Reduced Susceptibility of Laboratory-Derived *Staphylococcus Aureus* Mutants to Tigecycline." *Antimicrobial Agents and Chemotherapy* 49 (5): 1865–71. <https://doi.org/10.1128/AAC.49.5.1865-1871.2005>.
- McMullan, G., A. R. Faruqi, and R. Henderson. 2016. "Direct Electron Detectors." *Methods in Enzymology* 579: 1–17. <https://doi.org/10.1016/bs.mie.2016.05.056>.
- Measures, Planned. 2016. "Key Elements Key Elements," no. March: 1–3.
- Mehmood, Shahid, Valentina Corradi, Hassanul G. Choudhury, Rohanah Hussain, Patrick Becker, Danny Axford, Severine Zirah, et al. 2016. "Structural and Functional Basis for Lipid Synergy on the Activity of the Antibacterial Peptide ABC Transporter McjD." *The Journal of Biological Chemistry* 291 (41): 21656–68. <https://doi.org/10.1074/jbc.M116.732107>.
- Mehmood, Shahid, Carmen Domene, Eric Forest, and Jean Michel Jault. 2012. "Dynamics of a Bacterial Multidrug ABC Transporter in the Inward- and Outward-Facing Conformations." *Proceedings of the National Academy of Sciences of the United States of America* 109 (27): 10832–36. <https://doi.org/10.1073/pnas.1204067109>.

- Mi, Wei, Yanyan Li, Sung Hwan Yoon, Robert K. Ernst, Thomas Walz, and Maofu Liao. 2017. "Structural Basis of MsbA-Mediated Lipopolysaccharide Transport." *Nature* 549 (7671): 233–37. <https://doi.org/10.1038/nature23649>.
- Miroux, B., and J. E. Walker. 1996. "Over-Production of Proteins in Escherichia Coli: Mutant Hosts That Allow Synthesis of Some Membrane Proteins and Globular Proteins at High Levels." *Journal of Molecular Biology* 260 (3): 289–98. <https://doi.org/10.1006/jmbi.1996.0399>.
- Mittal, Anshumali, Simon Böhm, Markus G. Grütter, Enrica Bordignon, and Markus A. Seeger. 2012. "Asymmetry in the Homodimeric ABC Transporter MsbA Recognized by a DARPIn." *The Journal of Biological Chemistry* 287 (24): 20395–406. <https://doi.org/10.1074/jbc.M112.359794>.
- Miyake, K., L. Mickley, T. Litman, Z. Zhan, R. Robey, B. Cristensen, M. Brangi, et al. 1999. "Molecular Cloning of cDNAs Which Are Highly Overexpressed in Mitoxantrone-Resistant Cells: Demonstration of Homology to ABC Transport Genes." *Cancer Research* 59 (1): 8–13.
- Miyazawa, Atsuo, Yoshinori Fujiyoshi, and Nigel Unwin. 2003. "Structure and Gating Mechanism of the Acetylcholine Receptor Pore." *Nature* 423 (6943): 949–55. <https://doi.org/10.1038/nature01748>.
- Moallem, Minoo. 2009. "The Revolution Will Not Be Fabricated." *Radical History Review*, no. 105: 123–31. <https://doi.org/10.1215/01636545-2009-008>.
- Moeller, Arne, Sung Chang Lee, Houchao Tao, Jeffrey A. Speir, Geoffrey Chang, Ina L. Urbatsch, Clinton S. Potter, Bridget Carragher, and Qinghai Zhang. 2015. "Distinct Conformational Spectrum of Homologous Multidrug ABC Transporters." *Structure (London, England : 1993)* 23 (3): 450–60. <https://doi.org/10.1016/j.str.2014.12.013>.
- Morita, Yuji, Kazuyo Kodama, Sumiko Shiota, Tomoyuki Mine, Atsuko Kataoka, Tohru Mizushima, and Tomofusa Tsuchiya. 1998. "NorM, a Putative Multidrug Efflux Protein, of *Vibrio Parahaemolyticus* and Its Homolog in *Escherichia Coli*." *Antimicrobial Agents and Chemotherapy* 42 (7): 1778–82.
- Nagle, John F., and Stephanie Tristram-Nagle. 2000. "Structure of Lipid Bilayers." *Biochimica et Biophysica Acta* 1469 (3): 159–95.
- Nakatani-Webster, Eri, Shiu-Lok Hu, William M. Atkins, and Carlos Enrique Catalano. 2015. "Assembly and Characterization of Gp160-Nanodiscs: A New Platform for Biochemical Characterization of HIV Envelope Spikes." *Journal of Virological Methods* 226 (December): 15–24. <https://doi.org/10.1016/j.jviromet.2015.09.011>.
- Neill, Jim O'. 2014. "Antimicrobial Resistance: Tackling a Crisis for the Health and Wealth of Nations The Review on Antimicrobial Resistance Chaired," no. December.
- Nguyen, Kim-Anh, Marine Peuchmaur, Sandrine Magnard, Romain Haudecoeur, Cédric Boyère, Saravanan Mounien, Ikram Benammar, et al. 2018. "Glycosyl-Substituted Dicarboxylates as Detergents for the Extraction, Overstabilization, and Crystallization of Membrane Proteins." *Angewandte Chemie (International Ed. in English)* 57 (11): 2948–52. <https://doi.org/10.1002/anie.201713395>.
- Nicklisch, Sascha C. T., Steven D. Rees, Aaron P. McGrath, Tufan Gökirmak, Lindsay T. Bonito, Lydia M. Vermeer, Cristina Cregger, et al. 2016. "Global Marine Pollutants Inhibit P-Glycoprotein: Environmental Levels, Inhibitory Effects, and Cocrystal Structure." *Science Advances* 2 (4): e1600001. <https://doi.org/10.1126/sciadv.1600001>.
- Nöll, Anne, Christoph Thomas, Valentina Herbring, Tina Zollmann, Katja Barth, Ahmad Reza Mehdipour, Thomas M. Tomasiak, et al. 2017. "Crystal Structure and Mechanistic Basis of a Functional Homolog of the Antigen Transporter TAP." *Proceedings of the National Academy of Sciences of the United States of America* 114 (4): E438–47. <https://doi.org/10.1073/pnas.1620009114>.
- O'neill, Jim. 2015. "Antimicrobials in Agriculture and the Environment: Reducing Unnecessary Use and Waste the Review on Antimicrobial Resistance," no. December.
- Ogawara, Hiroshi. 2016. "Self-Resistance in *Streptomyces*, with Special Reference to  $\beta$ -Lactam Antibiotics." *Molecules* 21 (5). <https://doi.org/10.3390/molecules21050605>.



- Oldham, Michael L., Nikolaus Grigorieff, and Jue Chen. 2016. "Structure of the Transporter Associated with Antigen Processing Trapped by Herpes Simplex Virus." *ELife* 5. <https://doi.org/10.7554/eLife.21829>.
- Oluwole, Abraham Olusegun, Bartholomäus Danielczak, Annette Meister, Jonathan Oyebamiji Babalola, Carolyn Vargas, and Sandro Keller. 2017. "Solubilization of Membrane Proteins into Functional Lipid-Bilayer Nanodiscs Using a Diisobutylene/Maleic Acid Copolymer." *Angewandte Chemie (International Ed. in English)* 56 (7): 1919–24. <https://doi.org/10.1002/anie.201610778>.
- Omote, Hiroshi, Miki Hiasa, Takuya Matsumoto, Masato Otsuka, and Yoshinori Moriyama. 2006. "The MATE Proteins as Fundamental Transporters of Metabolic and Xenobiotic Organic Cations." *Trends in Pharmacological Sciences* 27 (11): 587–93. <https://doi.org/10.1016/j.tips.2006.09.001>.
- Orelle, C, F Gubellini, a Durand, S Marco, D Levy, P Gros, a Di Pietro, and J M Jault. 2008. "Conformational Change Induced by ATP Binding in the Multidrug ATP-Binding Cassette Transporter BmrA." *Biochemistry* 47 (8): 2404–12. <https://doi.org/10.1021/bi702303s>.
- Orelle, Cédric, Olivier Dalmas, Philippe Gros, Attilio Di Pietro, and Jean Michel Jault. 2003. "The Conserved Glutamate Residue Adjacent to the Walker-B Motif Is the Catalytic Base for ATP Hydrolysis in the ATP-Binding Cassette Transporter BmrA." *Journal of Biological Chemistry* 278 (47): 47002–8. <https://doi.org/10.1074/jbc.M308268200>.
- Orelle, Cédric, Khadija Mathieu, and Jean-Michel Jault. 2019. "Multidrug ABC Transporters in Bacteria." *Research in Microbiology* 170 (8): 381–91. <https://doi.org/10.1016/j.resmic.2019.06.001>.
- Orlando, Benjamin J., and Maofu Liao. 2020. "ABCG2 Transports Anticancer Drugs via a Closed-to-Open Switch." *Nature Communications* 11 (1): 2264. <https://doi.org/10.1038/s41467-020-16155-2>.
- Ostermeier, C., and H. Michel. 1997. "Crystallization of Membrane Proteins." *Current Opinion in Structural Biology* 7 (5): 697–701. [https://doi.org/10.1016/s0959-440x\(97\)80080-2](https://doi.org/10.1016/s0959-440x(97)80080-2).
- Overington, John P, Bissan Al-Lazikani, and Andrew L Hopkins. 2006. "How Many Drug Targets Are There?" *Nat. Rev. Drug Discovery* 5 (12): 993–96. <https://doi.org/10.1038/nrd2199>.
- Pasipanodya, Jotam G., and Tawanda Gumbo. 2011. "A New Evolutionary and Pharmacokinetic-Pharmacodynamic Scenario for Rapid Emergence of Resistance to Single and Multiple Anti-Tuberculosis Drugs." *Current Opinion in Pharmacology* 11 (5): 457–63. <https://doi.org/10.1016/j.coph.2011.07.001>.
- Paulsen, Ian T. 2003. "Multidrug Efflux Pumps and Resistance: Regulation and Evolution." *Current Opinion in Microbiology* 6 (5): 446–51. <https://doi.org/10.1016/j.mib.2003.08.005>.
- Pebay-Peyroula, E., R. M. Garavito, J. P. Rosenbusch, M. Zulauf, and P. A. Timmins. 1995. "Detergent Structure in Tetragonal Crystals of OmpF Porin." *Structure (London, England: 1993)* 3 (10): 1051–59. [https://doi.org/10.1016/s0969-2126\(01\)00241-6](https://doi.org/10.1016/s0969-2126(01)00241-6).
- Pebay-Peyroula, Eva, Cécile Dahout-Gonzalez, Richard Kahn, Véronique Trézéguet, Guy J.-M. Lauquin, and Gérard Brandolin. 2003. "Structure of Mitochondrial ADP/ATP Carrier in Complex with Carboxyatractyloside." *Nature* 426 (6962): 39–44. <https://doi.org/10.1038/nature02056>.
- Poole, K., and R. Srikumar. 2001. "Multidrug Efflux in Pseudomonas Aeruginosa: Components, Mechanisms and Clinical Significance." *Current Topics in Medicinal Chemistry* 1 (1): 59–71. <https://doi.org/10.2174/1568026013395605>.
- Popot, Jean-Luc. 2010. "Amphipols, Nanodiscs, and Fluorinated Surfactants: Three Nonconventional Approaches to Studying Membrane Proteins in Aqueous Solutions." *Annual Review of Biochemistry* 79: 737–75. <https://doi.org/10.1146/annurev.biochem.052208.114057>.
- Popot, J.-L., T. Althoff, D. Bagnard, J.-L. Banères, P. Bazzacco, E. Billon-Denis, L. J. Catoire, et al. 2011. "Amphipols from A to Z." *Annual Review of Biophysics* 40: 379–408. <https://doi.org/10.1146/annurev-biophys-042910-155219>.
- Pos, Klaas M. 2009. "Drug Transport Mechanism of the AcrB Efflux Pump." *Biochimica Et Biophysica Acta* 1794 (5): 782–93. <https://doi.org/10.1016/j.bbapap.2008.12.015>.

- Pumroy, Ruth A., Amrita Samanta, Yuhang Liu, Taylor Et Hughes, Siyuan Zhao, Yevgen Yudin, Tibor Rohacs, Seungil Han, and Vera Y. Moiseenkova-Bell. 2019. "Molecular Mechanism of TRPV2 Channel Modulation by Cannabidiol." *ELife* 8. <https://doi.org/10.7554/eLife.48792>.
- Punjani, Ali, John L. Rubinstein, David J. Fleet, and Marcus A. Brubaker. 2017. "CryoSPARC: Algorithms for Rapid Unsupervised Cryo-EM Structure Determination." *Nature Methods* 14 (3): 290–96. <https://doi.org/10.1038/nmeth.4169>.
- Qian, Hongwu, Xin Zhao, Pingping Cao, Jianlin Lei, Nieng Yan, and Xin Gong. 2017. "Structure of the Human Lipid Exporter ABCA1." *Cell* 169 (7): 1228-1239.e10. <https://doi.org/10.1016/j.cell.2017.05.020>.
- Qiu, Weihua, Ziao Fu, Guoyan G. Xu, Robert A. Grassucci, Yan Zhang, Joachim Frank, Wayne A. Hendrickson, and Youzhong Guo. 2018. "Structure and Activity of Lipid Bilayer within a Membrane-Protein Transporter." *Proceedings of the National Academy of Sciences of the United States of America* 115 (51): 12985–90. <https://doi.org/10.1073/pnas.1812526115>.
- Ravaud, Stéphanie, Marie-Ange Do Cao, Marie Jidenko, Christine Ebel, Marc Le Maire, Jean-Michel Jault, Attilio Di Pietro, Richard Haser, and Nushin Aghajari. 2006. "The ABC Transporter BmrA from *Bacillus Subtilis* Is a Functional Dimer When in a Detergent-Solubilized State." *Biochemical Journal* 395 (2): 345–53. <https://doi.org/10.1042/BJ20051719>.
- Redfield, Robert R. 2019. "Antibiotic Resistance Threats in the United States." *Centers for Disease Control and Prevention*, 148. <https://doi.org/CS239559-B>.
- Rees, Douglas C., Eric Johnson, and Oded Lewinson. 2009. "ABC Transporters: The Power to Change." *Nature Reviews Molecular Cell Biology* 10 (3): 218–27. <https://doi.org/10.1038/nrm2646>.
- Robert, Xavier, Josiane Kassis-Sahyoun, Nicoletta Ceres, Juliette Martin, Michael R. Sawaya, Randy J. Read, Patrice Gouet, Pierre Falson, and Vincent Chaptal. 2017. "X-Ray Diffraction Reveals the Intrinsic Difference in the Physical Properties of Membrane and Soluble Proteins." *Scientific Reports* 7 (1): 17013. <https://doi.org/10.1038/s41598-017-17216-1>.
- Royant, Antoine, Peter Nollert, Karl Edman, Richard Neutze, Ehud M. Landau, Eva Pebay-Peyroula, and Javier Navarro. 2001. "X-Ray Structure of Sensory Rhodopsin II at 2.1-Å Resolution." *Proceedings of the National Academy of Sciences of the United States of America* 98 (18): 10131–36. <https://doi.org/10.1073/pnas.181203898>.
- Sauna, Zuben E., In-Wha Kim, Krishnamachary Nandigama, Stephan Kopp, Peter Chiba, and Suresh V. Ambudkar. 2007. "Catalytic Cycle of ATP Hydrolysis by P-Glycoprotein: Evidence for Formation of the E-S Reaction Intermediate with ATP- $\gamma$ -S, a Nonhydrolyzable Analogue of ATP." *Biochemistry* 46 (48): 13787–99. <https://doi.org/10.1021/bi701385t>.
- Saxton, W. O., and J. Frank. 1976. "Motif Detection in Quantum Noise-Limited Electron Micrographs by Cross-Correlation." *Ultramicroscopy* 2 (January): 219–27. [https://doi.org/10.1016/S0304-3991\(76\)91385-1](https://doi.org/10.1016/S0304-3991(76)91385-1).
- Scheres, Sjors H.W. 2012. "RELION: Implementation of a Bayesian Approach to Cryo-EM Structure Determination." *Journal of Structural Biology* 180 (3): 519–30. <https://doi.org/10.1016/j.jsb.2012.09.006>.
- Schmalstieg, Aurelia M., Shashikant Srivastava, Serkan Belkaya, Devyani Deshpande, Claudia Meek, Richard Leff, Nicolai S.C. Van Oers, and Tawanda Gumbo. 2012. "The Antibiotic Resistance Arrow of Time: Efflux Pump Induction Is a General First Step in the Evolution of Mycobacterial Drug Resistance." *Antimicrobial Agents and Chemotherapy* 56 (9): 4806–15. <https://doi.org/10.1128/AAC.05546-11>.
- Seddon, Annela M., Paul Curnow, and Paula J. Booth. 2004. "Membrane Proteins, Lipids and Detergents: Not Just a Soap Opera." *Biochimica et Biophysica Acta (BBA) - Biomembranes, Lipid-Protein Interactions*, 1666 (1): 105–17. <https://doi.org/10.1016/j.bbamem.2004.04.011>.
- Sgro, Germán G., and Tiago R. D. Costa. 2018. "Cryo-EM Grid Preparation of Membrane Protein Samples for Single Particle Analysis." *Frontiers in Molecular Biosciences* 5. <https://doi.org/10.3389/fmolb.2018.00074>.

- Shapiro, A. B., and V. Ling. 1997. "Positively Cooperative Sites for Drug Transport by P-Glycoprotein with Distinct Drug Specificities." *European Journal of Biochemistry* 250 (1): 130–37. <https://doi.org/10.1111/j.1432-1033.1997.00130.x>.
- Sharom, Frances Jane. 2014. "Complex Interplay between the P-Glycoprotein Multidrug Efflux Pump and the Membrane: Its Role in Modulating Protein Function." *Frontiers in Oncology* 4 (March). <https://doi.org/10.3389/fonc.2014.00041>.
- Shintre, C. A., A. C. W. Pike, Q. Li, J.-I. Kim, A. J. Barr, S. Goubin, L. Shrestha, et al. 2013. "Structures of ABCB10, a Human ATP-Binding Cassette Transporter in Apo- and Nucleotide-Bound States." *Proceedings of the National Academy of Sciences* 110 (24): 9710–15. <https://doi.org/10.1073/pnas.1217042110>.
- Srinivasan, Vasundara, Antonio J. Pierik, and Roland Lill. 2014. "Crystal Structures of Nucleotide-Free and Glutathione-Bound Mitochondrial ABC Transporter Atm1." *Science (New York, N.Y.)* 343 (6175): 1137–40. <https://doi.org/10.1126/science.1246729>.
- Steinfels, Emmanuelle, Cédric Orelle, Olivier Dalmas, François Penin, Bruno Miroux, Attilio Di Pietro, and Jean Michel Jault. 2002. "Highly Efficient Over-Production in E. Coli of YvcC, a Multidrug-like ATP-Binding Cassette Transporter from Bacillus Subtilis." *Biochimica et Biophysica Acta - Biomembranes* 1565 (1): 1–5. [https://doi.org/10.1016/S0005-2736\(02\)00515-1](https://doi.org/10.1016/S0005-2736(02)00515-1).
- Steinfels, Emmanuelle, Cédric Orelle, Jean Raphaël Fantino, Olivier Dalmas, Jean Louis Rigaud, François Denizot, Attilio Di Pietro, and Jean Michel Jault. 2004. "Characterization of YvcC (BmrA), a Multidrug ABC Transporter Constitutively Expressed in Bacillus Subtilis." *Biochemistry* 43 (23): 7491–7502. <https://doi.org/10.1021/bi0362018>.
- Sugimoto, K., T. Senda, H. Aoshima, E. Masai, M. Fukuda, and Y. Mitsui. 1999. "Crystal Structure of an Aromatic Ring Opening Dioxygenase LigAB, a Protocatechuate 4,5-Dioxygenase, under Aerobic Conditions." *Structure (London, England: 1993)* 7 (8): 953–65. [https://doi.org/10.1016/s0969-2126\(99\)80122-1](https://doi.org/10.1016/s0969-2126(99)80122-1).
- Sun, Chang, Samir Benlekbir, Padmaja Venkatakrishnan, Yuhang Wang, Sangjin Hong, Jonathan Hosler, Emad Tajkhorshid, John L. Rubinstein, and Robert B. Gennis. 2018. "Structure of the Alternative Complex III in a Supercomplex with Cytochrome Oxidase." *Nature* 557 (7703): 123–26. <https://doi.org/10.1038/s41586-018-0061-y>.
- Szewczyk, Paul, Houchao Tao, Aaron P. McGrath, Mark Villaluz, Steven D. Rees, Sung Chang Lee, Rupak Doshi, Ina L. Urbatsch, Qinghai Zhang, and Geoffrey Chang. 2015. "Snapshots of Ligand Entry, Malleable Binding and Induced Helical Movement in P-Glycoprotein." *Acta Crystallographica. Section D, Biological Crystallography* 71 (Pt 3): 732–41. <https://doi.org/10.1107/S1399004715000978>.
- Tanwar, Jyoti, Shrayanee Das, Zeeshan Fatima, and Saif Hameed. 2014. "Multidrug Resistance: An Emerging Crisis." *Interdisciplinary Perspectives on Infectious Diseases* 2014. <https://doi.org/10.1155/2014/541340>.
- Taylor, Nicholas M I, Ioannis Manolaridis, Scott M Jackson, Julia Kowal, Henning Stahlberg, and P Kaspar. 2017. "Structure of the Human Multidrug Transporter ABCG2." *Nature Publishing Group* 546 (7659): 504–9. <https://doi.org/10.1038/nature22345>.
- Taylor, Patrick K., Amy T. Y. Yeung, and Robert E. W. Hancock. 2014. "Antibiotic Resistance in Pseudomonas Aeruginosa Biofilms: Towards the Development of Novel Anti-Biofilm Therapies." *Journal of Biotechnology* 191 (December): 121–30. <https://doi.org/10.1016/j.jbiotec.2014.09.003>.
- Theuretzbacher, Ursula, Kevin Outtersson, Aleks Engel, and Anders Karlén. 2019. "The Global Preclinical Antibacterial Pipeline." *Nature Reviews Microbiology* 18 (May): 275–85. <https://doi.org/10.1038/s41579-019-0288-0>.
- Thomas, Christoph, and Robert Tampé. 2018. "Multifaceted Structures and Mechanisms of ABC Transport Systems in Health and Disease." *Current Opinion in Structural Biology* 51 (August): 116–28. <https://doi.org/10.1016/j.sbi.2018.03.016>.
- Thonghin, Nopnithi, Richard F. Collins, Alessandro Barbieri, Talha Shafi, Alistair Siebert, and Robert C. Ford. 2018. "Novel Features in the Structure of P-Glycoprotein (ABCB1) in the Post-Hydrolytic

- State as Determined at 7.9 Å Resolution." *BMC Structural Biology* 18 (1): 17.  
<https://doi.org/10.1186/s12900-018-0098-z>.
- Tribet, Christophe, Roland Audebert, and Jean-Luc Popot. 1996. "Amphipols: Polymers That Keep Membrane Proteins Soluble in Aqueous Solutions." *Proceedings of the National Academy of Sciences of the United States of America* 93 (26): 15047–50.
- Tseng, T. T., K. S. Gratwick, J. Kollman, D. Park, D. H. Nies, A. Goffeau, and M. H. Saier. 1999. "The RND Permease Superfamily: An Ancient, Ubiquitous and Diverse Family That Includes Human Disease and Development Proteins." *Journal of Molecular Microbiology and Biotechnology* 1 (1): 107–25.
- Veal, W. L. 2003. "Identification of a Cell Envelope Protein (MtrF) Involved in Hydrophobic Antimicrobial Resistance in *Neisseria Gonorrhoeae*." *Journal of Antimicrobial Chemotherapy* 51 (1): 27–37. <https://doi.org/10.1093/jac/dkg031>.
- Venkatesan, Nandakumar, Govindaraj Perumal, and Mukesh Doble. 2015. "Bacterial Resistance in Biofilm-Associated Bacteria." *Future Microbiology* 10 (11): 1743–50.  
<https://doi.org/10.2217/fmb.15.69>.
- Ventola, C. Lee. 2015. "Antibiotic Resistance Crisis." *International Journal of Medicine in Developing Countries* 40 (4): 277–83. <https://doi.org/10.24911/ijmdc.51-1549060699>.
- Vera, Laura, and Enrico A. Stura. 2014. "Strategies for Protein Cryocrystallography." *Crystal Growth & Design* 14 (2): 427–35. <https://doi.org/10.1021/cg301531f>.
- Vetter, I. R., and A. Wittinghofer. 1999. "Nucleoside Triphosphate-Binding Proteins: Different Scaffolds to Achieve Phosphoryl Transfer." *Quarterly Reviews of Biophysics* 32 (1): 1–56.  
<https://doi.org/10.1017/s0033583599003480>.
- Wagenknecht, T, J M Carazo, M Radermacher, and J Frank. 1989. "Three-Dimensional Reconstruction of the Ribosome from *Escherichia Coli*." *Biophysical Journal* 55 (3): 455–64.
- Wallin, Erik, and Gunnar Von Heijne. 2008. "Genome-Wide Analysis of Integral Membrane Proteins from Eubacterial, Archaeal, and Eukaryotic Organisms." *Protein Science* 7 (4): 1029–38.  
<https://doi.org/10.1002/pro.5560070420>.
- Ward, A. B., P. Szewczyk, V. Grimard, C.-W. Lee, L. Martinez, R. Doshi, A. Caya, et al. 2013. "Structures of P-Glycoprotein Reveal Its Conformational Flexibility and an Epitope on the Nucleotide-Binding Domain." *Proceedings of the National Academy of Sciences* 110 (33): 13386–91.  
<https://doi.org/10.1073/pnas.1309275110>.
- Ward, Andrew, Christopher L Reyes, Jodie Yu, Christopher B Roth, and Geoffrey Chang. 2007. "Flexibility in the ABC Transporter MsbA : Alternating Access with a Twist" 2007.
- "WHO Publishes List of Bacteria for Which New Antibiotics Are Urgently Needed." n.d. Accessed October 8, 2020. <https://www.who.int/news-room/detail/27-02-2017-who-publishes-list-of-bacteria-for-which-new-antibiotics-are-urgently-needed>.
- Wise, E M, and J T Park. 1965. "Penicillin: Its Basic Site of Action as an Inhibitor of a Peptide Cross-Linking Reaction in Cell Wall Mucopolysaccharide Synthesis." *Proceedings of the National Academy of Sciences of the United States of America* 54 (1): 75–81.
- Wiseman, Benjamin, Arnaud Kilburg, Vincent Chaptal, Gina Catalina Reyes-Mejia, Jonathan Sarwan, Pierre Falson, and Jean Michel Jault. 2014. "Stubborn Contaminants: Influence of Detergents on the Purity of the Multidrug ABC Transporter BmrA." *PLoS ONE* 9 (12): 1–25.  
<https://doi.org/10.1371/journal.pone.0114864>.
- Wright, Gerard D. 2000. "Resisting Resistance : New Chemical Strategies for Battling Superbugs," 127–32.
- Zhang, Zhe, and Jue Chen. 2016. "Atomic Structure of the Cystic Fibrosis Transmembrane Conductance Regulator." *Cell* 167 (6): 1586-1597.e9.  
<https://doi.org/10.1016/j.cell.2016.11.014>.
- Zhang, Zhe, Fangyu Liu, and Jue Chen. 2017. "Conformational Changes of CFTR upon Phosphorylation and ATP Binding." *Cell* 170 (3): 483-491.e8. <https://doi.org/10.1016/j.cell.2017.06.041>.

Zoonens, Manuela, and Jean-Luc Popot. 2014. "Amphipols for Each Season." *The Journal of Membrane Biology* 247 (0): 759–96. <https://doi.org/10.1007/s00232-014-9666-8>.



# APPENDIX





## Membrane Proteins

International Edition: DOI: 10.1002/anie.201713395

German Edition: DOI: 10.1002/ange.201713395

## Glycosyl-Substituted Dicarboxylates as Detergents for the Extraction, Overstabilization, and Crystallization of Membrane Proteins

Kim-Anh Nguyen<sup>†</sup>, Marine Peuchmaur<sup>†</sup>, Sandrine Magnard<sup>†</sup>, Romain Haudecoeur, Cédric Boyère, Saravanan Mounien, Ikram Benammar, Veronica Zampieri, Sébastien Igonet, Vincent Chaptal, Anass Jawhari, Ahcène Boumendjel,<sup>\*</sup> and Pierre Falson<sup>\*</sup>

**Abstract:** To tackle the problems associated with membrane protein (MP) instability in detergent solutions, we designed a series of glycosyl-substituted dicarboxylate detergents (DCODs) in which we optimized the polar head to clamp the membrane domain by including, on one side, two carboxyl groups that form salt bridges with basic residues abundant at the membrane–cytoplasm interface of MPs and, on the other side, a sugar to form hydrogen bonds. Upon extraction, the DCODs **8b**, **8c**, and **9b** preserved the ATPase function of *BmrA*, an ATP-binding cassette pump, much more efficiently than reference or recently designed detergents. The DCODs **8a**, **8b**, **8f**, **9a**, and **9b** induced thermal shifts of 20 to 29 °C for *BmrA* and of 13 to 21 °C for the native version of the G-protein-coupled adenosine receptor *A<sub>2A</sub>R*. Compounds **8f** and **8g** improved the diffraction resolution of *BmrA* crystals from 6 to 4 Å. DCODs are therefore considered to be promising and powerful tools for the structural biology of MPs.

Membrane proteins (MPs) play key roles in the transport and export of a wide range of substances in cells. Indeed, they account for 60% and 80% of all current and estimated pharmaceutical targets, respectively.<sup>[1,2]</sup> Unfortunately, MPs represent less than 1% of 3D-resolved structures,<sup>[3]</sup> irrespective of the approach used for obtaining these structures (X-ray diffraction or cryo-electron microscopy (cryo-EM)), despite recent progress for the latter.<sup>[4]</sup> A major challenge encountered with MPs during extraction, purification, and structural experiments is the change from the native lipophilic environment to an aqueous one, which can lead to the loss of the active conformation.<sup>[5]</sup> Detergents, commonly used to extract MPs, are amphiphathic molecules with a polar head and

a hydrophobic counterpart. They form complexes with MPs,<sup>[6]</sup> preventing irreversible aggregation in aqueous solution. However, being more exchangeable than lipids,<sup>[7]</sup> detergents tend to expose hydrophobic patches of the membrane domain of MPs<sup>[6]</sup> to water, which contributes to reducing their stability and promotes aggregation. In recent years, various clinically relevant MPs have been isolated and structurally resolved by detergent-aided extraction protocols; nevertheless, the conformation of proteins in micelles can be very different from the native conformation, leading to alterations in structure and function.<sup>[8]</sup>

One efficient strategy to overcome stability-related problems was mainly developed for GPCRs, rendering them thermostable with a gain of 17–21 °C by either introducing 6–17 mutations,<sup>[9,10]</sup> removing flexible loops, or combining them with proteins,<sup>[11]</sup> antibodies,<sup>[12]</sup> or nanobodies.<sup>[13]</sup> MP structures were successfully resolved by using a handful of detergents, especially the very popular *n*-dodecyl β-D-maltoside (DDM)<sup>[14]</sup> and, more recently, a dimer-like derivative, lauryl maltose neopentyl glycol (LMNG), with which Chae and co-workers achieved 11 °C of thermostabilization.<sup>[15,16]</sup> Cholate derivatives (facial amphiphiles, FA) also display remarkable stabilization properties when used as detergents.<sup>[17]</sup> Despite these technological advances, efforts must be made for the large majority of MPs that remain unstable once complexed to detergents. For example, we pioneered the generation of salt bridges between the polar head of the detergent and basic residues,<sup>[18]</sup> which are abundant in almost all MPs at their membrane–cytoplasm interface.<sup>[19]</sup> Herein, we further improved on this concept by designing new compounds that increase the thermostability of tested MPs.

We designed DCODs that share three structural features, namely a lipophilic tail, a polar head bearing two negatively charged carboxylates, and a sugar (glucoside or maltoside; Scheme 1). We used serine as a molecular platform flanked by one lipophilic tail linked to the amino group with a saccharide group grafted onto the hydroxy moiety, and two carboxylates derived from glutamic acid were attached to the carboxylic acid of serine. Direct glycosylation at the hydroxy group of serine was hampered by a β-elimination reaction, as already reported.<sup>[20,21]</sup> We achieved the synthesis through the introduction of a propargyl moiety on *N*-Boc serine, coupling with glutamic acid esters, and click chemistry with either protected glucosyl or maltosyl groups bearing an azido group, followed by deprotection of the benzyl and acetate groups. We prepared compounds with either a short (**8c**, **8d**), medium (**8b**, **9b**), or long aliphatic tail (**8a**, **9a**). We also introduced branched chains (**8e**, **8f**) and chains bearing a hydrophobic

[\*] Dr. K.-A. Nguyen,<sup>[†]</sup> Dr. M. Peuchmaur,<sup>[†]</sup> Dr. R. Haudecoeur, Dr. C. Boyère, S. Mounien, I. Benammar, Prof. A. Boumendjel  
DPM UMR 5063, Univ Grenoble-Alpes/CNRS  
38041 Grenoble (France)

E-mail: Ahcene.Boumendjel@univ-grenoble-alpes.fr

S. Magnard,<sup>[†]</sup> V. Zampieri, Dr. V. Chaptal, Dr. P. Falson  
DRMP group, IBCP UMR 5086 (MMSB), CNRS/Lyon I University  
69367 Lyon (France)

E-mail: Pierre.Falson@ibcp.fr

Dr. S. Igonet, Dr. A. Jawhari

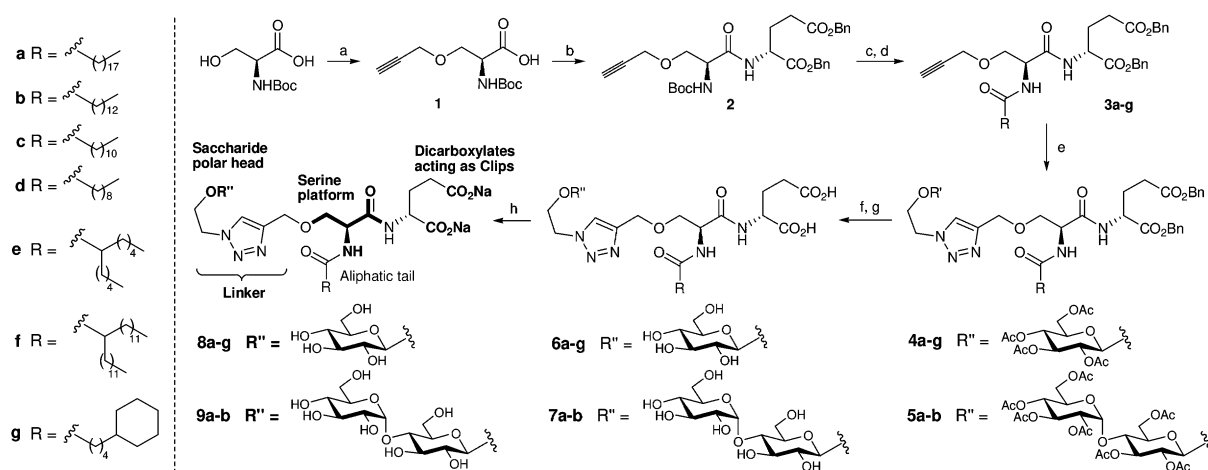
CALIXAR

60 avenue Rockefeller, 69008 Lyon (France)

[†] These authors contributed equally to this work.

Supporting information and the ORCID identification number(s) for the author(s) of this article can be found under:

<https://doi.org/10.1002/anie.201713395>.



**Scheme 1.** Synthesis of the DCODs **8a–8g**, **9a**, and **9b**. Reagents and conditions: a) propargyl bromide, NaH, DMF, RT, overnight; b) H-D-Glu(OBn)-OBn, *para*-tosylate, TBTU, DIPEA, DMF, RT, 3 h; c) TFA, CH<sub>2</sub>Cl<sub>2</sub>, 0 °C, 4–5 h; d) RCOCl, DMAP, pyridine, CH<sub>2</sub>Cl<sub>2</sub>, rt, overnight; e) glucosyl/maltosyl-OCH<sub>2</sub>CH<sub>2</sub>-N<sub>3</sub>, CuSO<sub>4</sub>·5H<sub>2</sub>O, sodium ascorbate, DMF, microwave, 140 °C, 30–60 min; f) MeONa, MeOH, RT, overnight; g) LiOH, THF/H<sub>2</sub>O, RT, 4 h; h) MeONa, MeOH, RT. DIPEA = diisopropylethylamine, DMAP = 4-dimethylaminopyridine, DMF = *N,N*-dimethylformamide, TBTU = 2-(1*H*-benzotriazol-1-yl)-1,1,3,3-tetramethyluronium tetrafluoroborate, TFA = trifluoroacetic acid.

cyclic ring (**8g**). All DCODs (see the Supporting Information, Figures S1 and S2) were fully water-soluble and could be prepared on gram scale.

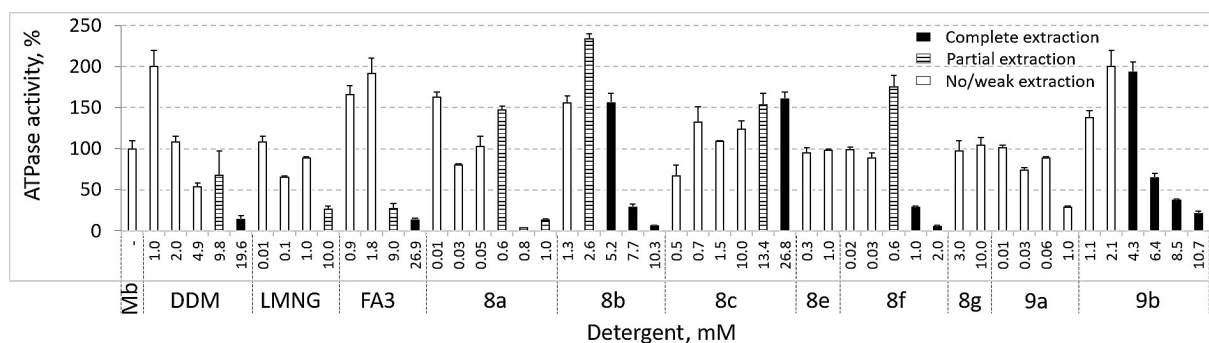
As expected, the critical micellar concentration (CMC) of the DCODs (Figures S2 and S3) correlated with the length of the hydrophobic chain and the nature of the polar head group. The lowest values were obtained with a C<sub>18</sub> alkyl tail irrespective of the glucoside or maltoside present in the polar head group (**8a**, **9a**). Branched alkyl chains such as CH(C<sub>5</sub>H<sub>11</sub>)<sub>2</sub> and CH(C<sub>12</sub>H<sub>25</sub>)<sub>2</sub> (**8e**, **8f**) did not show added value compared to linear ones. Compared to DDM, the CMCs of the C<sub>13</sub> alkyl-tail DCODs were much higher, in the millimolar range, depending on the sugar whereas the C<sub>18</sub> alkyl-tail DCODs gave CMCs in the micromolar range, indicating their tendency to self-assemble. Dynamic light scattering (DLS) experiments (Figures S2 and S4) showed that DCOD micelles are either quite large (20–30 nm; **8d**, **8c**, **8f**), suggesting that they may generate tube-shaped objects, or very small (0.25–2.5 nm; **8b**, **8a**, **9b**, **9a**), indicating a low aggregation number.

We evaluated the capacity of DCODs to extract two polytopic drug efflux pumps, namely BmrA,<sup>[22]</sup> which is a homodimer, and the acriflavine resistance protein AcrB, a homotrimer belonging to the random nodule division (RND) family.<sup>[23]</sup> We carried out their extraction by incubating the membranes with a fivefold excess (w/w) of the detergent (see the Supporting Information). The supernatants were clarified by centrifugation and analyzed by SDS-PAGE (Figure S5). Without solubilizing supports, BmrA and AcrB were faintly detected. However, in the presence of detergents, both MPs were found in the supernatants in different ranges, depending on the DCOD concentration. DCODs **8b**, **9a**, and, to a lesser extent, **8a** and **8f** efficiently extracted BmrA, while **8b**, **8a**, **9b**, and **9a** showed good extraction capacities for AcrB.

We then addressed the functionality of MPs extracted with DCODs by comparison with DDM, LMNG,<sup>[15]</sup> and

FA3.<sup>[17]</sup> We probed whether the ATPase activity of BmrA, which is coupled to drug efflux in membranes, is maintained in solution (Figure 1). As generally observed with BmrA, the addition of sub-solubilizing concentrations of a mild detergent is not deleterious for the protein, but a further increase to solubilizing concentrations leads to its partial/complete inactivation. This was the case for DDM, LMNG, and FA3, with which BmrA lost up to 85% functionality at full extraction. DCOD **8f** displayed the same pattern, while **9a**, **8e**, and **8g** did not extract BmrA, and **8a** only partially extracted it (Figure 1). On the contrary, **8c**, **8b**, and **9b** provided BmrA with functional stabilization, even at solubilizing concentrations. The best functional stabilization was reached with the maltoside derivative **9b**. It is worth noting that a longer hydrophobic tail, typically C<sub>18</sub>, as in **8a** and **9a**, appeared not to be beneficial, while a branched chain as in **8f** was. Finally, we checked with **8b** that BmrA remained functional in the supernatant fraction after extraction and centrifugation (Figure S7).

We then studied the stability as a function of time and temperature. We compared DCOD **8b** with DDM and FA3, for which stability properties over time were recently reported together with their use in generating well-diffracting crystals of MsbA,<sup>[17]</sup> a homologue of BmrA. We mixed DDM, FA3, or DCOD **8b** with DDM-purified BmrA aliquots, adding them at 10% (0.09 mM) of the total (BmrA-bound + free) DDM concentration (0.9 mM). The amount of DDM in complex with BmrA can be estimated to be about 400 ± 40 mol mol<sup>-1</sup>.<sup>[6]</sup> To test the capacity of the detergents to maintain their stabilizing effect despite a large excess of DDM, we diluted the detergents after incubation by adding 300% of DDM to reach a final total DDM concentration of 2.7 mM, which is about 30 times higher than that of **8b** or FA3. We stored the aliquots for up to 40 days, and tightened the conditions of the test by setting the temperature to 18 °C. The ATPase activity of BmrA was probed during this time. As observed (Figure 2A), BmrA incubated with DDM and **8b**



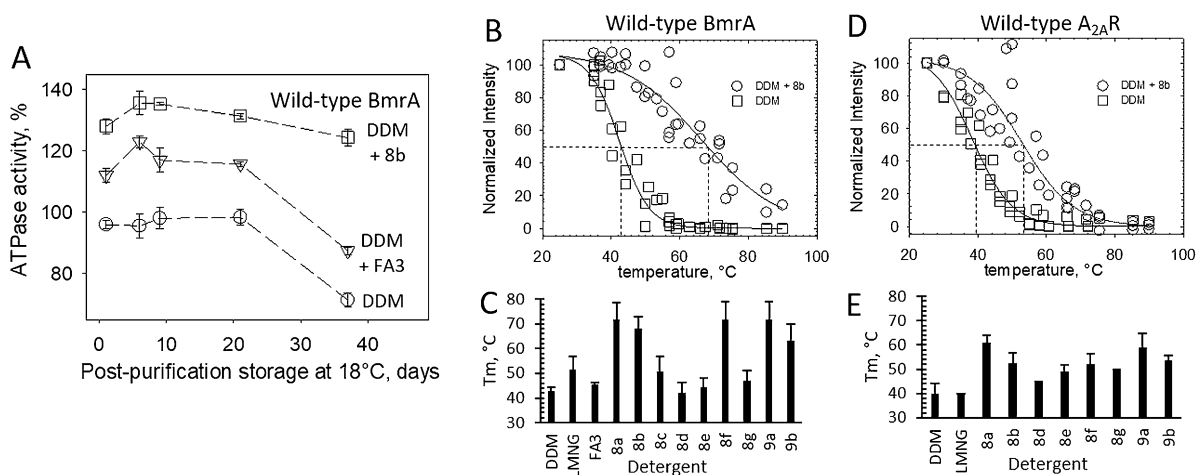
**Figure 1.** ATPase activity of BmrA with DCODs. Values are normalized to the assay without detergent (Mb,  $0.7 \mu\text{mol ATP min}^{-1} \text{mg}^{-1}$ , 3 independent experiments). Black, gray, and white bars correspond to the detergent concentration at which BmrA is either fully, partially, or not solubilized, as deduced from Figure S6.

remained fully stable at this temperature (at which crystallization occurs in 2–3 days compared to three weeks at  $4^\circ\text{C}$ ). In contrast, BmrA displayed a significant loss of activity when incubated with DDM alone or with DDM and FA3.

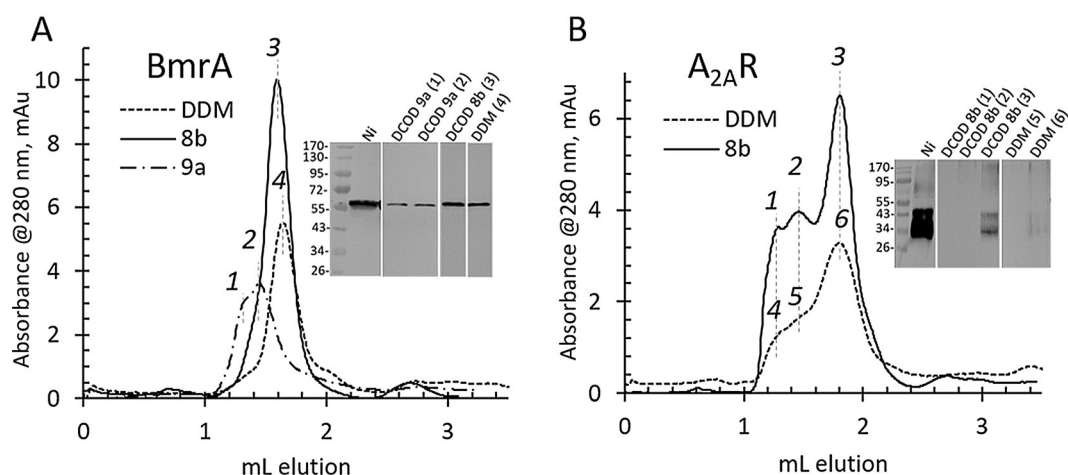
We then evaluated the stability of MPs with temperature in the presence or absence of DCODs (Figure 2B–E). We tested them on BmrA (B,C) and on the native version of the adenosine  $A_{2A}$  receptor ( $A_{2A}R$ ; D,E), that is, without any truncation, mutation, or fusion designed to increase its stability.<sup>[9,10]</sup> MPs were extracted with 10 mM DDM, with or without 1 mM of a DCOD or a commercial detergent, then clarified by centrifugation, and further subjected to 30 min incubation at 25 to  $90^\circ\text{C}$ .<sup>[24]</sup> The aggregated material was then removed by centrifugation and the supernatant submitted to SDS-PAGE and Western blot analysis to quantify the remaining solubilized MPs. A full experiment is displayed in Figure 2B and D for each protein fraction incubated with **8b**, allowing the apparent melting temperatures,  $T_m$ , at which 50% of BmrA or  $A_{2A}R$  remains in solution (dotted lines), to be estimated. Other  $T_m$  values are given in Figure 2C,E. As

shown, the DCODs **8a**, **8b**, **8f**, **9a**, and **9b** induced a thermal shift of 20 to  $29^\circ\text{C}$  for BmrA and of 13 to  $21^\circ\text{C}$  for  $A_{2A}R$  while the others did not produced a marked shift. A clear effect was observed with respect to the hydrophobic component, namely the larger, the better. Note that this gain in thermostability is equivalent to that obtained previously by introducing 17 mutations in a maltose-binding protein– $A_{2A}R$  fusion protein with a C-terminal 96 residue truncation.<sup>[9]</sup> This result positions DCODs at the forefront of the very small set of stabilizing detergents, such as LMNG,<sup>[15]</sup> FA3,<sup>[17]</sup> and the recently published norbornane-based maltosides (NBMs),<sup>[25]</sup> that are able to generate an increase in  $T_m$  of more than one log unit.

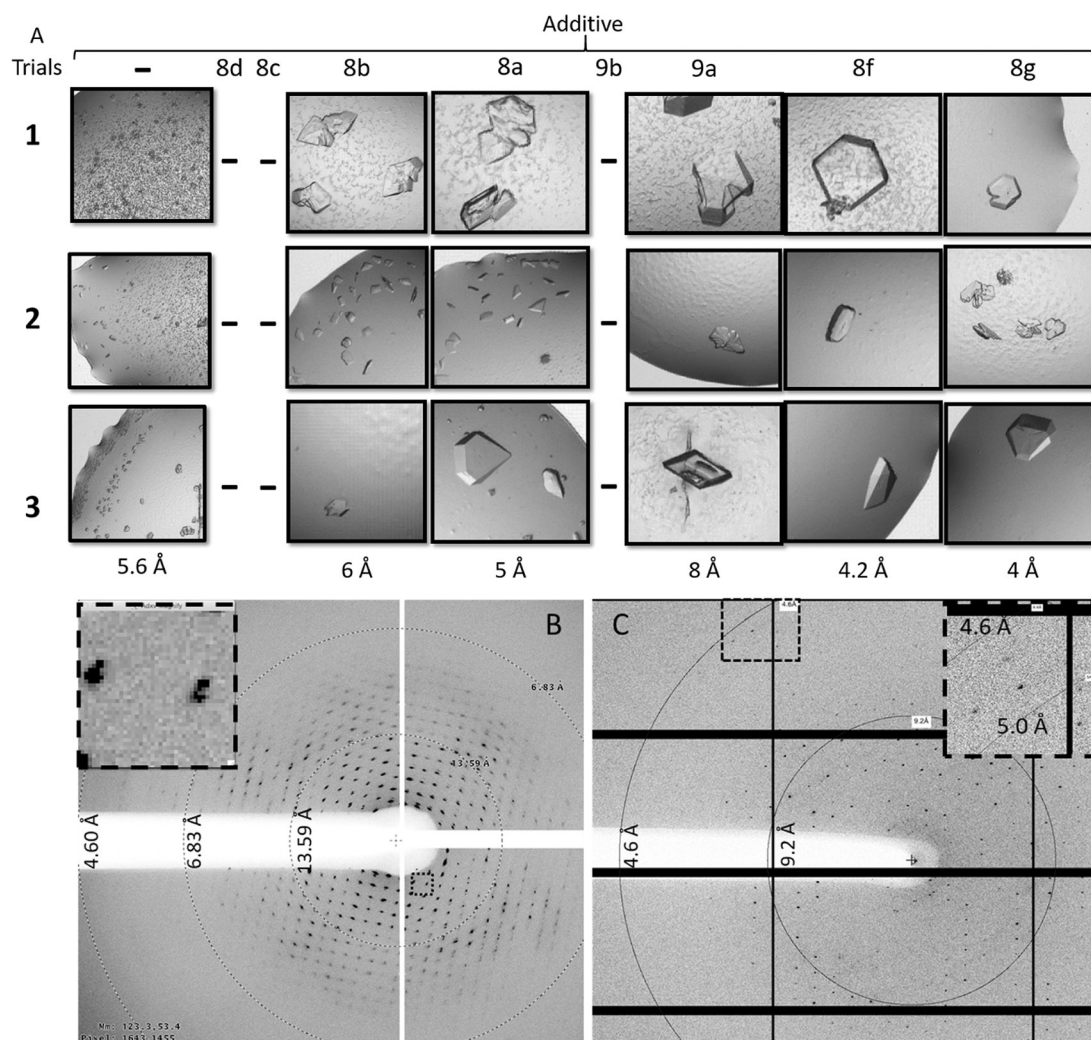
We then studied the behavior of BmrA and the native  $A_{2A}$  receptor in solution with DCODs, which was probed by size exclusion chromatography (SEC). We carried out the experiments either with BmrA in solution with DCOD **8b** (glucosyl and  $C_{13}$  tail) or **9a** (maltoside and  $C_{18}$  tail), or with  $A_{2A}R$  in solution with DCOD **8b**, and compared the results to the use of DDM (maltoside and  $C_{12}$  tail). The MPs were extracted and



**Figure 2.** Stability of MPs with DCODs. A) Stability with time of DDM-purified BmrA with DDM, DCOD **8b**, and FA3. BmrA was purified in DDM, and the last SEC pool was diluted to  $1.5 \mu\text{M}$  BmrA and  $0.3 \text{ mM}$  free DDM, to which  $0.1 \text{ mM}$  of DDM, FA3, or **8b** was added, followed by  $2.7 \text{ mM}$  DDM. Samples were stored at  $18^\circ\text{C}$ , and the ATPase activity of BmrA was measured with time (2 measurements). B–E) Thermostabilization of BmrA (B,C) and  $A_{2A}R$  (D,E) by DCODs. Membrane fractions were extracted with 10 mM DDM with or without 1 mM detergent, clarified, and heated at the indicated temperature for 30 min followed by centrifugation. The remaining MPs were quantified by SDS-PAGE and Western blot analysis (2–4 experiments).



**Figure 3.** SEC of BmrA and A<sub>2A</sub>R with DCODs or DDM. Proteins were extracted and purified in DDM by nickel affinity chromatography and SEC (Superdex 200 10/300), and aliquots were reloaded onto a nickel affinity column for exchanging DDM either with itself or with DCOD **8b** or **9a**, and then eluted through a Superdex 200 5/150 equilibrated with each detergent (calibration in Figure S8).



**Figure 4.** BmrA-E504A crystallization and crystal diffraction with DCODs. Three independent experiments from three separate purifications; statistics in Figure S9. B, C) Diffraction of BmrA crystals without (B, ESRF beamline ID30A on a Pilatus detector, rendered using Adxv software) and with (C, SOLEIL beamline PX2 on an Eiger detector rendered using Albula Dextris software) DCOD **8f**. Diffraction spots are visible up to 5.6 Å (B) or 4.6 Å (C) resolution but could only be processed in the latter (Figure S9) owing to multiplicity in the former.

purified in DDM by nickel affinity chromatography followed by SEC carried out on a Superdex 200 10/300, and then reloaded onto nickel resin on which detergents were exchanged followed by SEC carried out with a Superdex 200 5/150 (Figure 3). We determined by matrix-assisted laser desorption/ionization (MALDI) mass spectrometry, as we recently set up,<sup>[6]</sup> that most of the DDM had indeed been exchanged by this procedure (not shown). As observed, both proteins gave similar profiles with DCOD **8b** and DDM, with a main peak (3 and 4 for BmrA and 3 and 6 for A<sub>2A</sub>R) corresponding to the dimeric state of BmrA and the monomeric state of A<sub>2A</sub>R, respectively. Whatever the detergent, DCOD **8b** or DDM, A<sub>2A</sub>R gave two other species (peaks 1 and 4 and 2 and 5 in panel B) corresponding to higher oligomeric forms. BmrA in solution with DCOD **9a** mainly led to higher oligomeric forms in agreement with a dimer (peak 2, panel A) and tetramer (peak 1, panel A) of the homodimer. Consequently, the behavior of DCOD **8b** is equivalent to that of DDM for both proteins while DCOD **9b** stabilizes bigger oligomers, a property that is probably due to its longer aliphatic tail.

Finally, we looked at the capacity of DCODs to promote crystallization and to improve the crystal resolution of MPs. For this purpose, we tested DCODs on BmrA, for which we attempted to solve the 3D structure, and that we purified as previously reported.<sup>[22]</sup> BmrA crystallizes routinely in the presence of PEG 1000, giving crystals that diffract to 6–8 Å. We tested the DCODs as crystallization additives by adding each at 1 CMC in the crystallization drop from a 10× concentrated solution. Crystals appeared after three days at 18°C and were grown for one week.

As shown in Figure 4, DCODs bearing a glucoside moiety (compounds **8**) promoted crystallization much better than those bearing a maltoside (compounds **9**), and the larger the hydrophobic component, the better (**8f** > **8a** > **8b** > **9a**). Indeed, **8f** promoted the formation of well-organized crystals diffracting to up to 4 Å. Most importantly, DCOD additives improved the quality of the diffraction pattern (Figure 4B vs. C). While crystals generated without additives appeared morphologically to be monocrystalline, the diffraction pattern displayed split spots synonymous to multiple crystals and crystal packing defects, preventing data processing (Figure 4B). The presence of **8f** or **8g** allowed for better and bigger crystals to form, which diffracted with single spots and allowed for data processing (Figure 4C).

According to this study, the DCODs **8b**, **8c**, and **9b** can be considered as highly promising compounds for extracting and stabilizing flexible MPs while **8f** and **8g** can be used for improving MP crystallization.

## Acknowledgements

K.-A.N., M.P., R.H., and A.B. are grateful to the Agence Nationale pour la Recherche for financial support (Labex Arcane ANR-11-LABX-0003-01). K.-A.N., M.P., S.M., V.C., A.B., and P.F. are also thankful to ANR for financial support

(ANR Blanc CLAMPS 2014-17). P.F. warmly thanks Prof. Léa Payen for access to her MALDI apparatus. P.F., V.C., and V.Z. also thank ESRF and SOLEIL synchrotrons for the time and the help they gave for crystal diffraction and analyses.

## Conflict of interest

K.-A.N., M.P., S.M., A.B., and P.F. are inventors of a patent (patent being filed) covering some of the results reported in this study.

**Keywords:** amphiphiles · detergents · glycosides · membrane proteins · stabilization

**How to cite:** *Angew. Chem. Int. Ed.* **2018**, *57*, 2948–2952  
*Angew. Chem.* **2018**, *130*, 2998–3002

- [1] P. Imming, C. Sinning, A. Meyer, *Nat. Rev. Drug Discovery* **2006**, *5*, 821–835.
- [2] J. P. Overington, B. Al-lazikani, A. L. Hopkins, *Nat. Rev. Drug Discovery* **2006**, *5*, 993–996.
- [3] Membrane proteins of known 3D structure, <http://blanco.biomol.uci.edu/mpstruc> (accessed Apr 12, **2017**).
- [4] W. Kühlbrandt, *Elife* **2014**, *3*, e03678.
- [5] G. G. Privé, *Methods* **2007**, *41*, 388–397.
- [6] V. Chaptal et al., *Sci. Rep.* **2017**, *7*, 41751.
- [7] J. N. Israelachvili, D. J. Mitchell, B. W. Ninham, *Biochim. Biophys. Acta Biomembr.* **1977**, *470*, 185–201.
- [8] M. Zoonens, J. Comer, S. Masscheleyn, E. Pebay-Peyroula, C. Chipot, B. Miroux, F. Dehez, *J. Am. Chem. Soc.* **2013**, *135*, 15174–15182.
- [9] F. Magnani, Y. Shibata, M. J. Serrano-Vega, C. G. Tate, *Proc. Natl. Acad. Sci. USA* **2008**, *105*, 10744–10749.
- [10] M. J. Serrano-Vega, F. Magnani, Y. Shibata, C. G. Tate, *Proc. Natl. Acad. Sci. USA* **2008**, *105*, 877–882.
- [11] G. Lebon, T. Warne, P. C. Edwards, K. Bennett, C. J. Langmead, A. G. W. Leslie, C. G. Tate, *Nature* **2011**, *474*, 521–525.
- [12] T. Hino et al., *Nature* **2012**, *482*, 237–240.
- [13] A. M. Ring, A. Manglik, A. C. Kruse, M. D. Enos, W. I. Weis, K. C. Garcia, B. K. Kobilka, *Nature* **2013**, *502*, 575–579.
- [14] P. Rosevear, T. VanAken, J. Baxter, S. Ferguson-Miller, *Biochemistry* **1980**, *19*, 4108–4115.
- [15] P. S. Chae et al., *Nat. Methods* **2010**, *7*, 1003–1008.
- [16] S. G. F. Rasmussen et al., *Nature* **2007**, *450*, 383–387.
- [17] S. C. Lee et al., *Proc. Natl. Acad. Sci. USA* **2013**, *110*, E1203–E1211.
- [18] R. Matar-Merheb et al., *PLoS One* **2011**, *6*, e18036.
- [19] G. von Heijne, *Nat. Rev. Mol. Cell Biol.* **2006**, *7*, 909–918.
- [20] P. Sjölin et al., *J. Chem. Soc. Perkin Trans. 1* **1999**, 1731–1742.
- [21] P. Sjölin, J. Kihlberg, *J. Org. Chem.* **2001**, *66*, 2957–2965.
- [22] B. Wiseman, A. Kilburg, V. Chaptal, G. C. Reyes-Mejia, J. Sarwan, P. Falson, J.-M. Jault, *PLoS One* **2014**, *9*, e114864.
- [23] L. Daury et al., *Nat. Commun.* **2016**, *7*, 10731.
- [24] Y. Ashok, R. Nanekar, V.-P. Jaakola, *Protein Eng. Des. Sel.* **2015**, *28*, 539–542.
- [25] M. Das et al., *J. Am. Chem. Soc.* **2017**, *139*, 3072–3081.

Manuscript received: December 30, 2017

Accepted manuscript online: January 29, 2018

Version of record online: February 13, 2018